

6-30-2017

Porphyrinoids with Designed Properties

Michael P. Luciano

University of Connecticut - Storrs, michael.luciano@uconn.edu

Follow this and additional works at: <https://opencommons.uconn.edu/dissertations>

Recommended Citation

Luciano, Michael P., "Porphyrinoids with Designed Properties" (2017). *Doctoral Dissertations*. 1501.
<https://opencommons.uconn.edu/dissertations/1501>

Porphyrinoids with Designed Properties

Michael P. Luciano, Ph.D.

University of Connecticut, 2017

This thesis focuses on the development of new synthetic methodologies toward porphyrinoids with properties designed for various applications. Among the chromophores studied are the quinoline-annulated porphyrins, a relatively unexplored class of π -extended porphyrinoids that absorb light in the near-infrared region (NIR). Another class studied are the pyrrole-modified porphyrins (PMPs), (hydro)porphyrin analogues containing a non-pyrrolic building block.

The synthesis of chlorin and chlorin-analogues of the quinoline-annulated porphyrins are described that are characterized by even more red-shifted optical spectra than regular quinoline-annulated porphyrins (**Chapter 2**). The NIR-emitting platinum(II) complexes of the quinoline-annulated porphyrins suggest potential *in vivo* O₂ sensing applications (**Chapter 3**). Photophysical studies of the free-base quinoline-annulated porphyrins, along with *ex vivo* photoacoustic imaging (PAI) studies, revealed their promise as novel PAI contrast agents. The preparation of water-soluble derivatives and their evaluation *in vivo* for the PAI imaging of an implanted tumor in a mouse model is described (**Chapter 4**).

A new methodology toward hitherto inaccessible PMPs incorporating medium-sized rings is also delineated (**Chapter 5**). Initial experiments toward this class of PMPs resulted in a serendipitous finding of a more efficient route toward a known class of PMPs containing an imidazolone moiety, the porpholactams. The conversion of the porpholactam to a number of chelator-substituted imidazoloporphyrins toward the goal of generating metal-ion chemosensors for the selective and sensitive detection of M²⁺ cations is also delineated (**Chapter 6**).

Porphyrinoids with Designed Properties

Michael P. Luciano

B.S., Merrimack College, 2012

A Dissertation

Submitted in Partial Fulfillment of the

Requirements for the Degree of

Doctor of Philosophy

at the

University of Connecticut

2017

Copyright by
Michael P. Luciano

2017

APPROVAL PAGE

Porphyrinoids with Designed Properties

Presented by

Michael P. Luciano, B.S.

Major Advisor

Christian Brückner

Associate Advisor

Amy Howell

Associate Advisor

Mark Peczu

Associate Advisor

Edward Neth

University of Connecticut

2017

Acknowledgements

First and foremost, I would like to thank my advisor Prof. Christian Brückner, for his support and mentorship throughout the years. I am grateful for the opportunity to join your lab and I am excited to take what I have learned from you and apply it to the next step in my career. I could not have asked for a better mentor. I would also like to thank Dr. Mark Peczu, Dr. Amy Howell and Dr. Edward Neth for their mentorship and for being a part of my advisory committee.

Much of the work presented here would not be possible without the help from the staff in the chemistry department and my collaborators. I'd like to thank Dr. You-Jun Fu for providing MS services, Dr. Vitaly Gorbatyuk and Dr. Nick Eddy for NMR assistance and Charlene Fuller, Ashley Butler and Emilie Hogrebe for making life as a graduate student more manageable. I also want to thank my collaborators Mohsen Erfanzadeh, Feifei Zhou and Dr. Quing Zhu in the department of biomedical engineering for performing the photoacoustic imaging experiments and Randy Hamchand for performing the chemosensing experiments. I would also like to thank the external collaborators I have worked with including Dr. Matthias Zeller at Purdue University, who solved all of the beautiful crystal structures presented in this thesis as well as Beate Röder and her group at Humboldt-Universität zu Berlin for providing the photophysical measurements.

Throughout the years I have had the pleasure of working with some great people in the Brückner lab. A special thank you to Joshua Akhigbe and Lalith Samankumara for their mentorship when I first started. I would also like to thank my friends Meenakshi, Ruoshi and Nisansala who I traveled all the way across the world with to the International Conference of Porphyrins and Phthalocyanines and Corey, Randy, Damaris and Carly. I would also like to acknowledge the talented undergraduates I have mentored throughout the years: Wes Tardie, Justin Hua and Jiaming Ding for their contributions and good times hanging out in the lab.

In graduate school, I met the special person I will be spending the rest of my days with. Jaci, you are truly the best and I would not be where I am today without you. You were there for me through thick and thin and I can't wait to start the next chapter with you. Finally, I want to thank my family, especially my parents, Joni and Joe who brought me into this world and taught me how to work hard and chase my dreams.

Table of Contents

1	Introduction	1
1.1	Porphyrins and Hydroporphyrins	1
1.2	Quinoline-Annulated Porphyrins	4
1.3	The Breaking and Mending Approach.....	8
1.4	Modifications of Porphyrins and Hydroporphyrins for their Solubilization in Aqueous Media.....	9
1.4.1	Water-Soluble Porphyrins Bearing Cationic Substituents	11
1.4.2	Water-Soluble Porphyrins Bearing Anionic Substituents	29
1.4.3	Water-Soluble Porphyrins with Neutral Groups.....	47
1.4.4	Summary and Outlook.....	66
1.5	Notes and References.....	67
2	Quinoline-Annulated Chlorins and Chlorin Analogues.....	77
2.1	Results and Discussion	79
2.1.1	OsO ₄ -Mediated dihydroxylation of quinoline-annulated porphyrins 10 and 11	79
2.1.2	Periodinane-mediated oxidation of quinoline-annulated dihydroxychlorin 13	82
2.2	Conclusions.....	84
2.3	Experimental Section.....	86
2.3.1	Materials and Instruments	86
2.3.2	Synthesis and Characterization.....	86
2.4	References	97
3	Platinum Complexes of Quinoline-Annulated Porphyrins as NIR Emitters ...	100
3.1	Results and Discussion.....	101
3.1.1	Synthesis.....	101
3.1.2	Optical Properties and Photophysics	102
3.2	Conclusions.....	103
3.3	Experimental Section.....	104
3.3.1	Materials and Instruments	104
3.3.2	Synthesis and Characterization.....	104
3.4	References	114
4	<i>in vivo</i> Photoacoustic Tumor Tomography Using a Quinoline-Annulated Porphyrin as NIR Molecular Contrast Agent.....	115
4.1	Results and Discussion	119
4.1.1	Synthesis of a Freely Water-Soluble Quinoline-Annulated Porphyrin	119
4.1.2	Photophysical Properties and Solubility of PEGylated Quinoline-Annulated Porphyrins 4d and 4e	121
4.1.3	<i>ex vivo</i> Photoacoustic Signal Generation of Water-Soluble Quinoline-Annulated Porphyrin 4e	123
4.1.4	Toxicity of PEGylated Quinoline-Annulated Porphyrin 4e	124

4.1.5	The Use of Quinoline-Annulated Porphyrin 4e as an <i>in vivo</i> PAI Contrast Agent..	125
4.1.6	Renal Filtration of Quinoline-Annulated Porphyrin 4e	127
4.1.7	Fluorescent-Tagging of Quinoline-Annulated Porphyrin 4e	127
4.1.8	Biodistribution Study of BODIPY-Tagged Quinoline-Annulated Porphyrin 4g ..	130
4.2	Conclusions	131
4.3	Experimental Section	131
4.3.1	Materials and Instruments	131
4.3.2	Synthesis and Characterization.....	132
4.3.3	Co-registered pulse-echo-photoacoustic tomography.....	171
4.3.4	Animal protocols.....	172
4.3.5	Toxicity test	172
4.3.6	Tumor model	172
4.3.7	<i>In vivo</i> PAT of murine tumor.....	173
4.3.8	<i>Ex vivo</i> fluorescent imaging.....	174
4.3.9	Photophysical measurements	174
4.4	References	175
5	Supersizing Pyrrole-Modified Porphyrins by Reversal of the Breaking and Mending Strategy	178
5.1	Results and Discussion	180
5.1.1	Formation of a Novel Pyrrole-modified Porphyrin by Replacement of a Pyrrole with a 1,3,6-Triazocine-2,4,8-Trione Ring	180
5.1.2	Synthesis of Thioxo-Supersized Pyrrole-modified Porphyrin 14	184
5.1.3	Modification of TPP-dione with semicarbazide and thiosemicarbazide.....	187
5.1.4	Formation of Adducts using Malonamide derivatives and their oxidative cleavage	190
5.2	Conclusions	195
5.3	Experimental Section	196
5.3.1	Materials and Instruments	196
5.3.2	Synthesis and Characterization.....	196
5.4	References	250
6	Substituted Imidazoloporphyrins	252
6.1	Results and Discussion	256
6.1.1	An Efficient Synthesis of Porpholactam 9	256
6.1.2	Conversion of Porpholactam 8 to Reactive Imidazoloporphyrin Triflate 12	258
6.1.3	Modification of Imidazoloporphyrin with Potential Chelating Motifs.....	261
6.1.4	Interaction of iminodiacetic acid-substituted imidazoloporphyrin 16 with Zn ²⁺ ..	263
6.2	Conclusions	265
6.3	Experimental Section	266
6.3.1	Materials and Instruments	266
6.3.2	Synthesis and Characterization.....	266
6.4	References	291

Table of Schemes

1. Introduction

Scheme 1-1. Adler synthesis of <i>meso</i> -aryl porphyrins.	2
Scheme 1-2. Synthesis of synthetic handles for the modification of <i>meso</i> -tetraarylporphyrins.	3
Scheme 1-3. The two independent paths toward bisquinoline-annulated porphyrin 7H ₂ developed by Ruppert (1Ni → 5Ni → 7H₂) and Brückner (1H₂ → 10H₂ → 7H₂).	6
Scheme 1-4. The breaking and mending approach toward pyrrole-modified porphyrins (PMPs).	8
Scheme 1-5. Scope of the ‘breaking and mending approach’	8
Scheme 1-6. Principle strategies toward hydrophilic porphyrin derivatives.	11
Scheme 1-7. Spermine- and spermidine-porphyrin conjugates.	13
Scheme 1-8. Chlorin and bacteriochlorin polyamines derived from <i>Spirulina maxima</i> and <i>Rhodobacter spaeroides</i> , respectively.	14
Scheme 1-9. Cationic esters of chlorin e6 with terminal ammonium groups.	15
Scheme 1-10. β-substituted cationic ammonium bacteriochlorin derivatives. ⁵⁷	15
Scheme 1-11. β-Substituted cationic ammonium bacteriochlorin derivatives prepared by Suzuki coupling.	17
Scheme 1-12. <i>meso</i> -Aryl-ammonium bis-acetylene linked porphyrin dimers prepared via Senge arylation.	18
Scheme 1-13. Quarternization options of <i>meso</i> -tetrakis(4-pyridyl)porphyrin.	19
Scheme 1-14. M-Arene complexes of <i>meso</i> -tetra(4-pyridyl)porphyrin.	21
Scheme 1-15. A ₃ B tri-pyridyl porphyrins prepared by Adler synthesis and subsequent synthetic modification.	22
Scheme 1-16. Water-soluble AB ₃ phosphorus porphyrins.	24
Scheme 1-17. Amphiphilic <i>meso</i> -pyridyl chlorins and bacteriochlorins.	25
Scheme 1-18. Preparation of a <i>meso</i> -pyridinium-functionalized bis-acetylene linked porphyrin dimer.	26
Scheme 1-19. An octapyridiniumporphyrin.	27
Scheme 1-20. <i>meso</i> -Imidazolium porphyrins.	28
Scheme 1-21. Increasing water-solubility of the naturally occurring porphyrins with increasing number of carboxylic acid functionalities.	29

Scheme 1-22. Carboxylated <i>meso</i> -aryl porphyrins.	30
Scheme 1-23. Carboxylated benzoporphyrins.	30
Scheme 1-24. Porphyrin dimers and trimers bearing carboxylate groups in the <i>meso</i> -positions.	31
Scheme 1-25. Carboxylated <i>trans</i> -AB porphyrins.	32
Scheme 1-26. Dendritic carboxylated porphyrins.	33
Scheme 1-27. Dendritic polycarboxylated porphyrins.	34
Scheme 1-28. Core-modified carboxylated porphyrin.	35
Scheme 1-29. Octacarboxylated porphyrin 84	35
Scheme 1-30. Carboxylated bis-acetylene linked porphyrin dimers.	36
Scheme 1-31. Tetracarboxybacteriochlorins.	37
Scheme 1-32. Sulfonated <i>N</i> -confused porphyrin.	38
Scheme 1-33. Sulfonated A ₃ B porphyrin bearing DPA substituents for fluorescence sensing of Zn ²⁺	39
Scheme 1-34. Sulfonated isoindoline nitroxide-functionalized A ₃ B porphyrin.	40
Scheme 1-35. Chlorosulfonated porphyrins and their hydrolysis and reduction products.	41
Scheme 1-36. Sulfonated Pd-bacteriopheophorbide.	42
Scheme 1-37. Phosphonated <i>b</i> -alkyl porphyrin derivatives.	44
Scheme 1-38. <i>trans</i> -AB Porphyrins bearing swallowtail phosphonate motifs.	44
Scheme 1-39. Synthetic chlorins bearing phosphonate swallowtail motifs.	45
Scheme 1-40. <i>trans</i> -AB porphyrins bearing phosphate swallowtail motifs.	46
Scheme 1-41. A ₃ B porphyrin carrying three short PEG chains.	48
Scheme 1-42. Hydrophilic bis-acetylene linked porphyrin dimers carrying PEG chains and various other solubilizing motifs.	49
Scheme 1-43. PEGylated synthetic chlorins using PEGylated building blocks.	50
Scheme 1-44. PEGylated derivatives of <i>meso</i> -tetrakis(3-hydroxyphenyl)chlorin.	51
Scheme 1-45. PEGylated derivatives of <i>meso</i> -tetra(4-hydroxyphenyl)porphyrin.	52
Scheme 1-46. Amphiphilic porphyrin with a PEG-dendrimer.	52
Scheme 1-47. PEGylated <i>meso</i> -aryl porphyrins by benzylation of a PEG with tetra(<i>p</i> -bromomethylphenyl)porphyrin.	53

Scheme 1-48. PEGylated porphyrins derived from <i>meso</i> -tetrakis(4-carboxyphenyl)porphyrin using a PEG-amine.....	53
Scheme 1-49. PEGylated AB ₃ porphyrin with carboxylic acid bioconjugation handle.....	55
Scheme 1-50. Porphyrin-PEG dendrimer conjugates..	55
Scheme 1-51. PEGylated A ₂ B ₂ porphyrin..	56
Scheme 1-52. PEGylated quinoline-annulated porphyrins.....	57
Scheme 1-53. PEGylated porpholactone derived from <i>meso</i> -tetrakis(pentafluorophenyl)porphyrin derivatives.....	58
Scheme 1-54. PEGylated derivatives of chlorin e6.....	59
Scheme 1-55. PEGylated protoporphyrin and its zinc complex.....	59
Scheme 1-56. PEGylated hematoporphyrin.....	60
Scheme 1-57. Hydrophilic bacteriochlorin cycloimides.....	60
Scheme 1-58. PEGylated bacteriochlorins formed by reductive amination.....	61
Scheme 1-59. β -Substituted PEGylated synthetic bacteriochlorins <i>via</i> Suzuki coupling.....	62
Scheme 1-60. PEGylated porphyrins and chlorins prepared through click chemistry.....	64
Scheme 1-61. PEGylated chlorins prepared by Aldol-condensation of β -diformyl chlorin..	65
Scheme 1-62. PEGylated bacteriochlorins bearing a bioconjugatable tether prepared by amide coupling.....	65
2. Quinoline-Annulated Chlorins and Chlorin Analogues	
Scheme 2-1. Synthesis of quinoline-annulated porphyrin 10 and its quinoline- <i>N</i> -oxide 11 ..	78
Scheme 2-2. OsO ₄ -Mediated dihydroxylation of quinoline-annulated porphyrins 10 and 11	80
Scheme 2-3. Oxidations of quinoline-annulated dihydroxychlorin 13	82
3. Platinum Complexes of Quinoline-Annulated Porphyrins as NIR Emitters	
Scheme 3-1. Synthesis of quinoline-annulated porphyrin Pt-complexes	101
4. <i>in vivo</i> Photoacoustic Tumor Tomography Using a Quinoline-Annulated Porphyrin as NIR Molecular Contrast Agent	
Scheme 4-1. Synthesis of water-soluble quinoline-annulated porphyrins.....	120
Scheme 4-2. Synthesis of <i>meso</i> -phenoxy BODIPY derivative 11	128

Scheme 4-3. Synthesis of BODIPY-tagged water-soluble quinoline-annulated porphyrin 4g ..	128
5. Supersizing Pyrrole-Modified Porphyrins by Reversal of the Breaking and Mending Strategy	
Scheme 5-1. Example for the ‘breaking and mending of porphyrins’ approach toward porphyrinoids containing non-pyrrolic building blocks.....	179
Scheme 5-2. Synthesis of pyrrole-expanded porphyrazine 6 described by the groups of Barrett and Hoffman. ¹⁰	179
Scheme 5-3. Synthesis of urea chlorindiol adducts 8 and 9 , and the outcomes of the oxidative diol cleavage.....	181
Scheme 5-4. Synthesis of Ni-complexes and thioxo derivatives of the supersized pyrrole-modified porphyrins.....	185
Scheme 5-5. Synthesis of 6-membered ring adducts..	188
Scheme 5-6. Synthesis of malonamide adducts..	191
Scheme 5-7. Proposed mechanism for the formation of oxidative cleavage products 21 and 22	193
6. Substituted Imidazoloporphyrins	
Scheme 6-1. Known synthesis of imidazoloporphyrin 3 and porpholactam 9	255
Scheme 6-2. Conversion of porpholactam 9 to imidazoloporphyrin β -substituted derivatives.	260
Scheme 6-3. Proposed mode of binding of substituted-imidazoloporphyrin 16 with M^{2+} cations in MeOH solution.	264

Table of Figures

1. Introduction

Figure 1-1. Numbering and naming of porphyrins and hydroporphyrins.....	1
Figure 1-2. UV-vis spectra of free-base porphyrin and chlorin (solid traces) and metalloporphyrin and metallochlorin (dotted traces).	2
Figure 1-3. UV-vis spectra (CH_2Cl_2) of mono- and bis-quinoline annulated porphyrins.	7

2. Quinoline-Annulated Chlorins and Chlorin-Analogues

Figure 2-1. Two other theoretical isomers of diol 13 , highlighting the arguments against their existence, and the observed NOe correlation seen in 12	81
Figure 2-2. UV-vis spectra (CH_2Cl_2) of the compounds indicated.	82
Figure 2-3. UV-vis spectra (CH_2Cl_2) of the compounds indicated.	83

Figure 2-4. UV-vis spectra (CH ₂ Cl ₂) of the compounds indicated.....	84
Figure 2-5. UV-vis spectrum (CH ₂ Cl ₂) of 12	87
Figure 2-6. ¹ H NMR spectrum (400 MHz, CDCl ₃) of 13	89
Figure 2-7. ¹³ C NMR (100 MHz, CDCl ₃) of 13	90
Figure 2-8. ¹ H- ¹ H NOESY spectrum (CDCl ₃) of 13	91
Figure 2-9. ¹ H NMR (400 MHz, CDCl ₃) of 14	93
Figure 2-10. ¹³ C NMR spectrum (100 MHz, CDCl ₃) of 14	94
Figure 2-11. ¹ H NMR spectrum (400 MHz, CDCl ₃) of 15	96
3. Platinum Complexes of Quinoline-Annulated Porphyrins as NIR Emitters	
Figure 3-1. UV-vis spectrum (CH ₂ Cl ₂) of 7Pt	105
Figure 3-2. ¹ H NMR spectrum (400 MHz, CDCl ₃) of 7Pt	106
Figure 3-3. ¹³ C NMR spectrum (100 MHz, CDCl ₃) of 7Pt	107
Figure 3-4. UV-vis spectrum (CH ₂ Cl ₂) of 8Pt	108
Figure 3-5. ¹ H NMR spectrum (400 MHz, CDCl ₃) of 8Pt	109
Figure 3-6. ¹³ C NMR spectrum (100 MHz, CDCl ₃) of 8Pt	110
Figure 3-7. UV-vis spectrum (CH ₂ Cl ₂) of 10Pt	111
Figure 3-8. ¹ H NMR spectrum (400 MHz, CDCl ₃) of 10Pt	112
Figure 3-9. ¹³ C NMR spectrum (100 MHz, CD ₂ Cl ₂) of 10Pt	113
4. <i>in vivo</i> Photoacoustic Tumor Tomography Using a Quinoline-Annulated Porphyrin as NIR Molecular Contrast Agent	
Figure 4-1. UV-vis spectra (A: CH ₂ Cl ₂ , B: H ₂ O) of the compounds indicated.	122
Figure 4-2. Co-registered PE-PAT images of polyethylene tubes (inner/outer \varnothing = 0.58/0.96 mm) filled with (A and C) one-day-old rat blood and (B and D) with a solution of PEG-ylated quinoline-annulated porphyrin 4e at a concentration in which the sample possessed the identical absolute absorbance value at 790 nm as the undiluted blood (see ESI).	124
Figure 4-3. Co-registered PE-PAT images before injection of the contrast agent (A) and ICG (C) and after the systemic injection of 4e (B) and ICG (D)..	126
Figure 4-4. Time-dependence of the relative enhancement of the PAT max value following the injection of 100 μ L of the dye 4e (\sim 33.3 mM, $\lambda_{\text{excitation}}$ = 790 nm) and ICG (1.33 mM, $\lambda_{\text{excitation}}$ = 780 nm) at identical absorbance value.	126

Figure 4-5. A. PEG-ylated quinoline-annulated dye 4e dissolved in PBS (~33.3 mM) in a microcuvette. B. Mouse urine collected after ~45 min after injection of 4e in a capillary tube.	127
Figure 4-6. A. UV-vis spectra of 4f (black) and 11 (red) (solid lines), and fluorescence emission (red broken line; $\lambda_{\text{excitation}} = 441 \text{ nm}$) for phenoxy-BODIPY 11 (all MeOH). B. UV-vis (solid line) and fluorescence emission (broken line; $\lambda_{\text{excitation}} = 441 \text{ nm}$) spectra of quinoline-annulated porphyrin-BODIPY dyad 4g (MeOH)).	130
Figure 4-7. ^1H NMR spectrum (400 MHz, CD_2Cl_2) of 8	133
Figure 4-8. ^{13}C NMR spectrum (100 MHz, CD_2Cl_2) of 8	134
Figure 4-9. UV-vis spectrum (CH_2Cl_2) of 8	135
Figure 4-10. FT-IR spectrum (neat, diamond ATR) of 8	135
Figure 4-11. ^1H NMR spectrum (400 MHz, CD_2Cl_2) of 9	137
Figure 4-12. ^{13}C NMR spectrum (100 MHz, CD_2Cl_2) of 9	138
Figure 4-13. UV-vis spectrum (CH_2Cl_2) of 9	139
Figure 4-14. FT-IR spectrum (neat, diamond ATR) of 9	139
Figure 4-15. ^1H NMR spectrum (400 MHz, CDCl_3) of 5b	141
Figure 4-16. ^{13}C NMR spectrum (100 MHz, CDCl_3) of 5b	142
Figure 4-17. UV-vis spectrum (CH_2Cl_2) of 5b	143
Figure 4-18. FT-IR spectrum (neat, diamond ATR) of 5b	143
Figure 4-19. ^1H NMR spectrum (400 MHz, CD_2Cl_2) of 4b	145
Figure 4-20. ^{13}C NMR spectrum (100 MHz, CD_2Cl_2) of 4b	146
Figure 4-21. UV-vis spectrum (CH_2Cl_2) of 4b	147
Figure 4-22. FT-IR spectrum (neat, diamond ATR) of 4b	147
Figure 4-23. ^1H NMR spectrum (400 MHz, DMSO-d_6) of 4c	149
Figure 4-24. ^{13}C NMR spectrum (100 MHz, DMSO-d_6) of 4c	150
Figure 4-25. UV-vis spectrum (MeOH) of 4c	151
Figure 4-26. FT-IR spectrum (neat, diamond ATR) of 4c	151
Figure 4-27. ^1H NMR spectrum (500 MHz, CD_2Cl_2) of 4d	153
Figure 4-28. ^{13}C NMR spectrum (125 MHz, CD_2Cl_2) of 4d	154
Figure 4-29. UV-vis spectrum (CH_2Cl_2) of 4d	155
Figure 2-30. ^1H NMR spectrum (400 MHz, CD_2Cl_2) of 4e	156

Figure 4-31. UV-vis spectrum (H ₂ O) of 4e .	157
Figure 4-32. Absorption spectra of 4e (PQP) in CH ₂ Cl ₂ , H ₂ O and H ₂ O-Triton-X solutions.	157
Figure 4-33. HR-MS (ESI ⁺ , 100% CH ₃ CN, TOF) of 4e .	158
Figure 4-34. ¹ H NMR spectrum (400 MHz, DMSO-d ₆) of 4c^{Zn} .	160
Figure 4-35. ¹³ C NMR spectrum (100 MHz, CD ₂ Cl ₂ /10% MeOD) of 4c^{Zn} .	161
Figure 4-36. UV-vis spectrum (MeOH) of 4c^{Zn} .	162
Figure 4-37. FT-IR spectrum (neat, diamond ATR) of 4c^{Zn} .	162
Figure 4-38. ¹ H NMR spectrum (500 MHz, DMSO-d ₆) of 4f .	164
Figure 4-39. ¹⁹ F NMR spectrum (470 MHz, DMSO-d ₆) of 4f .	165
Figure 4-40. UV-vis and Fluorescence emission spectrum (MeOH, λ _{excitation} = 441 nm) of 4f .	165
Figure 4-41. ¹ H NMR spectrum (400 MHz, CD ₂ Cl ₂ , pre-saturated at 3.6 ppm) of 4g .	167
Figure 4-42. ¹⁹ F NMR spectrum (376 MHz, CD ₂ Cl ₂) of 4g .	168
Figure 4-43. UV-vis and Fluorescence emission spectrum (MeOH, λ _{excitation} = 441 nm) of 4g .	168
Figure 4-44. MALDI-TOF spectrum (100% DHBA) of 4g .	169
Figure 4-45. LC-MS of mouse urine extract (CH ₂ Cl ₂), obtained after injection of 4e .	170
Figure 4-46. UV-vis spectrum (CH ₂ Cl ₂) of mouse (diluted) urine obtained after injection of 4e .	171
Figure 4-47. <i>In vivo</i> PAT experiment setup.	174
5. Supersizing Pyrrole-Modified Porphyrins by Reversal of the Breaking and Mending Strategy	
Figure 5-1. UV-vis spectra (CH ₂ Cl ₂) of the compounds indicated.	182
Figure 5-2. Stick representation of the single crystal X-ray structure of 11 (top) and 11Ni (bottom).	183
Figure 5-3. A: UV-vis spectra (CH ₂ Cl ₂) of 11 (green trace) and thioxo-derivative 14 (blue trace). B: X-ray crystal structure and measured C _β -C _α -C _α -C _β dihedral angles of 11 and 14 .	186
Figure 5-4. ¹ H NMR spectra (CDCl ₃ , 298 K) of the compounds indicated.	189
Figure 5-5. UV-vis spectra (CH ₂ Cl ₂) of dione 7 (blue trace) and semicarbazone 18 (orange trace).	190
Figure 5-6. X-ray crystal structure of spiro-barbiturate 22 .	192
Figure 5-7. X-ray crystal structure of diol 23 . Hydrogens removed for clarity.	193

Figure 5-8. UV-vis spectra of diol 24 (black trace, CH ₂ Cl ₂) and reaction mixture 7 minutes after treatment with Pb(OAc) ₄ in dry THF at r.t. (red trace, THF).	195
Figure 5-9. UV-vis spectrum (CH ₂ Cl ₂) of 8	197
Figure 5-10. ¹ H NMR spectrum (400 MHz, CDCl ₃) of 8	198
Figure 5-11. ¹³ C NMR spectrum (100 MHz, CDCl ₃) of 8	199
Figure 5-12. UV-vis spectrum (CH ₂ Cl ₂) of 9	200
Figure 5-13. ¹ H NMR spectrum (400 MHz, CDCl ₃) of 9	201
Figure 5-14. ¹³ C NMR spectrum (100 MHz, CDCl ₃) of 9	202
Figure 5-15. UV-vis spectrum (CH ₂ Cl ₂) of 10	203
Figure 5-16. ¹ H NMR (400 MHz, CDCl ₃) of 10	204
Figure 5-17. UV-vis spectrum (CH ₂ Cl ₂) of 11	205
Figure 5-18. ¹ H NMR (400 MHz, CDCl ₃) of 11	206
Figure 5-19. ¹³ C NMR (100 MHz, CDCl ₃) of 11	207
Figure 5-20. UV-vis spectrum (CH ₂ Cl ₂) of 8Ni	208
Figure 5-21. ¹ H NMR spectrum (400 MHz, CDCl ₃) of 8Ni	209
Figure 5-22. ¹³ C NMR spectrum (400 MHz, CDCl ₃) of 8Ni	210
Figure 5-23. UV-vis spectrum (CH ₂ Cl ₂) of 9Ni	211
Figure 5-24. ¹ H NMR spectrum (400 MHz, CDCl ₃) of 9Ni	212
Figure 5-25. ¹³ C NMR spectrum (500 MHz, CDCl ₃) of 9Ni	213
Figure 5-26. ¹ H NMR (400 MHz, CDCl ₃) of 10Ni	215
Figure 5-27. UV-vis spectrum (CH ₂ Cl ₂) of 11Ni	216
Figure 5-28. ¹ H NMR (400 MHz, CDCl ₃) of 11Ni	217
Figure 5-29. ¹³ C NMR spectrum (100 MHz, CDCl ₃) of 11Ni	218
Figure 5-30. ¹ H NMR spectrum (400 MHz, CDCl ₃) of 12	219
Figure 5-31. UV-vis spectrum (CH ₂ Cl ₂) of 13	220
Figure 5-32. ¹ H NMR spectrum (400 MHz, CDCl ₃) of 13	221
Figure 5-33. ¹³ C NMR spectrum (125 MHz, CDCl ₃) of 13	222
Figure 5-34. UV-vis spectrum (CH ₂ Cl ₂) of 14	223
Figure 5-35. ¹ H NMR spectrum (400 MHz, CDCl ₃) of 14	224

Figure 5-36. ^{13}C NMR spectrum (125 MHz, CDCl_3) of 14 .	225
Figure 5-37. UV-vis spectrum (CH_2Cl_2) of 18 .	226
Figure 5-38. ^1H NMR spectrum (400 MHz, CDCl_3) of 18 .	227
Figure 5-39. ^1H NMR spectrum (100 MHz, CDCl_3) of 18 .	228
Figure 5-40. Partial ^1H - ^1H -NOESY spectrum (CDCl_3) of 18 .	229
Figure 5-41. ^{15}N - ^1H HSQC spectrum (CDCl_3) of 18 .	229
Figure 5-42. HMBC spectrum (CDCl_3) of 18 .	230
Figure 5-43. UV-vis spectrum (CH_2Cl_2) of 19 .	231
Figure 5-44. ^1H NMR spectrum (400 MHz, CDCl_3) of 19 .	232
Figure 5-45. ^{13}C NMR spectrum (100 MHz, CDCl_3) of 19 .	233
Figure 5-46. UV-vis spectrum (CH_2Cl_2) of 20 .	234
Figure 5-47. ^1H NMR spectrum (500 MHz, CDCl_3) of 20 .	235
Figure 5-48. ^{13}C NMR spectrum (125 MHz, CDCl_3) of 20 .	236
Figure 5-49. Partial ^{13}C - ^1H HSQC spectrum (CDCl_3) of 20 .	237
Figure 5-50. HMBC spectrum (CDCl_3) of 20 .	237
Figure 5-51. UV-vis spectrum (CH_2Cl_2) of 23 .	239
Figure 5-52. UV-vis spectrum (CH_2Cl_2) of 24 .	239
Figure 5-53. ^1H NMR spectrum (500 MHz, CDCl_3) of 23 .	240
Figure 5-54. ^{13}C NMR spectrum (125 MHz, CDCl_3) of 23 .	241
Figure 5-55. ^{13}C - ^1H HSQC spectrum (CDCl_3) of 23 .	242
Figure 5-56. ^1H - ^1H COSY spectrum (CDCl_3) of 23 .	242
Figure 5-57. ^1H NMR spectrum (500 MHz, CDCl_3) of 24 .	243
Figure 5-58. ^{13}C NMR spectrum (125 MHz, CDCl_3) of 24 .	244
Figure 5-59. Partial ^{13}C - ^1H HSQC spectrum (CDCl_3) of 24 .	245
Figure 5-60. UV-vis spectrum (CH_2Cl_2) of 21 .	246
Figure 5-61. ^1H NMR spectrum (400 MHz, CDCl_3) of 21 .	247
Figure 5-62. ^{13}C NMR spectrum (100 MHz, CDCl_3) of 21 .	248
Figure 5-63. ^{15}N - ^1H HSQC spectrum (CDCl_3) of 21 .	249

6. Substituted Imidazoloporphyrins

Figure 6-1. UV-vis spectra (CH ₂ Cl ₂) of dione 7 (blue trace) and dihydroxychlorin 8 (red trace).....	256
Figure 6-2. UV-vis spectrum (CH ₂ Cl ₂) of the compound indicated.....	257
Figure 6-3. UV-vis spectra (CH ₂ Cl ₂) of the compounds indicated.....	259
Figure 6-4. UV-vis spectra (CH ₂ Cl ₂) of the compounds indicated.....	261
Figure 6-5. X-ray structure of substituted imidazoloporphyrin 15	262
Figure 6-6. Absorbance titration of 16 with Zn ²⁺	264
Figure 6-7. UV-vis spectrum (CH ₂ Cl ₂) of 14	268
Figure 6-8. ¹ H NMR spectrum (125 MHz, CDCl ₃) of 14	269
Figure 6-9. ¹³ C NMR spectrum (125 MHz, CDCl ₃) of 14	270
Figure 6-10. UV-vis spectrum (CH ₂ Cl ₂) of 15	271
Figure 6-11. ¹ H NMR spectrum (500 MHz, CDCl ₃) of 15	272
Figure 6-12. ¹³ C NMR spectrum (125 MHz, CDCl ₃) of 15	273
Figure 6-13. UV-vis spectrum (MeOH) of 16	275
Figure 6-14. ¹ H NMR spectrum (400 MHz, CD ₂ Cl ₂ /10% MeOD) of 16	276
Figure 6-15. ¹³ C NMR spectrum (125 MHz, CD ₂ Cl ₂ /10% MeOH) of 16	277
Figure 6-16. UV-vis spectrum of 17 in CH ₂ Cl ₂ (solid trace) and CH ₂ Cl ₂ + 10% TFA (broken trace).....	279
Figure 6-17. ¹ H NMR (125 MHz, CDCl ₃) of 17	280
Figure 6-18. Partial H-H COSY spectrum (CDCl ₃) of 17	281
Figure 6-19. ¹³ C NMR (125 MHz, CDCl ₃) of 17	282
Figure 6-20. UV-vis spectrum of 18 in CH ₂ Cl ₂ (solid trace) and CH ₂ Cl ₂ + 10% TFA (broken trace).....	284
Figure 6-21. ¹ H NMR spectrum (500 MHz, CDCl ₃) of 18	285
Figure 6-22. ¹³ C NMR spectrum (125 MHz, CDCl ₃) of 18	286
Figure 6-23. UV-vis spectrum of 19 in CH ₂ Cl ₂ (solid trace) and CH ₂ Cl ₂ + 10% TFA (broken trace).....	287
Figure 6-24. ¹ H NMR spectrum (125 MHz, CDCl ₃) of 19	288
Figure 6-25. Partial ¹ H- ¹ H COSY spectrum (CDCl ₃) of 19	289
Figure 6-26. ¹³ C NMR (125 MHz, CDCl ₃) of 19	290

List of Tables

Table 1-1. Comparison of the retention times of hydrophilic porphyrin dimers shown in Scheme 1-42.⁶³ 49

Table 1-2. Comparison of relevant properties concerning hydrophilicity of a series of structurally similar synthetic bacteriochlorins, as described by the group of Lindsey.⁵⁹ 63

List of Abbreviations

aq	aqueous
Boc	<i>t</i> -butyloxycarbonyl
conc	concentrated
COSY	Correlation spectroscopy
d	doublet
dach	1,2-diaminocyclohexane
CTAP	Cetyltrimethylammonium permanganate
dba	dibenzylideneacetone
DCC	<i>N,N'</i> -dicyclohexyl carbodiimide
DCE	1,2-dichloroethane
DDQ	2,3-dichloro-5,6-dicyano benzoquinone
DIEA	diisopropylethylamine
DMAP	4-dimethylaminopyridine
DMF	dimethyl formamide
DMP	Dess-Martin periodinane
dmpda	<i>N,N'</i> -dimethyl-1,3-propanediamine
DMSO	dimethyl sulfoxide
DPA	Di-(2-picolyl)amine
EDC	1-Ethyl-3-(3-dimethylaminopropyl)carbodiimide
ESI	electrospray ionization
equiv	equivalents

FI	Fluorescence
FTIR	Fourier transform infrared spectroscopy
fwhm	full width half maximum
h	hour
Hz	Hertz
HBtu	(2-(1 <i>H</i> -benzotriazol-1-yl)-1,1,3,3-tetramethyluronium hexafluorophosphate
HOBt	1-hydroxybenzotriazole
ICG	indocyanine green
λ_{max}	wavelength of maximum absorption
m	multiplet
min	minute
MRI	magnetic resonance imaging
NOESY	Nuclear Overhauser effect spectroscopy
PAI	photoacoustic imaging
PAT	photoacoustic tomography
PDT	photodynamic therapy
PEG	polyethylene glycol
PBS	phosphate buffered saline
PMP	pyrrole-modified porphyrin
<i>p</i> -TSA	<i>p</i> -toluenesulfonic acid
py	pyridine
NBS	<i>N</i> -bromosuccinimide

NIR	near-infrared region
NHS	<i>N</i> -hydroxysuccinimide
NMR	nuclear magnetic resonance
s	singlet
t	triplet
TBTU	<i>O</i> -(benzotriazol-1-yl)- <i>N,N,N',N'</i> -tetramethyluronium tetrafluoroborate
TFA	trifluoroacetic acid
THF	tetrahydrofuran
TLC	thin-layer chromatography
TMAD	<i>N,N,N',N'</i> -tetramethylazodicarboxamide
TMPI	2,2,6,6-tetramethylpiperidine
TPP	<i>meso</i> -tetraphenylporphyrin
UV-vis	Ultraviolet-visible

Sections of this thesis have been, and will be, published as follows:

- Luciano, M.; Akhigbe, J.; Ding, J.; Thuita, D.; Hamchand, R.; Zeller, M.; Brückner, C. 'Functionalization of the Imidazoloporphyrin Imidazole Moiety toward the Generation of Metal Ion Chemosensors' in preparation for *J. Org. Chem.*, to be submitted summer 2017.
Contributions: JA: early porpholactam studies; JD: Undergraduate researcher under the tutelage of ML; RH: Spectrophotometric titrations; MZ: Crystallography.
- Akhigbe, J.; Luciano, M.; Jockusch, S.; Brückner, C. 'Quinoline-Annulated Porphyrin Platinum Complexes as NIR Emitters' manuscript in preparation for *Phys. Chem. Chem. Phys.*, to be submitted summer 2017.
Contributions: JA: Mono-quinoline Pt complexes; ML: Bis-quinoline Pt complex; SJ: Photophysical measurements.
- Luciano, M.; Tardie, W.; Zeller, M.; Brückner, C. 'Supersized Pyrrole-modified Porphyrins', in preparation for *Chem. Sci.* to be submitted summer 2017 (full paper to the *Chem. Commun.* preliminary report)
Contributions: WT: Undergraduate researcher under the tutelage of ML; MZ: Crystallography.
- Luciano, M.; Brückner, C.; 'Modifications of Porphyrins and Hydroporphyrins for their Solubilization in Aqueous Media' *Molecules* **2017**, accepted for publication. (invited review)
- Luciano, M.; Erfanzadeh, M.; Zhou, F.; Hua, Z.; Bornhütter, T.; Röder, B.; Zhu, Q.; Brückner, C. '*in vivo* Photoacoustic Tumor Tomography Using a Quinoline-Annulated Porphyrin as NIR Molecular Contrast Agent' *Org. Biomol. Chem.* **2017**, *15*, 972-983.
Contributions: ME and FZ: Imaging experiments and animal studies; ZH: Undergraduate researcher under the tutelage of ML; TB and BR: Photophysical measurements.
- Luciano, M.; Tardie, W.; Zeller, M.; Brückner, C. 'Supersizing Pyrrole-modified Porphyrins by Reversal of the 'Breaking and Mending' Strategy' *Chem. Commun.* **2016**, *52*, 10133-10136.
Contributions: WT: Undergraduate researcher under the tutelage of ML; MZ: Crystallography.

- Akhigbe, J.; Yang, M.; Luciano, M.; Brückner, C. Quinoline-Annulated Chlorins and Chlorin-Analogues *J. Porphyrins Phthalocyanines*, **2016**, *20*, 265-273.
Contributions: JA: quinolin-annulated porphyrin osmylation, breaking and mending chemistry; MY: Undergraduate researcher under the tutelage of JA; ML: quinoline-annulated chlorin oxidations.
- Akhigbe, J.; Luciano, M.; Zeller, M.; Brückner, C. Mono- and Bisquinoline-Annulated Porphyrins from Porphyrin β,β' -Dione Oximes, *J. Org. Chem.* **2015**, *80*, 499-511.
Contributions: ML: bis-quinoline M complexes, out of plane plots; JA: Initiated preparation of quinoline-annulated porphyrins; MZ: Crystallography.

1 Introduction

1.1 Porphyrins and Hydroporphyrins

Synthetic dyes that absorb light in the near-infrared region (NIR) have valuable applications in the biomedical sciences, particularly as novel bioimaging contrast agents,¹ as drugs for photodynamic therapy (PDT)² and as chromophores for *in vivo* molecular recognition.³ Among the commonly investigated synthetic dyes, porphyrins and porphyrin analogues are the most promising candidates due to their high molar extinction coefficient, and fluorescence and singlet oxygen quantum yields.

Porphyrins are tetrapyrrolic aromatic heterocycles in which four pyrrolic subunits are linked by methine bridges. A porphyrin has an 18π conjugated aromatic system cross-conjugated with two additional double bonds, making it an $18 + 4\pi$ aromatic system. The numbering and positions of a porphyrin according to the IUPAC naming convention are shown in Figure 1-1.

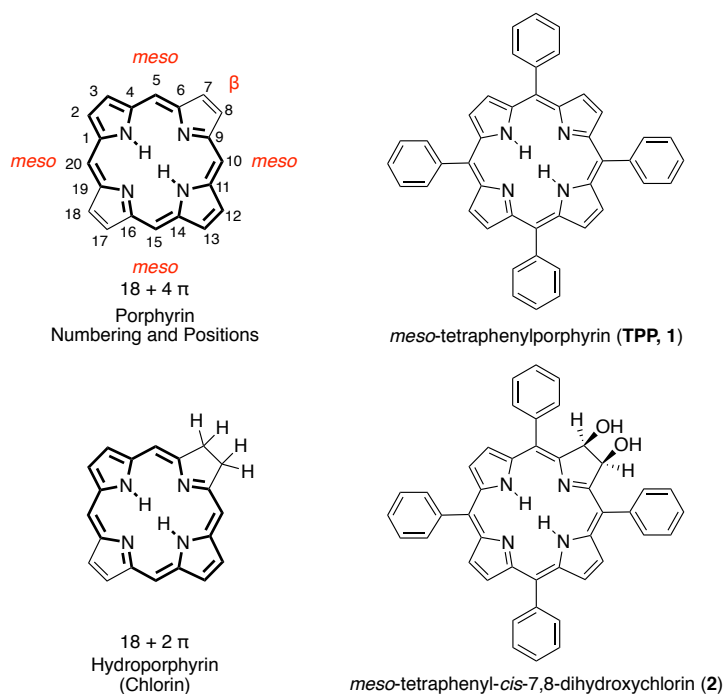


Figure 1-1. Numbering and naming of porphyrins and hydroporphyrins.

The two cross-conjugated β,β' bonds of a porphyrin can be reduced to produce hydroporphyrins. A hydroporphyrin with one cross-conjugated β,β' -bond reduced is called a chlorin. The conversion of a porphyrin to a chlorin results in a bathochromic shift in the longest wavelength of absorption (Figure 1-2).

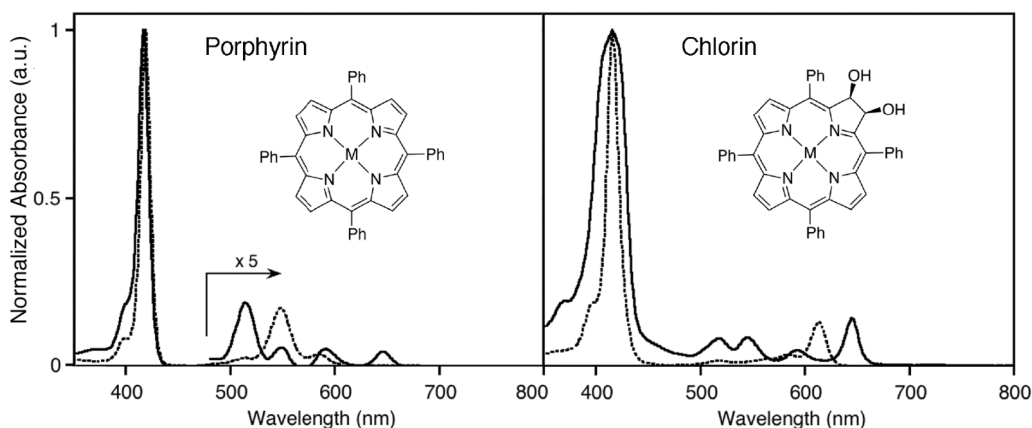
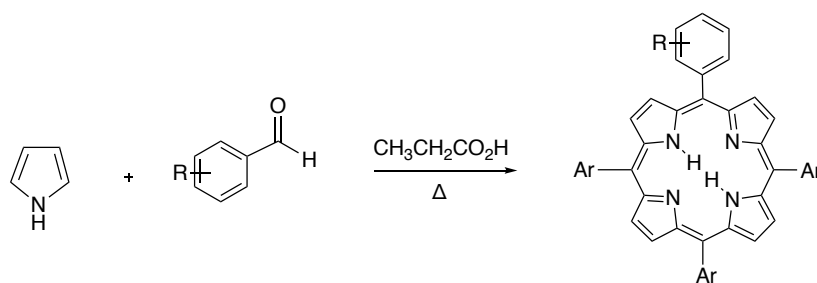


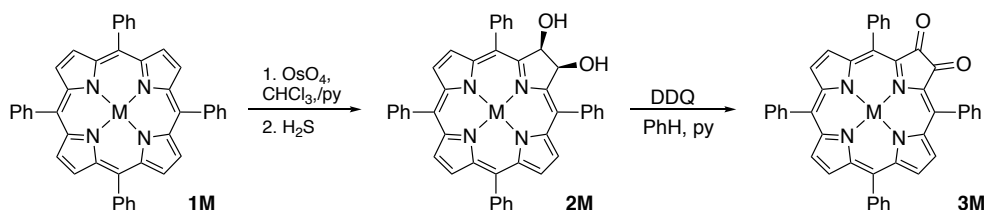
Figure 1-2. UV-vis spectra of free-base porphyrin and chlorin (solid traces) and metalloporphyrin and metallochlorin (dotted traces).

The synthesis of porphyrin analogues has been achieved by semisynthetic methods, starting from extracts of naturally derived porphyrinoids as well as total synthesis methods. Alternatively, synthetic methods toward new porphyrinoids have been achieved using model synthetic systems such as *meso*-tetraphenylporphyrin (**1**), which can be prepared by the Adler procedure (Scheme 1-1).⁴ The Adler procedure is flexible with respect to introducing different *meso*-substituents to the porphyrin, by using the appropriate benzaldehyde derivative.



Scheme 1-1. Adler synthesis of *meso*-aryl porphyrins.

We have demonstrated in our lab the OsO_4 -mediated regioselective dihydroxylation of the β,β' bond of TPP to form the *vic-cis*-diol (OH_2TPP) (Scheme 1-2).⁵ This particular chlorin now has a *vic-cis*-diol synthetic handle and is thus amenable to a wide variety of modifications at the β,β' position. The diol **2M** can also be further oxidized to the dione **3M** by treatment with DDQ. The diol **2M** and dione **3M**, or similar *meso*-aryl analogues, serve as the ultimate starting materials for all of the porphyrinoids described in this dissertation.



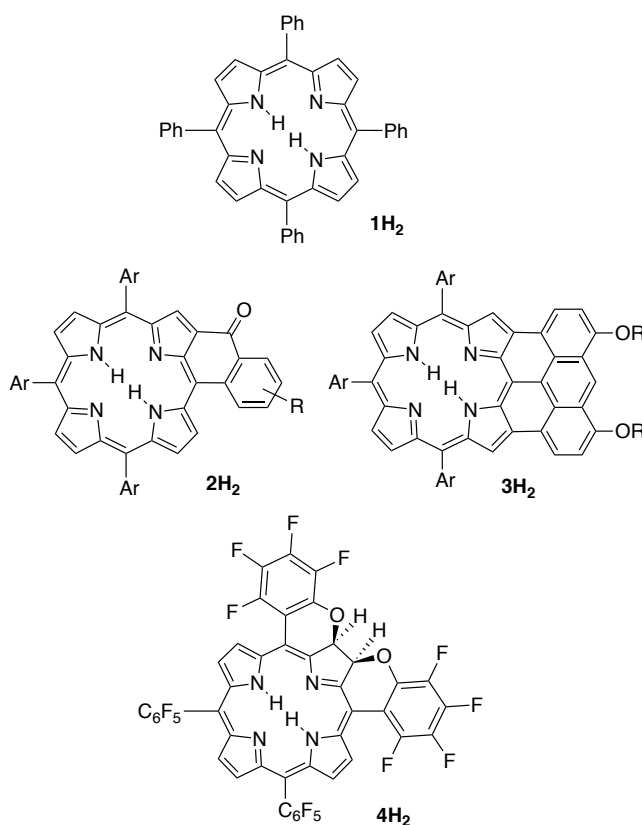
Scheme 1-2. Synthesis of synthetic handles for the modification of *meso*-tetraarylporphyrins.

1.2 Quinoline-Annulated Porphyrins

Even though the high extinction coefficients, fluorescence and singlet oxygen photosensitization quantum yields of regular porphyrins and chlorins are potentially attractive for their use in biomedical applications, e.g., as photochemotherapeutics,⁶ photoantimicrobials,⁷ photoantifungals,⁸ or fluorescent markers,^{6c,9} most regular porphyrins and chlorins do not absorb light within the ~700-900 nm wavelength regime referred to as the ‘optical window’ of tissue.¹⁰ For instance, the maximum wavelength of absorbance (λ_{max}) for regular porphyrins, such as *meso*-tetraphenylporphyrin **1H₂**, rarely exceeds 650 nm. In comparison, the wavelength of maximum penetration of breast tissue is ~725 nm; whole blood has an absorption minimum at ~710 nm.¹¹ Regular porphyrins are thus unsuitable for biomedical *in vivo* applications. Non-emitting chromophores may also be attractive as photoacoustic imaging agents but,¹² again, only if they also absorb light within the optical window of tissue.¹³ Light-harvesting applications also benefit from NIR-absorbing dyes as a large portion of the irradiance energy of sunlight falls into this range. Panchromatic absorbers are also most desirable for light harvesting as these chromophores collect the maximum amount of energy.¹⁴

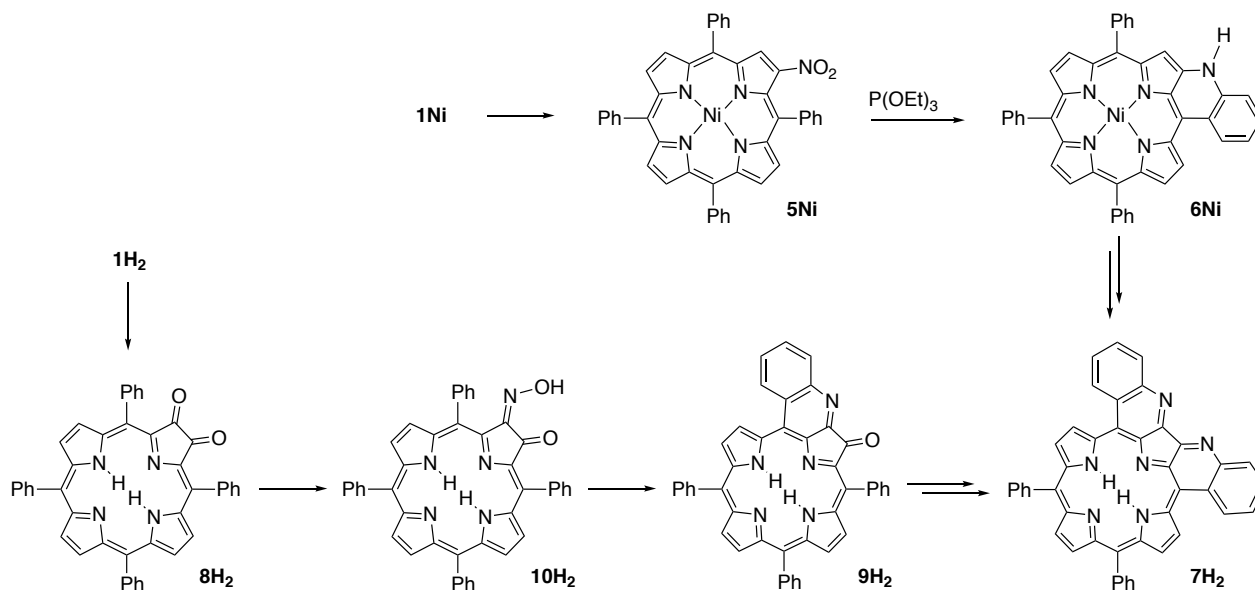
A number of strategies have been employed to achieve this goal. For instance, the expansion of the conjugated π -system by increasing the number of conjugated pyrroles was highly successful, as the many examples of NIR absorbing expanded porphyrins demonstrate.¹⁵ One other strategy is the establishment of π -systems that are annulated to the porphyrinic chromophore.^{14d,16} Among the latter class of porphyrins may be *meso*-arylporphyrin derivatives that bear a covalent linkage between one or more β -positions and the flanking *meso*-phenyl/aryl groups.¹⁷ In the absence of the linkage, a H _{β} -pyrrole-H_O-phenyl steric interaction prevents the *meso*-aryl groups from adopting low-energy coplanar conformations. The linkage removes this interaction but needs to be short enough to force the phenyl group(s) into (idealized) coplanarity with the porphyrinic chromophore, thereby extending the π -conjugation pathway. This

linkage may be a ketone functionality, itself in conjugation with the chromophore (**2H₂**).¹⁸ The resulting bathochromic shift of λ_{max} of **2H₂** compared to **1H₂** is a respectable ~76 nm. On the other hand, the fusion of one through four anthracenes to a porphyrin, as in **3H₂**, results in an enormous perturbation of their UV-vis spectra, with λ_{max} values red-shifted ~300 nm upon fusion of a single anthracene; the corresponding nickel(II) complex with four anthracenes shifted the λ_{max} by more than 900 nm, to 1417 nm.¹⁹ Few examples exist in which a chlorin chromophore incorporates an annulated ring, as in bischromene-annulated chlorin **4H₂**, leading to a 24 nm-shifted λ_{max} compared to the parent chlorin.²⁰



In 2011, Jeandon and Ruppert, building on the extensive work by Ruppert, Callot, and co-workers in the construction of peripheral conjugated chelates,²¹ published the formation of bisquinoline-annulated porphyrin **7H₂** from nickel porphyrin **1Ni** via a multi-step sequence (Scheme 1-3).²² The key β -to-o-linkage formation step involved a Cadogan reaction of

nitroporphyrin **5Ni** to form the amine-linked porphyrin **6Ni**. Subsequent nitrogen protection, regioselective nitration, thermally induced oxidation and ring-closure, and acid-induced demetallation produced the bisquinoline-annulated system **7H₂** in good yield.



Scheme 1-3. The two independent paths toward bisquinoline-annulated porphyrin **7H₂** developed by Ruppert (**1Ni** → **5Ni** → **7H₂**) and Brückner (**1H₂** → **10H₂** → **7H₂**).

Concurrently with Jeandon and Ruppert, we independently described in a preliminary report the conversion of free base porphyrin **1H₂** to free base bisquinoline-annulated porphyrin **7H₂**.²³ The key steps were two consecutive acid-mediated electrophilic aromatic substitution reactions of oximes, such as **10H₂**, formed from the corresponding ketone **8H₂**. We prepared this well-known dione **8H₂** along a dihydroxylation-diol oxidation sequence from porphyrin **1H₂**,²⁴ but this product can be made along a number of alternative routes.²⁵

The quinoline-annulated porphyrins are characterized by their significantly red-shifted optical spectra, with λ_{max} values in their absorption spectra in the realm of 750 – 800 nm (Figure 1-3). We attribute the dramatic shift in the optical spectrum of these chromophores to the increase of π -conjugation established by the annulation reaction, as well as a marked increase in the non-planarity of the macrocycles, as observed in their solid-state structures.²⁶

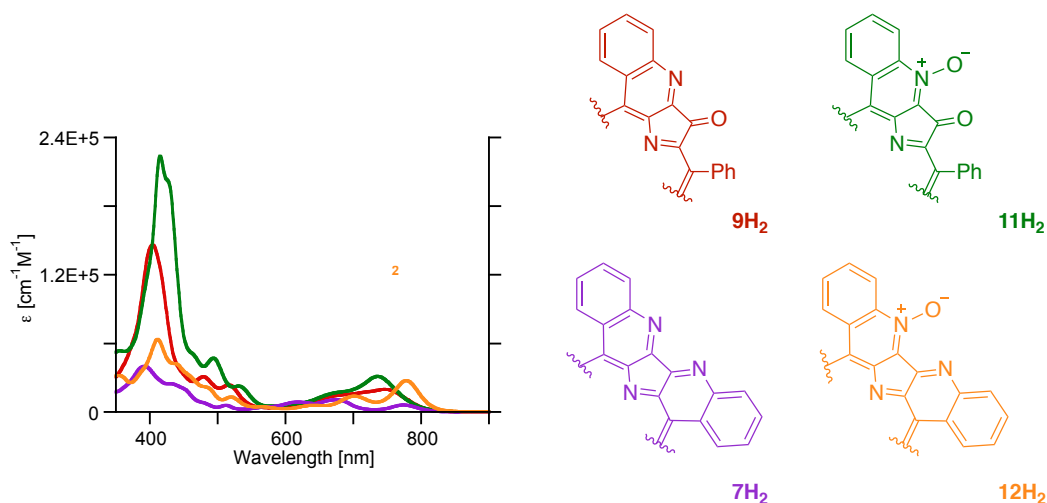


Figure 1-3. UV-vis spectra (CH_2Cl_2) of mono- and bis-quinoline annulated porphyrins.

The broad and intense absorption of the quinoline-annulated porphyrins in the NIR region suggests their use in biomedical applications. However, their very low fluorescence and singlet oxygen quantum yields prevent their use as PDT agents. Taking these properties into consideration, we were able to show that these NIR absorbers are excellent *in vitro* contrast agents for photoacoustic imaging applications.¹³ Further evaluation of the quinoline-annulated porphyrin platinum complexes, particularly **7Pt**, also suggests their use as O_2 sensors for their NIR emission and long phosphorescence lifetimes. Unfortunately, their insolubility in aqueous systems prevents the evaluation of these dyes in biological contexts.

Step 1: **Activating**

Step 2: **Breaking**

Step 3: **Mending**

Step 4: **Derivatization**

Porphyrin

Activated Chlorin (or Porphyrin)

Secochlorin

Pyrrole-modified Porphyrin (PMP)

8

1.4 Modifications of Porphyrins and Hydroporphyrins for their Solubilization in Aqueous Media

The utility of porphyrins and hydroporphyrins (chlorins and bacteriochlorins) in a variety of biomedical applications was demonstrated.²⁹ These include photodynamic cancer therapy,^{6b,6c,30} antifungal photodynamic therapy,⁸ their use as photoantimicrobials,⁷ as fluorescence and photoacoustic imaging agents,^{6c,9,12a,31} (single) cell imaging³² and fluorescence labelling,³³ and as *in vivo* chemosensors.³⁴ In addition, they have shown value in a number of technical applications, such as chemosensing,^{34a} electronic devices and materials,³⁵ catalysis,³⁶ photocatalysis,³⁷ and light harvesting.³⁸ These applications rest on the favorable optical, chemical and electronic properties of these porphyrinoids: Their intense absorbance in the visible to near infrared (NIR) region, high fluorescence or singlet oxygen quantum yields, good photoacoustic signal generation efficiency, ease of ejection of a photo-excited electron, etc. Many of these applications will greatly benefit from an inherent solubility of the porphyrins in aqueous media, i.e., not requiring any surfactants or liposome vesicles to mediate solubility. However, even though the methodologies toward synthetic porphyrins,³⁹ hydroporphyrins,^{6b,40} and their analogues,^{28,40d,41} have advanced enormously in the past decades, the vast majority of the synthetic porphyrinoids presented are not naturally water-soluble, preventing—or at least complicating—their utilization in, for example, biological contexts.

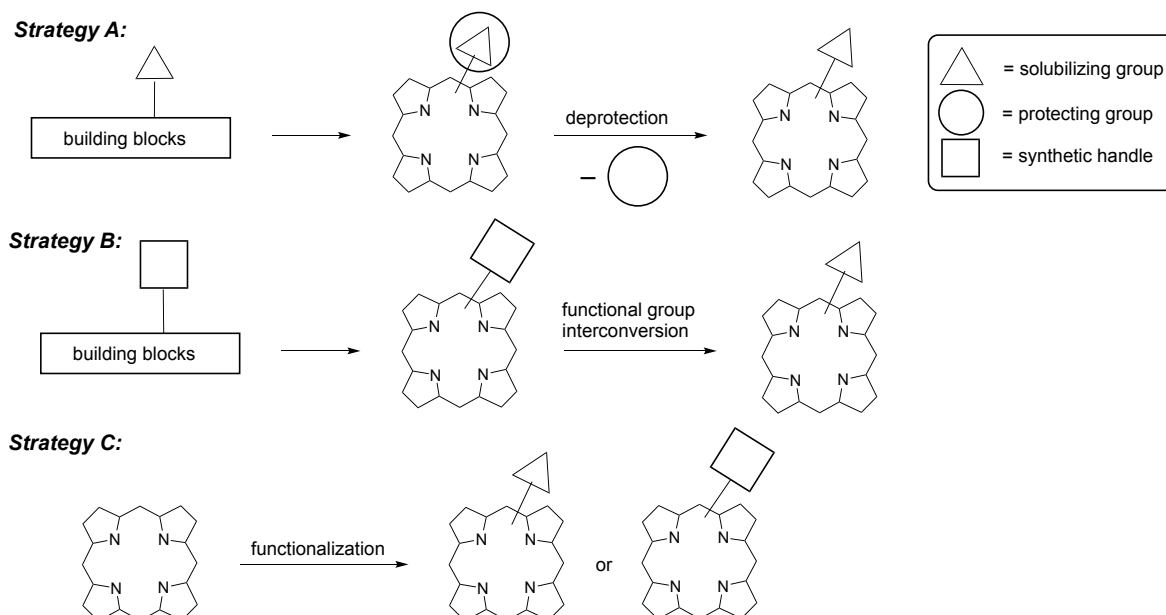
Initial efforts to impart water-solubility relied on the utilization of *meso*-pyridyl and *meso-p*-sulfonatophenyl-substituents in (mostly) symmetric porphyrins. These porphyrins were based on Adler syntheses of tetrapyrrolyl- and tetraphenylporphyrin, followed by quarternization with a suitable alkyl halide or direct sulfonation, respectively. Albeit simple, both methods have drawbacks. They are difficult to translate to β -alkyl-substituted porphyrins, the sulfonation reaction conditions are harsh and therefore incompatible with many hydroporphyrin chromophores or substituents that convey desirable properties onto the porphyrin. This led to the development of

a range of alternative methods to impart water-solubility that are mild, selective, and that generate the water-soluble porphyrin derivative late in the synthetic sequence, thus facilitating its isolation and purification.

Rather than attempting to be comprehensive, we aim to present here a tutorial-style review that highlights recent (since ~2000) synthetic strategies. Where data is available, we compare the resulting solubilities and report on other notable practical considerations. This summary extends a review on water-soluble porphyrins published in the year 2000⁴² that provides a detailed account of the acid-base properties and aggregation behavior of conventional water-soluble porphyrins. A 2014 review on amphiphilic porphyrins by Gryko and co-workers⁴³ is also available; overlap with this review is minimized and these reviews are thus complementary. Porphyrins linked to sugars, many of which are also water-soluble, have been reported.⁴³⁻⁴⁴ We chose not to include them here because glycosylation strategies are frequently not driven by achieving water-solubility but to increase tumor targeting; they were also reviewed in the context of amphiphilic porphyrins.⁴³ Water-soluble porphyrins conjugated to biomolecules (e.g., oligonucleotides and peptides), appended to functionalities such as cyclodextrans,⁴⁵ crown ethers,⁴⁶ porphyrin nanoparticles,⁴⁷ or porphyrins that were solubilized with the help of surfactants or vesicles⁴⁸ are also beyond the scope of this discussion. Likewise, we do not cover the solubilization of expanded porphyrins or most other porphyrinoids.

The review is organized along the charge the solubilization groups introduce: Cationic (amine/ammonium, pyridyl/pyridinium), anionic (sulfonate, phosphonate, carboxylic acid/carboxylate) and neutral (polyethylene glycol (PEG) chains). Each section discusses the examples loosely in increasing order of complexity and the position of the solubilizing group. Three principle strategies for the introduction of solubilizing groups can be distinguished (Scheme 1-6). **Strategy A** encompasses the synthesis of porphyrin macrocycle using building blocks bearing solubilizing groups (protected or not). **Strategy B** involves the synthesis of a

porphyrin macrocycle with precursor functionalities that can later be manipulated to hydrophilic groups. **Strategy C** employs synthetic modifications of an already-formed porphyrin to impart water solubility.



Scheme 1-6. Principle strategies toward hydrophilic porphyrin derivatives.

1.4.1 Water-Soluble Porphyrins Bearing Cationic Substituents

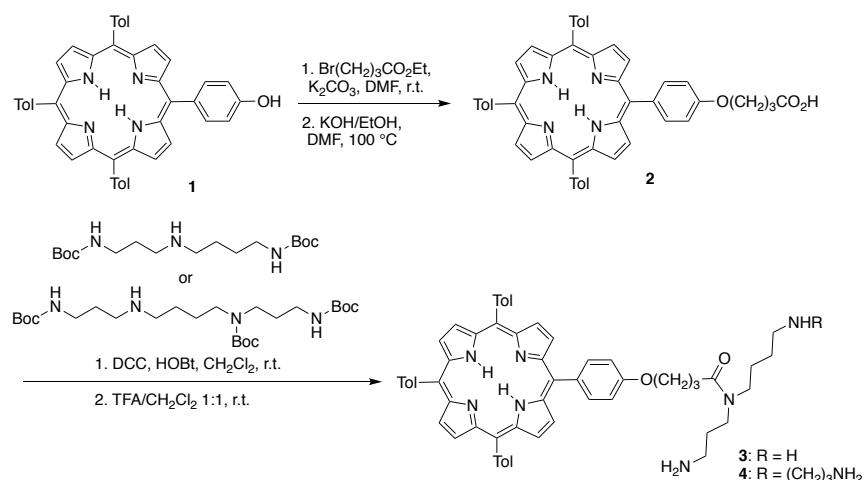
Cationic porphyrins were among the first synthetic water-soluble porphyrins to be discovered.⁴⁹ These early methods of solubilization relied on the *N*-alkylation of *meso*-tetrapyrrolylporphyrins and their metal complexes (see also section 1.4.1.2).⁴³ These types of cationic porphyrins were widely studied for their association with the polyanion DNA,⁵⁰ as part of the quest for new photosensitizers for photodynamic therapy (PDT), and for their promise as photo-antimicrobials for gram positive and gram negative bacteria.⁵¹ Tetra-pyrrolyl/pyridiniumporphyrins are also commercially available.⁵²

1.4.1.1 Amine/Ammonium functionalized porphyrins

One possibility for the preparation of cationic water-soluble porphyrins and hydroporphyrins is through derivatization with amines or polyamines. Porphyrinoids with amine functional groups may be soluble in aqueous media at low pH, but quarternization of the amines with suitable electrophiles is frequently employed to furnish freely water-soluble derivatives. The resulting (poly)cationic derivatives are usually purified by crystallization protocols or reverse phase chromatography. Ion-exchange chromatography offers an option to subsequently exchange the halide counterion (typically Br⁻ or I⁻) to another anion.⁵³

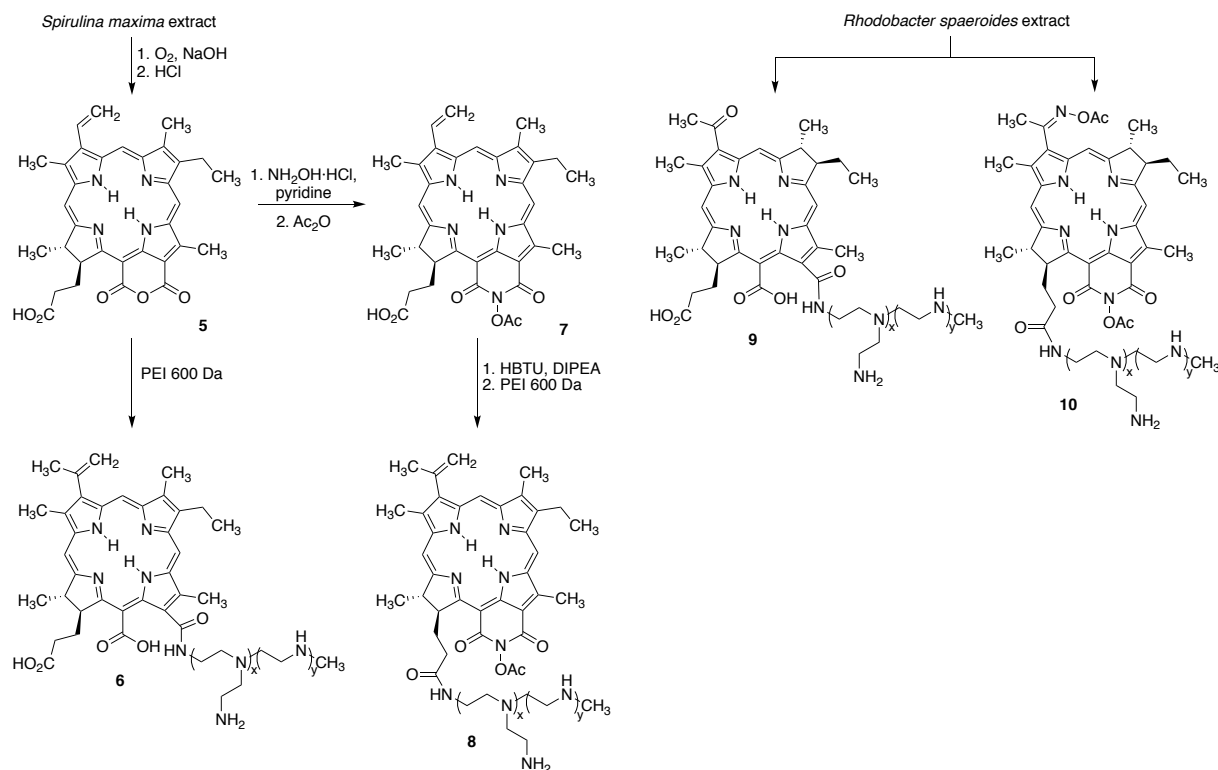
A number of symmetric and asymmetric amphiphilic *meso*-aryl porphyrins bearing amine functional groups have been reported.⁴³ The strategies toward their generation often rely on Adler or Lindsey porphyrin syntheses incorporating amine-containing building blocks or through modification of other functionalities, such as phenols.

Krausz and co-workers, for example, synthesized polyamine- *meso*-arylporphyrin conjugates by DCC-mediated amide-coupling of carboxylic acid-functionalized A₃B porphyrin **2**, made by functionalization of phenol **1** with di-Boc-protected-spermidine or tri-Boc-protected-spermine (Scheme 1-7).⁵⁴ The ultimate starting A₃B porphyrin **1** was synthesized using a mixed aldehyde Adler condensation, followed by alkylation of the phenolic oxygen with ethyl 4-bromobutanoate and saponification. The thus generated polyamines were submitted to standard Boc-deprotection conditions to afford the polyamine-porphyrin conjugates **3** and **4**, respectively.



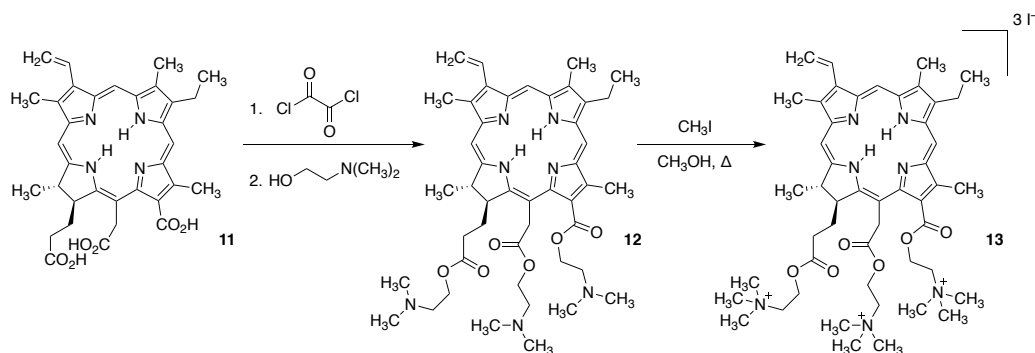
Scheme 1-7. Spermine- and spermidine-porphyrin conjugates, as described by the group of Krausz.⁵⁴

Bacteriochlorins derived from natural sources and bearing an anhydride functionality could also be derivatized by amide formation with polyamines.⁵⁵ Sol and co-workers prepared water-soluble chlorin polyamine derivative **6** through amidation of a chlorin extracted from *Spirulina maxima* (Scheme 1-8). The polyamine groups were introduced by nucleophilic ring opening of anhydride **5** with polyethylenimine (PEI, MW 600 Da). Alternatively, polyamination was performed at the propionic acid side chain. The anhydride moiety in chlorin **5** was first converted to an acetate-protected cycloimide chlorin **7** by treatment with hydroxylamine, followed by acylation. The subsequent polyamination at the propionic acid side chain required activation of the carboxylic acid moiety, followed by reaction with PEI. In a similar fashion, water-soluble polyaminated bacteriochlorins **9** and **10** were prepared starting from bacteriochlorins extracted from *Rhodobacter spaeroides*. In water, the resulting compounds exhibited split and/or broadened Soret bands, indicating some degree of aggregation.

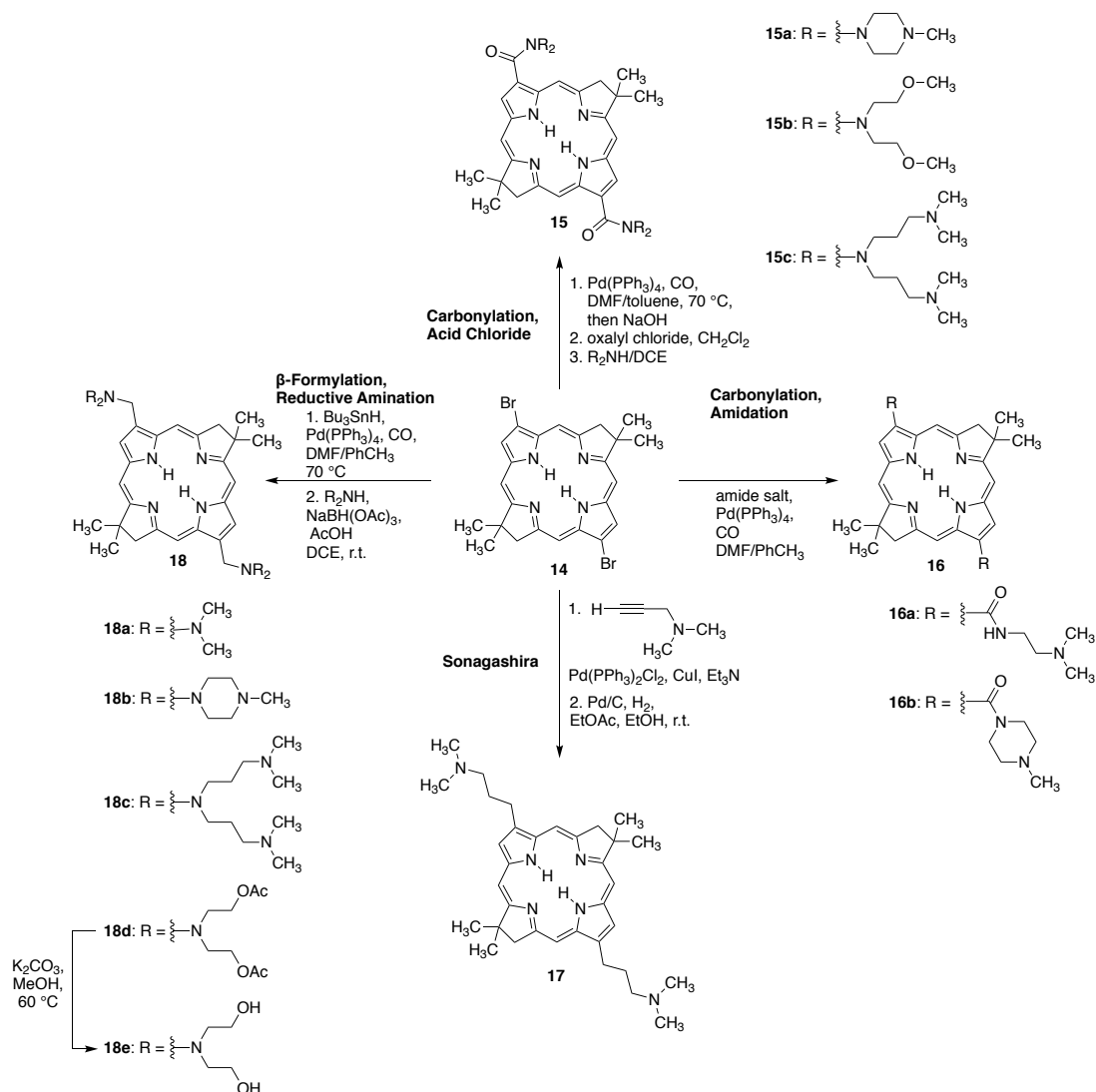


Scheme 1-8. Chlorin and bacteriochlorin polyamines derived from *Spirulina maxima* and *Rhodobacter spaeroides*, respectively, as described by the group of Sol.⁵⁵

Amine groups were also introduced to porphyrins bearing carboxylic acid groups by esterification with an amino-alcohol. An example of this strategy was the preparation of a tricationic water-soluble ester of chlorin e6 **11** (Scheme 1-9).⁵⁶ Methyl pheophorbide **a** was saponified, and the acid groups in product **11** were activated as acid chlorides and esterified with *N,N*-dimethylaminoethanol to provide triamine **12**. Quarternization by reaction with CH_3I gave the tricationic water-soluble chlorin derivative **13**.⁵⁶



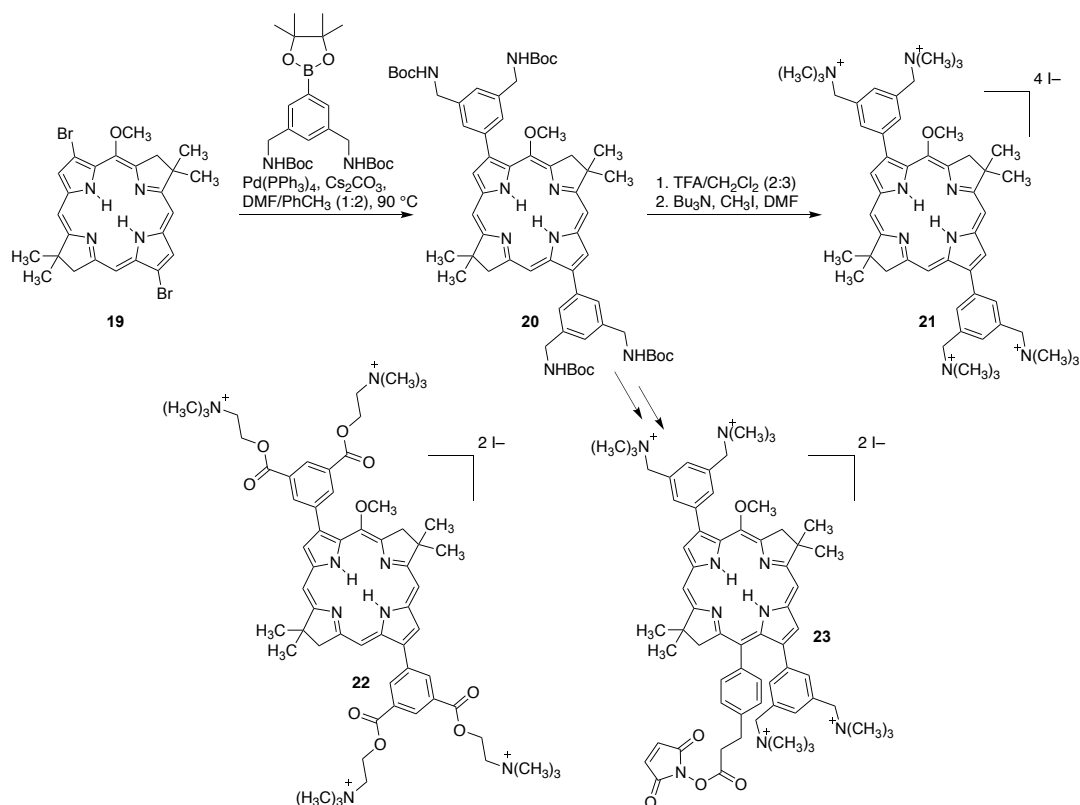
Scheme 1-9. Cationic esters of chlorin e6 with terminal ammonium groups, as described by the group of Inoue.⁵⁶



Scheme 1-10. β -substituted cationic ammonium bacteriochlorin derivatives, as described by the group of Lindsey.⁵⁷

Amine groups have been introduced to the β -positions of hydroporphyrins by transition metal-mediated coupling strategies using β -bromo precursors. Thus, Lindsey and co-workers prepared a range of water-soluble cationic bacteriochlorin derivatives utilizing the versatile 3,13 dibromobacteriochlorin building block **14**. The bromo groups are susceptible to a variety of transition metal-mediated C-C bond forming coupling reactions (Scheme 1-10).⁵⁷ For example, bacteriochlorins **15a-15c** were prepared from **14** through a carbonylation \rightarrow acid chloride reaction with secondary amines. Additionally, reaction of amide salts with **14** in a carbonylation \rightarrow amidation sequence gave the amino-bacteriochlorins **16a** and **16b**. Sonogashira coupling of **14** with an ethynyl-amine, followed by reduction, gave the bacteriochlorin **17** with amine-terminated alkyl chains. Lastly, a variety of secondary amines was employed in a β -formylation \rightarrow reductive-amination strategy to produce amine-functionalized bacteriochlorins **18a-18e**. The resulting amines were amenable to purification by silica gel column chromatography (EtOAc or CH₂Cl₂/MeOH/NH₄OH as eluents). Subsequent *N*-alkylation of the amines was achieved using standard conditions, and the water-soluble cationic products that precipitated from the CHCl₃ reaction mixtures were isolated by precipitation and centrifugation. Some of these compounds were investigated for their efficacy as antimicrobial photosensitizers.⁵⁸

Lindsey and co-workers also used similar dibromobacteriochlorin **19** to directly introduce arylamines to the β -positions *via* Suzuki couplings (Scheme 1-11).⁵⁹ After the coupling of dibromobacteriochlorin **19** with an aryl boronic ester bearing two Boc-protected amines, the Boc groups in product **20** were removed, and the free amine quarternized by treatment with CH₃I to afford the final ammonium-functionalized bacteriochlorin product **21**.

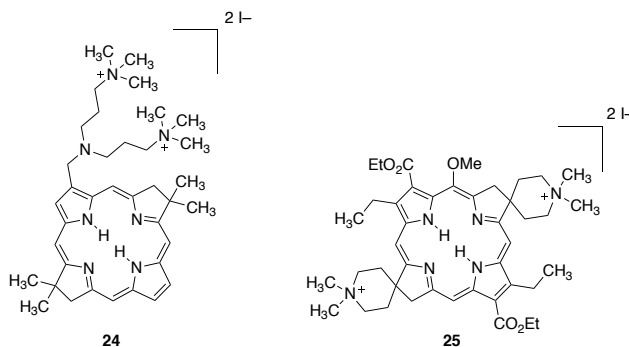


Scheme 1-11. β -Substituted cationic ammonium bacteriochlorin derivatives prepared by Suzuki coupling, as described by the group of Lindsey.⁵⁹

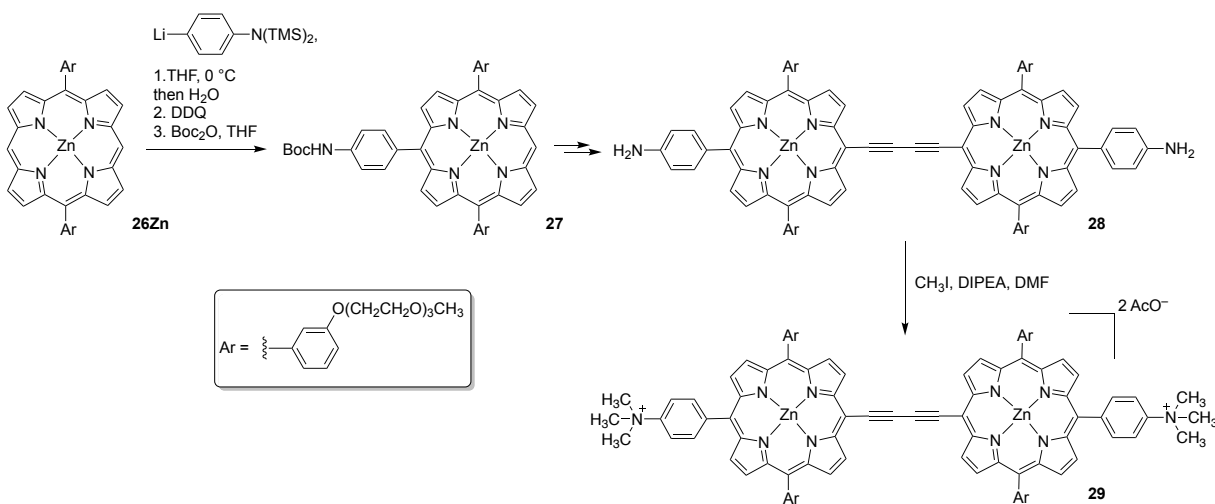
Related compounds with terminal amine functional groups, such as 3,13-diaryl bacteriochlorin **22**, were prepared using similar Suzuki coupling strategies. Bioconjugatable derivatives of these compounds carrying an NHS-ester functional group, such as **23**, were also prepared by a regioselective *meso*-bromination \rightarrow Suzuki coupling sequence (see also Section 2.2.2).⁵⁹

The Lindsey group also prepared a range of amphiphilic bacteriochlorins of limited aqueous solubility bearing one amine side chain by reductive amination of a β -formylated bacteriochlorin (see also Scheme 1-10).⁶⁰ A representative example is bacteriochlorin **24**, which possesses an ammonium-terminated dialkyl chain, a so-called swallowtail functionality. This moiety was designed to project solubilizing groups above and below the plane of the macrocycle, leading to facial encumbrance that inhibits macrocycle stacking and increases hydrophilicity. A similar

strategy was used to solubilize *meso*-aryl porphyrins in organic solvents.⁶¹ Other ammonium-based water-soluble derivatives were also prepared by the Lindsey group by introduction of spiro-linked piperidine moieties at the β -positions of a bacteriochlorin.⁶² The integral spiro-piperidine functional groups were quarternized using standard conditions to furnish water-soluble derivatives, such as bacteriochlorin **25**.



The direct introduction of ammonium groups using a nucleophilic Senge arylation strategy was performed by Anderson and co-workers on 1,15 diaryl porphyrin **26Zn** (Scheme 1-12).⁶³ Porphyrin **26** was functionalized at the *meso*-position with a Boc-protected amino-phenyl group. The resulting derivative **27** was carried through multiple steps to afford porphyrin dimer **28** that was rendered water-soluble by quarternization of the amine functionality with CH_3I .

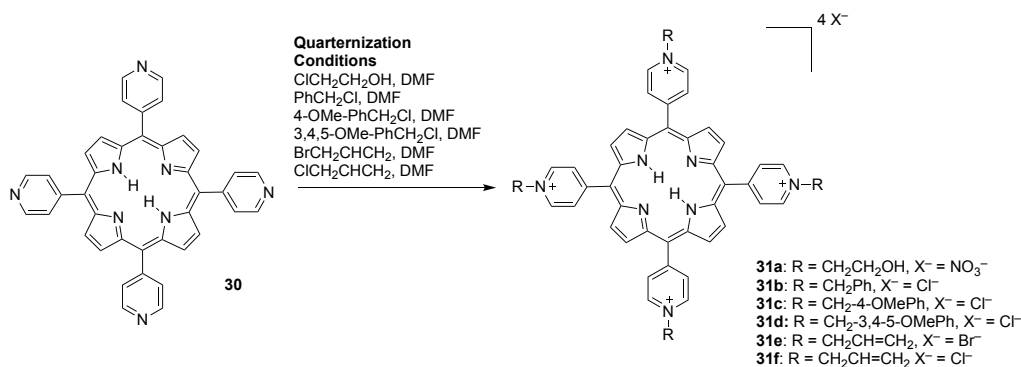


Scheme 1-12. *meso*-Aryl-ammonium bis-acetylene linked porphyrin dimers prepared via Senge arylation, as described by the group of Anderson.⁶³

1.4.1.2 Porphyrins Carrying Pyridyl/Pyridinium Groups

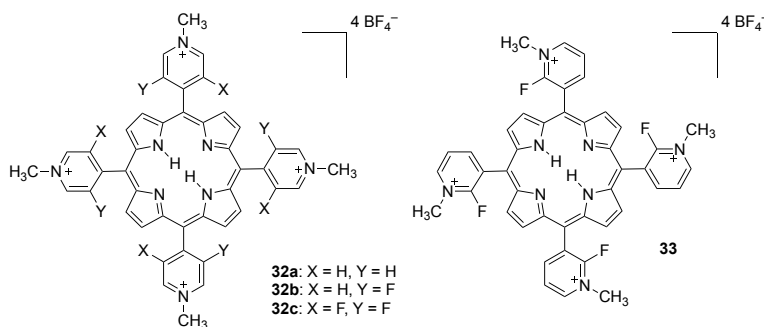
meso-Tetrakispyridiniumporphyrins

meso-Tetrapyridylporphyrins and the corresponding *meso*-tetrakis(methylpyridinium)porphyrins are long known, and their intercalation into DNA was studied in detail.⁵⁰ Pyridinium porphyrins continue to attract attention as next generation photosensitizers for PDT. Various new *meso*-tetrakispyridiniumporphyrin derivatives were prepared using a range of electrophiles to quarternize the pyridine nitrogens (Scheme 1-13). Orlandi and co-workers prepared *meso*-tetrakis(4-pyridinium)porphyrins (**31**) by reaction of *meso*-tetra(4-pyridyl)porphyrin (**30**) with various benzyl chlorides to study the effect of polar alkylating groups on their antibacterial activity.⁶⁴ The benzylation conditions required were more vigorous (reflux in DMF for 24 h) than typical for pyridine alkylations using alkyl halides. The water-soluble products were recovered by precipitation with Et₂O and filtration. Similarly, Ghazaryan and co-workers prepared a variety of *meso*-substituted *N*-substituted tetrapyridiniumporphyrins with different central metals (Ag, Zn, Co and Fe) and alkylating agents (allyl-, oxyethyl-, butyl- and methallyl-substituted derivatives).⁶⁵

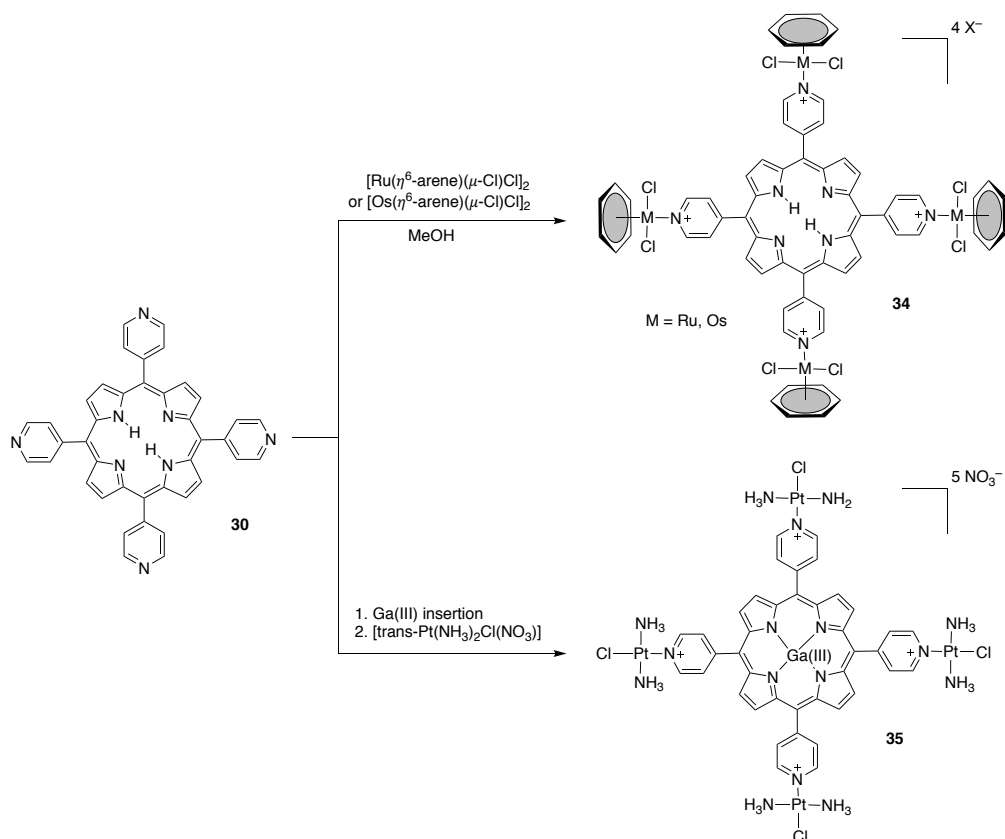


Scheme 1-13. Quarternization options of *meso*-tetrakis(4-pyridyl)porphyrin.

Fluorinated derivatives of *m*- or *p*-linked *meso*-pyridyl porphyrins were prepared along Adler synthesis routes.⁶⁶ *N*-Alkylation of the pyridyl substituents by treatment with $(\text{CH}_3)_3\text{O}^+\text{BF}_4^-$ afforded the tetra-alkylated products **32** and **33**, respectively as their tetrafluoroborate salts.



In search of dual-action photo- and cyto-toxic anti-cancer agents, various metal complexes were coordinated to the outer pyridyl nitrogens in tetrapyrrolylporphyrins (Scheme 1-14). Ruthenium, rhodium and iridium complexes were thus prepared by Therrien and co-workers⁶⁷ by treatment of *meso*-tetrapyrrolylporphyrin (**30**) with various metal arene salts to afford the water-soluble organic metallic complexes of type **34**. They also prepared mixed arene-ruthenium substituted porphyrins in a similar manner, producing mono- and tetrametallated derivatives of 3- and 4-tetrapyrrolylporphyrins.⁶⁸ Both *cis*- and *trans*-platin conjugates of porphyrins were prepared by treatment of **30** with *cis*- or *trans*-Pt(II) complexes, respectively.⁶⁸ The gallium complexes of these compounds (such as **35**) were prepared by Odani and co-workers⁶⁹ and also tested as photosensitizers for cancer therapy. In addition, tetrapyrrolylporphyrins with ruthenium nitrosyl groups substituted at their periphery were reported by the group of Alessio, generated by reaction of **30** with ruthenium nitrosyls and purified by column chromatography ($\text{CHCl}_3/5\% \text{ EtOH}$ as eluent).⁷⁰

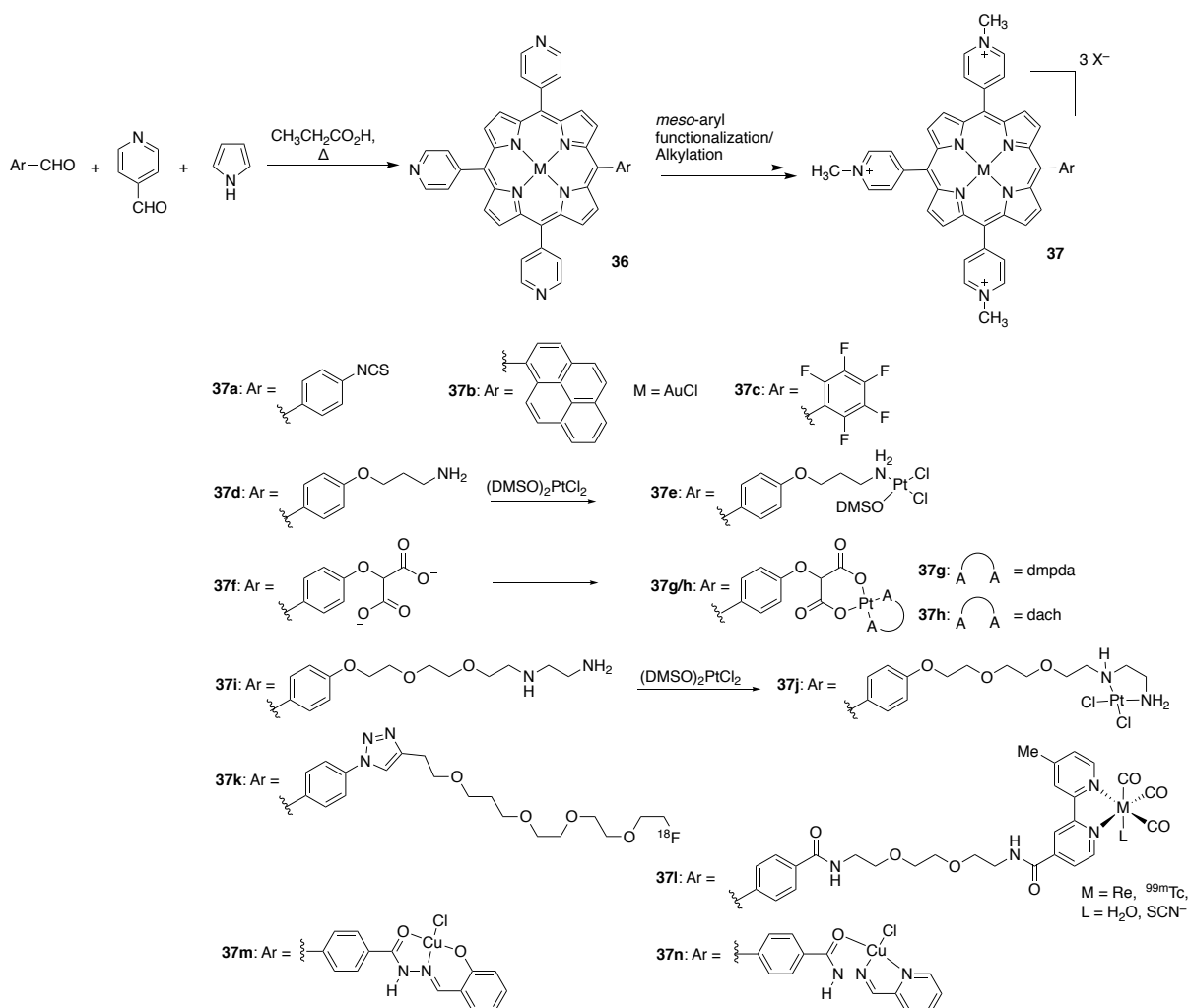


Scheme 1-14. M-Arene complexes of *meso*-tetra(4-pyridyl)porphyrin, as described by the groups of Therrien,⁶⁷⁻⁶⁸ and Odani.⁶⁹

***A₃B* and Other *meso*-Pyridiniumporphyrins**

A number of symmetrically substituted pyridylporphyrins have been prepared in the search for the next generation of anticancer PDT agents. However, to further optimize their tumor-targeting and biodistribution properties, the porphyrin needs to be amenable to further modifications that will allow, for example, the conjugation of the porphyrin to a targeting molecule. Thus, a variety of examples emerged that use *A₃B* porphyrins bearing three *meso*-pyridinium groups as the water-soluble framework of the chromophore, with the fourth *meso*-aryl ring available for further manipulations (Scheme 1-15). The parent *A₃B* porphyrins are typically synthesized as statistical mixtures by Adler condensation of pyridylaldehyde, the desired arylaldehydes, and pyrrole, followed by chromatographic separation of the product mixture. The

A₃B porphyrin precursors are functionalized at the remaining *meso*-aryl group and *N*-alkylated with CH₃I, with the order of these operations depending on the functionality present (see below).

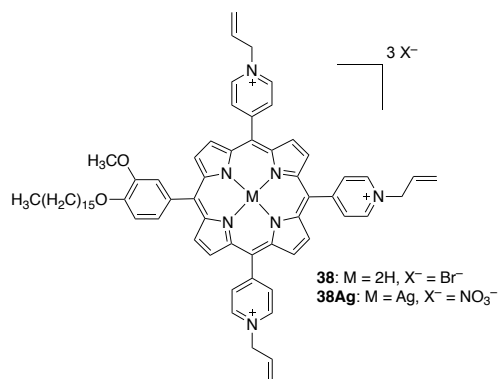


Scheme 1-15. A₃B tri-pyridyl porphyrins prepared by Adler synthesis and subsequent synthetic modification.

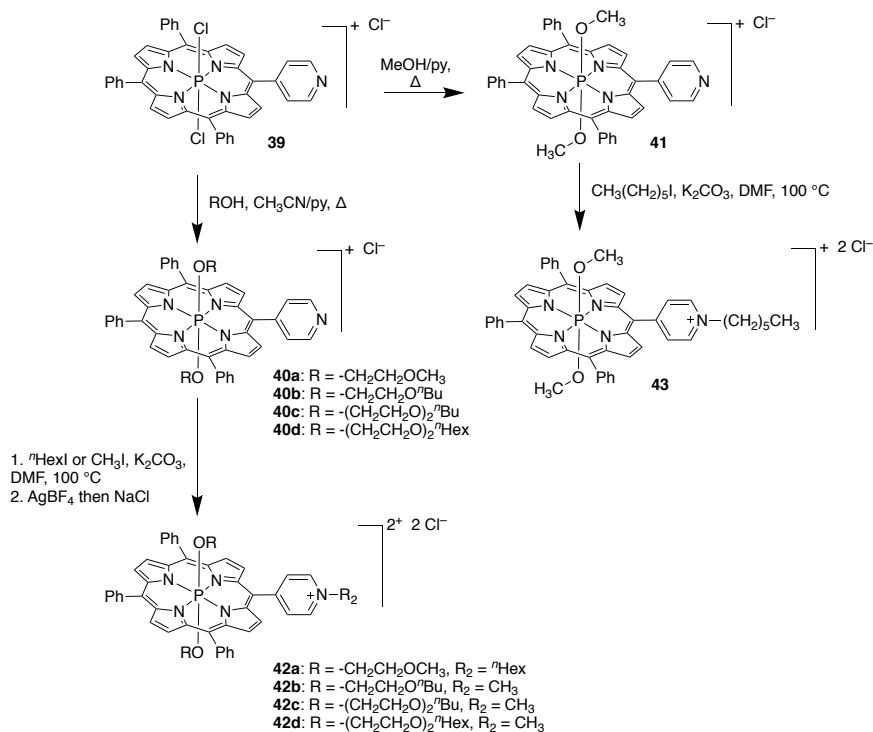
Using this strategy, a pyrene-substituted trispyridyl A₃B porphyrin could be prepared.⁷¹ Its *N*-alkylation with methyl *p*-toluenesulfonate in refluxing CHCl₃/CH₃NO₂ afforded the tris-*N*-methyl pyridiniumporphyrin **37b**. The Boyle group synthesized tripyridyl A₃B porphyrin **37a** with the fourth aryl ring bearing a bioconjugatable isocyanate group. The *N*-alkylation step (standard CH₃I alkylation conditions) needed to be performed after the formation of the isocyanate group to avoid unwanted *N*-alkylation of the amine precursors.⁷² A number of *p*-substituted phenyl

derivatives allowed a wide range of functionalizations. For instance, Song *et al.* synthesized A₃B pyridyl porphyrin **37j** with the fourth aryl group bearing a Pt(II) complex linked to the hydroxyl group of the *meso*-phenol group by a triethylene glycol linker.⁷³ *N*-Alkylation of the three pyridyl groups, followed by Boc-deprotection and complexation with the Pt(II) precursor, yielded the A₃B platinum-porphyrin conjugate **37j**. A similar approach was taken by the group of Alessio to synthesize water-soluble ^{99m}Tc(I)/Re(I)-porphyrin conjugates, such as **37l**, utilizing an amide-linked spacer between the aryl group and the ^{99m}Tc(I)/Re(I) ion.⁷⁴ The water-soluble derivatives were purified by normal phase silica gel column chromatography (CH₂Cl₂/MeOH mixtures). These types of compounds can also be conjugated to cancer-targeting peptides for use in cancer therapy.⁷⁵ Cu(II)-based acylhydrazone porphyrin-derivatives **37m** and **37n** could be obtained using a similar strategy.⁷⁶ The Boyle group synthesized an A₃B porphyrin that could be further functionalized to establish an azide group.⁷⁷ The azide functionality was used in a click reaction to introduce an ¹⁸F-terminated short PEG chain to generate water-soluble porphyrin **37k** for PDT/PET theranostic applications.⁷⁷ After *N*-methylation of the pyridyl nitrogens, the subsequent synthetic steps required precipitation of the product using Et₂O/MeOH mixtures. The final products were purified by passing through a column of neutral alumina.

Gasparyan and co-workers synthesized an A₃B amphiphilic trispyridylporphyrin with one *meso*-aryl group carrying a long alkyl chain using a mixed aldehyde Adler condensation.⁷⁸ Quaternization of the pyridyl groups with 3-bromopropene provided the water-soluble vinyl-substituted trispyridiniumporphyrins **38** and **38Ag** that were isolated by precipitation with acetone.

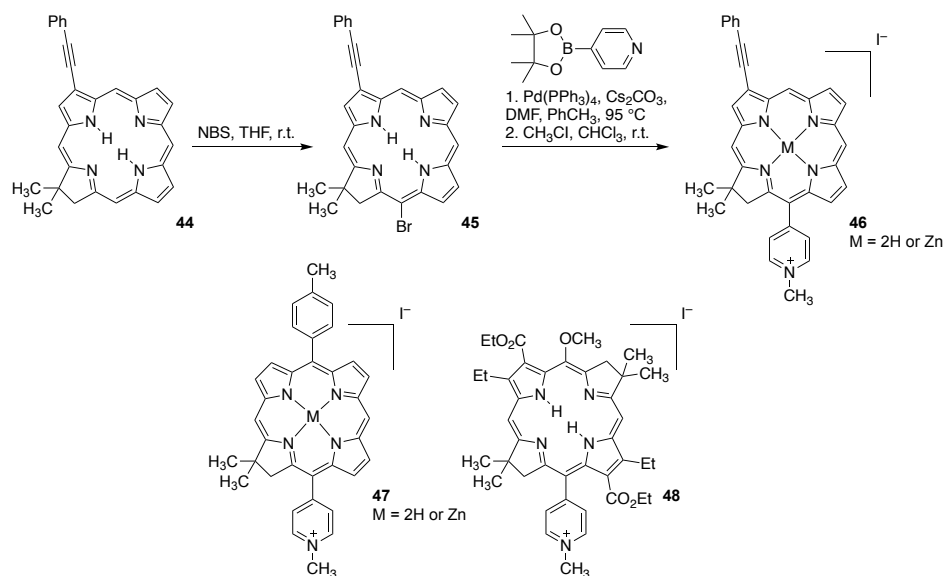


Yasuda and co-workers prepared AB₃ phosphorus porphyrin **39**.⁷⁹ Its axial chloro-ligands could be exchanged for simple alcohols and oligoethylene glycol chains to generate hydrophilic phosphorus porphyrins **40** and **41**. *N*-Alkylation of the *meso*-pyridyl group in **40a-40d** or **41** then furnished water-soluble derivatives, with solubility in water of around ~10 mM for compounds **42a-42d** and **43**. (Scheme 1-16).⁷⁹ An equivalent methodology was used to introduce axial PEG chains.⁸⁰



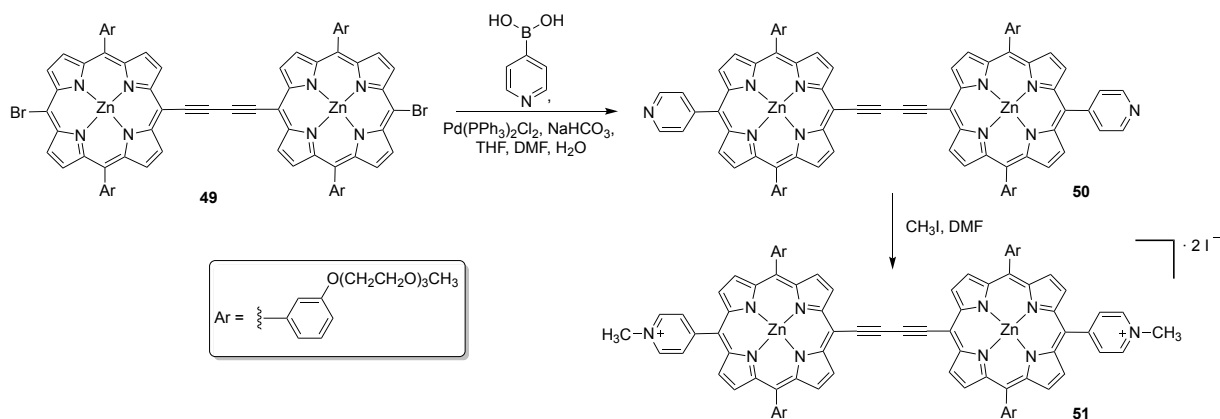
Scheme 1-16. Water-soluble AB₃ phosphorus porphyrins, as described by the group of Yasuda.⁷⁹

Using a fundamentally different strategy toward *meso*-pyridyl porphyrins, pyridyl substituents can be introduced to *meso*-brominated porphyrins by using Suzuki couplings. For instance, the Lindsey group reported the synthesis of a series of amphiphilic hydroporphyrins prepared by Suzuki coupling of a pyridyl boronic ester with *meso*-bromo-chlorins or bacteriochlorins.^{40d} Key chlorin building block **45** was prepared by regioselective *meso*-bromination of chlorin **44** using NBS (Scheme 1-17).⁸¹ In the final step of the synthesis, the pyridyl functional group was quarternized with CH₃I to furnish bacteriochlorin **46**. This strategy is flexible and tolerant of a number of other substituents on the hydroporphyrin framework. Thus, chlorin **47** and bacteriochlorin **48** were prepared along analogous routes.



Scheme 1-17. Amphiphilic *meso*-pyridyl chlorins and bacteriochlorins, as described by the group of Lindsey.⁸¹

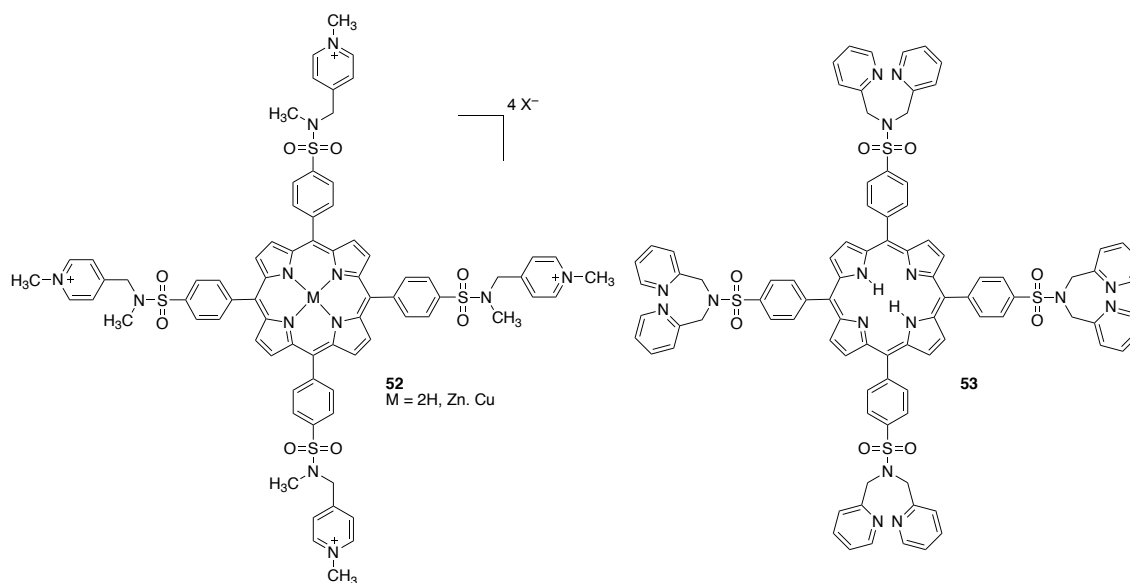
In an analogous manner, Anderson and co-workers employed a Suzuki coupling strategy to introduce pyridyl functional groups to *meso*-dibrominated bis-acetylene linked porphyrin dimer **49** (Scheme 1-18).⁶³ After coupling with 4-pyridinylboronic acid, both *meso*-pyridyl functional groups in **50** were methylated under standard conditions to afford the dicationic product **51**. This water-soluble porphyrin dimer was purified by precipitation from DMF/Et₂O.



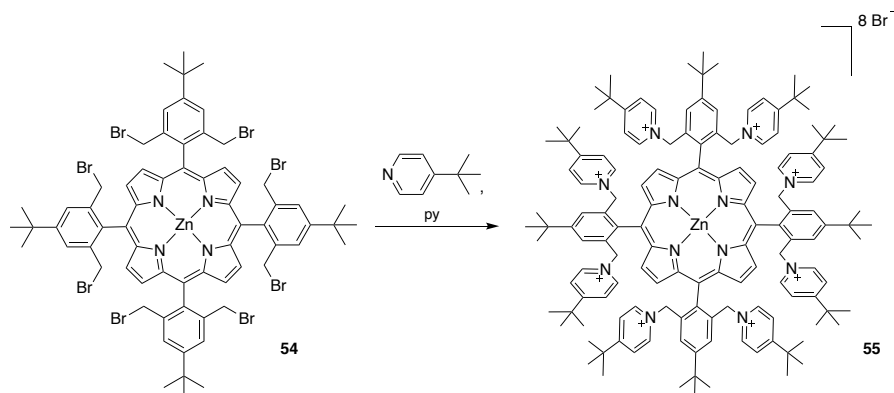
Scheme 1-18. Preparation of a *meso*-pyridinium-functionalized bis-acetylene linked porphyrin dimer, as described by the group of Anderson.⁶³

Other Pyridyl-Substituted Porphyrins

Porphyrins bearing alkylated pyridinium substituents in positions not directly linked to the *meso*- or β -positions of the macrocycle were also prepared. For example, Marzilli and co-workers synthesized porphyrins with the pyridyl groups linked through sulfonamide linkages (**52**) to the *p*-phenyl positions of *meso*-tetraarylporphyrins.^{53,82} They investigated whether distant pyridinium groups are equally competent in mediating DNA-intercalation. Dipicolylamine (DPA) substituents could also be linked through the sulfonamide group (**53**).⁸³

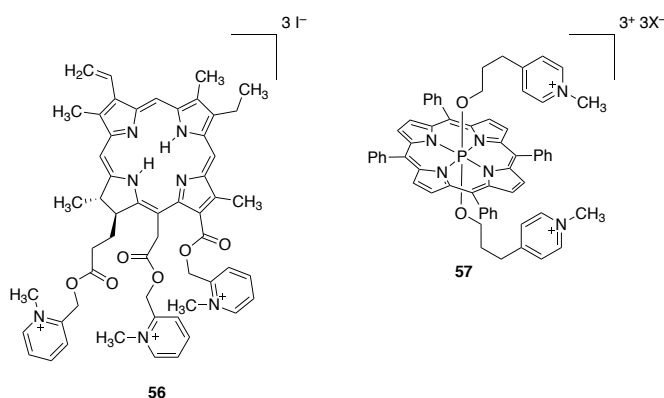


A remarkable octapyridiniumporphyrin **55** was prepared by Prato and co-workers⁸⁴ by treatment of *meso*-tetrakis(2,6-bis-(bromomethyl)-4-*t*-butylphenyl) porphyrin **54** with *t*-butyl pyridine (Scheme 1-19). The octapyridyl porphyrin **55** was purified by crystallization from Et₂O/MeOH. The octacationic compound **55** was used in studies toward assemblies for light-harvesting applications.



Scheme 1-19. An octapyridiniumporphyrin, as described by the group of Prato.⁸⁴

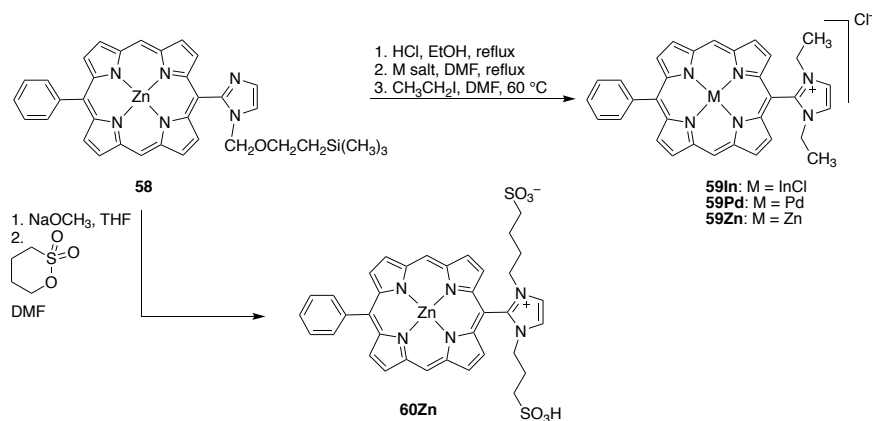
The introduction of pyridinium groups can also be achieved by esterification of a β -alkylester with a suitable pyridine-derivatized alcohol. Thus, cationic water-soluble ester **56** was prepared from chlorin e6 (**11**) by esterification with 2-(2-hydroxyethyl)pyridine, followed by quaternization with CH₃I (cf. Scheme 1-9).⁵⁶ Derivatives **56** and related **13** possess sharp absorbance spectra in Tris-HCl buffer at pH 7.6, indicating little aggregation of the chromophores.



Pyridinium substituents have also been introduced in the axial positions of phosphorus and antimony *meso*-tetraphenyl porphyrins by axial exchange using a pyridine-derivatized alcohol (cf. to Scheme 1-16).^{79,85} Alkylation of the axial pyridyl moiety with a range of alkyl bromides furnished derivatives such as **57**, with a water-solubility of ~3 mM.⁷⁹

meso-Imidazolium Porphyrins

The synthesis of porphyrins carrying *N*-alkylated *meso*-imidazolyl functionalities represents another strategy for the preparation of cationic porphyrins.⁸⁶ Lindsey and co-workers prepared porphyrins with one or two *meso*-imidazolyl groups by starting from imidazole-functionalized dipyrromethane precursors.⁸⁷ Mono-imidazolyl porphyrin **58** was alkylated with various alkylating reagents. The resulting imidazolium porphyrins were studied for their use in photodynamic therapy. The zwitterionic imidazolium sulfonate porphyrin **60Zn**, for example, is the product obtained when 1,4-butane sultone was used as the alkylating reagent (Scheme 1-20).^{87a}

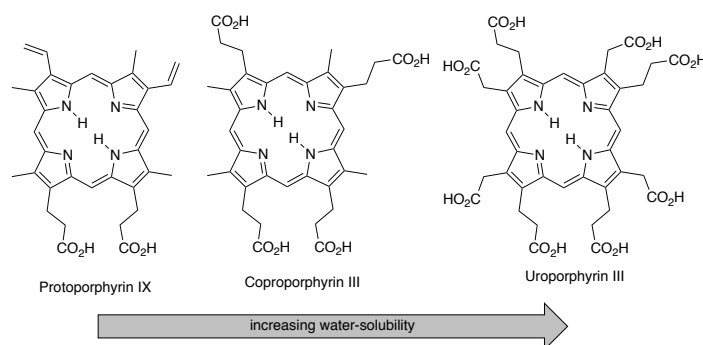


Scheme 1-20. *meso*-Imidazolium porphyrins, as described by the groups of Lindsey and Hamblin.⁸⁷

1.4.2 Water-Soluble Porphyrins Bearing Anionic Substituents

1.4.2.1 Porphyrins with Carboxylate Functional Groups

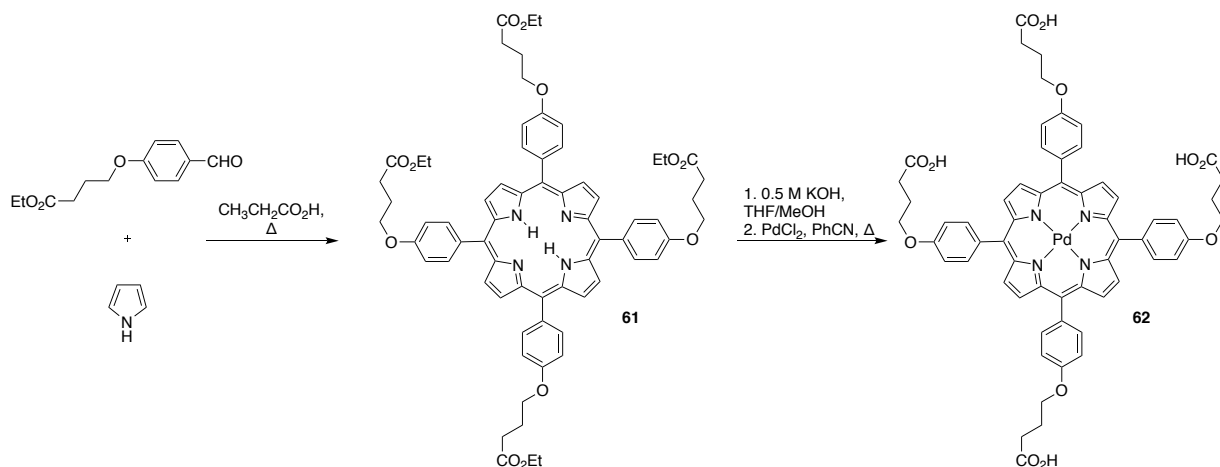
Many naturally occurring porphyrins contain acetic acid or propionic acid side chains.⁸⁸ With increasing number of acid side chains, their solubility in aqueous solution increases, with the uroporphyrins being freely soluble, particularly in solutions of basic pH (Scheme 1-21).⁸⁸



Scheme 1-21. Increasing water-solubility of the naturally occurring porphyrins with increasing number of carboxylic acid functionalities.

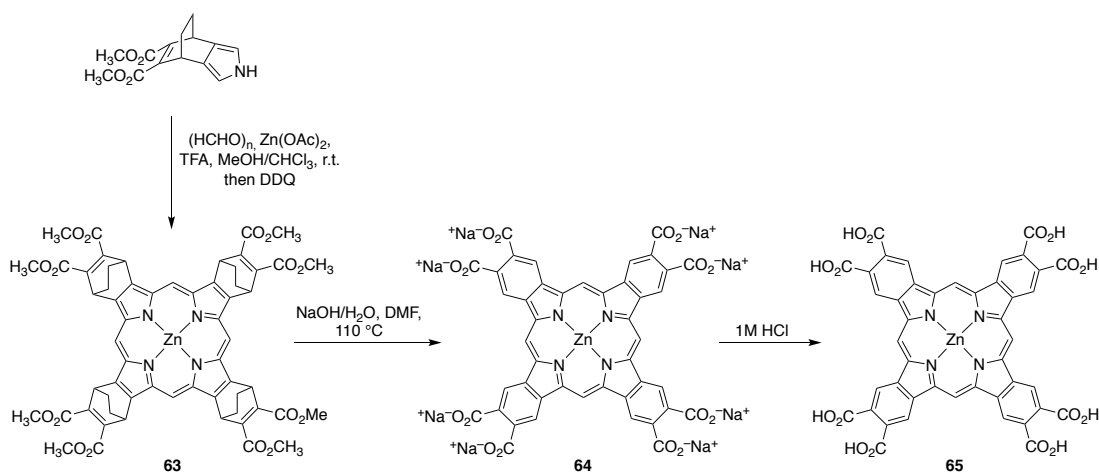
This suggests that the introduction of carboxylic acid functional groups to the periphery of porphyrins might be an effective way of furnishing water-soluble derivatives. This is, in fact, also observed. To simplify the purification of the porphyrins, the carboxylate groups are often masked throughout the synthesis as esters and are revealed by saponification in the final step.

meso-Tetrakis(4-carboxyphenyl)porphyrin, and its tetraester, are well known, and readily synthesized by condensation of the corresponding aldehydes with pyrrole.⁸⁹ They are also commercially available.⁵² Carboxylate groups may also be introduced to the porphyrin by starting with more elaborate building blocks containing esters. Classic carboxylated *meso*-aryl porphyrins, such as *meso*-tetrakis(4-carboxyphenyl)porphyrin, have been prepared by Adler synthesis with ester-substituted benzaldehydes followed by saponification of the esters.⁴² Tetracarboxylated palladium porphyrin **62** was prepared by this approach (Scheme 1-22).⁹⁰



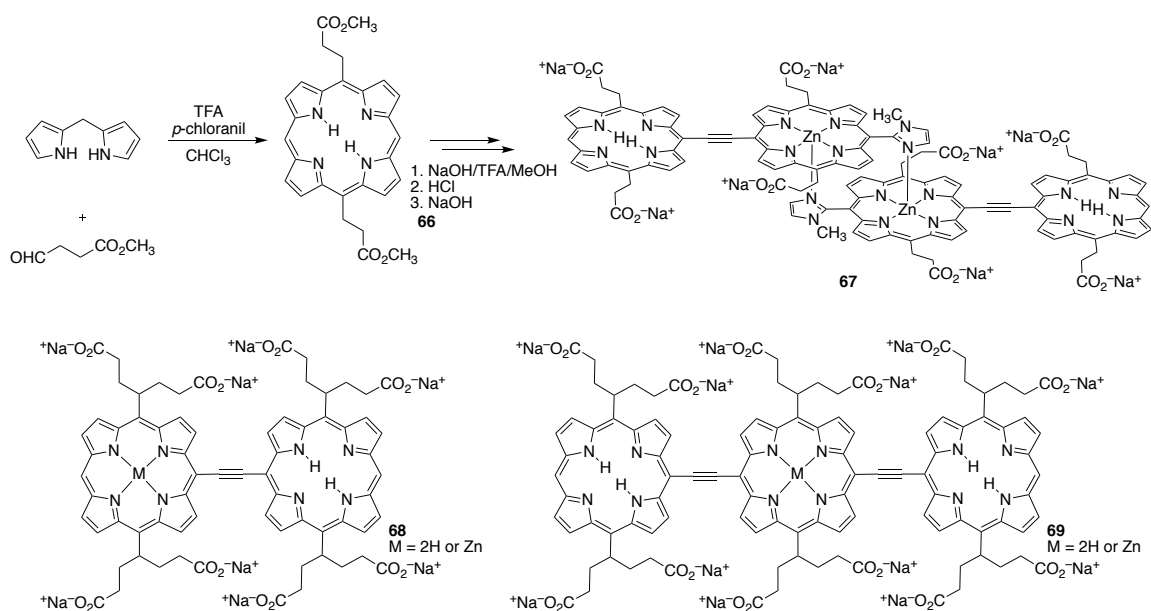
Scheme 1-22. Carboxylated *meso*-aryl porphyrins, as described by the group of Skondra.⁹⁰

An introduction of esters to the β -positions of a porphyrin from ester-substituted building blocks is also possible, as illustrated by the synthesis of carboxylated benzoporphyrins starting from an ester-functionalized isoindole (Scheme 1-23).⁹¹ A retro-Diels-Alder reaction of **63** with concomitant saponification of the methyl esters afforded octacarboxylate **64**. Protonation provided the octaacid **65** that also precipitated under these conditions. The water-solubility of the sodium salt **64** was determined to be 0.111 M.⁹¹



Scheme 1-23. Carboxylated benzoporphyrins, as described by the group of Sugimoto.⁹¹

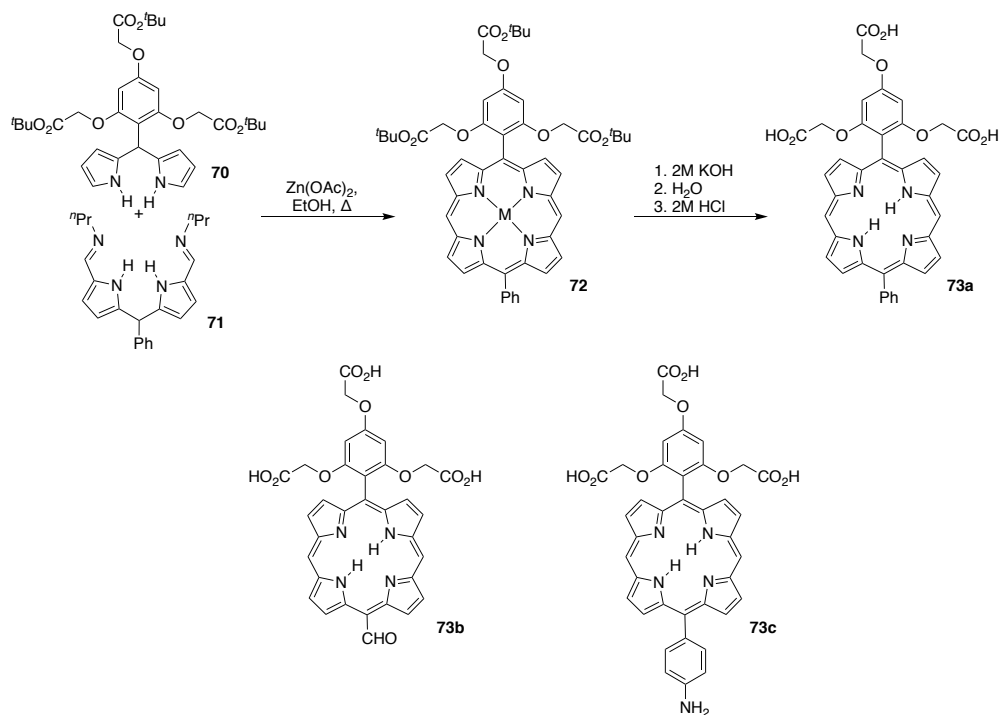
Water-soluble acetylene-linked bis(imidazolylporphyrins) were prepared from starting materials bearing protected acid functionalities. Thus, ester-functionalized aldehyde and dipyrromethane were condensed and oxidized to synthesize porphyrin **66** bearing ester-terminated alkyl chains in the *meso*-positions. The ester moieties were carried through the entire synthesis of the porphyrin dimer, and the carboxylates were only deprotected in the last step (Scheme 1-24).⁹² Using this strategy, bulky bis(carboxylethyl)methyl substituents could also be introduced to the *meso*-positions early in the synthesis to furnish dimers of type **68** and trimers of type **69**, which showed less aggregation in water.⁹³



Scheme 1-24. Porphyrin dimers and trimers bearing carboxylate groups in the *meso*-positions, as described by the group of Kobuke.⁹²⁻⁹³

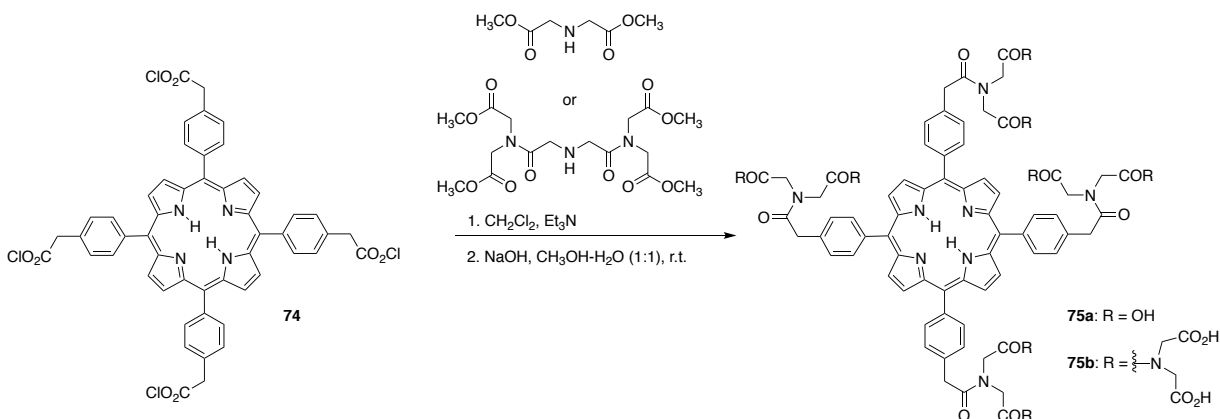
Lindsey and co-workers prepared carboxylated *trans*-AB porphyrins using a 2+2 dipyrromethane condensation strategy, using dipyrromethane **70** carrying a protected 2,4,6-triester-substituted *meso*-phenyl group (Scheme 1-25).⁹⁴ The condensation of **70** and counterpart **71** in the presence of zinc afforded the zinc-porphyrin triester **72**, which could be saponified and protonated to afford the tricarboxylic acid **73a**. Along an analogous route, *trans*-

AB porphyrins **73b** and **73c** bearing bioconjugatable groups at the *meso*-position opposite the solubilizing groups were prepared.



Scheme 1-25. Carboxylated *trans*-AB porphyrins, as described by the group of Lindsey.⁹⁴

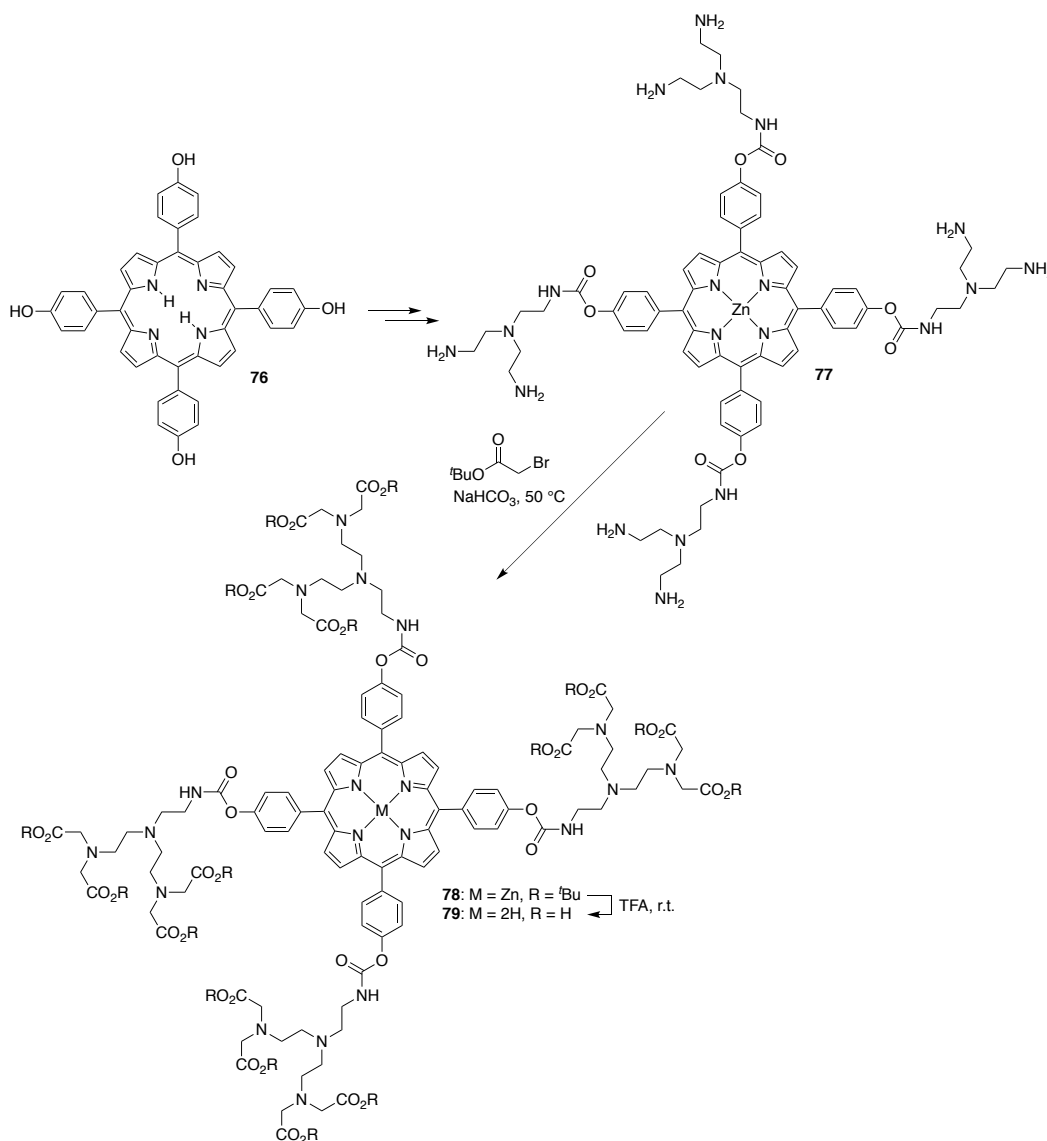
To maximize the number of carboxylic acid groups introduced, carboxylic acid ester-terminated dendritic components can be utilized, often bound to the porphyrin through amide linkages. For instance, treatment of tetraphenylporphyrin acid chloride **74** with dimethyl iminodiacetate or its second generation dendrimer analogue, followed by saponification of the esters, afforded the polyacid porphyrins **75a** or **75b**, respectively (Scheme 1-26).⁹⁵ They were purified by precipitation and filtration.



Scheme 1-26. Dendritic carboxylated porphyrins, as described by the group of Mukhtar.⁹⁵

meso-Tetrakis(4-hydroxyphenyl)porphyrin (**76**) is a versatile starting material for the synthesis of hydrophilic derivatives since the *p*-phenolic oxygens can react with a variety of solubilizing groups. A₄-Porphyrin **76** is synthesized through the Adler procedure, generally as its 4-methoxy derivative, that can be purified and handled easily. It is subsequently deprotected using BBr_3 ^{31e} (see also below, Scheme 1-28 and Scheme 1-52).

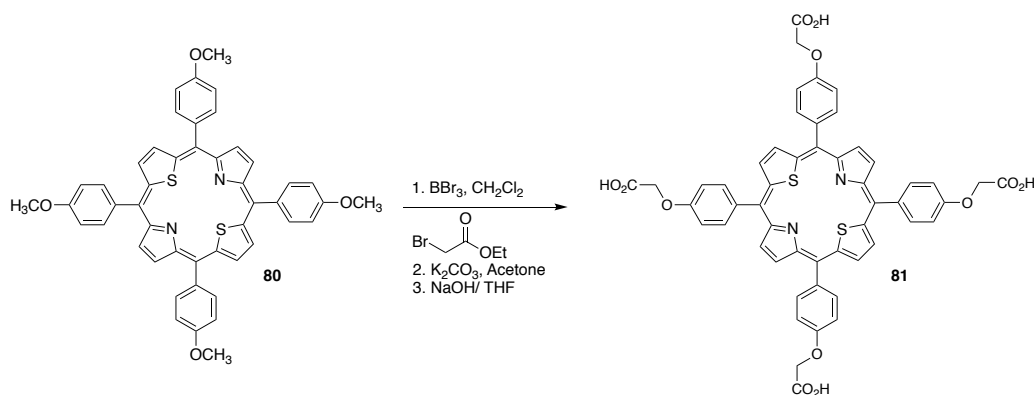
Using tetraphenol **76**, Chen and co-workers also synthesized porphyrins bearing dendritic carboxylate groups, albeit their synthesis was less convergent than that of Mukhtar and co-workers,⁹⁶ since the dendrimer generations were built up on the porphyrin core. Thus, **76** was converted to polyamine-derivatized porphyrin **77** in three steps. Reaction of the amines in **77** with bromoacetic acid ethyl ester provided the protected porphyrin **78**; hydrolysis with TFA gave the free acid **79** (Scheme 1-27)⁹⁶ that was isolated by precipitation (addition of a MeOH solution of **79** to Et_2O).



Scheme 1-27. Dendritic polycarboxylated porphyrins, as described by the group of Chen.⁹⁶

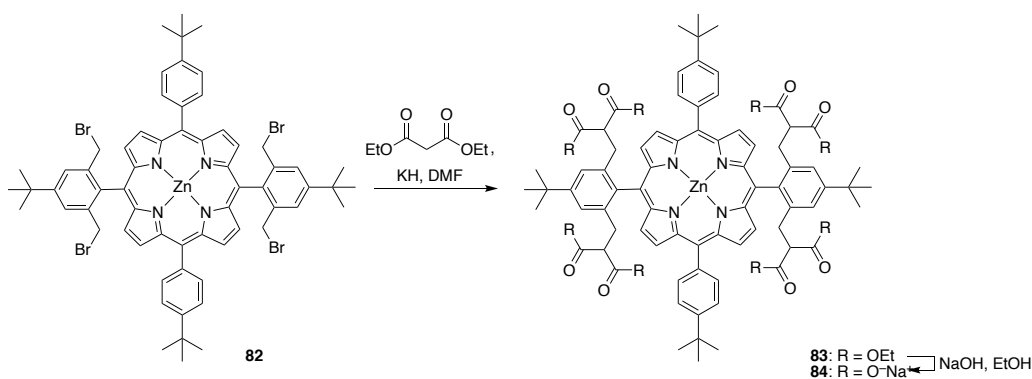
Alkylation strategies have also been employed for the introduction of carboxylates. For instance, various carboxylated core-modified porphyrins were prepared by O-alkylation of the phenolic oxygens of a *meso*-4-hydroxyphenyl-substituted core-modified dithiaporphyrin. Like their aza-analogues, the requisite core-modified porphyrins were synthesized with a methyl-ether protecting group in the *p*-position of one or more phenyl groups and deprotected using the standard BBr₃ method. The phenolic oxygens were then alkylated with ethylbromoacetate.

Saponification of the installed esters furnished the dithiaporphyrin **81** bearing carboxylic acid functional groups (Scheme 1-28).⁹⁷



Scheme 1-28. Core-modified carboxylated porphyrin, as described by the group of Detty.⁹⁷

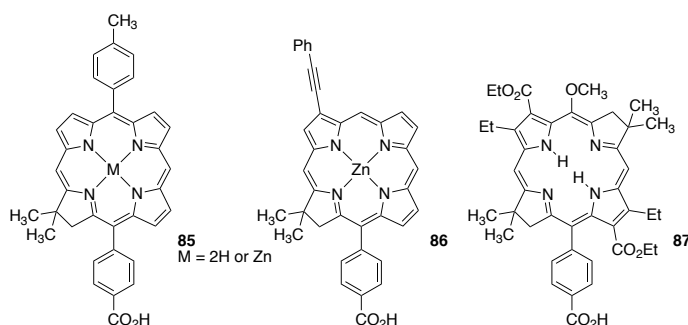
Prato and co-workers also used an alkylation strategy to synthesize octacarboxylated porphyrin **84**, starting from a tetrabromomethyl-substituted porphyrin. Alkylation of porphyrin **82** with diethyl malonate afforded the tetramalonic ester-derivatized porphyrin **83**, which was saponified to free the eight carboxylate moieties (Scheme 1-29).⁸⁴ Octacarboxylate **84** precipitated under the saponification conditions and was isolated by filtration to afford the pure product.



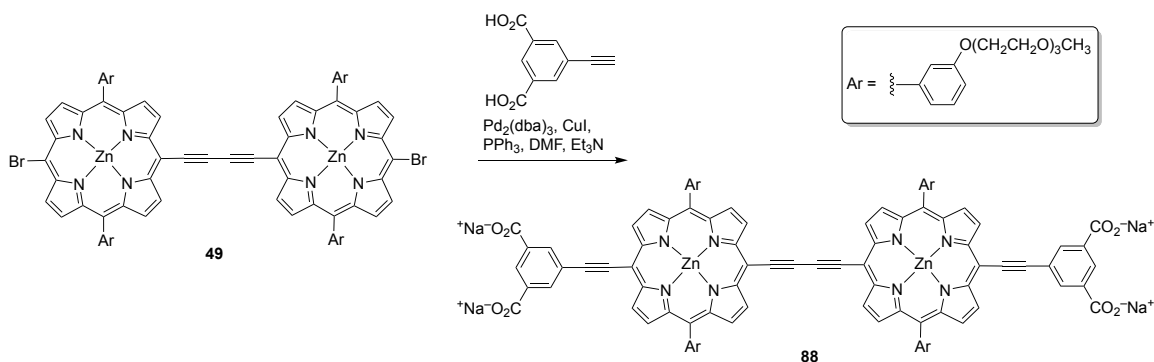
Scheme 1-29. Octacarboxylated porphyrin **84**, as described by the group of Prato.⁸⁴

Carboxyphenyl substituents can also be directly introduced to the *meso*-positions of synthetic chlorins and bacteriochlorins by Suzuki coupling of suitable *meso*-bromo-substituted

porphyrins with boronic esters derived from benzoic acid. Using the same Suzuki coupling approach that was used to introduce pyridyl substituents to the *meso*-position (cf. Scheme 1-17), chlorins **85**, **86** and the bacteriochlorin **87** were prepared.⁸¹ The carboxylate functionality was introduced in the free acid form, eliminating the need for the utilization of protecting groups.



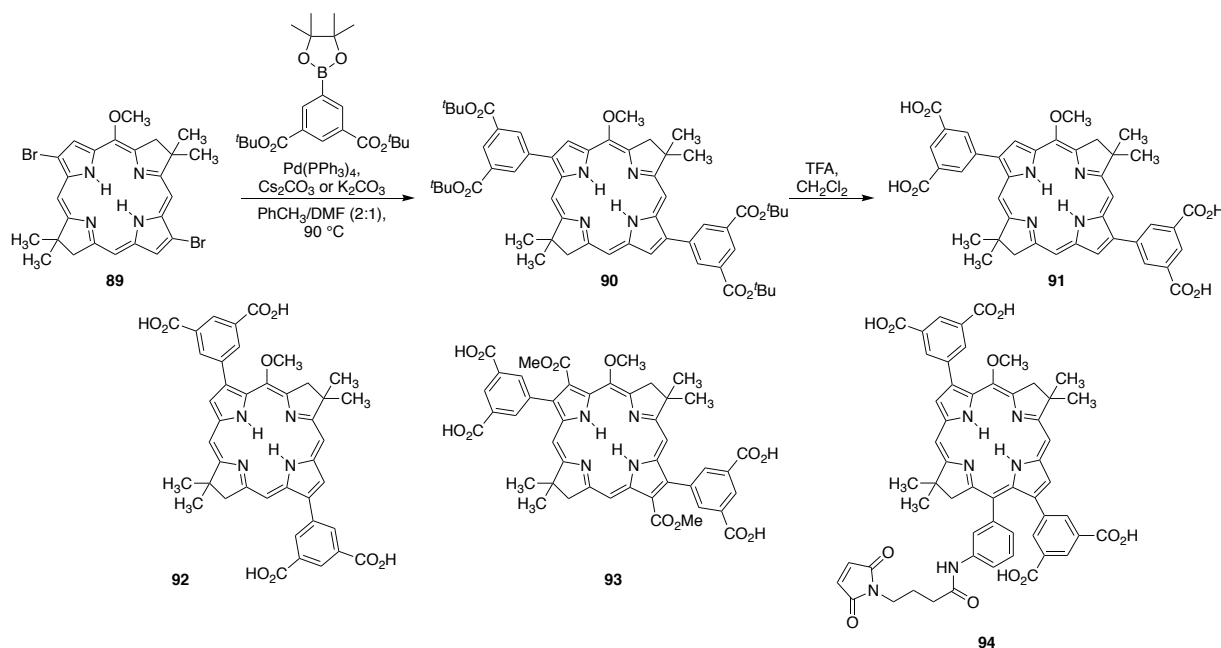
Starting from *meso*-brominated precursors, the group of Anderson used a Sonogashira coupling strategy to functionalize the *meso*-positions of a PEGylated porphyrin dimer with carboxylate groups. *meso*-Dibromoporphyrin dimer **49** was coupled with 5-ethynyl-1,3-benzenedicarboxylic acid to form the tetracarboxylated water-soluble porphyrin dimer **88** (Scheme 1-30).⁶³ Again, it is noteworthy that the acid functionality was introduced in unprotected form.



Scheme 1-30. Carboxylated bis-acetylene linked porphyrin dimers, as described by the group of Anderson.⁶³ dba = dibenzylacetone.

Functionalization of the β -position of bacteriochlorins with carboxyphenyl groups was also achieved by Suzuki coupling, albeit this method required the use of protected boronic ester

carboxylates.⁹⁸ Thus, β -dibromoporphyrin **89** was functionalized using the boronic ester of the *t*-butyl ester-protected 3,5-carboxyphenyl substituents (Scheme 1-31). The protecting groups were removed at the last step of the synthesis by acid treatment. Furthermore, the option for bioconjugation was demonstrated in these systems by Suzuki coupling of a *meso*-bromobacteriochlorin, generated by regioselective bromination of the parent bacteriochlorin, to produce hydrophilic tetracarboxylbacteriochlorin **94**.⁹⁸



Scheme 1-31. Tetracarboxybacteriochlorins, as described by the group of Lindsey.⁹⁸

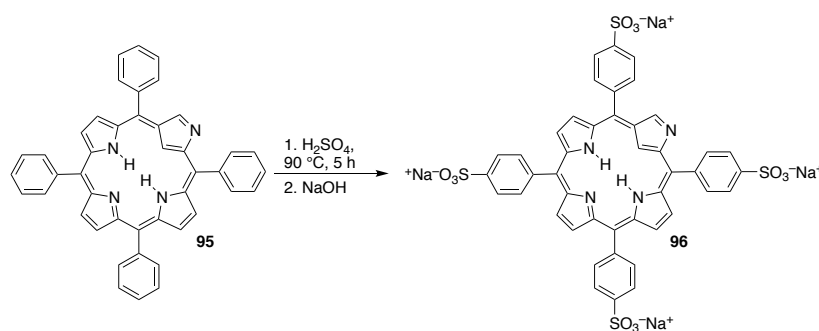
1.4.2.2 Sulfonated Porphyrins

Sulfonation of *meso*-tetraphenylporphyrin proceeds regioselectively at the *para*-positions of the *meso*-phenyl rings.⁹⁹ This reaction led to the earliest examples of water-soluble *meso*-tetra-arylporphyrins.⁴² A number of sulfonated A₄ porphyrins were prepared by direct sulfonation methods⁴² and are commercially available.⁵² However, this solubilization strategy has drawbacks, not the least of which are the harsh reaction conditions (conc. H₂SO₄, Δ) required for the sulfonation step and the difficulty in purifying the target compound. On the other hand,

sulfonation readily leads to the solubilization of porphyrins in aqueous media. Interestingly, the porphyrin is protonated during the sulfonation step and is thus protected by the dicationic charge from getting sulfonated at the β -positions.¹⁰⁰

One particular challenge faced by using sulfonation procedures is the incorporation of other functional groups since they may be incompatible with the harsh sulfonation conditions. The sulfonation step is often employed directly after porphyrin formation; then, subsequent modification of the porphyrin is performed. The drawback of this strategy is the difficulty in handling and purification of the sulfonated porphyrins.

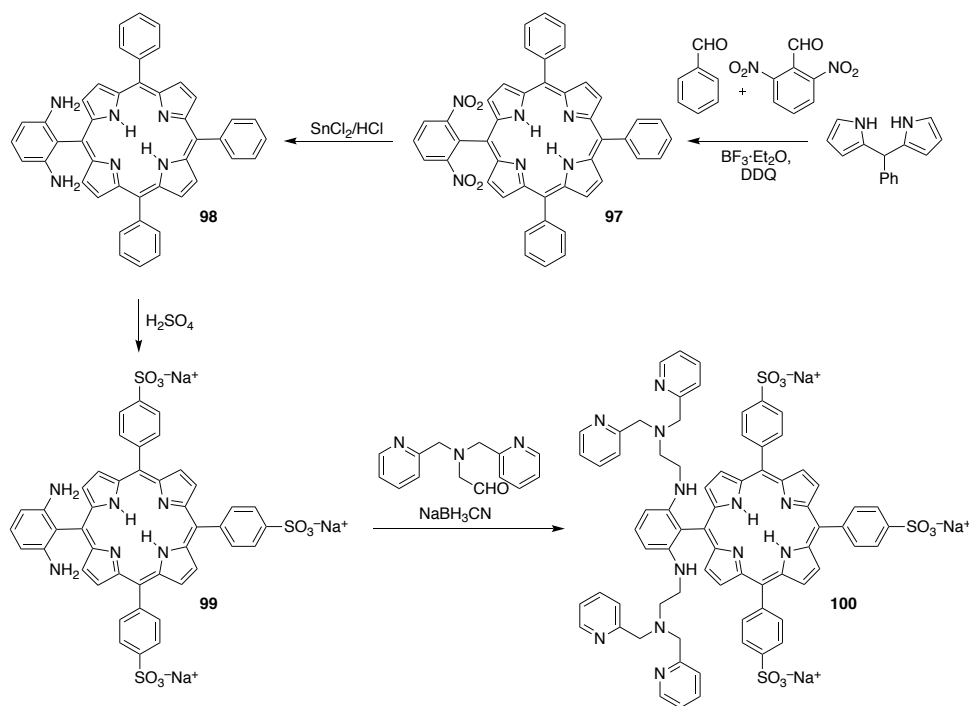
Despite these disadvantages, the traditional direct sulfonation method was employed by Pillai and co-workers to regioselectively introduce sulfonate groups to the *meso-p*-phenyl positions of *N*-confused porphyrins (Scheme 1-32).¹⁰¹ Sulfonation of *N*-confused porphyrin **95** by treatment with H₂SO₄ at elevated temperature over several hours afforded tetrasulfonated porphyrin **96** that was tested as a photosensitizer for PDT.¹⁰¹ The product was purified by precipitation and continuous Soxhlet extraction with MeOH. No further functionalizations of this porphyrin derivative were reported.



Scheme 1-32. Sulfonated *N*-confused porphyrin, as described by the group of Pillai.¹⁰¹

Likewise, asymmetric *meso*-aryl porphyrins were also subjected to sulfonation reactions. For instance, A₃B porphyrin *meso*-trisphenyl-4-pyridylporphyrin, made by mixed aldehyde

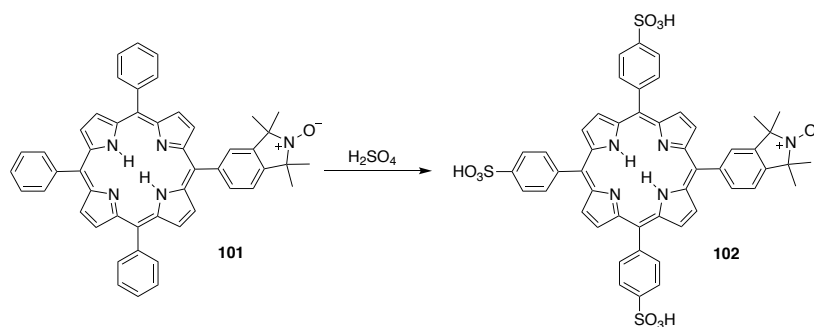
condensation, could be trisulfonated using oleum at 80 °C.¹⁰² The pure product was obtained by precipitation and centrifugation after neutralization of the acid. The pyridyl moiety could then be functionalized with a platinum complex for study as a tumor targeting photosensitizer. The Lippard group prepared the A₃B porphyrin *meso*-trisphenyl-(2,6-nitrophenyl)porphyrin **97** (Scheme 1-33). Reduction of the nitro group afforded 2,6-diaminophenyl porphyrin **98** that was subjected to sulfonation. The water-soluble product **99** was purified and isolated by reverse phase chromatography (RP-18). The purified free amine could then be functionalized with DPA for its use as a Zn²⁺ chemosensor.¹⁰³ Furthermore, the manganese complex of **100** was prepared and used as a dual function contrast agent for the fluorescence imaging of Zn²⁺ and MRI in biological contexts.¹⁰³



Scheme 1-33. Sulfonated A₃B porphyrin bearing DPA substituents for fluorescence sensing of Zn²⁺, as described by the group of Lippard.¹⁰³

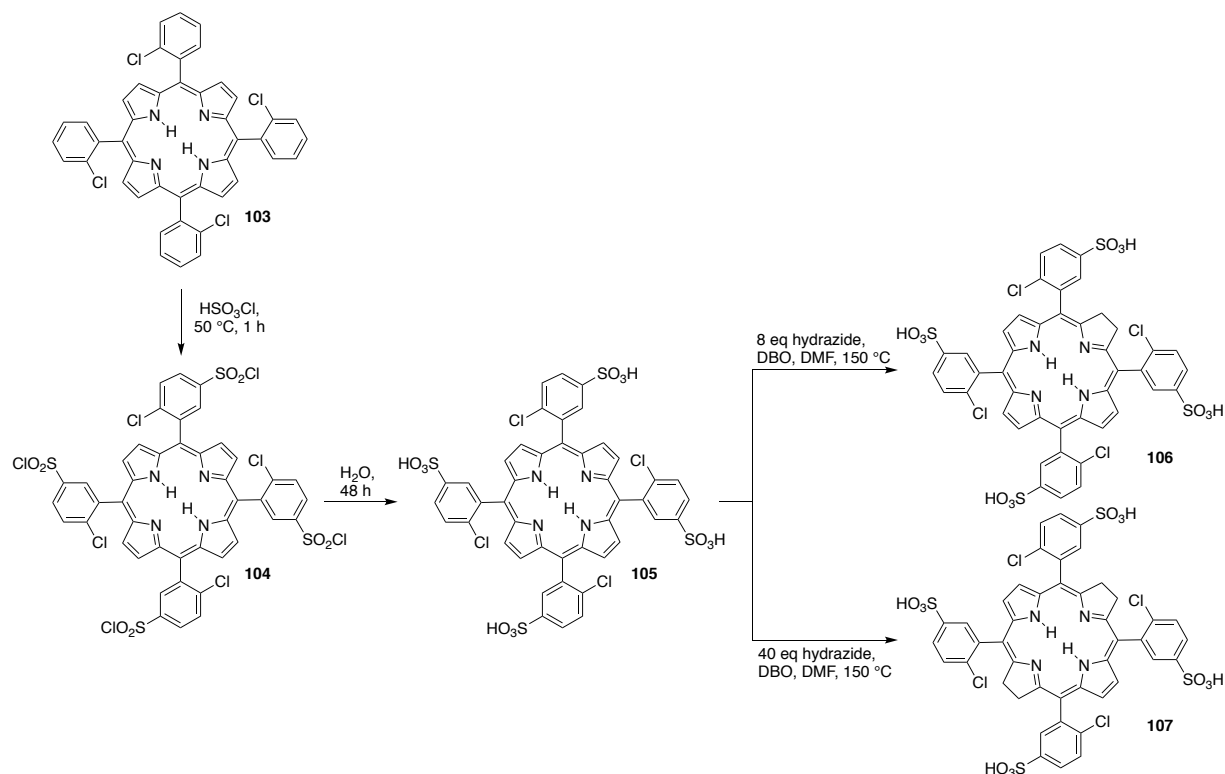
As the previous examples have shown, some functionalities tolerate the sulfonation conditions. Surprisingly, this is also the case for isoindoline nitroxide-functionalized A₃B

porphyrin **101**. The three phenyl substituents could be sulfonated by treatment with H_2SO_4 with retention of the isoindoline nitroxide (Scheme 1-34); albeit the yield for the water-soluble final product **102** was low ($\sim 30\%$).¹⁰⁴



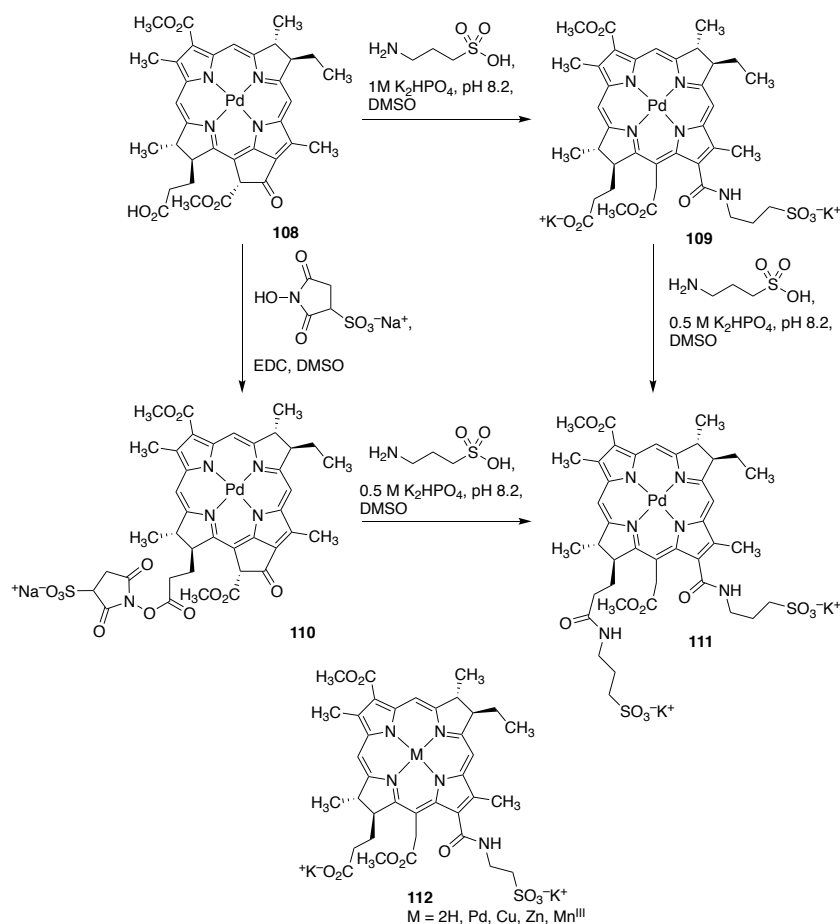
Scheme 1-34. Sulfonated isoindoline nitroxide-functionalized A₃B porphyrin, as described by the group of Yang.¹⁰⁴

A chlorosulfonation method has been used for the introduction of sulfonic acid groups to a number of halogenated *meso*-aryl porphyrins by the group of Wyatt and co-workers (Scheme 1-35).¹⁰⁵ Treatment of chlorinated porphyrin **103**, for example, with chlorosulfonic acid afforded chlorosulfonation product **104** that was hydrolyzed by suspension in H_2O to provide the corresponding sulfonic acid product **105**. Alternatively, the chlorosulfonate could be converted to sulfonamide derivatives by reaction with amines.¹⁰⁵ The corresponding chlorin and bacteriochlorin **106** and **107**, respectively, were made by diimide reduction of sulfonated porphyrin **105**, and were tested as photosensitizers for the PDT of tumors (Scheme 1-35).¹⁰⁶



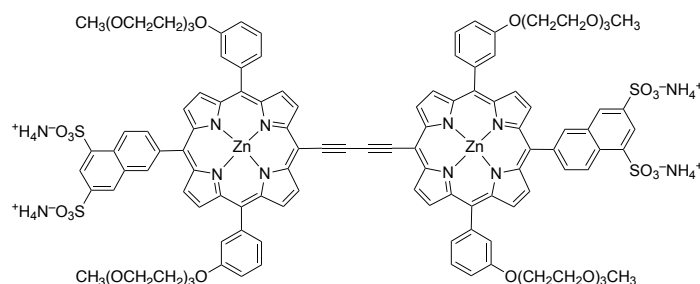
Scheme 1-35. Chlorosulfonated porphyrins and their hydrolysis and reduction products, as described by the group of Wyatt.¹⁰⁵ DBO = 1,4-diazobicyclo[2.2.2]octane.

The attachment of sulfonated groups to the β -positions of a tetrapyrrolic macrocycle is an alternative method toward the generation of hydrophilic sulfonated derivatives. This approach was applied to the generation of alkylsulfonated bacteriochlorins.¹⁰⁷ For example, sulfonated bacteriochlorophyll derivatives were prepared by reaction of Pd-bacteriopheophorbide (**108**) with homotaurine (Scheme 1-36).¹⁰⁷ Treatment of either **109** or the sulfo-NHS ester **110** with a second equivalent of homotaurine also yielded the bis-sulfonated product **111** (with the trisulfonated compound arising from imine formation with the β -acetyl group as a minor product). Bacteriochlorin **112M** could also be prepared using a similar procedure using taurine as the nucleophile. All the sulfonated derivatives were found to possess high solubility in water (up to 40 mg/mL).¹⁰⁸ The products were either purified by HPLC (MeOH/phosphate-buffer solvent systems) or by silica gel chromatography (4:1 CHCl_3 :MeOH).



Scheme 1-36. Sulfonated Pd-bacteriopheophorbide, as described by the group of Scherz.¹⁰⁸ EDC = 1-ethyl-3-(3-dimethylaminopropyl)carbodiimide.

Sulfonate functionalities may also be introduced at a late stage in the porphyrin synthesis by transition metal-mediated cross-coupling strategies. For instance, Anderson and co-workers introduced sulfonate groups to the *meso*-positions of a *meso*-brominated PEGylated conjugated porphyrin dimer using a Suzuki coupling with a sulfonated arylboronic acid, a strategy similar to the introduction of pyridine functionalities described above (cf. Scheme 1-18).⁶³ The tetra-sulfonated porphyrin dimer **113** was purified using semi-preparative reverse-phase HPLC.

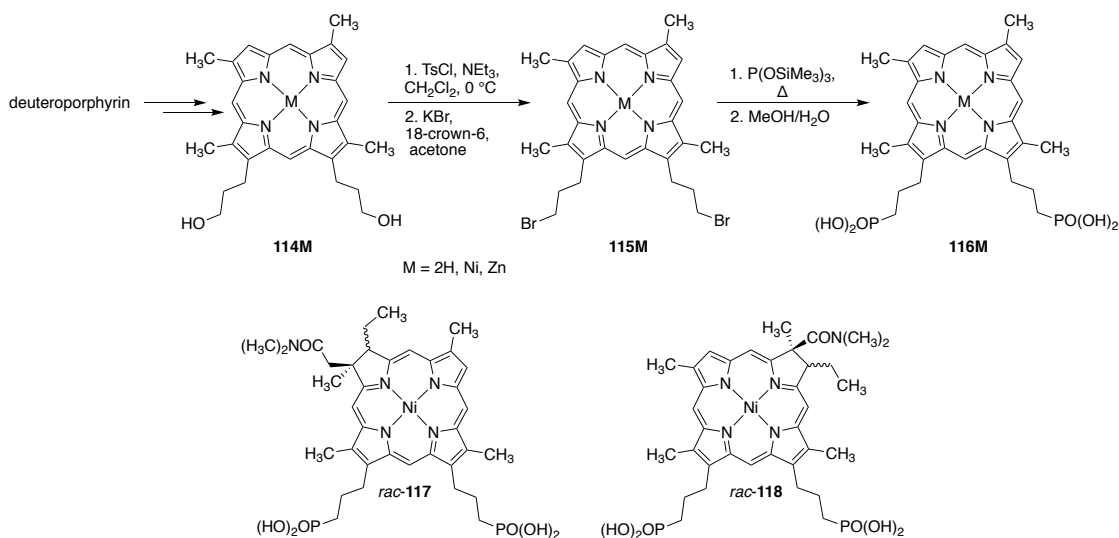


113

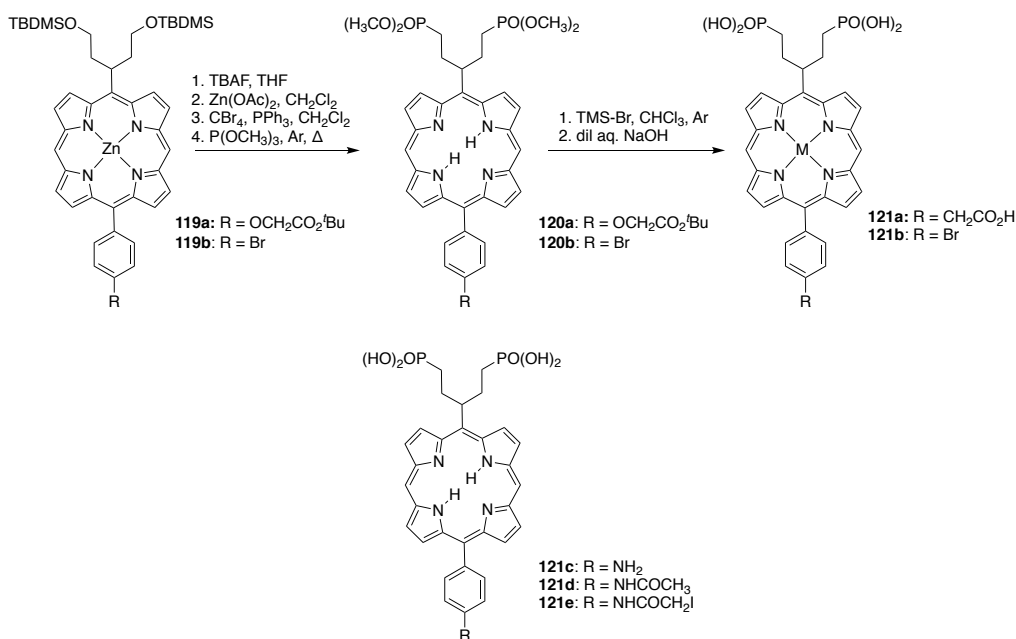
1.4.2.3 Porphyrins With Phosphate/Phosphonate Functional Groups

The introduction of alkylphosphonate functional groups to the periphery of a porphyrin is another strategy to impart hydrophilicity to porphyrins and hydroporphyrins. Phosphate groups have also been employed, but because of the increased hydrolytic lability of the phosphate group, only rarely. Alkyl phosphonates have been introduced to the porphyrin by modification of a porphyrin or by the synthesis of the porphyrin macrocycle with protected phosphonate/phosphate or alcohol building blocks. Deprotection and subsequent modification of the porphyrin furnished the water-soluble phosphonated derivatives.

One of the first examples of porphyrins bearing phosphonate groups was introduced by the Montforts group.¹⁰⁹ They prepared water-soluble metalloporphyrins by phosphonation of the primary alkyl alcohols in deuteroporphyrin derivative **114M** (Scheme 1-37).¹⁰⁹ Their strategy involved the conversion of the alcohols in **114M** to brominated derivative **115M**, followed by reaction with $\text{P}(\text{OSiMe}_3)_3$, and subsequent hydrolysis of the intermediate with $\text{MeOH}/\text{H}_2\text{O}$ to afford phosphonate **116M**. The free phosphonate functional groups were used to attach these derivatives to electrode surfaces.¹⁰⁹ Using a similar strategy, diphosphonated chlorin derivatives **rac-117** and **rac-118** were also prepared (Scheme 1-37).



Scheme 1-37. Phosphonated β -alkyl porphyrin derivatives, as described the group of Montforts.¹⁰⁹

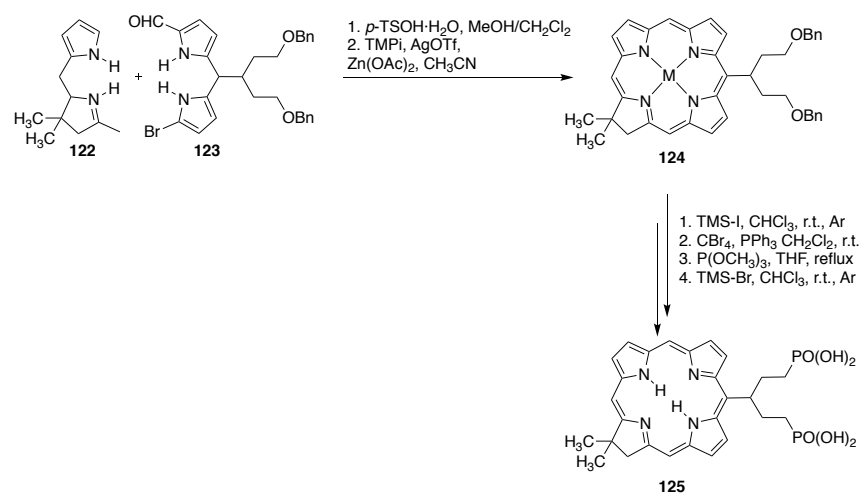


Scheme 1-38. *trans*-AB Porphyrins bearing swallowtail phosphonate motifs, as described by the group of Lindsey.¹¹⁰

While the requisite alkyl alcohols for phosphonation in **114M** were generated by functional group manipulation of the propionic acid side chains present in the natural product precursors, the requisite alcohols can also be introduced (in free or protected form) at the porphyrin synthesis stage. For instance, Lindsey and co-workers prepared *trans*-AB porphyrin **119** by

using a dipyrromethane precursor bearing two *t*-butyldimethylsilyl (TBDMS) protected hydroxyl groups (Scheme 1-38).^{110a} After removal of the protecting groups, the hydroxyl groups could be derivatized in a similar manner as described by Montforts¹⁰⁹ to provide the protected phosphonate ester **120**. Ester hydrolysis revealed the free phosphonate groups, conferring water-solubility. The corresponding zinc complexes were also prepared.

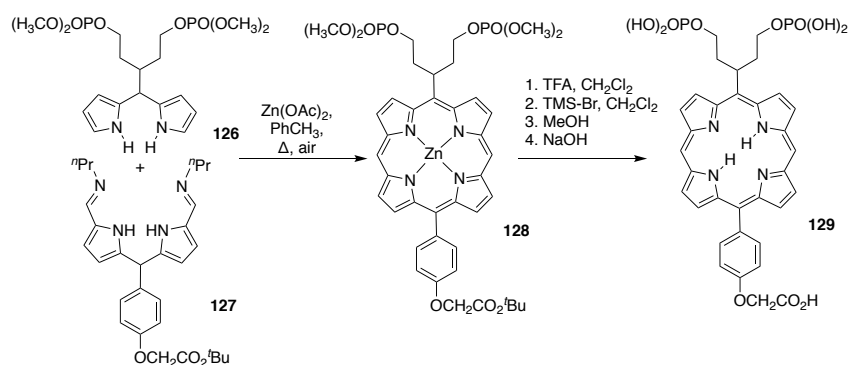
Along analogous pathways, *trans*-AB porphyrins bearing amino (**121c**), acetamido (**121d**), and iodoacetamido (**121e**) bioconjugatable tethers at the *meso*-phenyl position opposite the solubilizing group also became accessible (Scheme 1-38).^{110b} This approach is suitable for the synthesis of phosphonated chlorins, synthesized by using dipyrromethane building block **123**, bearing two protected alcohols (Scheme 1-39).^{110b} After condensation of **122** and **123**, the benzyl ether protecting groups in **124** were removed, and the alcohols were brominated and phosphonated. The phosphonate ester was then treated with TMS-Br to furnish the free phosphonates **125**.



Scheme 1-39. Synthetic chlorins bearing phosphonate swallowtail motifs, as described by the group of Lindsey.¹¹¹

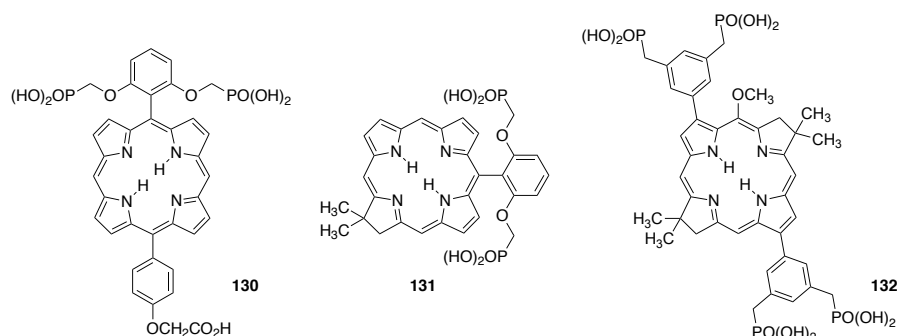
Lindsey and co-workers also prepared *trans*-AB porphyrins incorporating phosphate groups, though in this instance they started with a dipyrromethane precursor already bearing phosphate

esters (Scheme 1-40).^{110a} In the last steps, the protected phosphate groups were subjected to hydrolysis to afford the free phosphate groups.



Scheme 1-40. *trans*-AB porphyrins bearing phosphate swallowtail motifs, as described by the group of Lindsey.^{110a}

Phosphonate groups can also be introduced to the porphyrin by starting with dipyrromethane precursors bearing protected phosphonate functional groups. Using this strategy, *trans*-AB porphyrin **130** was synthesized by condensation using a dipyrromethane precursor carrying a 2,6-diphosphonated aryl ring that projects the solubilizing groups above and below the plane of the macrocycle target (cf. Scheme 1-40).¹¹² Hydrolysis of the phosphonate esters and saponification affords the *trans*-AB porphyrin bearing both the phosphonate solubilization groups and a carboxylic acid bioconjugatable tether. Using a similar strategy as for chlorin **125**, this 2,6-aryl-phosphonate motif was also incorporated into chlorin **131**.¹¹¹ Again, the Suzuki coupling strategy of β -dibromobacteriochlorins proved versatile enough to be applicable to the introduction of β -aryl-phosphonate groups (cf. Scheme 1-11). Lindsey and co-workers coupled two aryl-diposphonate esters by a Suzuki coupling strategy to afford, after hydrolysis of the phosphonate esters, water-soluble bacteriochlorin **132**.



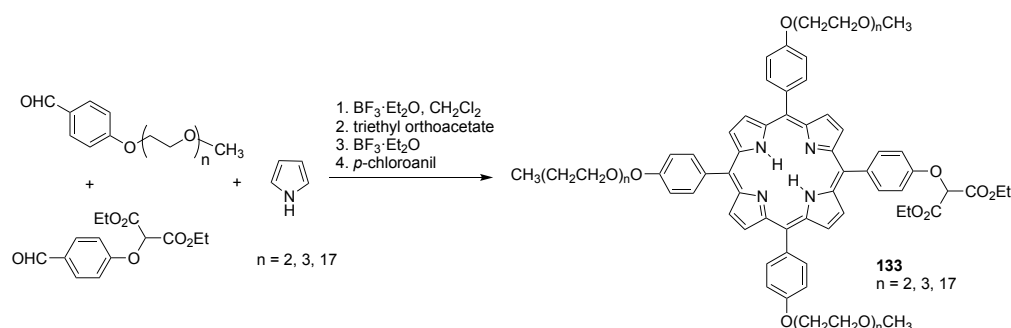
1.4.3 Water-Soluble Porphyrins with Neutral Groups

1.4.3.1 PEGylated porphyrins

PEGylation has emerged as a strategy for the preparation of neutral water-soluble porphyrins and hydroporphyrins. It has many benefits over traditional means using ionic groups. For instance, PEGylation strategies are more flexible with respect to where in the synthetic sequence they are introduced. This is because the PEG functional group is not very reactive once installed. Unwanted reactivity to form oligomeric species is also suppressed by using heterobifunctional PEG chains, in which one end of the PEG chain often has a methyl cap. PEGylated porphyrins are also much more amenable to traditional aqueous work-up conditions, as they may partition favorably in organic solvents such as CH_2Cl_2 and EtOAc.¹¹³ Often times PEGylated porphyrins can be purified by normal silica-gel chromatography.^{31e,114}

Porphyrinoid Macrocycle Total Synthesis Using PEGylated Building Blocks

Despite these advantages, the multistep manipulation of porphyrins with PEG-groups present throughout the synthesis is relatively rare. For instance, Brunner and co-workers presented such an example. They synthesized the A_3B porphyrin **133** by mixed condensation of two arylaldehydes and pyrrole, with one of the aryl aldehydes carrying a PEG chain ($n = 2, 3$ or 17) (Scheme 1-41).¹¹⁵ The resulting A_3B PEGylated porphyrins **133a-133c** were purified using ordinary silica gel chromatography ($\text{CH}_2\text{Cl}_2/\text{MeOH}$ mixtures).



Scheme 1-41. A₃B porphyrin carrying three short PEG chains, as described by the group of Brunner.¹¹⁵

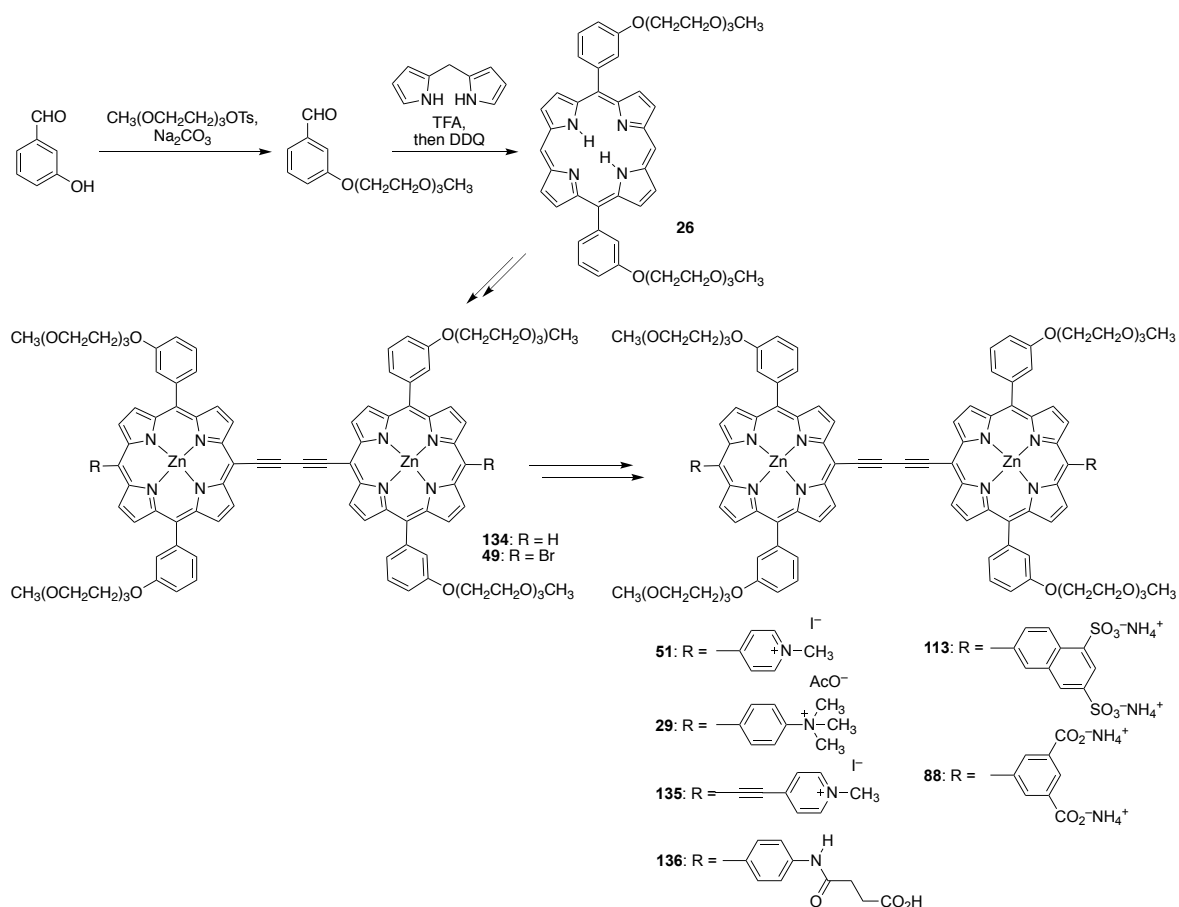
Another example for the early introduction of PEGylated building blocks was reported by the Anderson group.⁶³ Using a PEGylated benzaldehyde, porphyrin **26** bearing two methyl-capped tetraethylene glycol (TEG) groups on opposite *meso*-phenylgroups was prepared. Leaving the PEG chains intact, it was converted to the bis-acetylene linked porphyrin dimer **134**. Porphyrin dimer **134** was found not to be sufficiently soluble in aqueous media for biological application. Therefore, these materials were further derivatized with additional solubilizing groups, all while the PEG functional groups remained intact (Scheme 1-42).⁶³

Starting from *meso*-dibromo dimer **49**, cationic (pyridinium; cf. Scheme 1-18), anionic (sulfonate) and carboxylate (cf. Scheme 1-30) groups were introduced using either Suzuki or Sonogashira coupling strategies. The Senge-arylation method was also used to introduce ammonium and pyridyl solubilizing groups (cf. Scheme 1-12). The dimers were separated by either recrystallization (DMF, Et_2O) or by semi-preparative reverse phase HPLC. Due to insufficient solubility of the compounds in regular reverse-phase HPLC solvents (such as CH_3CN , MeOH, water), DMF, DMSO, or THF were used. Also due to solubility issues, the authors could not measure logP values for these compounds in octanol:water. However, they did compare the relative polarity of some derivatives by means of their retention times under reverse-phase HPLC conditions (Table 1-1).

Table 1-1. Comparison of the retention times of hydrophilic porphyrin dimers⁶³

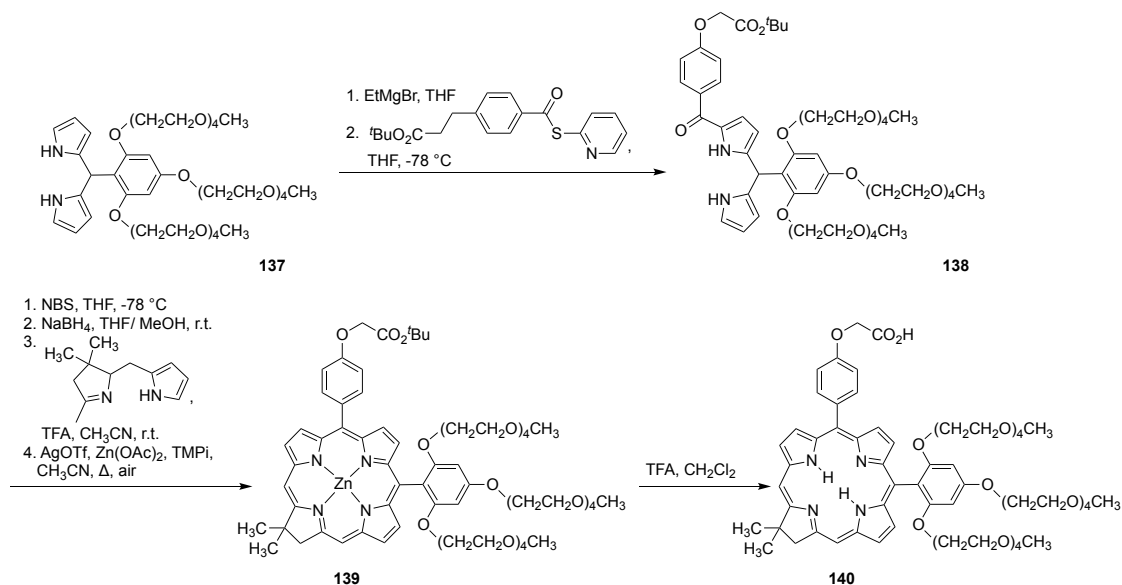
Porphyrin dimer	Retention time/min
51	6.2
29	6.8
135	7.6
136	15.6
88	18.0

HPLC Conditions: C₈ column (5 μ m, 3.9 \times 150 mm) , 1 mL/ min flow rate, solvent A: 1% aqueous acetic acid, solvent B: THF, linear gradient

**Scheme 1-42.** Hydrophilic bis-acetylene linked porphyrin dimers carrying PEG chains and various other solubilizing motifs, as described by the group of Anderson.⁶³

PEG-substituted dipyrromethanes also found use in the early introduction of solubilizing groups. The Lindsey group was able to synthesize chlorins from a PEGylated dipyrromethane

precursor (Scheme 1-43).^{113b} This strategy also incorporated a bioconjugatable tether at another *meso*-position, the precursor of which was also introduced at the dipyrromethane stage.



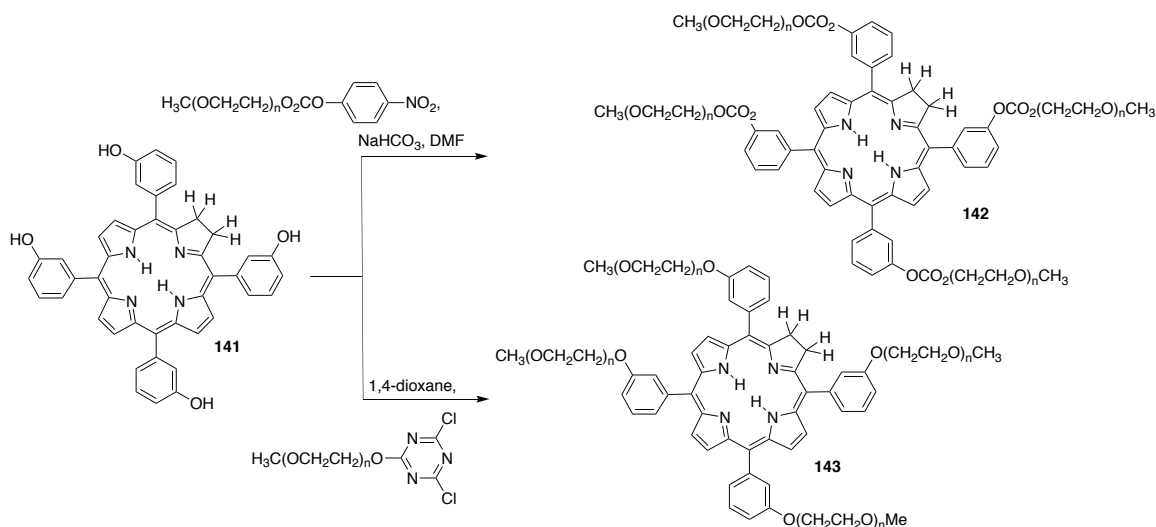
Scheme 1-43. PEGylated synthetic chlorins using PEGylated building blocks, as described by the group of Lindsey.^{113b}

PEGylation of *meso*-aryl Porphyrins

A number of *meso*-tetraphenylporphyrins bearing PEG groups have been synthesized by PEGylation of porphyrins incorporating suitable linker functionalities on the aryl groups. These porphyrins are usually prepared *via* Adler or Lindsey methods, and the PEG groups can be linked by various methods, including etherification, amidation or esterification reactions. Particularly popular linking groups for the PEGylation of porphyrins are *meso*-phenol substituents. PEGylation of various *meso*-tetrahydroxyphenyl porphyrin derivatives with a suitably functionalized PEG precursor yields water-soluble porphyrins, with activation of the PEG group often required.

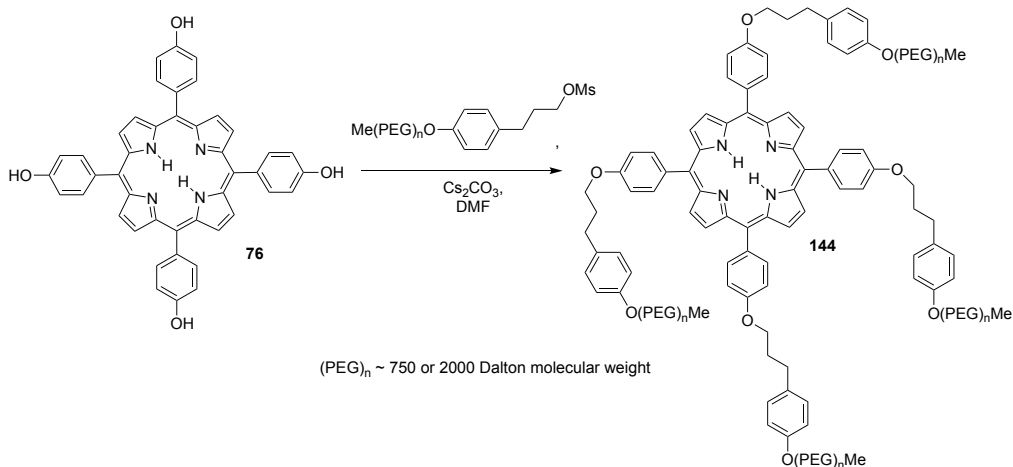
For example, *meso*-tetrakis(3-hydroxyphenyl)chlorin (**141**) was rendered water-soluble by introducing PEG groups through two different etherification strategies. Tetraphenylporphyrin **141** was treated with methoxypolyethylene glycol-*p*-nitrophenylcarbonate or cyanuric chloride-

activated methoxypolyethyleneglycol to afford the water-soluble PEGylated porphyrins **142** or **143**, respectively (Scheme 1-44. **PEGylated derivatives of *meso*-tetrakis(3-hydroxyphenyl)chlorin**, as described by the group of Sinn.¹¹⁶).¹¹⁶

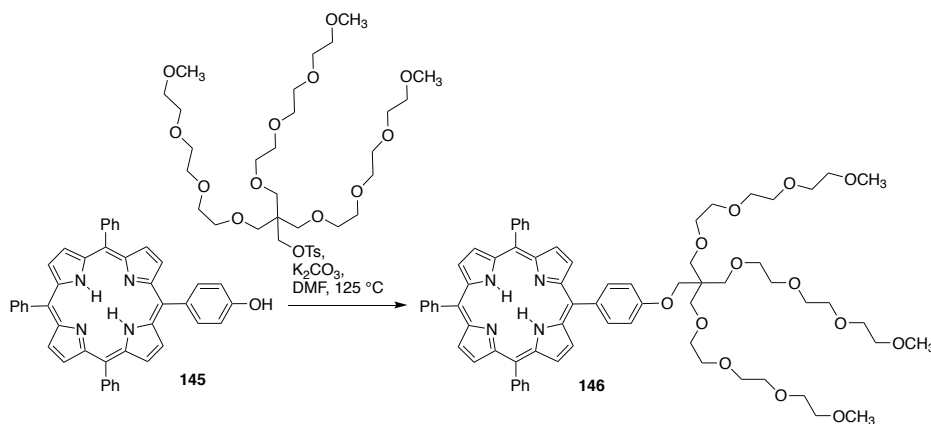


Scheme 1-44. PEGylated derivatives of *meso*-tetrakis(3-hydroxyphenyl)chlorin, as described by the group of Sinn.¹¹⁶

meso-Tetrakis(4-hydroxyphenyl)porphyrin (**76**) can also be alkylated using various activated PEGs. For instance, this procedure has been employed to alkylate **76** by treatment with PEG-mesylates to form **144**. (Scheme 1-45).^{114a} Under similar conditions, single PEG chains or PEG-dendrimers (Scheme 1-46)¹¹⁷ can also be introduced into asymmetric *meso*-hydroxyphenylporphyrins.¹¹⁸ Vitalini and co-workers prepared PEGylated derivatives of **76** by alkylation of the phenolic oxygens with a chlorinated PEG.¹¹⁹ The PEG-functionalized porphyrins could be purified by adding a solution of the compound in CH_2Cl_2 to a cold solution of Et_2O to induce precipitation (for larger PEGs);^{114a,118a} porphyrins bearing smaller PEG-chains could also be purified by column chromatography (CH_2Cl_2 -acetone-MeOH or $\text{CH}_2\text{Cl}_2/\text{EtOH}$ mixtures).^{114a,117}

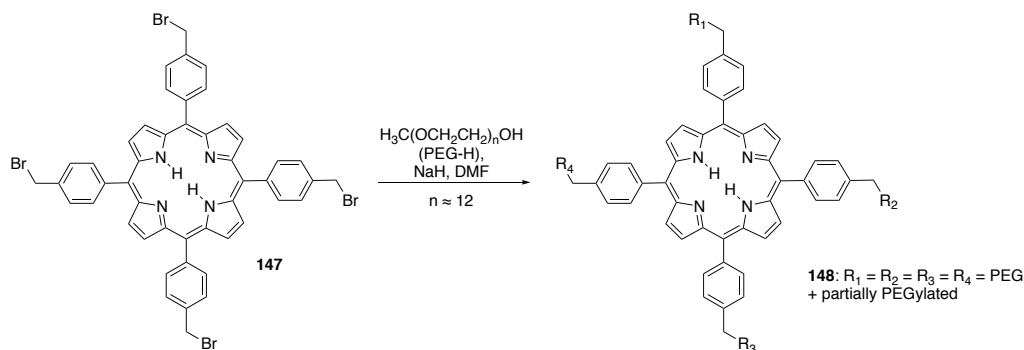


Scheme 1-45. PEGylated derivatives of *meso*-tetra(4-hydroxyphenyl)porphyrin, as described by the group of Pozzi.^{114a}



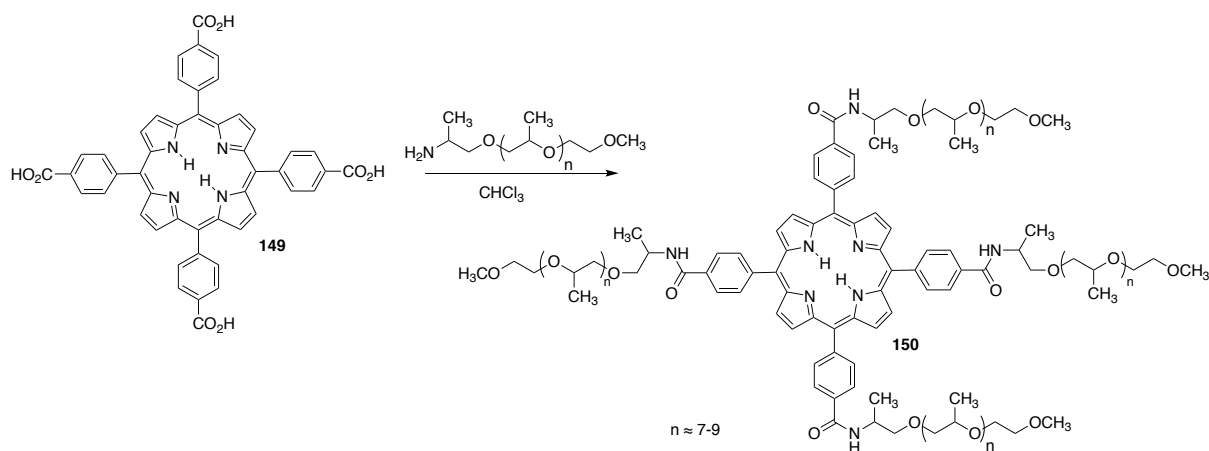
Scheme 1-46. Amiphilic porphyrin with a PEG-dendrimer, as described by the group of Dumoulin.¹¹⁷

PEGylation of *meso*-arylporphyrins was also achieved by inversion of the Williamson ether synthesis reaction partners, i.e., involving a halogenated porphyrin precursors and PEGs bearing a free alcohol. An example is the PEGylation of tetra(*p*-bromomethylphenyl)porphyrin (**147**) with a methyl-capped PEG alcohol ($M_n = 550$) that afforded the tetra-PEGylated porphyrin **148** as the main product, along with partially PEGylated porphyrins (Scheme 1-47). The porphyrin starting material was prepared by Lindsey porphyrin synthesis from 4-(bromomethyl)-benzaldehyde and pyrrole.¹²⁰ The PEGylated products were amenable to aqueous work-up (extraction with CH_2Cl_2) and were purified by HPLC.



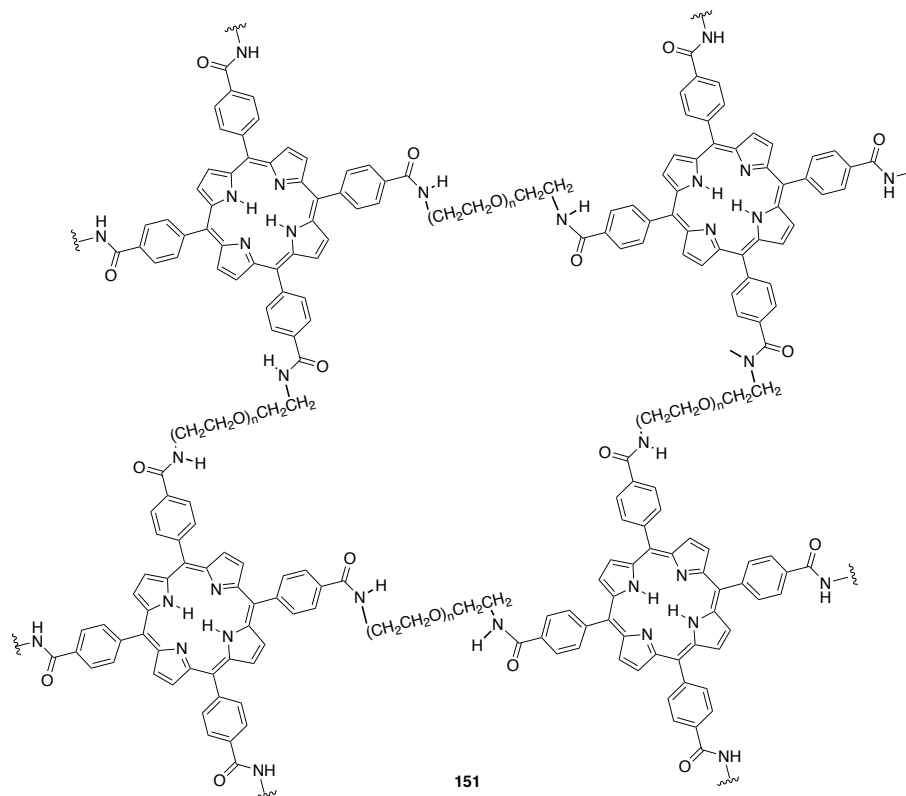
Scheme 1-47. PEGylated *meso*-aryl porphyrins by benzylation of a PEG with tetra(*p*-bromomethylphenyl)porphyrin, as described by the group of Lee.¹²⁰

meso-Aryl porphyrins bearing peripheral carboxylic acid functional groups can be PEGylated by amide formation using an amine-terminated PEG. For instance, Scolaro and co-workers prepared PEGylated derivatives of *meso*-tetrakis(4-carboxyphenyl)porphyrin (**149**) by treatment with Jeffamine M-600 ($n = 7-9$) (Scheme 1-48).¹²¹

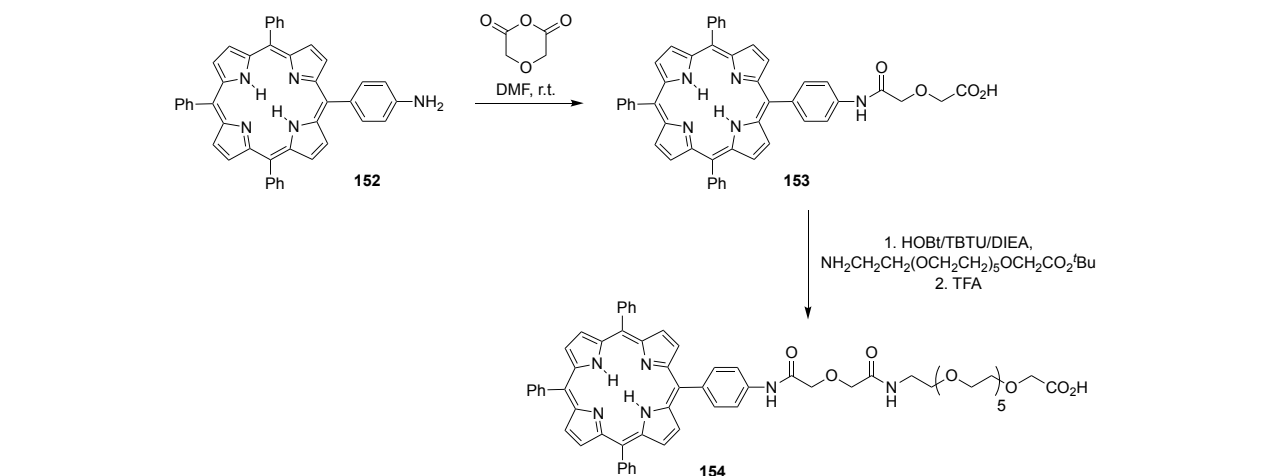


Scheme 1-48. PEGylated porphyrins derived from *meso*-tetrakis(4-carboxyphenyl)porphyrin using a PEG-amine, as described by the group of Scolaro.¹²¹

Also starting from tetraacid **149**, Lovell and co-workers reacted it with a variety of homobifunctional PEG-diamines (average Mw ranging from 150 Da to 10 kDa) to synthesize a PEG-linked porphyrin mesh **151**.¹²² This reaction illustrates the complex cross-linked structure formed when using PEGs capable of reacting at both ends. The porphyrin-PEG-mesh was purified by dialysis, followed by addition of citric acid to precipitate unreacted porphyrin.

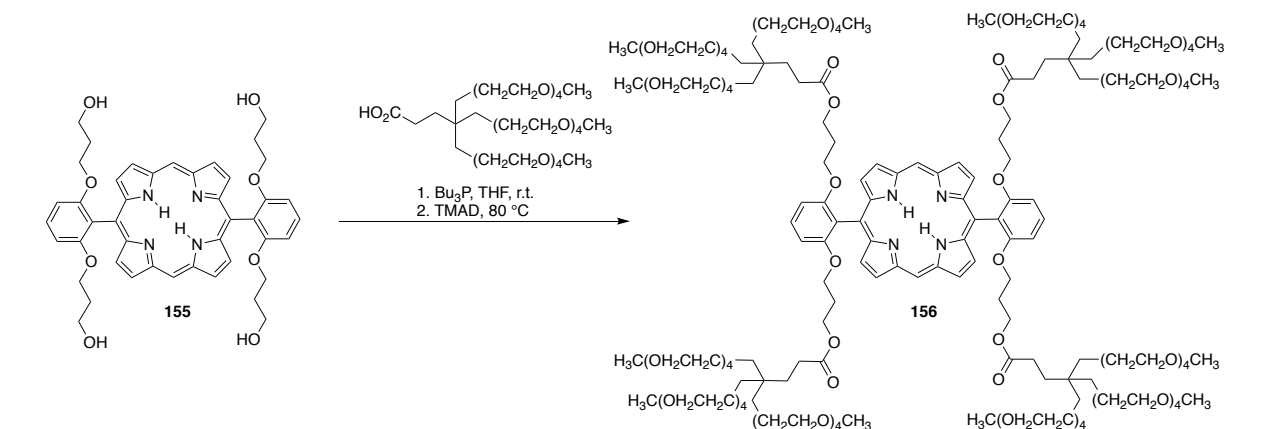


PEGylated porphyrins and hydroporphyrins with amide linkages can also be prepared starting with aminophenyl porphyrins. For instance, Peng *et al.* functionalized a chlorin with a poly(ϵ -caprolactone)-poly(ethyleneglycol) diblock copolymer.¹²³ Introduction of the PEG-polymer was achieved by treatment of *meso*-tetrakis(4-aminophenyl)chlorin with the acid-chloride of the diblock copolymer. The polymer-functionalized porphyrin was purified by precipitation with Et₂O, followed by a dialysis step in acetone. Vicente and co-workers prepared water-soluble porphyrin-peptide conjugates with a PEG linker on one *meso*-aryl group starting from an AB₃ porphyrin **152** bearing one *p*-aminophenyl group. The amine functionality in **152** was reacted with diglycolic anhydride, followed by amidecoupling using a PEG-amine and Boc-deprotection (Scheme 1-49). A peptidyl resin can be coupled to the hydroxybenzotriazole (HOBt) ester of the porphyrin **154**.¹²⁴ More hydrophilic PEGylated A₃B porphyrins bearing three carboxyphenyl groups were also prepared in a similar manner.¹²⁴



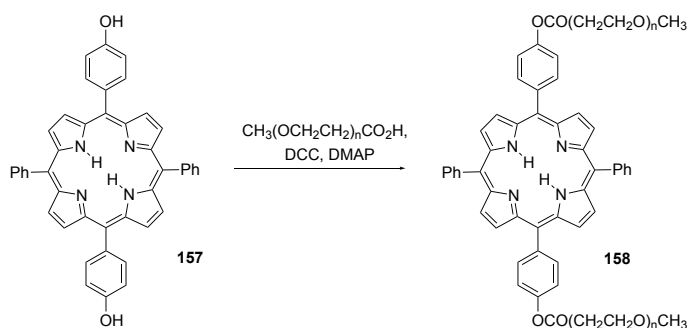
Scheme 1-49. PEGylated AB₃ porphyrin with carboxylic acid bioconjugation handle, as described by the group of Vicente.¹²⁴

Oligoethylene glycol amide-linkages have also been utilized as hydrophilic spacers in instances that require designed structures on the periphery of a hydrophilic porphyrin. Using this strategy, Alessio and co-workers have prepared ruthenium-porphyrin conjugates with oligoethylene glycol spacers.¹²⁵ This methodology has also been used to develop Rhenium (I)-porphyrin conjugates in a similar manner.¹²⁶ Lastly, PEGylation of *meso*-hydroxyphenyl-porphyrins can be achieved utilizing ester linkages. Thus, Diederich and co-workers prepared dendritic porphyrin **156** by esterification of porphyrin tetraol **155** (Scheme 1-50).¹²⁷



Scheme 1-50. Porphyrin-PEG dendrimer conjugates, as described by the group of Diederich.¹²⁷ TMAD = *N,N,N',N'*-tetramethylazodicarboxamide.

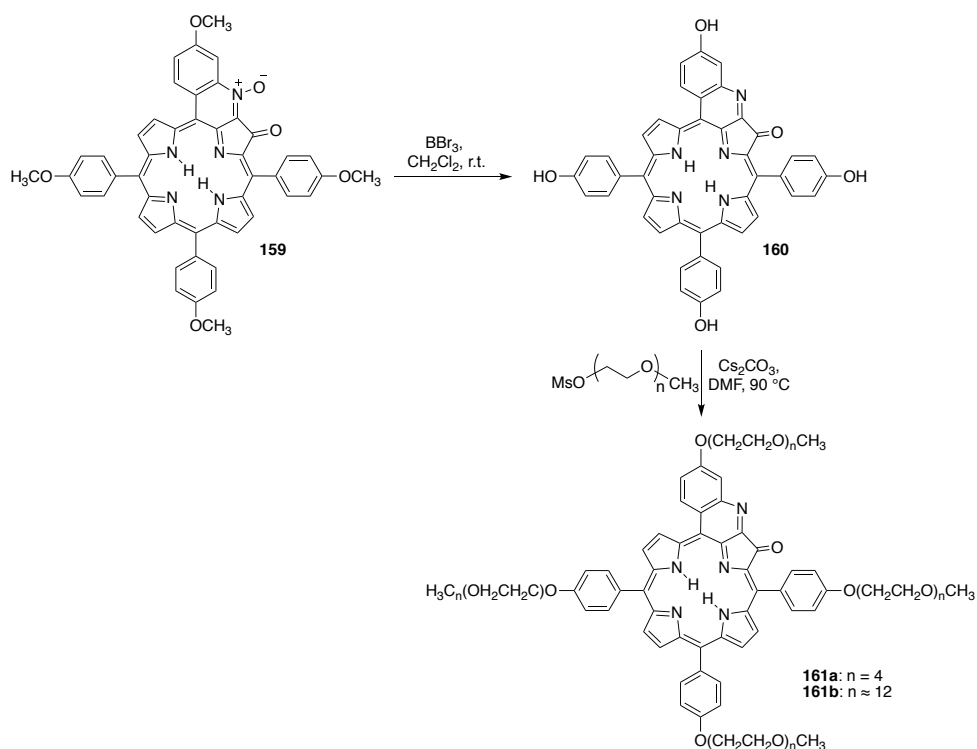
The extension of the reactive alcohol site from the phenolic position using an alkyl chain was employed to accommodate the bulky PEG-dendrimer substituents. The resulting porphyrin-dendrimers were purified by preparative gel permeation chromatography and were soluble in phosphate buffer at pH 7. Alternatively, the PEGylation of a *meso*-hydroxyphenyl A₂B₂ porphyrin by DCC/DMAP-mediated esterification with a PEG-carboxylic acid (1000 Da) was reported (Scheme 1-51).¹²⁸



Scheme 1-51. PEGylated A₂B₂ porphyrin, as described by the group of Nawaz.¹²⁸ DCC = dicyclohexylcarbodiimide, DMAP = 4-dimethylaminopyridine.

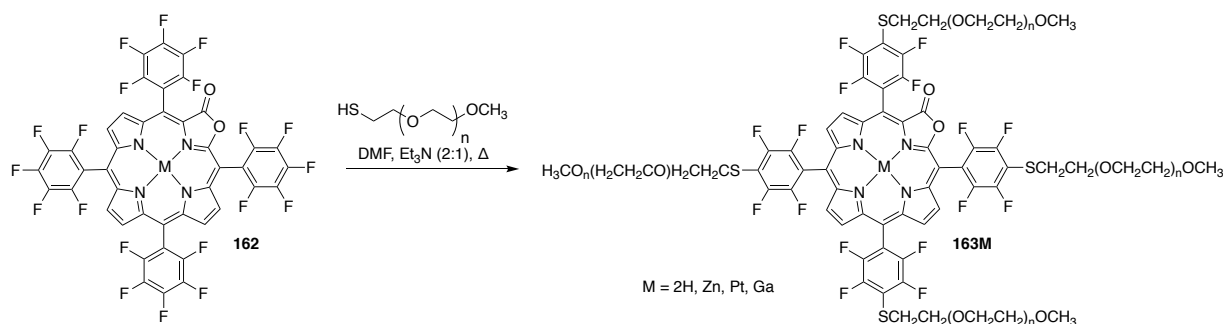
π -Extended porphyrin derivatives may also be subject to the same PEGylation strategies as seen for regular porphyrins. For instance, PEGylation of the phenolic oxygens in quinoline-annulated porphyrin **160** was reported by Luciano *et al.* (Scheme 1-52)^{31e} using a similar O-alkylation method as described for regular porphyrins (Scheme 1-45).

Precursor porphyrin **159** was prepared from *meso*-tetrakis(4-methoxyphenyl)porphyrin. A BBr₃-mediated deprotection was employed to deprotect the phenolic oxygens as the penultimate step of the synthesis. The phenol could then be PEGylated using either a short ($n = 4$) or long chain (avg. MW 550, $n \approx 12$) PEG-mesylate.^{31e} The short PEG chain derivative **161a** was found to be only slightly soluble in water. However, the derivative bearing long PEGs (**161b**) was soluble in PBS to form ~ 30 mM solutions and was used as photoacoustic imaging contrast agents for *in vivo* imaging of tumors in a mouse model.^{31e}



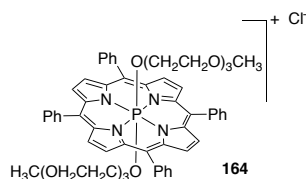
Scheme 1-52. PEGylated quinoline-annulated porphyrins, as described by the group of Brückner.^{31e}

Brückner and co-workers were able to take advantage of the well-known $\text{S}_{\text{N}}\text{Ar}$ reactivity of *meso*-pentafluorophenylporphyrins toward nucleophiles at the *p*-F positions to introduce PEG groups to pyrrole-modified porphyrins (PMPs) at a late stage of the synthetic sequence toward *meso*-arylmetalporpholactones^{114b,114c,129} (Scheme 1-53). This allowed the preparation of a variety of PEGylated porpholactone metal complexes (**163M**) that were used as optical high pH or cyanide sensors in water.^{114c} The PEGylated derivatives were purified by silica gel chromatography ($\text{CH}_2\text{Cl}_2/5\%$ MeOH). Similarly, thiol-functionalized sugars were introduced into *meso*-pentafluorophenylporphyrins using the $\text{S}_{\text{N}}\text{Ar}$ reaction, also resulting in their solubilization in aqueous solutions.¹³⁰



Scheme 1-53. PEGylated porpholactone derived from *meso*-tetrakis(pentafluorophenyl)porphyrin derivatives, as described by the group of Brückner.^{114c}

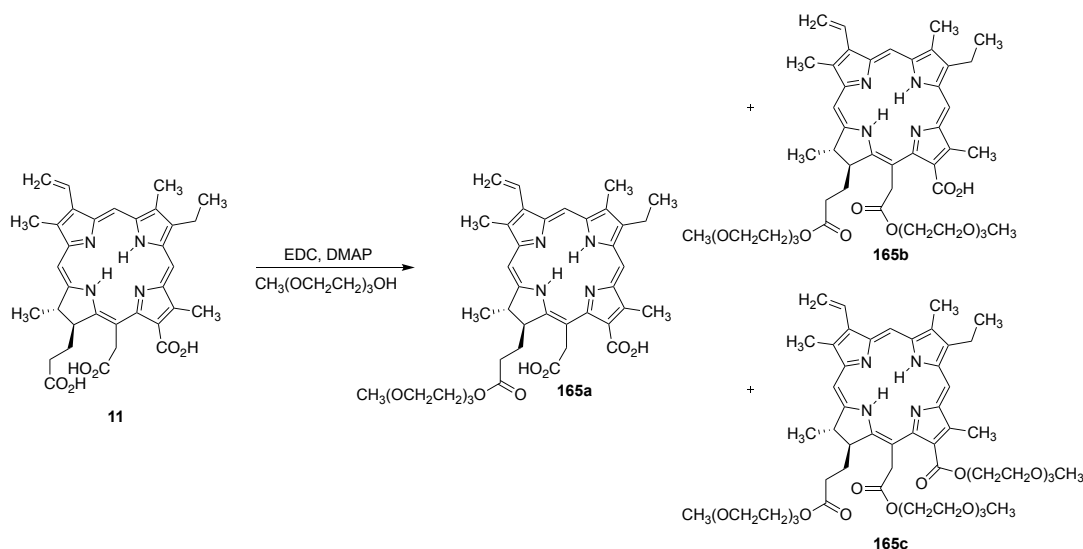
Building on previous efforts for the solubilization of antimony porphyrins by axial ligand exchange with alcohols (cf. Scheme 1-16), Yasuda and co-workers prepared hydrophilic PEGylated phosphorus porphyrins, such as tetraphenylporphyrin derivative **164**, by introduction of short PEGs as axial ligands. Incorporation of the axial-PEGs furnished highly water-soluble derivatives. Porphyrin **164**, for example, has a water-solubility of 17.3 mM.⁸⁰



Porphyrins PEGylated at their β -Positions

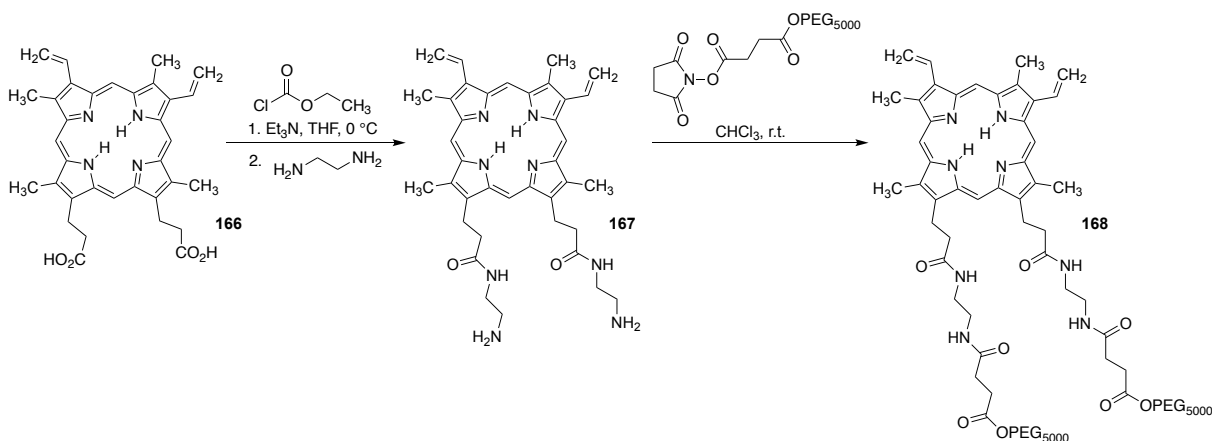
A number of PEGylated β -alkyl-porphyrins and chlorins were prepared. Representative of these are a number of PEGylated chlorin e6 derivatives, prepared first by Hamblin *et al.*¹³¹ The PEGylation increased tumor targeting of the photosensitizer. Mono-(**165a**), di-(**165b**), and tri-(**165c**) PEGylated derivatives of chlorin e6 were also prepared in which the PEG groups were introduced by esterification at one to three of its carboxylic acids using a short methyl-capped PEG (Scheme 1-54).¹³² Longer reaction times were needed to increase the yield of the tri-PEGylated product **165c**. The authors also measured the solubility of the compounds to be 1.8 ± 1.3 mM for **11**, 2.3 ± 1.0 mM for **165a**, 3.3 ± 0.9 mM for **165b**, and 3.9 ± 0.8 mM for **165c** in

1% (v/v) DMSO/water, indicating the increased aqueous solubility with the increase of the number of PEG chains.



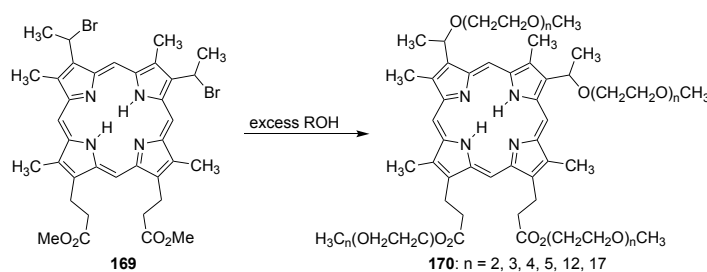
Scheme 1-54. PEGylated derivatives of chlorin e6, as described by the group of Greer.¹³² EDC = 1-ethyl3-(3-dimethylaminopropyl)carbodiimide,

The propionic side chains in protoporphyrin **166** could be functionalized with PEG-chains through amide linkages, whereby a short diamine established the requisite amine linkage sites. Amine intermediate **167** was then reacted with succinimidyl-PEG₅₀₀₀ to afford the water-soluble PEGylated protoporphyrin derivative **168** (Scheme 1-55), and its zinc complex.¹³³



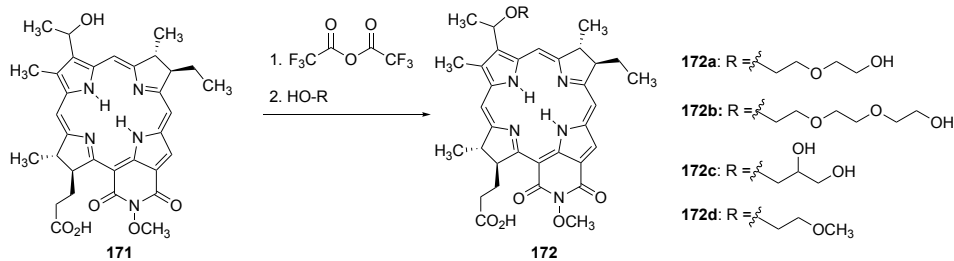
Scheme 1-55. PEGylated protoporphyrin and its zinc complex, as described by the group of Maeda.^{133a}

Other PEGylated porphyrins were prepared using ether linkages. For example, brominated hematoporphyrin derivative **169** was converted to the corresponding PEGylated compounds **170a-170f** by treatment with a stoichiometric excess of a methyl-capped PEG (Scheme 1-56).¹³⁴ Concomitantly, the propionic acid side chains were also derivatized with PEG chains. After hydrolysis of the propionic ester side chains, platinum-conjugates were prepared and evaluated for their antitumor phototoxicity and cytotoxicity.¹³⁴ The PEGylated derivatives were amenable to aqueous work-up and purified by alumina chromatography.



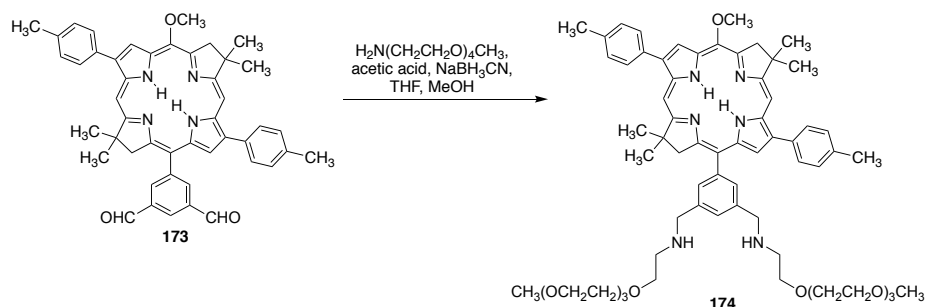
Scheme 1-56. PEGylated hematoporphyrin, as described by Brunner and Sohn.¹³⁴

Etherification conditions were also applied to cycloimide-bacteriochlorin alcohol derivative **171** (Scheme 1-57).¹³⁵ Activation of the hydroxyethyl substituent on bacteriochlorin **171** with trifluoroacetic anhydride, followed by treatment with hydroxyl-terminated short PEGs and diols of varying length, gave the corresponding derivatives **172a-172d**. The products were insoluble in water, but aqueous solutions were prepared with the help of 10% Cremophore EL, a PEGylated castor oil formulation vehicle.



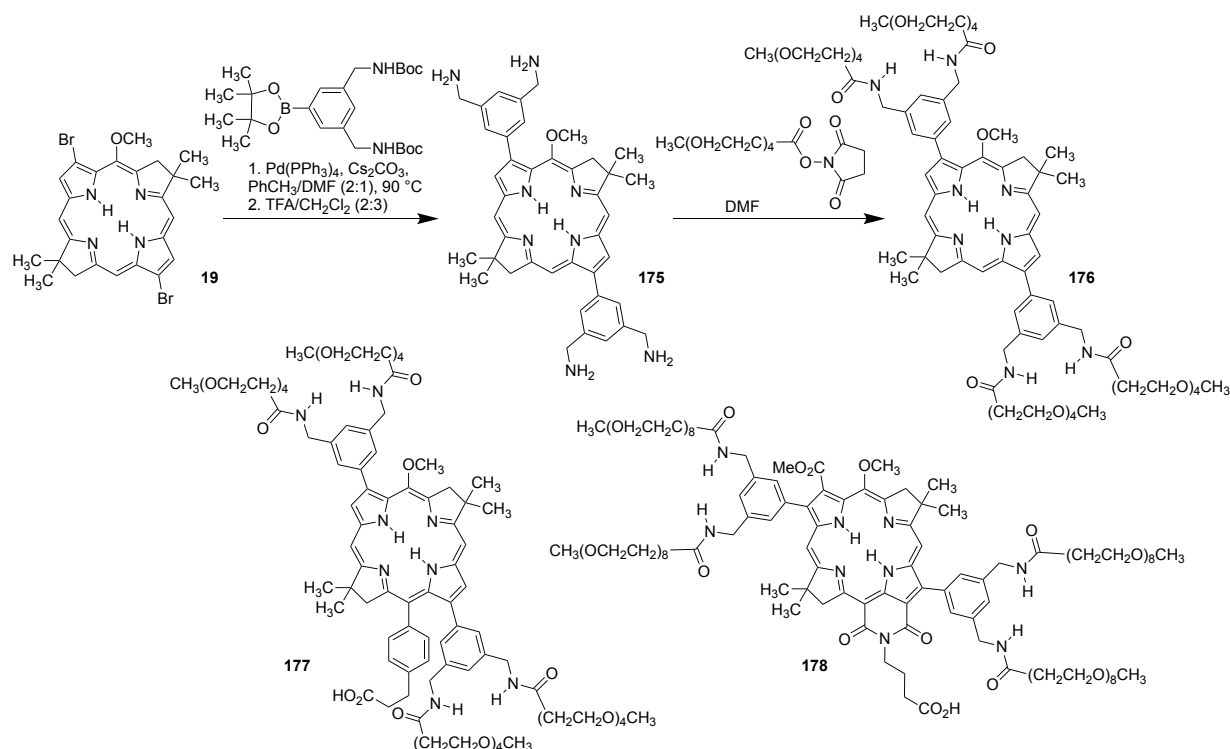
Scheme 1-57. Hydrophilic bacteriochlorin cycloimides, as described by the group of Feofanov.¹³⁵

The *meso*-Suzuki coupling method developed by Lindsey and co-workers was utilized for the introduction of PEG groups to bacteriochlorin **173** (Scheme 1-58).¹³⁶ Bacteriochlorin **173** was prepared by Suzuki coupling of the corresponding *meso*-bromo bacteriochlorin with an aryl-boronic ester bearing two unprotected aldehyde functional groups. The aldehyde functionalities were PEGylated by reductive amination with an amine-terminated PEG to afford water-soluble PEGylated bacteriochlorin **174**.



Scheme 1-58. PEGylated bacteriochlorins formed by reductive amination, as described by the group of Lindsey.¹³⁶

Another representative example for the introduction of PEG groups via Suzuki coupling of dibromobacteriochlorin **19** with a Boc-protected amine-derivatized boronic ester, followed by Boc-deprotection under standard conditions, afforded diaryl bacteriochlorin **175** carrying two amine groups. The amines were PEGylated by amide formation with a PEG-NHS ester to afford bacteriochlorin **176** (Scheme 1-59).^{113a} Derivatives bearing bioconjugatable tethers (**177**) and (**178**) were also prepared using a regioselective *meso*-bromination strategy, followed by similar coupling sequences.^{113a}



Scheme 1-59. β -Substituted PEGylated synthetic bacteriochlorins *via* Suzuki coupling, as described by the group of Lindsey.^{113a}

Due to the versatility of the 3,13-dibromobacteriochlorin building block (**19**), various solubilization motifs could be introduced to this scaffold. Thus, ammonium (**22** and **23**), carboxylate (**92**), phosphonate (**132**) and PEG (**176**) solubilizing motifs were introduced by coupling with suitable aryl-boronic esters as shown in Scheme 1-59. The products were compared by Lindsey and co-workers according to several notable parameters⁵⁹ (Table 1-2): The method of purification of the water-soluble adducts, the solubility of the compounds (as measured by the change in UV-vis absorption spectra over a 1000-fold concentration range), the full width at half-maximum (fwhm) of the longest wavelength of absorption and emission, and the stability of the chromophores in the light and dark. Overall, it was found that either the cationic ammonium or neutral-PEGylated species were the most promising derivatives because of their facile purification (precipitation), their amenability to further bioconjugation reactions, and good dark and light stabilities. The PEGylated derivatives were also shown to display very little

aggregation, as demonstrated by the sharp absorbance and emission peaks in their optical spectra over a 1000-fold concentration range.

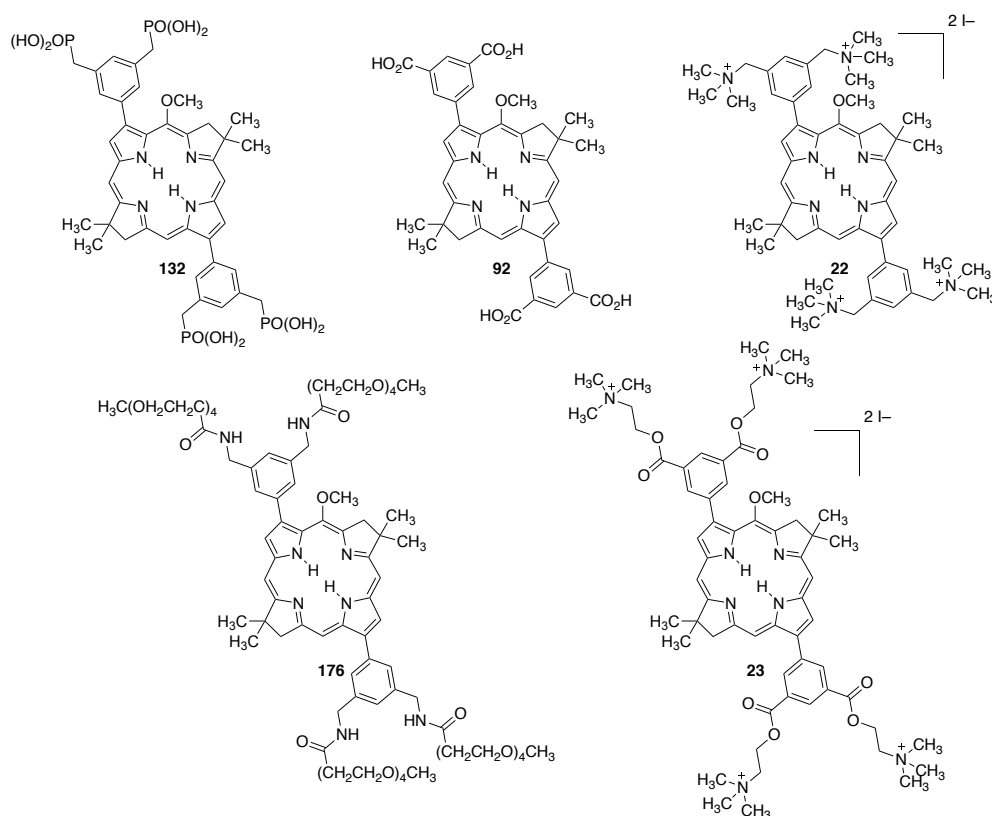


Table 1-2. Comparison of relevant properties concerning hydrophilicity of a series of structurally similar synthetic bacteriochlorins, as described by the group of Lindsey.⁵⁹

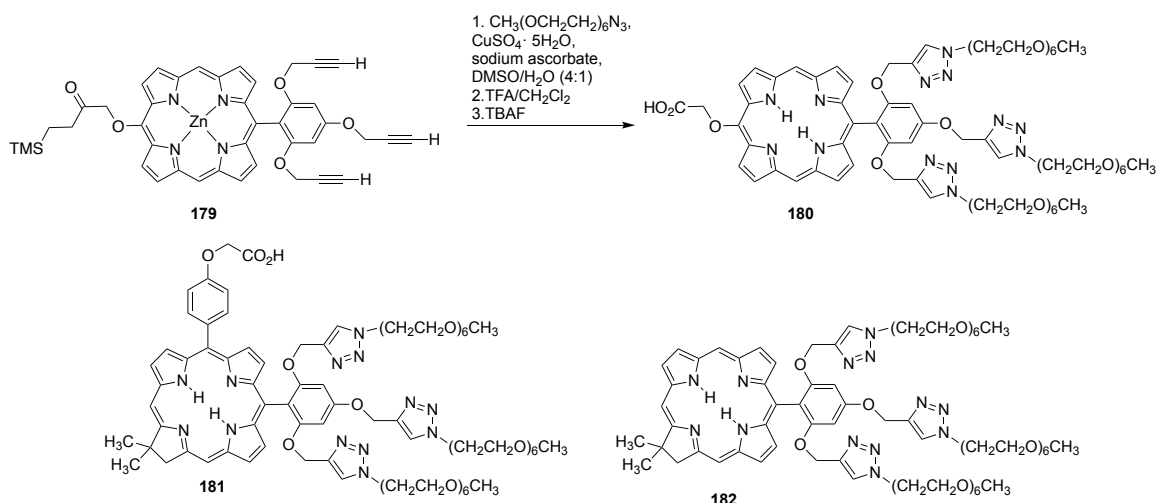
Compound	Purification method ^a	Water-Solubility ^b	fwhm (abs, fl) (nm) ^c	Stability in light (%) ^d	Stability in dark (%) ^e
132	reverse phase chromatography	0.46 μM – 460 μM	26, 30	85	> 95
92	ppt, washing with hexanes/MeOH (49:1)	0.32 μM – 320 μM	26, 26	96	> 95
22	ppt, washing with Et ₂ O/ THF (1:1)	0.24 μM – 240 μM	26, 26	82	> 95
23	ppt., washing with Et ₂ O/ THF (1:1)	0.18 μM – 180 μM	40, 26	96	> 95
176	ppt, washing with hexanes/CH ₂ Cl ₂ (19:1)	0.43 μM – 430 μM	22, 23	95	> 95

^a For the final step of the synthesis. ^b measured in aqueous media (PBs except **176**, water) by the absorption upon reciprocal change in concentration and pathlength. ^c 1 μM in PBS. fwhm = full width at half maximum of the longest wavelength band of absorption or emission, an indicator of aggregation. ^d The % remaining of a 1 μM solution in PBS

after several hours of absorption and fluorescence studies. ^e The % remaining of a 1 μ M solution in PBS allowed to stand in the dark at 4 °C for 48 h (as determined by absorption intensity of Q_y band).

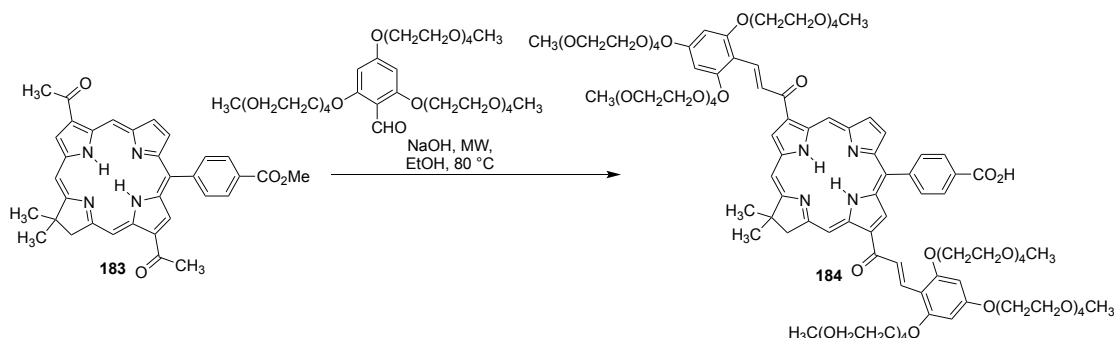
With the PEGylated derivatives appearing to be among the most promising motifs for solubilization, Lindsey and co-workers set out to prepare a series of PEGylated chlorins and bacteriochlorins (with options for bioconjugation) using a range of synthetic methodologies.¹¹³

One such example for the direct, late-stage PEGylation of chlorin derivatives was the azide-alkyne Huisgen-cycloaddition (click) reaction between an alkyne-substituted porphyrin or chlorin and an azide-terminated PEG. This strategy was employed to perform a direct PEGylation of *trans*-AB porphyrin **179** (Scheme 1-60) to afford the PEGylated porphyrin **180**.¹³⁷ Along analogous routes, synthetic chlorins **181** and **182** were prepared from alkyne-substituted *meso*-aryl groups and subsequent reactions with PEG-azides.^{113b}



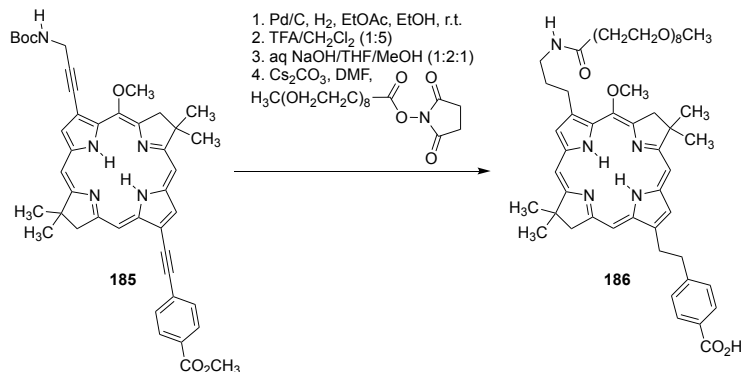
Scheme 1-60. PEGylated porphyrins and chlorins prepared through click chemistry, as described by the group of Lindsey.^{113b}

In addition, an aldol condensation method was developed to directly introduce an aryl group bearing three PEG chains to the β -positions of a β -diacetyl-substituted chlorin **183**. Reaction of **183** with a PEG-substituted aryl aldehyde formed the porphyrin-chalcone **184** (Scheme 1-61).^{113b} The absorption spectrum of the PEGylated chlorin-chalcone **184** was broadened in pure water, indicating its aggregation.



Scheme 1-61. PEGylated chlorins prepared by Aldol-condensation of β -diformyl chlorin, as described by the group of Lindsey.^{113b}

Lindsey and co-workers also used an amide coupling of an alkyl-amine substituted bacteriochlorin with a PEG-NHS ester to produce PEGylated bacteriochlorin **186** (Scheme 1-62).^{113a} The β -functionalized bacteriochlorin **185** was prepared by Sonogashira coupling and subsequent reduction of the alkynes. Boc-deprotection was followed by saponification to furnish the amine and acid-derivatized intermediate, which was reacted with a PEG-NHS ester to provide the PEGylated bacteriochlorin **186**. The carboxylic acid functionality on this chromophore is available for bioconjugation.



Scheme 1-62. PEGylated bacteriochlorins bearing a bioconjugatable tether prepared by amide coupling, as described by the group of Lindsey.^{113a}

1.4.4 Summary and Outlook

In summary, significant progress has been made in the past decades toward the preparation of water-soluble porphyrins and hydroporphyrins. A wide range of options is available for their solubilization in aqueous media. Cationic, anionic or neutral groups may be introduced in regio- and chemoselective fashion. Their number and positioning has major influences on the solubility of the derivatized porphyrin, whereby swallowtail approaches stand out as seemingly particularly effective in mediating water-solubility with a moderate concomitant increase in molecular weight. All solubilizing functionalities can be introduced at early stages of the synthesis of the target compound – generally in protected form – or at late stages. The late-state introduction of the solubilizing motif(s) reduces the number of difficult chromatographic steps needed in the synthetic sequence; these polar moieties and/or their water-solubility generally complicate their isolation and purification. Irrespective of the timing of the introduction of the solubilizing groups, multiple linking strategies are available. As far as flexibility and ease of implementation, PEGylation strategies stand out because they generate neutral chromophores of good solubility, the PEG chains are chemically stable, the versatility of the linking moieties can be used to link PEG chains to the chromophore, and the facility of the work-up conditions once the PEG chains are established. A combined approach using both ionic and PEG groups may also have its merits in cases where the introduction of short PEGs was not enough to solubilize the macrocycle. Even though the toolbox for the synthetic chemist to effect water-solubility is already extensive, the continued development of solubilizing strategies that are mild, selective, and introduce chemically robust solubilization motifs to porphyrins is vital to the field for these versatile chromophores to realize their full potential in the many technical and biomedical applications that take place in aqueous media.

1.5 Notes and References

- (1) Escobedo, J. O.; Rusin, O.; Lim, S.; Strongin, R. M. *Curr. Opin. Chem. Biol.* **2010**, *14*, 64.
- (2) Sternberg, E. D.; Dolphin, D.; Brückner, C. *Tetrahedron* **1998**, *54*, 4151.
- (3) Xu, Z.; Yoon, J.; Spring, D. R. *Chem. Soc. Rev.* **2010**, *39*, 1996.
- (4) Adler, A. D.; Longo, F. R.; Finarelli, J. D.; Goldmacher, J.; Assour, J.; Korsakoff, L. J. *Org. Chem.* **1967**, *32*, 476.
- (5) Brückner, C.; Dolphin, D. *Tetrahedron Lett.* **1995**, *36*, 3295.
- (6) a) Bonnett, R. *Chemical Aspects of Photodynamic Therapy*; Gordon & Breach: Langhorne, PA, 2000; b) Sternberg, E. D.; Dolphin, D.; Brückner, C. *Tetrahedron* **1998**, *54*, 4151; c) Ethirajan, M.; Chen, Y.; Joshi, P.; Pandey, R. K. *Chem. Soc. Rev.* **2011**, *40*, 340.
- (7) Wainwright, M. *Photodiagn. Photodyn. Ther.* **2009**, *6*, 167.
- (8) Donnelly, R. F.; McCarron, P. A.; Tunney, M. M. *Microbiol. Res.* **2008**, *163*, 1.
- (9) Weissleder, R.; Pittet, M. J. *Nature* **2008**, *452*, 580.
- (10) Wilson, P. C. *Photosensitizing Compounds: Their Chemistry, Biology and Clinical Use*; Wiley Interscience: Chichester, 1989.
- (11) Cerussi, A. E.; Berger, A. J.; Bevilacqua, F.; Shah, N.; Jakubowski, D.; Butler, J.; Holcombe, R. F.; Tromberg, B. J. *Acad. Radiol.* **2001**, *8*, 211.
- (12) a) Kim, C.; Favazza, C.; Wang, L. V. *Chem. Rev.* **2010**, *110*, 2756; b) Wang, L. V. *Nature Photonics* **2009**, *3*, 503.
- (13) Abuteen, A.; Zanganeh, S.; Akhigbe, J.; Samankumara, L. P.; Aguirre, A.; Biswal, N.; Braune, M.; Vollertsen, A.; Röder, B.; Brückner, C.; Zhu, Q. *Phys. Chem. Chem. Phys.* **2013**, *15*, 18502.
- (14) a) Harriman, A. *Photochem.* **1998**, *29*, 425; b) Gust, D.; Moore, T. A.; Moore, A. L. *Pure Appl. Chem.* **1998**, *70*, 2189; c) Ball, P. *New Sci.* **1999**, *161*, 38; d) Banala, S.; Rühl, T.; Santic, P.; Wurst, K.; Kräutler, B. *Angew. Chem. Int. Ed.* **2009**, *48*, 599.
- (15) a) Sessler, J. L.; Gebauer, A.; Weghorn, S. J. In *The Porphyrin Handbook*; Kadish, K. M., Smith, K. M., Guillard, R., Eds.; Academic Press: San Diego, 2000; Vol. 2, p 55; b) Sessler, J. L.; Davis, J. M. *Acc. Chem. Res.* **2001**, *34*, 989; c) Pareek, Y.; Ravikanth, M.; Chandrashekar, T. K. *Acc. Chem. Res.* **2012**, *45*, 1801.
- (16) a) Crossley, M. J.; King, L. G.; Newsom, I. A.; Sheehan, C. S. *Journal of the Chemical Society, Perkin Transactions 1: Organic and Bio-Organic Chemistry* **1996**, 2675; b)

- Kozyrev, A. N.; Suresh, V.; Das, S.; Senge, M. O.; Shibata, M.; Dougherty, T. J.; Pandey, R. K. *Tetrahedron* **2000**, *56*, 3353; c) Lash, T. D.; Werner, T. M.; Thompson, M. L.; Manley, J. M. *J. Org. Chem.* **2001**, *66*, 3152; d) Gill, H. S.; Harmjanz, M.; Santamaría, J.; Finger, I.; Scott, M. J. *Angew. Chem., Int. Ed.* **2004**, 485; e) McCarthy, J. R.; Hyland, M. A.; Brückner, C. *Org. Biomol. Chem.* **2004**, *2*, 1484; f) Nakamura, Y.; Aratani, N.; Shinokubo, H.; Takagi, A.; Kawai, T.; Matsumoto, T.; Yoon, Z. S.; Kim, D. Y.; Ahn, T. K.; Kim, D.; Muranaka, A.; Kobayashi, N.; Osuka, A. *J. Am. Chem. Soc.* **2006**, *128*, 4119; g) Diev, V. V.; Hanson, K.; Zimmerman, J. D.; Forrest, S. R.; Thompson, M. E. *Angew. Chem., Int. Ed.* **2010**, *49*, 5523; h) Jiao, C.; Huang, K.-W.; Guan, Z.; Xu, Q.-H.; Wu, J. *Org. Lett.* **2010**, *12*, 4046; i) Dudkin, S. V.; Makarova, E. A.; Fukuda, T.; Kobayashi, N.; Lukyanets, E. A. *Tetrahedron Lett.* **2011**, *52*, 2994; j) Krayner, M.; Yang, E.-K.; Diers, J. R.; Bocian, D. F.; Holten, D.; Lindsey, J. S. *New J. Chem.* **2011**, *35*, 587; k) Brückner, C.; Götz, D. C. G.; Fox, S. P.; Ryppa, C.; McCarthy, J. R.; Bruhn, T.; Akhigbe, J.; Banerjee, S.; Daddario, P.; Daniell, H. W.; Zeller, M.; Boyle, R. W.; Bringmann, G. *J. Am. Chem. Soc.* **2011**, *133*, 8740; l) Samankumara, L. P.; Wells, S.; Zeller, M.; Acuña, A. M.; Röder, B.; Brückner, C. *Angew. Chem. Int. Ed.* **2012**, *51*, 5757; m) Ishizuka, T.; Saegusa, Y.; Shiota, Y.; Ohtake, K.; Yoshizawa, K.; Kojima, T. *Chem. Commun.* **2013**, 49, 5939.
- (17) Fox, S.; Boyle, R. W. *Tetrahedron* **2006**, *62*, 10039.
- (18) a) Callot, H. J. *Tetrahedron* **1973**, *29*, 899; b) Barloy, L.; Dolphin, D.; Dupre, D.; Wijesekera, T. P. *Journal of Organic Chemistry* **1994**, *59*, 7976; c) Jeandon, C.; Ruppert, R.; Richeter, S.; Callot, H. J. *Org. Lett.* **2003**, *5*, 1487.
- (19) a) Davis, N. K. S.; Pawlicki, M.; Anderson, H. L. *Org. Lett.* **2008**, *10*, 3945; b) Davis, N. K. S.; Thompson, A. L.; Anderson, H. L. *Org. Lett.* **2010**, *12*, 2124; c) Davis, N. K. S.; Thompson, A. L.; Anderson, H. L. *J. Am. Chem. Soc.* **2011**, *133*, 30.
- (20) Hyland, M. A.; Morton, M. D.; Brückner, C. *J. Org. Chem.* **2012**, *77*, 3038.
- (21) a) Callot, H. J.; Ruppert, R.; Jeandon, C.; Richeter, S. *J. Porphyrins Phthalocyanines* **2004**, *8*, 111; b) Fouchet, J.; Jeandon, C.; Ruppert, R.; Callot, H. J. *Org. Lett.* **2005**, *7*, 5257; c) Jimenez, A. J.; Jeandon, C.; Gisselbrecht, J.-P.; Ruppert, R. *Eur. J. Org. Chem.* **2009**, 2009, 5725; d) Richeter, S.; Jeandon, C.; Gisselbrecht, J.-P.; Graff, R.; Ruppert, R.; Callot, H. J. *Inorg. Chem.* **2004**, *43*, 251; e) Richeter, S.; Jeandon, C.; Gisselbrecht, J.-P.; Ruppert, R.; Callot, H. J. *Inorg. Chem.* **2007**, *46*, 10241; f) Richeter, S.; Jeandon, C.; Kyritsakas, N.; Ruppert, R.; Callot, H. J. *J. Org. Chem.* **2003**, *68*, 9200; g) Sébastien,

- R.; Christophe, J.; Jean-Paul, G.; Romain, R. In *Handbook of Porphyrin Science*; World Scientific Publishing Company: 2010; Vol. Volume 3, p 429.
- (22) Jeandon, C.; Ruppert, R. *Eur. J. Org. Chem.* **2011**, 4098.
- (23) Akhigbe, J.; Zeller, M.; Brückner, C. *Org. Lett.* **2011**, 13, 1322.
- (24) Daniell, H. W.; Williams, S. C.; Jenkins, H. A.; Brückner, C. *Tetrahedron Lett.* **2003**, 44, 4045.
- (25) a) Crossley, M. J.; King, L. G. *Journal of the Chemical Society, Chemical Communications* **1984**, 920; b) Crossley, M. J.; Burn, P. L.; Langford, S. J.; Pyke, S. M.; Stark, A. G. *J. Chem. Soc., Chem. Commun.* **1991**, 1567; c) Starnes, S. D.; Arungundram, S.; Saunders, C. H. *Tetrahedron Lett.* **2002**, 43, 7785; d) Starnes, S. D.; Rudkevich, D. M.; Rebek, J., Jr. *Org. Lett.* **2000**, 2, 1995.
- (26) Akhigbe, J.; Luciano, M.; Zeller, M.; Brückner, C. *J. Org. Chem.* **2015**, 80, 499.
- (27) Brückner, C. *Acc. Chem. Res.* **2016**, 49, 1080.
- (28) Brückner, C. *Acc. Chem. Res.* **2016**, accepted for publication (DOI: 10.1021/ar.
- (29) Huang, H.; Song, W.; Rieffel, J.; Lovell, J. F. *Frontiers Phys.* **2015**, 3, Article #23.
- (30) a) Dolmans, D. E. J. G. J.; Fukumura, D.; Jain, R. K. *Nature Rev. Cancer* **2003**, 3, 380; b) Brandis, A. S.; Salomon, Y.; Scherz, A. In *Chlorophylls and Bacteriochlorophylls*; Grimm, B., Porra, R. J., Rüdinger, W., Scheer, H., Eds.; Springer: Dordrecht, NL, 2006, p 485.
- (31) a) Pandey, R. K.; James, N.; Chen, Y.; Dobhal, M. P. *Top. Heterocycl. Chem.* **2008**, 14, 41; b) Luo, S.; Zhang, E.; Su, Y.; Cheng, T.; Shi, C. *Biomaterials* **2011**, 32, 7127; c) Wang, L. V.; Hu, S. *Science* **2012**, 335, 1458; d) Weber, J.; Beard, P. C.; Bohndiek, S. E. *Nat. Methods* **2016**, 13, 639; e) Luciano, M.; Erfanzadeh, M.; Zhou, F.; Zhu, H.; Bornhütter, T.; Röder, B.; Zhu, Q.; Brückner, C. *Org. Biomol. Chem.* **2017**, 15, 972.
- (32) Stender, A. S.; Marchuk, K.; Liu, C.; Sander, S.; Meyer, M. W.; Smith, E. A.; Neupane, B.; Wang, G.; Li, J.; Cheng, J.-X.; Huang, B.; Fang, N. *Chem. Rev.* **2013**, 113, 2469.
- (33) Jiang, J.; Taniguchi, M.; Lindsey, J. S. *New J. Chem.* **2015**, 39, 4534.
- (34) a) Spencer, J. A.; Ferraro, F.; Roussakis, E.; Klein, A.; Wu, J.; Runnels, J. M.; Zaher, W.; Mortensen, L. J.; Alt, C.; Turcotte, R.; Yusuf, R.; Cote, D.; Vinogradov, S. A.; Scadden, D. T.; Lin, C. P. *Nature* **2014**, 508, 269; b) Lemon, C. M.; Karnas, E.; Han, X.; Bruns, O. T.; Kempa, T. J.; Fukumura, D.; Bawendi, M. G.; Jain, R. K.; Duda, D. G.; Nocera, D. G. *J. Am. Chem. Soc.* **2015**, 137, 9832.

- (35) a) Drain, C. M.; Varotto, A.; Radivojevic, I. *Chem. Rev.* **2009**, *109*, 1630; b) Jurow, M.; Schuckman, A. E.; Batteas, J. D.; Drain, C. M. *Coord. Chem. Rev.* **2010**, *254*, 2297; c) Tanaka, T.; Osuka, A. *Chem. Soc. Rev.* **2015**, *44*, 943.
- (36) Barona-Castano, J. C.; Carmona-Vargas, C. C.; Brocksom, T. J.; de Oliveira, K. T. *Molecules* **2016**, *21*.
- (37) a) Rybicka-Jasińska, K.; Ciszewski, Ł. W.; Gryko, D. *Adv. Synth. Catal.* **2016**, *358*, 1671; b) Rybicka-Jasińska, K.; Shan, W.; Zawada, K.; Kadish, K. M.; Gryko, D. *J. Am. Chem. Soc.* **2016**, *138*, 15451.
- (38) a) Panda, M. K.; Ladomenou, K.; Coutsolelos, A. G. *Coord. Chem. Rev.* **2012**, *256*, 2601; b) Urbani, M.; Grätzel, M.; Nazeeruddin, M. K.; Torres, T. *Chem. Rev.* **2014**, *114*, 12330; c) Kärkäs, M. D.; Verho, O.; Johnston, E. V.; Åkermark, B. *Chem. Rev.* **2014**, *114*, 11863; d) Hedley, G. J.; Ruseckas, A.; Samuel, I. D. W. *Chem. Rev.* **2017**, *117*, 796.
- (39) a) Smith, K. M. *New J. Chem.* **2016**, *40*, 5644; b) Hiroto, S.; Miyake, Y.; Shinokubo, H. *Chem. Rev.* **2016**.
- (40) a) Montforts, F.-P.; Gerlach, B.; Höper, F. *Chem. Rev.* **1994**, *94*, 327; b) Brückner, C.; Samankumara, L.; Ogikubo, J. In *Handbook of Porphyrin Science*; Kadish, K. M., Smith, K. M., Guillard, R., Eds.; World Scientific: River Edge, NY, 2012; Vol. 17 (Synthetic Developments, Part II; Chapter 76), p 1; c) Lindsey, J. S. *Chem. Rev.* **2015**, *115*, 6534; d) Taniguchi, M.; Lindsey, J. S. *Chem. Rev.* **2017**, *117*, 344.
- (41) a) Arnold, L.; Müllen, K. *J. Porphyrins Phthalocyanines* **2011**, *15*, 757; b) Brückner, C.; Akhigbe, J.; Samankumara, L. In *Handbook of Porphyrin Science*; Kadish, K. M., Smith, K. M., Guillard, R., Eds.; World Scientific: River Edge, NY, 2014; Vol. 31, p 1; c) Szyszko, B.; Latos-Grazynski, L. *Chem. Soc. Rev.* **2015**, *44*, 3588; d) Costa, L. D.; Costa, J. I.; Tome, A. C. *Molecules* **2016**, *21*.
- (42) Hambright, P. In *The Porphyrin Handbook*; Kadish, K. M., Smith, K. M., Guillard, R., Eds.; Academic Press: San Diego, 2000; Vol. 3, p 129.
- (43) Pisarek, S.; Maximova, K.; Gryko, D. *Tetrahedron* **2014**, *70*, 6685.
- (44) a) Singh, S.; Aggarwal, A.; Bhupathiraju, N. V.; Arianna, G.; Tiwari, K.; Drain, C. M. *Chem. Rev.* **2015**, *115*, 10261; b) Moylan, C.; Scanlan, E. M.; Senge, M. O. *Curr. Med. Chem.* **2015**, *22*, 2238.
- (45) Králová, J.; Kejík, Z.; Bříza, T.; Poučková, P.; Král, A.; Martásek, P.; Král, V. *J. Med. Chem.* **2010**, *53*, 128.

- (46) a) Gotardo, M. C. A. F.; Sacco, H. C.; Filho, J. C. S.; Ferreira, A. G.; Tedesco, A. C.; Assis, M. D. *J. Porphyrins Phthalocyanines* **2003**, *7*, 399; b) Welch, C.; Archibald, S. J.; Boyle, R. W. *Synthesis* **2009**, 551.
- (47) a) McCarthy, J. R.; Perez, M. J.; Brückner, C.; Weissleder, R. *Nano Lett.* **2005**, *5*, 2552; b) Paproski, R. J.; Forbrich, A.; Huynh, E.; Chen, J.; Lewis, J. D.; Zheng, G.; Zemp, R. J. *Small* **2016**, *12*, 371; c) da Silveira, J. M.; da Silva, A. R.; Senge, M. O.; Jorge, R. A. J. *Nanosci. Nanotechnol.* **2014**, *14*, 6274; d) Chouikrat, R.; Seve, A.; Vanderesse, R.; Benachour, H.; Barberi-Heyob, M.; Richeter, S.; Raehm, L.; Durand, J. O.; Verelst, M.; Frochot, C. *Curr. Med. Chem.* **2012**, *19*, 781.
- (48) a) Paszko, E.; Senge, M. O. *Curr. Med. Chem.* **2012**, *19*, 5239; b) Huynh, E.; Lovell, J. F.; Helfield, B. L.; Jeon, M.; Kim, C.; Goertz, D. E.; Wilson, B. C.; Zheng, G. *J. Am. Chem. Soc.* **2012**, *134*, 16464; c) Lovell, J. F.; Jin, C. S.; Huynh, E.; Jin, H.; Kim, C.; Rubinstein, J. L.; Chan, W. C. W.; Cao, W.; Wang, L. V.; Zheng, G. *Nat. Mater.* **2011**, *10*, 324.
- (49) Hambright, P.; Fleischer, E. B. *Inorg. Chem.* **1970**, *9*, 1757.
- (50) a) Wheelhouse, R. T.; Sun, D.; Han, H.; Han, F. X.; Hurley, L. H. *J. Am. Chem. Soc.* **1998**, *120*, 3261; b) McMillin, D. R.; Shelton, A. H.; Bejune, S. A.; Fanwick, P. E.; Wall, R. K. *Coord. Chem. Rev.* **2005**, *249*, 1451.
- (51) Merchat, M.; Bertolini, G.; Giacomini, P.; Villaneuva, A.; Jori, G. *J. Photochem. Photobiol. B* **1996**, *32*, 153.
- (52) Commercial suppliers of porphyrins, for example: Frontier Scientific, Logan, UT, U.S.A.; Sigma-Aldrich, St. Louis, MO, U.S.A.; PorphyChem SAS, Dijon, France; Porphyrin Systems GbR, Appen, Germany.
- (53) Manono, J.; Marzilli, P. A.; Marzilli, L. G. *Inorg. Chem.* **2009**, *48*, 5636.
- (54) Lamarche, F.; Sol, V.; Huang, Y.-M.; Granet, R.; Guilloton, M.; Krausz, P. *J. Porphyrins Phthalocyanines* **2002**, *6*, 130.
- (55) Drogat, N.; Gady, C.; Granet, R.; Sol, V. *Dyes Pigm.* **2013**, *98*, 609.
- (56) Taima, H.; Okubo, A.; Yoshioka, N.; Inoue, H. *Tetrahedron Lett.* **2005**, *46*, 4161.
- (57) Ruzié, C.; Krayner, M.; Balasubramanian, T.; Lindsey, J. S. *J. Org. Chem.* **2008**, *73*, 5806.
- (58) Huang, L.; Huang, Y. Y.; Mroz, P.; Tegos, G. P.; Zhiyentayev, T.; Sharma, S. K.; Lu, Z.; Balasubramanian, T.; Krayner, M.; Ruzie, C.; Yang, E.; Kee, H. L.; Kirmaier, C.; Diers, J. R.; Bocian, D. F.; Holten, D.; Lindsey, J. S.; Hamblin, M. R. *Antimicrob. Agents. Chemother.* **2010**, *54*, 3834.

- (59) Jiang, J.; Yang, E.; Reddy, K. R.; Niedzwiedzki, D. M.; Kirmaier, C.; Bocian, D. F.; Holten, D.; Lindsey, J. S. *New. J. Chem.* **2015**, 39, 5694.
- (60) Sharma, S. K.; Krayner, M.; Sperandio, F. F.; Huang, L.; Huang, Y. Y.; Holten, D.; Lindsey, J. S.; Hamblin, M. R. *J. Porphyrins Phthalocyanines* **2013**, 17, 73.
- (61) a) Thamyongkit, P.; Speckbacher, M.; Diers, J. R.; Kee, H. L.; Kirmaier, C.; Holten, D.; Bocian, D. F.; Lindsey, J. S. *J. Org. Chem.* **2004**, 69, 3700; b) Thamyongkit, P.; Lindsey, J. S. *J. Org. Chem.* **2004**, 69, 5796.
- (62) Reddy, K. R.; Lubian, E.; Pavan, M. P.; Kim, H.-J.; Yang, E.; Holten, D.; Lindsey, J. S. *New. J. Chem.* **2013**, 37, 1157.
- (63) Balaz, M.; Collins, H. A.; Dahlstedt, E.; Anderson, H. L. *Org. Biomol. Chem.* **2009**, 7, 874.
- (64) Banfi, S.; Caruso, E.; Buccafurni, L.; Battini, V.; Zazzaron, S.; Barbieri, P.; Orlandi, V. *J. Photochem. Photobiol. B* **2006**, 85, 28.
- (65) Tovmasyan, A. G.; Babayan, N. S.; Sahakyan, L. A.; Shahkhatuni, A. G.; Gasparyan, G. H.; Aroutiounian, R. M.; Ghazaryan, R. K. *J Porphyrins Phthalocyanines* **2008**, 12, 1100.
- (66) Ko, Y. J.; Yun, K. J.; Kang, M. S.; Park, J.; Lee, K. T.; Park, S. B.; Shin, J. H. *Bioorg. Med. Chem. Lett.* **2007**, 17, 2789.
- (67) Schmitt, F.; Govindaswamy, P.; Süß-Fink, G.; Ang, W. H.; Dyson, P. J.; Juillerat-Jeanneret, L.; Therrien, B. *J. Med. Chem.* **2008**, 51, 1811.
- (68) Schmitt, F.; Govindaswamy, P.; Zava, O.; Süß-Fink, G.; Juillerat-Jeanneret, L.; Therrien, B. *J. Biol. Inorg. Chem.* **2008**, 14, 101.
- (69) Hu, X.; Ogawa, K.; Kiwada, T.; Odani, A. *J. Inorg. Biochem.* **2017**, 170, 1.
- (70) Gianferrara, T.; Serli, B.; Zangrando, E.; Iengo, E.; Alessio, E. *New. J. Chem.* **2005**, 29, 895.
- (71) Haeubl, M.; Reith, L. M.; Gruber, B.; Karner, U.; Muller, N.; Knor, G.; Schoefberger, W. *J. Biol. Inorg. Chem.* **2009**, 14, 1037.
- (72) Sutton, J. M.; Clarke, O. J.; Fernandez, N.; Boyle, R. W. *Bioconjugate Chem.* **2002**, 13, 249.
- (73) Song, R.; Kim, Y.-S.; Lee, C. O.; Sohn, Y. S. *Tetrahedron Lett.* **2003**, 44, 1537.
- (74) a) Spagnul, C.; Alberto, R.; Gasser, G.; Ferrari, S.; Pierroz, V.; Bergamo, A.; Gianferrara, T.; Alessio, E. *J. Inorg. Biochem.* **2013**, 122, 57; b) Gianferrara, T.; Spagnul, C.; Alberto, R.; Gasser, G.; Ferrari, S.; Pierroz, V.; Bergamo, A.; Alessio, E. *ChemMedChem* **2014**, 9, 1231.

- (75) Mion, G.; Mari, C.; Da Ros, T.; Rubbiani, R.; Gasser, G.; Gianferrara, T. *ChemistrySelect* **2017**, 2, 190.
- (76) Feng, X.-X.; Zhang, J.-X.; Wu, Y.; Zhang, Q.; Liu, J.-C. *Dyes Pigm.* **2017**, 136, 773.
- (77) Entract, G. M.; Bryden, F.; Domarkas, J.; Savoie, H.; Allott, L.; Archibald, S. J.; Cawthorne, C.; Boyle, R. W. *Mol. Pharmaceutics* **2015**, 12, 4414.
- (78) Tovmasyan, A.; Babayan, N.; Poghosyan, D.; Margaryan, K.; Harutyunyan, B.; Grigoryan, R.; Sarkisyan, N.; Spasojevic, I.; Mamyán, S.; Sahakyan, L.; Aroutiounian, R.; Ghazaryan, R.; Gasparyan, G. *J. Inorg. Biochem.* **2014**, 140, 94.
- (79) Matsumoto, J.; Suemoto, Y.; Kanemaru, H.; Takemori, K.; Shigehara, M.; Miyamoto, A.; Yokoi, H.; Yasuda, M. *J. Photochem. Photobiol. B* **2017**, 168, 124.
- (80) Matsumoto, J.; Shinbara, T.; Tanimura, S.-i.; Matsumoto, T.; Shiragami, T.; Yokoi, H.; Nosaka, Y.; Okazaki, S.; Hirakawa, K.; Yasuda, M. *Photochem. Photobiol., A* **2011**, 218, 178.
- (81) Aravindu, K.; Mass, O.; Vairaprakash, P.; Springer, J. W.; Yang, E.; Niedzwiedzki, D. M.; Kirmaier, C.; Bocian, D. F.; Holten, D.; Lindsey, J. S. *Chem. Sci.* **2013**, 4, 3459.
- (82) Manono, J.; Marzilli, P. A.; Fronczek, F. R.; Marzilli, L. G. *Inorg. Chem.* **2009**, 48, 5626.
- (83) Perera, T.; Abhayawardhana, P.; Marzilli, P. A.; Fronczek, F. R.; Marzilli, L. G. *Inorg. Chem.* **2013**, 52, 2412.
- (84) Guldi, D. M.; Zilbermann, I.; Anderson, G.; Li, A.; Balbinot, D.; Jux, N.; Hatzimarinaki, M.; Hirsch, A.; Prato, M. *Chem. Commun.* **2004**, 726.
- (85) Matsumoto, J.; Kubo, T.; Shinbara, T.; Matsuda, N.; Shiragami, T.; Fujitsuka, M.; Majima, T.; Yasuda, M. *Bull. Chem. Soc. Jpn.* **2013**, 86, 1240.
- (86) Milgrom, L. R.; Bone, S.; Bruce, D. w.; Macdonald, M. P. *J. Mol. Electron.* **1991**, 7, 95.
- (87) a) Bhaumik, J.; Yao, Z.; Borbas, K. E.; Taniguchi, M.; Lindsey, J. S. *J. Org. Chem.* **2006**, 71, 8807; b) Mroz, P.; Bhaumik, J.; Dogutan, D. K.; Aly, Z.; Kamal, Z.; Khalid, L.; Kee, H. L.; Bocian, D. F.; Holten, D.; Lindsey, J. S.; Hamblin, M. R. *Cancer Lett.* **2009**, 282, 63.
- (88) Fuhrhop, J.-H.; Smith, K. M. *Laboratory Methods in Porphyrin and Metalloporphyrin Research*; Elsevier: Amsterdam, 1975.
- (89) a) Longo, F. R.; Finarelli, M. G.; Kim, J. B. *J. Heterocycl. Chem.* **1969**, 6, 927; b) Datta-Gupta, N.; Bardos, T. *J. Heterocycl. Chem.* **1966**, 3, 495; c) Lindsey, J. S.; Schreiman, I. C.; Hsu, H. C.; Kearney, P. C.; Marguerettaz, A. M. *J. Org. Chem.* **1987**, 52, 827.
- (90) Kostas, I. D.; Coutsolelos, A. G.; Charalambidis, G.; Skondra, A. *Tetrahedron Lett.* **2007**, 48, 6688.

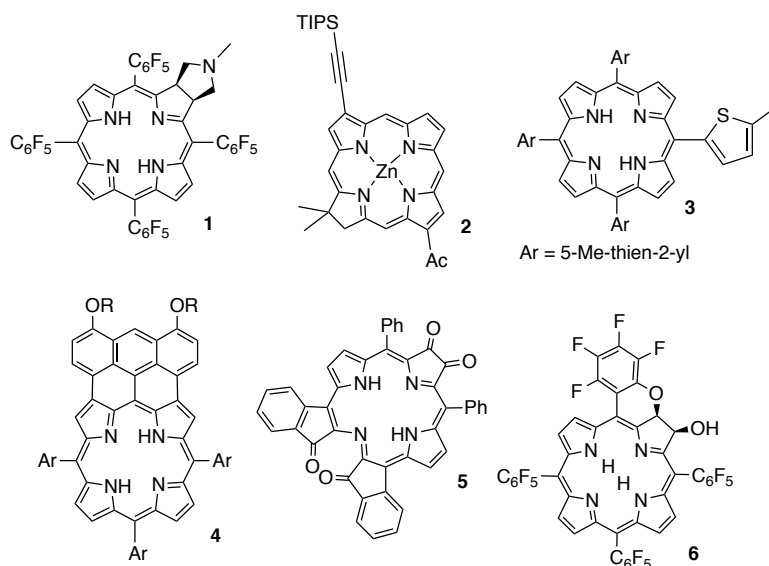
- (91) Murashima, T.; Tsujimoto, S.; Yamada, T.; Miyazawa, T.; Uno, H.; Ono, N.; Sugimoto, N. *Tetrahedron Lett.* **2005**, *46*, 113.
- (92) Ogawa, K.; Hasegawa, H.; Inaba, Y.; Kobuke, Y.; Inouye, H.; Kanemitsu, Y.; Kohno, E.; Hirano, T.; Ogura, S.; Okura, I. *J. Med. Chem.* **2006**, *49*, 2276.
- (93) Inaba, Y.; Ogawa, K.; Kobuke, Y. *J. Porphyrins Phthalocyanines* **2007**, *11*, 406.
- (94) Muresan, A. Z.; Lindsey, J. S. *Tetrahedron* **2008**, *64*, 11440.
- (95) Subbarayan, M.; Shetty, S. J.; Srivastava, T. S.; Noronha, O. P. D.; Samuel, A. M.; Mukhtar, H. *Biochem. Biophys. Res. Commun.* **2001**, *281*, 32.
- (96) Luo, J.; Chen, L.-F.; Hu, P.; Chen, Z.-N. *Inorg. Chem.* **2014**, *53*, 4184.
- (97) You, Y.; Gibson, S. L.; Hilf, R.; Davies, S. R.; Oseroff, A. R.; Roy, I.; Ohulchanskyy, T. Y.; Bergey, E. J.; Detty, M. R. *J. Med. Chem.* **2003**, *46*, 3734.
- (98) Jiang, J.; Vairaprakash, P.; Reddy, K. R.; Sahin, T.; Pavan, M. P.; Lubian, E.; Lindsey, J. S. *Org. Biomol. Chem.* **2014**, *12*, 86.
- (99) Srivastava, T. S.; Tsutsui, M. *J. Org. Chem.* **1973**, *38*, 2103.
- (100) a) Mahammed, A.; Goldberg, I.; Gross, Z. *Org. Lett.* **2001**, *3*, 3443; b) Saltsman, I.; Mahammed, A.; Goldberg, I.; Tkachenko, E.; Botoshansky, M.; Gross, Z. *J. Am. Chem. Soc.* **2002**, *124*, 7411; c) Vestfrid, J.; Kothari, R.; Kostenko, A.; Goldberg, I.; Tumanskii, B.; Gross, Z. *Inorg. Chem.* **2016**, *55*, 6061.
- (101) Thomas, A. P.; Saneesh Babu, P. S.; Asha Nair, S.; Ramakrishnan, S.; Ramaiah, D.; Chandrashekar, T. K.; Srinivasan, A.; Radhakrishna Pillai, M. *J. Med. Chem.* **2012**, *55*, 5110.
- (102) Song, R.; Kim, Y.-S.; Sohn, Y. S. *J. Inorg. Biochem.* **2002**, *83*, 83.
- (103) Zhang, X. A.; Lovejoy, K. S.; Jasanoff, A.; Lippard, S. J. *Proc. Natl. Acad. Sci. U. S. A.* **2007**, *104*, 10780.
- (104) Liu, F.; Zou, T. J.; Tan, Z. L.; Chen, S.; Wu, Z. H.; Yan, G. P.; Zhang, Q.; Liang, S. C.; Yang, J. *Org. Biomol. Chem.* **2017**, *15*, 1245.
- (105) Monteiro, C. J. P.; Pereira, M. M.; Pinto, S. M. A.; Simões, A. V. C.; Sá, G. F. F.; Arnaut, L. G.; Formosinho, S. J.; Simões, S.; Wyatt, M. F. *Tetrahedron* **2008**, *64*, 5132.
- (106) Dabrowski, J. M.; Arnaut, L. G.; Pereira, M. M.; Monteiro, C. J.; Urbanska, K.; Simoes, S.; Stochel, G. *ChemMedChem* **2010**, *5*, 1770.
- (107) Brandis, A.; Mazor, O.; Neumark, E.; Rosenbach-Belkin, V.; Salomon, Y.; Scherz, A. *Photochem. Photobiol.* **2005**, *81*, 983.
- (108) Brandis, A.; Mazor, O.; Neumark, E.; Rosenbach-Belkin, V.; Salomon, Y.; Scherz, A. *Photochem. Photobiol.* **2005**, *81*, 983.

- (109) Wedel, M.; Walter, A.; Montforts, F.-P. *Eur. J. Org. Chem.* **2001**, 1681.
- (110) a) Borbas, K. E.; Mroz, P.; Hamblin, M. R.; Lindsey, J. S. *Bioconjugate Chem.* **2006**, *17*, 638; b) Borbas, K. E.; Kee, H. L.; Holten, D.; Lindsey, J. S. *Org. Biomol. Chem.* **2008**, *6*, 187.
- (111) Borbas, K. E.; Chandrashaker, V.; Muthiah, C.; Kee, H. L.; Holten, D.; Lindsey, J. S. *J. Org. Chem.* **2008**, *73*, 3145.
- (112) Sahin, T.; Vairaprakash, P.; Borbas, K. E.; Balasubramanian, T.; Lindsey, J. S. *J. Porphyrins Pthalocyanines* **2015**, *19*, 663.
- (113) a) Zhang, N.; Jiang, J.; Liu, M.; Taniguchi, M.; Mandal, A. K.; Evans-Storms, R. B.; Pitner, J. B.; Bocian, D. F.; Holten, D.; Lindsey, J. S. *New. J. Chem.* **2016**, *40*, 7750; b) Liu, M.; Chen, C.-Y.; Mandal, A. K.; Chandrashaker, V.; Evans-Storms, R. B.; Pitner, J. B.; Bocian, D. F.; Holten, D.; Lindsey, J. S. *New. J. Chem.* **2016**, *40*, 7721.
- (114) a) Benaglia, M.; Danelli, T.; Fabris, F.; Sperandio, D.; Pozzi, G. *Org. Lett.* **2002**, *4*, 4229; b) Worlinsky, J. L.; Halepas, S.; Ghandehari, M.; Khalil, G.; Brückner, C. *Analyst* **2015**, *140*, 190; c) Worlinsky, J. L.; Halepas, S.; Brückner, C. *Org. Biomol. Chem.* **2014**, *12*, 3991.
- (115) Lottner, C.; Bart, K.-C.; Bernhardt, G.; Brunner, H. *J. Med. Chem.* **2002**, *45*, 2079.
- (116) Reuther, T.; Kübler, A. C.; Zillmann, U.; Flechtenmacher, C.; Sinn, H. *Lasers Surg. Med.* **2001**, *29*, 314.
- (117) Topkaya, D.; Lafont, D.; Poyer, F.; Garcia, G.; Albrieux, F.; Maillard, P.; Bretonnière, Y.; Dumoulin, F. *New. J. Chem.* **2016**, *40*, 2044.
- (118) a) Zhang, J.-L.; Che, C.-M. *Org. Lett.* **2002**, *4*, 1911; b) Nawalany, K.; Kozik, B.; Kepczynski, M.; Zapotoczny, S.; Kumorek, M.; Nowakowska, M.; Jachimska, B. *J. Phys. Chem. B.* **2008**, *112*, 12231.
- (119) Mineo, P.; Scamporrino, E.; Vitalini, D. *Macromol. Rapid Commun.* **2002**, *23*, 681.
- (120) Kim, W. J.; Kang, M. S.; Kim, H. K.; Kim, Y.; Chang, T.; Ohulchanskyy, T. Y.; Prasad, P. N.; Lee, K.-S. *J. Nanosci. Nanotechnol.* **2009**, *9*, 7130.
- (121) Castriciano, M. A.; Romeo, A.; Angelini, N.; Micali, N.; Longo, A.; Mazzaglia, A.; Scolaro, L. M. *Macromolecules* **2006**, *39*, 5489.
- (122) Lovell, J. F.; Roxin, A.; Ng, K. K.; Qi, Q.; McMullen, J. D.; DaCosta, R. S.; Zheng, G. *Biomacromolecules* **2011**, *12*, 3115.
- (123) Peng, C.-L.; Shieh, M.-J.; Tsai, M.-H.; Chang, C.-C.; Lai, P.-S. *Biomaterials* **2008**, *29*, 3599.

- (124) Sibrian-Vazquez, M.; Jensen, T. J.; Hammer, R. P.; Vicente, M. G. H. *J. Med. Chem.* **2006**, *49*, 1364.
- (125) Gianferrara, T.; Bergamo, A.; Bratsos, I.; Milani, B.; Spagnul, C.; Sava, G.; Alessio, E. *J. Med. Chem.* **2010**, *53*, 4678.
- (126) Mion, G.; Gianferrara, T.; Bergamo, A.; Gasser, G.; Pierroz, V.; Rubbiani, R.; Vilar, R.; Leczkowska, A.; Alessio, E. *ChemMedChem* **2015**, *10*, 1901.
- (127) Zingg, A.; Felber, B.; Gramlich, V.; Fu, L.; Collman, J. P.; Diederich, F. *Helv. Chim. Acta* **2002**, *85*, 333.
- (128) Akhtar, M. A.; Riaz, S.; Hayat, A.; Nasir, M.; Muhammad, N.; Rahim, A.; Nawaz, M. H. *J. Mol. Liq.* **2017**, *225*, 235.
- (129) Ogikubo, J.; Worlinsky, J. L.; Fu, Y.-J.; Brückner, C. *Tetrahedron Lett.* **2013**, *54*, 1707.
- (130) Ahmed, S.; Davoust, E.; Savoie, H.; Boa, A. N.; Boyle, R. W. *Tetrahedron Lett.* **2004**, *45*, 6045.
- (131) Hamblin, M. R.; Miller, J. L.; Rizvi, I.; Ortel, B.; Maytin, E. V.; Hasan, T. *Cancer Res.* **2001**, *61*, 7155.
- (132) Kimani, S.; Ghosh, G.; Ghogare, A.; Rudshteyn, B.; Bartusik, D.; Hasan, T.; Greer, A. *J. Org. Chem.* **2012**, *77*, 10638.
- (133) a) Sahoo, S. K.; Sawa, T.; Fang, J.; Tanaka, S.; Miyamoto, Y.; Akaike, T.; Maeda, H. *Bioconjugate Chem.* **2002**, *13*, 1031; b) Regehly, M.; Greish, K.; Rancan, F.; Maeda, H.; Böhm, F.; Röder, B. *Bioconjugate Chem.* **2007**, *18*, 494.
- (134) a) Lottner, C.; Bart, K.-C.; Bernhardt, G.; Brunner, H. *J. Med. Chem.* **2002**, *45*, 2064; b) Kim, Y.-S.; Song, R.; Hyun Kim, D.; Jun, M. J.; Sohn, Y. S. *Biorg. Med. Chem.* **2003**, *11*, 1753.
- (135) Sharonov, G. V.; Karmakova, T. A.; Kassies, R.; Pljutinskaya, A. D.; Grin, M. A.; Refregiers, M.; Yakubovskaya, R. I.; Mironov, A. F.; Maurizot, J.-C.; Vigny, P.; Otto, C.; Feofanov, A. V. *Free Radical Biol. Med.* **2006**, *40*, 407.
- (136) Fan, D.; Taniguchi, M.; Lindsey, J. S. *J. Org. Chem.* **2007**, *72*, 5350.
- (137) Mandal, A. K.; Sahin, T.; Liu, M.; Lindsey, J. S.; Bocian, D. F.; Holten, D. *New J. Chem.* **2016**, *40*, 9648.

2 Quinoline-Annulated Chlorins and Chlorin Analogues

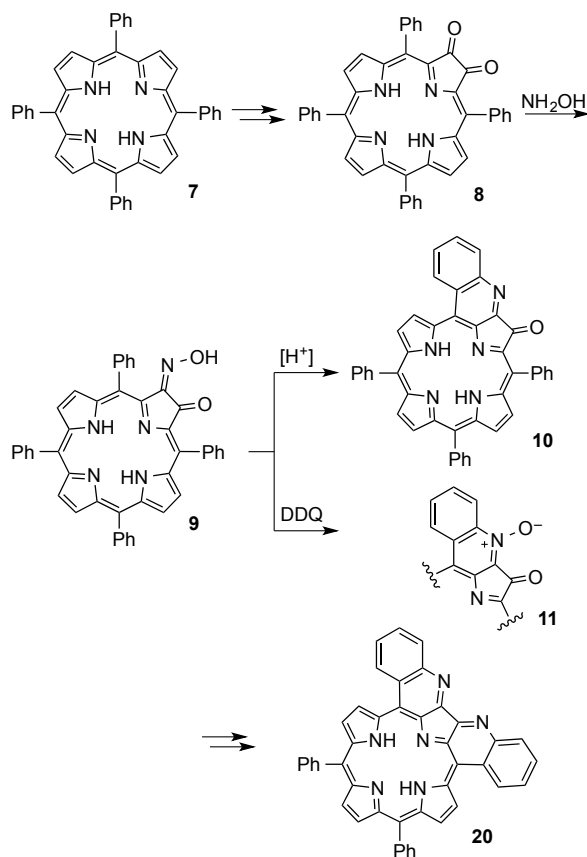
Hydroporphyrins (chlorins and bacteriochlorins) possess bathochromically hyperspectra compared to porphyrins, making them desirable targets for synthesis, either via total synthesis pathways or the reduction of porphyrins.¹ Examples of recently reported synthetic chlorins are **1**² and **2**,³ made by conversion of a porphyrin and total synthesis, respectively. The particular β -substituent patterns employed impart high chemical stabilities on these chlorins, whereas many 'simple' chlorins are frequently sensitive toward oxidations back to the parent porphyrin. Exceptions notwithstanding,⁴ derivatization of the phenyl-groups in *meso*-phenylporphyrins generally have no major effect on the optical properties of the porphyrin.⁵ A generally more significant effect is observed when the phenyl group is replaced by sterically smaller aryl group that allow a larger co-planar arrangement – and thus π -overlap – of the π -system of the aryl group and the porphyrinoid, as in the case of *meso*-thienyl-substituted porphyrinoids, such as **3**.⁶ Substituents that are conjugated to the chromophore also modulate the electronic properties of the chromophore.^{1f,7}



One related approach is to extend the porphyrinic π -systems through annulation reactions. Multiple examples were reported, including porphyrins **4**,⁸ **5**,⁹ and **6**.¹⁰ The distortion from

planarity of the chromophores is yet another synthetic approach to red-shift the spectra of porphyrins.¹¹ Incidentally, annulations also often introduce non-planarity.^{9-10,12} Indachlorindione **5**, for example, combines π -extension, non-planarity, and the presence of conjugated β -substituents to achieve a panchromatic absorption spectrum between 300 and >900 nm.⁹

Reported by us recently,¹²⁻¹³ quinoline-annulated porphyrins **10** and **11** are available in two steps from well-known 2,3-dioxochlorin **8**, itself accessible along a number of pathways from the ultimate porphyrinic starting material, *meso*-tetraphenylporphyrin **7** (Scheme 2-1).¹⁴ Depending on the reaction conditions, ring-closure of oxime **9** using either acidic or oxidative conditions yields **10** or **11**, respectively.¹²⁻¹³ A repeat of the reaction sequence on **10** generates a bis-quinoline-annulated porphyrin **20**.¹² An alternative reaction pathway to the bis-quinoline-annulated macrocycle was reported by Jeandon and Ruppert.¹⁵



Scheme 2-1. Synthesis of quinoline-annulated porphyrin **10** and its quinoline-*N*-oxide **11**.

All quinoline-annulated porphyrins possess unusually broadened and red-shifted optical spectra.¹²⁻¹³ They are also low emitting and are poor singlet oxygen sensitizers.¹⁶ Quinoline-annulated porphyrin **10** in particular has gained additional interest as a very attractive photoacoustic imaging (PAI) agent.¹⁶ PAI is a non-invasive biomedical imaging modality that combines optical and ultrasound imaging in such a way that its key characteristics are superior to each of the component imaging techniques. NIR absorbers displaying a strong photoacoustic effect are much sought-after,¹⁷ particularly if they are also non-phototoxic.

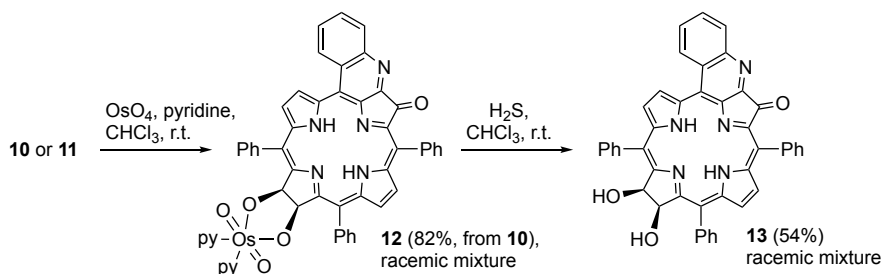
With the intriguing quinoline-annulated porphyrins at hand, the question arises whether the corresponding hydroporphyrin analogues can be formed. We also intended to expand the pool of quinoline-annulated porphyrin derivatives to screen them in PAI assays to help us better define structural motifs that lead to high PAI signals. In this contribution, we will show that the quinoline-annulated dihydroxychlorin can indeed be generated. Moreover, using our ‘porphyrin breaking and mending’ strategy, this dihydroxychlorin can also be converted to quinoline-annulated porphyrin and chlorin analogues in which a pyrroline moiety was formally replaced by a pyrroledione and oxazolone moiety, respectively. We will describe the dramatic effects these modifications have on the NIR absorbance properties of some of the derivatives.

2.1 Results and Discussion

2.1.1 OsO₄-Mediated dihydroxylation of quinoline-annulated porphyrins **10** and **11**.

Reaction of quinoline-annulated porphyrin **10** or its quinoline *N*-oxide **11** with stoichiometric amounts of OsO₄ under the standard porphyrin dihydroxylation conditions¹⁸ generated an identical product in high yields that, on account of its diagnostic signals in the ¹H NMR spectrum (*inter alia*, the signals for pyrroline hydrogens, d at 6.61 and 6.80 ppm), can be identified as the expected osmate ester **12** (Scheme 2-2). We observed the facile loss of the quinoline-*N*-oxide oxygen atom before, even under oxidizing conditions.¹⁹ Reduction of osmate ester **12** using H₂S generated the corresponding quinoline-annulated dihydroxychlorin **13**.¹⁸ All signals expected for

the quinoline and the pyrrole moiety can be identified. As commonly observed in the non-planar quinoline-annulated porphyrins, the signals for the inner NH protons are low-field shifted compared to regular porphyrins or chlorins, to 0.1 and 0.5 ppm, likely an effect of their non-planarity.¹²⁻¹³



Scheme 2-2. OsO₄-Mediated dihydroxylation of quinoline-annulated porphyrins **10** and **11**.

The absence of symmetry in diol ester **12** and diol **13** did not allow a direct confirmation of the site of dihydroxylation, by for instance, an inspection of the number and coupling patterns of the β -proton signals. However, we deduced that the connectivity of **12** and **13** was the result of a dihydroxylation of the β,β' -bond opposite the quinoline-annulated pyrrole based on other spectroscopic evidence, combined with correlations to precedent reactions of the related dioxochlorins. Considering, for example, the two tautomeric possibilities for isomer **A** and isomer **B**, all resulting from the reaction of one of the pyrroles adjacent to the quinoline-annulated pyrrole: This forces the inner NH protons into a high-energy adjacent isobacteriochlorin-type arrangement.²⁰ Any tautomer (like **A-I**) that places a proton on the quinoline-annulated pyrrole also interrupts ring aromaticity and is therefore highly unlikely. In addition, the pyrrole β -proton signals can be clearly made out in the ¹H NMR spectra of **12** and **13**, as can all the signals for the quinoline-annulated *meso*-phenyl group. Since in isomer **B**, one pyrrole β -proton is located very closely to a quinoline proton, a strong coupling between these protons should be seen in a NOESY spectrum of **13**, but no such correlation could be detected. On the other hand, the NOESY spectrum of **13** indicates a correlation between the pyrrole

hydrogens and two non-annulated phenyl groups (see experimental section), confirming the connectivity of the quinolone-annulated diol **13** as shown. Oxidation reactions of free base dioxochlorin **8** are also directed toward the pyrrole opposite the dioxopyrroline,²¹ and reductions of the somewhat related porpholactones and porpholactams also take place at the pyrrole opposite the oxazolone moiety.²² Thus, in its regioselective dihydroxylation, quinoline-annulated porphyrin **10** resemble chlorins.²³

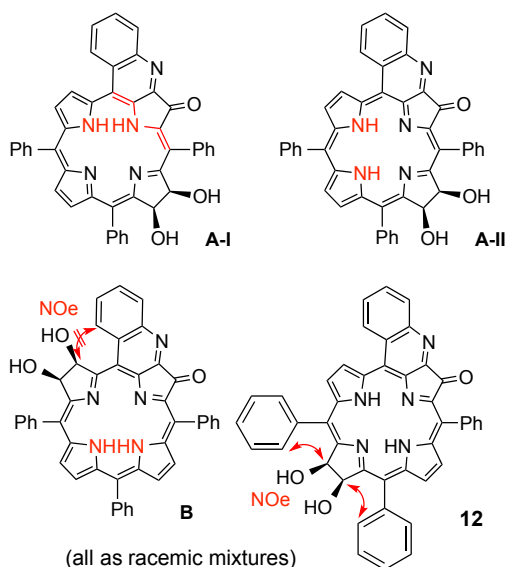


Figure 2-1. Two other theoretical isomers of diol **13**, highlighting the arguments against their existence, and the observed NOe correlation seen in **12**.

The UV-vis spectrum of the parent quinoline-annulated porphyrin **10** is, as described previously,¹²⁻¹³ much broadened and red-shifted ($\lambda_{\text{max}} = 750 \text{ nm}$) compared to that of a regular porphyrin ($\lambda_{\text{max}} \sim 650 \text{ nm}$) (Figure 2-2). In comparison, the spectrum of its dihydroxylated derivative **13** is nearly 100 nm red-shifted ($\lambda_{\text{max}} = 842 \text{ nm}$), with a slight enhancement of the λ_{max} band. These are the hallmarks of chlorins vs. porphyrins.²⁴ Thus, compound **13** can be referred to as a quinoline-annulated dihydroxychlorin.

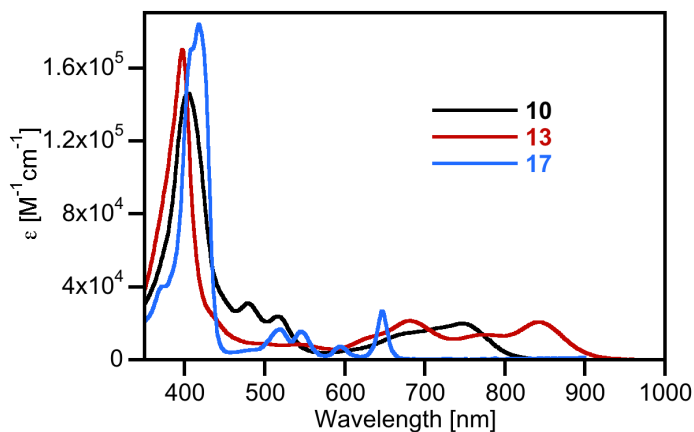
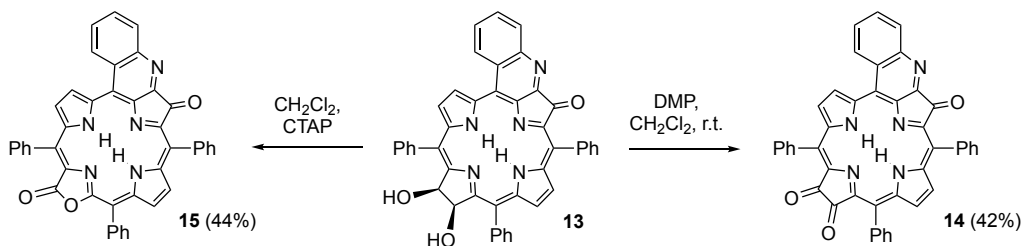


Figure 2-2. UV-vis spectra (CH_2Cl_2) of the compounds indicated.

2.1.2 Periodinane-mediated oxidation of quinoline-annulated dihydroxychlorin **13**

The oxidation of the *vic-cis*-diol moiety in dihydroxychlorins, tetrahydroxybacteriochlorins, or dihydroxypyrroline-bearing pyrrole-modified porphyrins to the corresponding diones and tetraones using 2,3-dichloro-5,6-dicyano-1,4-benzoquinone (DDQ) or 2-iodoxybenzoic acid (IBX) is well known.^{9,14a,25} We found that the hypervalent iodine-based oxidant Dess-Martin periodinane (DMP) is also well suited to accomplish this reaction on diol **13**, generating the corresponding quinoline-annulated dione **14**. The product shows all the expected analytical data (e.g., absence of the pyrroline-hydrogen signals in its ^1H NMR, appearance of two new ketone signals in its ^{13}C NMR at 186 and 187 ppm, and exhibiting a composition indicating the loss of four hydrogens, as per ESI+ HR-MS).



Scheme 2-3. Oxidations of quinoline-annulated dihydroxychlorin **13**.

The UV-vis spectrum of dione **14** shows the spectral broadening also observed for dione **8**^{14a} (Figure 2-3), attributed to the conjugated dione moiety.²⁶ Otherwise, the spectrum resembles more that of porphyrin **10** than chlorin **13**. An equivalent diol-to-dione conversion in an indachlorin led to significant red-shifts,⁹ not observed here, perhaps reflecting the spectral differences between dione-modified porphyrins and chlorin analogues.

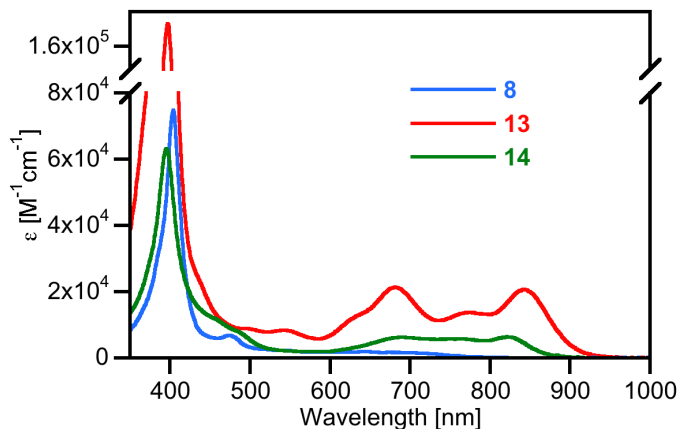


Figure 2-3. UV-vis spectra (CH₂Cl₂) of the compounds indicated.

The direct conversion of a pyrrole β,β' -bond to a lactone moiety under a number of oxidation conditions is well established,^{14b,27} whereby the two-step process *via* the diolchlorins is characterized by mild reaction conditions and high selectivity.^{19,28} This reaction could also be translated to pyrrole-modified porphyrins.^{9,29} Application of the standard cetyltrimethylammonium permanganate (CTAP) oxidation protocol to quinoline-annulated chlorin diol **13**, generates the low-polarity product **15** that showed all the expected spectroscopic signatures for its quinoline-annulated porpholactone structure. Its ESI+ HR-MS indicates the loss of a carbon and four hydrogen atoms and its IR spectrum shows the appearance of an additional, lactone-type, carbonyl group (at 1756 cm⁻¹). The ¹H NMR spectrum of **15** shows the expected disappearance of the pyrroline hydrogens and also reveals the presence of an inseparable 1:5 mixture of the two possible regioisomers **15-I** and **15-II**. We were, however, not able to assign which isomer is the major isomer. We,²⁹ and others,⁷ have observed before that the introduction

of a lactone moiety into non-symmetric pyrrole-modified porphyrins exhibits some degree of regioselectivity.

The UV-vis spectrum of quinoline-annulated porpholactone **15** is clearly different from that of the starting chlorin **13** and resembles that of quinoline-annulated porphyrin **10** (Figure 2-4). The ability of a lactone moiety to mimic a β,β' -bond was rationalized before.^{28b}

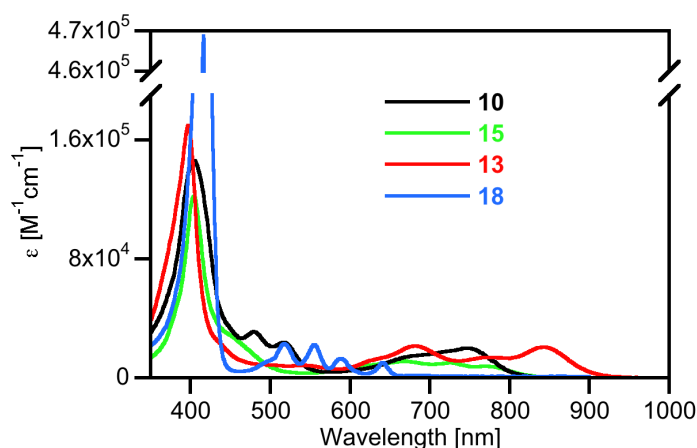
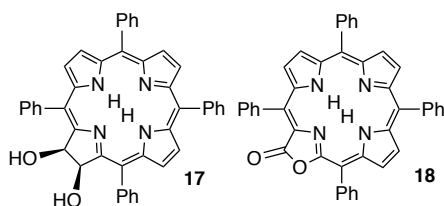


Figure 2-4. UV-vis spectra (CH_2Cl_2) of the compounds indicated.

2.2 Conclusions

In conclusion, quinoline-annulated porphyrin **10** can be dihydroxylated using OsO_4 like regular porphyrins or chlorins, with the regiochemical selectivity of a chlorin (dihydroxylation opposite the annulated dione moiety).²³ The dihydroxypyrroline moiety in quinoline-annulated dihydroxychlorin **13** is susceptible to the same conversions we previously demonstrated for dihydroxychlorins^{14a,28,30} and dihydroxychlorin analogues.^{9,29} Oxidations to the corresponding dione **14** and lactone **15** were also carried out. Likewise, the same general trends in the changes of their optical spectra are observed. Comparing the absolute λ_{max} values of the parent compounds (644 nm for dihydroxychlorin **17**;¹⁸ very broad Q-bands in dioxochlorin **8**,^{14a} Figure 2-3 and 640 nm for porpholactone **18**,^{28b} Figure 2-4 with those of the quinoline-annulated analogues, the large shifts induced by the quinoline-annulation become apparent. The

absorption maximum in all of the annulated chromophores was pushed well into the NIR, and all possess longer wavelengths absorptions than, for example, bisquinoline-annulated porphyrin **20**,^{12,15} though these are more readily accessible. Annulation causes a ~200 nm shift in diol **13** (Figure 2-2), a ~150 nm shift in dione **14** (Figure 2-3) and a ~130 nm shift in lactone **15** (Figure 2-4). This compares to the ~100 nm annulated porphyrin **10** is shifted compared to porphyrin **7**.¹² The magnitude of the shifts correlates with the flexibility of the frameworks, with the porphyrins tending to be more rigid and planar than hydroporphyrins.³¹ Evidently, the annulation introduces some strain into the macrocycle that can be alleviated through the adoption of non-planar conformation modes the more flexible the parent framework is. We attribute the general reduction in the extinction coefficient induced by the annulation also to their non-planarity. We are currently investigating the detailed photophysical properties of these intriguing NIR-absorbing chromophores, including their efficacy as PAI contrast agents.



2.3 Experimental Section

2.3.1 Materials and Instruments

Monoquinoline annulated porphyrin **10** was prepared according to the previously reported preparation.¹²⁻¹³ Aluminum-backed, silica gel 60, 250 μm thickness analytical plates were used for analytical TLC; 20 \times 20 cm, glass-backed, silica gel 60, 500 μm thickness preparative TLC plates, and standard grade, 60 Å, 32–63 μm flash column silica gel were used for preparative chromatography.

^1H and ^{13}C NMR spectra were recorded on a Bruker 400 MHz instrument in the solvents indicated, and were referenced to residual solvent peaks. High and low resolution mass spectra were provided by the Mass Spectrometry Facility, Department of Chemistry, University of Connecticut. The microwave synthesizer used was a discover microwave reactor.

2.3.2 Synthesis and Characterization

Quinoline-annulated osmate ester 12. Quinoline-annulated porphyrin **10** (250 mg, 3.83×10^{-5} mol) was dissolved in mixture of freshly distilled pyridine and EtOH-stabilized CHCl_3 (12 mL of CHCl_3 /30% pyridine) in a round-bottom flask equipped with a magnetic stir bar. The mixture was treated with OsO_4 (400 mg, 1.57×10^{-3} mol, 4 equiv; 4 mL of a stock solution prepared by dissolving a 1 g OsO_4 ampule in 10 mL pyridine) and the reaction flask was stoppered, shielded with aluminum foil from ambient light, and stirred at r.t. for four days. Once no further changes of the reaction mixture was detectable and the starting material was 95%+ consumed (by TLC), the solvent was removed by rotary evaporation and the residue was thoroughly dried under a gentle stream of N_2 . The crude material was loaded onto a silica gel column with a fine sand layer and eluted with CH_2Cl_2 /3% MeOH. The first fraction was a trace amount of unreacted starting material. The second olive-green fraction was collected, the solvent volume was reduced and solvent-exchanged with MeOH on the rotary evaporator. The precipitate was

collected and dried under vacuum to provide quinoline-fused dihydroxychlorin osmate ester **12** (339 mg, 3.21×10^{-4} mol, 82% yield) as a dark green, micro-crystalline material. R_f (silica- $\text{CH}_2\text{Cl}_2/2\%$ MeOH) = 0.21; ^1H NMR (400 MHz, CDCl_3): δ 8.98–8.92 (m, 3H), 8.66 (br s 2H), 8.58 (br s 2H), 8.18 (dd, $^3J = 4.9$, $^4J = 1.7$ Hz, 1H), 8.10 (dd, $^3J = 4.9$, $^4J = 1.8$ Hz, 2H), 8.03 (dd, $^3J = 4.9$, $^4J = 1.9$ Hz, 1H), 7.90–7.86 (m, 4H), 7.79 (br s, 3H), 7.70 (t, 2H), 7.64 (br s, 4H), 7.55–7.53 (d, $^3J = 5.0$ Hz, 3H), 7.44 (br s, 3H), 7.36 (br s, 3H), 6.79 (d, $^3J = 5.9$ Hz, 1H), 6.62 (d, $^3J = 5.6$ Hz, 1H), -0.08 (s, 1H, exchangeable with D_2O), -0.25 (s, 1H, exchangeable with D_2O) ppm; ^{13}C NMR: This compound possesses limited solubility, even at elevated temperature. UV-vis (CH_2Cl_2) λ_{max} (Rel. I.) 402 (1), 692 (0.14), 844 (0.12) nm; FT-IR (neat, diamond ATR): $\nu_{\text{C=O}} = 1715 \text{ cm}^{-1}$; for full spectrum, see Figure S2; HR-MS (ESI+, 100% CH_3CN , 30 V cone voltage): The molecular peak of this compound could not, like that of other osmate esters,³² not be detected.

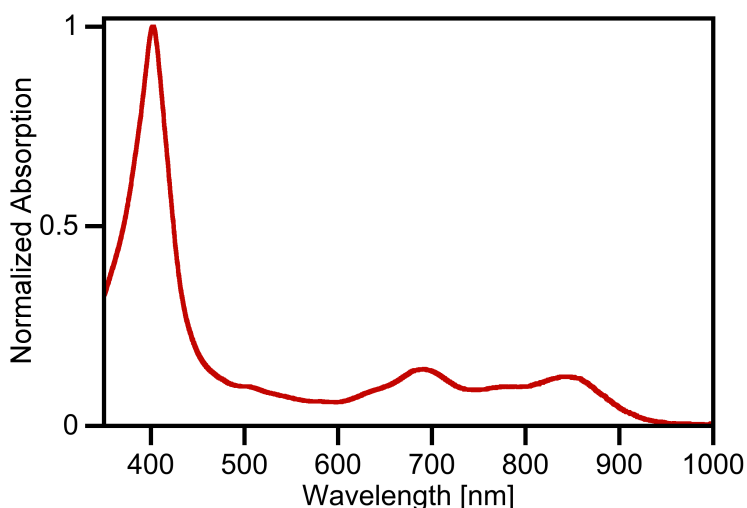


Figure 2-5. UV-vis spectrum (CH_2Cl_2) of **12**.

Quinoline-annulated dihydroxychlorin 13. Quinoline osmate ester **12** (378 mg) was dissolved in CHCl_3 /10% MeOH (50 ml) in a 100 ml round bottom flask equipped with a magnetic stir bar and a gas in- and outlet. A gentle stream of H_2S was passed into the flask for ~2 min (no bubbling through the solution! Caution: fume hood and bleach-filled H_2S scrubber!). Once TLC control indicated the consumption of all the starting material, the reaction mixture was thoroughly purged with nitrogen (fume hood and H_2S scrubber!), and then evaporated to dryness by rotary evaporation (air outlet of rotary evaporator vacuum pump in the fume hood!). The residue was separated by automated flash chromatography (silica gel–solvent gradient from 100% CH_2Cl_2 to CH_2Cl_2 /2% MeOH) to obtain **13** in 44% yield (~96 mg): R_f (silica- CH_2Cl_2 /2% MeOH) 0.38; ^1H NMR (400 MHz, CDCl_3): δ 8.78 (d, $^3J = 7.1$ Hz, 1H), 8.69 (br s, 1H), 8.24 (d, $^3J = 7.1$ Hz, 2H), 8.05 (dd, $^3J = 5.0$, $^4J = 1.8$ Hz, 1H), 8.00 (dd, $^3J = 5.0$, $^4J = 2.0$ Hz, 1H), 7.99 (d, $^3J = 4.4$ Hz, 2H), 7.77 (two overlapping dd, $^3J = 5.0$, $^4J = 1.8$ Hz, 2H), 7.68–7.60 (m, 13H), 6.07 (d, $^3J = 6.3$ Hz, 1H), 5.91 (d, $^3J = 6.3$ Hz, 1H), 3.54 (s, 1H), 3.32 (s, 1H), 0.48 (s, 1H, exchangeable with D_2O), 0.08 (s, 1H, exchangeable with D_2O) ppm; ^{13}C NMR (100 MHz, CDCl_3): δ 193.9, 162.7, 158.3, 149.7, 147.0, 145.0, 141.8, 140.9, 140.8, 140.3, 140.0, 138.2, 136.8, 133.7, 132.8, 132.5, 131.9, 130.7, 129.5, 128.5, 128.2, 128.0, 127.9, 127.8, 127.6, 127.5, 127.0, 122.2, 122.1, 120.9, 118.7, 114.6, 111.0, 74.5, 74.4 ppm; UV-vis (CH_2Cl_2) λ_{max} (log ϵ) 397 (5.23), 543 (3.93), 682 (4.33), 773 (4.14), 842 (4.32) nm; FT-IR (neat, diamond ATR): $\nu_{\text{C=O}} = 1710\text{ cm}^{-1}$; for full spectrum, see Figure S6; HR-MS (ESI^+ , cone voltage = 30 V, 100% CH_3CN) m/e calcd for $\text{C}_{44}\text{H}_{30}\text{N}_5\text{O}_3$ ($[\text{M}\cdot\text{H}]^+$) 676.2309, found 676.2322.

2. Quinoline-Annulated Chlorins and Chlorin Analogues

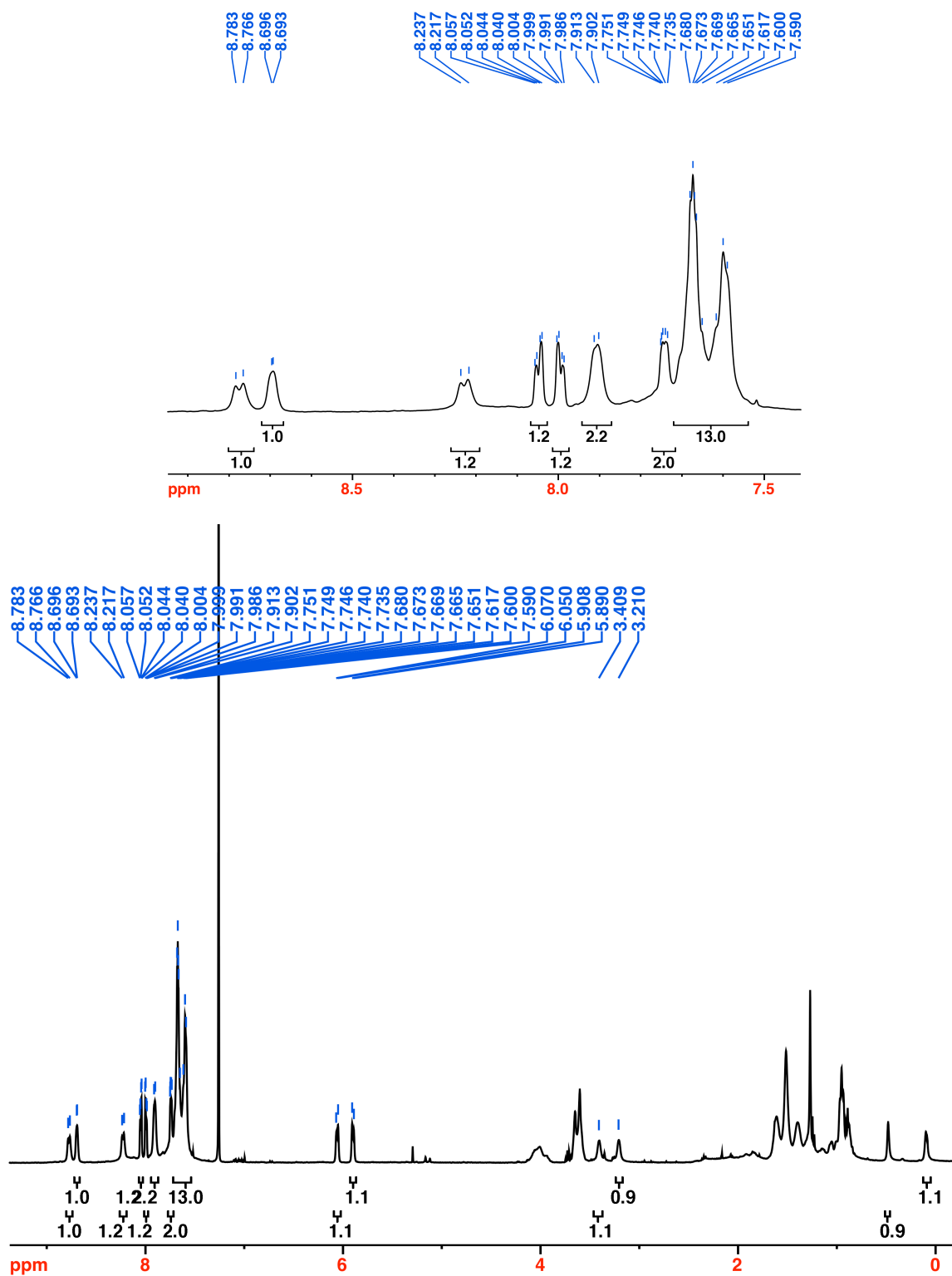


Figure 2-6. ^1H NMR spectrum (400 MHz, CDCl_3) of **13**.

2. Quinoline-Annulated Chlorins and Chlorin Analogues

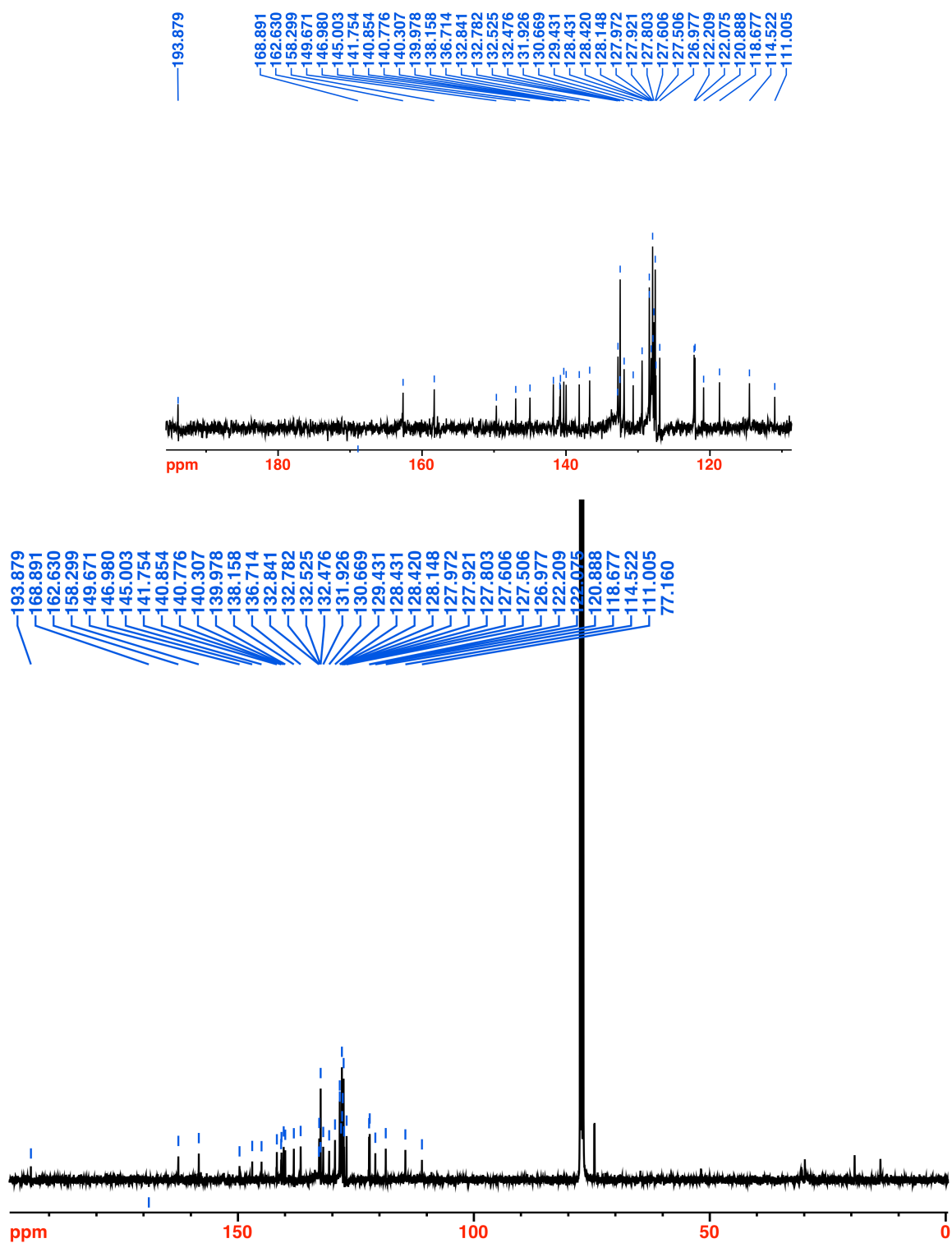


Figure 2-7. ^{13}C NMR (100 MHz, CDCl_3) of 13.

2. Quinoline-Annulated Chlorins and Chlorin Analogues

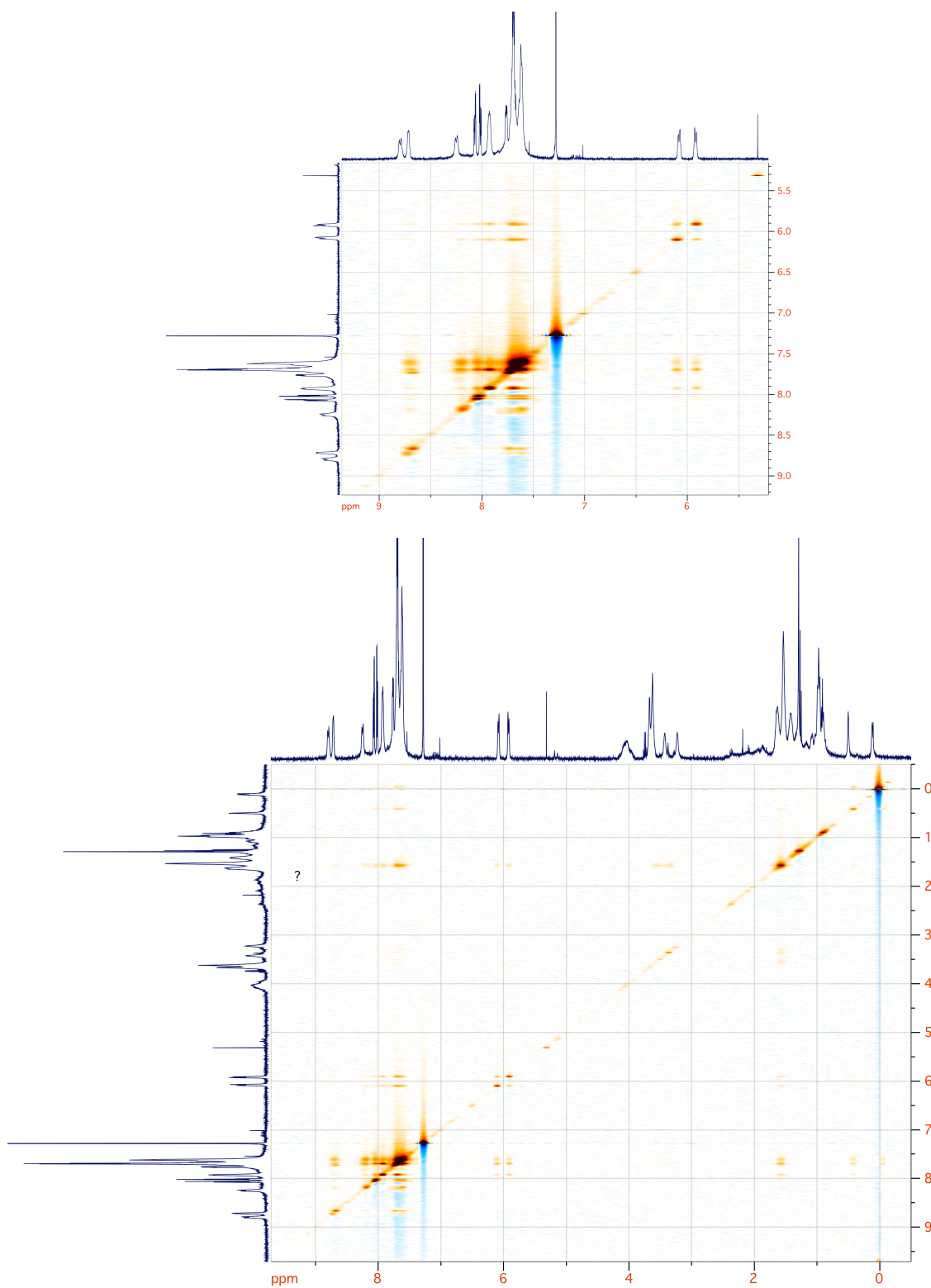


Figure 2-8. ^1H - ^1H NOESY spectrum (CDCl_3) of **13**.

Quinoline-annulated dioxoporphyrin 14. Diol **13** (10.6 mg, 1.6×10^{-5} mol) was dissolved in CH_2Cl_2 (9.0 mL) in a round-bottom flask equipped with a magnetic stir bar. Dess-Martin periodinane (DMP) (13.7 mg, 3.2×10^{-5} mol, 2 equiv) was added and the reaction mixture stirred at ambient temperature for 10 min. When TLC and UV-vis indicated the consumption of the starting material, a saturated $\text{Na}_2\text{S}_2\text{O}_3$ solution (5 mL) was added to the reaction mixture and vigorously stirred. After a few minutes, the mixture was extracted with CH_2Cl_2 ($3 \times \sim 10$ mL). The combined organic layers were washed with saturated Na_2CO_3 , followed by brine, then dried over Na_2SO_4 , and reduced to dryness. The residue was separated by preparative TLC (silica- CH_2Cl_2) to afford the dark green dioxoporphyrin **14** in 42% yield (4.4 mg): R_f (silica- CH_2Cl_2) = 0.32; ^1H NMR (400 MHz, CDCl_3): δ 9.02–8.98 (m, 2H), 8.53–8.51 (dd, $^3J = 8$, $^4J = 1.2$ Hz, 1H), 8.22 (m, 3H), 7.92–7.64 (m, 19H), 0.71 (s, 1H, exchangeable with D_2O), 0.52 (s, 1H, exchangeable with D_2O) ppm; ^{13}C NMR (100 MHz, CDCl_3): δ 193.8, 187.1, 185.7, 149.8, 149.3, 145.8, 144.4, 143.5, 142.6, 140.8, 138.3, 137.9, 137.5, 137.2, 135.5, 134.3, 133.3, 132.71, 132.55, 132.43, 130.45, 130.39, 128.89, 128.81, 128.62, 128.43, 127.84, 127.69, 127.64, 127.3, 123.3, 122.9, 117.1, 115.5, 111.7 ppm; UV-vis (CH_2Cl_2) λ_{max} (log ϵ) 395 (4.8), 463 (sh), 686 (3.8), 757 (sh), 825 (3.8) nm; FT-IR (neat, diamond ATR): $\nu_{\text{C=O}} = 1719 \text{ cm}^{-1}$; for full spectrum, see Figure S10; HR-MS (ESI $^+$, 100% CH_3CN , cone voltage = 30 V) m/e calcd for $\text{C}_{44}\text{H}_{26}\text{N}_5\text{O}_3$ ($[\text{M}\cdot\text{H}]^+$) 672.2056, found 672.2064.

2. Quinoline-Annulated Chlorins and Chlorin Analogues

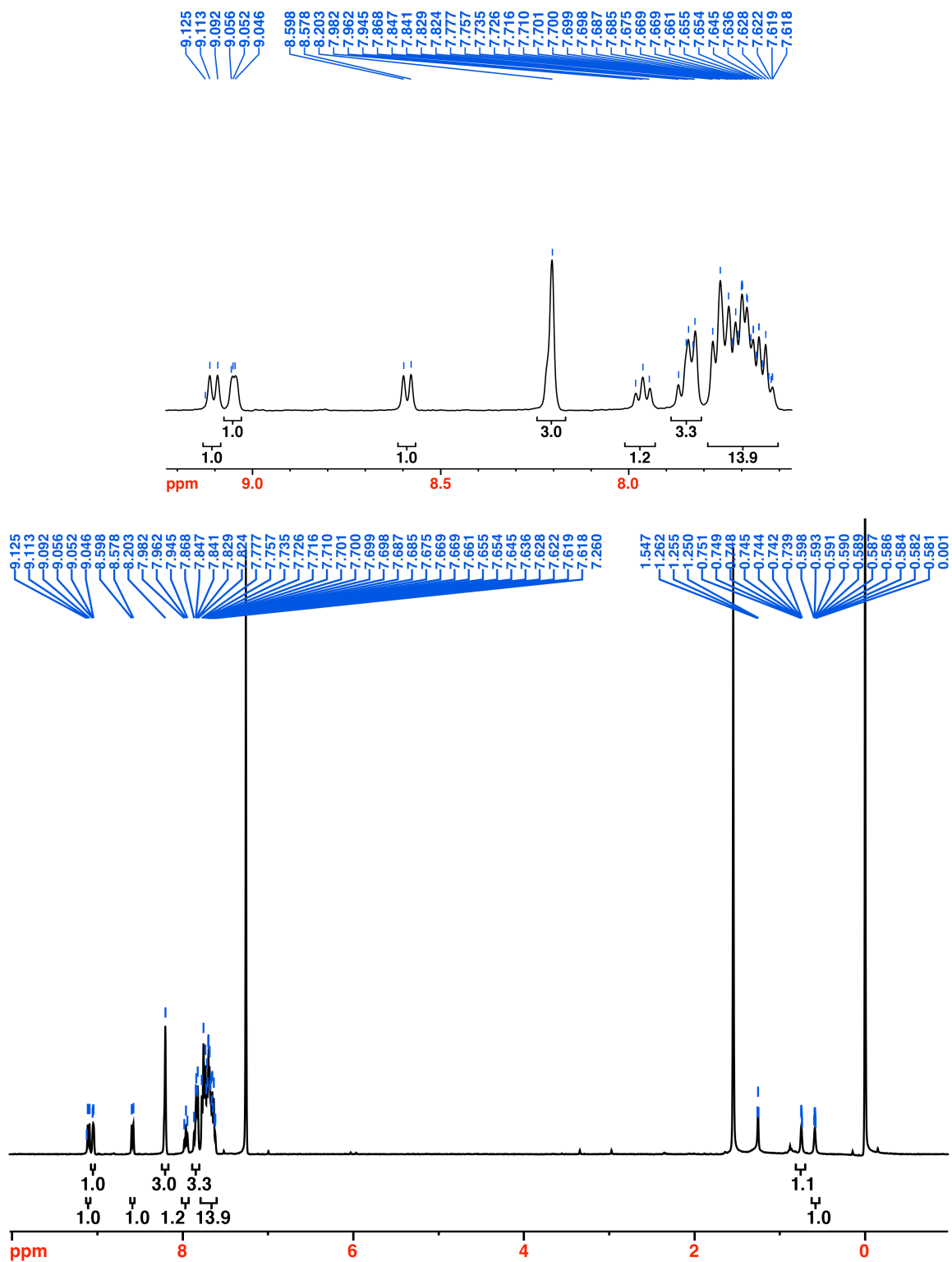


Figure 2-9. ^1H NMR (400 MHz, CDCl_3) of **14**

2. Quinoline-Annulated Chlorins and Chlorin Analogues

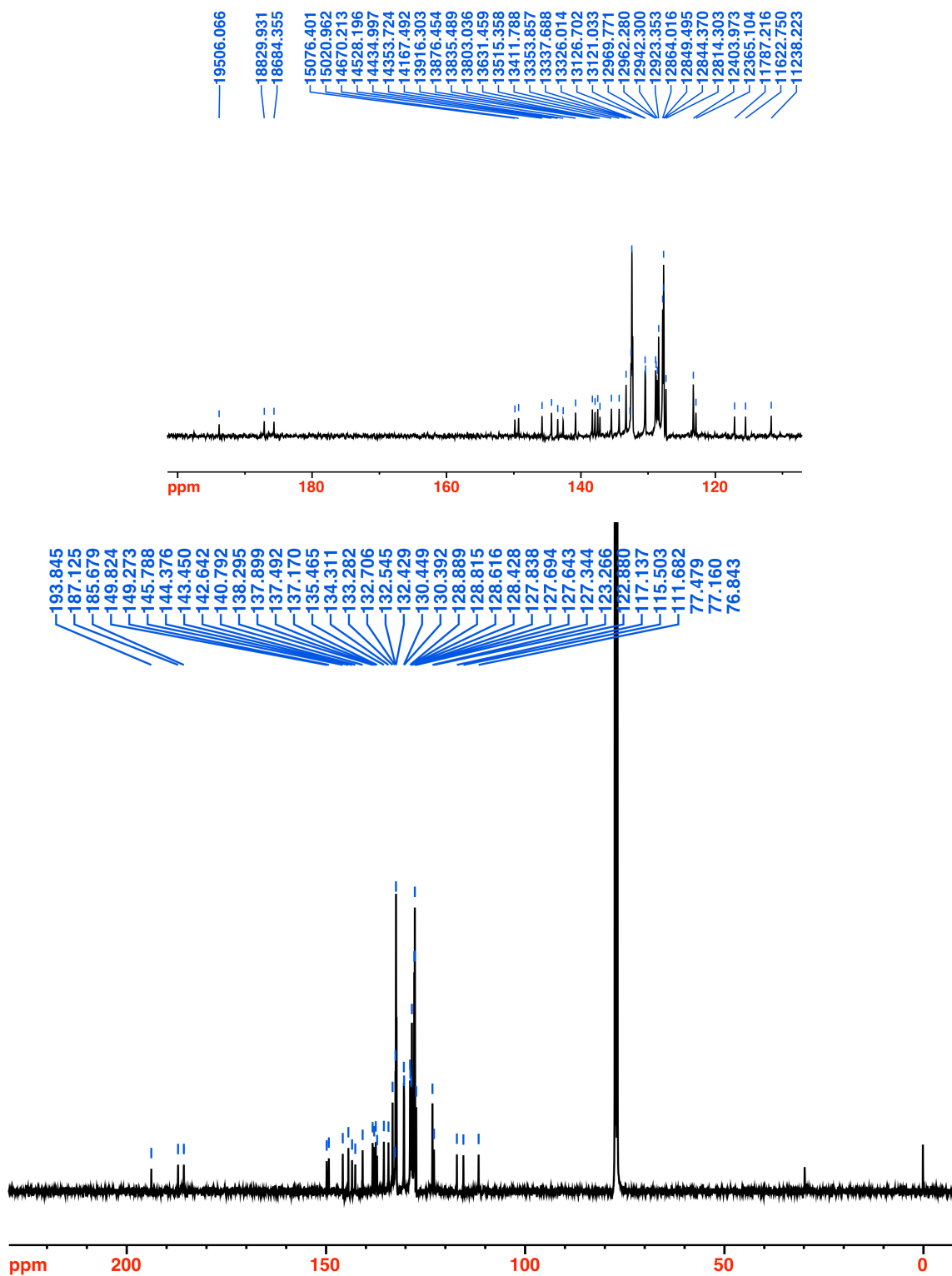


Figure 2-10. ^{13}C NMR spectrum (100 MHz, CDCl_3) of 14.

Quinoline-annulated porpholactone 15: To a solution of diol **13** (10.0 mg, 1.51×10^{-5} mol) in CHCl_3 (5 mL) in a round-bottom flask equipped with a stir bar was added cetyltrimethylammonium permanganate (CTAP,³³ 6.1 mg, 1.51×10^{-5} mol, ~5 equiv) and the mixture was stirred for 1 h at ambient temperature. The reaction was monitored by TLC for the disappearance of the starting material. If needed, additional oxidant was added after 1 h and until all starting material was consumed. The solution was then filtered through a short plug of silica gel, and the filter cake washed with CHCl_3 until the filtrate was colorless. The combined filtrates were evaporated to dryness by rotary evaporation. The residue was purified by preparative TLC (silica- CH_2Cl_2 /10% pet ether 30-60), followed by precipitation of the product by slow solvent exchange with pet ether 30-60 on the rotary evaporator to afford the 1:5 mixture of the two lactone isomers: R_f (silica- CH_2Cl_2) 0.47; ^1H NMR (400 MHz, CDCl_3): δ 9.20 (d, $^3J = 8.3$ Hz, 1H), 8.90 (two overlapping dd, $^3J = 4.5$, $^4J = 2.2$ Hz, 1H), 8.60 (dd, $^3J = 8.0$, $^4J = 1.1$ Hz, 1H), 8.22 (dd, $^3J = 5.2$, $^4J = 1.7$ Hz, 1H), 8.11 (dd, $^3J = 5.2$, $^4J = 1.7$ Hz, 1H), 8.04 (dd, $^3J = 4.6$, $^3J = 2.3$ Hz, 1H), 7.97–7.83 (m, 6H), 7.75–7.63 (m, 10H), 1.17 (s, 1H, exchangeable with D_2O), 1.60 (s, 1H, exchangeable with D_2O) ppm; ^{13}C NMR (100 MHz, CDCl_3): This compound possesses limited solubility even at elevated temperature, not allowing the recording of a well-resolved ^{13}C NMR spectrum; UV-vis (CH_2Cl_2) λ_{max} (log ϵ) 404 (5.09), 668 (4.05), 726 (4.00), 772 (3.89) nm; FT-IR (neat, diamond ATR): $\nu_{\text{C=O}} = 1756, 1724 \text{ cm}^{-1}$; for full spectrum, see Figure S13; HR-MS (ESI^+ , 100% CH_3CN , cone voltage = 30 V) m/e calcd for $\text{C}_{43}\text{H}_{26}\text{N}_5\text{O}_3$ ($[\text{M}\cdot\text{H}]^+$) 660.2036, found 660.2048.

2. Quinoline-Annulated Chlorins and Chlorin Analogues

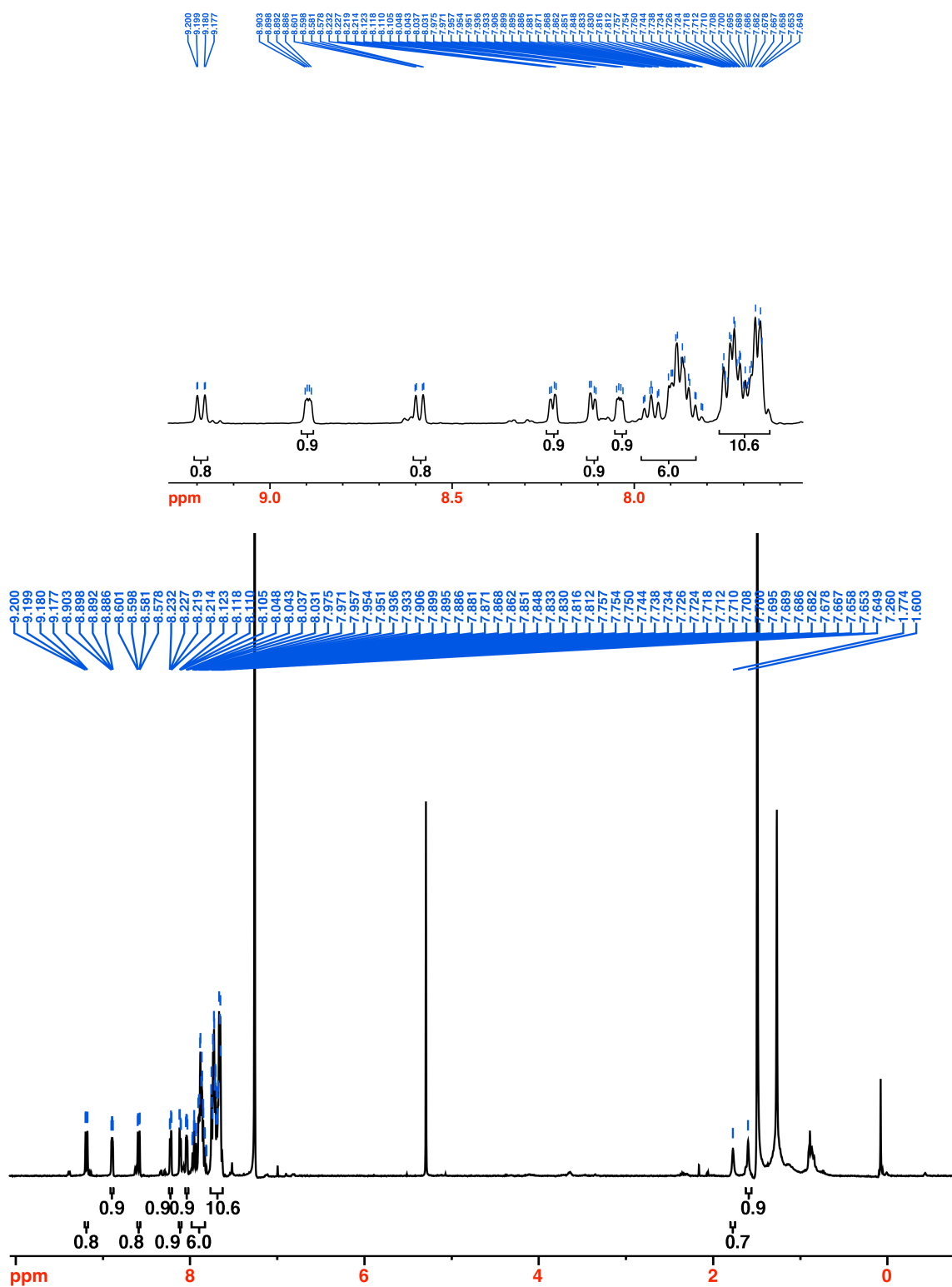


Figure 2-11. ^1H NMR spectrum (400 MHz, CDCl_3) of **15**.

2.4 References

- (1) a) Flitsch, W. *Adv. Heterocycl. Chem.* **1988**, *43*, 73; b) Montforts, F.-P.; Gerlach, B.; Hoeper, F. *Chem. Rev.* **1994**, *94*, 327; c) Montforts, F.-P.; Glasenapp-Breiling, M. *Prog. Heterocycl. Chem.* **1998**, *10*, 1; d) Galezowski, M.; Gryko, D. T. *Curr. Org. Chem.* **2007**, *11*, 1310; e) Brückner, C.; Samankumara, L.; Ogikubo, J. In *Handbook of Porphyrin Science*; Kadish, K. M., Smith, K. M., Guillard, R., Eds.; World Scientific: River Edge, NY, 2012; Vol. 17 (Synthetic Developments, Part II; Chapter 76), p 1; f) Lindsey, J. S. *Chem. Rev.* **2015**, *115*, 6534.
- (2) Silva, A. M. G.; Tome, A. C.; Neves, M. G. P. M. S.; Silva, A. M. S.; Cavaleiro, J. A. S. *J. Org. Chem.* **2005**, *70*, 2306.
- (3) Laha, J. K.; Muthiah, C.; Taniguchi, M.; McDowell, B. E.; Ptaszek, M.; Lindsey, J. S. *J. Org. Chem.* **2006**, *71*, 4092.
- (4) Vitasovic, M.; Gouterman, M.; Linschitz, H. *J. Porphyrins Phthalocyanines* **2001**, *5*, 191.
- (5) Lindsey, J. S. In *The Porphyrin Handbook*; Kadish, K. M., Smith, K. M., Guillard, R., Eds.; Academic Press: San Diego, 2000; Vol. 1, p 45.
- (6) a) Gupta, I.; Hung, C.-H.; Ravikanth, M. *Eur. J. Org. Chem.* **2003**, 4392; b) Gupta, I.; Ravikanth, M. *J. Photochem. Photobiol., A* **2006**, *177*, 156; c) Brückner, C.; Foss, P. C. D.; Sullivan, J. O.; Pelto, R.; Zeller, M.; Birge, R. R.; Crundwell, G. *Phys. Chem. Chem. Phys.* **2006**, *8*, 2402; d) Greco, J. A.; Rossi, A.; Birge, R. R.; Brückner, C. *Photochem. Photobiol.* **2014**, *90*, 402.
- (7) Ke, X.-S.; Chang, Y.; Chen, J.-Z.; Tian, J.; Mack, J.; Cheng, X.; Shen, Z.; Zhang, J.-L. *J. Am. Chem. Soc.* **2014**, *136*, 9598.
- (8) a) Davis, N. K. S.; Thompson, A. L.; Anderson, H. L. *Org. Lett.* **2010**, *12*, 2124; b) Davis, N. K. S.; Thompson, A. L.; Anderson, H. L. *J. Am. Chem. Soc.* **2011**, *133*, 30.
- (9) Samankumara, L. P.; Dorazio, S. J.; Akhigbe, J.; Li, R.; Nimthong-Roldán, A.; Zeller, M.; Brückner, C. *Chem. – Eur. J.* **2015**, *21*, 11118.
- (10) Hyland, M. A.; Morton, M. D.; Brückner, C. *J. Org. Chem.* **2012**, *77*, 3038.
- (11) a) Ravikanth, M.; Chandrashekar, T. K. *Struct. Bonding (Berlin)* **1995**, *82*, 105; b) Shelnutt, J. A.; Song, X.-Z.; Ma, J.-G.; Jentzen, W.; Medforth, C. J. *Chem. Soc. Rev.* **1998**, *27*, 31; c) Ryeng, H.; Ghosh, A. *J. Am. Chem. Soc.* **2002**, *124*, 8099.
- (12) Akhigbe, J.; Luciano, M.; Zeller, M.; Brückner, C. *J. Org. Chem.* **2015**, *80*, 499.
- (13) Akhigbe, J.; Zeller, M.; Brückner, C. *Org. Lett.* **2011**, *13*, 1322.

- (14) a) Daniell, H. W.; Williams, S. C.; Jenkins, H. A.; Brückner, C. *Tetrahedron Lett.* **2003**, *44*, 4045; b) Crossley, M. J.; King, L. G. *Journal of the Chemical Society, Chemical Communications* **1984**, 920; c) Crossley, M. J.; Burn, P. L.; Langford, S. J.; Pyke, S. M.; Stark, A. G. *J. Chem. Soc., Chem. Commun.* **1991**, 1567; d) Starnes, S. D.; Arungundram, S.; Saunders, C. H. *Tetrahedron Lett.* **2002**, *43*, 7785.
- (15) Jeandon, C.; Ruppert, R. *Eur. J. Org. Chem.* **2011**, 4098.
- (16) Abuteen, A.; Zanganeh, S.; Akhigbe, J.; Samankumara, L. P.; Aguirre, A.; Biswal, N.; Braune, M.; Vollertsen, A.; Röder, B.; Brückner, C.; Zhu, Q. *Phys. Chem. Chem. Phys.* **2013**, *15*, 18502.
- (17) a) Kim, C.; Favazza, C.; Wang, L. V. *Chem. Rev.* **2010**, *110*, 2756; b) Wang, L. V. *Nature Photonics* **2009**, *3*, 503.
- (18) Brückner, C.; Rettig, S. J.; Dolphin, D. *J. Org. Chem.* **1998**, *63*, 2094.
- (19) Banerjee, S.; Zeller, M.; Brückner, C. *J. Org. Chem.* **2010**, *75*, 1179.
- (20) a) Wu, Y.-D.; Chan, K. W. K.; Yip, C.-P.; Vogel, E.; Plattner, D. A.; Houk, K. N. *J. Org. Chem.* **1997**, *62*, 9240; b) Stepien, M.; Latos-Grazynski, L. *Top. Heterocycl. Chem.* **2009**, *19*, 83.
- (21) Imahori, H.; Iijima, H.; Hayashi, H.; Toude, Y.; Umeyama, T.; Matano, Y.; Ito, S. *ChemSusChem* **2011**, *4*, 797.
- (22) Akhigbe, J.; Haskoor, J. P.; Krause, J. A.; Zeller, M.; Brückner, C. *Org. Biomol. Chem.* **2013**, *11*, 3616.
- (23) Bruhn, T.; Brückner, C. *J. Org. Chem.* **2015**, *80*, 4861.
- (24) Gouterman, M. In *The Porphyrins*; Dolphin, D., Ed.; Academic Press: New York, 1978; Vol. 3, p 1.
- (25) Starnes, S. D.; Rudkevich, D. M.; Rebek Jr., J. *J. Am. Chem. Soc.* **2001**, *123*, 4659.
- (26) Brückner, C.; McCarthy, J. R.; Daniell, H. W.; Pendon, Z. D.; Ilagan, R. P.; Francis, T. M.; Ren, L.; Birge, R. R.; Frank, H. A. *Chem. Phys.* **2003**, *294*, 285.
- (27) a) Gouterman, M.; Hall, R. J.; Khalil, G. E.; Martin, P. C.; Shankland, E. G.; Cerny, R. L. *J. Am. Chem. Soc.* **1989**, *111*, 3702; b) Jayaraj, K.; Gold, A.; Austin, R. N.; Ball, L. M.; Turner, J.; Mandon, D.; Weiss, R.; Fischer, J.; DeCian, A.; Bill, E.; Müther, M.; Schünemann, V.; Trautwein, A. X. *Inorg. Chem.* **1997**, *36*, 4555; c) Lv, H.; Yang, B.; Jing, J.; Yu, Y.; Zhang, J.; Zhang, J.-L. *Dalton Trans.* **2012**, *41*, 3116; d) Yu, Y.; Lv, H.; Ke, X.; Yang, B.; Zhang, J.-L. *Adv. Synth. Catal.* **2012**, *354*, 3509.
- (28) a) McCarthy, J. R.; Jenkins, H. A.; Brückner, C. *Org. Lett.* **2003**, *5*, 19; b) Brückner, C.; Ogikubo, J.; McCarthy, J. R.; Akhigbe, J.; Hyland, M. A.; Daddario, P.; Worlinsky, J. L.;

- Zeller, M.; Engle, J. T.; Ziegler, C. J.; Ranaghan, M. J.; Sandberg, M. N.; Birge, R. R. *J. Org. Chem.* **2012**, *77*, 6480.
- (29) Ogikubo, J.; Meehan, E.; Engle, J. T.; Ziegler, C. J.; Brückner, C. *J. Org. Chem.* **2013**, *78*, 2840.
- (30) Akhigbe, J.; Ryppa, C.; Zeller, M.; Brückner, C. *J. Org. Chem.* **2009**, *74*, 4927.
- (31) Kratky, C.; Waditschatka, R.; Angst, C.; Johansen, J. E.; Plaquevent, J. C.; Schreiber, J.; Eschenmoser, A. *Helv. Chim. Acta* **1985**, *68*, 1312.
- (32) Samankumara, L. P.; Zeller, M.; Krause, J. A.; Brückner, C. *Org. Biomol. Chem.* **2010**, *8*, 1951.
- (33) Furniss, B.S.; Hannaford, A.J.; Smith, P.W.G.; Tatchell, A.R. *Vogel's Textbook of Practical Organic Chemistry*, Longman: Essex, GB, 5th Edition, 1989, p. 549.

3 Platinum Complexes of Quinoline-Annulated Porphyrins as NIR Emitters

Dyes with pO_2 -dependent emission are desirable for a number of applications such as luminophores in pressure-sensitive paints and as optical O_2 sensors in biomedical applications.¹ The Stern-Volmer relationship describes the underlying mechanism of function of these dyes: If a triplet-state dye collides with a triplet state oxygen molecule (3O_2), singlet oxygen (1O_2) is generated, and the regular phosphorescence of the dye is quenched. Platinum and palladium porphyrins in particular show promise as dyes to measure any O_2 tension due to their efficient intersystem crossing (ISC) quantum yields into the triplet state, long triplet excited state lifetimes and high quantum yields of phosphorescence.²

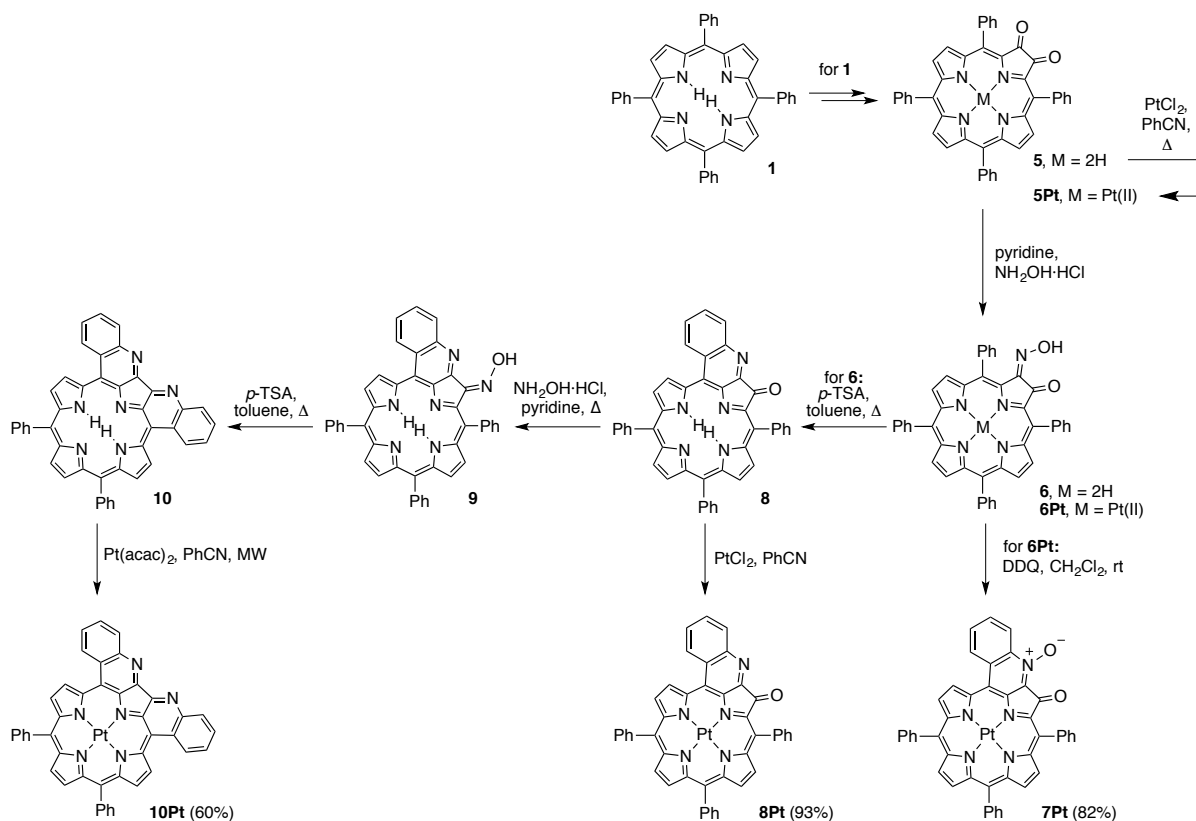
For a metalloporphyrin-based O_2 sensor to find use in biomedical applications *in vivo* it must absorb light within the optical window of tissue (i.e. > 700 nm), have emission in the NIR and have an excited-state that is quenched by O_2 . Toward this end, various Pt and Pd tetrabenzos- and tetranaphtholporphyrin derivatives have been prepared.³ However, difficult syntheses and poor solubility largely prevented the further evaluation of these types of chromophores.

We found that the platinum complexes of our own quinoline annulated porphyrins, which are prepared in two steps from the well-known dioxoporphyrin **5**,⁴ possess strong NIR emission (at 77 K). We report here the synthesis, characterization and photophysics for the quinoline-annulated porphyrin-Pt complexes as NIR emitters with the potential for use as novel O_2 sensors.

3.1 Results and Discussion

3.1.1 Synthesis

Insertion of platinum(II) into the known free bases tetraphenyl-2,3-dioxochlorin **5** and mono- and bisquinoline-annulated porphyrins **9** and **10**, all synthesized along established pathways,⁴ and using standard reaction conditions,⁵ generated the corresponding platinum complexes **5Pt**, **9Pt**, and **10Pt**, respectively (Scheme 1).



Scheme 3-1. Synthesis of quinoline-annulated porphyrin Pt-complexes.

Metal insertion was generally facile, likely assisted by the pronounced non-planarity of the chromophores.^{4b} When subjected to platinum(II) insertion conditions (or the insertion of nickel(II) or even zinc(II)), the *N*-oxide of the quinoline-annulated porphyrin *N*-oxide **7** is lost.^{4b,6} Hence, the synthesis of *N*-oxide platinum complex **7Pt** required a synthetic path that involved an early

insertion of platinum. Thus, [tetraphenyl-2,3-dioxochlorinato]platinum(II) **5Pt** served as the starting material. This metallodione was then manipulated along an established reaction sequence: Formation of oxime **6Pt**, followed by DDQ-induced oxidative ring-closure to form quinoline-annulated porphyrin *N*-oxide platinum(II) complex **7Pt**. The platinum complexes possessed all the expected spectroscopic properties. Most ^1H NMR spectroscopic data of the platinum complexes are very similar to those of the corresponding nickel(II) or palladium(II) complexes, also suggesting that the platinum complexes assume the non-planar conformations of their congeners.

3.1.2 Optical Properties and Photophysics

Similar to the observation for the free base species, the quinoline-annulated porphyrin platinum complexes **7Pt**, **8Pt**, **10Pt** all possess bathochromically shifted UV-vis spectra, which we attribute to the increase in π -conjugation of the chromophores, as well as their inferred non-planarity. Compared with the other previously prepared group 10 metal complexes (Ni, Pd) as well as the free base **8**, the UV-vis spectrum of **8Pt** is also relatively unchanged upon metal insertion, with no observed shift in the solet band and side bands. On the other hand, the bis-quinoline fused **10Pt** exhibits the expected reduction in the number of side bands, as well as a split solet band, similar to other group 10 metal complexes of **10**.^{4b}

Table 3-1. Photophysical data for dione **5Pt** and the quinoline-annulated porphyrin Pt complexes.

Compound	$\lambda_{\text{max,abs}}/\text{nm}^a$	$\log \epsilon$ at $\lambda_{\text{max}}/\text{cm}^{-1} \text{ M}^{-1a}$	$\lambda_{\text{max,em}}/\text{nm}^b$	$\phi_{\text{PH}}/\%^b$	$\tau_{\text{T1}}/\mu\text{s}^c$
5Pt	~524-815 ^d	- ^e	733	55	71
7Pt	702	4.33	1000	1	0.43
8Pt	720	4.05	945, 1062	2	0.53
10Pt	717	3.99	944, 1073	7	1.7

^a in CH_2Cl_2 , ^b $\lambda_{\text{excitation}} = \lambda_{\text{solet}}$ ^c EtOH, glass, 77K ^d broad, featureless absorption ^e not measured

3. Platinum Complexes of Quinoline-Annulated Porphyrins as NIR Emitters

Key photophysical properties for the platinum complexes are listed in Table 3-1. All of the quinoline-annulated porphyrin Pt complexes possess the NIR emission expected for Pt porphyrins,² with $\lambda_{\text{emission}}$ values well into the NIR region for quinoline-annulated porphyrin platinum complexes **7Pt**, **8Pt** and **10Pt**.

The ϕ_{Ph} and τ_{T1} were also determined for the Pt complexes. Of the quinoline-annulated porphyrin platinum complexes, **10Pt** stands out as a potentially useful luminophor for O₂ sensing applications due to its bright emission in the NIR with a phosphorescence quantum yield (ϕ_{Ph}) of 7%, and a long excited-state triplet lifetime (τ_{T1}) of 1.7 μs .

3.2 Conclusions

In conclusion, the platinum complexes of the NIR absorbing quinoline-annulated porphyrins were prepared using standard conditions. Like their free base counterparts, they possess long wavelength absorption within the optical window of tissue, and similar UV-vis spectra as the other previously prepared group 10 metal complexes. However, unlike their free base counterparts, they exhibit emission well into the NIR region. Particularly bis-quinoline-fused porphyrin **10Pt** possesses bright NIR emission and relatively long excited-state lifetime, suggesting it as a potentially most useful chromophore. The preparation of a water-soluble derivative of **10Pt** is currently underway for the biological testing of this novel NIR emitting and oxygen partial pressure-sensitive dye.

3.3 Experimental Section

3.3.1 Materials and Instruments

All reagents and solvents were from commercial sources and used without prior purification. Platinum dione **5Pt** and oxime **6Pt**⁷, free-base dione **5**⁸, and free-base annulated quinolines **8** and **9**^{4b} were prepared as described previously (Scheme 1). Aluminum-backed, silica gel 60, 250 μm thickness analytical plates were used for analytical TLC; 20 \times 20 cm, glass-backed, silica gel 60, 500 μm thickness preparative TLC plates, and standard grade, 60 Å, 32–63 μm flash column silica gel were used for preparative chromatography.

¹H and ¹³C NMR spectra were recorded on a Bruker 400 MHz instrument in the solvents indicated, and were referenced to residual solvent peaks. High and low resolution mass spectra were provided by the Mass Spectrometry Facility, Department of Chemistry, University of Connecticut. The microwave synthesizer used was a discover microwave reactor.

3.3.2 Synthesis and Characterization

[meso-Triphenyl-monoquinoline-annulated oxo-porphyrinato-*N*-oxide]platinum(II) (7Pt). Monooxime **6Pt** (20.2 mg, 2.37×10^{-5} mol) was dissolved in CH_2Cl_2 (10.0 mL) in a round-bottom flask equipped with a magnetic stirring bar. DDQ (11 mg, 4.7×10^{-5} mol, 2 equiv) was added and the mixture was stirred for 30 min. When the starting material was consumed (reaction control by TLC), the reaction mixture was filtered through a short plug of silica gel to removed excess DDQ/the corresponding hydroquinone. The filtrate was washed with water (2 \times 10 mL), dried over anhyd Na_2SO_4 , evaporated to dryness by rotary evaporation, and the residue was purified by preparative TLC (CH_2Cl_2 /2% MeOH). After solvent exchange of the extracted main green band with MeOH, **7Pt** was isolated by filtration in 82% yield as a green powder: R_f (silica- CH_2Cl_2 /5% MeOH) = 0.55; ¹H NMR (400 MHz, CDCl_3): δ 9.09 (d, ³ J = 5.2 Hz, 1H), 8.88, (d, ³ J = 8.5 Hz, 1H), 8.70 (d, ³ J = 8.1 Hz, 1H), 8.57 (d, ³ J = 5.0 Hz, 1H), 8.36, 8.33, 8.31 (three

3. Platinum Complexes of Quinoline-Annulated Porphyrins as NIR Emitters

overlapping d, $^3J = 5.0$ Hz, 3H), 8.21 (d, $^3J = 5.0$ Hz, 1H), 8.04 (dd, $^3J = 6.3$ Hz, $^4J = 1.5$ Hz, 2H), 7.99 (dd, $^3J = 6.2$ Hz, $^4J = 1.6$ Hz, 2H), 7.83 (t, $^3J = 7.8$ Hz, 1H) 7.77 – 7.66 (m, 12H) ppm; ^{13}C NMR (100 MHz, CDCl_3): δ 180.7, 147.5, 141.4, 141.0, 140.1, 140.0, 139.9, 138.2, 137.5, 136.2, 134.9, 134.6, 133.6, 133.4, 133.1, 131.9, 131.7, 130.9, 130.0, 129.9, 129.7, 129.5, 129.0, 128.7, 128.6, 128.4, 128.0, 127.9, 127.7, 127.5, 125.9, 121.6, 118.4, 103.3 ppm; UV-vis (CHCl_2) λ_{max} (log ϵ) 408 (5.33), 475 (4.59), 650 (sh), 702 (4.33) nm; FT-IR (neat, diamond ATR): 1695.4 ($\nu_{\text{C=O}}$) cm^{-1} ; MS (DART $^+$, orifice voltage = 20 V, 100% CH_3CN) m/e calcd for $\text{C}_{44}\text{H}_{25}\text{N}_5\text{O}_2\text{Pt}$ 851.1738 ($[\text{M.H}]^+$), found 851.1719.

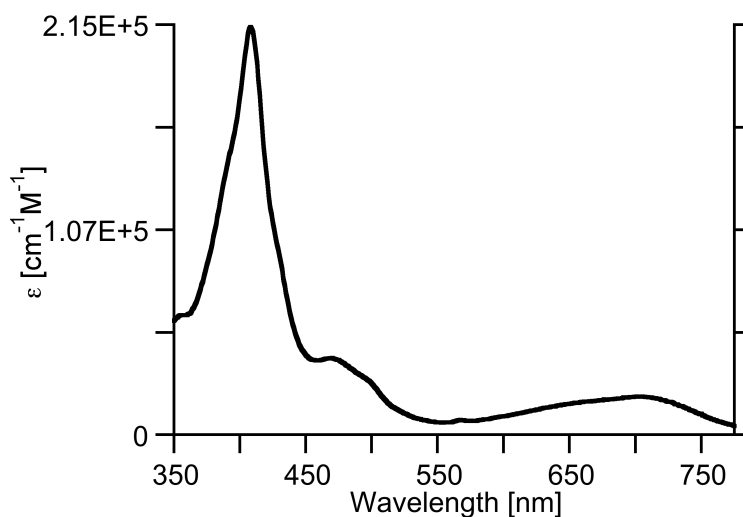


Figure 3-1. UV-vis spectrum (CH_2Cl_2) of **7Pt**.

3. Platinum Complexes of Quinoline-Annulated Porphyrins as NIR Emitters

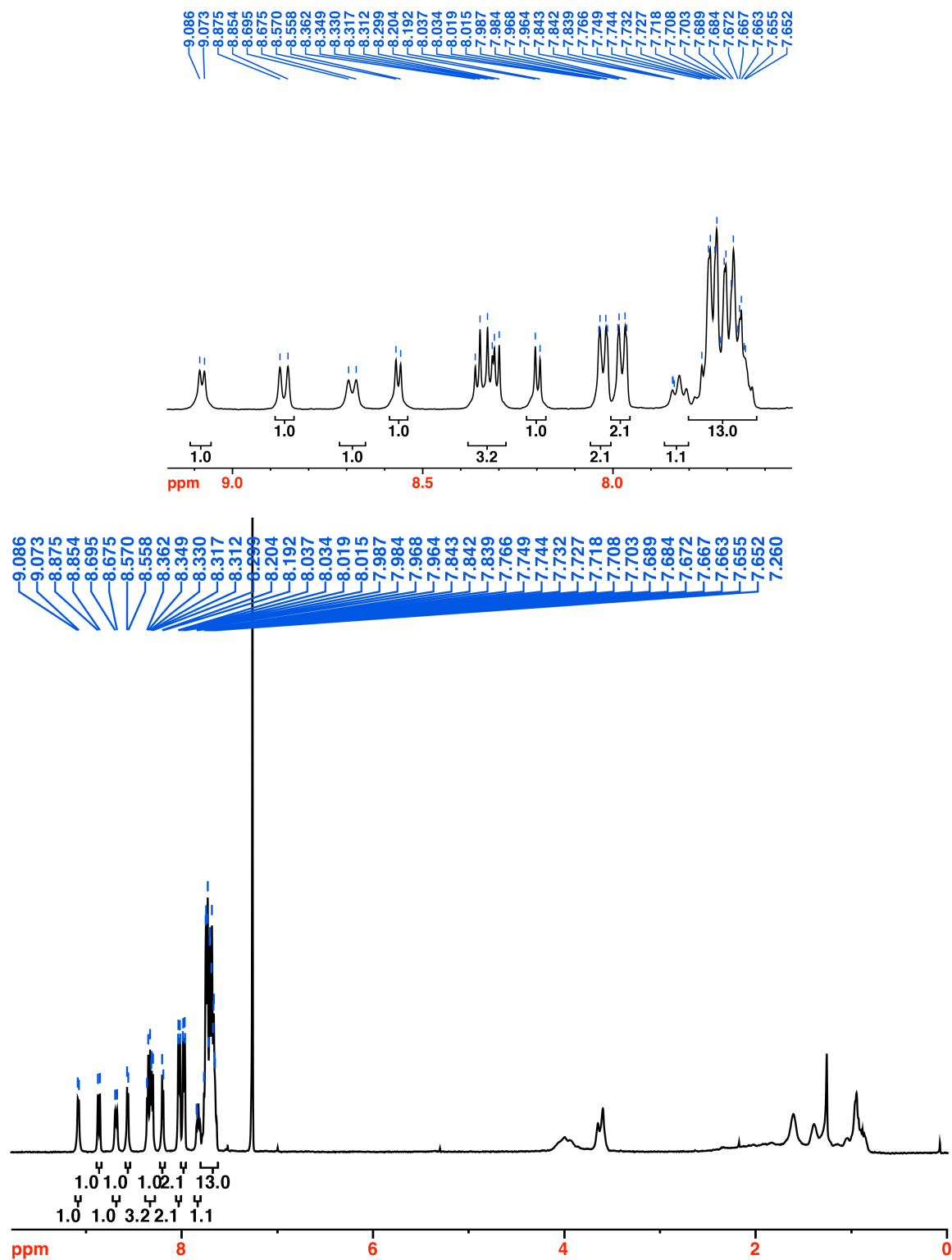


Figure 3-2. ^1H NMR spectrum (400 MHz, CDCl_3) of **7Pt**.

3. Platinum Complexes of Quinoline-Annulated Porphyrins as NIR Emitters

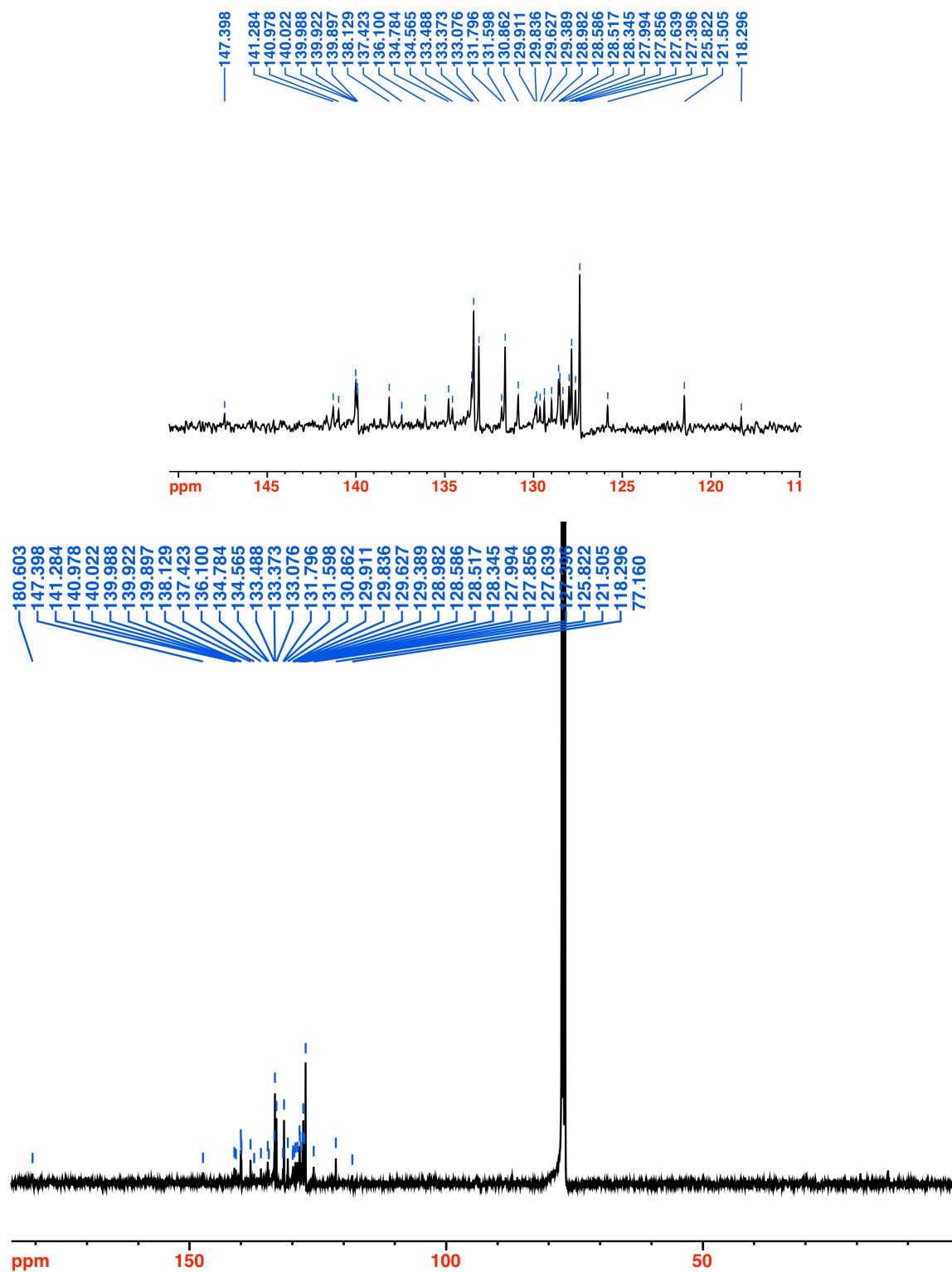


Figure 3-3. ^{13}C NMR spectrum (100 MHz, CDCl_3) of 7Pt.

[meso-Triphenyl-monoquinoline-fused oxoporphyrinato]platinum(II) (8Pt). Free base mono-quinoline-fused oxo-porphyrin **8** (17.7 mg, 2.76×10^{-5} mol) was dissolved in PhCN (5 mL) and added to a hot solution of PhCN (15 mL) and platinum(II) chloride (PtCl_2 , 29.3 mg, 1.10×10^{-4} mol, 4.0 equiv) in a round-bottom flask equipped with a magnetic stir bar and N_2 gas inlet. The mixture was heated to reflux for 2 h. When the starting material was consumed (reaction control by UV-vis and TLC), the resulting mixture was allowed to cool to room temperature, the solvent was removed in *vacuo* and taken up in CH_2Cl_2 . The main product was isolated and purified by a flash column chromatography ($\text{CH}_2\text{Cl}_2/0.5\%$ MeOH), followed by recrystallized by solvent exchange into MeOH to provide **8Pt** as a light green powder in 93% yield. R_f (silica- CH_2Cl_2) 0.30; ^1H NMR (400 MHz, CDCl_3): δ 8.98 (d, $^3J = 4.7$ Hz, 1H), 8.65 (d, $^3J = 8.2$ Hz, 1H), 8.42 (t, 2H), 8.24 – 8.19 (overlapping s and d, $^3J = 5.0$ Hz, 3H), 8.10 (d, $^3J = 5.0$ Hz, 1H), 8.00 (d, $^3J = 7.0$ Hz, 2H), 7.93 (d, $^3J = 6.7$ Hz, 2H), 7.74 – 7.60 (m, 13H) ppm; ^{13}C NMR (100 MHz, CDCl_3): δ 190.5, 150.0, 148.6, 145.2, 141.4, 140.5, 140.0, 139.9, 139.5, 138.0, 137.3, 135.5, 134.5, 134.1, 133.9, 133.3, 133.2, 133.1, 132.9, 132.8, 132.1, 131.8, 129.8, 129.3, 129.3, 129.1, 128.7, 128.6, 128.3, 128.1, 127.9, 127.8, 127.5, 127.3, 127.1, 125.3, 117.3, 110.8 ppm; UV-vis (CHCl_3) λ_{max} (log ϵ) 399 (5.07), 462 (4.38), 492 (4.24), 668 (sh), 720 (4.05) nm; FT-IR (neat, diamond ATR): 1714.7 ($\nu_{\text{C=O}}$) cm^{-1} ; MS (DART $^+$, orifice voltage = 20 V, 100% CH_3CN) m/e calcd for $\text{C}_{44}\text{H}_{25}\text{N}_5\text{OPt}$ 835.1788 ($[\text{M.H}]^+$), found 835.1779.

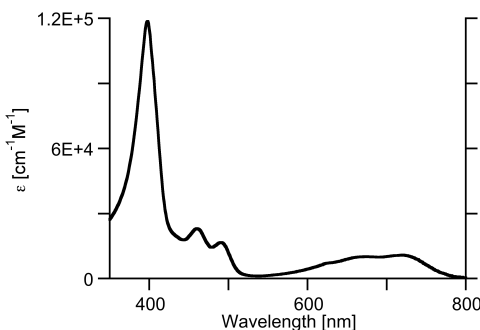


Figure 3-4. UV-vis spectrum (CH_2Cl_2) of **8Pt**.

3. Platinum Complexes of Quinoline-Annulated Porphyrins as NIR Emitters

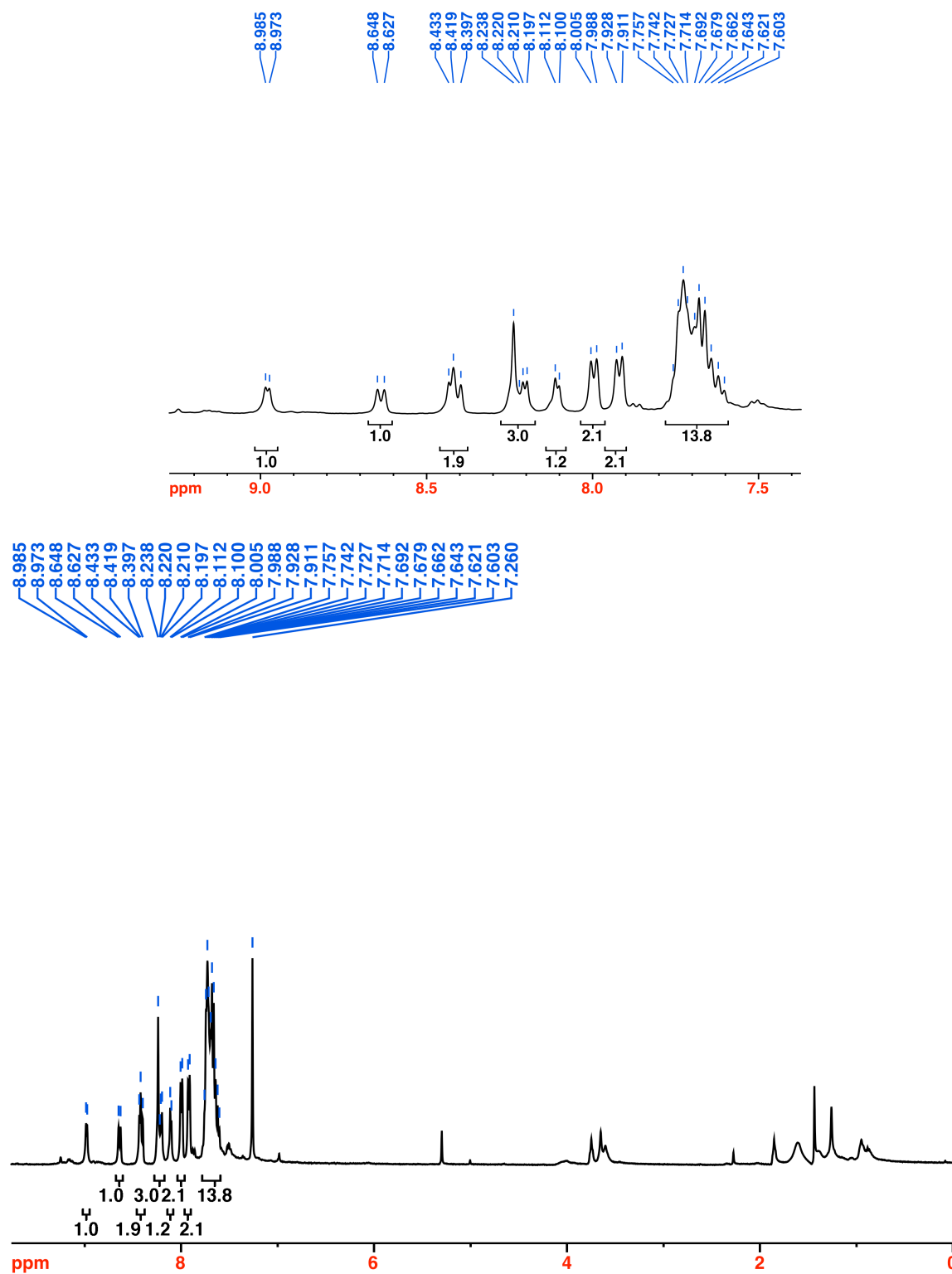


Figure 3-5. ^1H NMR spectrum (400 MHz, CDCl_3) of **8Pt**.

3. Platinum Complexes of Quinoline-Annulated Porphyrins as NIR Emitters

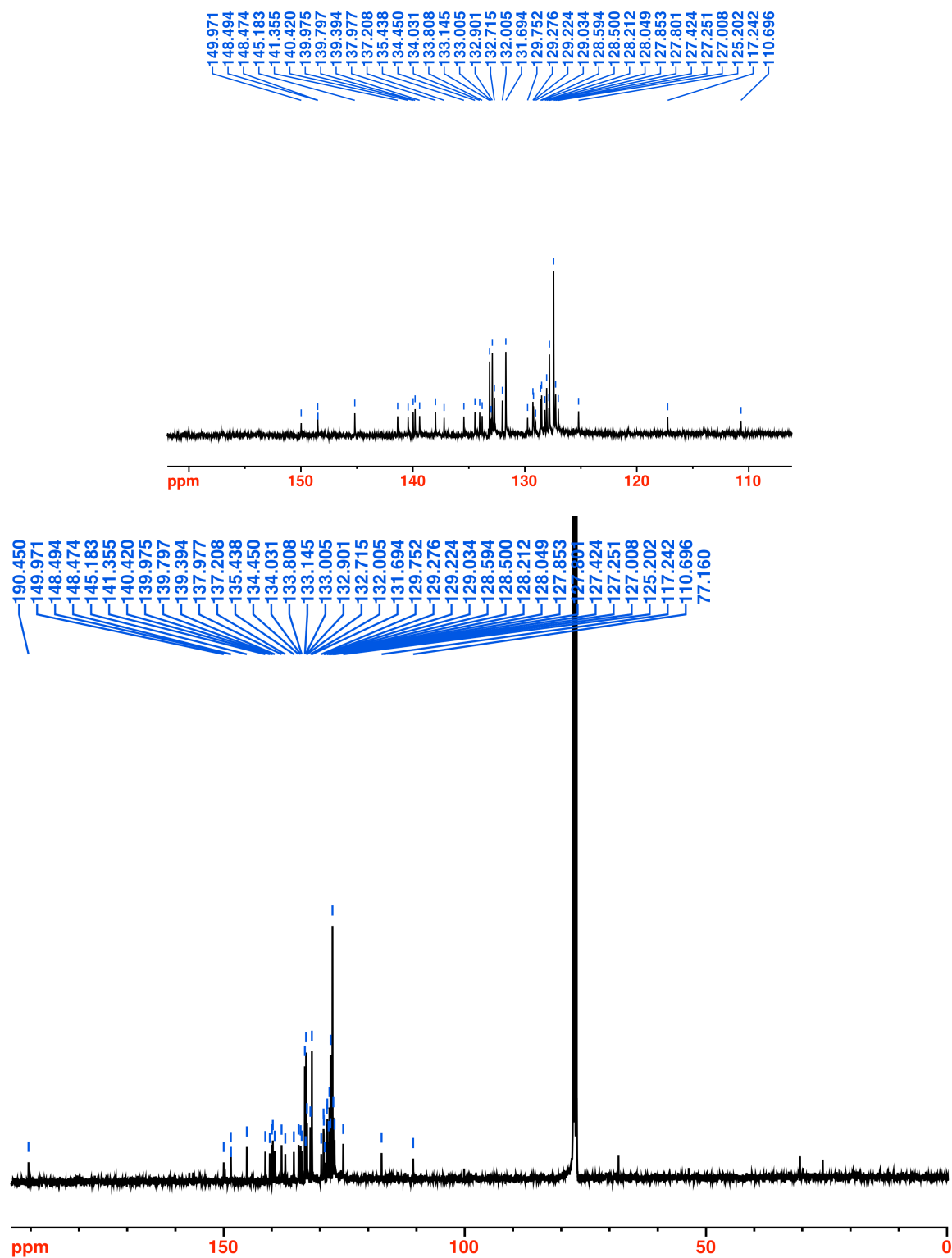


Figure 3-6. ¹³C NMR spectrum (100 MHz, CDCl₃) of 8Pt.

[meso-Diphenyl-bis-quinoline-fused porphyrinato]platinum(II) (10Pt). Free base bisquinoline-annulated porphyrin **10** (11.6 mg, 1.8×10^{-5} mol) was dissolved in PhCN (2.7 mL) in a thick-walled glass tube equipped with a magnetic stir bar. Pt(acac)₂ (22 mg, 5.4×10^{-5} mol, 3 equiv) was added, and the vessel was sealed and placed in a microwave cavity. Using an initial microwave power of 300 W, the contents of the reaction vessel were heated to 250 °C where it was held for 20 min. Upon completion, the vessel was cooled to ambient temperature. The solvent was evaporated and the residue was separated on a preparative TLC plate (CH₂Cl₂/5% MeOH) to provide **10Pt** as a bright green solid in 60% yield (9.1 mg). *R_f* (silica-CH₂Cl₂/5% MeOH) = 0.51; (400 MHz; CD₂Cl₂): δ 8.29 (d, ³*J* = 4.0 Hz, 1H), 8.21 (two overlapping d, ³*J* = 6.7 Hz, 2H), 7.83 (s, 1H), 7.76-7.61 (m, 8H) ppm; ¹³C NMR (100 MHz, CD₂Cl₂): δ 149.6, 143.89, 143.73, 139.3, 139.0, 134.27, 134.10, 133.0, 132.0, 131.4, 129.8, 129.0, 128.1, 127.5, 127.0, 126.9, 125.7, 124.3, 124.2, 108.6 ppm; UV-vis (CH₂Cl₂) λ_{max} (log ε) 399 (4.46), 455 (4.20), 658 (3.66), 717 (3.99) nm; HR-MS (ESI⁺, 100% CH₃CN, TOF) *m/z* calcd for C₄₄H₂₅N₆Pt ([M·H]⁺), 832.1792 found 832.1769.

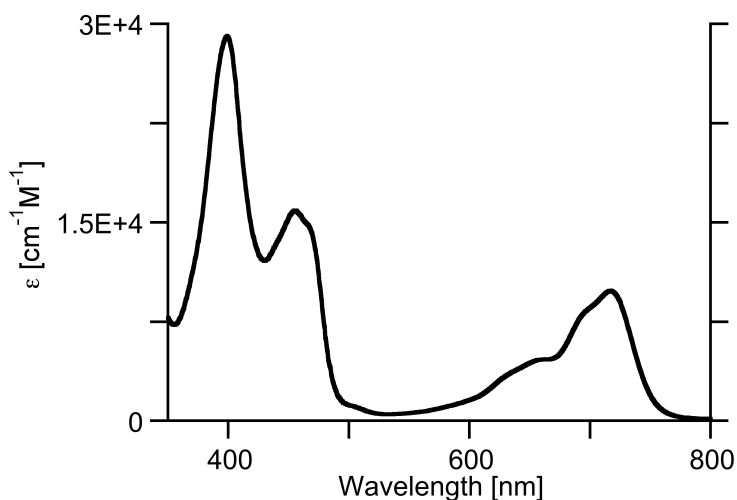


Figure 3-7. UV-vis spectrum (CH₂Cl₂) of **10Pt**.

3. Platinum Complexes of Quinoline-Annulated Porphyrins as NIR Emitters

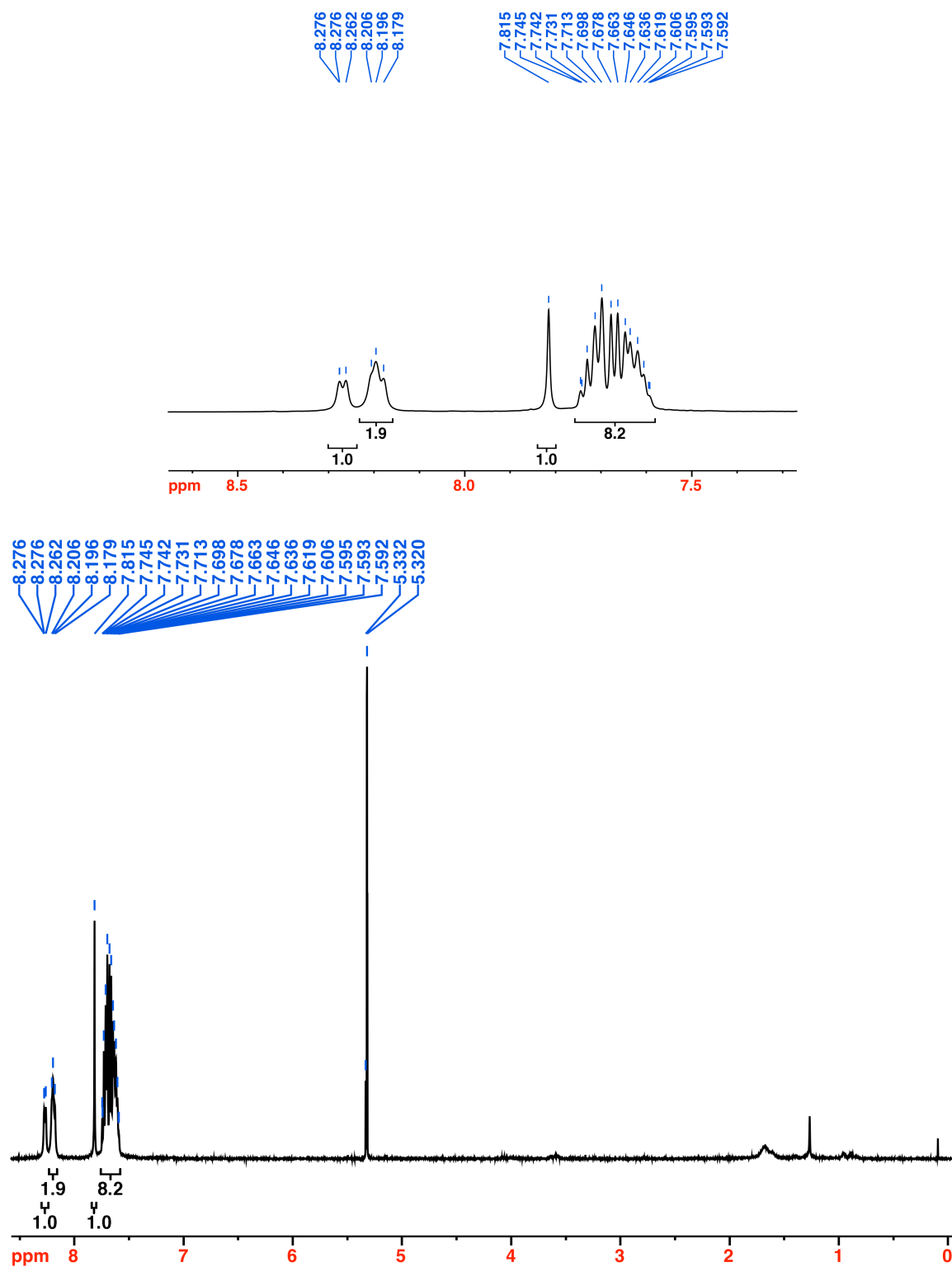


Figure 3-8. ^1H NMR spectrum (400 MHz, CDCl_3) of **10Pt**.

3. Platinum Complexes of Quinoline-Annulated Porphyrins as NIR Emitters

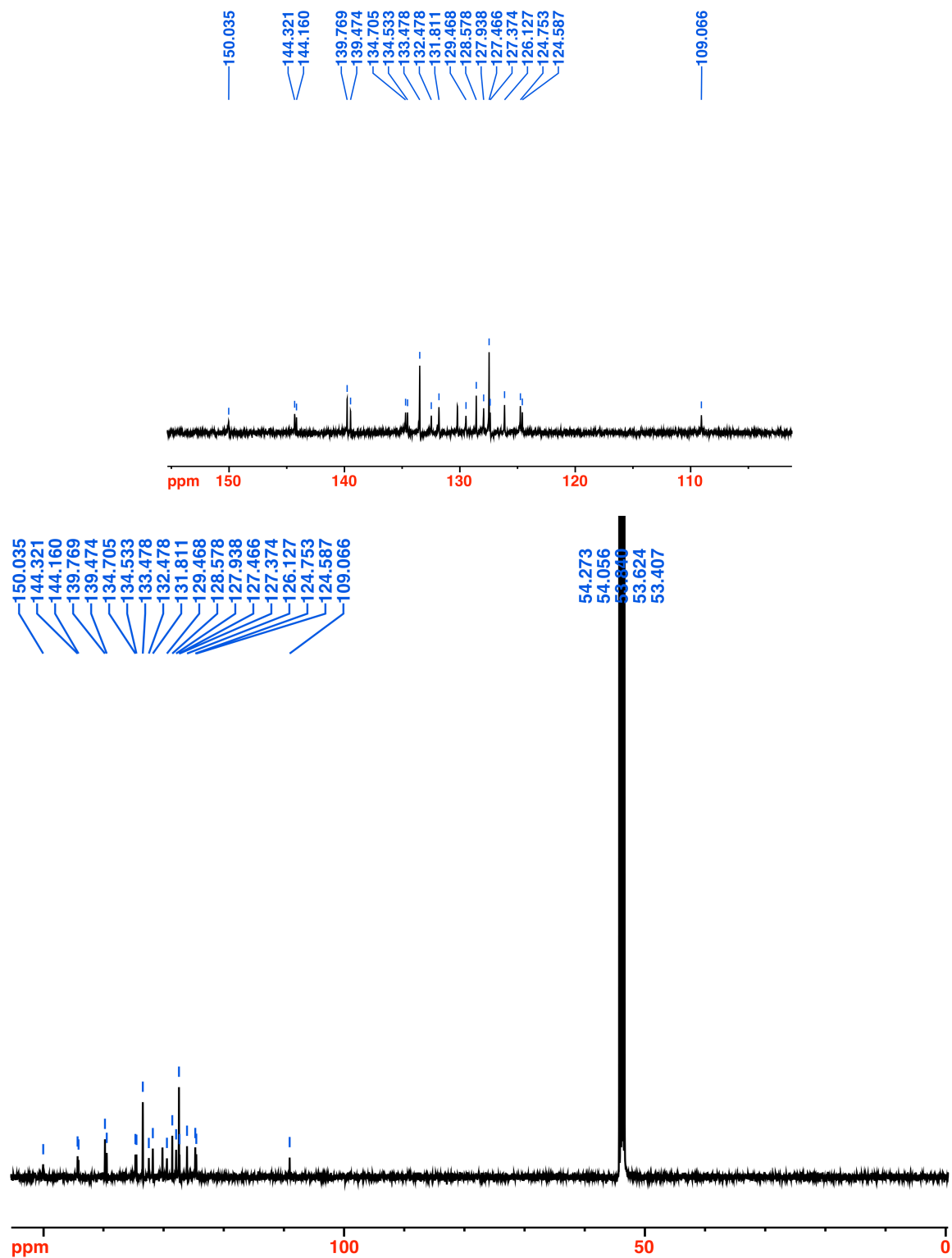


Figure 3-9. ^{13}C NMR spectrum (100 MHz, CD_2Cl_2) of **10Pt**.

3.4 References

- (1) a) Wang, X. D.; Wolfbeis, O. S. *Chem. Soc. Rev.* **2014**, *43*, 3666; b) Roussakis, E.; Li, Z.; Nichols, A. J.; Evans, C. L. *Angew. Chem. Int. Ed.* **2015**, *54*, 8340.
- (2) Eastwood, D.; Gouterman, M. *J. Mol. Spectrosc.* **1970**, *35*, 359.
- (3) a) Finikova, O. S.; Cheprakov, A. V.; Vinogradov, S. A. *J. Org. Chem.* **2005**, *70*, 9562; b) Niedermair, F.; Borisov, S. M.; Zenkl, G.; Hofmann, O. T.; Weber, H.; Saf, R.; Klimant, I. *Inorg. Chem.* **2010**, *49*, 9333; c) Borisov, S. M.; Nuss, G.; Haas, W.; Saf, R.; Schmuck, M.; Klimant, I. *J. Photochem. Photobiol., A* **2009**, *201*, 128; d) Borisov, S. M.; Papkovsky, D. B.; Ponomarev, G. V.; DeToma, A. S.; Saf, R.; Klimant, I. *Photochem. Photobiol., A* **2009**, *206*, 87; e) Borisov, S. M.; Nuss, G.; Klimant, I. *Anal. Chem.* **2008**, *80*, 9435.
- (4) a) Akhigbe, J.; Zeller, M.; Brückner, C. *Org. Lett.* **2011**, *13*, 1322; b) Akhigbe, J.; Luciano, M.; Zeller, M.; Brückner, C. *J. Org. Chem.* **2015**, *80*, 499.
- (5) a) Mei, E.; Vinogradov, S.; Hochstrasser, R. M. *J. Am. Chem. Soc.* **2003**, *125*, 13198; b) Dean, M. L.; Schmink, J. R.; Leadbeater, N. E.; Bruckner, C. *Dalton Transactions* **2008**, 1341.
- (6) Luciano, M.; Erfanzadeh, M.; Zhou, F.; Zhu, H.; Bornhütter, T.; Röder, B.; Zhu, Q.; Brückner, C. *Org. Biomol. Chem.* **2017**, *15*, 972.
- (7) Akhigbe, J.; Brückner, C. *Eur. J. Org. Chem.* **2013**, 3876.
- (8) Daniell, H. W.; Williams, S. C.; Jenkins, H. A.; Brückner, C. *Tetrahedron Lett.* **2003**, *44*, 4045.

4 *in vivo* Photoacoustic Tumor Tomography Using a Quinoline-Annulated Porphyrin as NIR Molecular Contrast Agent

The development of new—or the refinement of existing—imaging techniques of biological processes and tissue is arguably one of the leading driving forces in contemporary biomedical chemistry.¹ Photoacoustic imaging (PAI) is a rapid and non-invasive imaging modality that combines optical and ultrasound imaging.² Photoacoustic signals are optically generated and ultrasonically detected. PAI thus can take advantage of the optical window of tissue and provides the deep probing depth (multiple cm) and spatial resolution (sub-mm) of ultrasound.

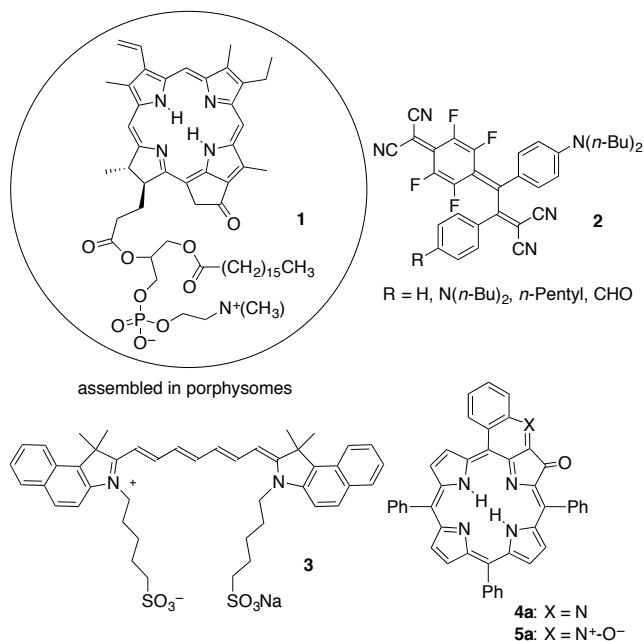
PAI is the consequence of a number of physical effects:^{2c} The absorption of a light pulse by a chromophore causes it to enter an excited state. Good PAI chromophores relax rapidly primarily along non-radiative pathways, causing a transient rise in temperature (in the mK regime) around the closest vicinity of the absorbing dye, leading to a localized thermal-elastic expansion. Thus, if the light source is a pulsed laser, light absorption generates a wideband ultrasonic wave. This signal can be acquired with standard ultrasonic transducers known from traditional ultrasound imaging. Furthermore, using wavelengths within the optical window of tissue (~700-1100 nm; the wavelength of maximum penetration of breast tissue is ~725 nm; whole blood has an absorption minimum at ~710 nm),³ dyes many centimeters deep within tissue can be probed. If such a NIR laser beam is scanned across an object, the photoacoustic data can be used to reconstruct 2D or 3D photoacoustic maps. The laser light energy used for *in vivo* imaging experiments is generally well below the standard thresholds above which tissue damages can be expected. Variants of PAI are photoacoustic tomography (PAT)^{2a} for large-scale imaging and photoacoustic microscopy (PAM)⁴ for small scale, high-resolution image generation.

Endogenous chromophores, primarily hemoglobin, can be used as PAI dyes.⁵ This allowed for the imaging of the blood content of the vascular network in rodent brains⁴ or cancer in breast⁶ and ovary tissues,⁷ the mapping of mesoscopic biological objects or whole animals.^{2a} However, particularly cancers in their early stages, cannot be detected by their intrinsic vascular contrast. Therefore, the use of exogenous contrast agents is required to achieve a suitable signal to noise ratio and to allow the PAI of deeply-seated organs or lesions.⁵

A number of nano- or micro-scale agents have been introduced as PAI or multimodal contrast agents in recent years, with some showing good *in vivo* imaging results.⁸ Among them are metal-based nanoparticles, combined with and without organic dyes, and nanotubes. However, the use of nanoparticles is not without problems with respect to biodistribution, toxicity, or homogeneity.⁹ Alternative approaches have been the use of molecular dyes assembled into vesicles, most prominent among them porphysomes made from chlorins or bacteriochlorins, such as pyropheophyrin derivative **1**,^{8b,10} microbubbles,^{8c,8d} or nanodroplets.^{8e} Also developed were photoacoustic probes that are generated in tissue.¹¹

Conspicuously rare in the contemporary literature are small molecular contrast agents designed for PAI.⁵ One example is **2**, shown to be a suitable contrast agent for imaging dissolved oxygen using photoacoustic lifetime imaging.¹² One of the oldest and best studied PAI contrast agents is the FDA-approved ocular angiographic dye indocyanine green (ICG, **3**), and related derivatives.¹³ ICG possesses NIR absorption ($\lambda_{\text{max}} \sim 800 \text{ nm}$) properties but is otherwise far from ideal. For instance, ICG is fluorescent. Thus, a portion of the absorbed light is not translated into a photoacoustic signal, diminishing its effectiveness as a PAI contrast agent. ICG is confined to the vasculature space, and it clears rapidly ($t_{1/2} < 4 \text{ min}$),¹⁴ complicating longitudinal *in vivo* studies. Irrespective of these shortcomings, the broad utilization of ICG suggests its use as a benchmark dye. The absence of the development of many molecular contrast agents highlights the fact that reliable structure-function relationships that might guide the

rational development of photoacoustic dyes suitable for their use in biological contexts has not been derived.



We recently reported the synthesis of *meso*-tetraphenylporphyrin-derived quinoline-annulated porphyrins, such as **4a** or **5a**.¹⁵ As a consequence of the extended π -conjugation and their annulation-induced non-planarity of the porphyrinic chromophore, the photophysical properties of quinoline-annulated porphyrins are significantly altered when compared to those of the parent porphyrin. While regular porphyrins generally do not absorb much past 650 nm, quinoline-annulated porphyrins possess λ_{max} bands in the 750 nm range. We have further shown that the bis-annulated systems and quinoline-annulated chlorins (in which another pyrrole was modified by a non-pyrrole heterocycle) are accessible by step-wise conversion of **5a**, further manipulating the optical properties of this family of porphyrinoids.¹⁵ Complementary syntheses of some of these derivatives and related chromophores are also known.¹⁶

Crucially, quinoline-annulated porphyrins **4a** and **5a** were shown to be primarily relaxing rapidly non-radiatively, making them very good photoacoustic dyes.¹⁷ We demonstrated a ~ 2.5 -

fold PAI contrast enhancement for **4a** over pure blood or ICG in phantom tissue experiments. The realization of a NIR-absorbing chromophores showing good photoacoustic signal generation efficiency is difficult, as the direct comparison of a number of NIR dyes absorbing in the same wavelength range has shown.¹⁷ Despite the promise of **4a** or **5a** as PAI contrast agents, however, their insolubility in aqueous solutions (in the absence of a formulation vehicle like Cremophore EL®) prevented their *in vivo* assessment.

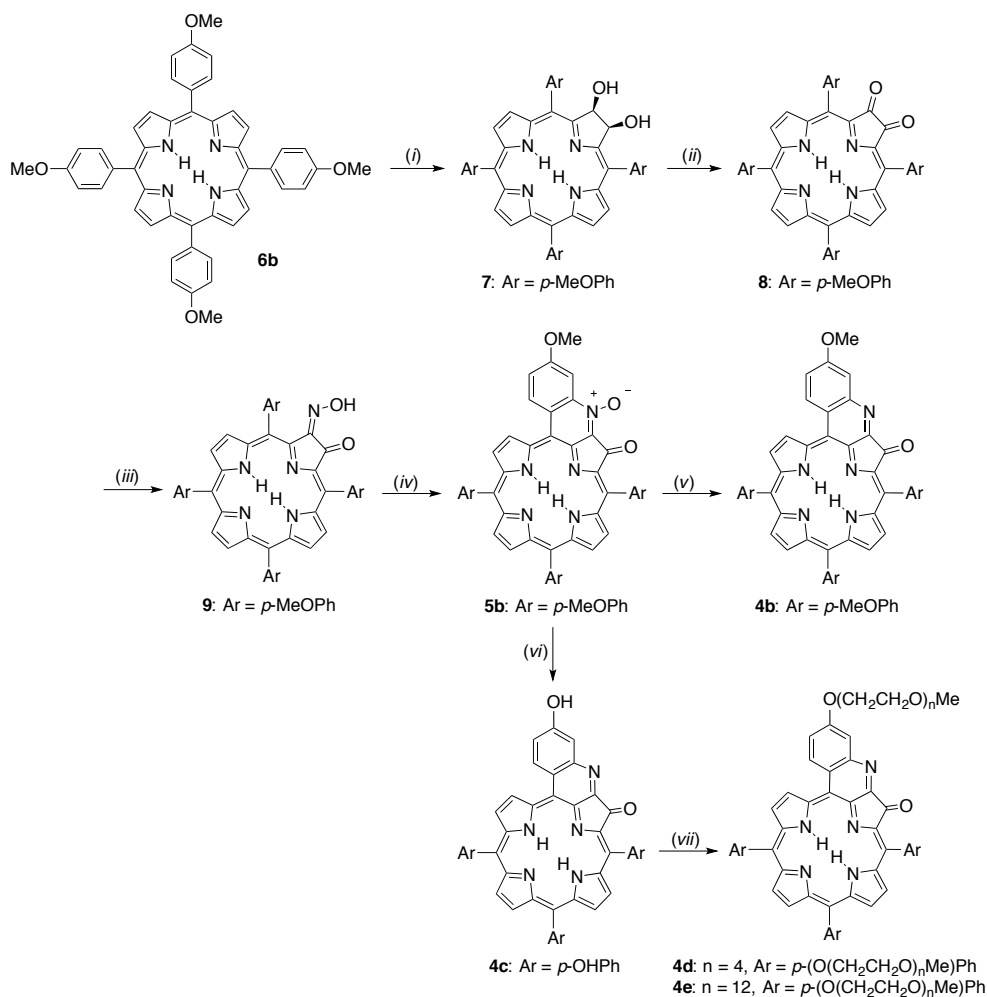
We report here the development of a quinoline-annulated porphyrin-based single-molecule, serum-soluble PAI contrast agent and the evaluation of its efficacy as an *in vivo* PAI contrast agent for the detection of implanted tumors in a mouse model. A multi-fold contrast enhancement when compared to ICG was found, a finding that could be traced to its photophysical properties. Its nontoxicity and renal clearance rates will be demonstrated. We also prepared a water-soluble quinoline-annulated derivative of the quinoline annulated porphyrin carrying a small fluorescent tag designed to facilitate the biodistribution studies of this intrinsically non-fluorescent chromophore. It was, however not fluorescent enough to be of utility. Nonetheless, the experiment demonstrated a facile and general conjugation strategy for these chromophores.

4.1 Results and Discussion

4.1.1 Synthesis of a Freely Water-Soluble Quinoline-Annulated Porphyrin

A number of strategies were established to render *meso*-arylporphyrins water-soluble.¹⁸ Among them are their functionalization with anionic (carboxylate, sulfonate, phosphonate) or cationic (pyridinium) groups or their decoration with (multiple) polyethylene glycol (PEG) chains. We chose the PEG-strategy for the charge neutrality of the final products and previous reports indicating their suitability for tumor targeting.^{18e,19} We found that quinoline-annulated porphyrin **4a** is chemically stable under the classic acidic methoxy deprotection conditions (BBr₃) but not to, for example, classic basic saponification reaction conditions (NaOH, wet THF). We thus chose the phenol-protected *meso*-tetrakis(*p*-methoxyphenyl)porphyrin **6b** as the basis for the formation of the quinoline-annulated porphyrin chromophore,^{15a} with the intent to deprotect and PEG-ylate the phenolic oxygens using standard Williamson alkylation strategies at the last stages of the dye synthesis pathway. This strategy was successful as demonstrated by the synthesis of the waters-soluble dyes **4d** and **4e** (Scheme 4-1).

4. *in vivo* PAI Using a Quinoline-Annulated Porphyrin as NIR Molecular Contrast Agent



Scheme 4-1. Synthesis of water-soluble quinoline-annulated porphyrins. Reaction conditions: (i) 1. 1 equiv. OsO₄, 30% pyridine/CHCl₃, r.t.; 2. H₂S (ii) 4 equiv. DMP, CH₂Cl₂, r.t. (iii) 100 equiv. NH₂OH·HCl, pyridine, N₂ atmosphere, r.t. (iv) DDQ, CH₂Cl₂, r.t. (v) pyridine, Δ (vi) 1. BBr₃, CH₂Cl₂ (vii) Me(OCH₂CH₂)_nOMs, Cs₂CO₃, DMF, 90 °C.

p-Methoxy-derivatized quinoline-annulated porphyrin **4b** was synthesized from meso-tetrakis(*p*-methoxyphenyl)porphyrin **6b** using the dihydroxylation → oxidation → oximation → annulation route established earlier for this chromophore class;^{15a} all intermediates showed the expected spectroscopic and analytical properties (see ESI). However, some notable deviations from the established protocols were implemented. The oxidation of diolchlorin **7** required the use of Dess-Martin Periodinane (DMP) for its smooth conversion to the corresponding 2,3-dioxochlorin **8**.²⁰ The generally used oxidant DDQ failed to produce this dione;²¹ instead dehydration to the corresponding enol was observed (the reaction was not further investigated).

Oxime **9** formed smoothly; its treatment with *p*-TSA under forcing conditions (toluene, reflux) produced the quinoline annulated porphyrin **4b** in acceptable yields, but this product was contaminated with the corresponding *N*-oxide **5b**. Because their separation was tedious, we treated oxime **9** with DDQ, thus forming *N*-oxide **5b** as the exclusive product in near-quantitative yields. We attribute the facile annulation and oxidation to the electron-rich nature of the *p*-OMe-substituted oxime. *N*-Oxide **5b** could be readily reduced to quinoline annulated porphyrin **4b** by heating to reflux in pyridine. Similar ready losses of the *N*-oxide were observed previously.^{15a} Quinoline-annulated porphyrin *N*-oxide **5b** was also susceptible to a BBr₃-mediated deprotection of the methoxy groups and concomitant reduction of the *N*-oxide, without any noticeable degradation of the macrocycle, generating the phenolic quinoline-annulated porphyrin **4c** in five linear steps from porphyrin **6b**.

Phenol-derivatized quinoline-annulated porphyrin **4c** could be PEG-ylated with a methoxy-capped PEG-mesylate using a short PEG chain (*n* = 4), forming **4d**, as well as a longer chain (avg. MW 550, *n* ~ 12), forming **4e**. ESI⁺ MS and ¹H NMR spectra of **4d** and **4e** confirmed that all four non-equivalent phenolic OH-groups were PEG-ylated. The mass spectra of **4e** reflect the chain length inhomogeneity of the longer PEG-chain (see experimental section). Because of the homogeneity of the shorter PEG derivative, we used this derivative for the determination of the photophysical properties of the water-soluble quinoline-annulated porphyrins.

4.1.2 Photophysical Properties and Solubility of PEGylated Quinoline-Annulated Porphyrins **4d** and **4e**

The presence of the four *p*-methoxy groups in **4b** (or the four *p*-OH groups in its deprotected derivative **4c**) is reflected in a slight red-shift of its optical spectrum (λ_{max} = 762 nm for **4b**, λ_{max} = 748 nm for **4c**) when compared to the spectrum of **4a** (λ_{max} = 728 nm), but the overall characteristics of the quinoline-annulated porphyrins are not altered (Figure 4-1A).¹⁷

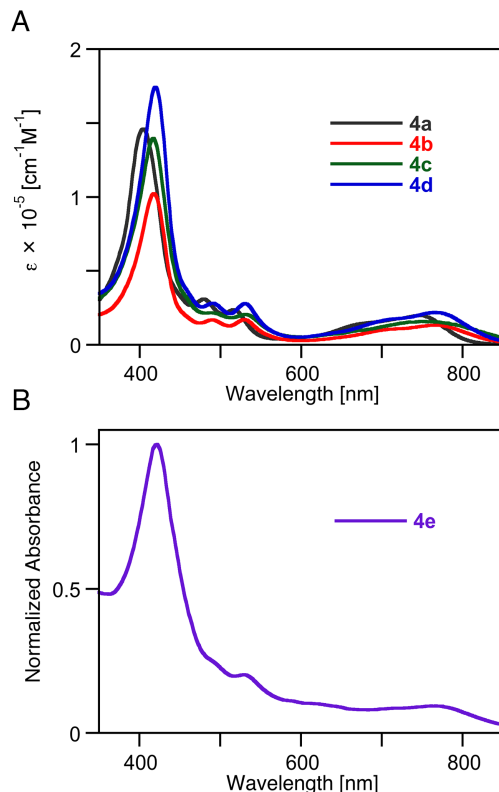


Figure 4-1. UV-vis spectra (A: CH₂Cl₂, B: H₂O) of the compounds indicated.

The shorter PEG derivative **4d** is highly soluble in CH₂Cl₂ as well as alcoholic solvents, but is only slightly soluble in pure water. The PEG-ylated quinoline-annulated porphyrin **4e** is freely soluble in alcohols, water, serum, and PBS buffer. As expected, the PEGylated derivatives **4d** and **4e** possess a λ_{max} value of 764 nm in CH₂Cl₂. Both compounds exhibit some modest degree of solvatochromism. The spectrum of **4e** in water, for example, is slightly blue-shifted and overall broadened (Figure 4-1B).

The dissolution of 100 mg **4e**/mL PBS was readily possible, forming a 33.3 mM solution. The solubility is therefore ~ 2 orders of magnitude higher than the reported value for ICG in water.²² The Lambert-Beer law is maintained for aqueous concentrations up to 0.03 mM (the upper limit we could measure in a 1 mm path length cell) but the addition of the surfactant TritonTM X-100 to dilute solutions slightly blue-shifts and enhances the Soret band (see

experimental), suggesting that **4e** is somewhat aggregated in aqueous solution. The solutions are stable; no significant changes were observed in the UV-vis spectra of the solutions over many hours, and with only the onset of minor shifts after two weeks (in the dark at 4 °C).

The fluorescence quantum yield ϕ for **4e** in CH₂Cl₂ as well as H₂O were determined to be significantly below 0.1%. Transient absorption spectra (in the range from 450 to 900 nm) for **4e** in both solvents with pump-probe delay times from 0 to 15000 ps delivered no reliable ISC-quantum yield or S₁-lifetime data. Correspondingly, **4e** in CH₂Cl₂, H₂O, as well as H₂O-Triton™ X-100 solutions showed no sign for the generation of singlet oxygen (¹O₂), as measured by the time-resolved NIR luminescence spectra of solutions of **4e** (at O.D. = 0.1 at the excitation λ of 532 nm) at 1270 and 1210 nm.

Thus, PEGylated quinoline-annulated porphyrin **4e**, like its parent compound,¹⁷ absorbs strongly within the spectroscopic window of tissue, is non-emissive, and does not generate ¹O₂. These are excellent properties for a photoacoustic imaging agent.

4.1.3 *ex vivo* Photoacoustic Signal Generation of Water-Soluble Quinoline-Annulated Porphyrin **4e**

The strength of a photoacoustic (PA) signal generated by an irradiated sample is dependent upon the excitation source, absorption coefficient of the sample, solvent, and its Grüneisen parameter that represents the efficiency of the photoacoustic signal generation.^{3b} The 2.5-fold increased PAI signal of quinoline-annulated porphyrin **4a** (dissolved in PBS–1% DMF–1% Cremophore EL®) over the signal resulting from blood at identical absorbance values in tissue phantom studies was demonstrated.¹⁷ Water-soluble quinoline-annulated porphyrin **4e** dissolved in water exhibits a similarly excellent performance: The relative *ex vivo* photoacoustic signal generation efficiency of the dye **4e** placed in a translucent polyethylene tube submerged in a water bath was compared against that of day-old rat blood in the same setup and otherwise

identical irradiation and detection conditions. The concentration of **4e** was adjusted so as to possess the identical absorbance value of the blood sample at 790 nm, the wavelength of the laser used to excite the dye. The co-registered pulse-echo and photoacoustic tomography (PE-PAT) images clearly show that the tube filled with **4e** generated a 4-fold stronger signal, thus generating a much higher contrast image than the blood sample (Figure 4-2A and Figure 4-2B).

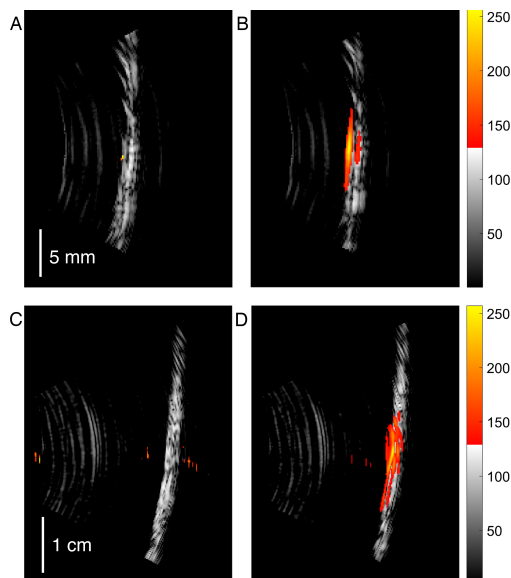


Figure 4-2. Co-registered PE-PAT images of polyethylene tubes (inner/outer $\phi = 0.58/0.96$ mm) filled with (A and C) one-day-old rat blood and (B and D) with a solution of PEG-ylated quinoline-annulated porphyrin **4e** at a concentration in which the sample possessed the identical absolute absorbance value at 790 nm as the undiluted blood (see ESI). In each image pair (A-B and C-D) the PAT signal was normalized to the maximum value recorded from the tube filled with **4e**. Samples immersed in water (A and B, PA signal dynamic range of -12 dB, the threshold is 25% of maximum) and Intralipid® (C and D, dynamic range of -15 dB, the threshold is 18% of maximum) at 1 cm (A and B) and 2.5 cm (C and D) scan depths, respectively. Vertical image axis is approximately parallel to the tube length and horizontal axis represents imaging depth.

In tissue, light is significantly scattered and absorbed. The fat emulsion Intralipid® provides a strongly scattering medium for light.²³ Thus, at 2.5 cm depth, only a small fraction of the light energy is delivered to the targets.^{3b} In fact, at the light level used in the experiment, the blood sample could not provide any PA signal higher than the noise level (Figure 4-2C), while the tube filled with **4e** still delivered well-resolved and high-contrast images (Figure 4-2D), demonstrating its potential as a PAI contrast agent.

4.1.4 Toxicity of PEGylated Quinoline-Annulated Porphyrin 4e

Anesthetized 6 week old BALB/c mice were treated with 100 μ L of a 33.3 mM PBS solution of **4e** via retro-orbital injection, and their heart rates were monitored for 3 h after injection. No signs of distress of the mice were observed. They also lived for several weeks after the injection with normal weight gain and showed no abnormal behavior. The majority of the dye is excreted via the renal pathway within the first hour after injection (see also below). These are all promising preliminary indications for the absence of any acute toxicity of the PEG-ylated quinoline-annulated porphyrin **4e**.

4.1.5 The Use of Quinoline-Annulated Porphyrin 4e as an *in vivo* PAI Contrast Agent

As a result of the solubility, apparent non-toxicity, and high PA signal generation efficiency of the PEG-ylated dye **4e**, we tested the efficacy of this dye as an *in vivo* PAT contrast agent in a mouse model. The dye **4e** (100 μ L of a 33.3 mM of **4e** in PBS) was administered via retro-orbital injection²⁴ to anesthetized BALB/c mice with tumors (7-10 mm) implanted in their flanks, and the PE and co-registered PE-PAT images were recorded, beginning 1 min after injection (Figure 4-3A and B). The PE image shows the outline of the tumor and serves as backdrop to the PA image. Before injection, only few pixels of the PA image possess high enough signal strength to exceed a threshold value (25% of the maximum PA signal after injection). Proximately after injection (1 min), a \sim 4-fold increase in the PAT signal strengths originating from the tumor site were recorded. The enhancement of the PA signal was monitored for 45 min after injection, seeing a gradual loss of the signal strength, but even after 45 min, an at least 2-fold PA signal enhancement was still achieved (Figure 4-4). The effect of PEG-ylation on increasing the blood circulation time of small molecules has been described.^{19,25}

4. *in vivo* PAI Using a Quinoline-Annulated Porphyrin as NIR Molecular Contrast Agent

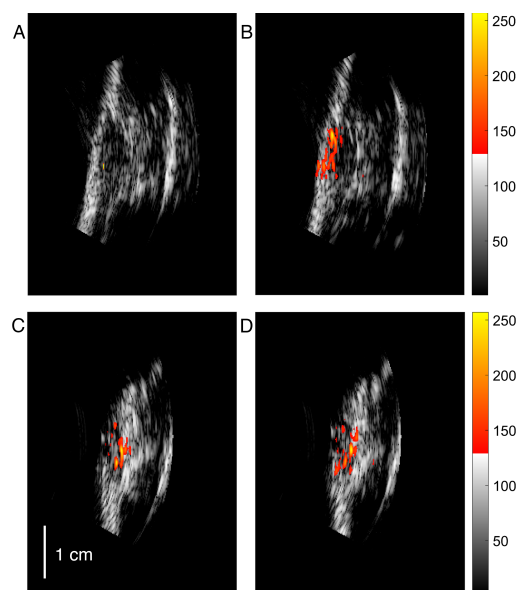


Figure 4-3. Co-registered PE-PAT images before injection of the contrast agent (A) and ICG (C) and after the systemic injection of **4e** (B) and ICG (D). In each image pair (A-B and C-D) the PAT signals were normalized to the same maximum value recorded after the injection; a similar dynamic range of -12 dB is applied to all images (the threshold is 25% of the maximum value). The vertical axis is approximately parallel to the surface of the mouse body and the horizontal axis represents the depth inside the body.

In comparison, injection of 100 μ L ICG solution of identical absorbance at 780 nm as **4e** at 790 nm ([ICG] = 1.33 mM) provided a significantly lower PA signal strength enhancement (\sim 1.6-fold) (Figures 3C-D), with no enhancement after less than 30 min (Figure 4-4). Thus, the rate at which dye **4e** is excreted (via renal pathways, see below) is significantly slower than the rapid excretion rate of ICG.¹⁴

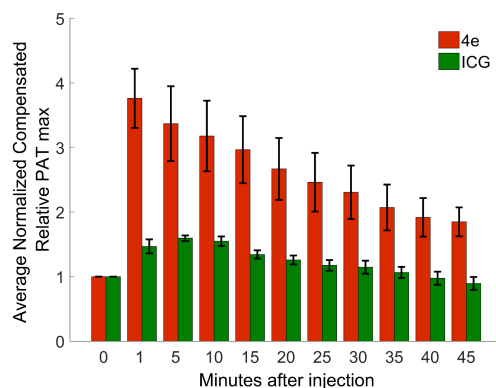


Figure 4-4. Time-dependence of the relative enhancement of the PAT max value following the injection of 100 μ L of the dye **4e** (\sim 33.3 mM, $\lambda_{\text{excitation}} = 790$ nm) and ICG (1.33 mM, $\lambda_{\text{excitation}} = 780$ nm) at identical absorbance value.

4.1.6 Renal Filtration of Quinoline-Annulated Porphyrin **4e**

An early indication for the biodistribution of dye **4e** was the observation of the color of the urine excreted by the mice immediately after the imaging experiments (after ~45 min) to the color of the dye (Figure 4-5). This suggested a very efficient renal filtration of the dye. Using UV-vis spectroscopic and HPLC-MS analyses of the urine extracts, we were able to show that **4e** was excreted in unaltered form.

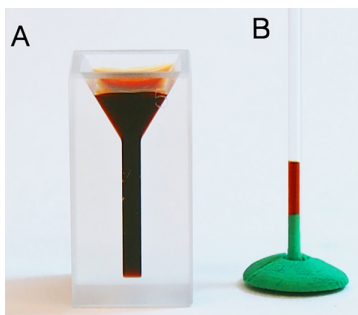


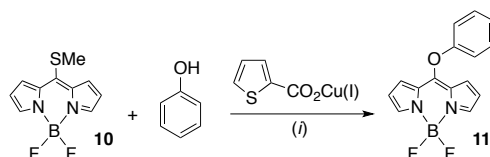
Figure 4-5. A. PEG-ylated quinoline-annulated dye **4e** dissolved in PBS (~33.3 mM) in a microcuvette. B. Mouse urine collected after ~45 min after injection of **4e** in a capillary tube.

4.1.7 Fluorescent-Tagging of Quinoline-Annulated Porphyrin **4e**

Quinoline-annulated porphyrin **4e** is non-fluorescent. However, the recording of fluorescent images of organs or the measurement of the dye-specific fluorescence of organ or biofluid extracts are convenient methodologies to track the biodistribution of any fluorophore. Thus, we opted to prepare a fluorophore-tagged derivative of quinoline-annulated porphyrin **4e**. Recognizing that FRET processes might be operative that quench the fluorescence of the tag at the absorption maxima of quinoline-annulated porphyrins, we looked for fluorophores that emit in an area of relative minor absorption of these chromophores (Figure 4-1).

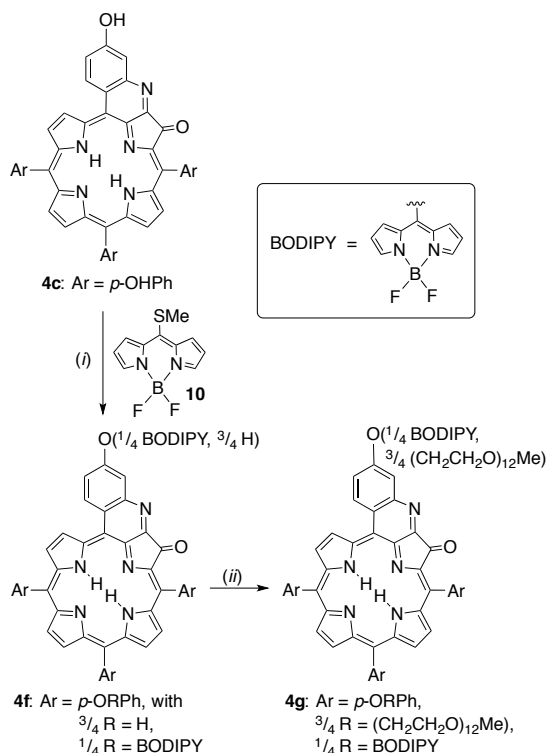
BODIPYs are well-established low molecular weight fluorophores of high brightness and multiple options to adjust their optical spectra.²⁶ Furthermore, a recent report describing the reaction of *meso*-mercapto-BODIPY derivative **10** with phenols to generate the *meso*-phenoxy-

BODIPY derivative **11** (Scheme 4-2)²⁷ seemed most suitable for our task of tagging a tetra-phenol-derived quinoline-annulated porphyrin. Moreover, the emission λ_{max} of 495 nm for **11** lies within the target range, and the attachment of the fluorophore at the most distal position to the porphyrinic chromophore would also reduce the chances for any FRET.



Scheme 4-2. Synthesis of *meso*-phenoxy BODIPY derivative **11**. Reaction Conditions: (i) Na₂CO₃, MeCN, 55 °C.

Thus, we chose to attach a single BODIPY moiety to one of the four phenolic oxygens of tetraol **4c**, followed by exhaustive PEG-ylation of the remaining three phenol functionalities (Scheme 4-3).



Scheme 4-3. Synthesis of BODIPY-tagged water-soluble quinoline-annulated porphyrin **4g**. Reaction conditions: (i) 1. Zn(OAc)₂·2H₂O, CH₂Cl₂/MeOH, Δ; 2. 1 equiv **10**, Na₂CO₃, CuTC, CH₃CN, 50 °C; 3. aq. HCl. (ii) Me(OCH₂CH₂)₁₂OMs, Cs₂CO₃, DMF, 90 °C.

In anticipation of the copper-catalyzed reaction chosen for the conjugation of the fluorescent tag to quinoline-annulated porphyrin **4c**, its central cavity was protected by insertion of zinc(II). A Cu(I) thiophene-carboxylate (CuTC)-mediated reaction of *meso*-mercapto-BODIPY **10**,²⁷ followed by an acid-mediated removal of the zinc protecting group using a mineral acid wash, generated quinoline-annulated porphyrin **4f** in which one of the phenolic oxygens was derivatized with the BODIPY group, while the other three groups remained unmodified (as per ESI⁺ MS). The lack of regioselectivity of this reaction is reflected in the complex ¹H NMR spectrum of this compound (see experimental section). The three phenolic oxygens of **4f** were then PEG-ylated using the long PEG mesylate as described above. Product **4g**, a deep yellow oil, shows the expected composition (as per MALDI MS). It is freely water-soluble. The presence of the BODIPY is seen in the (complex) ¹H NMR spectrum of **4g** by the observation of the diagnostic peaks for the α - and β -protons of the BODIPY moiety (at δ = 6.5-7.0 ppm). Its ¹⁹F NMR spectrum indicates the presence of fluorine atoms at δ = -146.4 to -146.6 ppm, the typical range for BODIPY fluorine atoms.

The UV-vis spectrum of non-PEGylated derivative **4f** is derived from a linear addition of the spectrum of tetraol **4c** and BODIPY **11** (Figure 4-6A), with only some minor shifts and broadening, likely derived from the presence of four regioisomers. Upon PEGylation of **4f**, the UV-vis spectrum is further broadened, with retention of the overall character of the quinoline-annulated derivatives (Figure 4-6B).

When dyad **4g** is excited at the λ_{max} value of the BODIPY moiety (at 441 nm), the molecule emits at 485 nm, this emission can be attributed to the BODIPY portion of **4g**.²⁷ However, the fluorescence yield ϕ for **4g** is estimated to lie below 0.3%, i.e., much lower than the fluorescence yield ϕ for **11**.²⁷

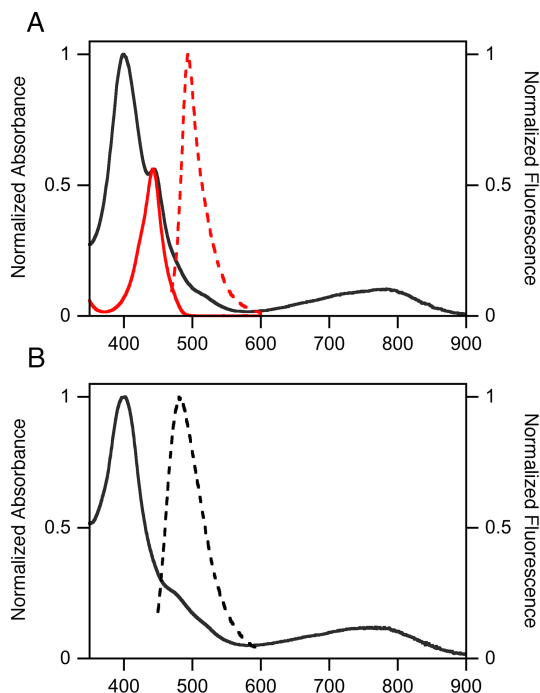


Figure 4-6. A. UV-vis spectra of **4f** (black) and **11** (red) (solid lines), and fluorescence emission (red broken line; $\lambda_{\text{excitation}} = 441$ nm) for phenoxy-BODIPY **11** (all MeOH). B. UV-vis (solid line) and fluorescence emission (broken line; $\lambda_{\text{excitation}} = 441$ nm) spectra of quinoline-annulated porphyrin-BODIPY dyad **4g** (MeOH)).

This suggests that some FRET (or other quenching) mechanisms are operative in **4g**, but that this quenching is not efficient enough to entirely switch off the fluorescence of the BODIPY moiety. The low fluorescence yield questions the possibility of tracking dyad **4g** in tissue using a fluorescence scanner.

4.1.8 Biodistribution Study of BODIPY-Tagged Quinoline-Annulated Porphyrin **4g**

The biodistribution of the BODIPY-labeled derivative **4g** in the tumor and other organs was studied by *ex vivo* fluorescent imaging, following the injection of **4g** into 4 BALB/c mice as described for **4e**. The mice were sacrificed 15 or 120 min after injection, the organs extracted, and their radiant efficiency fluorescent images recorded ($\lambda_{\text{exc}} = 465$ nm; GFP emission filter). Unfortunately, the high amount of tissue auto-fluorescence in that wavelength, did not allow the recording of high-contrast images. We note, however, that the tumor was yellow stained, suggesting an accumulation of the dye **4g** in the tumor.

4.2 Conclusions

In conclusion, we have demonstrated the *in vivo* efficacy of freely serum-soluble quinoline-annulated porphyrin derivative **4e** as a molecular contrast agent for photoacoustic tomography. The solubilization of the quinoline-annulated porphyrin followed a straight-forward PEGylation strategy, with the lengths of the PEG chains determining the solubility of the final product. The product appeared to be low acute toxicity, accumulated in the tumor site, and was rapidly excreted in unaltered fashion via renal pathways. The solubilisation strategy is conceivably also suitable to other quinoline-annulated porphyrin derivatives. Conjugation of the non-fluorescent PEGylated quinoline-annulated porphyrin to a fluorophore was also demonstrated, but the hopes to utilize this derivative for the tracking of the biodistribution of the contrast agent using fluorescence imaging was not fulfilled. Nonetheless, the flexible derivatization strategy points the way toward the conjugation to other molecules.

4.3 Experimental Section

4.3.1 Materials and Instruments

All solvents (Aldrich, Acros) and reagents MeO-PEG₄-OMs (Aldrich) and MeO-PEG₁₂-OMs (Creative Peg Works), CuTC (Aldrich) were reagent grade, or better, and were used as received. *meso*-Tetrakis(*p*-methoxyphenyl)-2,3-dihydroxychlorin (**7**)²⁸ and BODIPYs **10** and **11** were prepared as described previously.²⁷

Analytical (aluminum backed, silica gel 60, 250 µm thickness) and preparative (20 × 20 cm, glass backed, silica gel 60, 500 µm thickness) TLC plates, and the flash column silica gel (standard grade, 60 Å, 32-63 µm) used were provided by Sorbent Technologies, Atlanta, GA.

¹H and ¹³C NMR spectra were recorded on Bruker Avance II 400 and Bruker Avance I 500 instruments in the solvents indicated, and were referenced to residual solvent peaks. High and low resolution ESI mass spectra were provided by the Mass Spectrometry Facilities at the

Department of Chemistry, University of Connecticut. MALDI MS Spectra were provided by the Mass Spectrometry & Proteomics Facility at the University of Notre Dame. UV-vis and fluorescence spectra were recorded on Cary 50 and Cary Eclipse photospectrometers, Varian Inc, respectively, and IR spectra on a Bruker Alpha-P FT-IR spectrometer using a diamond ATR unit.

4.3.2 Synthesis and Characterization

meso-Tetrakis(*p*-methoxyphenyl)-2,3-dioxoporphyrin (8). Diol **7** (270 mg, 3.51×10^{-4} mol) was dissolved in CH₂Cl₂ (60.0 mL) in a round-bottom flask equipped with a magnetic stir bar. To the stirring solution was added Dess-Martin periodinane (590 mg, 1.39×10^{-3} mol, 4 equiv) in portions at ambient temperature. When the starting material was consumed (reaction control by UV-vis and TLC), the reaction was quenched by addition of a sat'd aq NaHCO₃ solution. The organic layer was isolated and washed with H₂O (3 × 30 mL). The organic layer was dried over anhyd Na₂SO₄ and evaporated to dryness by rotary evaporation, and the residue purified by column chromatography (silica-CH₂Cl₂) to yield **8** as a dark blue powder in yields ranging from 65 to 90% (243 mg): *R*_f (CH₂Cl₂-silica) = 0.52; ¹H NMR (400 MHz, CD₂Cl₂) δ 8.81 (d, ³*J* = 4.9 Hz, 1H), 8.65 (d, ³*J* = 4.9 Hz, 1H), 8.61 (s, 1H), 8.06 (d, ³*J* = 8.6 Hz, 2H), 7.84 (d, ³*J* = 8.6 Hz, 2H), 7.31-7.24 (m, 4H), 4.07 (two overlapping s, 6H), -1.90 (br s, 1H, exchangeable with D₂O); ¹³C NMR (100 MHz, CD₂Cl₂): δ 188.2, 159.9, 159.6, 155.64, 155.62, 155.59, 140.9, 140.2, 138.4, 135.3, 134.1, 133.8, 133.4, 131.8, 128.4, 128.0, 123.9, 113.4, 112.65, 112.54, 112.47, 55.5, 55.4 ppm; UV-vis (CH₂Cl₂) λ_{max} (log ε) 410 (5.26), 477 (4.26) nm; FT-IR (neat, diamond ATR) 1730 (ν_{C=O}) cm⁻¹; HR-MS (ESI⁺, 100% CH₃CN, TOF) *m/z* calcd for C₄₈H₃₇N₄O₆ ([M·H]⁺) 765.2713, found 765.2726.

4. *in vivo* PAI Using a Quinoline-Annulated Porphyrin as NIR Molecular Contrast Agent

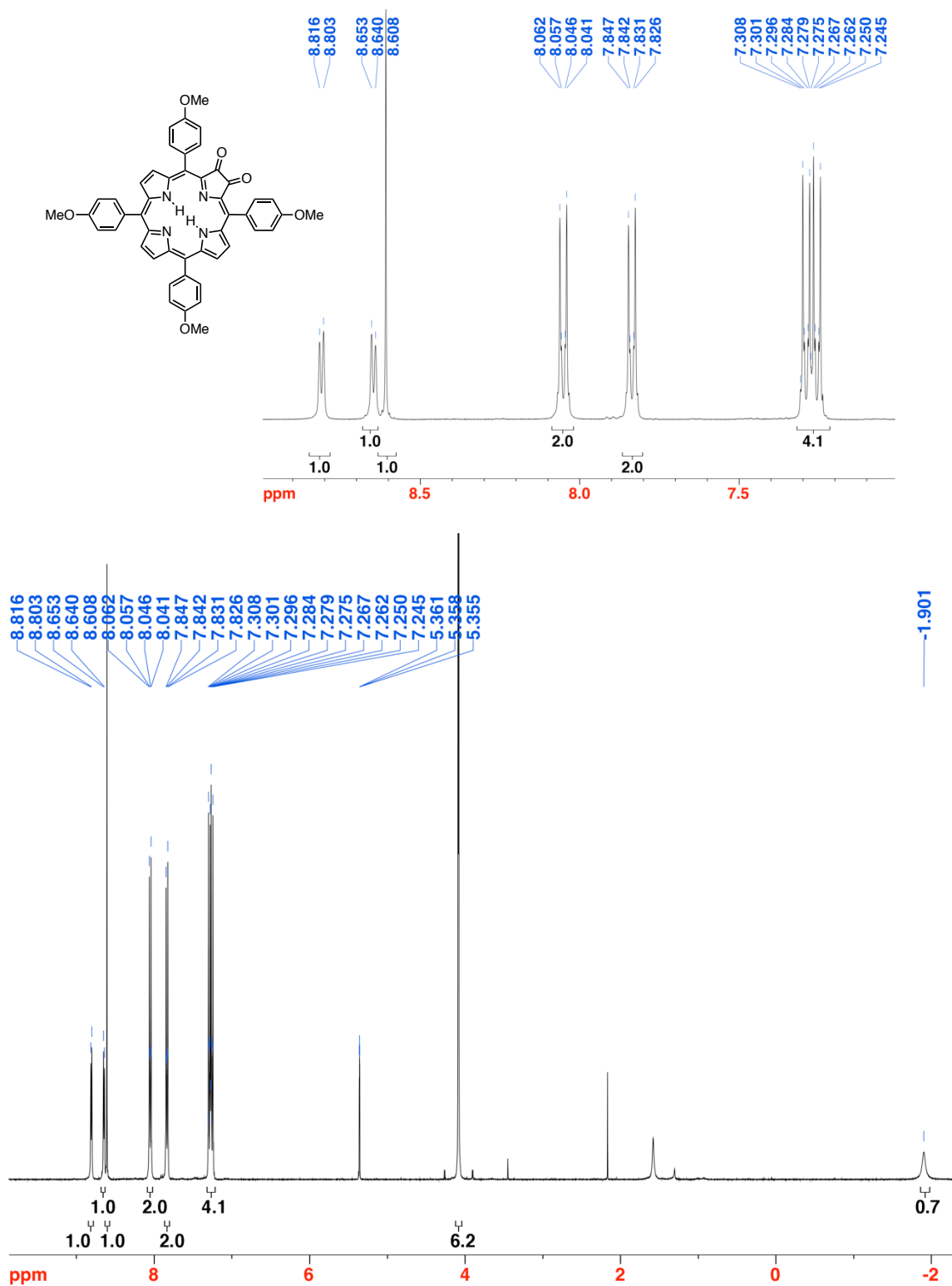


Figure 4-7. ^1H NMR spectrum (400 MHz, CD_2Cl_2) of 8.

4. *in vivo* PAI Using a Quinoline-Annulated Porphyrin as NIR Molecular Contrast Agent

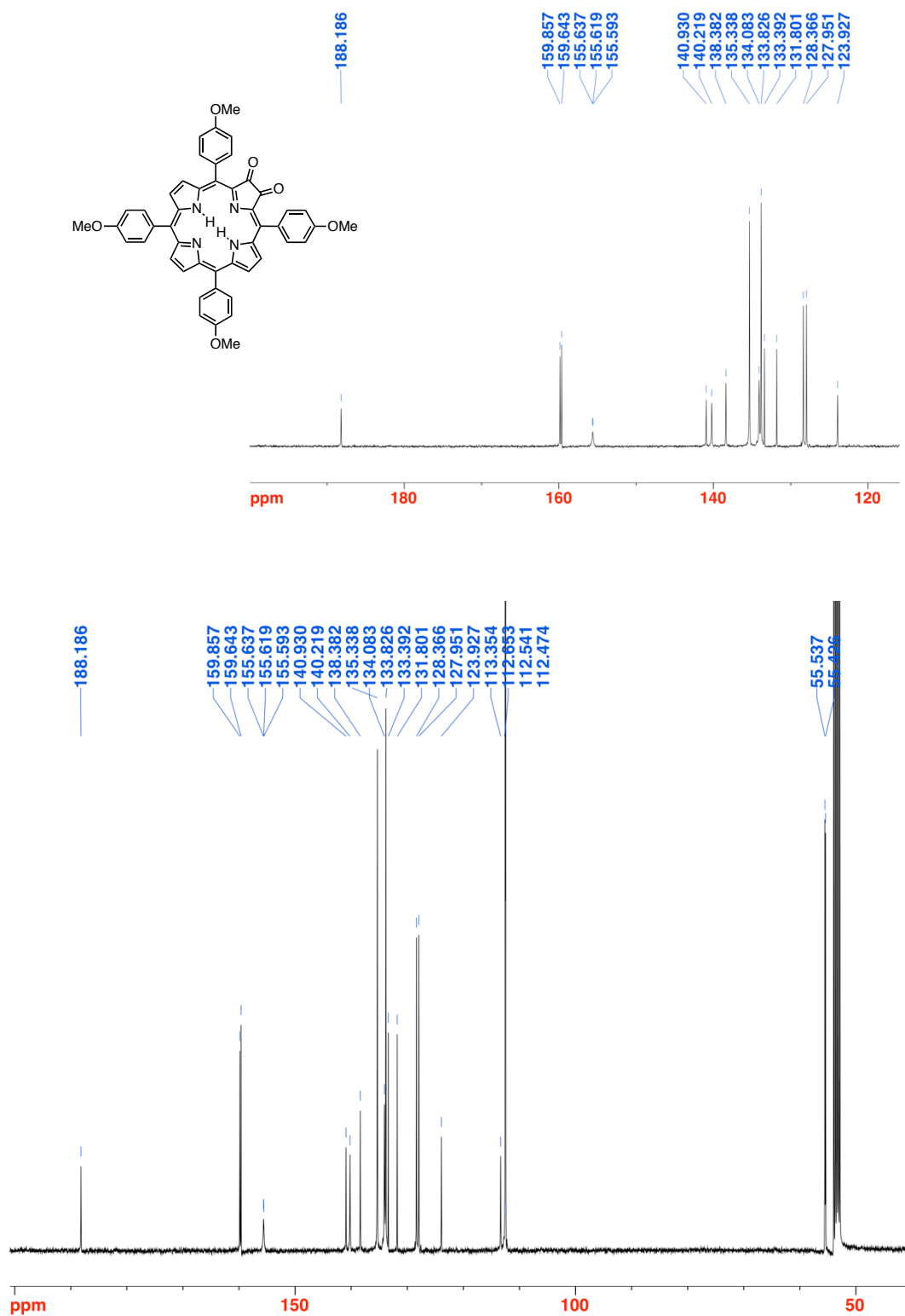


Figure 4-8. ¹³C NMR spectrum (100 MHz, CD₂Cl₂) of 8.

4. *in vivo* PAI Using a Quinoline-Annulated Porphyrin as NIR Molecular Contrast Agent

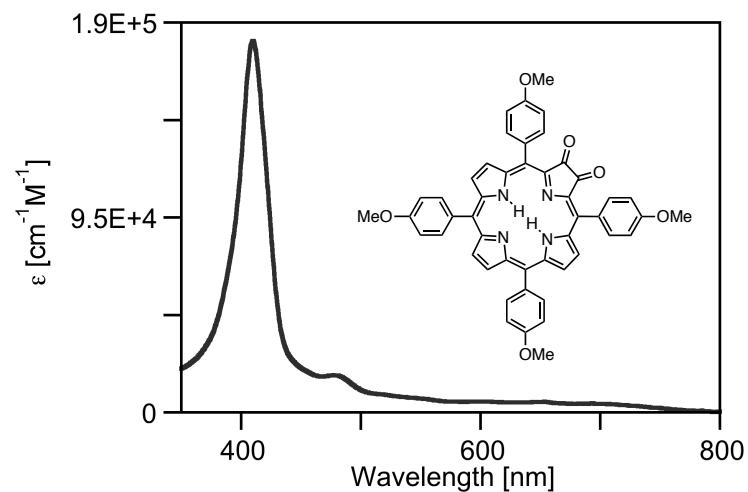


Figure 4-9. UV-vis spectrum (CH₂Cl₂) of **8**.

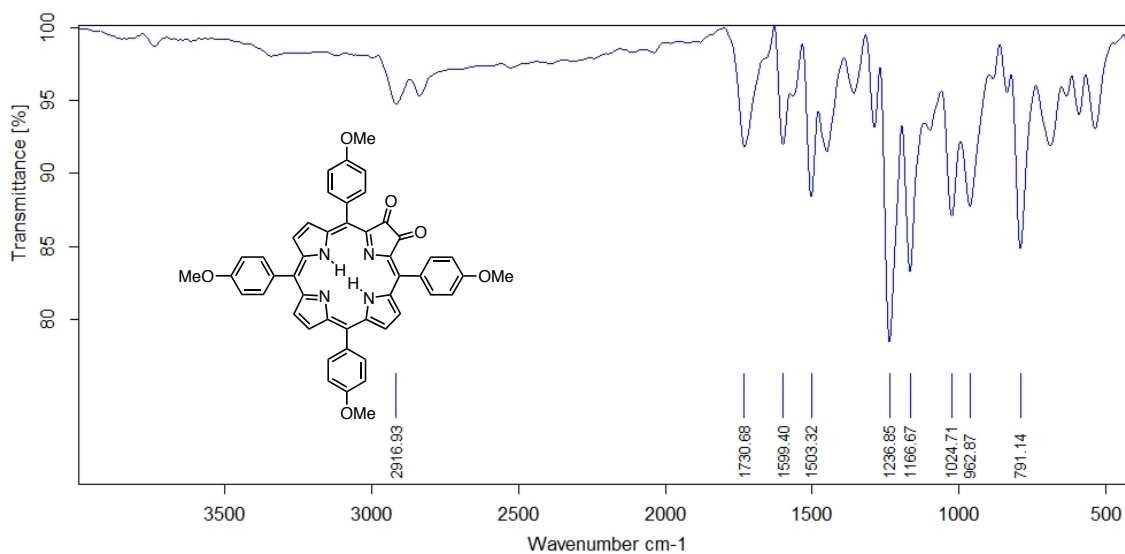


Figure 4-10. FT-IR spectrum (neat, diamond ATR) of **8**.

meso-Tetrakis(*p*-methoxyphenyl)-2-hydroxyimino-3-oxoporphyrin (9). Dione **8** (94 mg, 1.2×10^{-4} mol) was dissolved in pyridine (30.0 mL) in a round bottom flask equipped with a magnetic stir bar and N₂ inlet. Hydroxylamine hydrochloride (NH₂OH·HCl, 850 mg, ~100 equiv) was added, and the mixture was stirred at ambient temperature. When the starting material was consumed (after about 24 h; reaction control by TLC), the reaction mixture was evaporated to dryness by rotary evaporation. The residue was taken up in CH₂Cl₂ and filtered through a glass frit (M). The volume of the filtrate was reduced and submitted to column chromatography (silica-CH₂Cl₂/1% MeOH) to afford the olive-green product **9** in 60% yield, (58 mg): *R_f* (silica-CH₂Cl₂/1% MeOH) = 0.65; ¹H NMR (400 MHz, CD₂Cl₂) δ 15.78 (br s, 1H, exchangeable with D₂O), 8.81 (d, ³*J* = 5.7 Hz, 2H), 8.62 (t, ³*J* = 8.4 Hz, 4H), 8.03 (dd, ³*J* = 8.4, ⁴*J* = 2.0 Hz, 4H), 7.85 (dd, ³*J* = 8.4 Hz, 4H), 7.27-7.19 (m, 8H), 4.05 (s, 12H), -2.23 (br s, 1H exchangeable with D₂O), -2.36 (br s, 1H exchangeable with D₂O) ppm; ¹³C NMR (100 MHz, CD₂Cl₂) δ 188.2, 159.82, 159.75, 159.6, 156.4, 154.9, 151.9, 145.4, 141.1, 139.8, 138.9, 138.80, 137.98, 135.4, 134.4, 133.6, 133.50, 133.47, 132.1, 128.6, 128.4, 127.63, 127.57, 123.8, 121.8, 115.8, 113.0, 112.7, 112.4, 112.2, 55.5, 55.42, 55.39, 53.8 ppm; UV-vis (CH₂Cl₂) λ_{max} (log ε) 410 (5.44), 465 (sh), 613 (4.04), 670 (sh) nm; FT-IR (neat, diamond ATR): 1732 (ν_{C=O}) cm⁻¹; HR-MS (ESI⁺, 100% CH₃CN, TOF) *m/z* calcd for C₄₈H₃₈N₅O₆ ([M·H]⁺) 780.2822, found 780.2801.

4. *in vivo* PAI Using a Quinoline-Annulated Porphyrin as NIR Molecular Contrast Agent

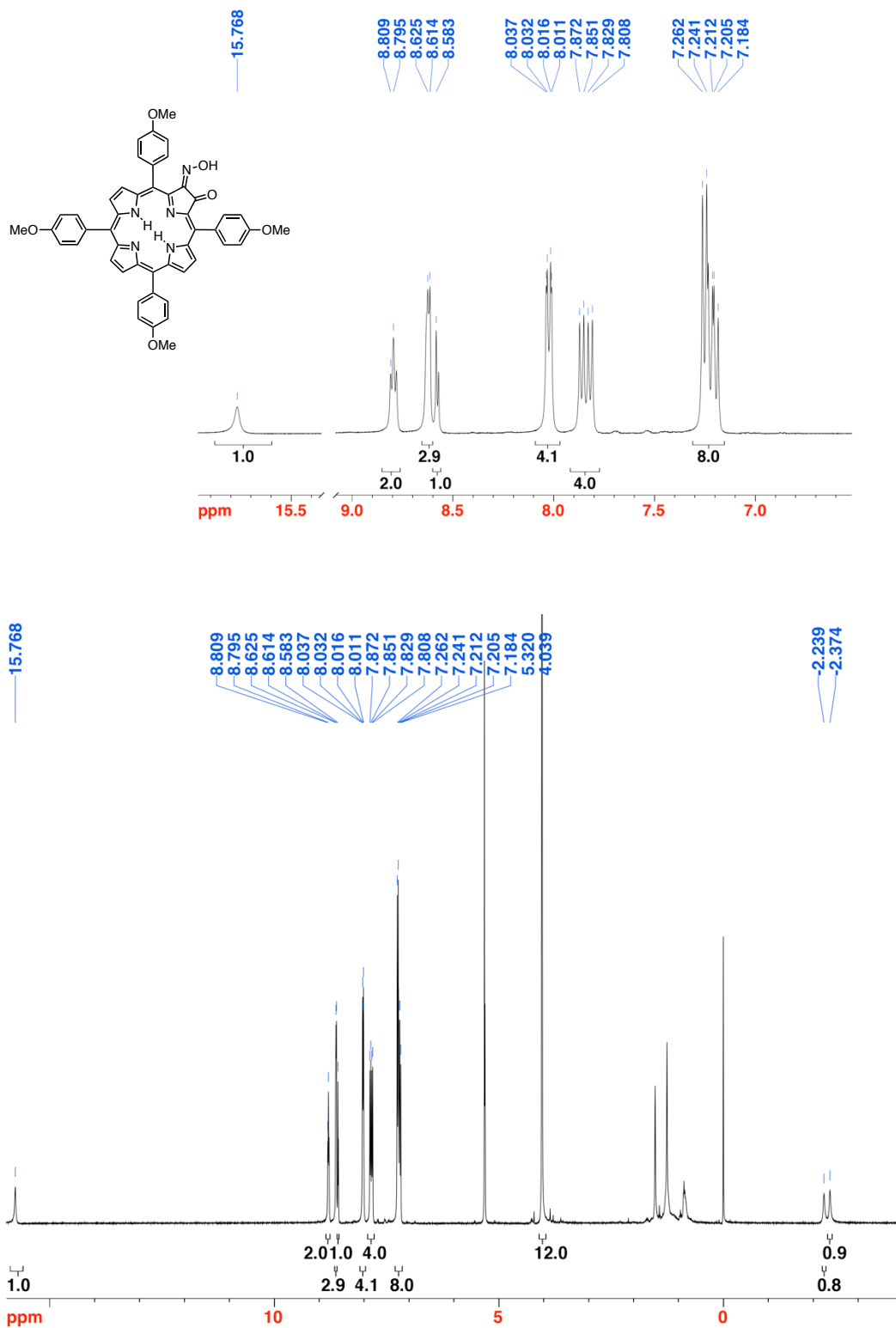


Figure 4-11. ^1H NMR spectrum (400 MHz, CD_2Cl_2) of **9**.

4. *in vivo* PAI Using a Quinoline-Annulated Porphyrin as NIR Molecular Contrast Agent

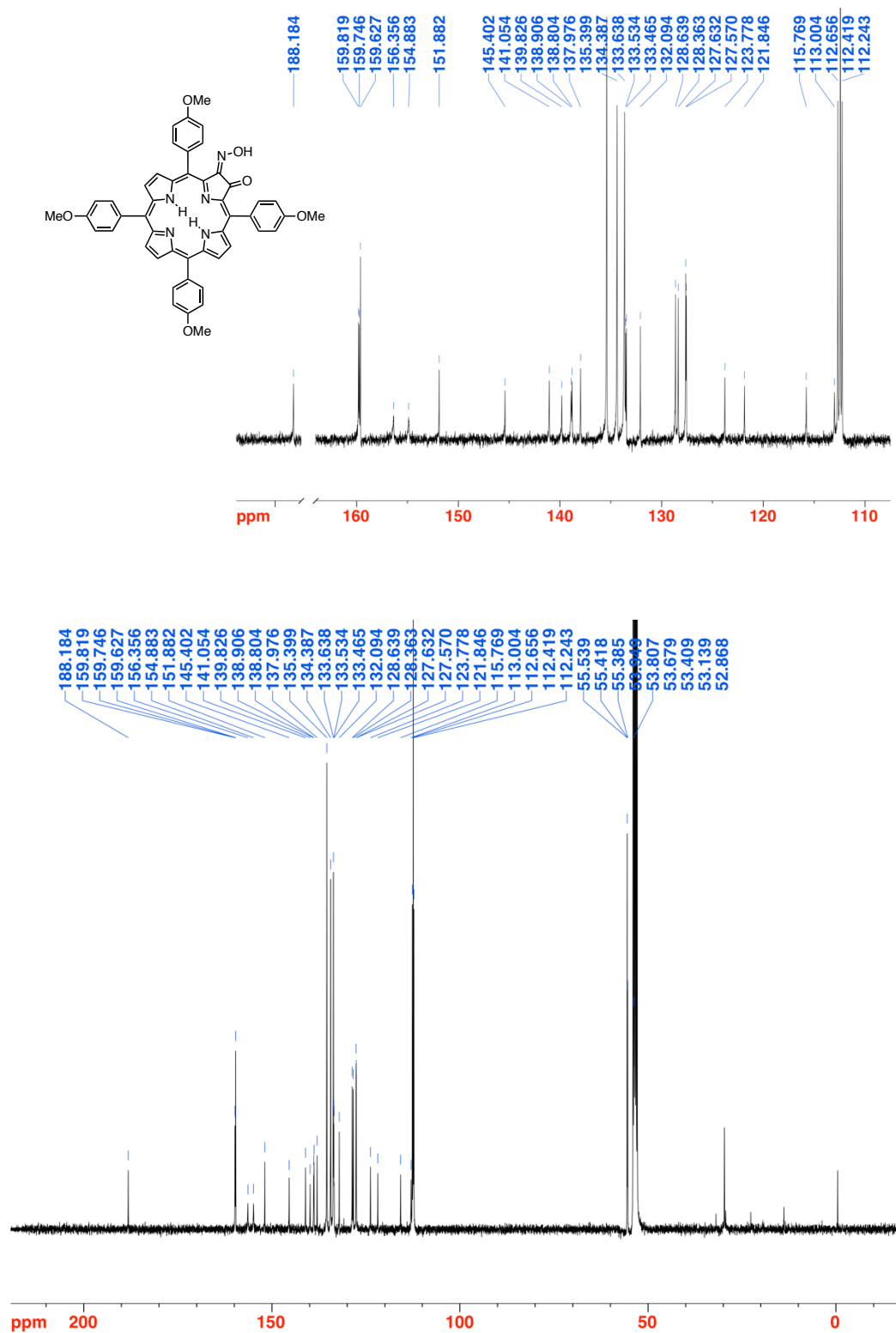


Figure 4-12. ^{13}C NMR spectrum (100 MHz, CD_2Cl_2) of **9**.

4. *in vivo* PAI Using a Quinoline-Annulated Porphyrin as NIR Molecular Contrast Agent

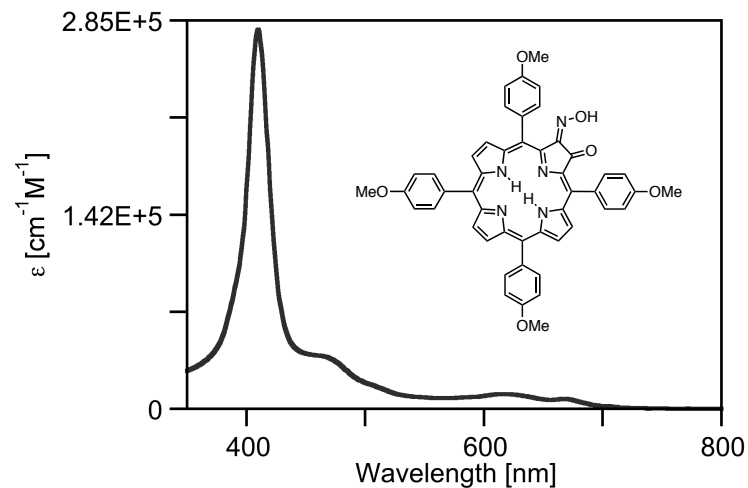


Figure 4-13. UV-vis spectrum (CH_2Cl_2) of **9**.

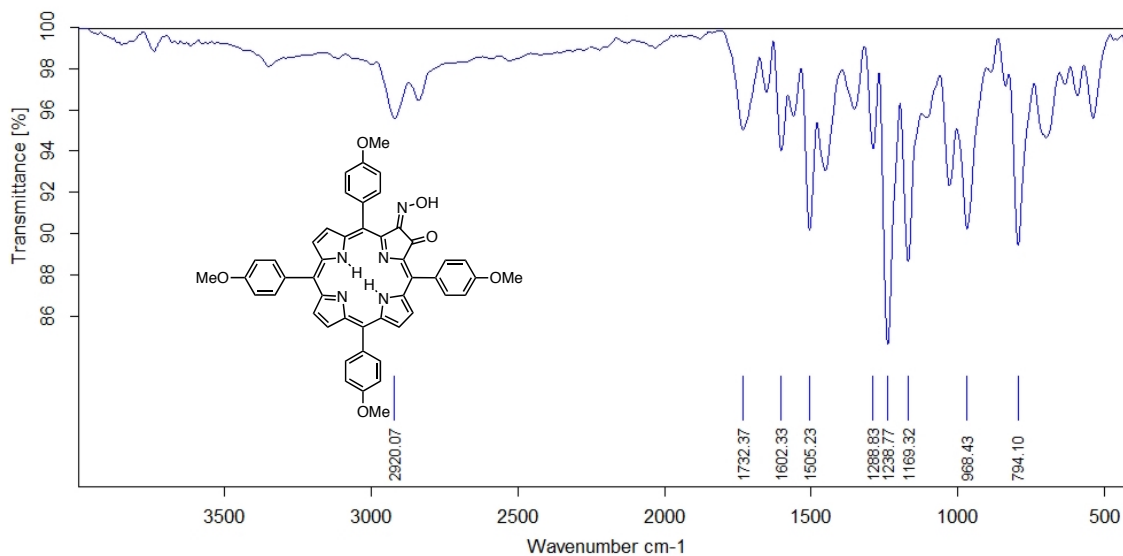


Figure 4-14. FT-IR spectrum (neat, diamond ATR) of **9**.

***meso*-Tris(*p*-methoxyphenyl)(*p*-methoxy)quinoline-annulated porphyrin *N*-Oxide (**5b**).**

Oxime **9** (14.7 mg, 1.88×10^{-5} mol) was dissolved in CH₂Cl₂ (10.0 mL) in a round bottom flask equipped with a magnetic stir bar. To the stirring solution was added 2,3-dichloro-5,6-dicyano-1,4-benzoquinone (DDQ, 9 mg, 2 equiv) and the mixture was stirred at ambient temperature. When the starting material was consumed (after 0.5 h; reaction control by UV-vis and TLC), the reaction mixture was filtered through a plug of silica gel. The filtrate was washed with water (2 × 10 mL), dried over anhyd Na₂SO₄, and evaporated to dryness by rotary evaporation. The resulting residue was purified by column chromatography (silica-CH₂Cl₂/1% MeOH) to afford the brown product **5b** in 97% yield (14 mg): *R*_f (silica-CH₂Cl₂/2% MeOH) = 0.22; ¹H NMR (400 MHz, CDCl₃) δ 8.54 (d, ³*J* = 4.2 Hz, 1H), 8.41 (d, ³*J* = 4.9 Hz, 1H), 8.35-8.28 (m, 3H), 8.19 (dd, ³*J* = 4.3 Hz, 2H), 8.03 (d, ³*J* = 2.0 Hz, 1H), 7.86-7.80 (m, 4H), 7.68-7.65 (m, 2H), 7.23-7.20 (m, 4H), 7.16-7.10 (m, 3H), 4.08-4.04 (m, 10H), 3.89 (s, 3H), -0.32 (br s, 2H, exchangeable with D₂O) ppm; ¹³C NMR (100 MHz, CDCl₃) δ 185.0, 159.9, 159.6, 159.3, 159.0, 155.9, 153.6, 145.9, 143.7, 143.5, 141.6, 138.2, 135.6, 135.5, 135.2, 134.9, 134.3, 133.7, 133.4, 133.3, 133.10, 132.98, 132.94, 131.0, 129.3, 127.7, 127.4, 127.3, 124.5, 123.8, 122.7, 120.9, 113.2, 113.1, 112.6, 112.5, 102.1, 101.9, 56.0, 55.6, 55.54, 55.47 ppm; UV-vis (CH₂Cl₂) λ_{max} (log ε) 422 (5.02), 504 (4.27), 543 (4.16), 751 (4.09) nm; FT-IR (neat, diamond ATR): 1686 (ν_{C=O}) cm⁻¹; HR-MS (ESI⁺, 100% CH₃CN, TOF) *m/z* calcd for C₄₈H₃₆N₅O₆ ([M·H]⁺), 778.2666, found 778.2693.

4. *in vivo* PAI Using a Quinoline-Annulated Porphyrin as NIR Molecular Contrast Agent

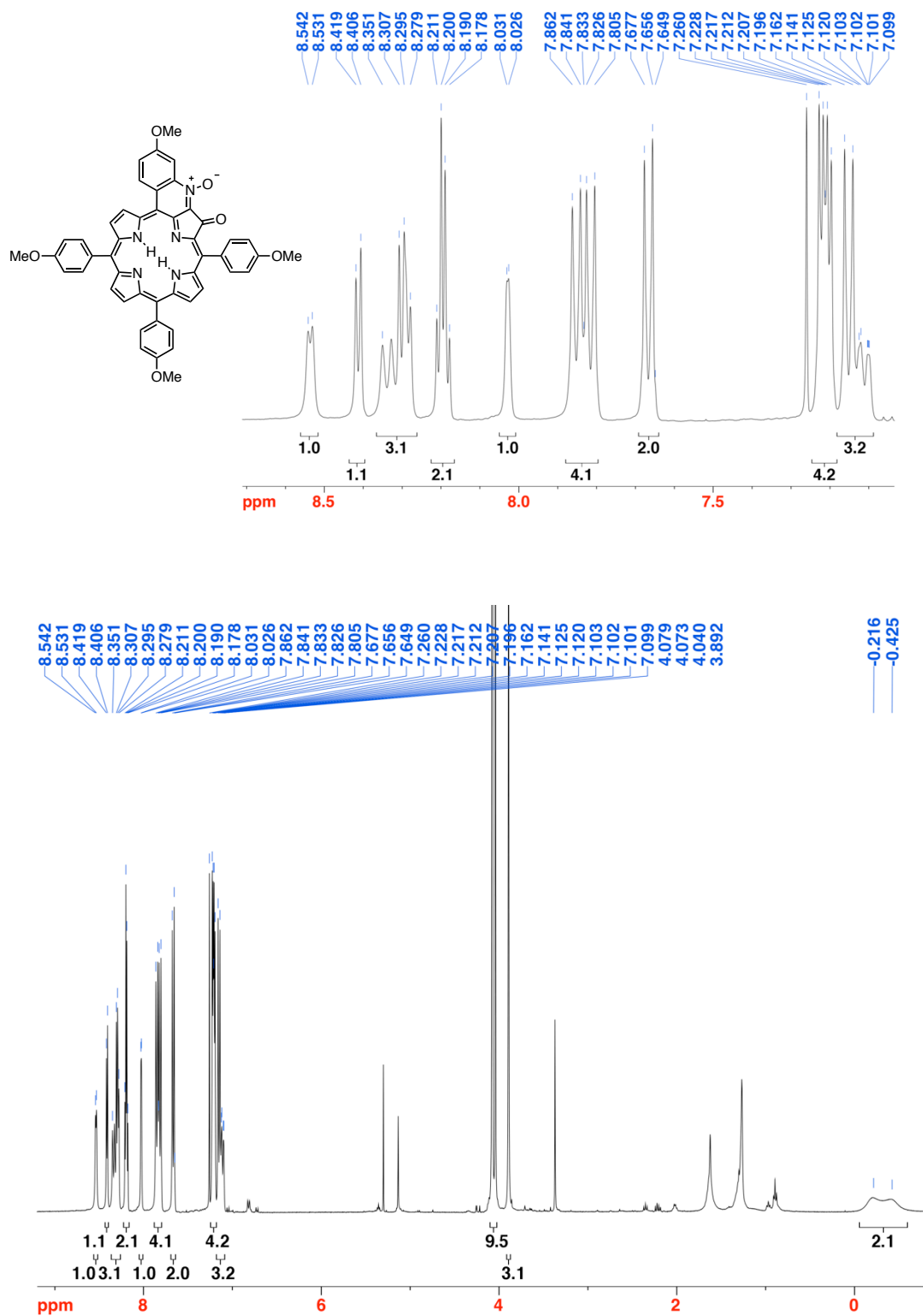


Figure 4-15. ^1H NMR spectrum (400 MHz, CDCl_3) of **5b**.

4. *in vivo* PAI Using a Quinoline-Annulated Porphyrin as NIR Molecular Contrast Agent

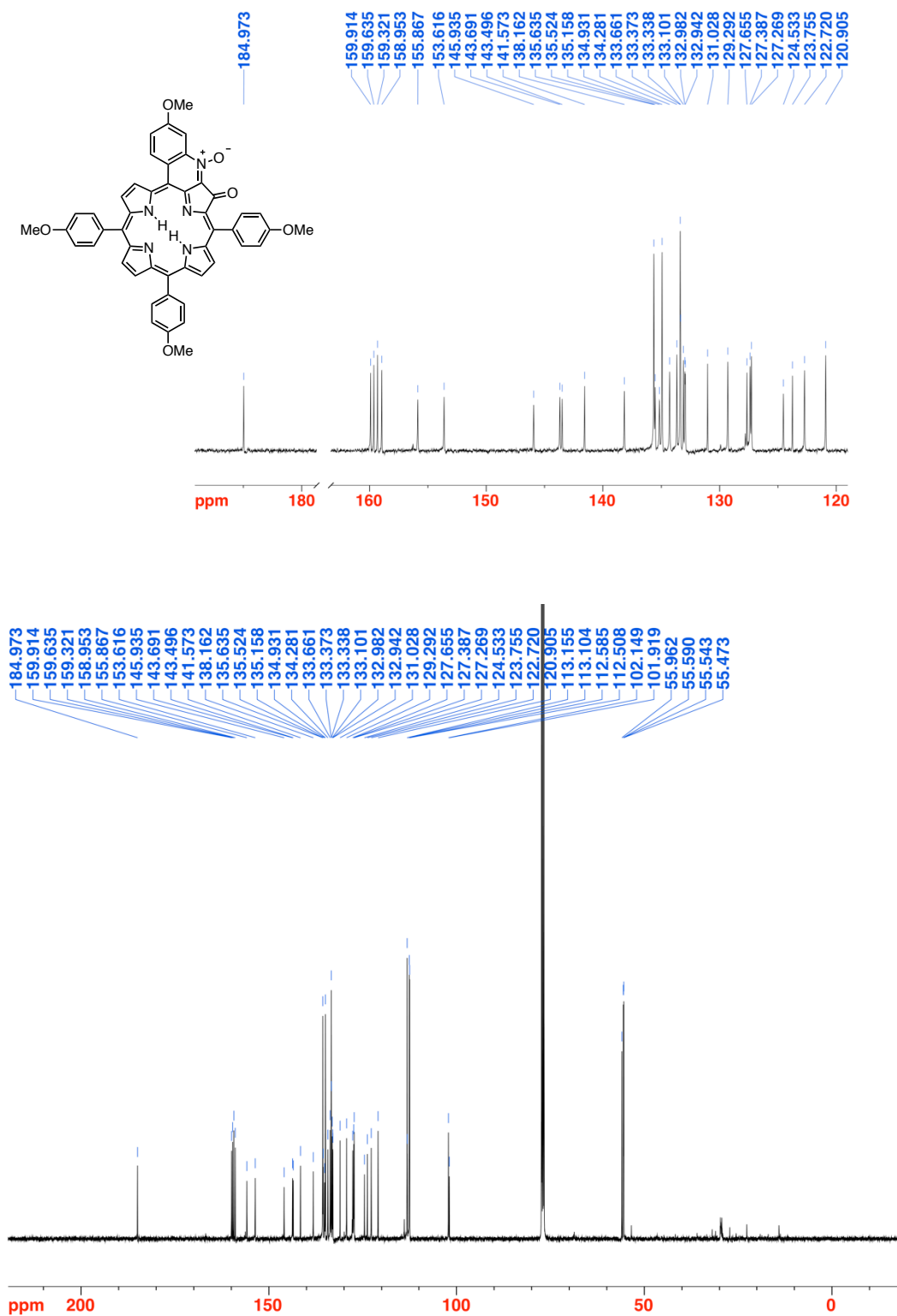


Figure 4-16. ^{13}C NMR spectrum (100 MHz, CDCl_3) of **5b**.

4. *in vivo* PAI Using a Quinoline-Annulated Porphyrin as NIR Molecular Contrast Agent

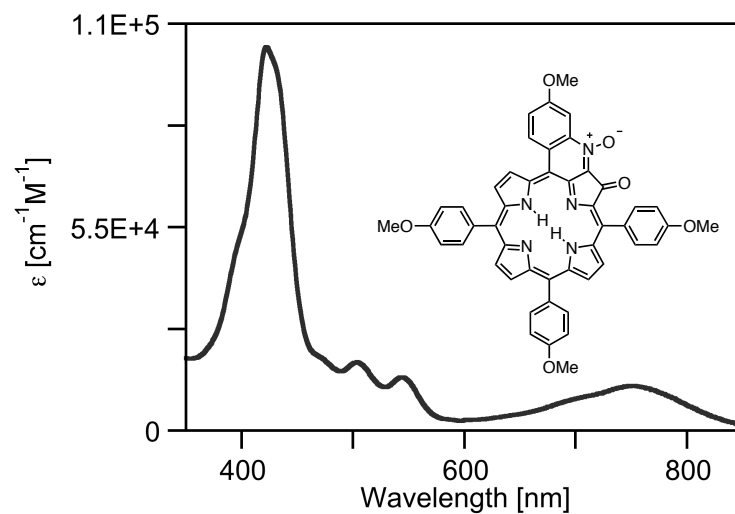


Figure 4-17. UV-vis spectrum (CH₂Cl₂) of **5b**.

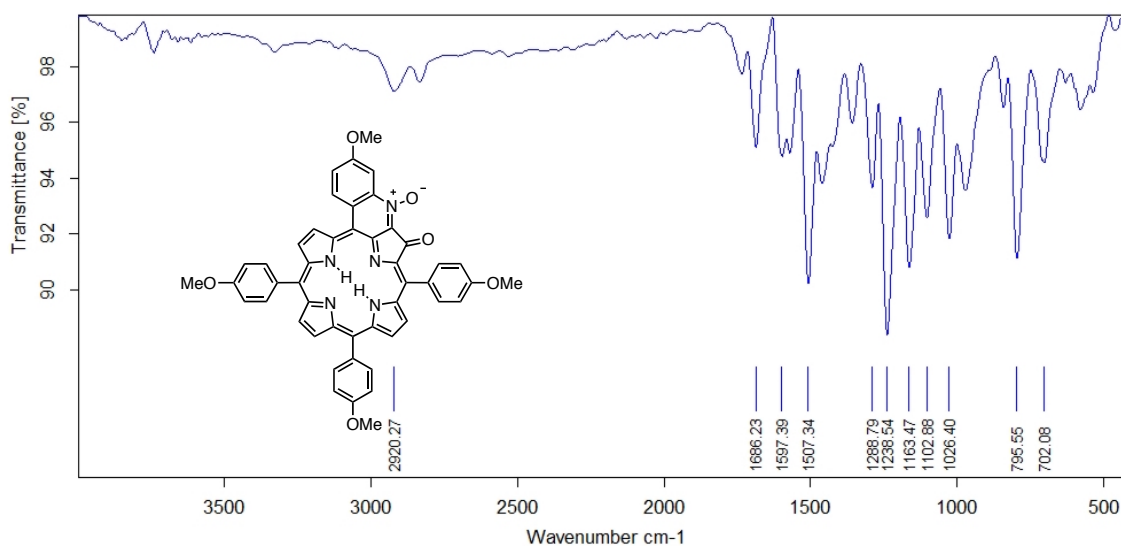


Figure 4-18. FT-IR spectrum (neat, diamond ATR) of **5b**.

meso-Tris(*p*-methoxyphenyl)(*p*-methoxy)quinoline-annulated porphyrin (4b). Quinoline *N*-oxide **5b** (23.7 mg, 3.05×10^{-5} mol) was dissolved in pyridine (25.0 mL) and heated to reflux. When the starting material was consumed (after 48 h; reaction control by TLC and UV-vis), the solvent was evaporated and the remaining residue was purified by preparative TLC (silica-CH₂Cl₂/2% MeOH) and solvent exchanged from CH₂Cl₂ to MeOH to afford the brown powder **4b** in 44% yield (10 mg): *R_f* (silica-CH₂Cl₂/2% MeOH) = 0.54; ¹H NMR (400 MHz, CD₂Cl₂): δ 8.97 (two overlapping d, ³*J* = 7.5 Hz, 2H), 8.37 (dd, ³*J* = 7.9, ⁴*J* = 4.9 Hz, 2H), 8.22 (d, ³*J* = 4.6 Hz, 1H), 8.16 (d, ³*J* = 4.4 Hz, 2H), 8.00-7.97 (m, 3H), 7.89 (d, ³*J* = 8.5 Hz, 2H), 7.73 (d, ³*J* = 8.4 Hz, 2H), 7.54 (dd, ³*J* = 9.1, ⁴*J* = 2.7 Hz, 1H), 7.28 (d, ³*J* = 8.5 Hz, 2H), 7.22 (dt, ³*J* = 5.3, ⁴*J* = 3.3 Hz, 4H), 4.09 (s, 3H), 4.06 (two overlapping singlets, 6H), 4.03 (s, 3H), 1.07 (s, 2H, exchangeable with D₂O); ¹³C NMR (100 MHz, CD₂Cl₂): δ 202.2, 180.4, 160.2, 159.8, 159.4, 159.0, 148.96, 148.85, 148.29, 148.21, 146.8, 146.56, 146.54, 145.7, 135.5, 134.7, 134.3, 133.5, 133.2, 132.9, 132.3, 131.0, 129.9, 127.5, 127.2, 122.9, 120.5, 113.0, 112.9, 112.8, 112.7, 112.6, 112.3, 110.0, 55.8, 55.6, 55.5, 55.4 ppm; UV-vis (CH₂Cl₂) λ_{max} (log ε) 418 (5.0), 490 (4.23), 529 (4.23), 701 (sh), 762 (4.12) nm; FT-IR (neat, diamond ATR): 1716 (ν_{C=O}) cm⁻¹; HR-MS (ESI⁺, 100% CH₃CN, TOF) *m/z* calcd for C₄₈H₃₆N₅O₅ ([M·H]⁺) 762.2716, found 762.2738.

4. *in vivo* PAI Using a Quinoline-Annulated Porphyrin as NIR Molecular Contrast Agent

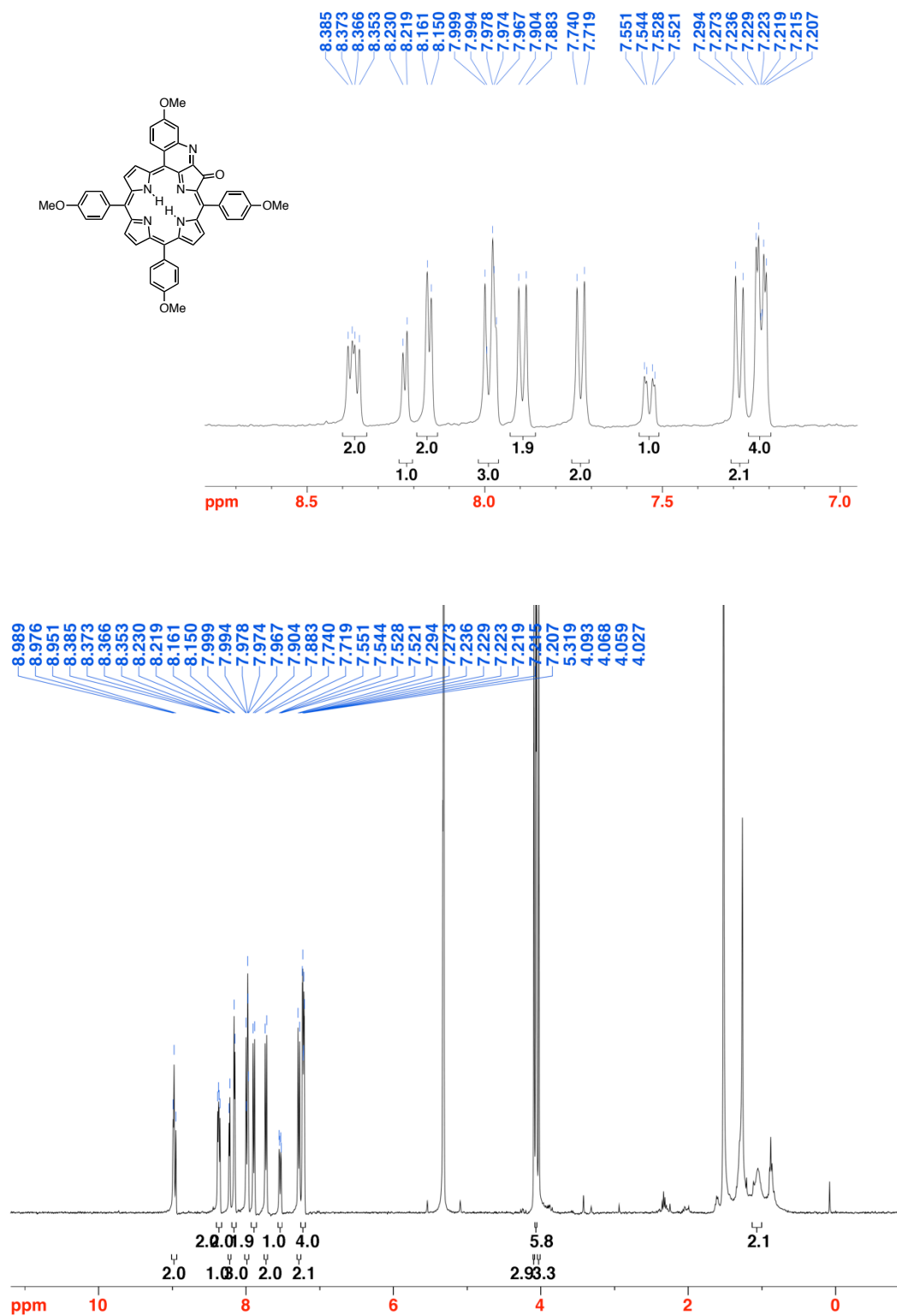


Figure 4-19. ¹H NMR spectrum (400 MHz, CD₂Cl₂) of **4b**.

4. *in vivo* PAI Using a Quinoline-Annulated Porphyrin as NIR Molecular Contrast Agent

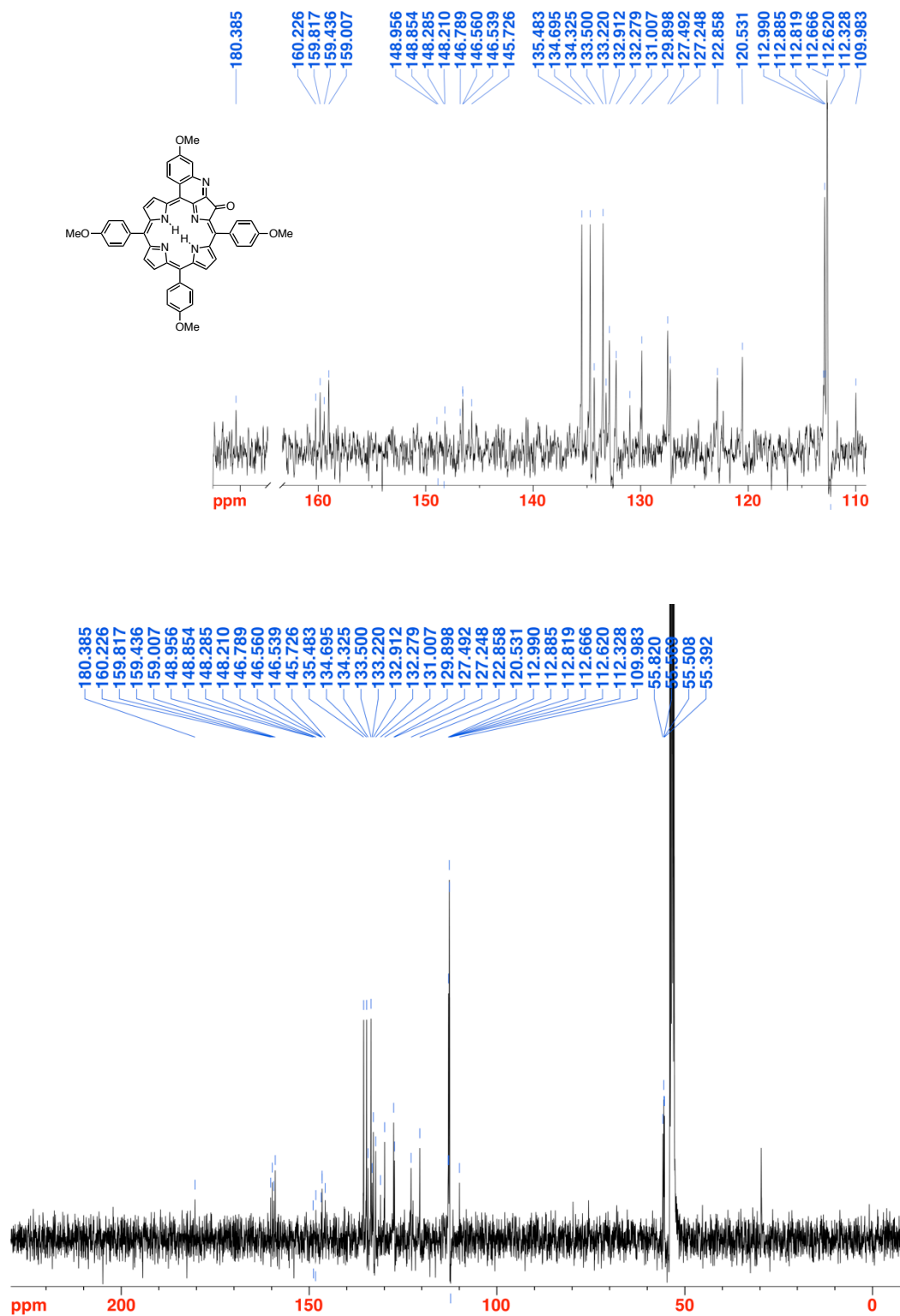


Figure 4-20. ^{13}C NMR spectrum (100 MHz, CD_2Cl_2) of **4b** (the compound has limited solubility).

4. *in vivo* PAI Using a Quinoline-Annulated Porphyrin as NIR Molecular Contrast Agent

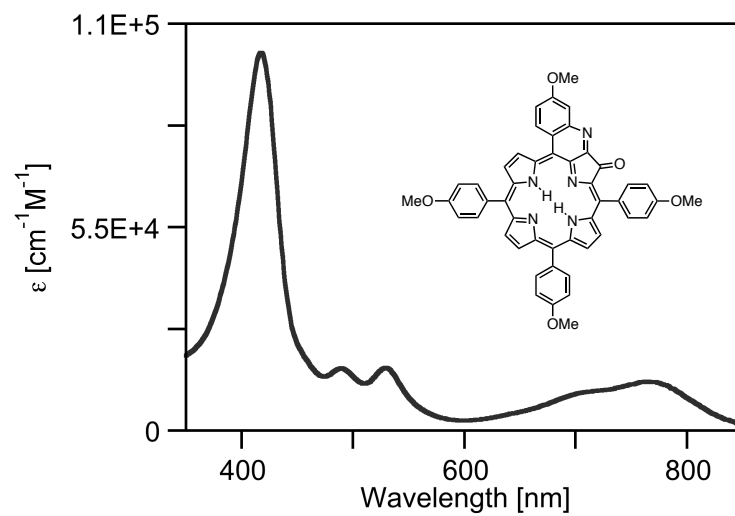


Figure 4-21. UV-vis spectrum (CH_2Cl_2) of **4b**.

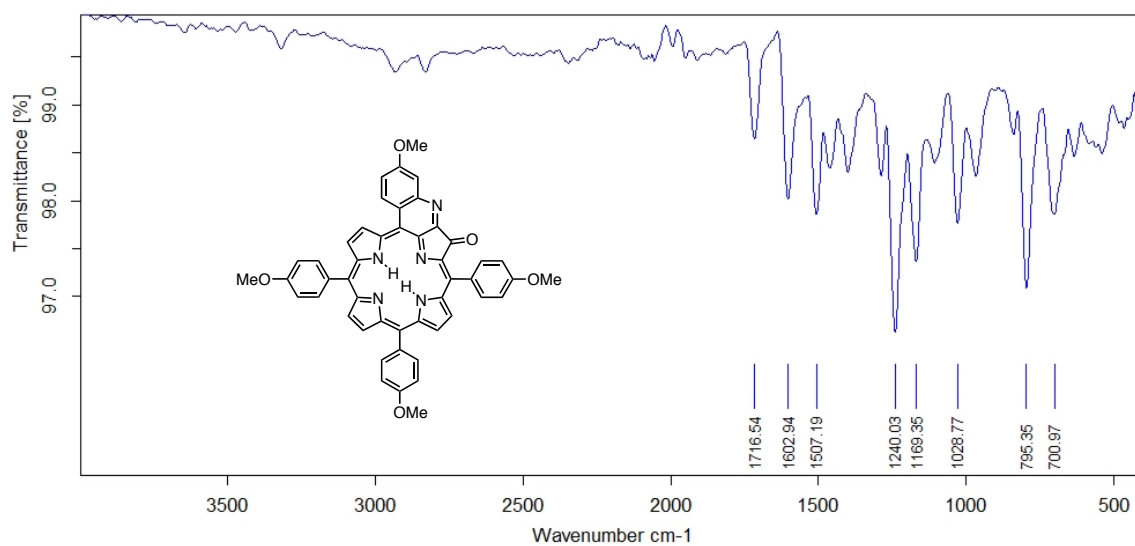


Figure 4-22. FT-IR spectrum (neat, diamond ATR) of **4b**.

meso-Tris(*p*-hydroxyphenyl)(*p*-hydroxy)quinoline-annulated porphyrin (4c). Quinoline *N*-oxide **5b** (26 mg, 3.3×10^{-5} mol) was dissolved in dry CH₂Cl₂ (5.5 mL) in a round bottom flask equipped with a magnetic stir bar and N₂ inlet. A 1.0 M solution of BBr₃ in CH₂Cl₂ (1.35 mL, ~40 equiv) was added drop-wise to the flask and the reaction mixture was stirred. When the starting material was consumed (after 24-48 h; reaction control by TLC), the excess BBr₃ was quenched by the careful addition of the reaction mixture to distilled water (10 mL). The resulting mixture was extracted with EtOAc (3 × 20 mL), washed with sat'd sodium bicarbonate solution and water (2 × 20 mL). The organic layer was then dried over anhydrous Na₂SO₄. The resulting residue was adsorbed onto silica gel and dry-loaded onto a silica gel column and purified by chromatography (silica-CH₂Cl₂/10% MeOH) to afford **4c** in 65% yield (18 mg): *R*_f (silica-CH₂Cl₂/10% MeOH) = 0.45; ¹H NMR (400 MHz, DMSO-*d*₆): δ 10.37 (s, 1H, exchangeable with D₂O), 10.09 (s, 1H, exchangeable with D₂O), 9.97 (s, 1H, exchangeable with D₂O), 9.71 (s, 1H, exchangeable with D₂O), 8.81 (s, 1H), 8.61 (s, 1H), 8.34 (s, 1H), 8.20 (s, 1H), 8.12 (d, ³*J* = 4.4 Hz, 1H), 8.03 (d, ³*J* = 5.8 Hz, 1H), 7.75 (d, ³*J* = 7.5, 3H), 7.58 (d, ³*J* = 7.8 Hz, 2H), 7.34 (d, ³*J* = 3.9 Hz, 1H), 7.16 (d, ³*J* = 7.9 Hz, 2H), 7.11 (d, ³*J* = 8.2 Hz, 2H), 7.04 (d, ³*J* = 8.4 Hz, 2H) ppm; ¹³C NMR (100 MHz, DMSO-*d*₆): δ 194.6, 158.6, 158.1, 157.5, 157.4, 150.51, 150.49, 150.47, 146.12, 146.10, 142.03, 141.96, 138.92, 138.89, 136.1, 135.8, 135.43, 135.39, 135.2, 134.7, 134.6, 134.03, 133.94, 133.4, 132.5, 131.4, 131.1, 130.6, 130.3, 130.10, 130.09, 129.4, 127.86, 127.83, 127.80, 127.32, 127.30, 127.27, 127.26, 124.59, 124.57, 123.29, 123.26, 123.20, 123.19, 120.98, 120.96, 120.95, 120.26, 120.25, 115.44, 115.41, 114.95, 114.92, 114.82, 114.76, 114.68, 111.9, 109.4, 100.0 ppm; UV-vis (MeOH) λ_{max} (log ε) 417 (5.15), 487 (sh), 531 (4.31), 748 (4.24) nm; FT-IR (neat, diamond ATR): 1705 (ν_{C=O}) cm⁻¹; HR-MS (ESI⁺, 100% CH₃CN, TOF) *m/z* calcd for C₄₄H₂₈N₅O₅ ([M·H]⁺) 706.2090, found 706.2061.

4. *in vivo* PAI Using a Quinoline-Annulated Porphyrin as NIR Molecular Contrast Agent

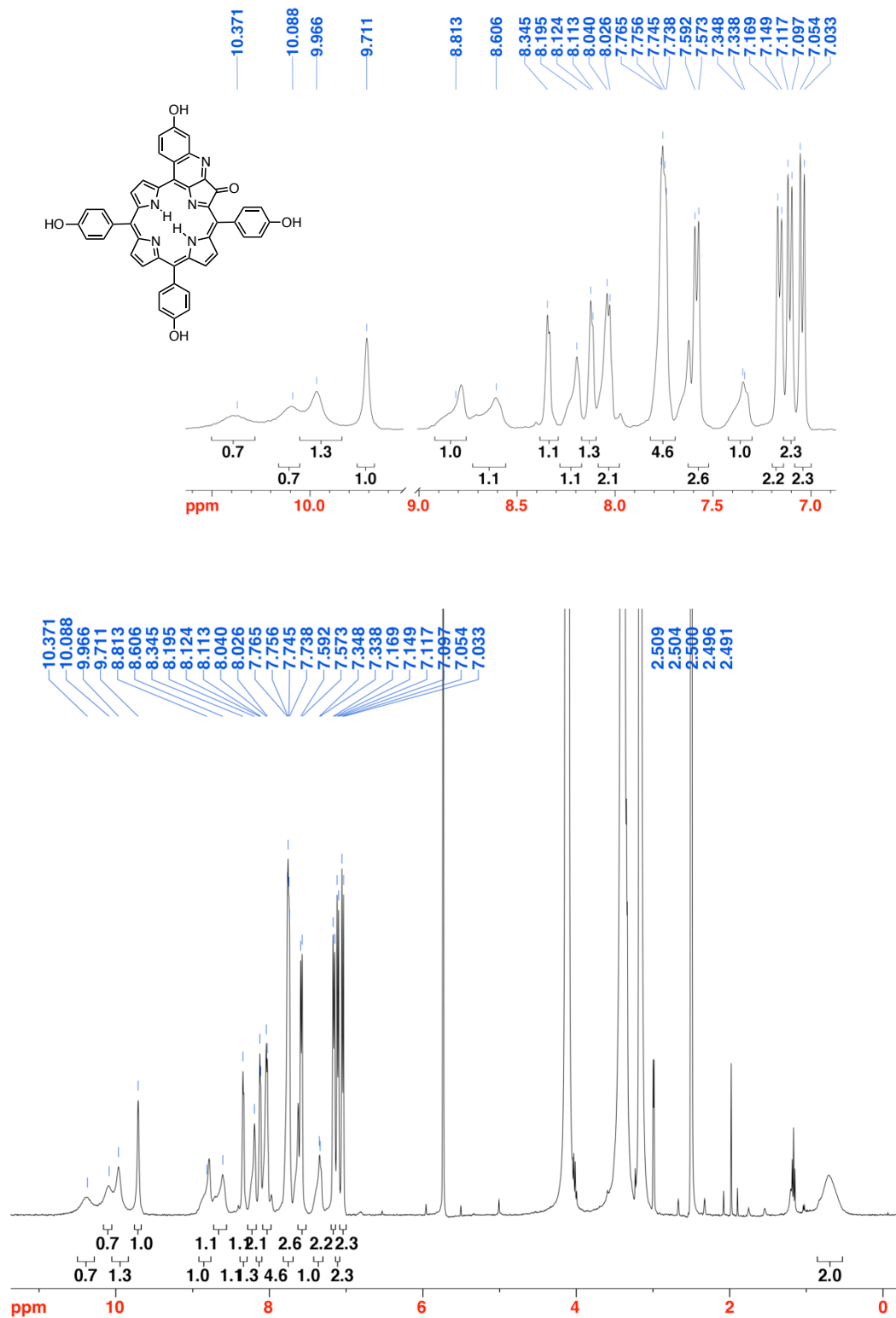


Figure 4-23. ^1H NMR spectrum (400 MHz, DMSO-d_6) of **4c**.

4. *in vivo* PAI Using a Quinoline-Annulated Porphyrin as NIR Molecular Contrast Agent

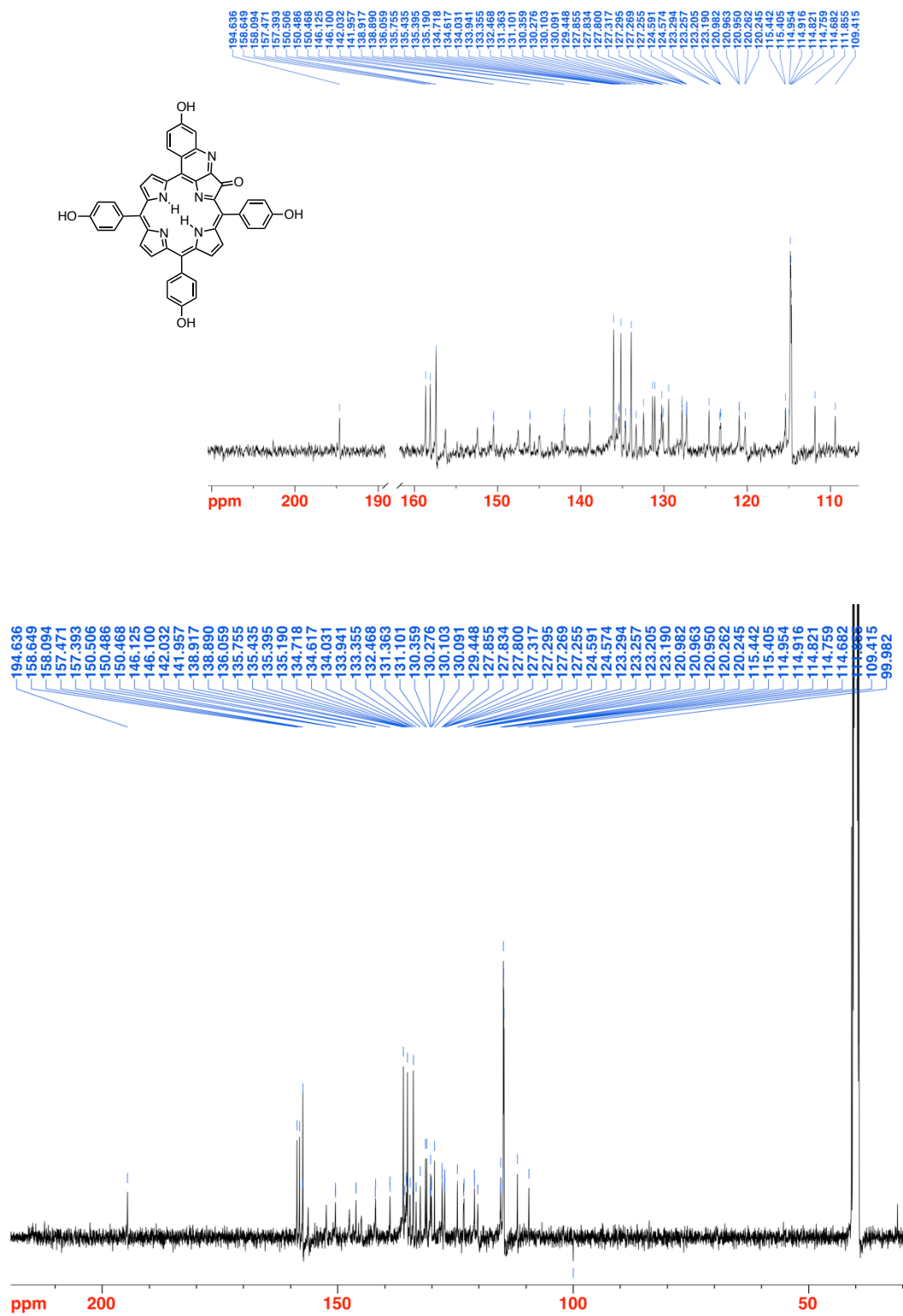


Figure 4-24. ¹³C NMR spectrum (100 MHz, DMSO-d₆) of 4c.

4. *in vivo* PAI Using a Quinoline-Annulated Porphyrin as NIR Molecular Contrast Agent

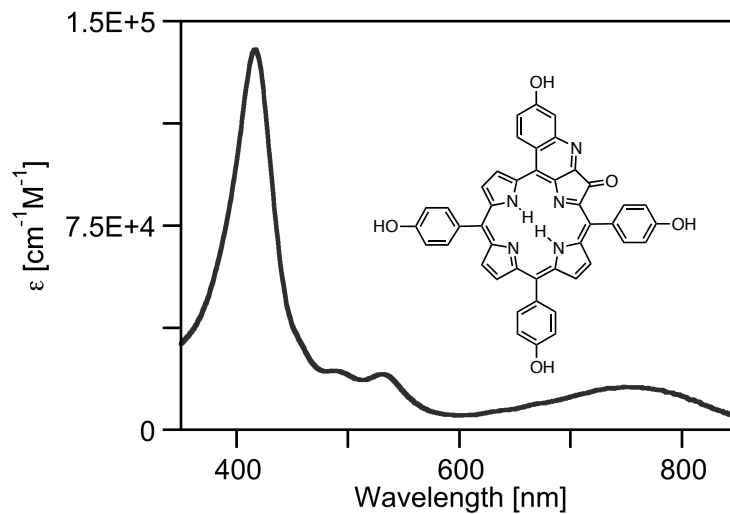


Figure 4-25. UV-vis spectrum (MeOH) of **4c**.

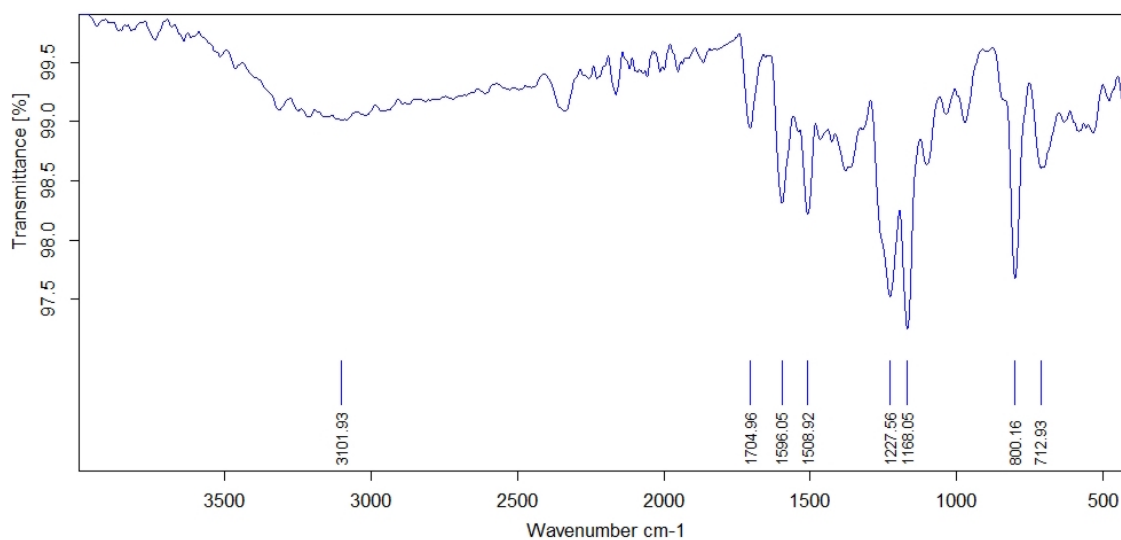


Figure 4-26. FT-IR spectrum (neat, diamond ATR) of **4c**.

***meso*-Tris(*p*-MeOPEG₄Ophenyl)(*p*-MeOPEG₄O)quinoline-annulated porphyrin (4d).**

Following a literature protocol for the PEGylation of a *meso*-(*p*-OH-phenyl)porphyrin,²⁹ quinoline--annulated porphyrin **4c** (10 mg, 1.4×10^{-5} mol) was dissolved in dry DMF (4.0 mL) in a two-neck round bottom flask equipped with a magnetic stir bar. MeO-PEG₄-OMs (25.0 mg, 8.9×10^{-5} mol, 6 equiv.) and Cs₂CO₃ (24.2 mg, 7.4×10^{-5} mol, 5.2 equiv.) were added and the reaction mixture was immersed in a preheated oil bath at ~100 °C. After consumption of the starting material after ~3 h (reaction control by TLC) the solvent was evaporated and the residue was partitioned between EtOAc (10 mL) and H₂O (10 mL). The organic layer was washed with H₂O (3 × 10 mL) and dried over Na₂SO₄. The brown residue was purified by column chromatography (silica-CH₂Cl₂/5% MeOH) to afford the tetra-PEGylated product **4d** as a yellow-brown oil in 56% yield (12 mg): *R*_f (silica-CH₂Cl₂/10% MeOH) = 0.56; ¹H NMR (500 MHz, CD₂Cl₂): δ 9.06-9.04 (m, 2H), 8.40 (d, ³*J* = 4.5 Hz, 1H), 8.36 (d, ³*J* = 5.0 Hz, 1H), 8.23 (d, ³*J* = 4.5 Hz, 1H), 8.16 (d, ³*J* = 4.5 Hz, 2H), 7.99 (d, ³*J* = 8.5 Hz, 3H), 7.89 (d, ³*J* = 8.5 Hz, 2H), 7.71 (d, ³*J* = 8.5 Hz, 2H), 7.63 (dd, ³*J* = 9.1, ⁴*J* = 2.5 Hz, 1H), 7.30 (d, ³*J* = 8.6 Hz, 2H), 7.23 (dd, ³*J* = 8.5, ⁴*J* = 1.8 Hz, 4H), 4.44 (t, ³*J* = 4.5 Hz, 2H), 4.38 (two overlapping t, ³*J* = 4.7 Hz, 4H), 4.35 (t, ³*J* = 4.6 Hz, 2H), 3.99 (dd, ³*J* = 8.8, ⁴*J* = 4.7 Hz, 6H), 3.82-3.77, (m, 8H), 3.72-3.57 (m, 34H), 3.55-3.50 (m, 8H), 3.35 (s, 3H), 3.34 (s, 3H), 3.33 (s, 3H), 3.31 (s, 3H) ppm; UV-vis (CH₂Cl₂) λ_{max} (log ε) 419 (5.2), 491 (4.5), 531 (4.4), 764 (4.3) nm; HR-MS (ESI⁺, 100% CH₃CN, TOF) *m/z* calcd for C₈₀H₁₀₀N₅O₂₁ ([M·H]⁺), 1466.6911, found 1466.6891.

4. *in vivo* PAI Using a Quinoline-Annulated Porphyrin as NIR Molecular Contrast Agent

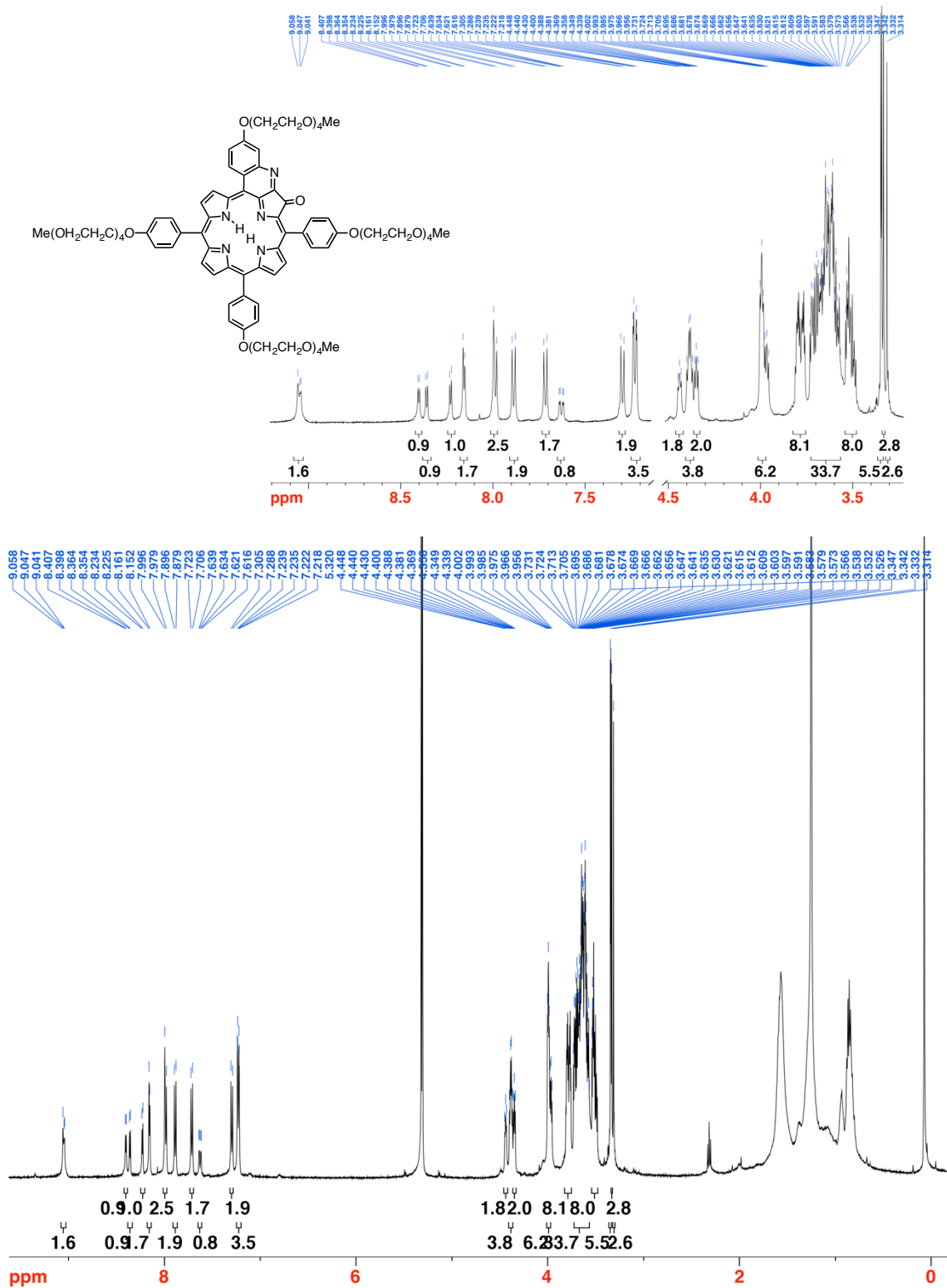


Figure 4-27. ^1H NMR spectrum (500 MHz, CD_2Cl_2) of **4d**.

4. *in vivo* PAI Using a Quinoline-Annulated Porphyrin as NIR Molecular Contrast Agent

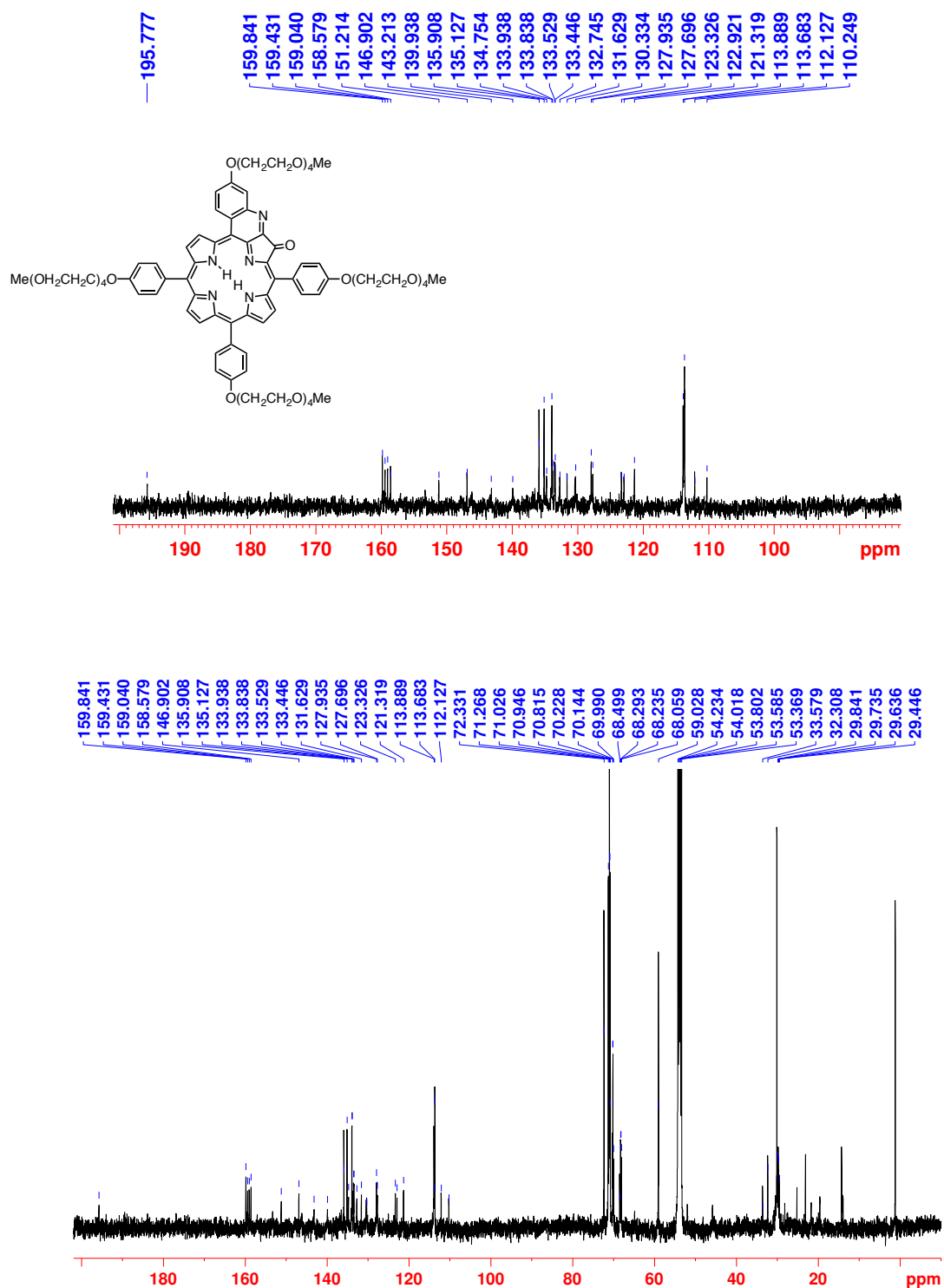


Figure 4-28. ¹³C NMR spectrum (125 MHz, CD₂Cl₂) of 4d.

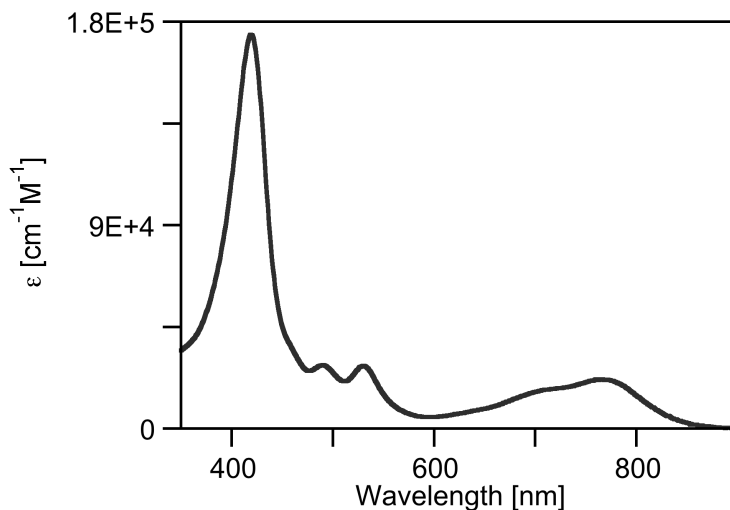


Figure 4-29. UV-vis spectrum (CH_2Cl_2) of **4d**.

***meso*-Tris(*p*-MeOPEG₁₂Ophenyl)(*p*-MeOPEG₁₂O)quinoline-annulated porphyrin (**4e**).**

Prepared from **4c** (22 mg, 3.1×10^{-5} mol) in dry DMF (10.0 mL), Cs_2CO_3 (80 mg, 1.6×10^{-4} mol, 5.2 equiv.), and MeO-PEG₁₂-OMs (80 mg, 1.2×10^{-4} mol, 4 equiv.) as described for the preparation of **4d**. Reaction time at 90 °C ~3 h. Purified by column chromatography (silica- CH_2Cl_2 /10% MeOH) to afford the tetra-PEGylated porphyrin **4e** as a brown oil in 90-99 % yield (81 mg-89 mg): ^1H NMR (400 MHz, CD_2Cl_2): δ 9.04 (s, 1H), 8.38 (two overlapping d, 2H), 8.19 (d, 3H), 7.98 (t, $^3J = 6.6$ Hz, 3H), 7.89 (d, $^3J = 8.3$ Hz, 3H), 7.72 (d, $^3J = 8.4$ Hz, 2H), 7.63 (d, $^3J = 8.3$ Hz, 1H), 7.31 (d, $^3J = 8.5$ Hz, 3H), 7.24 (dd, $^3J = 8.6$, $^4J = 2.2$ Hz, 4H), 3.34 (four overlapping s, 12H) ppm; UV-vis (CH_2Cl_2) λ_{max} (rel I.) 422 (1.0) 529 (0.20) 763 (0.09) nm; HR-MS (ESI⁺, 100% CH_3CN , TOF) cluster of peaks corresponding to addition of four PEG groups, see ESI.

4. *in vivo* PAI Using a Quinoline-Annulated Porphyrin as NIR Molecular Contrast Agent

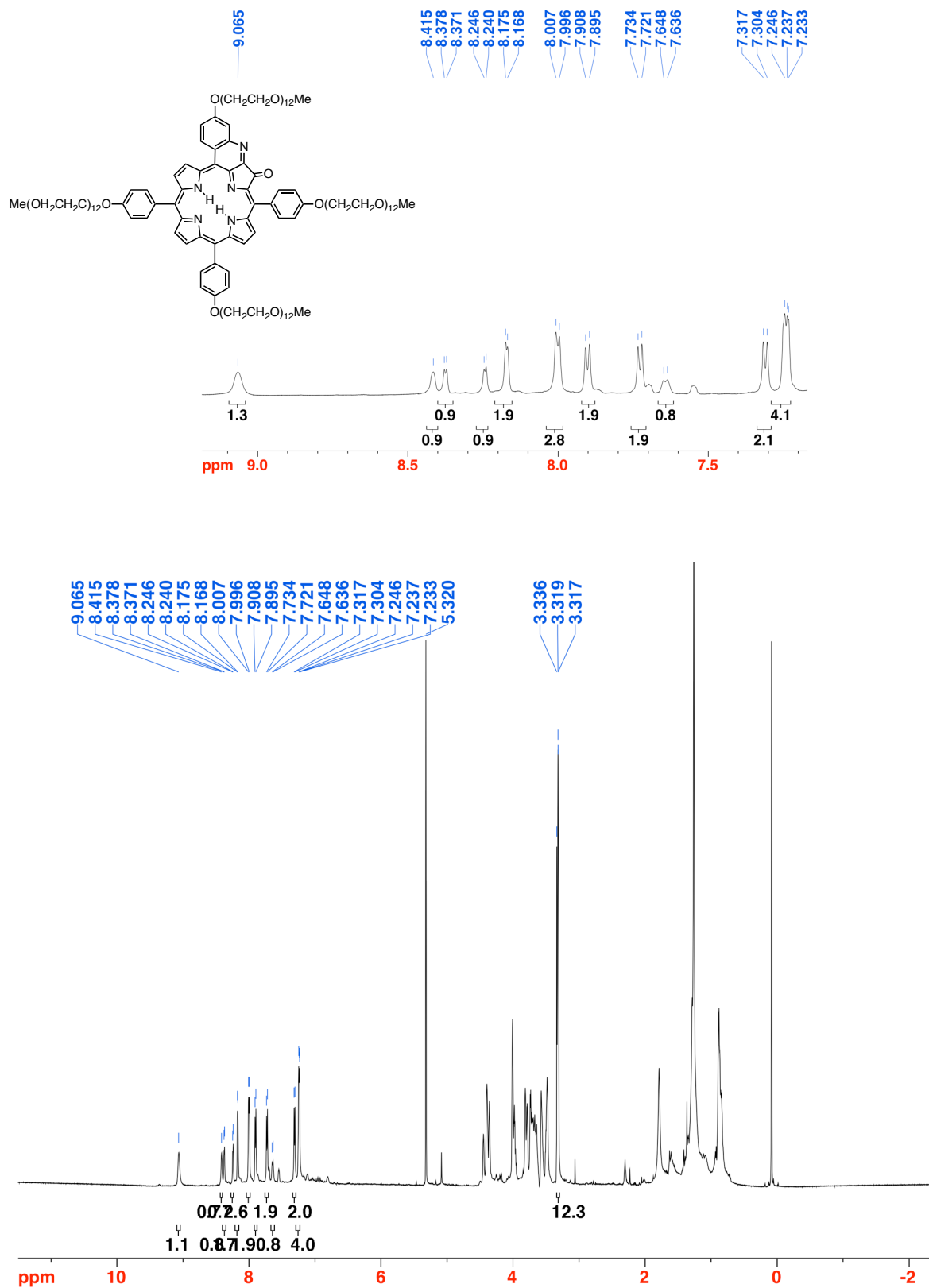


Figure 2-30. ^1H NMR spectrum (400 MHz, CD_2Cl_2) of **4e**.

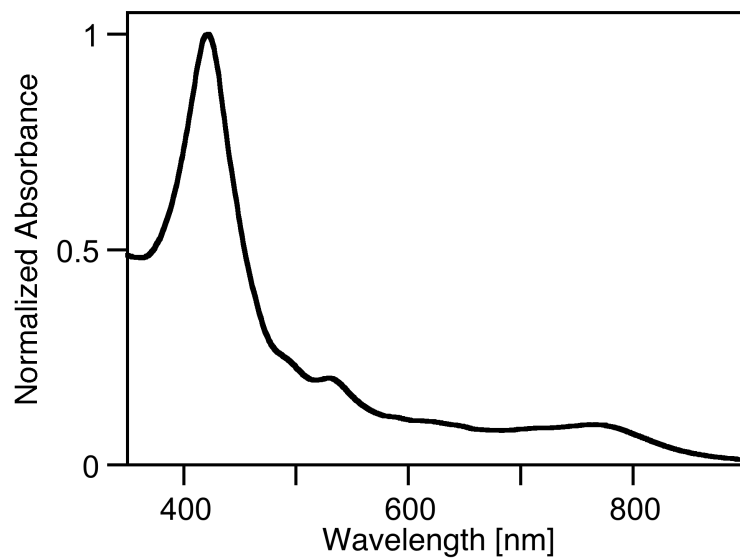


Figure 4-31. UV-vis spectrum (H_2O) of **4e**.

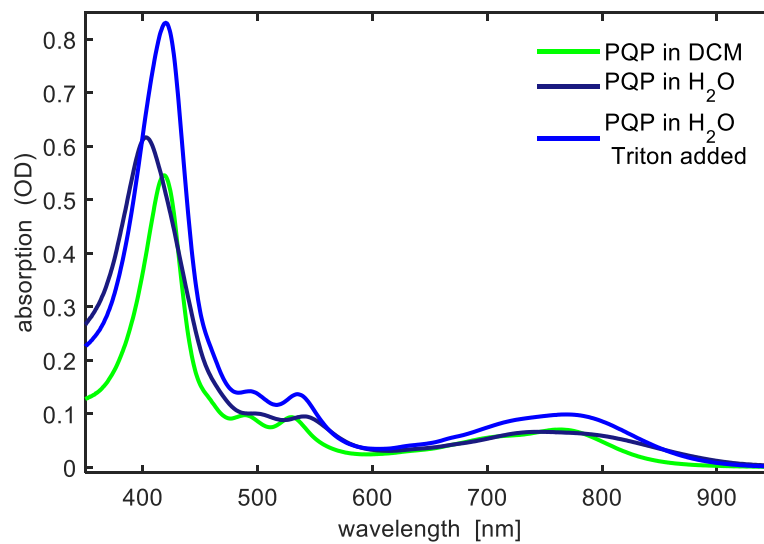


Figure 4-32. Absorption spectra of **4e** (PQP) in CH_2Cl_2 , H_2O and H_2O -Triton-X solutions. The change of the absorption spectrum of **4e** in H_2O after adding triton indicates that **4e** is somewhat aggregated in pure aqueous solution.

4. *in vivo* PAI Using a Quinoline-Annulated Porphyrin as NIR Molecular Contrast Agent

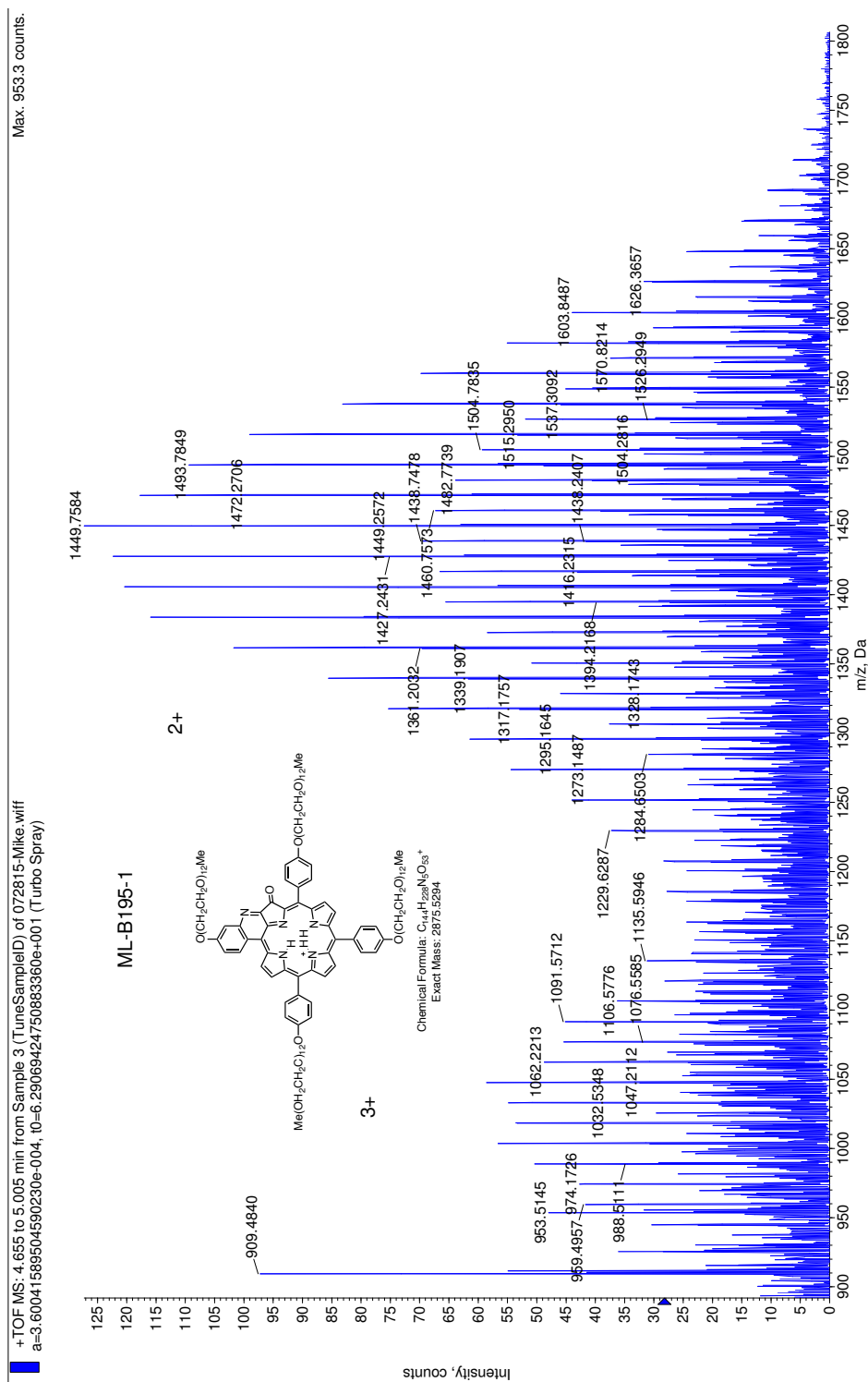


Figure 4-33. HR-MS (ESI⁺, 100% CH₃CN, TOF) of **4e**.

[*meso*-Tris(*p*-hydroxyphenyl)(*p*-hydroxy)quinoline-annulated porphyrinato]Zinc(II) (4cZn**).**

Quinoline-annulated porphyrin **4c** (19 mg, 2.7×10^{-5} mol) was dissolved in CH₂Cl₂/10% MeOH (7.0 mL) in a round bottom flask equipped with a magnetic stir bar. Zn(OAc)₂·2H₂O (18 mg, 8.1×10^{-5} mol, 3 equiv.) was added and the reaction was gently warmed. When the starting material was consumed (after 10 min; reaction control by TLC and UV-vis), the solvents were evaporated, and the residue was taken up in EtOAc and washed with water (3 × 20 mL). The organic layer was dried over anhydrous Na₂SO₄ and evaporated to dryness by rotary evaporation to afford **4cZn** as an orange solid in near-quantitative yield (21 mg): *R*_f (silica-CH₂Cl₂/10% MeOH) = 0.39; ¹H NMR (400 MHz, DMSO-*d*₆): δ 10.23 (s, 1H, exchangeable with D₂O), 9.94 (s, 1H, exchangeable with D₂O), 9.85 (s, 1H, exchangeable with D₂O), 9.57 (s, 1H, exchangeable with D₂O), 8.90 (t, ³*J* = 7.9 Hz, 2H), 8.19 (d, ³*J* = 4.5 Hz, 1H), 8.05 (d, ³*J* = 4.6 Hz, 1H), 7.99 (dd, ³*J* = 12.1, ⁴*J* = 4.4 Hz, 2H), 7.76 (t, ³*J* = 6.4 Hz, 4H), 7.70 (d, ³*J* = 8.2 Hz, 2H), 7.56 (dd, ³*J* = 9.0, ⁴*J* = 2.4 Hz, 1H), 7.47 (d, ³*J* = 8.2 Hz, 2H), 7.13 (d, ³*J* = 8.3 Hz, 2H), 7.07 (d, ³*J* = 8.3 Hz, 2H), 7.00 (d, ³*J* = 8.2 Hz, 2H) ppm; ¹³C NMR (100 MHz CD₂Cl₂/10% MeOD): δ 195.7, 159.8, 158.1, 157.8, 157.0, 156.6, 152.7, 152.1, 150.9, 150.5, 150.1, 148.0, 146.3, 143.3, 142.7, 135.6, 135.4, 134.8, 134.6, 133.8, 133.7, 133.6, 133.52, 133.47, 133.2, 132.0, 131.2, 131.06, 130.13, 130.0, 126.7, 123.7, 121.0, 115.6, 115.0, 114.7, 114.5, 111.9 ppm; UV-vis (MeOH) λ_{max} (log ε) 420 (5.13), 484 (sh), 518 (sh), 737 (sh), 816 (4.25) nm; FT-IR (neat, diamond ATR): ~1750 (ν_{C=O}) cm⁻¹; HR-MS (ESI⁺, 100% CH₃CN, TOF) *m/z* calcd for C₄₄H₂₆N₅O₅Zn ([M·H]⁺) 768.1225, found 768.1222.

4. *in vivo* PAI Using a Quinoline-Annulated Porphyrin as NIR Molecular Contrast Agent

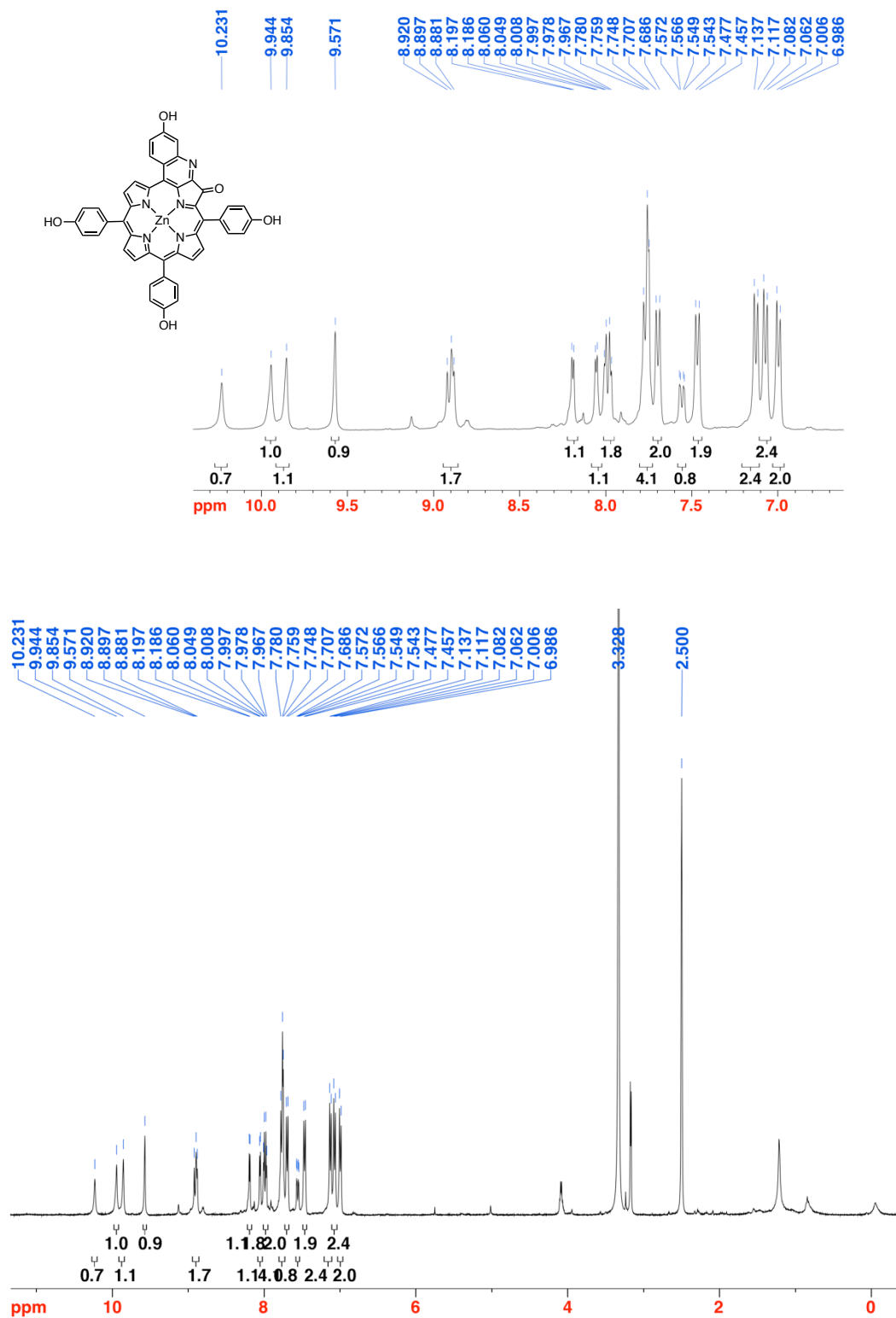


Figure 4-34. ¹H NMR spectrum (400 MHz, DMSO-d₆) of **4c^{Zn}**.

4. *in vivo* PAI Using a Quinoline-Annulated Porphyrin as NIR Molecular Contrast Agent

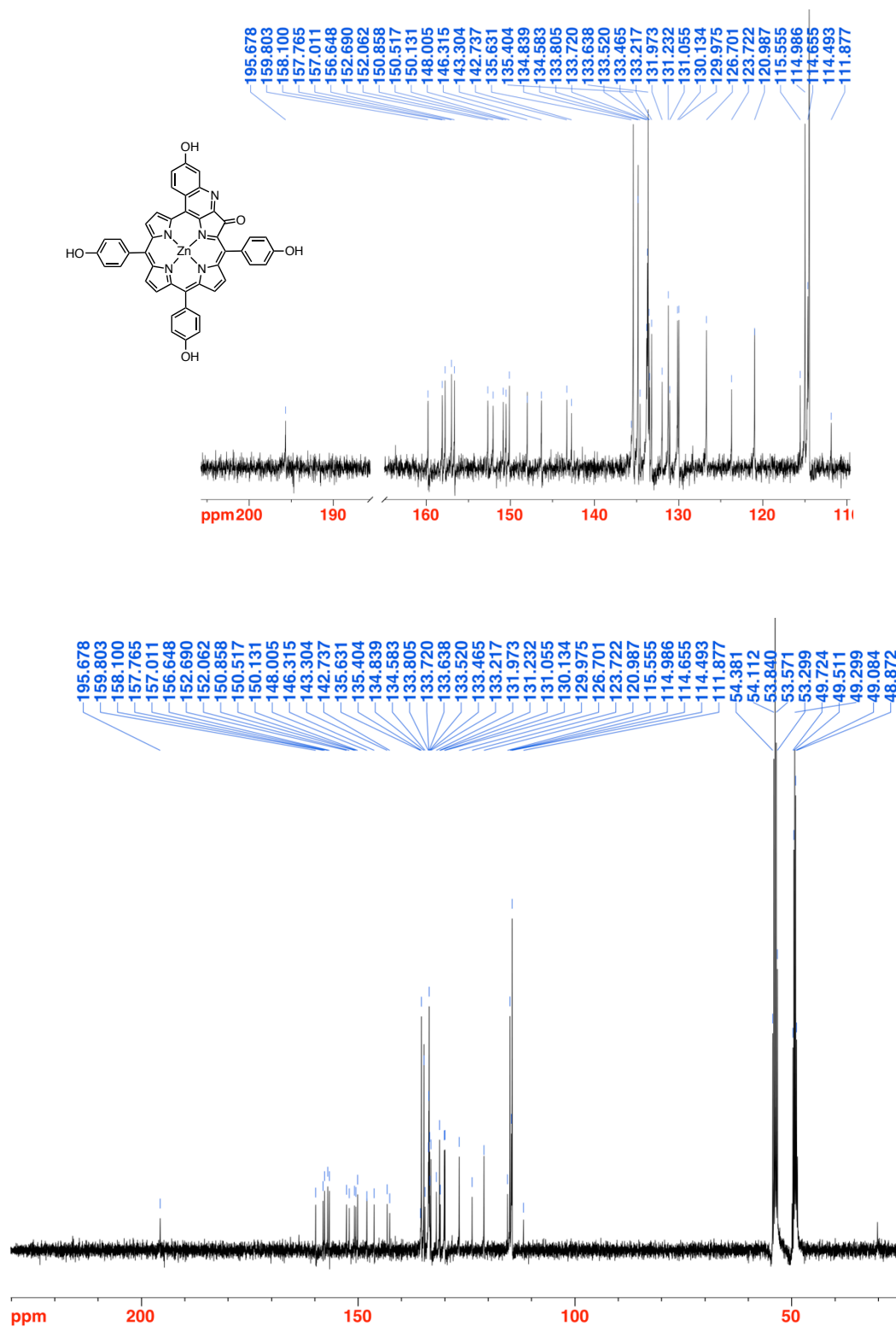


Figure 4-35. ¹³C NMR spectrum (100 MHz, CD₂Cl₂/10% MeOD) of **4c^{Zn}**.

4. *in vivo* PAI Using a Quinoline-Annulated Porphyrin as NIR Molecular Contrast Agent

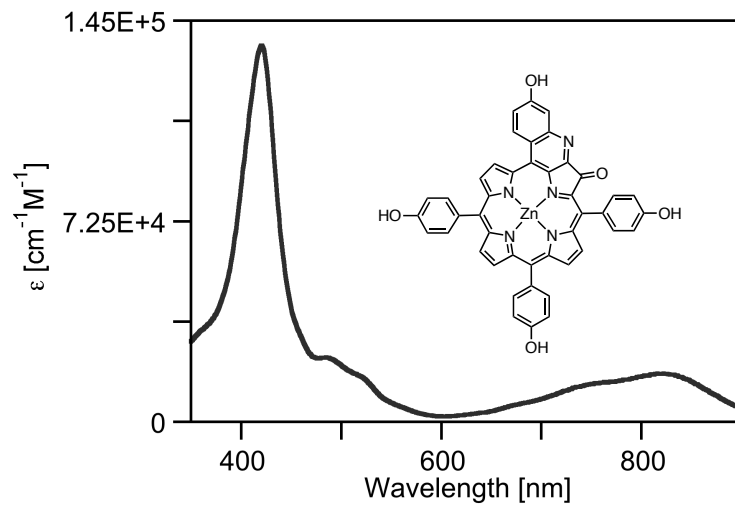


Figure 4-36. UV-vis spectrum (MeOH) of **4c^{Zn}**.

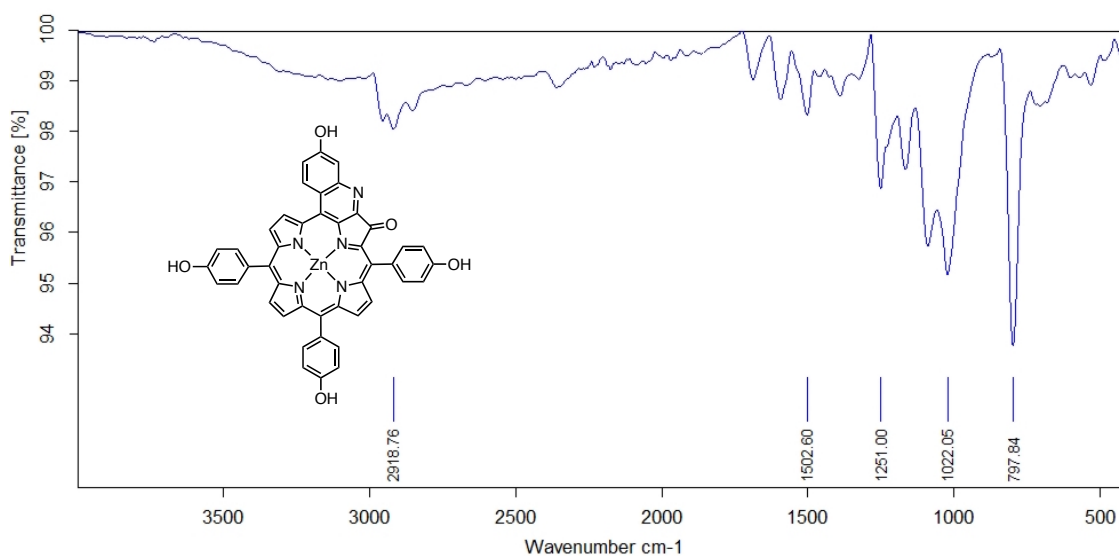


Figure 4-37. FT-IR spectrum (neat, diamond ATR) of **4c^{Zn}**.

***p*-(BODIPY)-tris-*p*-(OH)-quinoline-annulated porphyrin, mixture of regioisomers (4f).**

meso-thiomethyl-4,4,-difluoro-4-bora-3a,4a-diaza-s-indacene **10** (6 mg, 2.7×10^{-5} mol) was dissolved in dry CH₃CN (3.0 mL) in a round bottom flask equipped with a magnetic stir bar under N₂ atmosphere. Tetraol **4cZn** (21 mg, 2.7×10^{-5} mol, 1 equiv) was added and the mixture was stirred for 5 min under N₂. Copper(I) thiophene-2-carboxylate (CuTC) (5 mg, 2.7×10^{-5} mol, 1 equiv.) and Na₂CO₃ (3 mg, 2.7×10^{-5} mol, 1 equiv.) were added and the reaction mixture was immersed in a pre-heated oil bath at 50 °C and stirred.²⁷ After 48 h, a saturated aqueous NH₄Cl solution was added and the reaction mixture was stirred for several hours. The resulting biphasic mixture was extracted with EtOAc (3 × 10 mL), washed with H₂O (2 × 10 mL), and dried over Na₂SO₄. The remaining residue was purified by column chromatography (silica-CH₂Cl₂/10% MeOH) to afford recovered **4cZn** (6 mg) and the mono-BODIPY-tagged product **4f** as a series of closely running yellow fractions. The combined yellow fractions were dissolved in EtOAc (5.0 mL) and treated with 3 M HCl (5.0 mL) until the UV-vis spectrum of a neutralized aliquot indicated full demetallation. The organic layer was then washed with a sat'd aq. NaHCO₃ solution and H₂O, and was dried over anhyd. Na₂SO₄ to provide **4f** as a yellow film in 30% yield (7 mg): *R*_f (silica-CH₂Cl₂/10% MeOH) = 0.21; ¹H-NMR (500 MHz, DMSO-*d*₆): δ 10.09-10.07 (m, 1H, exchangeable with D₂O), 9.95-9.93 (m, 1H, exchangeable with D₂O), 9.69-9.64 (m, 1H, exchangeable with D₂O), 9.10 (br s, 1H), 8.45 (d, ³*J* = 4.4 Hz, 1H), 8.4-8.37 (m, 1H), 8.18 (d, ³*J* = 5.2 Hz, 2H), 8.13-8.10 (m, 2H) 8.08-7.95 (m, 3H), 7.92-7.88 (m, 3H), 7.80-7.77 (m, 4H), 7.60-7.59 (m, 1H), 7.31 (s, 1H), 7.19 (d, *J* = 6.0 Hz, 2H), 7.12 (two overlapping d, ³*J* = 7.8 Hz, 2H), 7.05-7.03 (m, 2H), 6.81 (d, *J* = 6.1 Hz, 2H), 6.76-6.72 (m, 1H) ppm; ¹⁹F NMR (470 MHz, DMSO-*d*₆): δ -142.1 to -142.2, (m) ppm; UV-vis (MeOH) λ_{max} (rel I.) 400 (1.0), 443 (0.56), 510 (sh), 784 (0.1) nm; FI (MeOH, λ_{excitation} = 441 nm) λ_{max} 488 nm, φ (EtOAc) = 0.01; HR-MS (ESI⁺, 100% CH₃CN, TOF) *m/z* calcd for C₅₃H₃₃BF₂N₇O₅ ([M·H]⁺) 896.2613, found 896.2613.

4. *in vivo* PAI Using a Quinoline-Annulated Porphyrin as NIR Molecular Contrast Agent

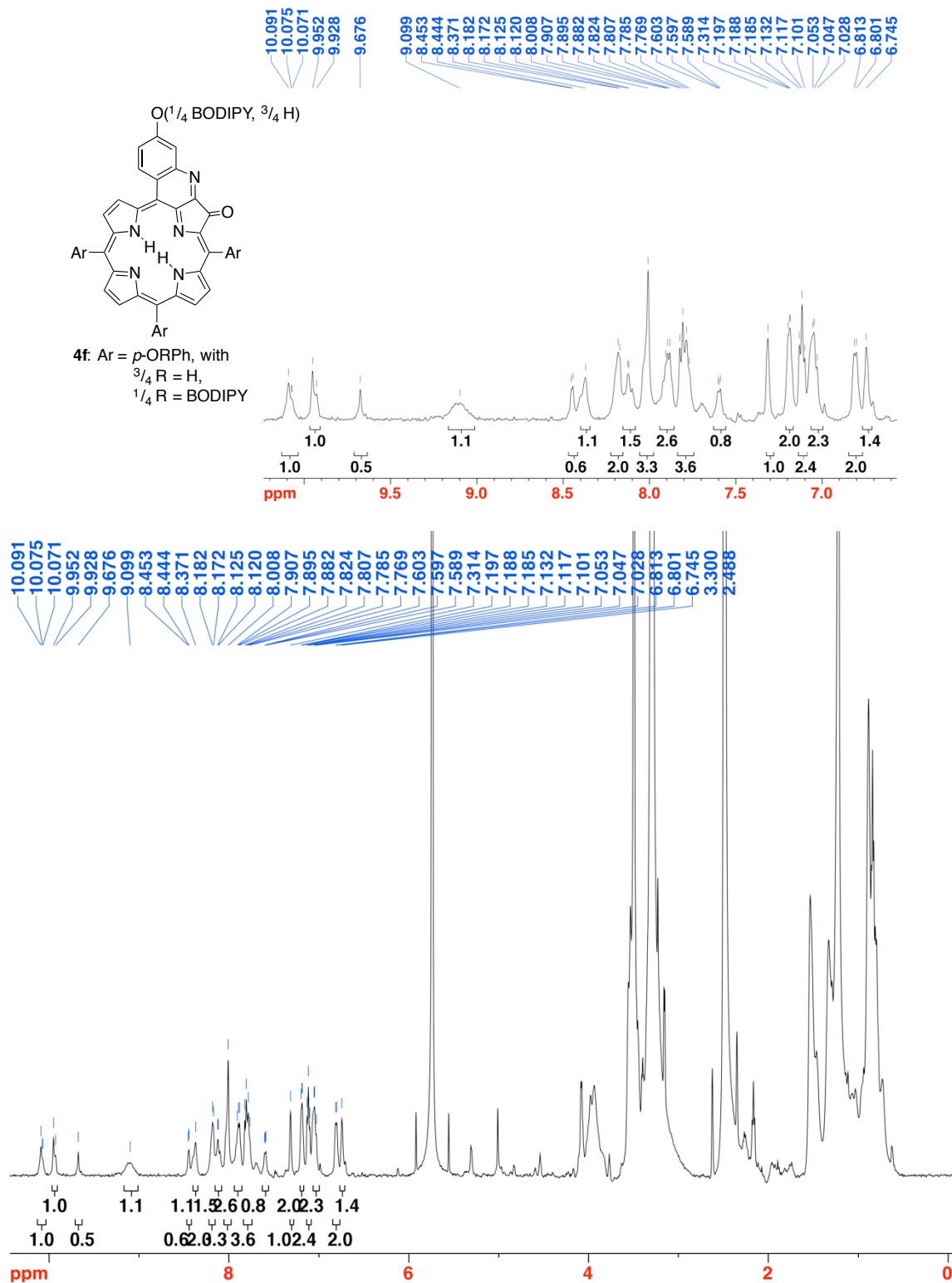


Figure 4-38. ^1H NMR spectrum (500 MHz, DMSO-d_6) of **4f**.

4. *in vivo* PAI Using a Quinoline-Annulated Porphyrin as NIR Molecular Contrast Agent

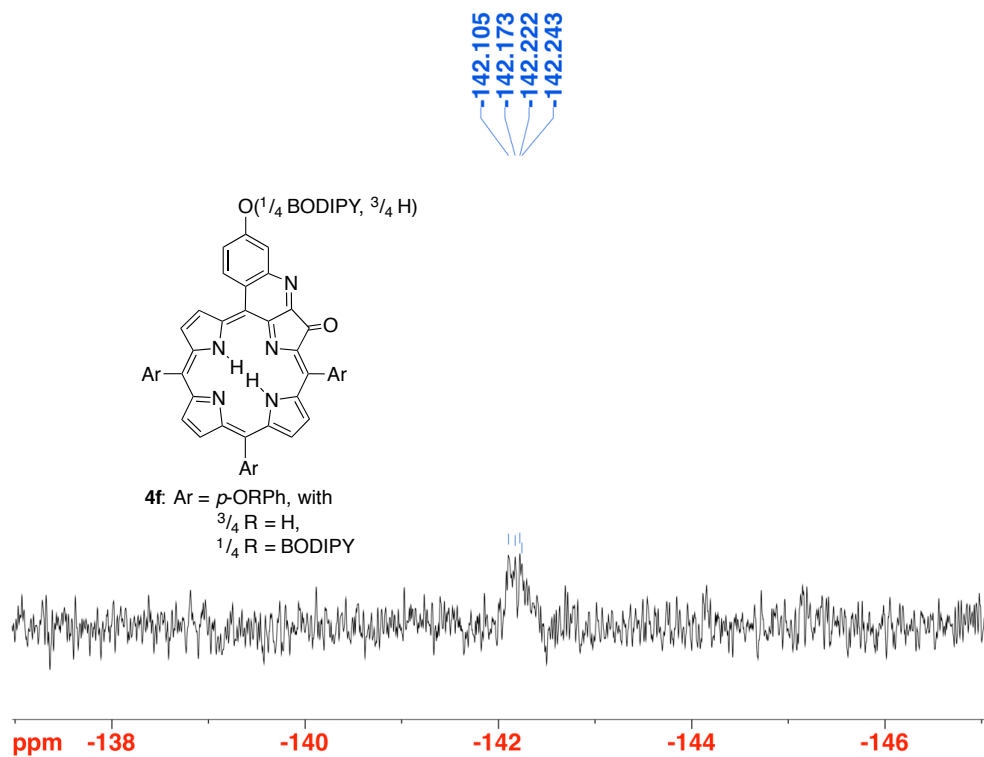


Figure 4-39. ^{19}F NMR spectrum (470 MHz, DMSO- d_6) of **4f**.

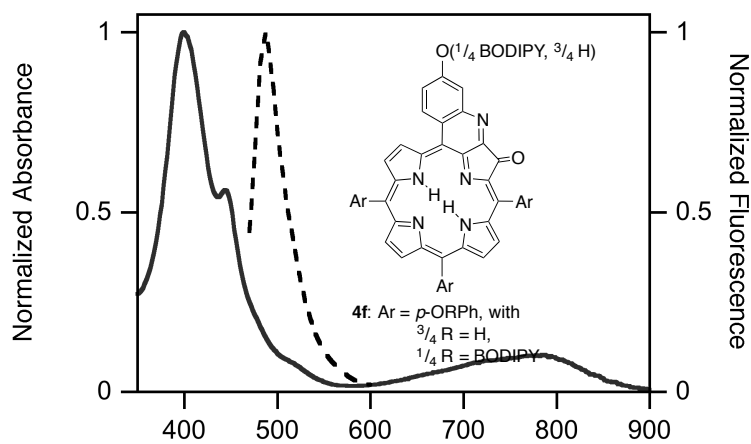


Figure 4-40. UV-vis and Fluorescence emission spectrum (MeOH, $\lambda_{\text{excitation}} = 441 \text{ nm}$) of **4f**.

***p*-(BODIPY)-tris-*p*-(OPEG12)-quinoline-annulated porphyrin, mixture of regioisomers (4g).**

Prepared according to the procedure for **4e** from **4d** (10 mg, 1.1×10^{-5} mol), MeO-PEG₅₅₀-OMs (22 mg, 3.4×10^{-5} mol, 3 equiv.), 14 mg of Cs₂CO₃ (4.4×10^{-5} mol, 3.9 equiv.) in DMF (2.0 mL) to afford **4g** as a yellow oil in 56% yield (16 mg): ¹H NMR (400 MHz, CD₂Cl₂): δ 9.14 (s, 1H), 8.45 (s, 1H), 8.38 (d, ³*J* = 4.6 Hz, 1H), 8.21 (d, 4H), 8.01 (d, ³*J* = 6.8 Hz, 3H), 7.91 (d, ³*J* = 7.6 Hz, 2H), 7.73 (d, ³*J* = 7.2 Hz, 3H), 7.52 (s, 1H), 7.31 (d, ³*J* = 8.0 Hz, 4H), 7.25 (d, ³*J* = 5.0 Hz, 5H), 7.13-7.11 (m, 2H), 6.82 (d, ³*J* = 5.7 Hz, 1H), 6.46 (s, 1H), 3.35-3.3 (three overlapping s, 9H) ppm; ¹⁹F NMR (470 MHz, CD₂Cl₂): δ -142.1 to -142.2, (m) ppm; UV-vis (MeOH) λ_{max} (rel I.) 402 (1.0), 473 (sh), 510, (sh), 769 (0.12) nm; FI (MeOH, λ_{excitation} = 441 nm) λ_{max} 485 nm, φ (EtOAc) < 0.003; HR-MS (MALDI, 100% DHBA) cluster of peaks corresponding to addition of three PEG groups, see ESI.

4. *in vivo* PAI Using a Quinoline-Annulated Porphyrin as NIR Molecular Contrast Agent

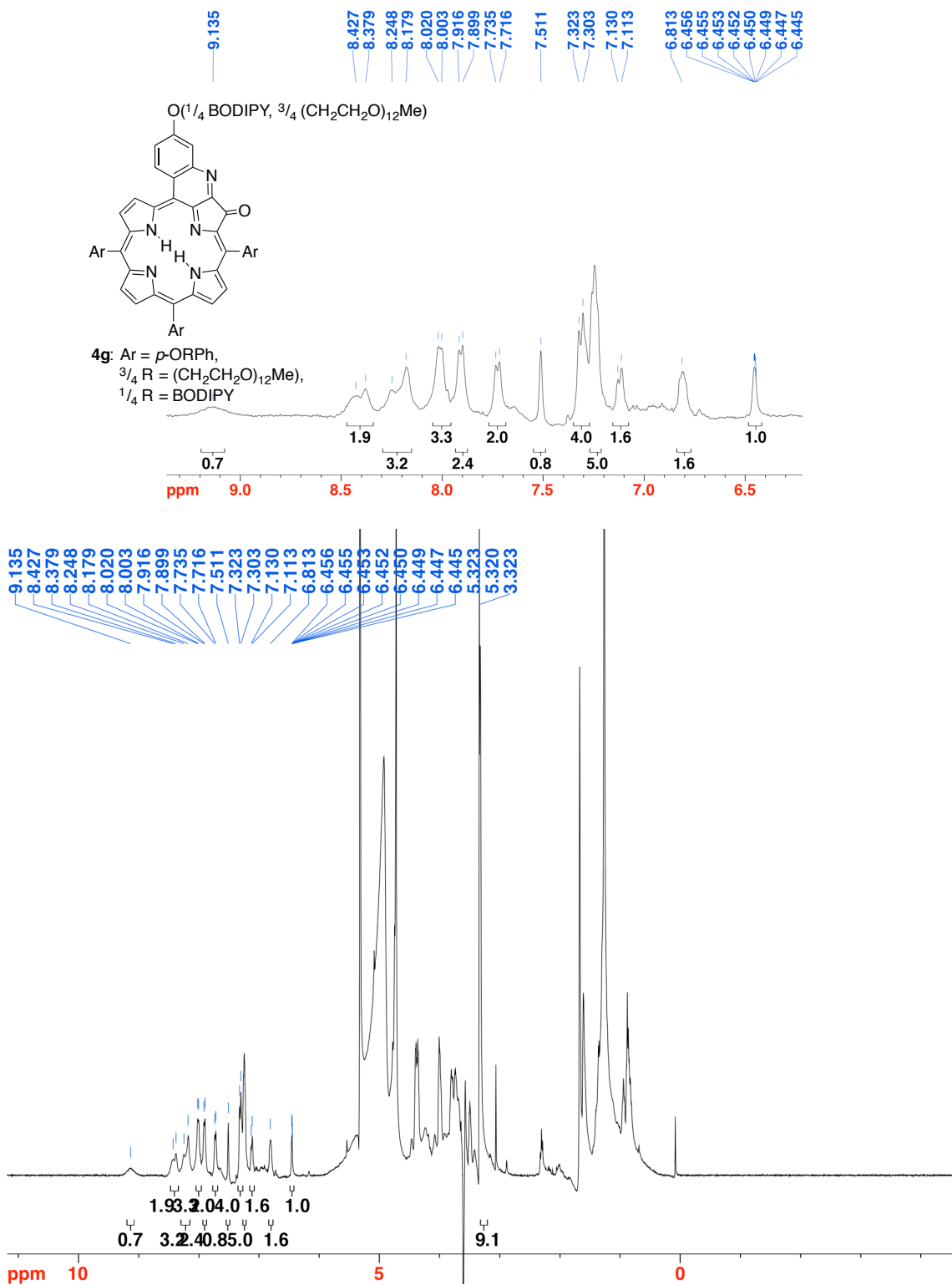


Figure 4-41. ¹H NMR spectrum (400 MHz, CD₂Cl₂, pre-saturated at 3.6 ppm) of **4g**.

4. *in vivo* PAI Using a Quinoline-Annulated Porphyrin as NIR Molecular Contrast Agent

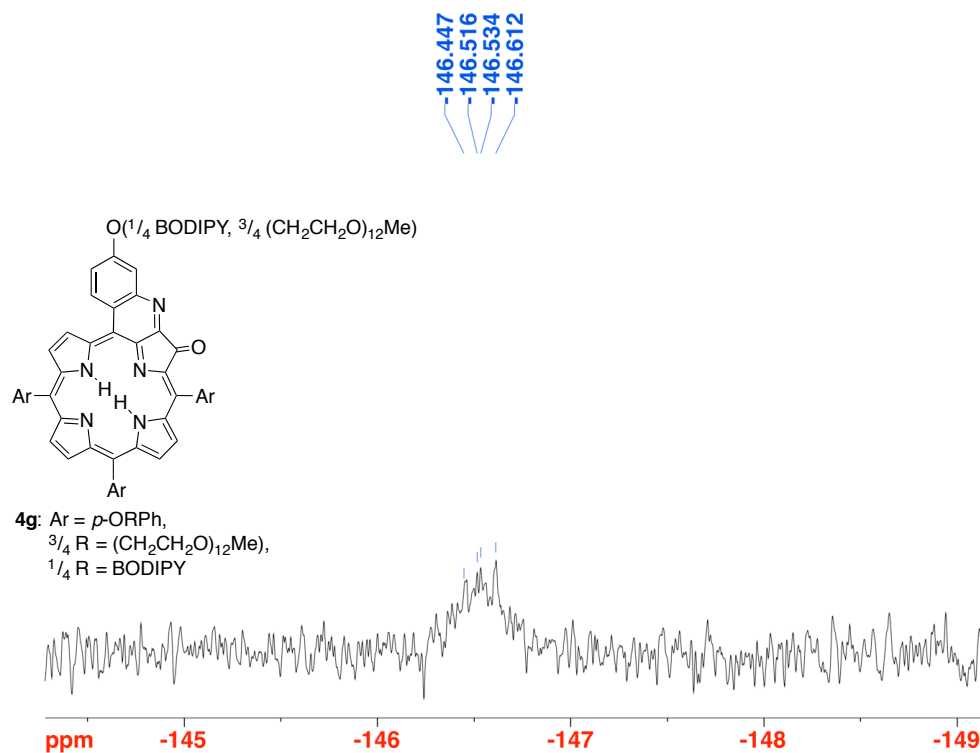


Figure 4-42. ¹⁹F NMR spectrum (376 MHz, CD₂Cl₂) of **4g**.

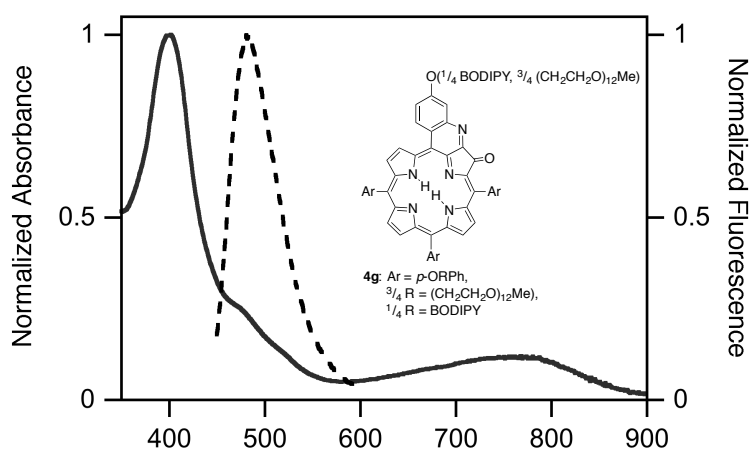


Figure 4-43. UV-vis and Fluorescence emission spectrum (MeOH, $\lambda_{\text{excitation}} = 441$ nm) of **4g**.

4. *in vivo* PAI Using a Quinoline-Annulated Porphyrin as NIR Molecular Contrast Agent

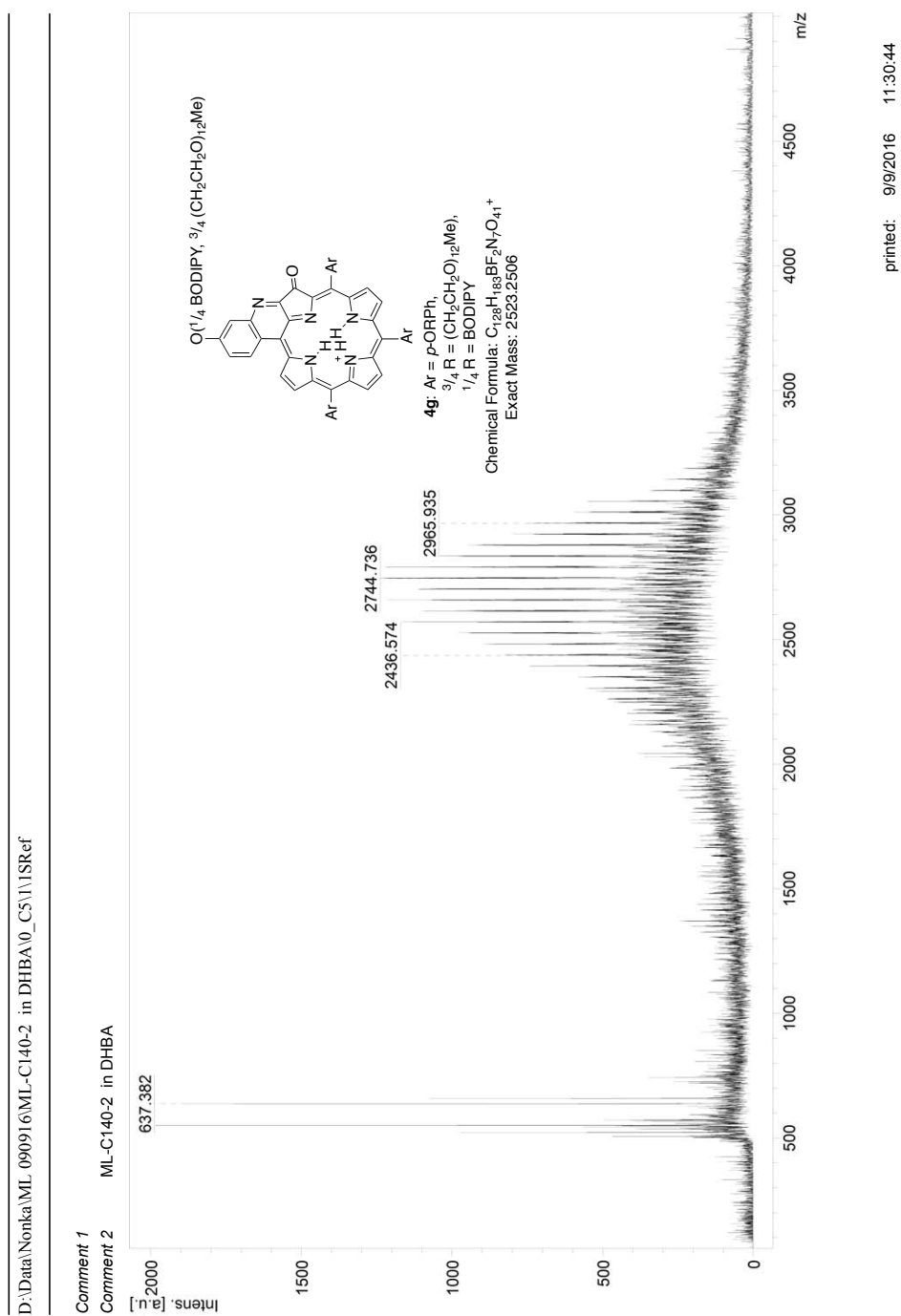


Figure 4-44. MALDI-TOF spectrum (100% DHBA) of **4g**.

4. *in vivo* PAI Using a Quinoline-Annulated Porphyrin as NIR Molecular Contrast Agent

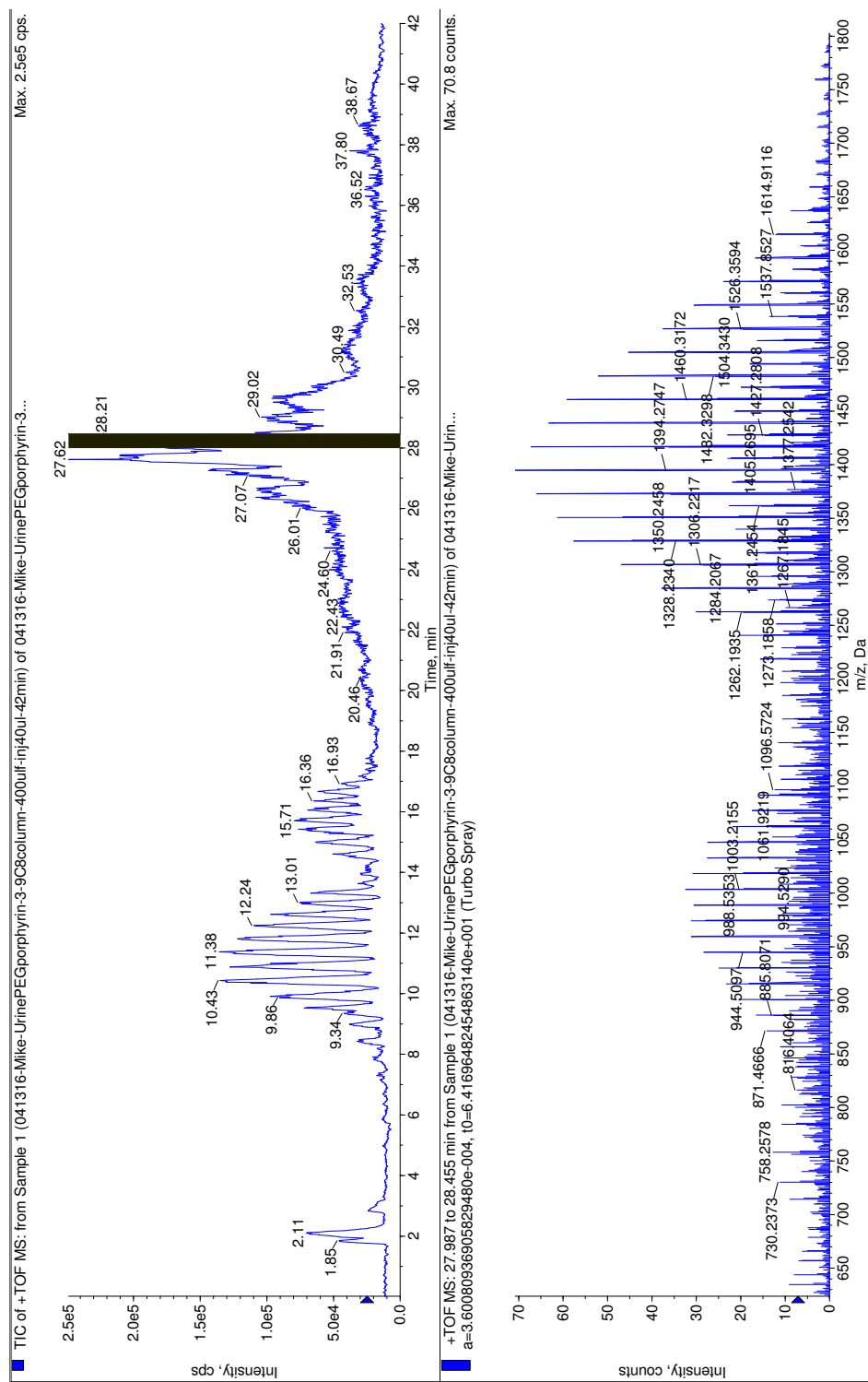


Figure 4-45. LC-MS of mouse urine extract (CH_2Cl_2), obtained after injection of **4e**.

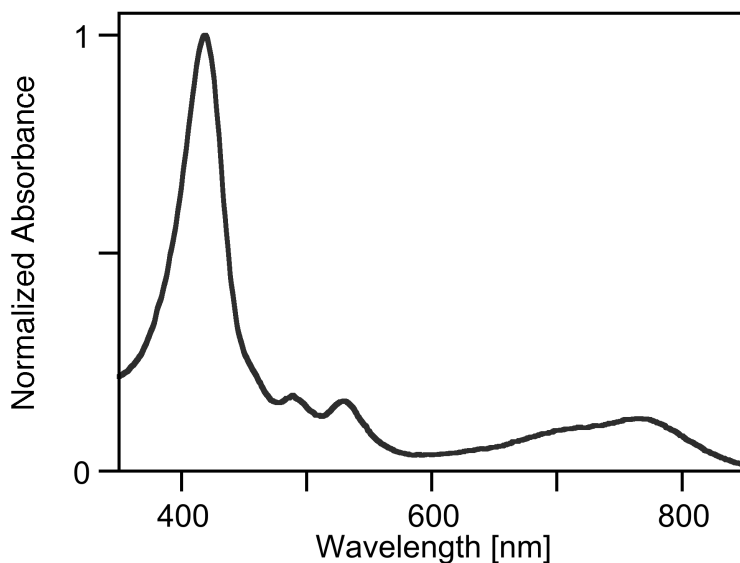


Figure 4-46. UV-vis spectrum (CH_2Cl_2) of mouse (diluted) urine obtained after injection of **4e**.

4.3.3 Co-registered pulse-echo-photoacoustic tomography

The details to the 64 channel co-registered ultrasound pulse echo-photoacoustic tomography (PE-PAT) system is described elsewhere.²⁹ Briefly, the system utilizes a unique field-programmable gate array (FPGA) technology that allows for real-time acquisition of ultrasound and photoacoustic signals. The photoacoustic signal is generated by a 15 Hz, 12 ns pulse width light of a tunable Ti-Sapphire laser (LT-2211, Symphotics TII Corp, Camarillo, CA) pumped by a second harmonic Nd:YAG laser (LS-2134, Symphotics TII Corp). Free space illumination is used for light delivery. The laser light is expanded by a combination of concave and convex lenses and shone on the sample using mirrors. A small portion of the beam is separated by a beam splitter (BSN11, Thorlabs) and is focused on a single element ultrasound transducer for monitoring the fluctuations in laser energy during the experiment.³⁰ The pulse-echo (PE) ultrasound signal is generated and received by the system in synchrony with the laser pulses. The PE and PAT images are formed by a beamforming algorithm. The data

sampling is performed at 40 MHz. A 64 channel ultrasound transducer with a center frequency of 3.5 MHz, a bandwidth of 80%, and a sector scan type is utilized for acquiring the co-registered PE-PAT images. Ultrasound and PAT images are overlapped to form the co-registered images. The effects of laser energy fluctuations are compensated for in the data analysis.

The setup was also used for the phantom photoacoustic signal generation efficiency evaluation of the dyes, as described previously.¹⁷

4.3.4 Animal protocols

All experiments involving mice were performed as approved by the Institutional Animal Care and Use Committee (IACUC) of the University of Connecticut under license #A15-047. The purity of contrast agents **4e** and **4g** was assessed by HPLC (see ESI). Solutions of **4e** and **4g** were also filtered through a syringe filter (nylon membrane, pore size 0.22 μ m) prior to injection.

4.3.5 Toxicity test

100 μ L of PBS based solution of **4e** with 33.3 mM concentration was injected into anesthetized 6 week old BALB/c mice (n = 2). The heart rates of the mice were monitored by a pulse oximeter (MouseStat, Kent Scientific) before injection and during a 3 h period after injection.

4.3.6 Tumor model

Tumor cell preparation was adopted from the literature.³¹ Briefly, 4T1 Luc cells were cultured at 37 °C with 5% CO₂ in a T75 flask (BD Biosciences, Bedford, MA); DMEM (Dulbecco's Modified Eagle's medium, Gibco, USA) medium supplemented with 10% FBS and 50 U/mL penicillin/streptomycin. After 3 passes, the cells were suspended in the DMEM and 1×10^5 cells were injected subcutaneously on top of the right leg of female BALB/c mice (6-8 weeks old,

body weight ~20 g). The mice were monitored for approximately two weeks post-inoculation until the tumor size was between 7-10 mm.

4.3.7 *In vivo* PAT of murine tumor

Prior to the *in vivo* imaging, the mice were anaesthetized (1.5 L/min oxygen with 1.5% isoflurane) and the tumor area depilated. The position of the mouse was fixed. Ultrasound gel was applied on the tumor area and a bag of water was placed on top of the tumor for acoustic wave coupling. The pulsed laser at 790 nm of the pulse-echo-photoacoustic tomography (PE-PAT) setup described above (780 nm for ICG) was shone on the tumor through the water bag; surface optical fluence on the tissue was always maintained below the maximum permissible exposure according to the ANSI safety standard.³² The transducer position was adjusted by a three-dimensional mechanical stage to reach a suitable imaging condition. The pre-injection PAT image of the tumor was acquired. Then 100 μ L of the PBS based solution of the dye **4e** (~33.3 mM concentration) or ICG was injected via retro-orbital injection.²⁴ Care was taken to avoid any changes in the position of the mouse, transducer, and light beam as a result of the injection. The PAT images of the tumor were acquired during the 45 min period following injection. The PAT images and the maximum PA signal levels were compared before and after the injection. The p-values in a student t-test between the results obtained for the dye and ICG are less than 0.005 for all instances, indicating statistical significance. The schematic of the *in vivo* experiment setup is illustrated in Figure 4-47.

4. *in vivo* PAI Using a Quinoline-Annulated Porphyrin as NIR Molecular Contrast Agent

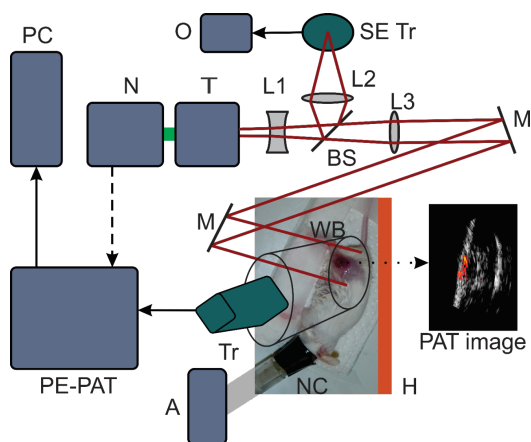


Figure 4-47. *In vivo* PAT experiment setup. N: Nd:YAG second harmonic laser, T: tunable Ti:sapphire laser, L1, L2, L3: lenses, BS: beam splitter, SE Tr: single element transducer for monitoring laser fluctuations, O: oscilloscope, M: mirror, WB: water bag, Tr: transducer, H: heater, NC: nose cone, A: anesthesia compound (1.5 L/min oxygen with 1.5 % isoflurane), PE-PAT: the co-registered PE-PAT system, PC: computer.

4.3.8 *Ex vivo* fluorescent imaging

100 μ L of **4g** (3 mM in PBS) was injected to three BALB/c mice of similar weight and similar tumor size. The mice were sacrificed 15 and 120 min after the injection. Tumor, liver, kidneys, heart, lung, and spleen were harvested, washed twice in PBS, and imaged using an IVIS® Lumina II fluorescent imaging system (Caliper Life Sciences, Hopkinton, MA); $\lambda_{\text{excitation}} = 465$ nm, GFP emission filter.

4.3.9 Photophysical measurements

The photophysical measurements were performed as described previously.¹⁷

4.4 References

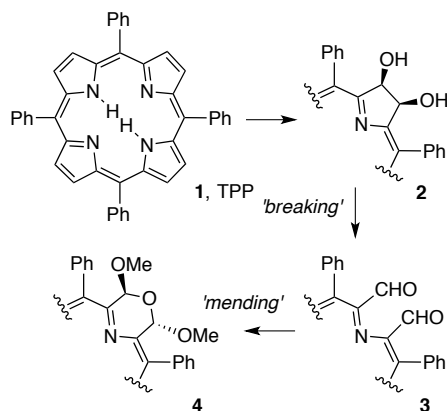
- (1) a) Weissleder, R.; Pittet, M. J. *Nature* **2008**, *452*, 580; b) Ethirajan, M.; Chen, Y.; Joshi, P.; Pandey, R. K. *Chem. Soc. Rev.* **2011**, *40*, 340; c) Schäferling, M. *Angew. Chem. Int. Ed.* **2012**, *51*, 3532; d) Stender, A. S.; Marchuk, K.; Liu, C.; Sander, S.; Meyer, M. W.; Smith, E. A.; Neupane, B.; Wang, G.; Li, J.; Cheng, J.-X.; Huang, B.; Fang, N. *Chem. Rev.* **2013**, *113*, 2469; e) Huang, H.; Song, W.; Rieffel, J.; Lovell, J. F. *Frontiers Phys.* **2015**, *3*, Article #23; f) Chang, C. J.; Gunnlaugsson, T.; James, T. D. *Chem. Soc. Rev.* **2015**, *44*, 4484.
- (2) a) Wang, L. V.; Hu, S. *Science* **2012**, *335*, 1458; b) Beard, P. *Interface Focus* **2011**, *1*, 602; c) Zhou, Y.; Yao, J.; Wang, L. V. *J. Biomed. Opt.* **2016**, *21*, Article # 061007.
- (3) a) Cerussi, A. E.; Berger, A. J.; Bevilacqua, F.; Shah, N.; Jakubowski, D.; Butler, J.; Holcombe, R. F.; Tromberg, B. J. *Acad. Radiol.* **2001**, *8*, 211; b) Wang, L. V.; Wu, H.-i. *Biomedical Optics: Principles and Imaging*; John Wiley & Sons: Hoboken, NJ, 2012.
- (4) Yao, J.; Wang, L.; Yang, J. M.; Maslov, K. I.; Wong, T. T.; Li, L.; Huang, C. H.; Zou, J.; Wang, L. V. *Nat. Methods* **2015**, *12*, 407.
- (5) Weber, J.; Beard, P. C.; Bohndiek, S. E. *Nat. Methods* **2016**, *13*, 639.
- (6) Heijblom, M.; Piras, D.; Xia, W.; van Hespén, J. C. G.; Klaase, J. M.; van den Engh, F. M.; van Leeuwen, T. G.; Steenbergen, W.; Manohar, S. *Opt. Express* **2012**, *20*, 11582.
- (7) a) Salehi, H. S.; Li, H.; Merkulov, A.; Kumavor, P. D.; Vavadi, H.; Sanders, M.; Kueck, A.; Brewer, M. A.; Zhu, Q. *J. Biomed. Opt.* **2016**, *21*, Article # 046006; b) Wang, T.; Yang, Y.; Alqasemi, U.; Kumavor, P. D.; Wang, X.; Sanders, M.; Brewer, M.; Zhu, Q. *Biomed. Opt. Express* **2013**, *4*, 2763.
- (8) a) Peer, D.; Karp, J. M.; Hong, S.; Farokhzad, O. C.; Margalit, R.; Langer, R. *Nat. Nanotechnol.* **2007**, *2*, 751; b) Wang, L.; Yang, P.-P.; Zhao, X.-X.; Wang, H. *Nanoscale* **2016**, *8*, 2488; c) Huynh, E.; Lovell, J. F.; Helfield, B. L.; Jeon, M.; Kim, C.; Goertz, D. E.; Wilson, B. C.; Zheng, G. *J. Am. Chem. Soc.* **2012**, *134*, 16464; d) Huynh, E.; Jin, C. S.; Wilson, B. C.; Zheng, G. *Bioconjugate Chem.* **2014**, *25*, 796; e) Paproski, R. J.; Forbrich, A.; Huynh, E.; Chen, J.; Lewis, J. D.; Zheng, G.; Zemp, R. J. *Small* **2016**, *12*, 371; f) Ho, C. J. H.; Balasundaram, G.; Driessen, W.; McLaren, R.; Wong, C. L.; Dinis, U. S.; Attia, A. B. E.; Ntziachristos, V.; Olivo, M. *Sci. Rep.* **2014**, *4*, Article # 5342.
- (9) a) Lewinski, N.; Colvin, V.; Dreze, R. *Small* **2008**, *4*, 26; b) Gnach, A.; Lipinski, T.; Bednarkiewicz, A.; Rybka, J.; Capobianco, J. A. *Chem. Soc. Rev.* **2015**, *44*, 1561; c) Srivastava, V.; Gusain, D.; Sharma, Y. C. *Ind. Eng. Chem. Res.* **2015**, *54*, 6209.

- (10) Lovell, J. F.; Jin, C. S.; Huynh, E.; Jin, H.; Kim, C.; Rubinstein, J. L.; Chan, W. C. W.; Cao, W.; Wang, L. V.; Zheng, G. *Nat. Mater.* **2011**, *10*, 324.
- (11) a) Filonov, G. S.; Krumholz, A.; Xia, J.; Yao, J.; Wang, L. V.; Verkhusha, V. V. *Angew. Chem. Int. Ed.* **2011**, *51*, 1448; b) Zhang, Y.; Cai, X.; Wang, Y.; Zhang, C.; Li, L.; Choi, S.-W.; Wang, L. V.; Xia, Y. *Angew. Chem. Int. Ed.* **2011**, *50*, 7359.
- (12) Ashkenazi, S. *J. Biomed. Optics* **2010**, *15*, Article # 040501.
- (13) a) Zanganeh, S.; Li, H.; Kumavor, P. D.; Alqasemi, U.; Aguirre, A.; Mohammad, I.; Stanford, C.; Smith, M. B.; Zhu, Q. *J. Biomed. Opt.* **2013**, *18*, Article # 096006; b) Abuteen, A.; Zanganeh, S.; Akhigbe, J.; Samankumara, L. P.; Aguirre, A.; Biswal, N.; Braune, M.; Vollertsen, A.; Röder, B.; Brückner, C.; Zhu, Q. *Phys. Chem. Chem. Phys.* **2013**, *15*, 18502.
- (14) a) Klibanov, A. L.; Maruyama, K.; Torchilin, V. P.; Huang, L. *FEBS Lett.* **1990**, *268*, 235; b) Desmettre, T.; Devoisselle, J.; Mordon, S. *Surv. Ophthalmol.* **2000**, *45*, 15.
- (15) a) Akhigbe, J.; Luciano, M.; Zeller, M.; Brückner, C. *J. Org. Chem.* **2015**, *80*, 499; b) Akhigbe, J.; Yang, M.; Luciano, M.; Brückner, C. *J. Porphyrins Phthalocyanines* **2016**, *20*, 265; c) Akhigbe, J.; Zeller, M.; Brückner, C. *Org. Lett.* **2011**, *13*, 1322.
- (16) a) Richeter, S.; Christophe, J.; Jean-Paul, G.; Romain, R. In *Handbook of Porphyrin Science*; Kadish, K. M., Smith, K. M., Guillard, R., Eds.; World Scientific Publishing Company: Hackensack, New Jersey, 2010; Vol. Volume 3, p 429; b) Jeandon, C.; Ruppert, R. *Eur. J. Org. Chem.* **2011**, 4098.
- (17) Abuteen, A.; Zanganeh, S.; Akhigbe, J.; Samankumara, L. P.; Aguirre, A.; Biswal, N.; Braune, M.; Vollertsen, A.; Röder, B.; Brückner, C.; Zhu, Q. *Phys. Chem. Chem. Phys.* **2013**, *15*, 18502.
- (18) a) Hambright, P. In *The Porphyrin Handbook*; Kadish, K. M., Smith, K. M., Guillard, R., Eds.; Academic Press: San Diego, 2000; Vol. 3, p 129; b) Brandis, A.; Mazor, O.; Neumark, E.; Rosenbach-Belkin, V.; Salomon, Y.; Scherz, A. *Photochem. Photobiol.* **2005**, *81*, 983; c) Borbas, K. E.; Mroz, P.; Hamblin, M. R.; Lindsey, J. S. *Bioconjugate Chem.* **2006**, *17*, 638; d) Borbas, K. E.; Chandrashaker, V.; Muthiah, C.; Kee, H. L.; Holten, D.; Lindsey, J. S. *J. Org. Chem.* **2008**, *73*, 3145; e) Li, Y.; Wang, J.; Zhang, X.; Guo, W.; Li, F.; Yu, M.; Kong, X.; Wu, W.; Hong, Z. *Org. Biomol. Chem.* **2015**, *13*, 7681; f) Mandal, A. K.; Sahin, T.; Liu, M.; Lindsey, J. S.; Bocian, D. F.; Holten, D. *New J. Chem.* **2016**, *40*, 9648.
- (19) Veronese, F. M.; Pasut, G. *Drug Discovery Today* **2005**, *10*, 1451.
- (20) Starnes, S. D.; Rudkevich, D. M.; Rebek Jr., J. *J. Am. Chem. Soc.* **2001**, *123*, 4659.

- (21) Daniell, H. W.; Williams, S. C.; Jenkins, H. A.; Brückner, C. *Tetrahedron Lett.* **2003**, *44*, 4045.
- (22) Aldrich, S. 2003.
- (23) Flock, S. T.; Jacques, S. L.; Wilson, B. C.; Star, W. M.; van Gemert, M. J. C. *Lasers Surg. Med.* **1992**, *12*, 510.
- (24) Steel, C. D.; Stephens, A. L.; Hahto, S. M.; Singletary, S. J.; Ciavarra, R. P. *Lab Animal* **2008**, *37*, 26.
- (25) Huang, H.; Wang, D.; Zhang, Y.; Zhou, Y.; Geng, J.; Chitgupi, U.; Cook, T. R.; Xia, J.; Lovell, J. F. *Bioconjugate Chem.* **2016**, *27*, 1574.
- (26) Boens, N.; Leen, V.; Dehaen, W. *Chem. Soc. Rev.* **2012**, *41*, 1130.
- (27) Flores-Rizo, J. O.; Esnal, I.; Osorio-Martinez, C. A.; Gomez-Duran, C. F.; Banuelos, J.; Lopez Arbeloa, I.; Pannell, K. H.; Metta-Magana, A. J.; Pena-Cabrera, E. *J. Org. Chem.* **2013**, *78*, 5867.
- (28) a) MacAlpine, J. K.; Boch, R.; Dolphin, D. *Journal of Porphyrins and Phthalocyanines* **2002**, *6*, 146; b) Brückner, C.; Ogikubo, J.; McCarthy, J. R.; Akhigbe, J.; Hyland, M. A.; Daddario, P.; Worlinsky, J. L.; Zeller, M.; Engle, J. T.; Ziegler, C. J.; Ranaghan, M. J.; Sandberg, M. N.; Birge, R. R. *J. Org. Chem.* **2012**, *77*, 6480.
- (29) Alqasemi, U.; Li, H.; Aguirre, A.; Zhu, Q. *IEEE Trans. Sonics Ultrason.* **2012**, *59*, 1344.
- (30) Salehi, H. S.; Wang, T.; Kumavor, P. D.; Li, H.; Zhu, Q. *Biomed. Opt. Express* **2014**, *5*, Article # 3074.
- (31) a) Xu, Y.; Zanganeh, S.; Mohammad, I.; Aguirre, A.; Wang, T.; Yang, Y.; Kuhn, L.; Smith, M. B.; Zhu, Q. *J. Biomed. Opt.* **2013**, *18*, Article # 066009; b) Zhou, F.; Zanganeh, S.; Mohammad, I.; Dietz, C.; Abuteen, A.; Smith, M. B.; Zhu, Q. *Org. Biomol. Chem.* **2015**, *13*, 11220.
- (32) ANSI Z136.1-2007: American National Standard for Safe Use of Lasers, American National Standards Institute Inc. 2007.

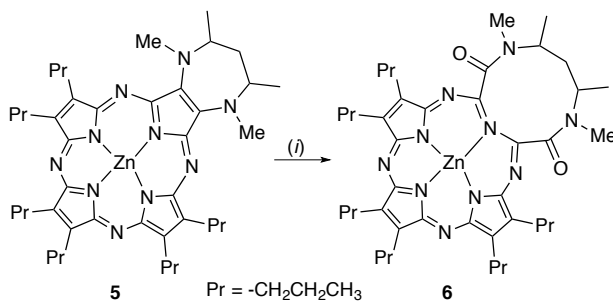
5 Supersizing Pyrrole-Modified Porphyrins by Reversal of the Breaking and Mending Strategy

The synthesis of porphyrin analogues has contributed to the understanding of the concept of aromaticity,¹ provided macrocycles with valuable molecular recognition or catalytic properties,² and has provided a large number of dyes with optical properties that are inaccessible with regular porphyrins or hydroporphyrins.³ The majority of porphyrin analogues were prepared by total synthesis.⁴ In an approach we dubbed ‘the breaking and mending of porphyrins’, we,⁵ and others,^{4e} prepared a wide variety of porphyrin analogues containing one or two non-pyrrolic heterocycles by step-wise conversion of a porphyrin. To illustrate the approach, *meso*-tetraphenylporphyrin **1**, for example, was dihydroxylated; the diol functionality was then used as a synthetic handle for further functionalizations (Scheme 5-1).⁵ Diol cleavage in the ‘breaking’ step resulted in the formation of a secochlorin **3** that could be cyclized in the ‘mending’ step to, e.g., provide a morpholinochlorin incorporating a 6-membered morpholine moiety.⁶ Attempts to generate 7-membered rings (1,4,5-triazaazepines or 1,3-diaza-5-oxaazepines) by cyclization of **3** with hydrazine or hydroxylamine, respectively, failed.⁷ In all likelihood, the analogues formed but then rapidly extruded a small molecule (N₂ or CO₂, respectively), regenerating the porphyrin or a porphyrin-like arrangement of four five-membered rings. This highlights the large stability of the natural porphyrinic architecture, but also identifies a limitation of our ‘breaking and mending’ approach toward pyrrole-modified porphyrins containing medium-sized rings.



Scheme 5-1. Example for the 'breaking and mending of porphyrins' approach toward porphyrinoids containing non-pyrrolic building blocks.

Albeit rare, porphyrinoids prepared by total synthesis containing 7-membered rings are stable.^{4e} The best investigated systems are the tropiporphyrins, a family of carbaporphyrins.^{4d} Azepipthalocyanines were also reported.⁸ Medium-sized rings can, in principle, be accessed by the cleavage of the linkage between two annulated smaller rings.⁹ In the realm of porphyrinoid chemistry, a single such example was provided in 2003 by the groups of Barrett and Hoffman (Scheme 5-2).¹⁰



Scheme 5-2. Synthesis of pyrrole-expanded porphyrazine **6** described by the groups of Barrett and Hoffman.
Reaction conditions: (i) KMnO₄, CH₂Cl₂ (44% yield).¹⁰

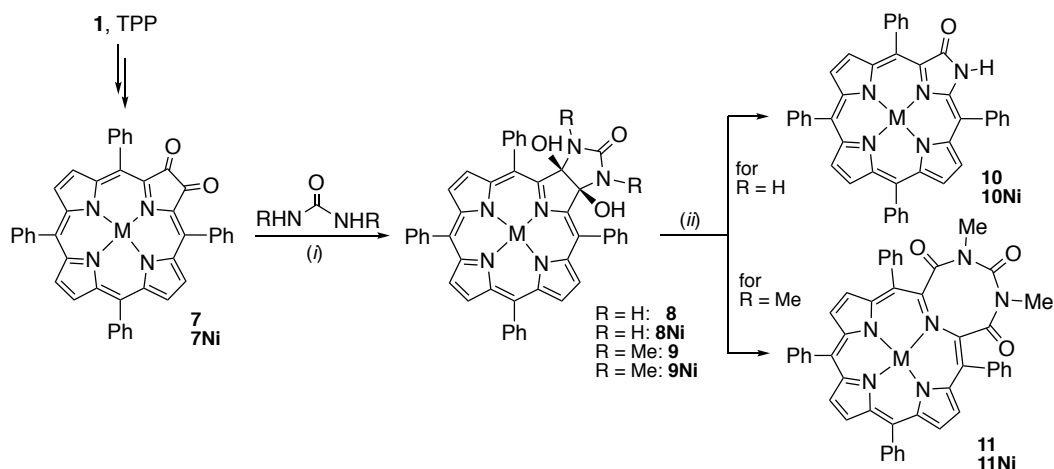
Diazaphthalocyanine **5** was prepared by total synthesis. Subsequently, the β,β' -bond linking the two heterocycles was cleaved, forming the pyrrole-expanded porphyrazine **6** containing a 10-membered heterocycle.¹⁰

With this precedent in mind, we set out to test whether a reversal of our traditional methodology, i.e., a ‘mending and breaking’ approach can be developed into a possibly general approach toward the synthesis of pyrrole-modified porphyrins with medium-sized heterocyclic rings that can also take advantage of some of the reaction types well established by us. This contribution will demonstrate that this is indeed the case, but it will also point at some limitations to this approach.

5.1 Results and Discussion

5.1.1 Formation of a Novel Pyrrole-modified Porphyrin by Replacement of a Pyrrole with a 1,3,6-Triazocine-2,4,8-Trione Ring

meso-Tetraarylporphyrin diones, such as **7**, are accessible from TPP (**1**) along a number of complimentary routes.¹¹ The regular ketone reactivity of the diones was previously demonstrated,^{11b} including in reactions generating pyrrole-modified porphyrins.¹² It is well-known that reaction of dione **7** with diamines generates diimines,¹³ but we found that the reaction of **7** with urea or *N,N'*-dimethylurea generated dihydroxychlorins **8** and **9**, respectively, containing imidazolidinone moieties annulated at the β,β' -positions. Diagnostic for the formation of the dihydroxychlorin structure are the preservation of the two-fold symmetry of the adducts as seen in their NMR spectra, the pyrroline carbon signals in their ¹³C NMR spectra (found at δ = 158.5 ppm for **8**), their regular chlorin-like spectra compared to the much broadened spectra for dione **7**¹⁴ (Figure 5-1A), and their expected composition (as per HR-MS). The presence of the lactam moieties in the annulated ring are indicated in the ¹³C NMR spectra of the products (for **8** at δ = 159.5 and 161.5 ppm for **9**) and IR spectra ($\nu_{C=O}$ at 1715 cm⁻¹ for **8**).



Scheme 5-3. Synthesis of urea chlorindiol adducts **8** and **9**, and the outcomes of the oxidative diol cleavage. *Reaction conditions:* (i) 20 equiv. urea derivative, pyridine, Δ (85% yield for **8**; 54% yield for **9**; 75% yield for **8Ni**; 68% yield for **9Ni**); (ii) 1-1.7 equiv. Pb(OAc)₄, THF, (Et₃N for preparation of **10** and **10Ni**), r.t., (69% yield for **10**; 71% yield for **11**; 45% yield for **10Ni**; 71% yield for **11Ni**).

We previously reported multiple methods for the oxidative cleavage of the pyrroline β,β' -bond of dihydroxychlorins.¹⁵ Thus, treatment of the polar magenta diol **8** under classic diol cleavage reaction conditions (Pb(OAc)₄)^{15b,16} resulted in the formation of a red non-polar compound in good yields (69%). Its porphyrin-like UV-vis spectrum (Figure 5-1B), NMR spectra, and its composition as determined by HR-MS identified it to be the known porpholactam **10**.¹⁷ Once again, the expulsion of smaller fragments from the putative medium-ring derivative establishing a stable 'tetrapyrrolic' architecture thwarted the formation of the target medium-sized ring-expanded compound. On the bright side, this 3-step pathway toward **10** is more convenient and significantly higher yielding (overall 29% from diol **2** at a 50 mg scale) than the previously described 3-step synthesis (~13%).¹⁷ Performing the same dione **7** \rightarrow diol **8** \rightarrow lactam **9** synthetic sequence after inserting Ni to the dione **7** results also in the fragmentation to the lactam **9Ni** from **8Ni**. The Ni complexes show the expected spectroscopic properties for metal-inserted species.

While we did not know the fragmentation mechanism of the putative intermediate resulting from the oxidative cleavage of **8** or **8Ni**, we suspected that the replacement of the amide

protons might hinder the fragmentation by, for instance, blocking amide-iminol-type equilibria. Indeed, oxidative diol cleavage of dimethylurea adduct **9** generated a compound in good yields possessing a composition of two hydrogen atoms less than the starting material (as per HR-MS). Moreover, it was characterized by a significantly red-shifted chlorin-type optical spectrum (Figure 5-1B). The general red-shift of the spectrum and particularly the much reduced extinction coefficient of its Soret band observed suggest the increase in non-planarity of the chromophore, while its general broadening suggest an increase of conformational flexibility.¹⁸

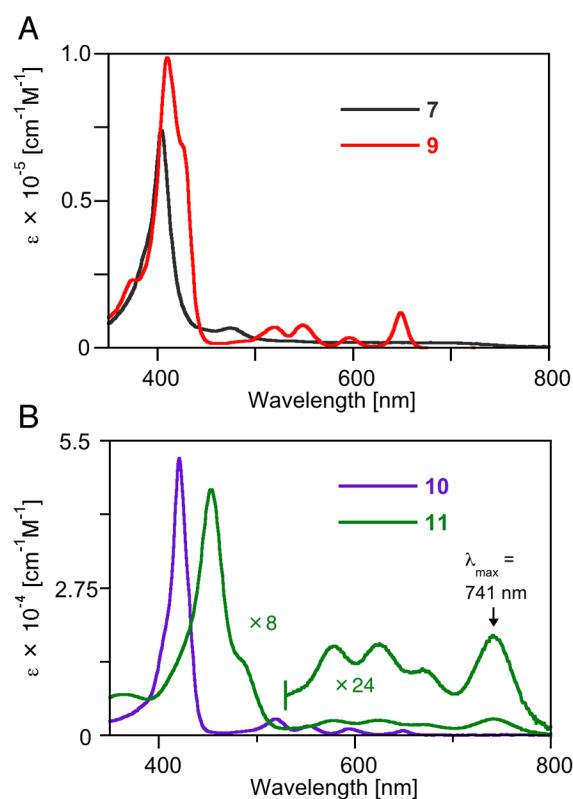


Figure 5-1. UV-vis spectra (CH_2Cl_2) of the compounds indicated.

Its NMR spectra retained the two-fold symmetry of the starting material with an upfield shift of the inner protons ($\delta = 1.88$ ppm) suggestive of a non-planar chromophore, and the presence of two lactam carbon atoms in different environments ($\delta = 173.1$ and 155.1 ppm). Thus all spectroscopic evidence point toward the successful formation of the target expanded pyrrole-

modified porphyrin **11**. Oxidative cleavage of diol **9Ni** also generated the corresponding supersized pyrrole-modified porphyrin **11Ni**, showing the expected analytical properties.

A single crystal X-ray structure analysis of **11** provided the final proof for the unique connectivity of this porphyrinoid (Figure 5-2). The pyrroline β,β' -bond was, as designed, oxidatively cleaved, and both β -carbons were converted in due process to lactam moieties that are incorporated into an 1,3,6-triazocine-2,4,8-trione ring. This 8-membered ring is, as designed, the result of a fusion of the three annulated dimethylurea atoms with the five pyrroline atoms. The non-pyrrolic moiety assumes a significantly non-planar conformation with an almost 90° twist along its long axis. This twist translates into the porphyrinic framework, leading to a mildly ruffled conformation.

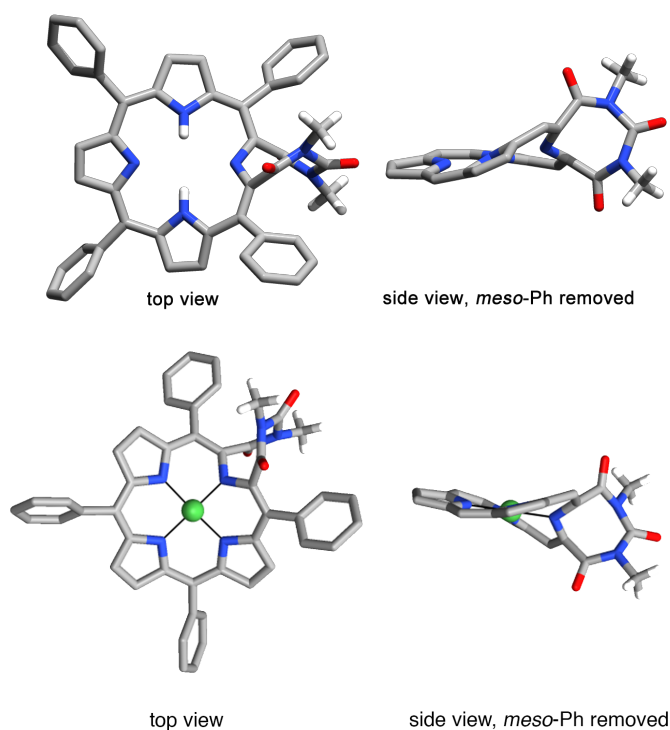


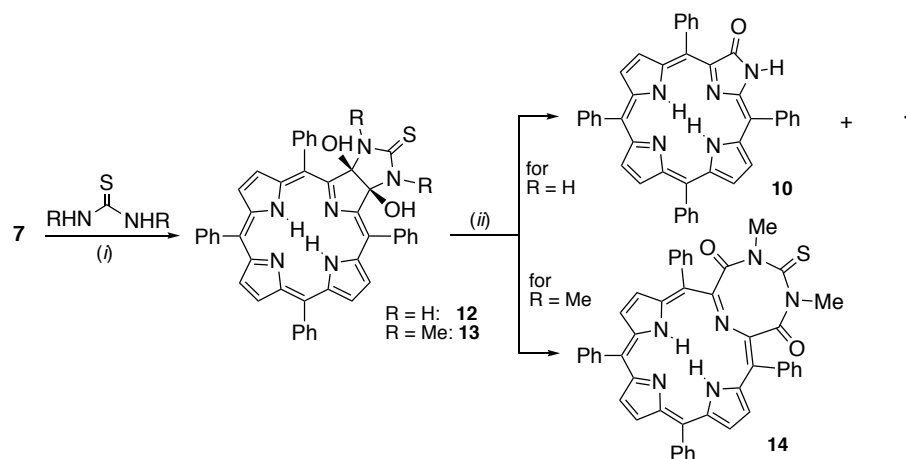
Figure 5-2. Stick representation of the single crystal X-ray structure of **11** (top) and **11Ni** (bottom). All disorder, solvent molecules, and sp^2 -CH hydrogens were omitted for clarity. For details, see experimental section.

The corresponding Ni complex **11Ni** could also be crystallized (Figure 5-2), and also exhibits a non-planar conformation of the non-pyrrolic moiety with an overall ruffled conformation of the chromophore. The solid-state conformation of **11Ni** also translates to a red-shifted metallochlorin-like UV-vis spectrum of this compound (see experimental section).

The structures rationalize all spectroscopic findings, but the question is also raised whether a larger than 8-membered ring will assume a figure-eight conformation that then will have a much weaker conformational effect on the remainder of the chromophore. This might rationalize why, for example, pyrrole-expanded porphyrazine **6** possesses a surprisingly regular chlorin-like optical spectrum (its solid state structure was not reported).¹⁰

5.1.2 Synthesis of Thiono-Supersized Pyrrole-modified Porphyrin **14**

Treatment of **7** with thiourea smoothly produced a polar red product with all the hallmarks of an annulated-chlorin (chlorin-like UV-vis spectrum, 2-fold symmetric ¹H NMR spectrum with exchangeable O-H and N-H protons) (Scheme 5-4). However, isolation of a pure sample of this compound proved difficult due to its preferential reversion back to the dione starting material **7**. Treatment of a crude sample of imidazolidinethione-annulated chlorin **12** under the same oxidative cleavage conditions (Pb(OAc)₄, Et₃N, dry THF) afforded again the known porpholactam **10** as the major product, along with some of the reversion product dione **7**. This reaction allows two conclusions to be made: The use of thiourea does not lead to the stabilization of the adduct of the putative eight-membered ring. It further suggests that the lactam oxygen in porpholactam **10** was unlikely to have been derived from the urea moiety, unless a rapid thionolactam-to-lactam conversion took place under the reaction conditions.



Scheme 5-4. Synthesis of thiono derivatives of the supersized pyrrole-modified porphyrins. Reaction conditions: (i) thiourea or *N,N'*-dimethylthiourea, pyridine, Δ (ii) $\text{Pb}(\text{OAc})_4$, THF, Et_3N .

Exchange of thiourea with *N,N'*-dimethylthiourea furnished the corresponding chlorin diol **13** in very good yields (89%), and this was much more stable to work-up and chromatographic separation. $\text{Pb}(\text{OAc})_4$ cleavage of **13** in dry THF led mostly to a reversion of the addition reaction, and diketone **7** was observed as the major product. However, traces of a less-polar green product were also isolated, and we suspected it to be the desired supersized pyrrole-modified porphyrin **14**. The extensive reversion of the addition reaction is likely due to the instability of diol-chlorin **13** toward the residual acid in $\text{Pb}(\text{OAc})_4$. Thus, the reaction was repeated with Et_3N in the reaction mixture to suppress the (presumably acid-catalyzed) reversion back to dione **7**. This suppression was indeed observed and the nonpolar green fraction ($R_f = 0.59$, silica- CH_2Cl_2) was now isolated as the main product in good yield. The HR-MS (ESI+, TOF) of this product indicated the loss of four hydrogen atoms, suggesting successful oxidative cleavage to supersized PMP **14** had taken place. The ^1H NMR spectrum of **14** is similar to that of the corresponding triazocine-trione-modified porphyrin **11**, but with some slight shifting in the aromatic region. As expected, the thionolactam carbon is significantly downfield shifted (187 ppm) with respect to the amide version **11** (173 ppm).

A single crystal suitable for X-ray analysis could be grown by slow vapor diffusion of MeOH into a solution of **14** in CH₂Cl₂, ultimately confirming the connectivity of the pyrrole-modified porphyrin with an 8-membered 1,3,6-triazocine-2-thione-4,8-dione moiety.

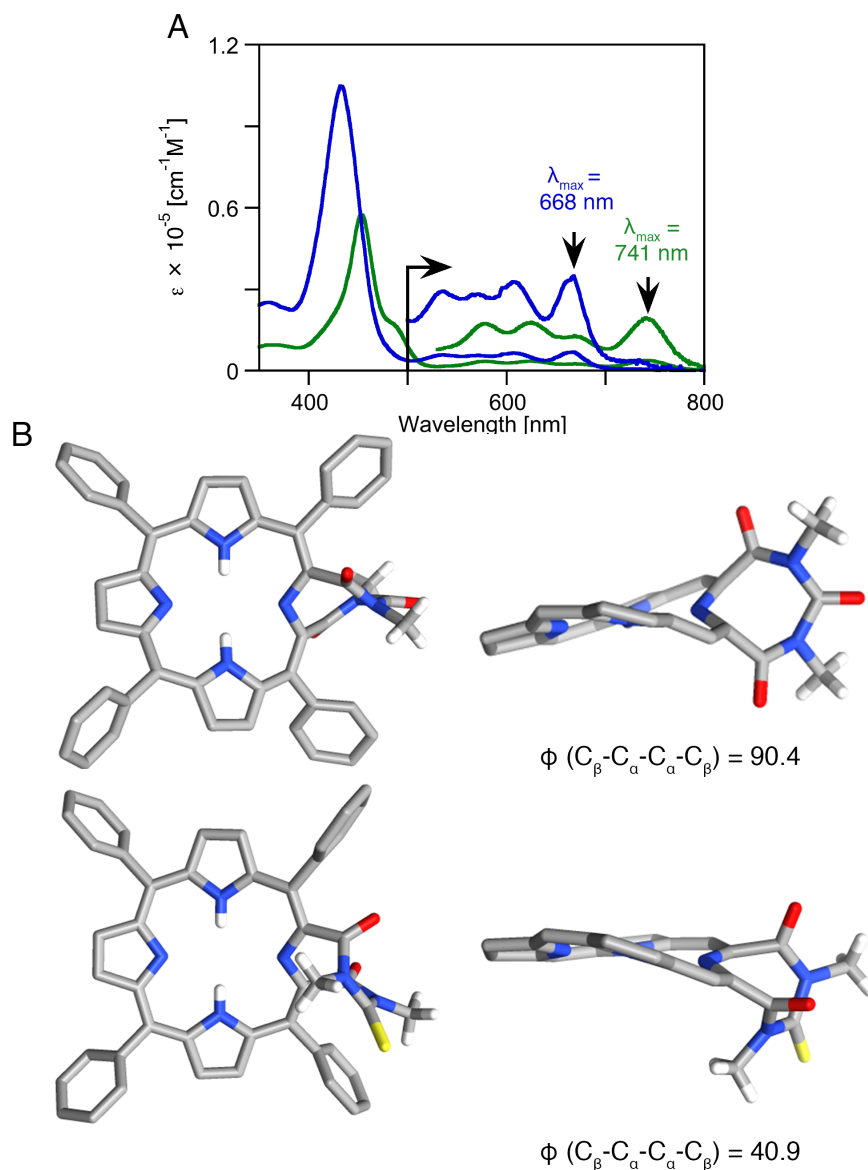


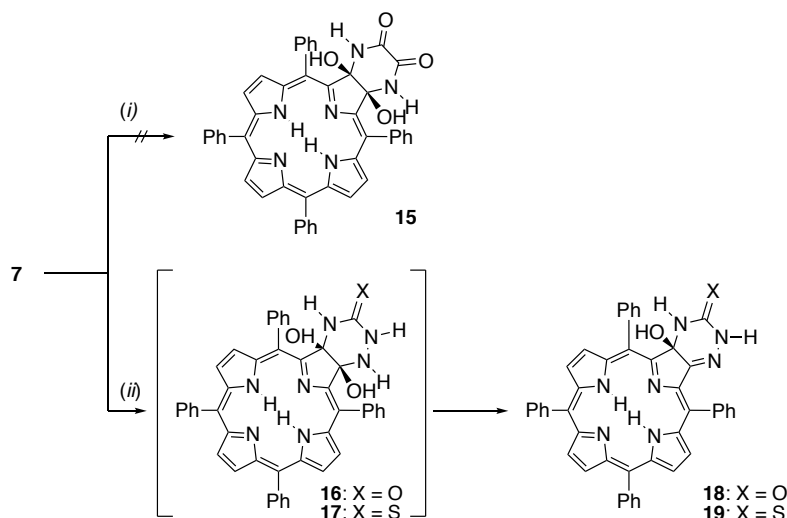
Figure 5-3. A: UV-vis spectra (CH₂Cl₂) of **11** (green trace) and thioxo-derivative **14** (blue trace). B: X-ray crystal structure and measured C _{β} -C _{α} -C _{α} -C _{β} dihedral angles of **11** and **14**.

Surprisingly, swapping out the oxygen atom for a sulfur atom has a rather drastic effect on the solid-state configuration of the pyrrole-modified porphyrin **14**. The modified pyrrole is much

less twisted with respect to the porphyrin axis as compared to **11**, translating into a milder ruffling of the macrocycle. The distortion of the pyrrole-modified porphyrins **11** and **14** was also assessed by measuring the $C_\beta-C_\alpha-C_\alpha-C_\beta$ dihedral angle of the modified pyrrole, a metric well suited to predict the red-shifted optical spectra in morpholinobacteriochlorins; the larger this angle, the more red-shifted the corresponding spectrum.¹⁹ This dihedral angle for the thio-derivative **14** is 40.9° compared to 90.4° for the urea-derived supersized pyrrole-modified porphyrin **11** (Figure 5-3A). This is also reflected in the much more red-shifted spectrum for **11** (λ_{\max} = 741 nm) than for **14** (λ_{\max} = 668 nm) (Figure 5-3B).

5.1.3 Modification of TPP-dione with semicarbazide and thiosemicarbazide

The preparation of analogues with 6-membered rings annulated to the β,β' bond of the porphyrin was also explored (Scheme 5-5). Unfortunately, reaction of dione **7** with an excess of oxamide yielded no product even after reflux for several days in pyridine. On the other hand, addition of an excess of semicarbazide·HCl yielded, within minutes at ambient temperature, a polar red and chemically unstable product with a UV-vis spectrum resembling that of a chlorin. Upon attempted isolation, this product **16** dehydrates to an isolable, stable and less polar green product **18**. Its composition, as determined by HR-MS (ESI+, TOF), indicated successful addition of semicarbazide accompanied by a loss of a water molecule. The ^1H NMR spectrum of the semicarbazide adduct **18** showed the presence of an asymmetric product with a sharp signal downfield at ~13 ppm that is exchangeable with D_2O , as well as a pair of exchangeable protons at 4.5 and 5.3 ppm (Figure 5-4).



Scheme 5-5. Synthesis of 6-membered ring adducts. Reaction conditions: (i) oxamide, pyridine, Δ
(ii) semicarbazide·HCl or thiosemicarbazide, pyridine, r.t. or $\text{Et}_3\text{N}/\text{THF}$, r.t..

An ^1H - ^1H NOESY of the compound revealed that the two exchangeable protons at 4.5 and 5.3 ppm are close to each other in space, but not neighboring the downfield-shifted exchangeable proton at 13 ppm, suggesting that they are on opposite sides of the annulated six-membered ring. A ^{15}N - ^1H HSQC experiment revealed that the peak at 13 ppm corresponds to an N-H proton. An HMBC experiment showed that this proton is correlating with two carbons, further supporting the structure of semicarbazone **18** as the isolated product.

The semicarbazide reaction can also be carried out using $\text{Et}_3\text{N}/\text{THF}$ instead of pyridine, successfully forming the putative chlorin species **16** *in situ* (by UV-vis). The attempted one-pot oxidative cleavage of this compound failed to produce the target supersized PMP, producing the ketone starting material **7** as well as semicarbazone **18** as a minor product.

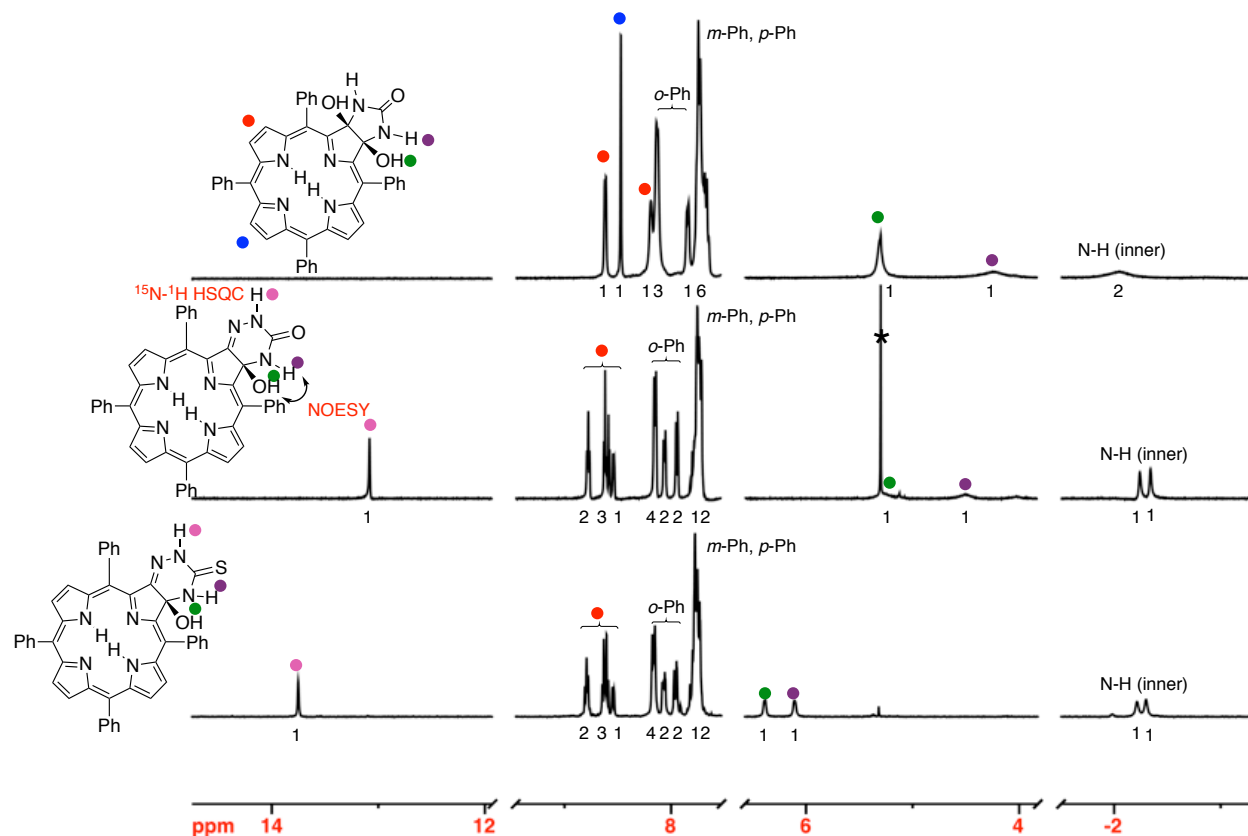


Figure 5-4. ^1H NMR spectra (CDCl₃, 298 K) of the compounds indicated. * = residual solvent

Similarly, the corresponding thiosemicarbazone **20** could be prepared by treatment of **7** with thiosemicarbazide, albeit in lower yields (~45%). The spectroscopic properties of thione derivative **20** were very similar to those of oxo-derivative **19**, with three slightly shifted diagnostic exchangeable proton peaks in its ^1H NMR spectrum (13.8 ppm, 6.4 and 6.1 ppm). Both the semicarbazone and thiosemicarbazone adducts possess relatively broadened featureless UV-vis spectra, similar to the spectrum of dione **7** (Figure 5-5), likely an effect of the sp^2 -hybridized β -position of the adduct. Further exploration of the chemistry of the carbazone derivatives, particularly the semicarbazone **18**, is currently underway.

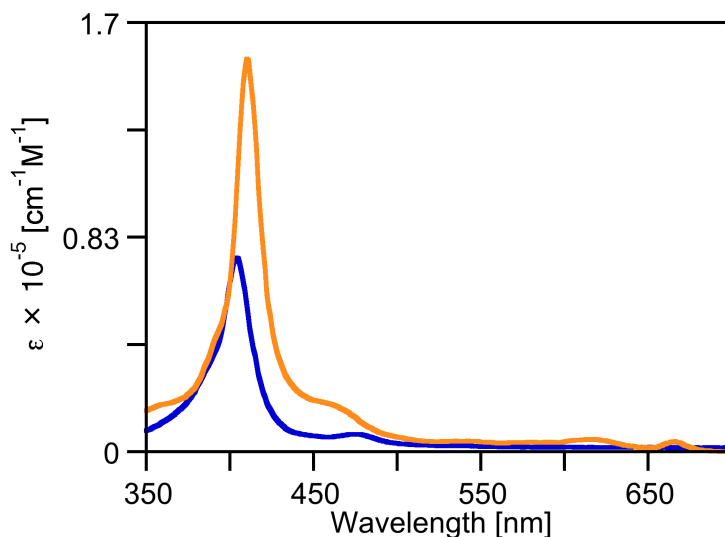
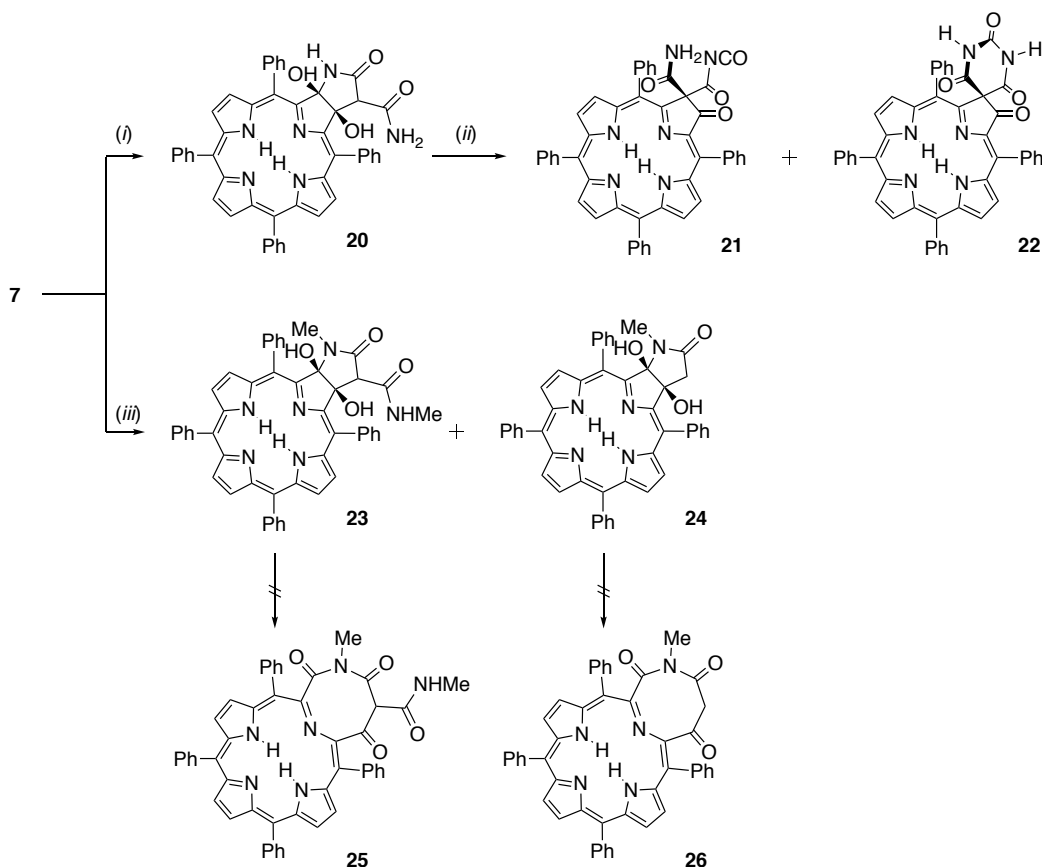


Figure 5-5. UV-vis spectra (CH_2Cl_2) of dione **7** (blue trace) and semicarbazone **18** (orange trace).

5.1.4 Formation of Adducts using Malonamide derivatives and their oxidative cleavage

The addition of malonamide derivatives to diketones to form 7-membered rings has been reported.²⁰ Thus, treatment of the diketone **7** with malonamide under the same reaction conditions afforded a very polar magenta product **20** ($R_f = 0.38$, 5% MeOH/ CH_2Cl_2) in high yields (~96%), with a chlorin-like UV-vis spectrum (Scheme 5-6). HR-MS showed a mass corresponding to the addition of malonamide to the porphyrin, with no subsequent dehydration. However, the formation of the simple, symmetric and desired adduct can be excluded, as its ^1H NMR spectrum is complex, indicating an asymmetric addition of malonamide. A total of five exchangeable protons were observed, with one downfield-shifted at 9.0 ppm. The other four exchangeable protons were observed in the range of 5-7 ppm, the range expected for pyrroline O-H or N-H signals. The ^{13}C NMR of the product revealed the expected signals for the annulated pyrrole moiety, as well as an upfield-shifted carbon at 55 ppm. ^{13}C - ^1H HSQC analysis showed that this carbon correlates with a peak integrating to a single proton at 4.2 ppm. Taken together, the spectroscopic data suggest that the diol species is formed by asymmetric attack of malonamide, with one linkage formed, as desired, from the amide- NH_2 end, but the other arising

from the malonyl position. An HMBC spectrum of this compound further strengthens this assignment, showing the expected multiple-bond correlations of the pyrroline carbons at 85 and 94 ppm with the exchangeable protons (see experimental section).



Scheme 5-6. Synthesis of malonamide adducts. Reaction conditions (i) malonamide, pyridine, Δ (ii) $\text{Pb}(\text{OAc})_4$, THF, r.t. (iii) *N,N'*-dimethylmalonamide, pyridine, Δ .

Oxidative cleavage of the diol **20** with $\text{Pb}(\text{OAc})_4$ in dry THF afforded a nonpolar purple product with a porphyrin like UV-vis spectrum in moderate yields (~60%). A ^1H NMR analysis of this compound revealed that it is a mixture of two compounds, with the second compound only a minor component. In our hands, these compounds proved inseparable. On the bright side, when we attempted to crystallize the mixture, crystals suitable for single crystal X-ray analysis of the minor component formed. This identified product **22** as an unprecedented spirobarbiturate.

Porphyrins with spiro-linked heterocycles at the β -positions prepared by modification of a porphyrin are generally rare.²¹

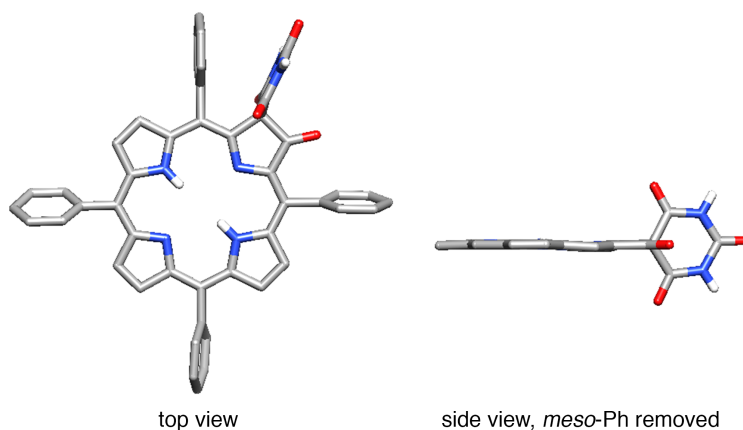
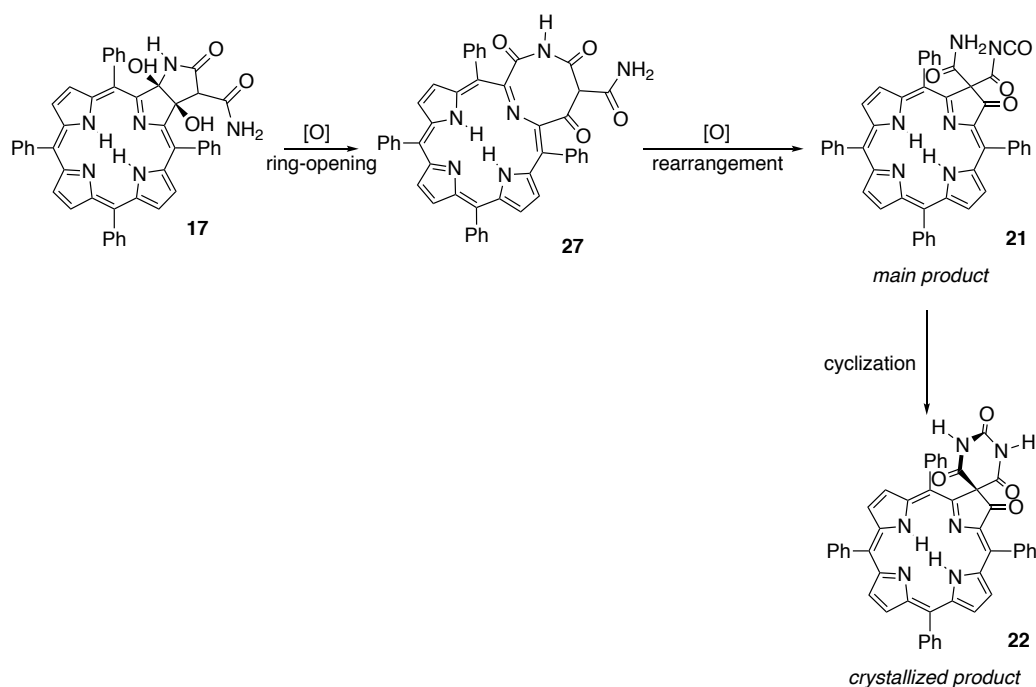


Figure 5-6. X-ray crystal structure of spiro-barbiturate **22**. Hydrogens removed for clarity.

The formation of spirobarbiturate **22** can be rationalized *via* the putative ring-opened intermediate **27** (Scheme 5-7). After an oxidative rearrangement of **27** to **21**, intramolecular cyclization by amide attack on the isocyanate provides spirobarbiturate **22**.

An examination of the spectroscopic data for **21** shows that its ^1H NMR shows only two exchangeable protons at 5.4 and 6.9 ppm while no malonyl proton can be observed (as in chlorindiol **20**). A ^{15}N - ^1H HSQC spectrum revealed that these two exchangeable protons are attached to the same nitrogen atom, further strengthening the connectivity assignment of product **21**. Attempts to grow crystals of the major component **21** suitable for a single crystal X-ray structure analysis are ongoing.



Scheme 5-7. Proposed mechanism for the formation of oxidative cleavage products **21** and **22**.

N,N'-dimethylmalonamide also reacts with dione **7** to generate the corresponding *N,N'*-dimethyl-pyrrolidinone-annulated dihydroxychlorin **23**, showing all expected analytical properties. A single crystal of this compound was grown, ultimately proving its connectivity (and, by extension, that of the diol **20** derived from malonamide). The chlorin chromophore in **23** surprises by possessing an uncommonly saddled conformation (Figure 5-7).

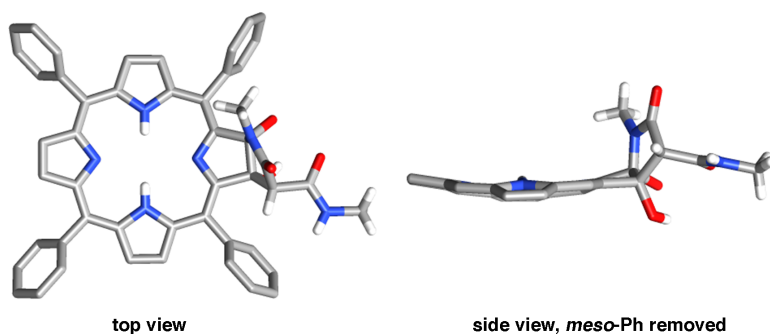


Figure 5-7. X-ray crystal structure of diol **23**. Hydrogens removed for clarity.

Next to the major *N,N'*-dimethylmalonamide addition product **23** was isolated a polar red product that also had a chlorin-like UV-vis spectrum. Its composition, as determined by HR-MS (ESI+, TOF), indicated the loss of a CONHMe fragment from the major chlorin product. An inspection of the ^1H NMR spectrum of this compound revealed that this could be supported: one methyl group as well as one N-H were missing, replaced by a pair of diastereotopic protons ($^2J = 17.5$ Hz) at 3.2 and 2.8 ppm. A ^{13}C - ^1H HSQC spectrum confirmed that the two peaks are connected to the same carbon.

Unfortunately, both diols **23** and **24** derived from *N,N'*-dimethylmalonamide failed to produce ring-opened products by action of $\text{Pb}(\text{OAc})_4$; instead only the formation of complex reaction mixtures was observed. Treatment of diols **23** and **24** with NaIO_4 heterogenized on silica gel in CH_2Cl_2 also failed to produce any products after several days. It is, however, likely that the target PMPs **25** and **26** formed by reaction of **23** and **24** with $\text{Pb}(\text{OAc})_4$, but that the constraints of the porphyrinic macrocycle led to rapid and non-specific degradation of the putative 10-membered ring PMPs. The decomposition of diol **24** was slow enough that we could measure a UV-vis spectrum of the reaction mixture. The UV-vis spectrum of **24** treated with $\text{Pb}(\text{OAc})_4$ in dry THF after 7 minutes indicated the hallmarks of a ring-opened product (red-shifted λ_{max} and broadened and red-shifted Soret band) (Figure 5-8), but the products **25** and **26** ultimately proved intractable.

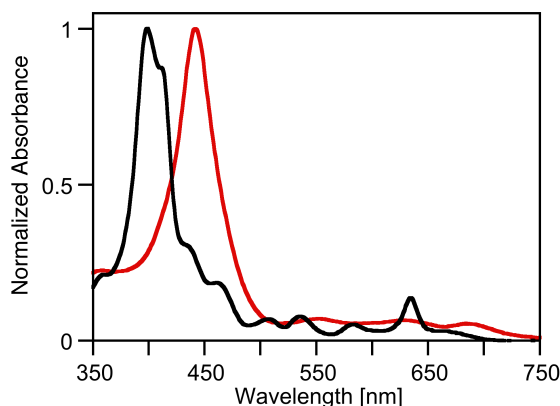


Figure 5-8. UV-vis spectra of diol **24** (black trace, CH₂Cl₂) and reaction mixture 7 minutes after treatment with Pb(OAc)₄ in dry THF at r.t. (red trace, THF).

5.2 Conclusions

In conclusion, a novel class of ring-expanded pyrrole-modified porphyrins incorporating an 8-membered heterocycle could be accessed by using an annulation → oxidative cleavage strategy, i.e., using a reversal of our well-established ‘breaking and mending strategy’. The synthesis of the corresponding thiono-analogue provided further insight into the validity of a recent proposal that the optical properties of a porphyrinic macrocycle are to a large degree determined by the C_β-C_α-C_α-C_β dihedral angle of the modified pyrrole.¹⁹ The attempted preparation of analogues of greater ring-sizes proved unsuccessful, as all attempts were thwarted by various degradation pathways. Nevertheless, the exploration of the reactivity of dione **7** toward other bifunctional nucleophiles offered a glimpse into rich chemistry with the possibility of generating previously inaccessible pyrrole-modified porphyrins with medium ring sizes and other β-functionalized porphyrinic chromophores.

5.3 Experimental Section

5.3.1 Materials and Instruments

Urea, thiourea, *N,N'*-dimethylurea, *N,N'*-dimethyl thiourea, semicarbazide·HCl, thiosemicarbazide, malonamide and Pb(OAc)₄ were purchased from Sigma-Aldrich and were used without further purification. THF (dry) was distilled from sodium benzophenone ketyl prior to use. Oxoporphyrin **7**^{11a} and *N,N*-dimethylmalonamide²² were prepared according to literature procedures.

Aluminum-backed, silica gel 60, 250 μm thickness analytical plates were used for analytical TLC; 20 × 20 cm, glass-backed, silica gel 60, 500 μm thickness preparative TLC plates, and standard grade, 60 Å, 32–63 μm flash column silica gel were used for preparative chromatography.

¹H and ¹³C NMR spectra were recorded on a Bruker 400 MHz instrument in the solvents indicated, and were referenced to residual solvent peaks. High and low resolution mass spectra were provided by the Mass Spectrometry Facility, Department of Chemistry, University of Connecticut. The microwave synthesizer used was a discover microwave reactor.

5.3.2 Synthesis and Characterization

meso-Tetraphenyl imidazolidinone-annulated dihydroxychlorin 8. Porphyrin Dione **7** (118.0 mg, 1.83×10^{-4} mol) was dissolved in pyridine (25.0 mL) in a RBF equipped with a magnetic stir bar. Urea (245 mg, 0.0041 mol, 22 equiv) was added and the mixture was heated to reflux for 30 min under a N₂ atmosphere. The solvent was evaporated *in vacuo*. The remaining residue was taken up in CHCl₃ and filtered through a glass frit. The filtrate was washed with 5 × 25 mL distilled water and dried over Na₂SO₄. The dried residue was separated by column chromatography (CH₂Cl₂-5% MeOH) recovering dione **7** in 8% yield (9 mg), followed by the magenta product **8** in 85% yield (111 mg): *R*_f (silica-CH₂Cl₂/5% MeOH) = 0.36; ¹H NMR

(400 MHz, CDCl_3): δ 8.64 (d, $^3J = 4.7$ Hz, H), 8.49 (s, 1H), 8.21 (s, 1H), 8.14 (d, $^3J = 5.8$ Hz, 3H), 7.86 (d, $^3J = 6.8$ Hz, 1H), 7.72 (m, 6H), 5.34 (br s, 1H, exchangeable with D_2O), 4.26 (br s, 1H, exchangeable with D_2O), -2.03 (br s, 1H, exchangeable with D_2O) ppm; ^{13}C NMR (100 MHz, DMSO-d_6): δ 159.5, 158.5, 152.8, 141.4, 141.1, 140.0, 135.4, 135.2, 134.12, 134.10, 134.08, 134.06, 133.18, 133.13, 128.55, 128.44, 127.50, 127.33, 127.26, 125.7, 123.1, 112.9, 93.5 ppm; UV-vis (CH_2Cl_2) λ_{max} (log ϵ) 406 (5.29), 512 (4.12), 541 (4.22), 591 (4.00), 642 (4.44) nm; FT-IR (neat, diamond ATR): $\nu_{\text{C=O}} = 1715.7 \text{ cm}^{-1}$; MS (ESI $^+$, 100% CH_3CN , TOF) m/z calcd for $\text{C}_{45}\text{H}_{33}\text{N}_6\text{O}_3$ ($[\text{M}\cdot\text{H}]^+$) 705.2609, found 705.2605.

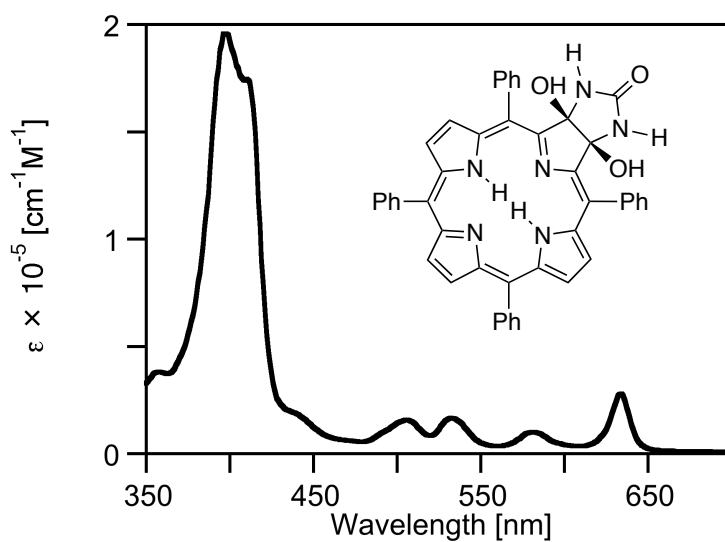


Figure 5-9. UV-vis spectrum (CH_2Cl_2) of **8**.

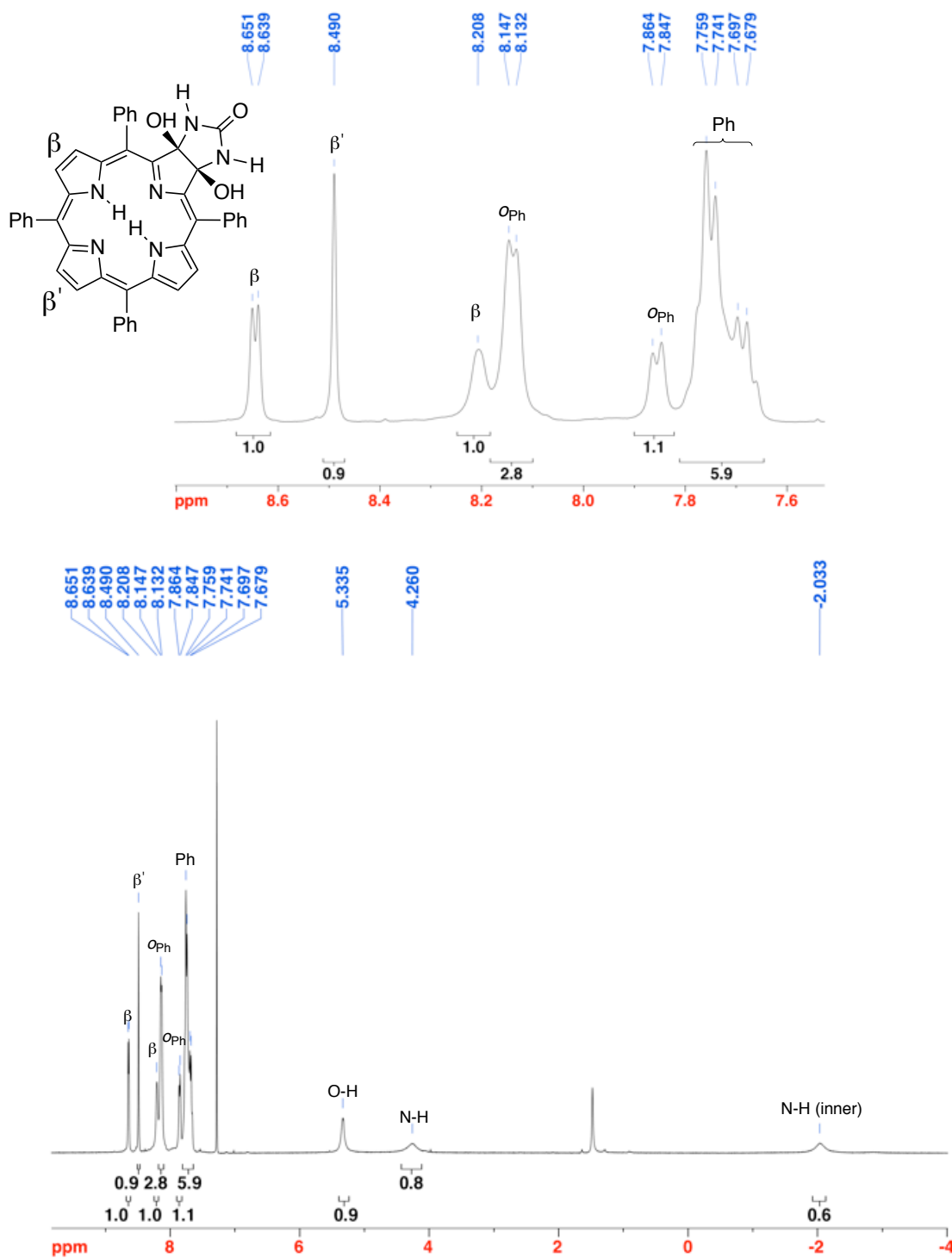


Figure 5-10. ^1H NMR spectrum (400 MHz, CDCl_3) of **8**.

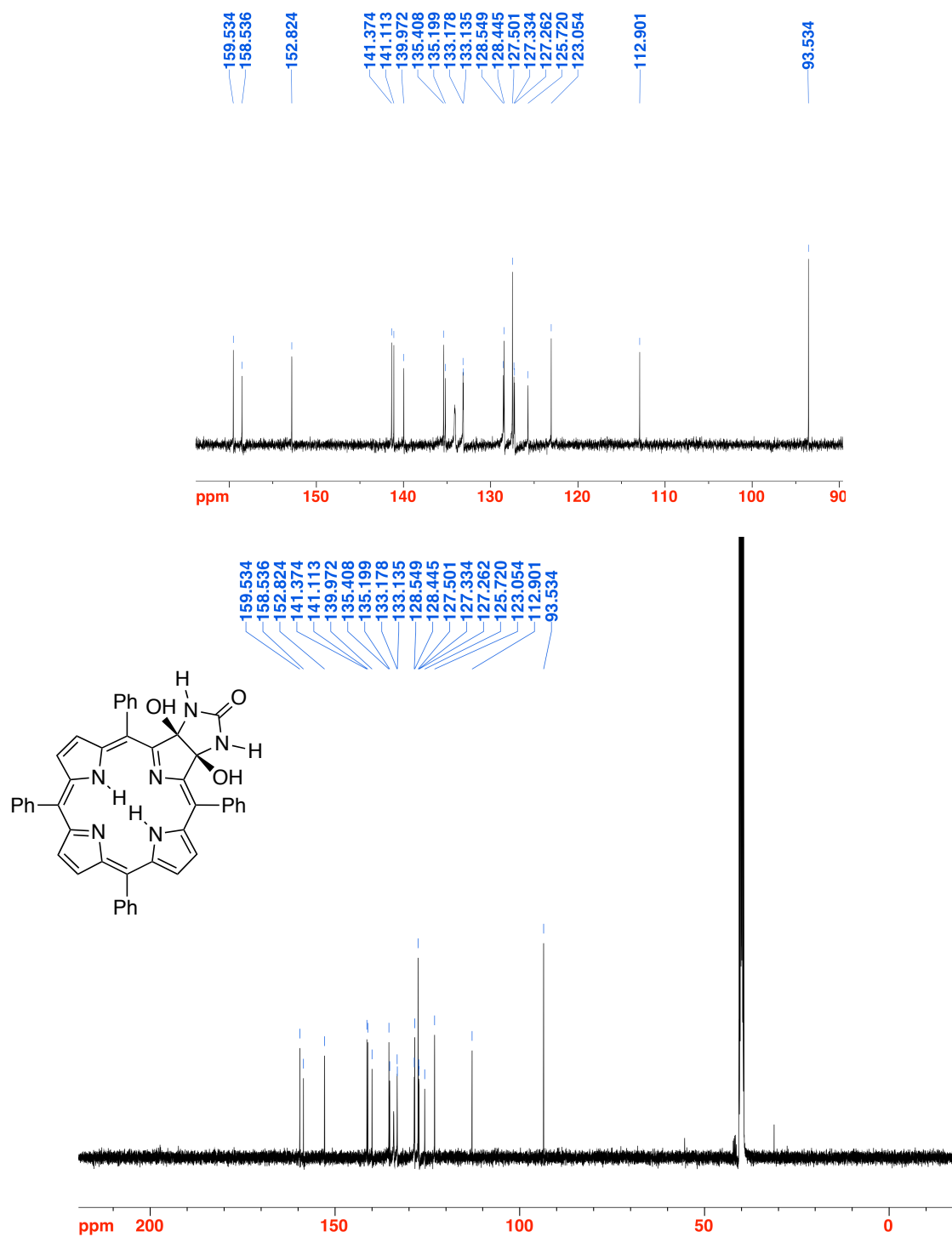


Figure 5-11. ^{13}C NMR spectrum (100 MHz, CDCl_3) of 8.

meso-Tetraphenyl-*N,N'*-dimethylimidazolidnone-annulated dihydroxychlorin 9.

Prepared from **7** (30.0 mg, 4.65×10^{-5} mol) in pyridine (8.0 mL) as described for **8** using *N,N'*-dimethylurea (82 mg, 9.31×10^{-4} mol, 20 equiv.) to afford the red dihydroxychlorin **9** in 54% yield (18.5 mg): R_f (silica-CH₂Cl₂/3% MeOH) = 0.56; ¹H NMR (400 MHz, CDCl₃): δ 8.57 (d, ³*J* = 4.9 Hz, 1H), 8.45 (s, 1H), 8.16 (d, ³*J* = 6.7 Hz, 1H), 8.07 (d, ³*J* = 5.2 Hz, 4H), 7.78-7.67 (m, 6H), 4.55 (s, 1H, exchangeable with D₂O), 2.28 (s, 3H), -1.75 (s, 1H, exchangeable with D₂O) ppm; ¹³C NMR (100 MHz, CDCl₃): δ 161.4, 154.2, 153.5, 141.4, 139.8, 136.0, 135.4, 134.1, 132.9, 128.7, 127.97, 127.88, 127.6, 127.3, 126.81, 126.73, 125.3, 123.7, 112.8, 97.1, 26.4 ppm; UV-vis (CH₂Cl₂) λ_{max} (log ϵ) 410 (4.99), 520 (3.84), 549 (3.88), 596 (3.53), 649 (4.08) nm; FT-IR (neat, diamond ATR): $\nu_{\text{C=O}}$ = 1680.4 cm⁻¹; HR-MS (ESI⁺, 100% CH₃CN, TOF) *m/z* calcd for C₄₇H₃₇N₆O₃ ([M·H]⁺) 733.2927, found 733.2941.

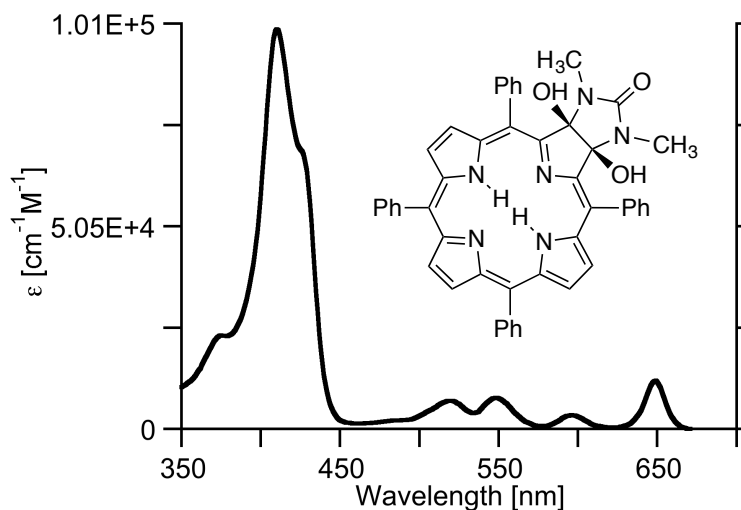


Figure 5-12. UV-vis spectrum (CH₂Cl₂) of **9**.

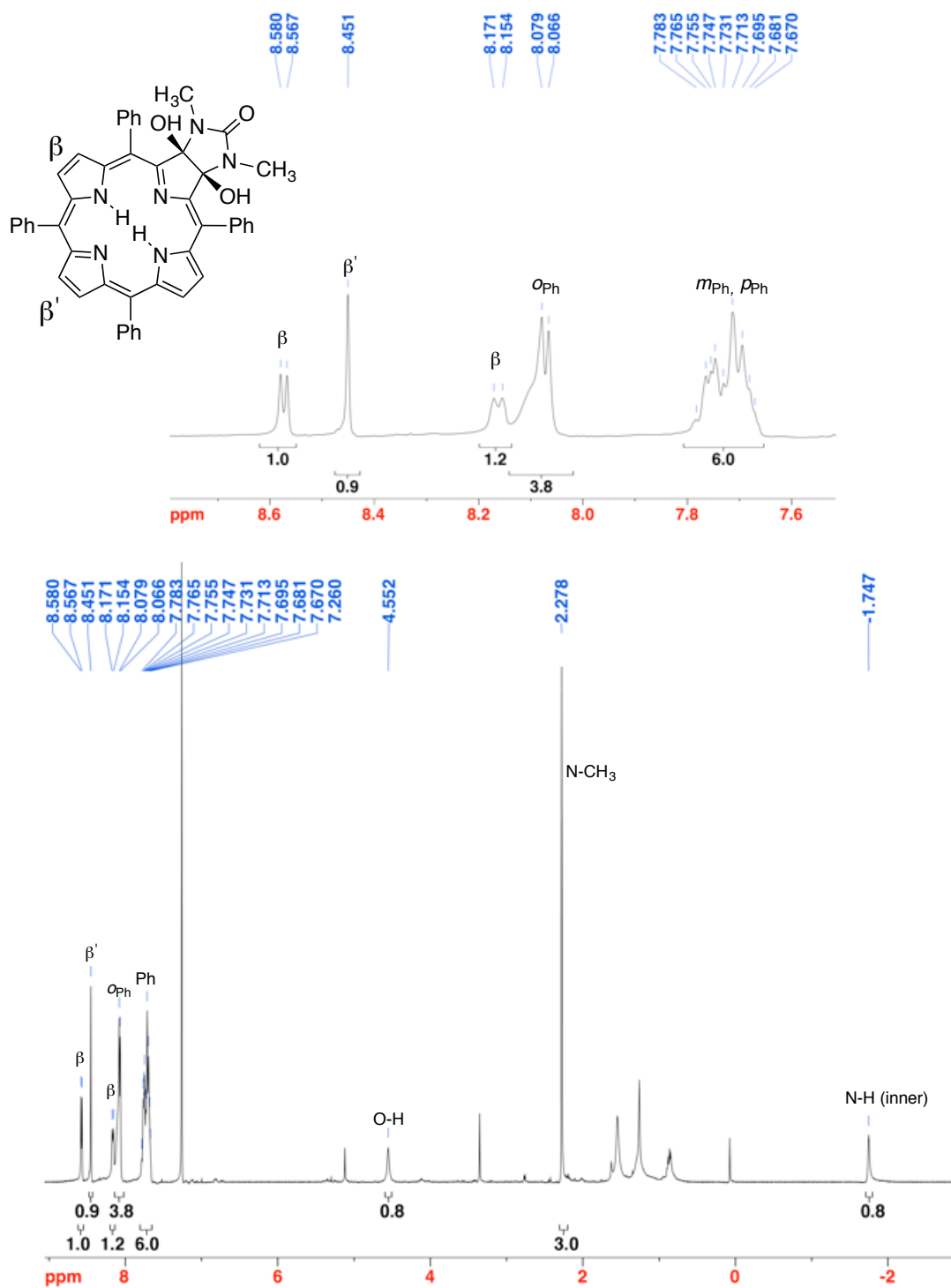


Figure 5-13. ¹H NMR spectrum (400 MHz, CDCl₃) of **9**.

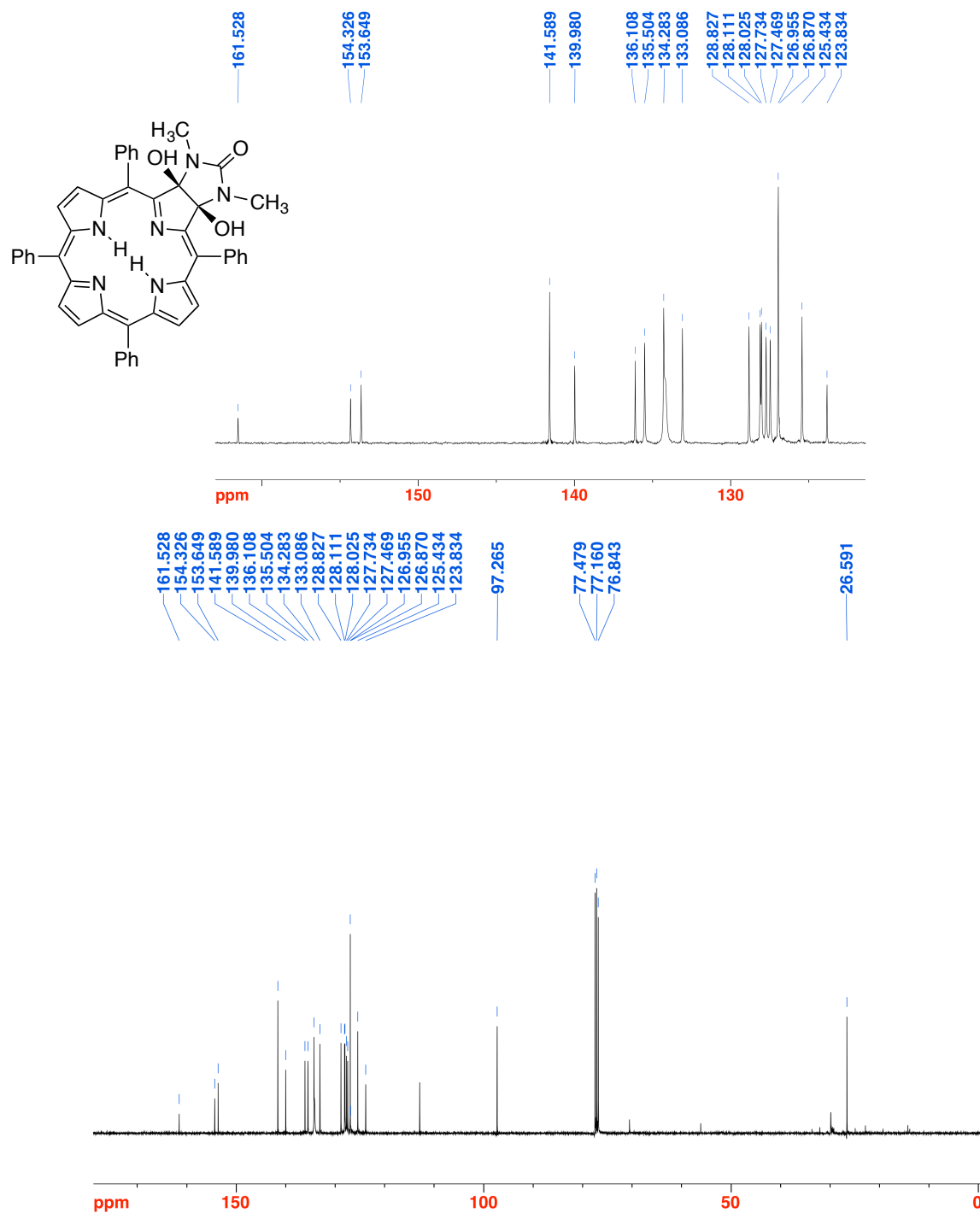


Figure 5-14. ^{13}C NMR spectrum (100 MHz, CDCl_3) of 9.

meso-Tetraphenyl-2-aza-3-oxoporphyrin xx. Dihydroxychlorin **8** (28.8 mg, 4.6×10^{-5} mol) was dissolved in dry THF (11.0 mL) and Et₃N (5-6 drops) in a RBF equipped with a magnetic stir bar. Pb(OAc)₄ (31.4 mg, 7.1×10^{-5} mol, 1.7 equiv.) was added in portions and the reaction mixture was stirred at ambient temperature. When the starting material was consumed (reaction control by UV-vis and TLC), the solvent was removed by rotary evaporation and the remaining residue was purified by preparative TLC (silica-CH₂Cl₂/1% MeOH) to afford well-known (J. Akhigbe, J. P. Haskoor, J. A. Krause, M. Zeller and C. Brückner, *Org. Biomol. Chem.*, 2013, **11**, 3616–3628.) porpholactam **10** in 69% yield (17.8 mg): ¹H NMR (400 MHz, CDCl₃): δ 9.65 (s, 1H, exchangeable with D₂O), 8.79 (d, ³J = 5.0 Hz, 1H), 8.71 (d, ³J = 4.7 Hz, 1H), 8.64 (d, ³J = 5.0 Hz, 1H), 8.61-8.54 (m, 3H), 8.16-8.12 (m, 4H), 8.10-8.07 (m, 2H), 7.99 (m, 2H), 7.81 (m, 3H), 7.77-7.69 (m, 9H), -1.87 (s, 1H, exchangeable with D₂O), -2.14 (s, 1H, exchangeable with D₂O) ppm.

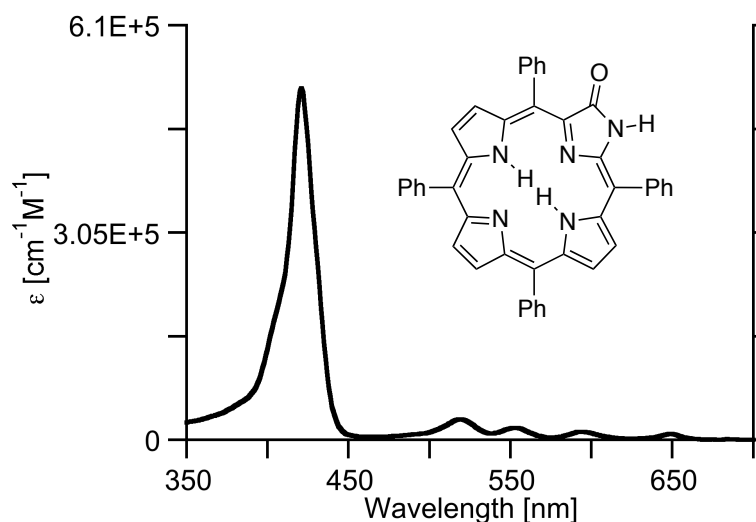


Figure 5-15. UV-vis spectrum (CH₂Cl₂) of **10**.

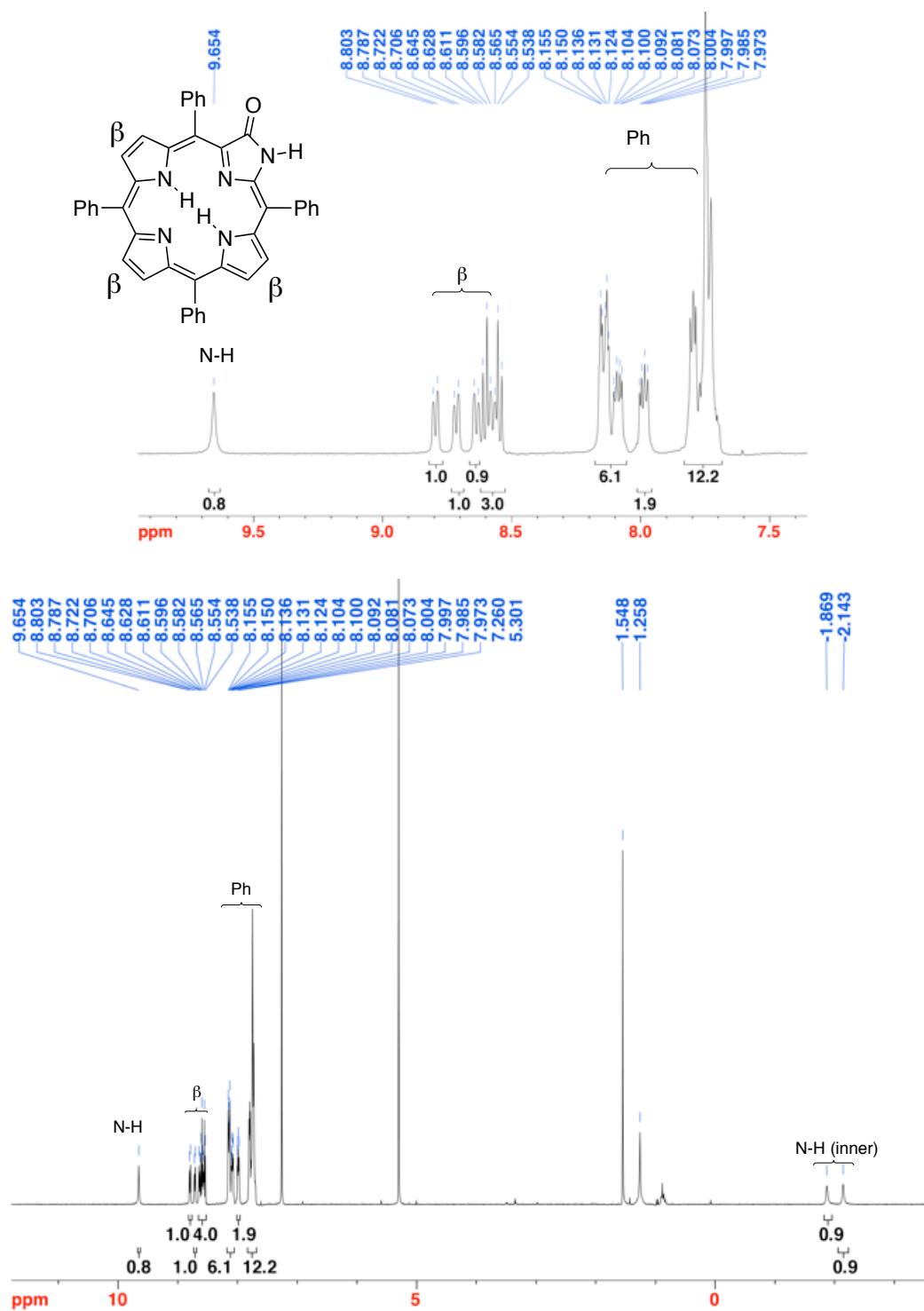


Figure 5-16. ^1H NMR (400 MHz, CDCl_3) of **10**.

1,3,6-Triazocine-2,4-8-trione-based Pyrrole-modified Porphyrin 11. Dihydroxychlorin-dimethylurea adduct **9** was dissolved in dry THF (5.0 mL) in a RBF equipped with a magnetic stir bar. $\text{Pb}(\text{OAc})_4$ (13.3 mg, 3.00×10^{-5} mol) was added and the reaction mixture was stirred at ambient temperature. When the starting material was consumed (reaction control by UV-vis and TLC), the solvent was evaporated and the residue separated by preparative TLC (silica- CH_2Cl_2 /3% MeOH) to afford **11** as a bright green solid in 71% yield (14.1 mg): R_f (silica- CH_2Cl_2 /2% MeOH) = 0.66; ^1H NMR (400 MHz, CDCl_3): δ 8.35 (d, $^3J = 4.9$ Hz, 1H), 8.28 (br s, 1H), 8.16 (s, 1H), 8.04 (d, $^3J = 4.9$ Hz, 1H), 7.99 (br s, 2H), 7.70 (m, 4H), 7.56 (t, $^3J = 7.5$ Hz, 1H), 7.43 (br s, 1H), 7.10 (br s, 1H), 3.28-3.15 (s, 3H), 1.88 (s, 1H, exchangeable with D_2O) ppm; ^{13}C NMR (100 MHz, CDCl_3): δ 173.1, 155.5, 155.1, 147.3, 140.9, 140.21, 140.08, 136.5, 135.5, 133.6, 131.9, 129.2, 128.41, 128.32, 128.13, 127.4, 126.3, 125.5, 119.5, 32.9 ppm; UV-vis (CH_2Cl_2) λ_{max} (log ϵ) 365 (3.98) 454 (4.76), 578 (3.54), 625 (3.55), 670 (3.40), 741 (3.59) nm; FT-IR (neat, diamond ATR): $\nu_{\text{C=O}} = 1709.6, 1614.8 \text{ cm}^{-1}$; HR-MS (ESI $^+$, 100% CH_3CN , TOF) m/z calcd for $\text{C}_{47}\text{H}_{34}\text{O}_6\text{N}_3$ ($[\text{M}\cdot\text{H}]^+$), 731.2771 found 731.2775.

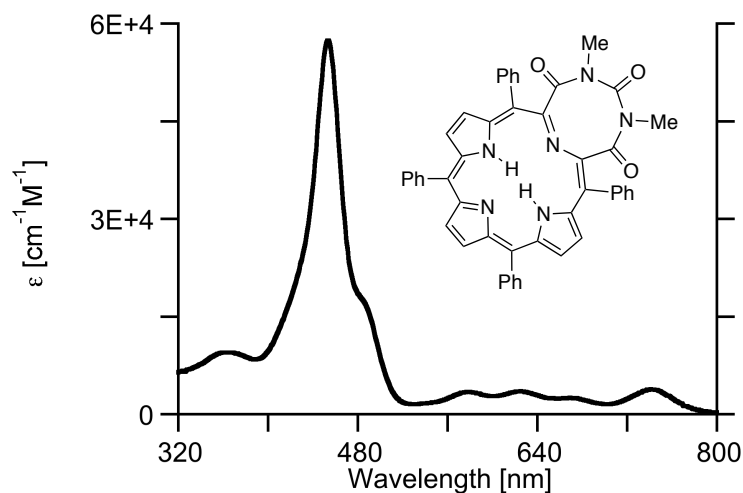


Figure 5-17. UV-vis spectrum (CH_2Cl_2) of **11**.

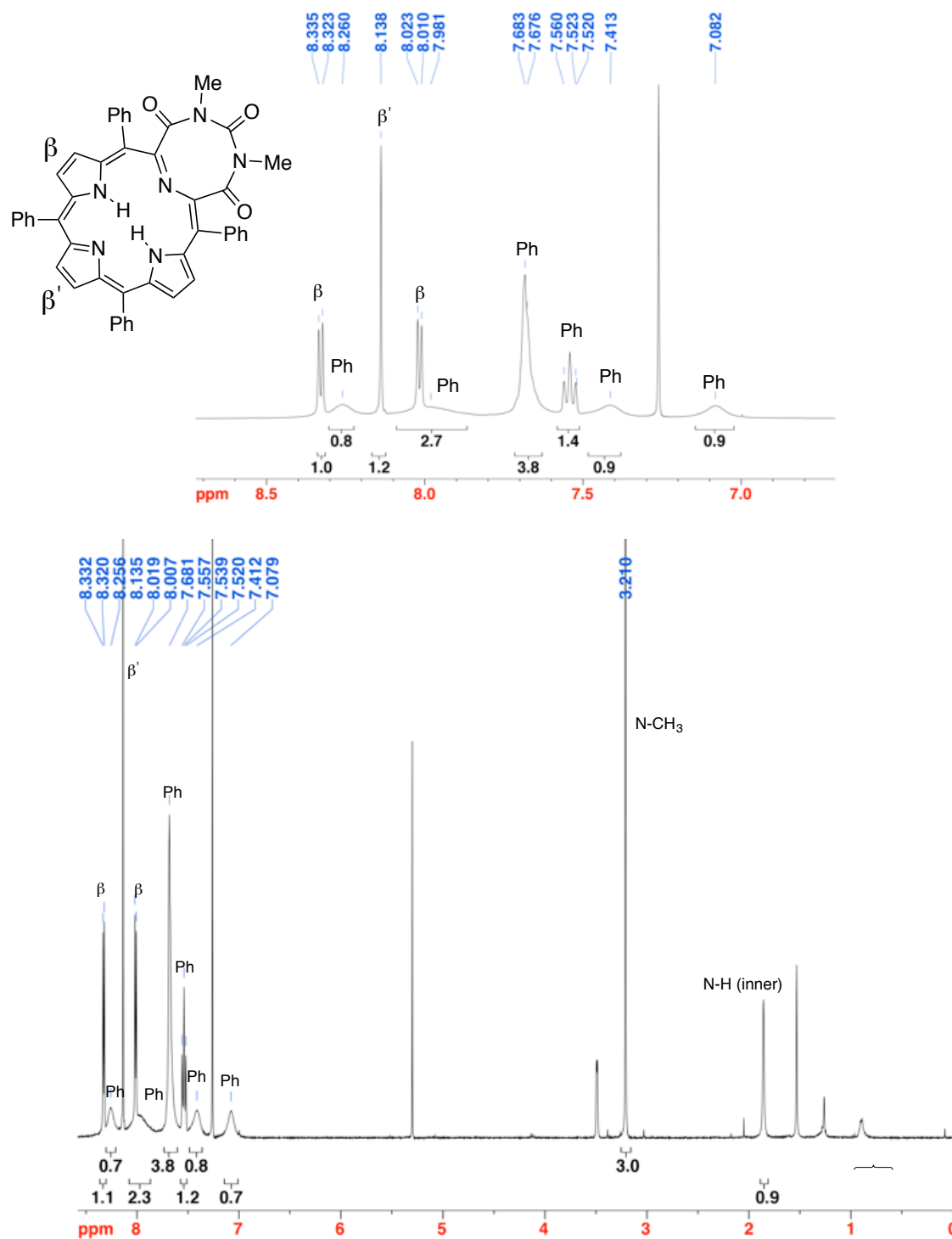


Figure 5 18. ^1H NMR (400 MHz, CDCl_3) of **11**.

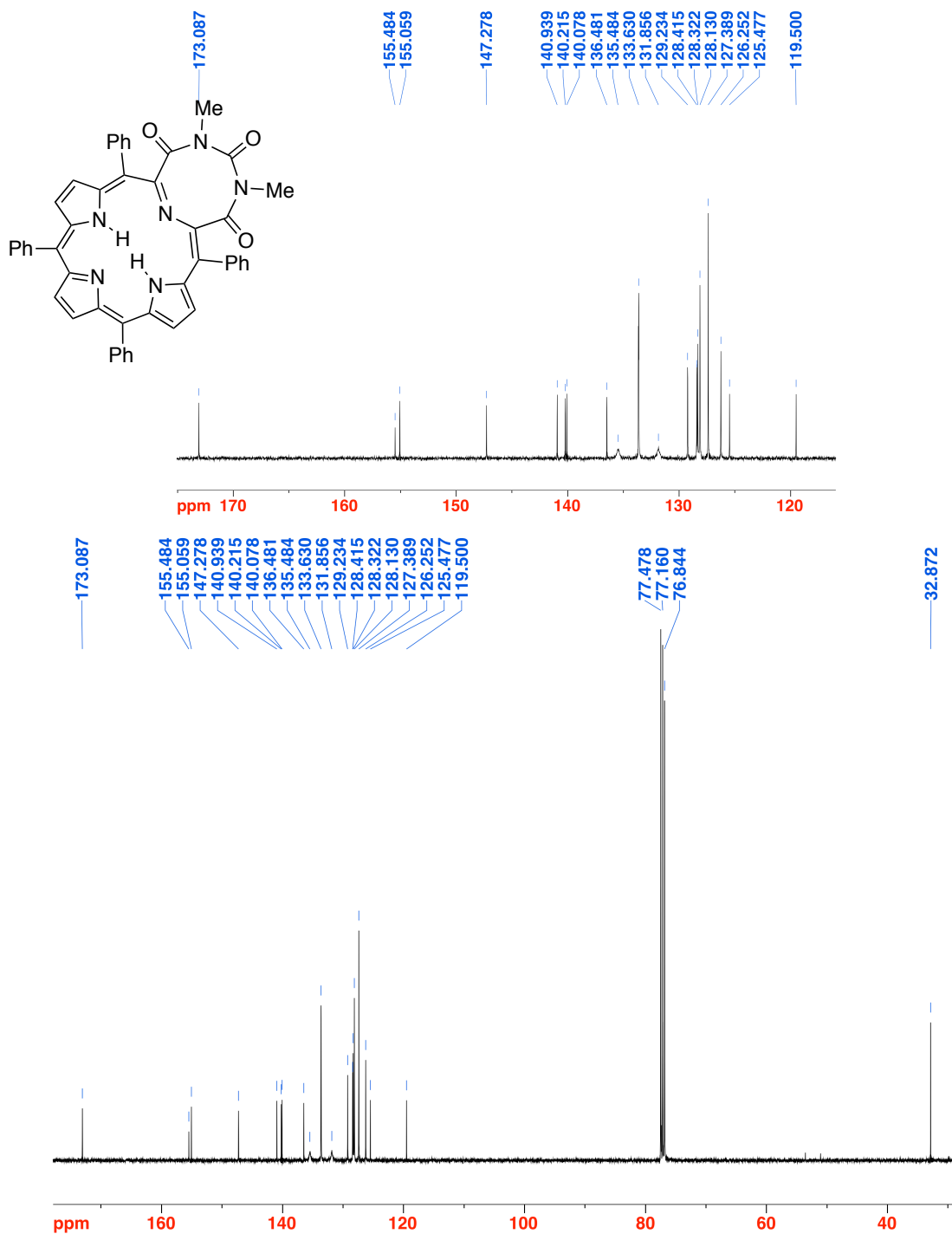


Figure 5-19. ^{13}C NMR (100 MHz, CDCl_3) of 11.

(8Ni). Prepared from **7Ni** (143 mg, 2.0×10^{-4} mol) as described for **8** using urea (234 mg, 0.004 mol, 19 equiv) to afford recovered dione **7Ni** (15 mg, 10%) and the blue dihydroxychlorin **8Ni** in 75% yield (116 mg): R_f (silica-CH₂Cl₂/5% MeOH) = 0.29; ¹H NMR (400 MHz, DMSO-d₆): δ 8.29 (d, ³*J* = 3.9 Hz, 2H), 8.15 (s, 1H), 7.82 (two overlapping d, ³*J* = 3.7 Hz, 2H), 7.69-7.65 (m, 5H), 7.59-7.54 (m, 3H), 6.74 (br s, 1H, exchangeable with D₂O), 5.88 (br s, 1H, exchangeable with D₂O) ppm; ¹³C NMR (100 MHz, DMSO-d₆): δ 159.2, 146.4, 146.1, 140.9, 139.4, 137.99, 137.88, 133.8, 133.03, 132.97, 129.6, 128.7, 128.04, 128.01, 127.97, 127.85, 123.8, 110.9, 94.2 ppm; UV-vis (CH₂Cl₂) λ_{\max} (log ϵ) 415 (4.26), 575 (sh), 607 (3.49) nm; HR-MS (ESI⁺, 100% CH₃CN, TOF) *m/z* calcd for C₄₅H₂₉N₆O₃ ([M·H]⁺), 759.1655 found 759.1640.

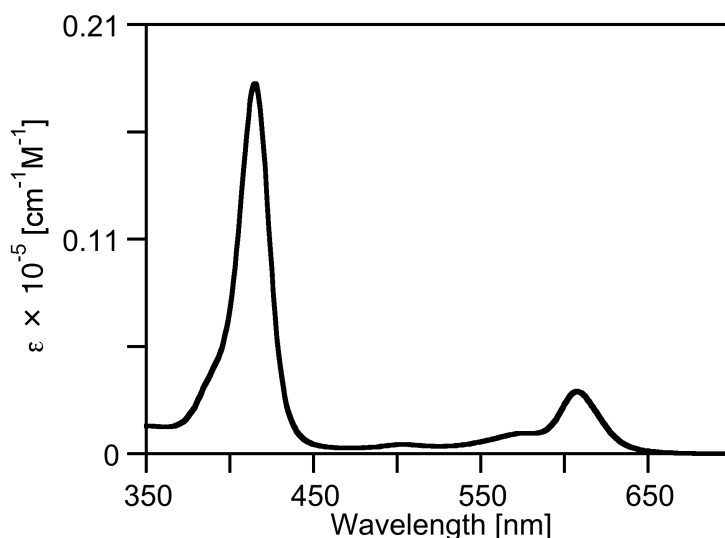
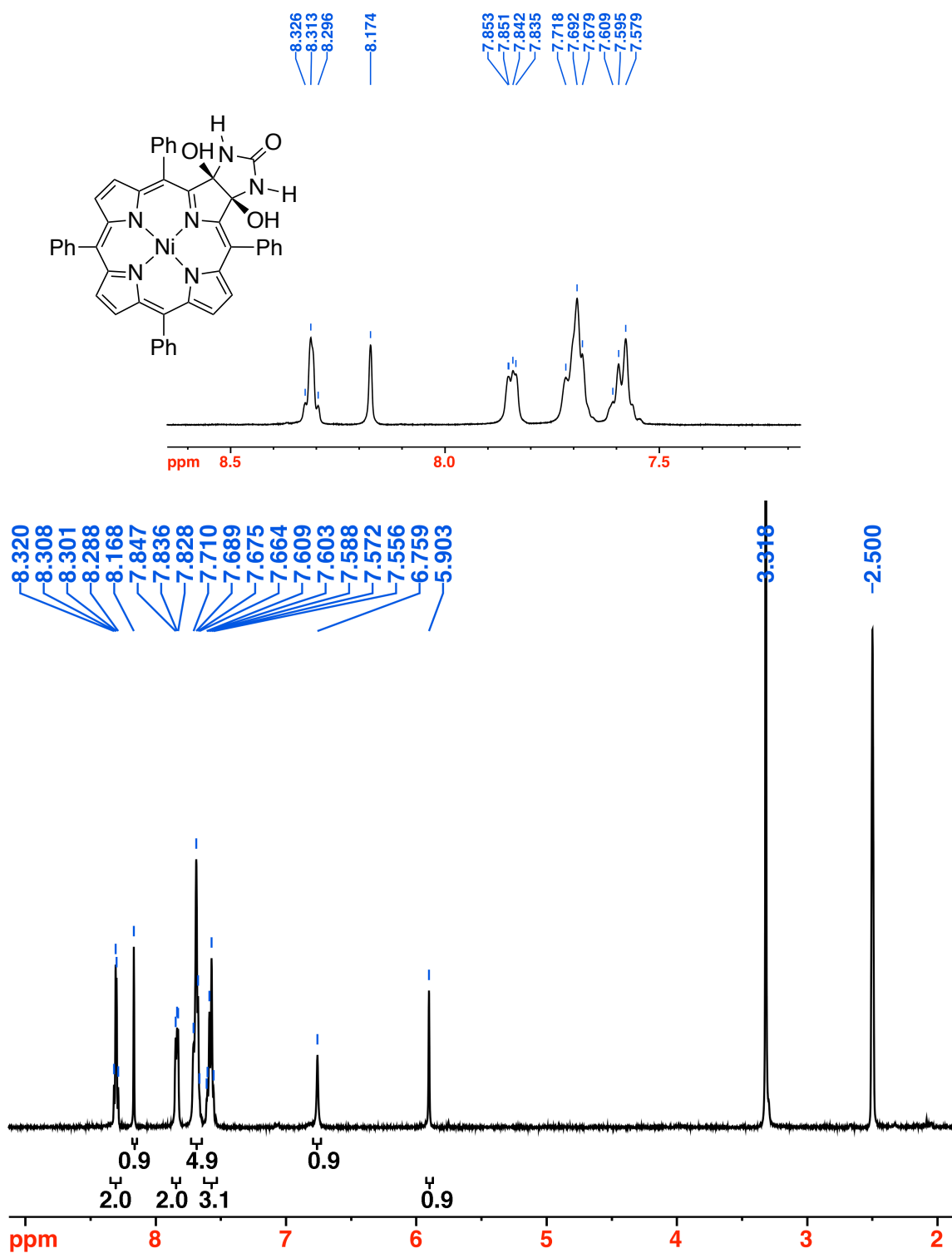


Figure 5-20. UV-vis spectrum (CH₂Cl₂) of **8Ni**.

Figure 5-21. ^1H NMR spectrum (400 MHz, CDCl_3) of **8Ni**.

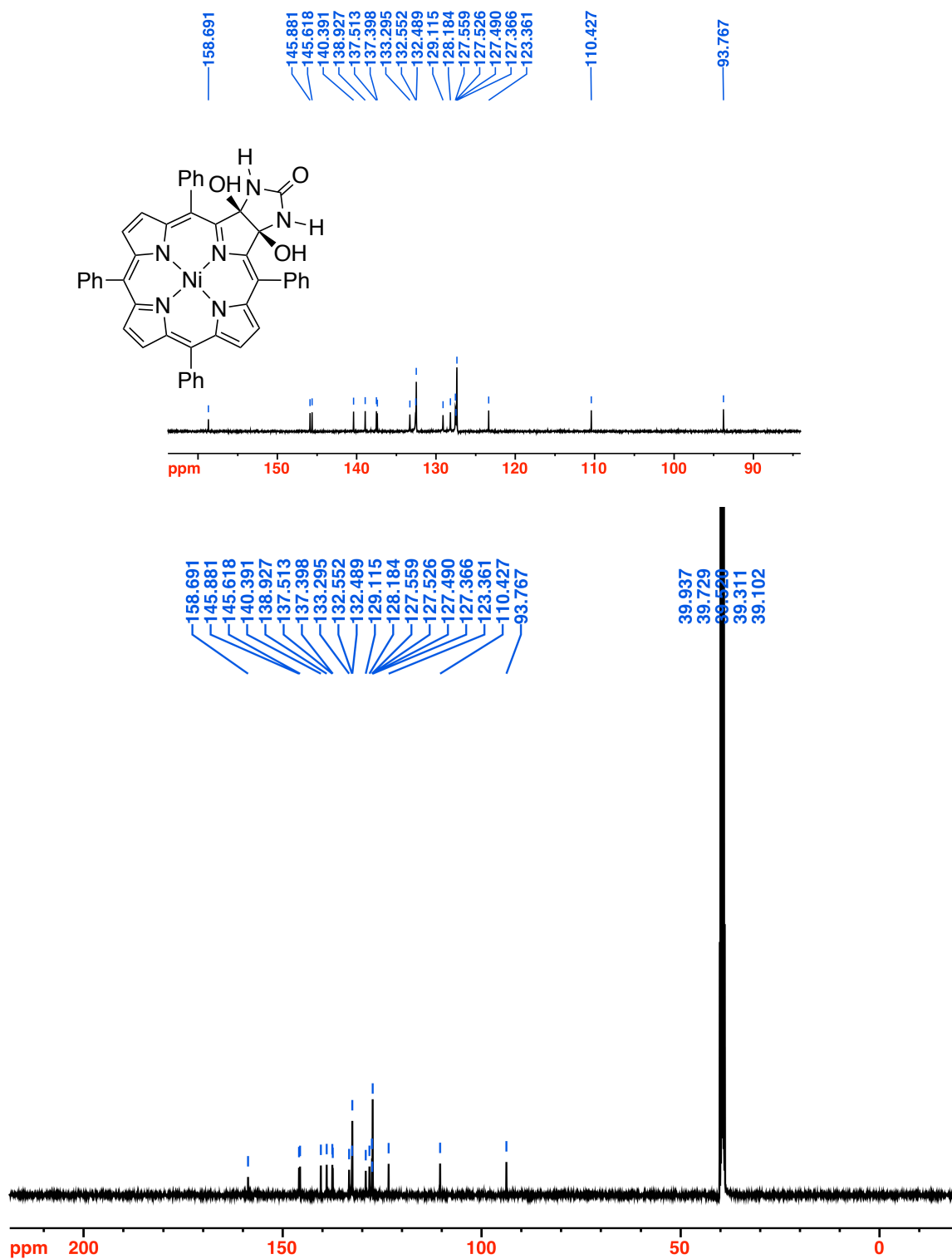


Figure 5-22. ^{13}C NMR spectrum (400 MHz, CDCl_3) of **8Ni**.

(9Ni). Prepared from **7Ni** (47.4 mg, 6.7×10^{-5} mol) in pyridine (20.0 mL) as described for **8** using *N,N'*-dimethylurea (119 mg, 1.3×10^{-3} mol, 20 equiv.) and purified by preparative TLC (silica-CH₂Cl₂/5% MeOH) to afford the blue-green dihydroxymetallochlorin **9Ni** in 68% yield (36.5 mg): *R_f* (silica-CH₂Cl₂/5% MeOH) = 0.28; ¹H NMR (500 MHz, CDCl₃): δ 8.29 (d, ³*J* = 4.9 Hz, 1H), 8.16 (s, 1H), 8.02 (d, ³*J* = 4.9 Hz, 1H), 7.83 (dd, ³*J* = 7.7, ⁴*J* = 1.6 Hz, 2H), 7.74-7.72 (m, 2H), 7.63-7.57 (m, 6H), 4.29 (s, 1H, exchangeable with D₂O), 2.17 (s, 3H) ppm; ¹³C NMR (125 MHz, CDCl₃): δ 161.4, 147.0, 142.3, 141.7, 139.5, 138.4, 137.5, 133.4, 132.79, 132.73, 129.5, 128.5, 127.98, 127.94, 127.86, 127.80, 127.1, 125.0, 110.7, 97.2, 26.4 ppm; UV-vis (CH₂Cl₂) λ_{max} (log ε) 409 (5.16), 562 (sh), 607 (4.38) nm; FT-IR (neat, diamond ATR): HR-MS (ESI⁺, 100 % CH₃CN, TOF) *m/z* calcd for C₄₇H₃₄N₆NiO₃⁺ ([M]⁺) 788.2045, found 788.2062.

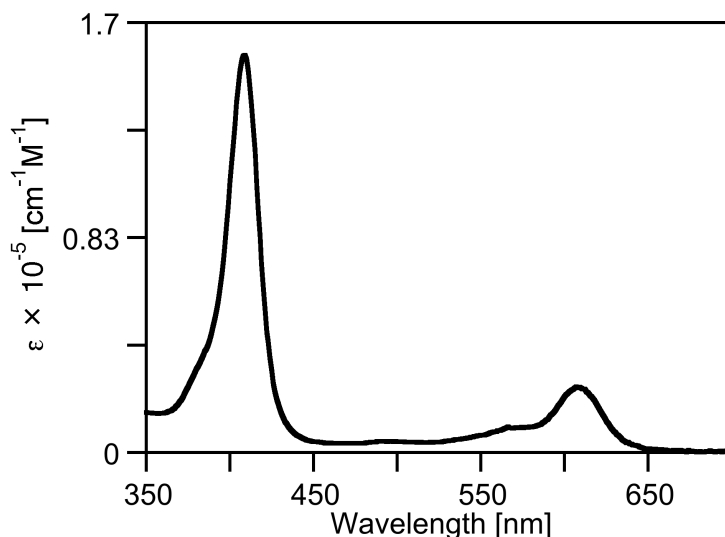


Figure 5-23. UV-vis spectrum (CH₂Cl₂) of **9Ni**.

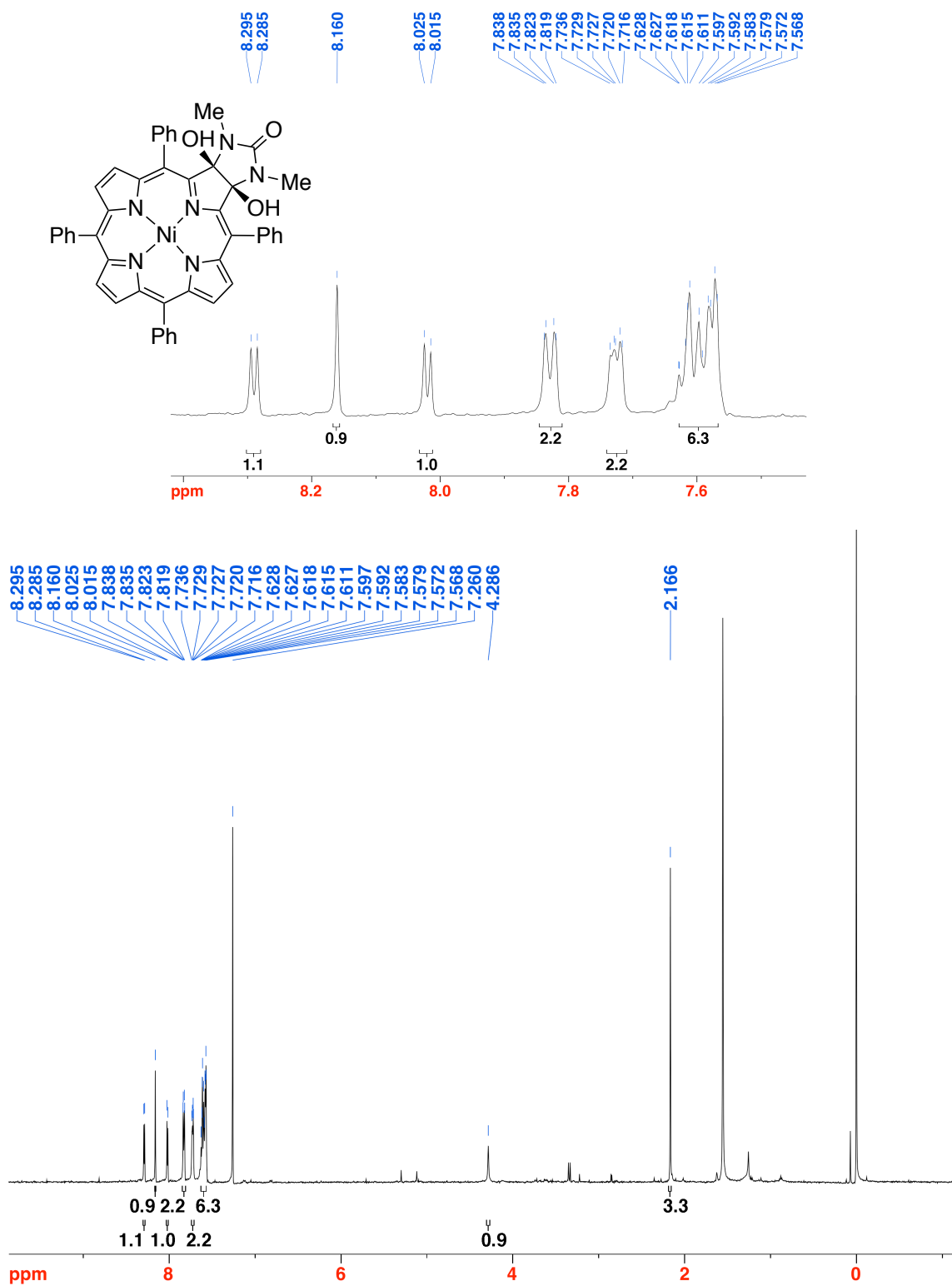


Figure 5-24. ^1H NMR spectrum (400 MHz, CDCl_3) of **9Ni**.

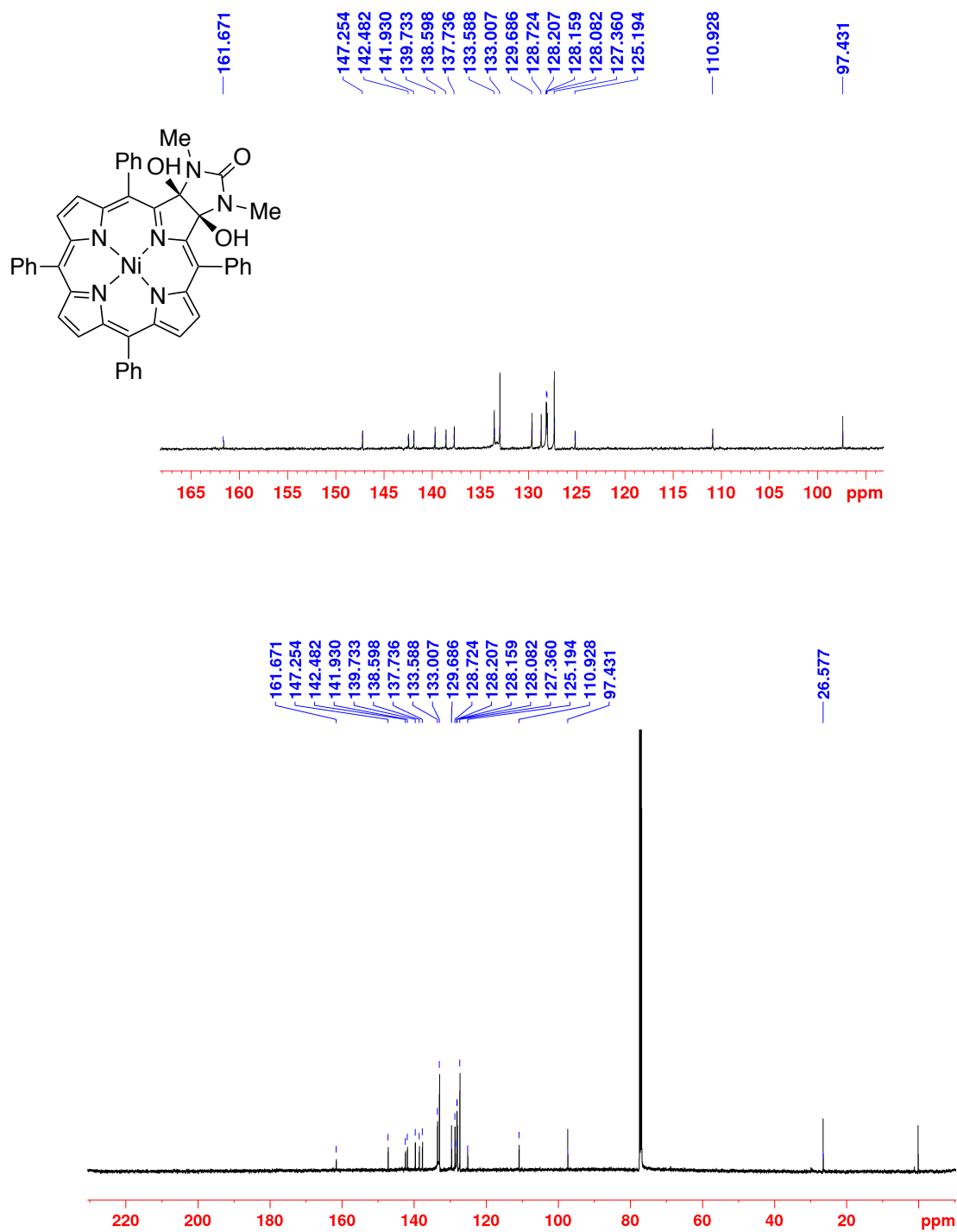
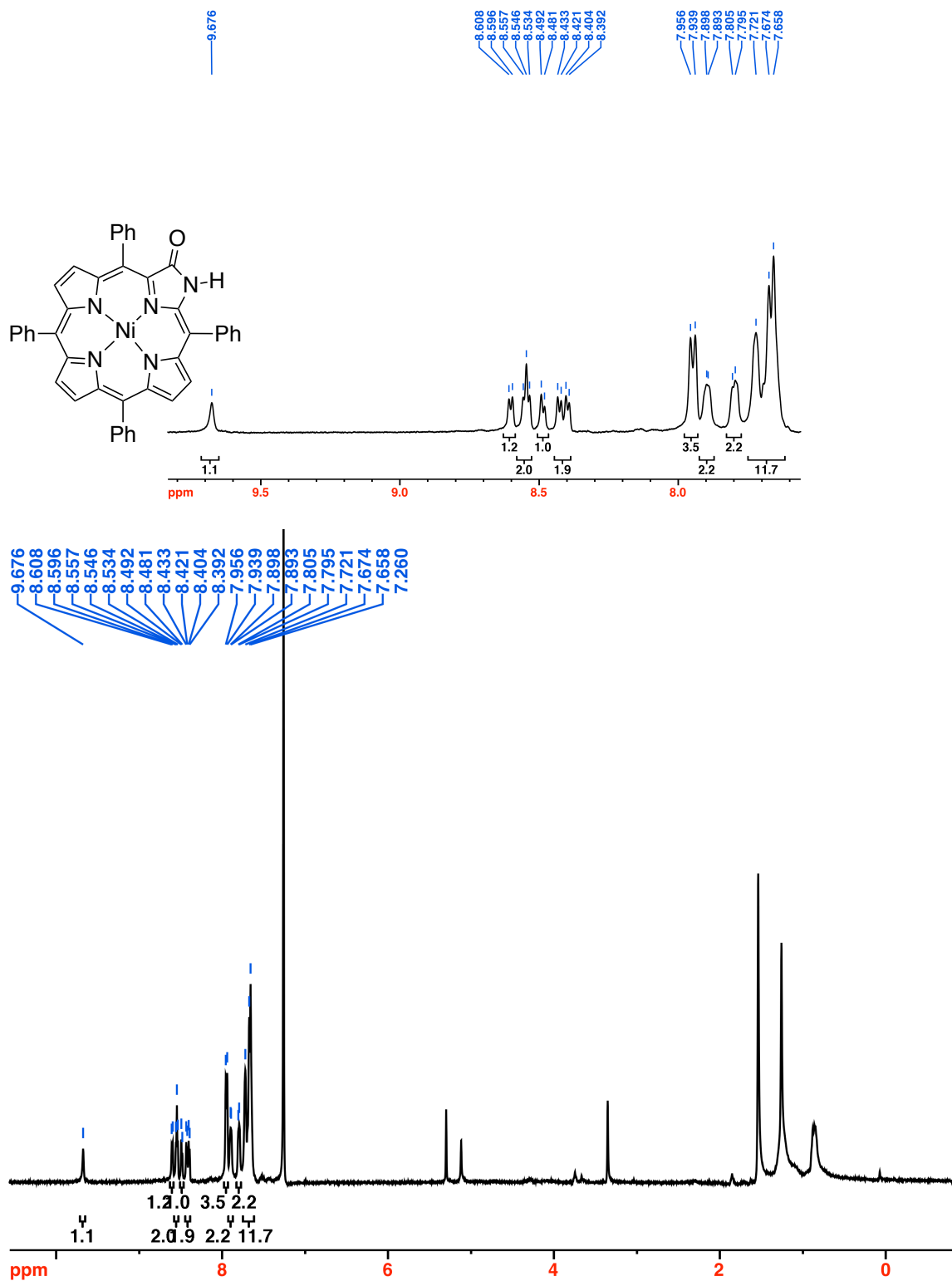


Figure 5-25. ^{13}C NMR spectrum (500 MHz, CDCl_3) of **9Ni**.

(10Ni.) Prepared as described for **10** on using **8Ni** (19.5 mg, 2.6×10^{-5} mol), Pb(OAc)₄ (12.6 mg, 2.8×10^{-5} mol, 1.1 equiv.) and dry THF (6.5 mL) to afford the red **10Ni** in 45% yield (9 mg); ¹H NMR (400 MHz, CDCl₃): δ 9.68 (s, 1H, exchangeable with D₂O), 8.60 (d, ³J = 5.0 Hz, 1H), 8.55 (two overlapping doublets, ³J = 4.5 Hz, 2H), 8.49 (d, ³J = 4.6 Hz, 1H), 8.41 (dd, ³J = 11.7, 4.8 Hz, 2H), 7.95 (d, ³J = 6.8 Hz, 3H), 7.92-7.88 (m, 2H), 7.80 (d, ³J = 4.1 Hz, 2H), 7.75-7.6 (m, 12H) ppm; UV-vis (CH₂Cl₂) λ_{max} (rel I.) 417 (1.0), 545 (sh), 589 (0.14) nm; ν_{C=O} = 1712.5; HR-MS (ESI⁺, 100% CH₃CN, TOF) *m/z* calcd for C₄₃H₂₈N₅NiO ([M·H]⁺), 688.1642 found 688.1573.

Figure 5-26. ¹H NMR (400 MHz, CDCl₃) of 10Ni.

(11Ni). Prepared according to the procedure for **11**, starting from **(9Ni)** (36.5 mg, 4.6×10^{-5} mol) in dry THF (12.0 mL) with Pb(OAc)₄ (41 mg, 9.2×10^{-6} mol, 2 equiv.) and purified by column chromatography (silica-CH₂Cl₂) to afford the green **11Ni** in 71% yield (26.0 mg): *R_f* (silica-CH₂Cl₂) = 0.52; ¹H-NMR (400 MHz; CDCl₃): δ 8.23 (d, ³*J* = 4.8 Hz, 1H), 8.06 (s, 1H), 7.88 (d, ³*J* = 4.8 Hz, 1H), 7.84 (br s, 1H), 7.65-7.60 (br m, 3H), 7.48 (br s, 3H), 3.21 (s, 3H) ppm; ¹³C NMR (100 MHz; CDCl₃): δ 171.7, 155.2, 148.3, 144.5, 140.6, 138.9, 137.8, 137.2, 134.4, 132.96, 132.92, 131.0, 130.1, 128.4, 127.5, 118.4, 33.1; UV-vis (CH₂Cl₂) λ_{max} (log ε) 441 (4.45), 661 (3.72) nm; HR-MS (ESI⁺, 100% CH₃CN, TOF) *m/z* calcd for C₄₇H₃₃N₆NiO₃ ([M·H]⁺), 787.1968 found 787.1979.

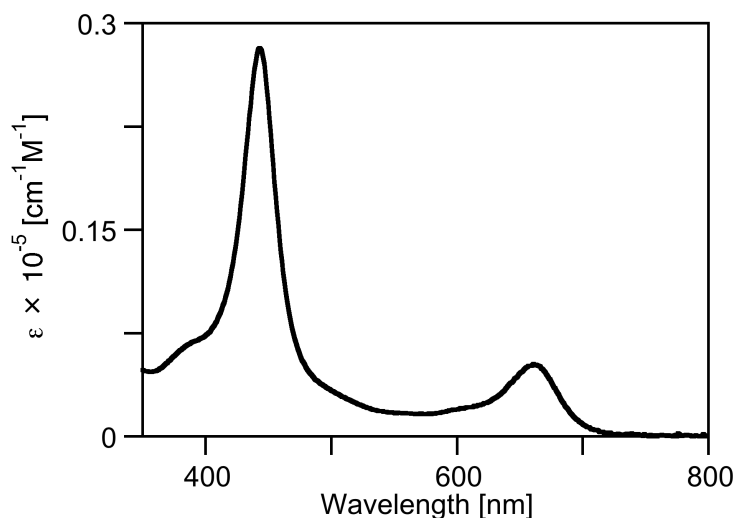


Figure 5-27. UV-vis spectrum (CH₂Cl₂) of **11Ni**.

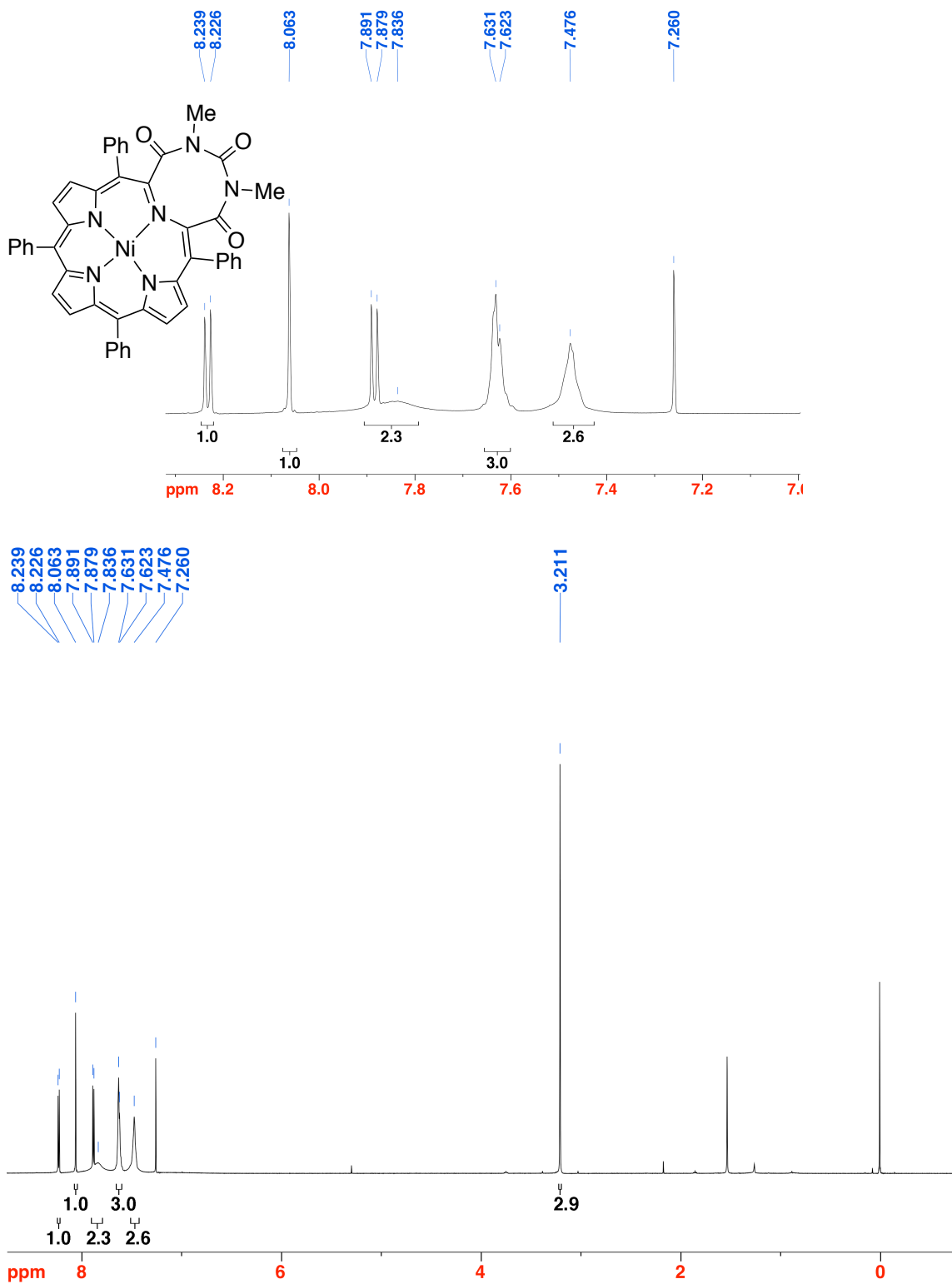


Figure 5-28. ^1H NMR (400 MHz, CDCl_3) of **11Ni**.

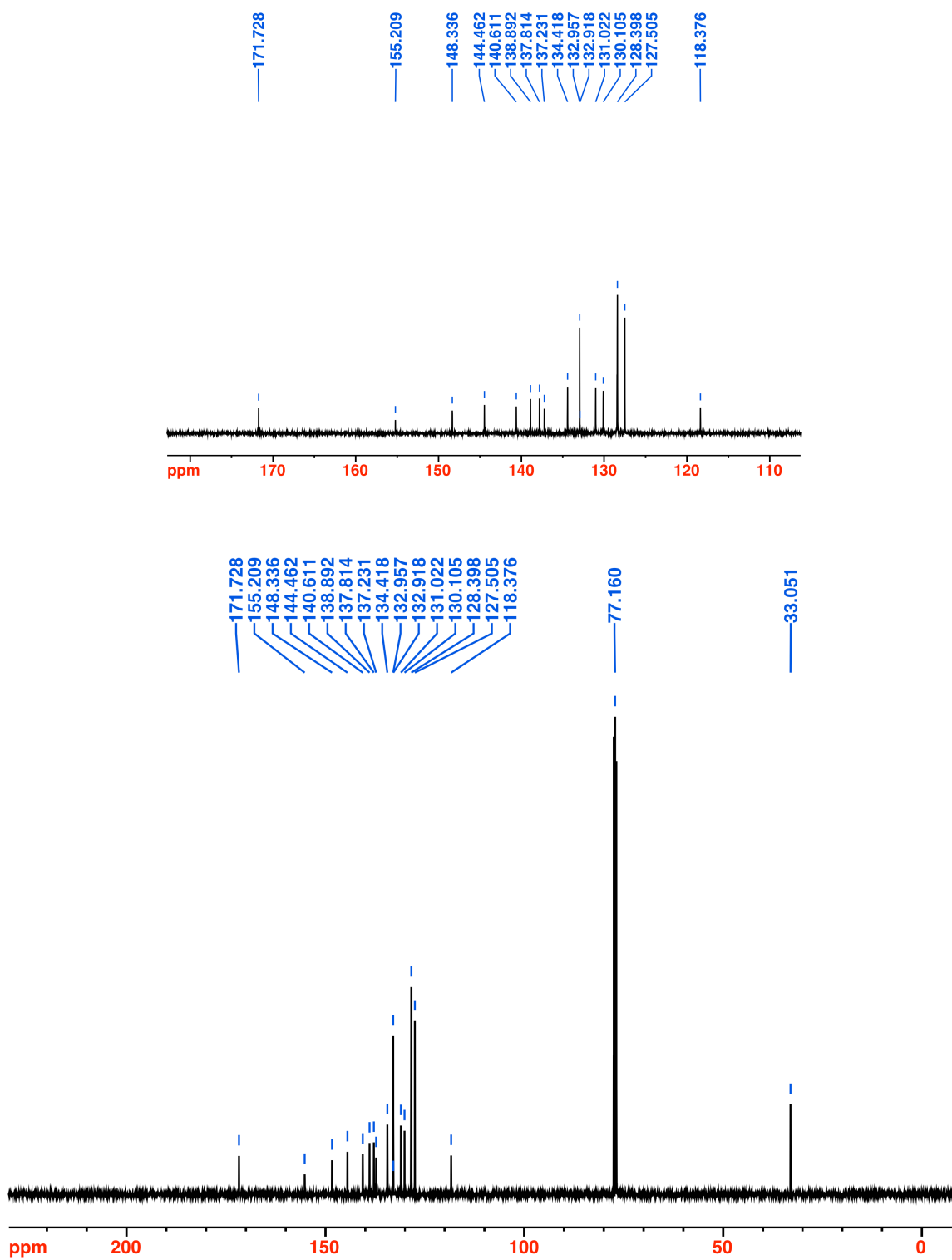


Figure 5-29. ¹³C NMR spectrum (100 MHz, CDCl₃) of **11Ni**.



meso-Tetraphenyl-*N,N'*-dimethyl-2-thioxo-imidazole-annulated dihydroxychlorin 13.

Prepared from **7** (92.0 mg, 1.42×10^{-4} mol) in pyridine (32.0 mL) as described for **8** using *N,N'*-dimethylthiourea (297 mg, 2.9×10^{-3} mol) and purified by column chromatography (silica-CH₂Cl₂/5% MeOH) to afford the dark red solid **13** in 89% yield (95.4 mg): *R_f* (silica-CH₂Cl₂/5% MeOH) = 0.65; ¹H NMR (400 MHz, CDCl₃): δ 8.59 (d, ³*J* = 5.0 Hz, 1H), 8.47 (s, 1H), 8.18 (d, ³*J* = 7.3 Hz, 1H), 8.08 (t, ³*J* = 7.6 Hz, 4H), 7.80-7.68 (m, 6H), 4.58 (s, 1H, exchangeable with D₂O), 2.58 (s, 3H), -1.75 (s, 1H, exchangeable with D₂O) ppm; ¹³C NMR (125 MHz, CDCl₃): δ 185.7, 153.8, 152.6, 141.40, 141.35, 139.5, 136.1, 135.3, 134.4, 134.1, 133.1, 132.7, 129.0, 128.5, 128.21, 128.15, 128.11, 127.97, 127.94, 127.5, 127.2, 126.98, 126.86, 125.4, 124.1, 112.8, 100.3, 30.5 ppm; UV-vis (CH₂Cl₂) λ_{max} (log ε) 400 (5.31), 510 (4.16), 539 (4.21), 585, (3.91), 638 (4.38) nm; HR-MS (ESI⁺, 100% CH₃CN, TOF) *m/z* calcd for C₄₇H₃₇N₆O₂S ([M·H]⁺), 749.2699 found 749.2684.

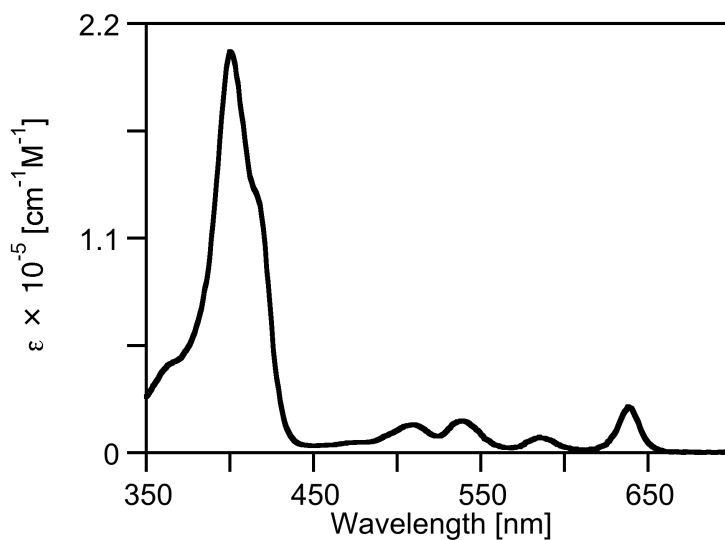
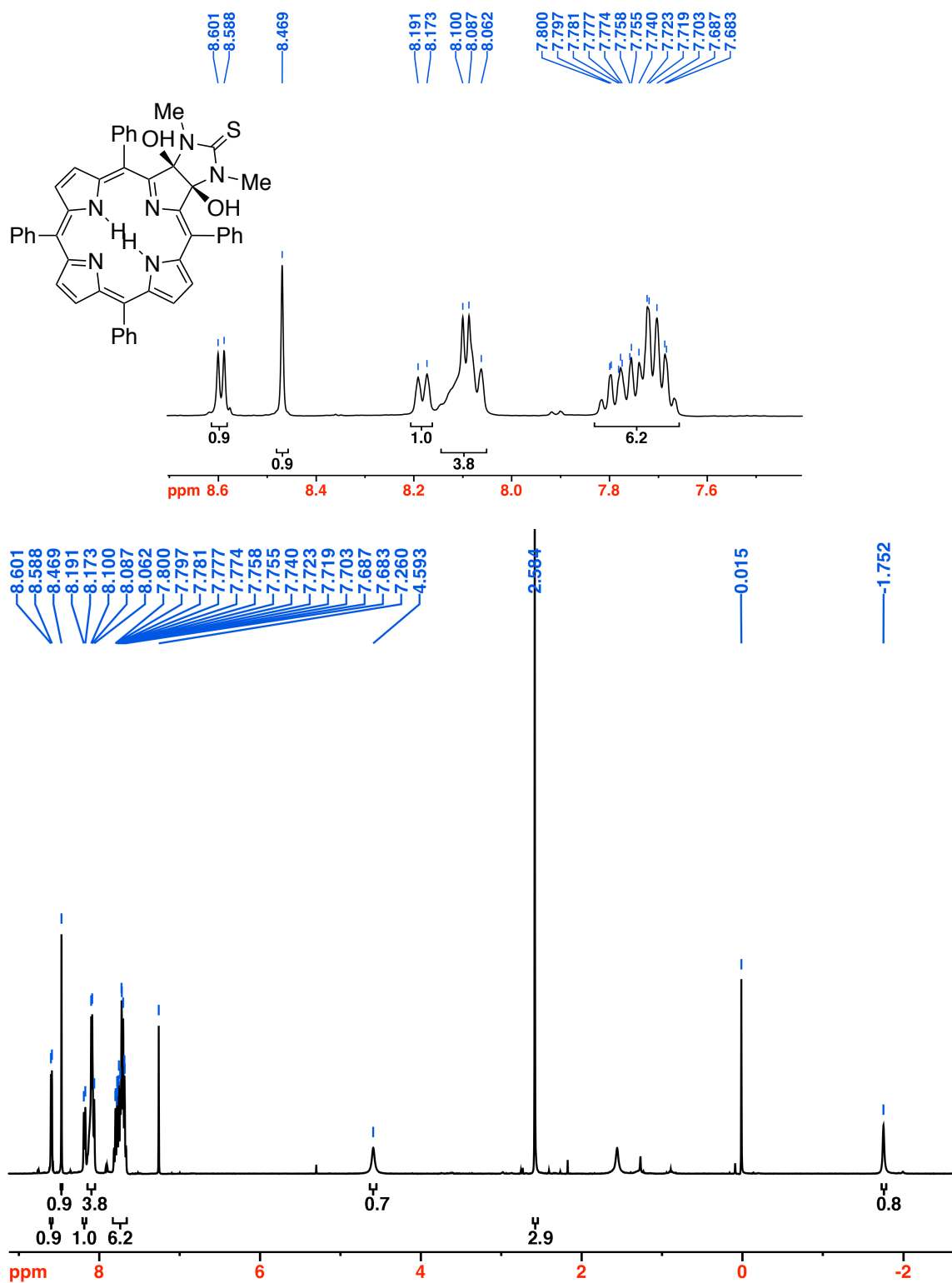


Figure 5-31. UV-vis spectrum (CH₂Cl₂) of **13**.

Figure 5-32. ^1H NMR spectrum (400 MHz, CDCl_3) of **13**.

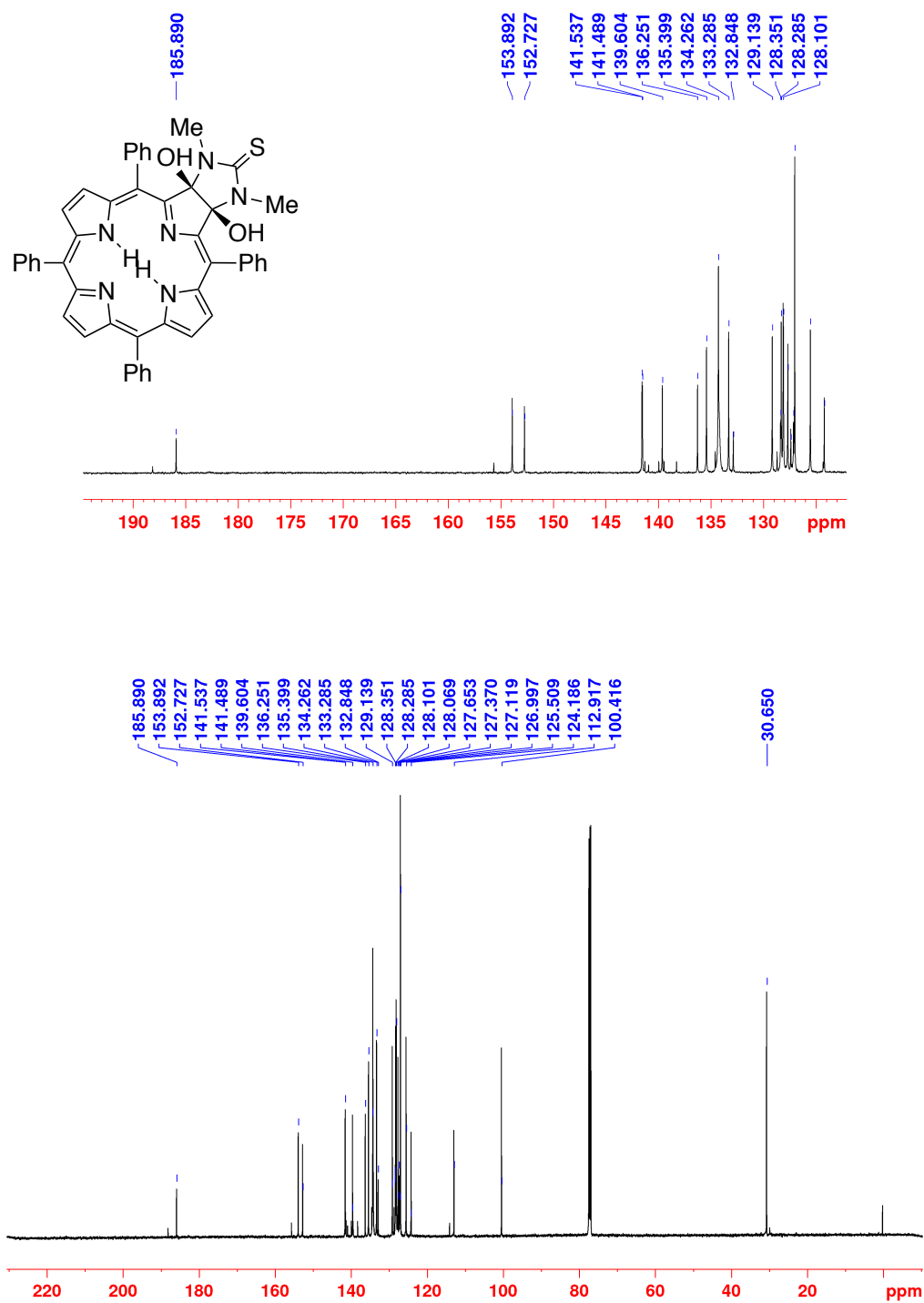


Figure 5-33. ¹³C NMR spectrum (125 MHz, CDCl₃) of 13.

Oxidative cleavage of 13. Prepared according to the procedure for **10**, starting from (**13**) (26.4 mg, 3.5×10^{-5} mol) in dry THF (10.0 mL) with $\text{Pb}(\text{OAc})_4$ (49.6 mg, 1.1×10^{-4} mol, 3.1 equiv.) and purified by preparative TLC (silica- CH_2Cl_2) to afford the known diketone **7** (2.0 mg, 9% yield) and the green **14** in 67 % yield (17.6 mg): R_f (silica- CH_2Cl_2) = 0.59; ^1H NMR (400 MHz, CD_2Cl_2): δ 8.56 (s, 1H), 8.50 (d, $^3J = 5.0$ Hz, 1H), 8.34 (s, 1H), 8.18 (d, $^3J = 5.0$ Hz, 1H), 8.03 (s, 1H), 7.75-7.68 (m, 4H), 7.59 (t, $^3J = 7.5$ Hz, 1H), 7.35 (s, 1H), 6.85 (s, 1H), 2.69 (s, 3H), -0.22 (s, 1H, exchangeable with D_2O) ppm; ^{13}C NMR (125 MHz, CD_2Cl_2): δ 186.9, 171.8, 155.4, 148.3, 140.81, 140.78, 140.68, 140.03, 140.01, 137.4, 134.5, 134.20, 134.11, 134.06, 134.01, 133.90, 133.86, 132.43, 132.39, 129.3, 128.61, 128.55, 128.51, 128.3, 127.8, 127.53, 127.41, 127.37, 125.4, 115.2, 109.80, 109.69, 109.65, 109.56, 109.51, 109.48, 109.43, 109.37, 109.31, 109.22, 109.16, 109.02, 108.96, 108.91, 108.88, 108.86, 35.6 ppm; UV-vis (CH_2Cl_2) λ_{max} (log ϵ) 360 (4.4), 432 (5.02), 536 (3.77), 572 (3.75), 607 (3.82), 668 (3.85) nm; HR-MS (ESI^+ , 100% CH_3CN , TOF) m/z calcd for $\text{C}_{47}\text{H}_{35}\text{N}_6\text{O}_2\text{S}$ ($[\text{M}\cdot\text{H}]^+$), 747.2542 found 747.2558.

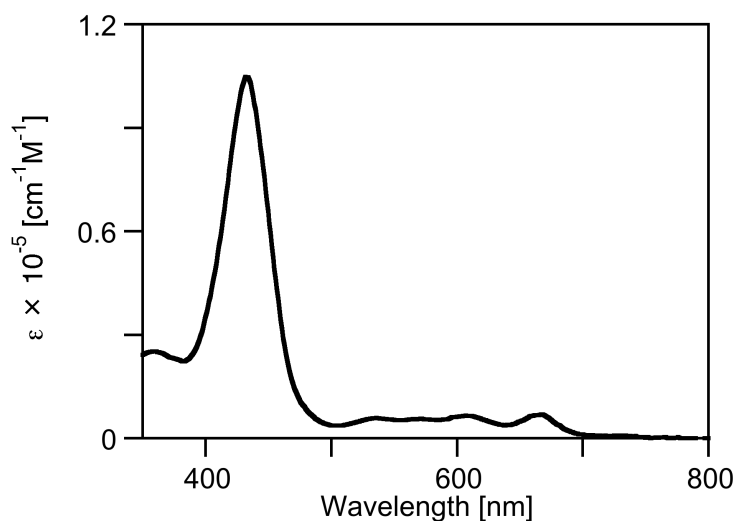


Figure 5-34. UV-vis spectrum (CH_2Cl_2) of **14**.

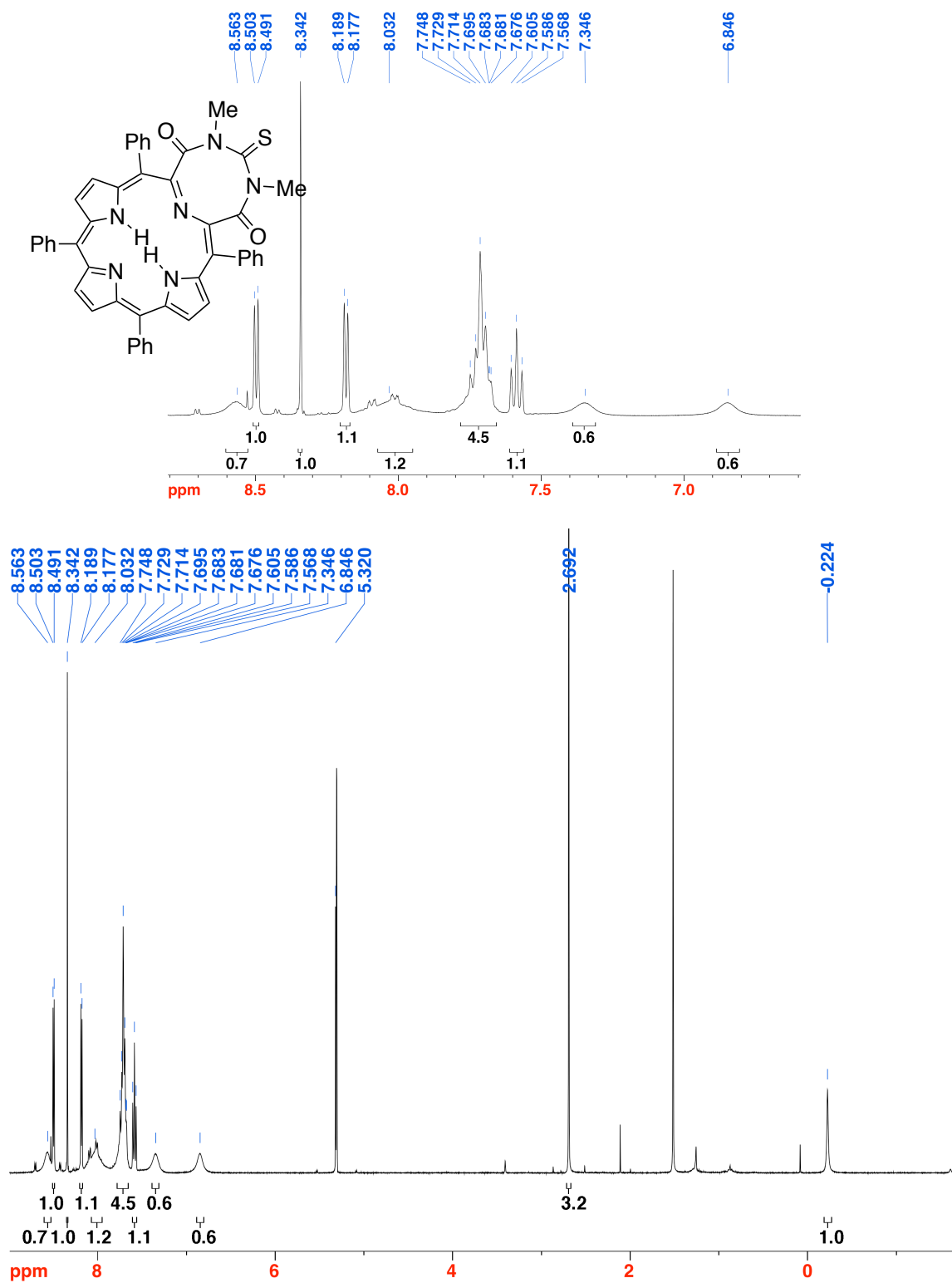


Figure 5-35. ^1H NMR spectrum (400 MHz, CDCl_3) of **14**.

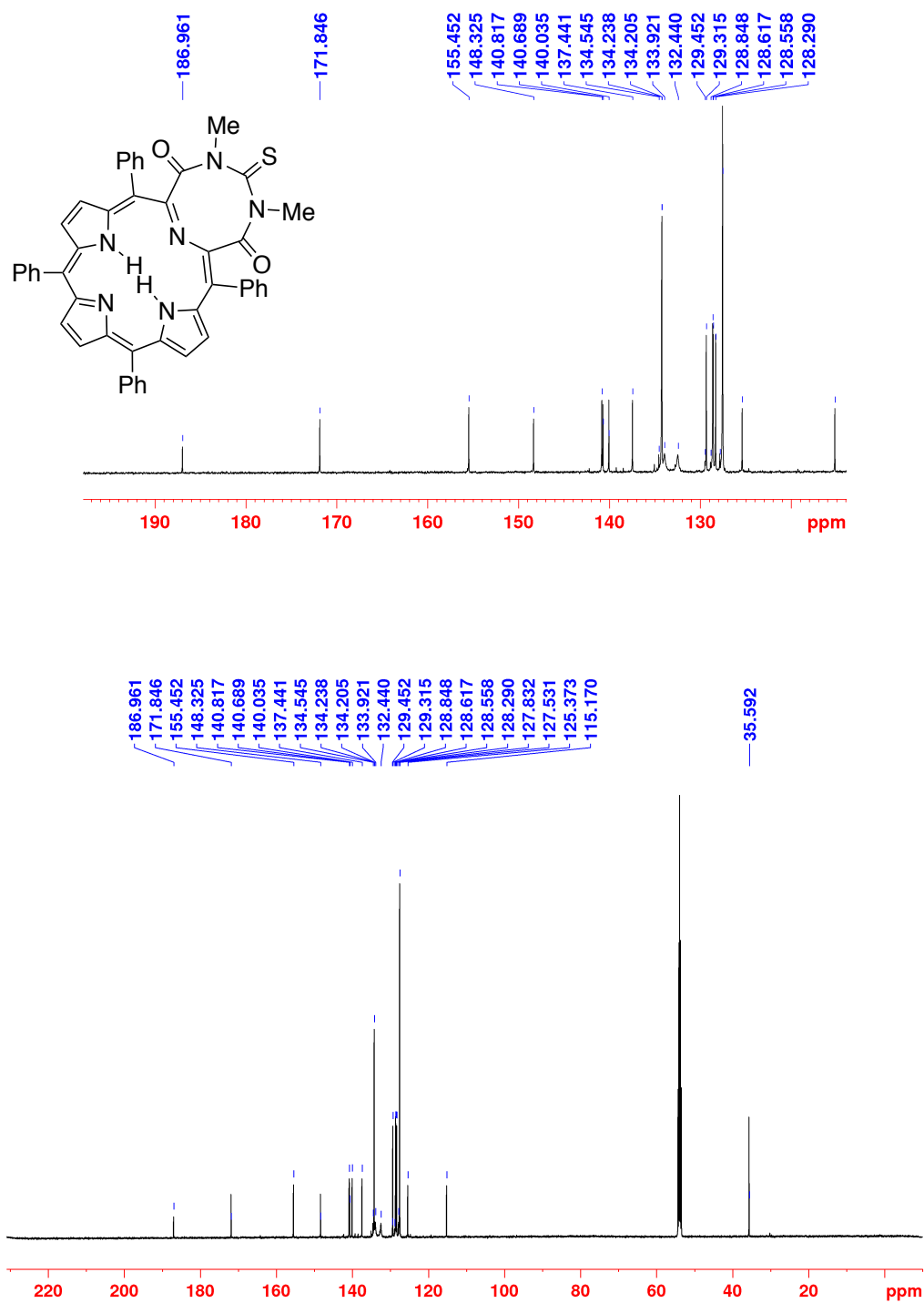


Figure 5-36. ^{13}C NMR spectrum (125 MHz, CDCl_3) of **14**.

Semicarbazide adduct (18). Prepared from **7** in 51% yield (16.5 mg) on a 4.65×10^{-5} mol (30.0 mg) scale using 103.8 mg (9.31×10^{-4} mol, 20 equiv.) of semicarbazide·HCl according to the general procedure except at r.t. and purified by column chromatography: R_f (silica-CH₂Cl₂/3% MeOH) = 0.44; ¹H NMR (400 MHz, CDCl₃): δ 13.08 (s, 1H, exchangeable with D₂O), 8.78 (two overlapping doublets, ³*J* = 5.2 Hz, 2H), 8.62 (two overlapping doublets, ³*J* = 4.9 Hz, 2H), 8.58 (d, ³*J* = 4.7 Hz, 1H), 8.54 (d, ³*J* = 5.7 Hz, 1H), 8.15 (dd, ³*J* = 5.9, ⁴*J* = 1.8 Hz, 4H), 8.07-8.05 (m, 2H), 7.96-7.94 (m, 2H), 7.82-7.70 (m, 12H), 5.27 (s, exchangeable with D₂O), 4.50 (s, exchangeable with D₂O), -2.24 (s, 1H exchangeable with D₂O), -2.34 (s, 1H, exchangeable with D₂O) ppm; ¹³C NMR (100 MHz, CDCl₃): δ 187.7, 155.7, 155.4, 154.4, 146.5, 142.4, 141.62, 141.48, 141.34, 140.4, 140.2, 138.9, 138.1, 137.6, 137.4, 134.4, 134.23, 134.18, 133.8, 133.4, 132.4, 128.7, 128.07, 127.99, 127.92, 127.79, 127.55, 127.49, 127.29, 127.22, 126.88, 126.84, 123.9, 122.0, 115.5, 112.2 ppm; UV-vis (CH₂Cl₂) λ_{\max} (log ϵ) 410 (5.17), 465 (sh), 613 (sh), 666, (3.6) nm; FT-IR (neat, diamond ATR) $\nu_{\text{C=O}}$ = 1667.1; HR-MS (ESI⁺, 100% CH₃CN, TOF) *m/z* calcd for C₄₅H₃₂N₇O₂ ([M·H]⁺), 702.2617 found 702.2618.

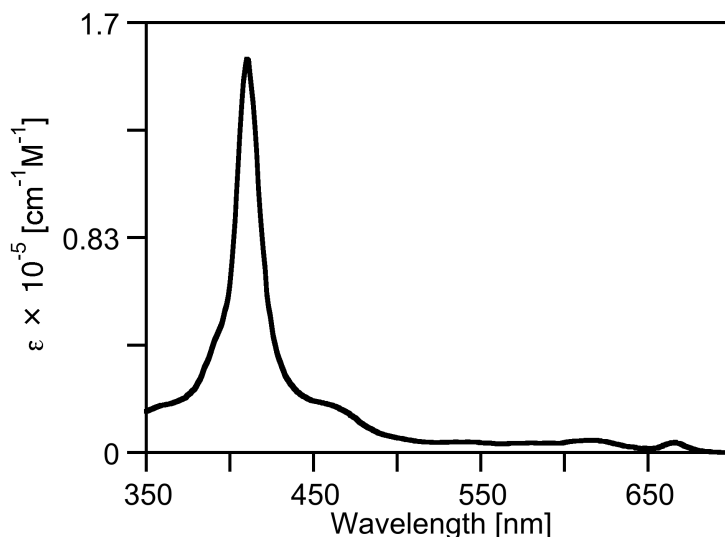
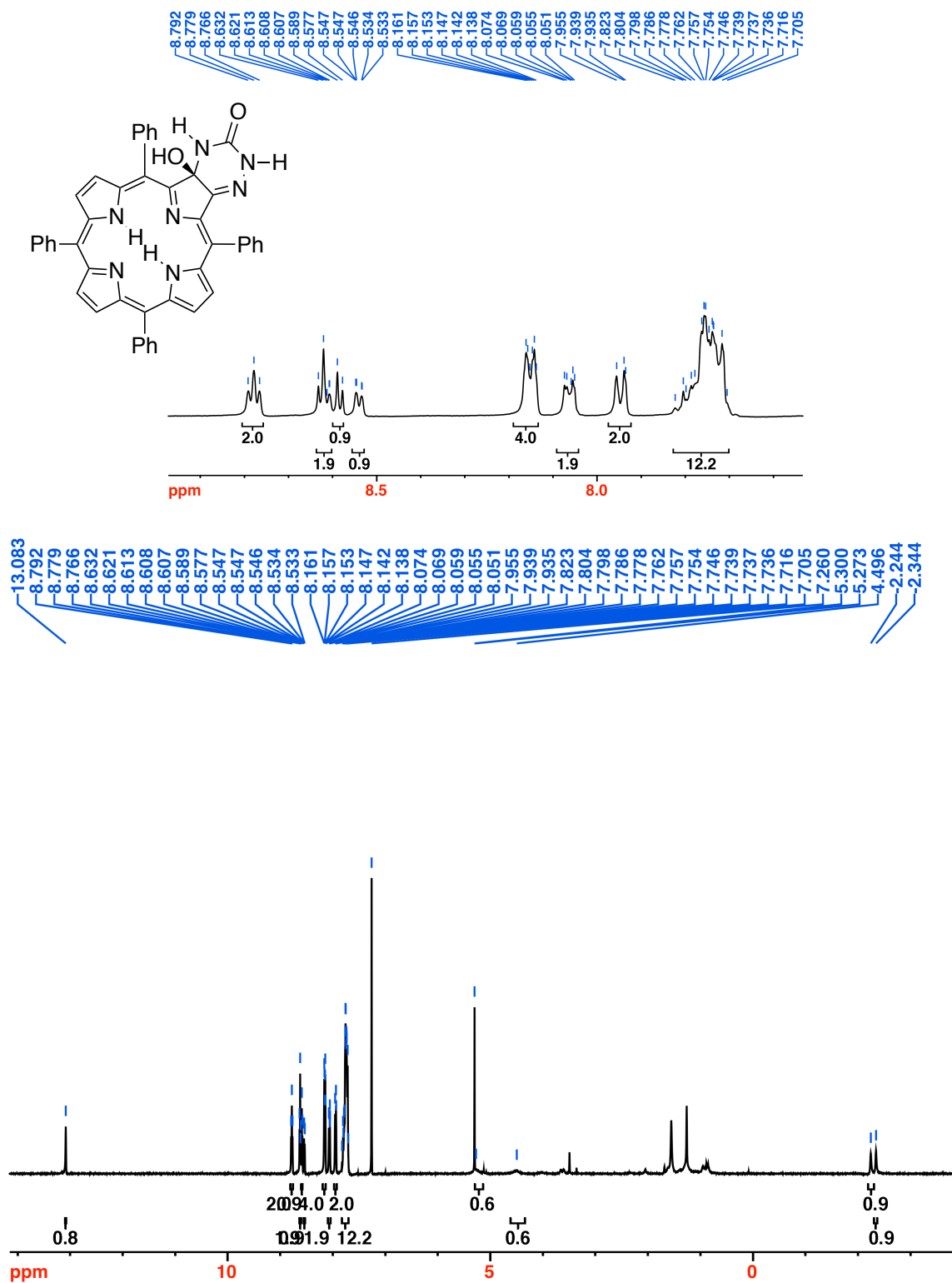
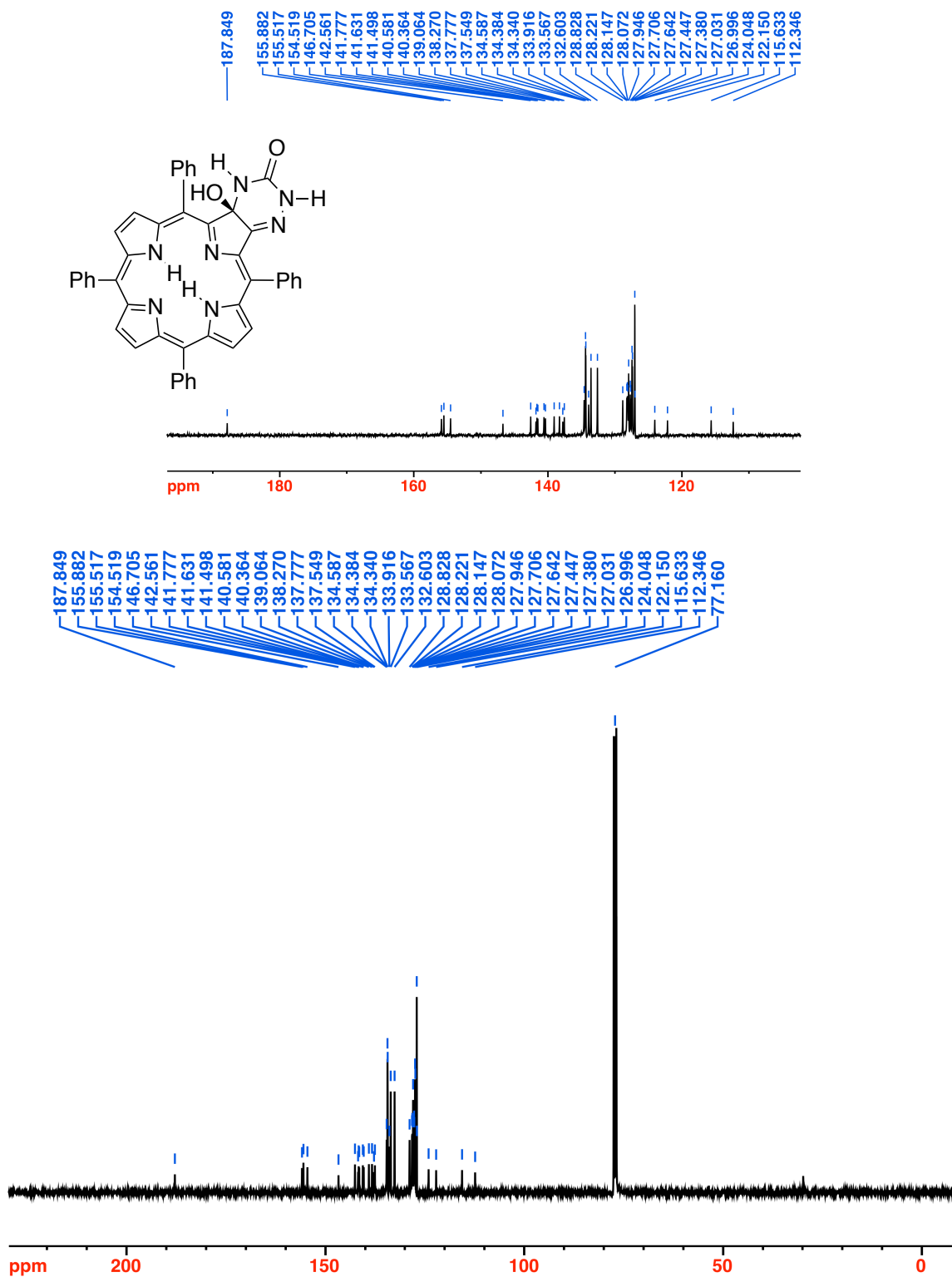


Figure 5-37. UV-vis spectrum (CH₂Cl₂) of **18**.

Figure 5-38. ^1H NMR spectrum (400 MHz, CDCl_3) of 18.

Figure 5-39. ^1H NMR spectrum (100 MHz, CDCl_3) of 18.

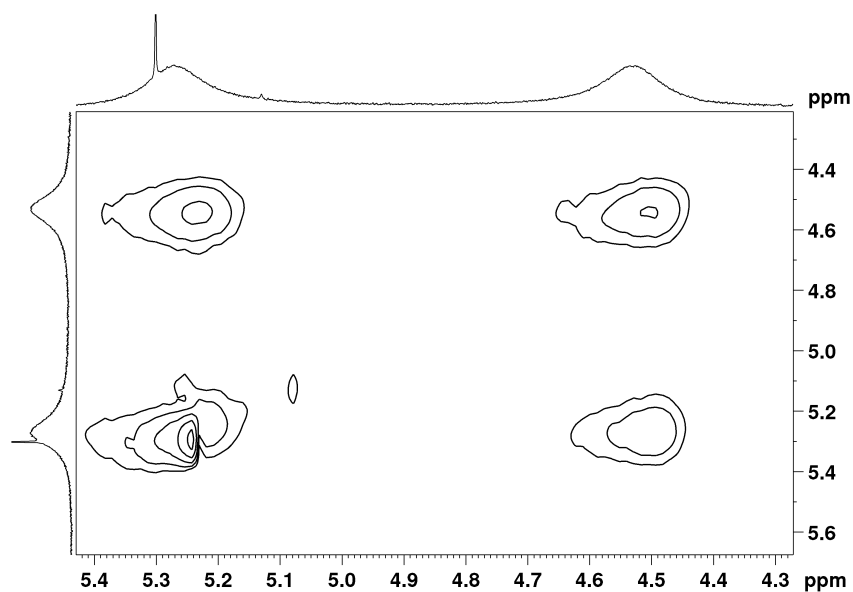


Figure 5-40. Partial ^1H - ^1H -NOESY spectrum (CDCl_3) of **18**.

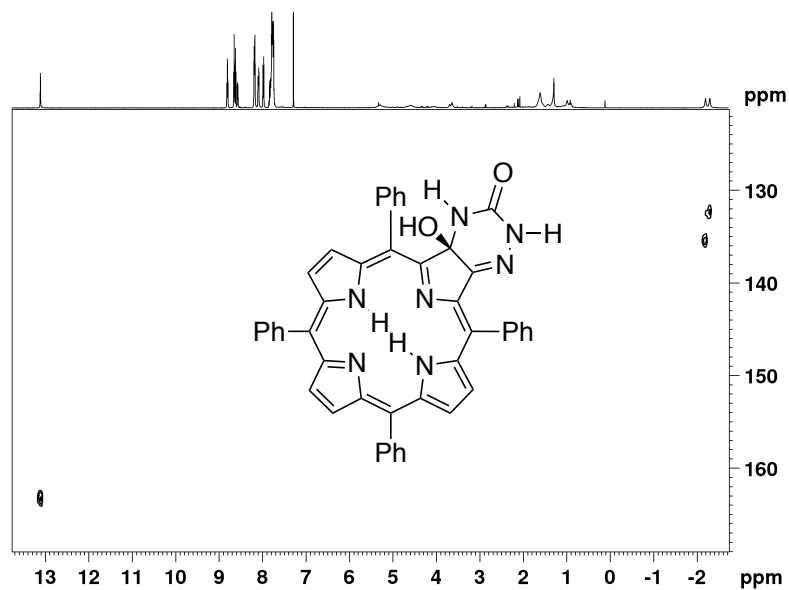


Figure 5-41. ^{15}N - ^1H HSQC spectrum (CDCl_3) of **18**.

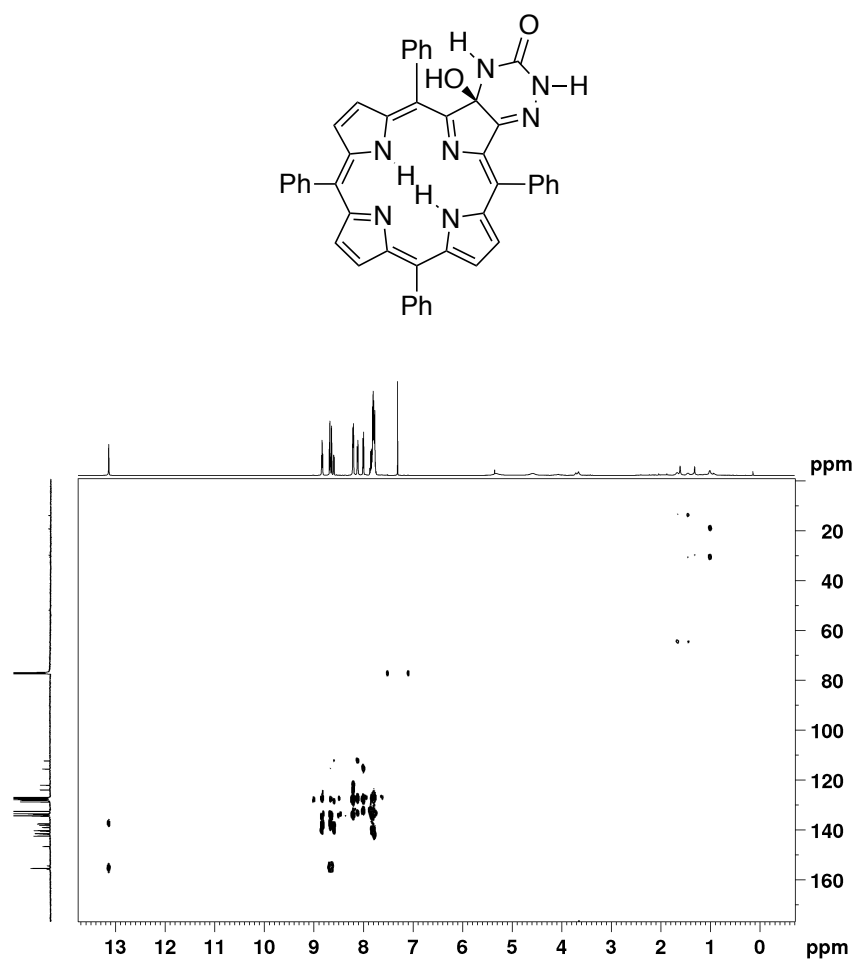


Figure 5-42. HMBC spectrum (CDCl₃) of **18**.

Thiosemicarbazide-fused adduct (19). Prepared from **7** in 45% (5.0 mg) yield on a 1.7×10^{-5} mol (10.0 mg) scale using 28.0 mg (3.1×10^{-4} mol, 20 equiv.) of thiosemicarbazide according to the general procedure for **8** except at r.t. and purified by column chromatography: R_f (silica- CH_2Cl_2) = 0.31; ^1H NMR (400 MHz, CDCl_3): δ 13.75 (s, 1H, exchangeable with D_2O), 8.80 (t, $^3J = 5.3$ Hz, 2H), 8.62 (m, 3H), 8.55 (d, $^3J = 4.9$ Hz, 1H), 8.17 (dd, $^3J = 6.2$, $^4J = 1.4$ Hz, 4H), 8.07 (dd, $^3J = 7.4$, $^4J = 1.6$ Hz, 2H), 7.97-7.95 (m, 2H), 7.84-7.72 (m, 12H), 6.39 (s, 1H, exchangeable with D_2O), 6.09 (s, 1H, exchangeable with D_2O), -2.22 (s, 1H, exchangeable with D_2O), -2.30 (s, 1H, exchangeable with D_2O) ppm; ^{13}C NMR (100 MHz, CDCl_3): δ 187.4, 180.9, 155.8, 154.5, 145.9, 142.4, 141.54, 141.39, 141.27, 140.3, 140.0, 139.0, 138.2, 137.5, 137.1, 134.5, 134.22, 134.18, 133.9, 133.3, 132.5, 128.7, 128.19, 128.10, 128.03, 128.00, 127.90, 127.80, 127.70, 127.49, 127.39, 127.33, 126.89, 126.76, 124.0, 122.3, 115.5, 112.2, ppm; UV-vis (CH_2Cl_2) λ_{max} (log ϵ) 414 (5.07), 480 (sh), 614 (3.59), 671 (3.59) nm.

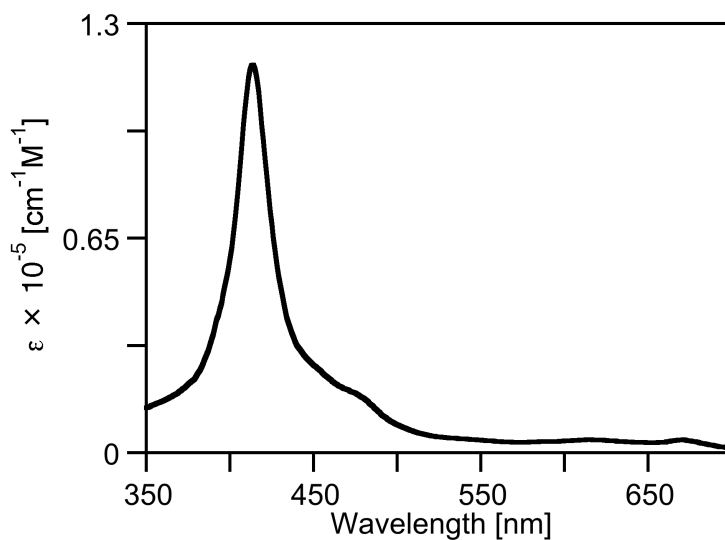
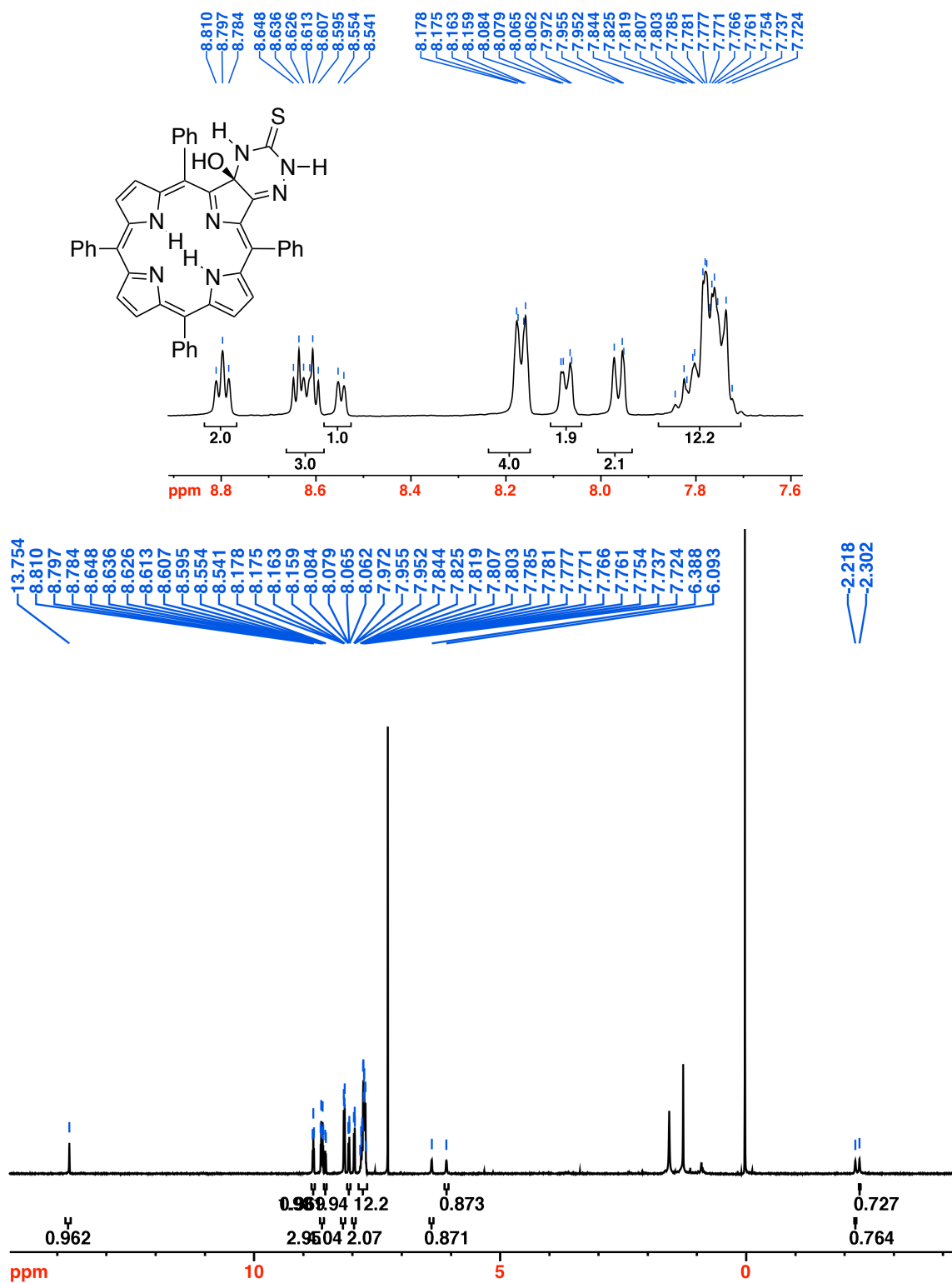


Figure 5-43. UV-vis spectrum (CH_2Cl_2) of **19**.

Figure 5-44. ^1H NMR spectrum (400 MHz, CDCl_3) of **19**.

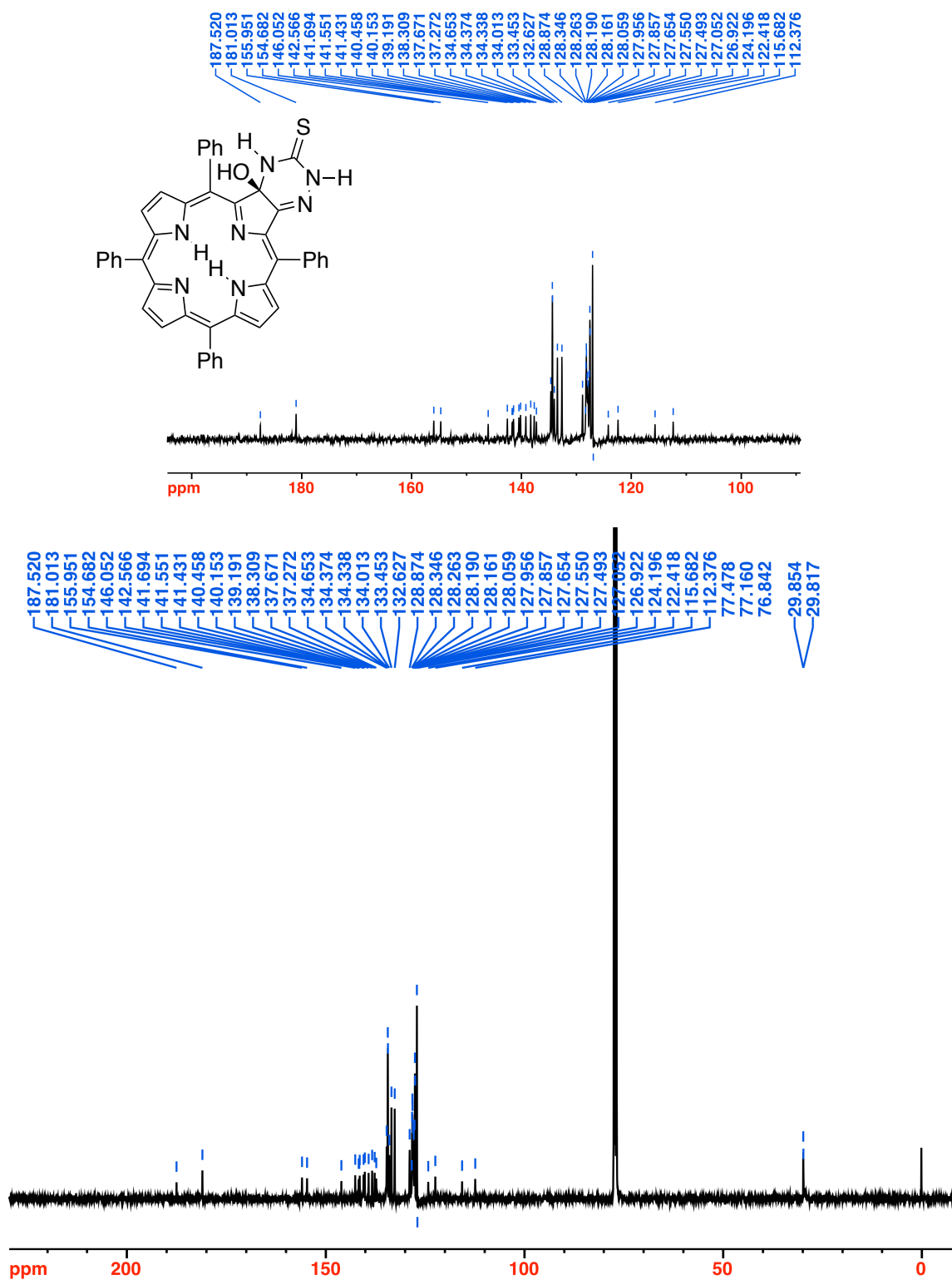


Figure 5-45. ¹³C NMR spectrum (100 MHz, CDCl₃) of 19.

Malonamide adduct 20. Prepared from **7** (71.0 mg, 1.1×10^{-4} mol) in pyridine (25 mL) as described for **8** using malonamide (225 mg, 2.2×10^{-3} mol) and purified by column chromatography (silica-CH₂Cl₂/5% MeOH) to afford the magenta solid **20** in 96.1% yield (79 mg): R_f (silica-CH₂Cl₂/5% MeOH) = 0.38; ¹H NMR (300 MHz, CDCl₃): δ 8.97 (s, 1H, exchangeable with D₂O), 8.65 (two overlapping doublets, ³ J = 5.8 Hz, 2H), 8.50 (s, 2H), 8.32-8.22 (m, 3H), 8.17 (d, ³ J = 4.8 Hz, 1H), 8.11 (d, ³ J = 5.8 Hz, 4H), 7.84-7.60 (m, 15H), 6.77 (s, 1H, exchangeable with D₂O), 6.36 (s, 1H, exchangeable with D₂O), 5.75 (s, 1H, exchangeable with D₂O), 5.40 (s, 1H, exchangeable with D₂O), -2.15 (s, 2H, exchangeable with D₂O) ppm; ¹³C NMR (100 MHz, DMSO-d₆): δ 171.0, 170.3, 159.5, 157.7, 152.89, 152.81, 141.37, 141.25, 141.0, 140.5, 139.8, 135.52, 135.43, 135.25, 134.6, 134.12, 134.04, 133.30, 133.24, 133.18, 128.57, 128.48, 128.38, 128.24, 127.66, 127.52, 127.50, 127.3, 127.02, 126.97, 125.9, 123.1, 114.6, 113.2, 95.5, 86.4, 55.4, 55.0 ppm; UV-vis (CH₂Cl₂) λ_{\max} (log ϵ) 408 (5.01), 516 (3.90), 542 (3.90), 542 (3.90), 590 (3.56), 642 (4.13) nm; HR-MS (ESI⁺, 100% CH₃CN, TOF) m/z calcd for C₄₇H₃₅N₆O₄ ([M·H]⁺), 747.2720 found 747.2706.

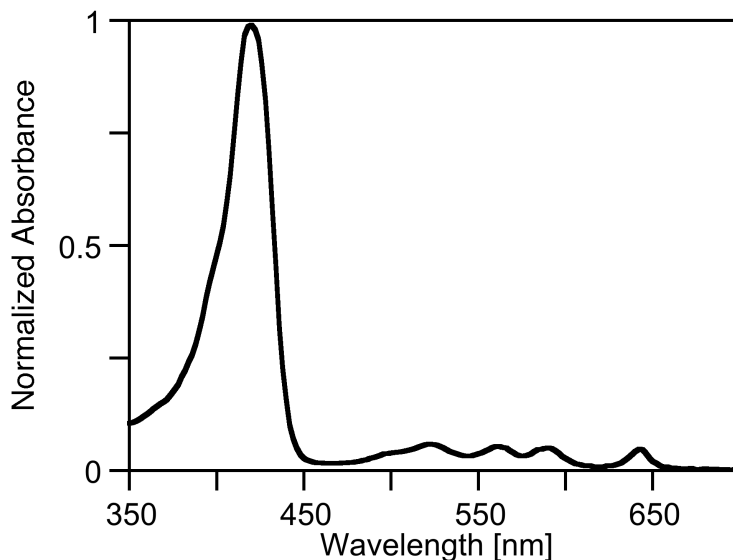
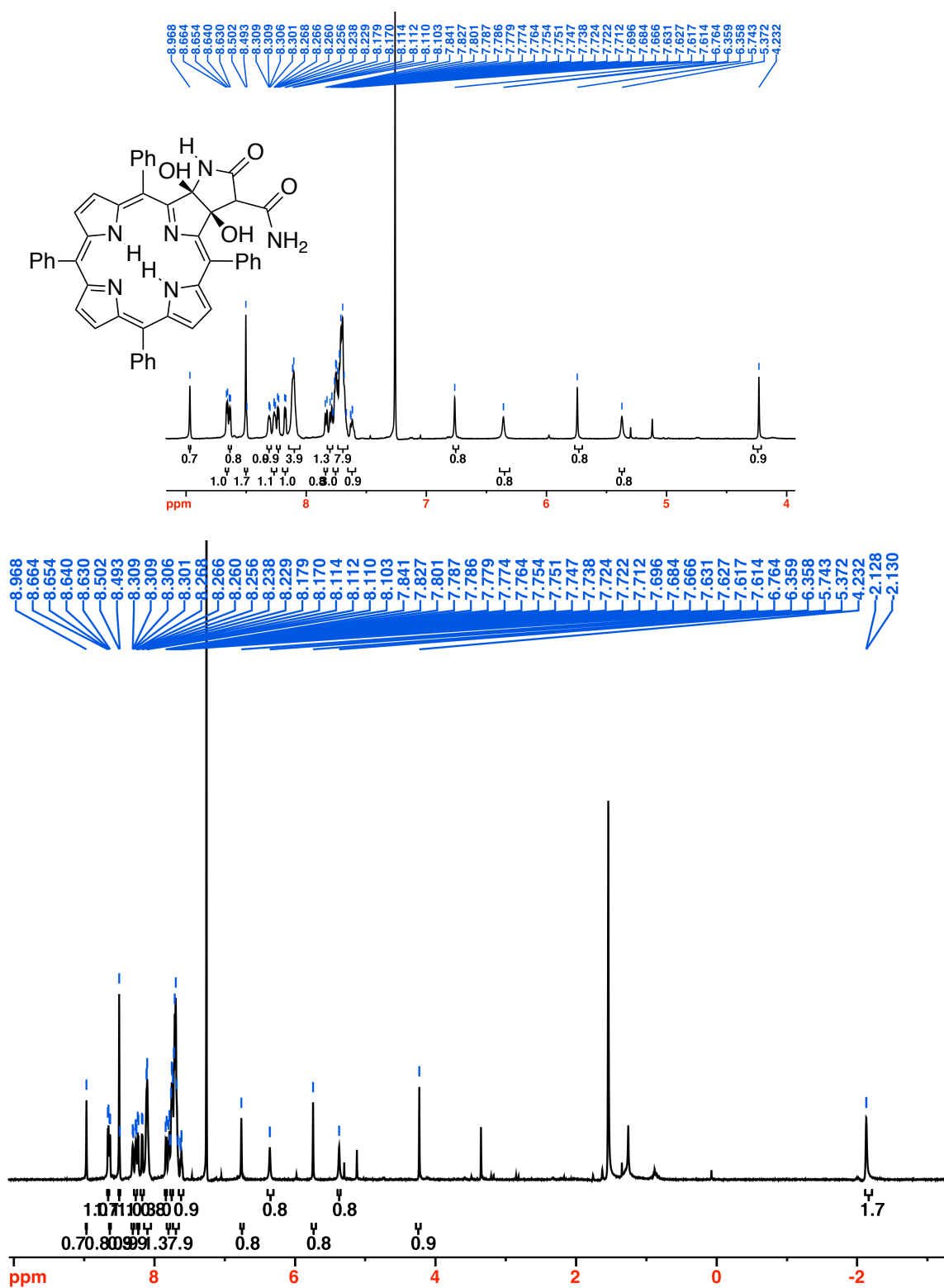


Figure 5-46. UV-vis spectrum (CH₂Cl₂) of **20**.

Figure 5-47. ^1H NMR spectrum (500 MHz, CDCl_3) of 20.

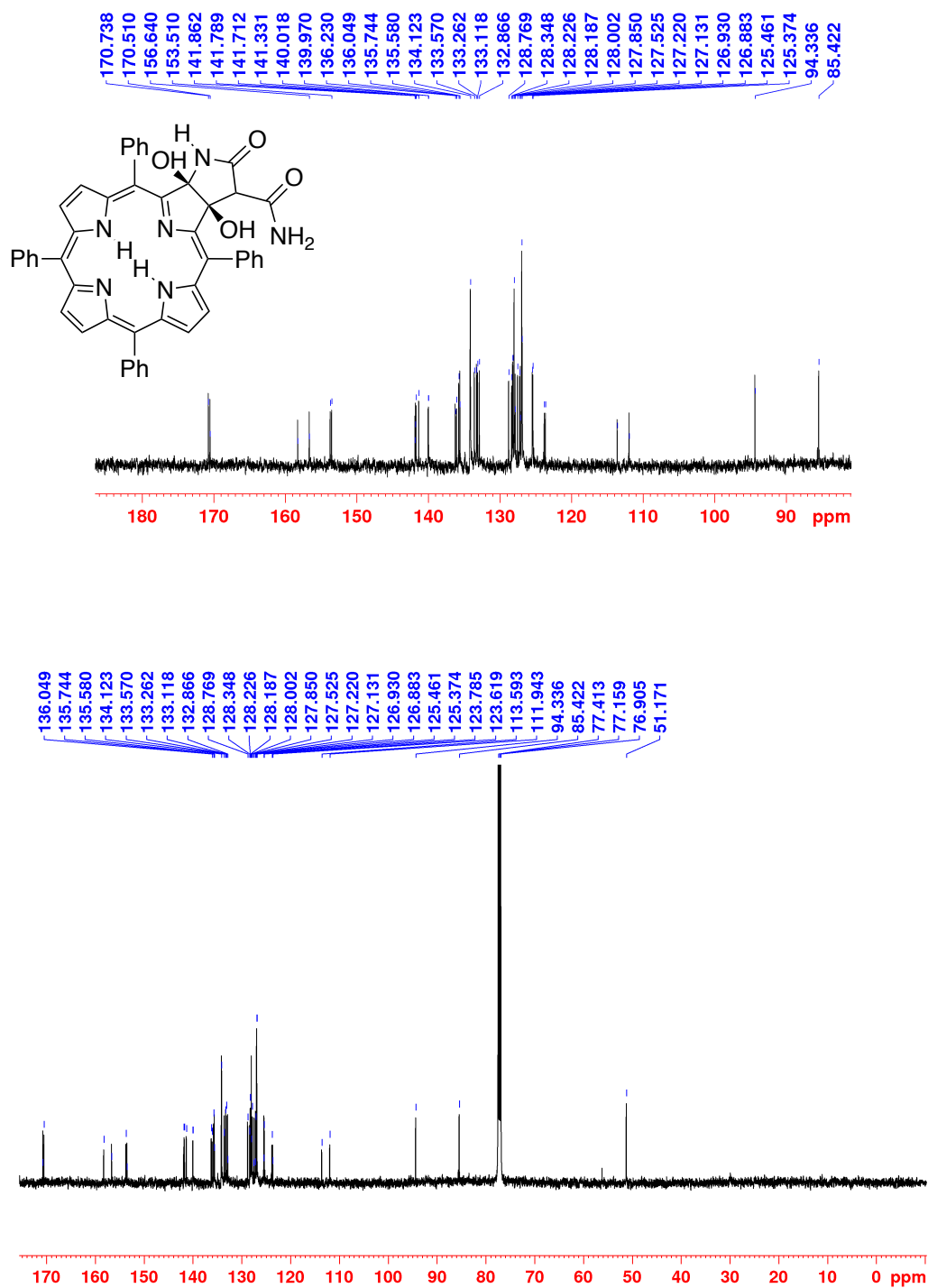


Figure 5-48. ^{13}C NMR spectrum (125 MHz, CDCl_3) of **20**.

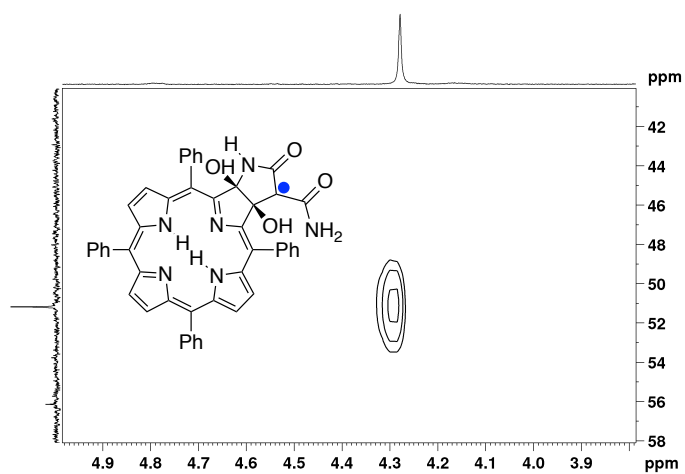


Figure 5-49. Partial ^{13}C - ^1H HSQC spectrum (CDCl_3) of **20**.

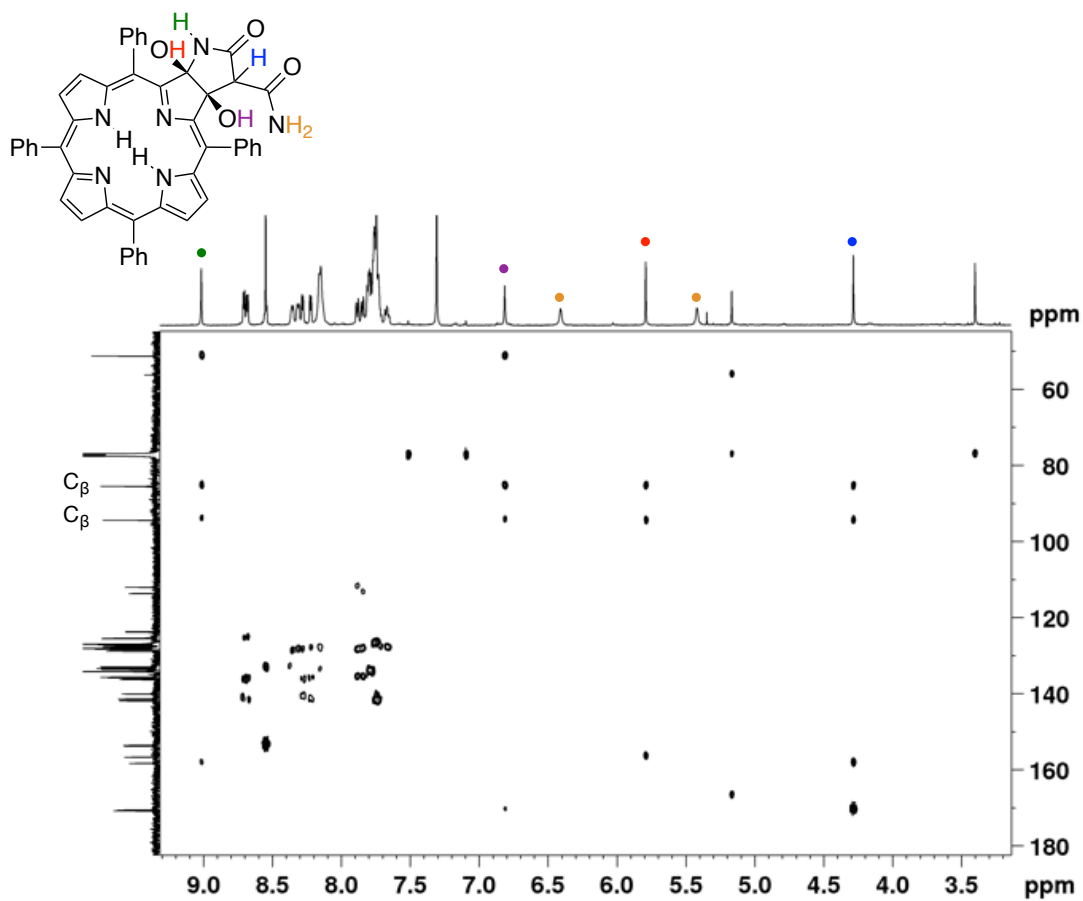


Figure 5-50. HMBC spectrum (CDCl_3) of **20**.

Dimethyl malonamide adducts 23 and 24. Prepared from **7** (50.0 mg, 7.8×10^{-5} mol) in pyridine (20 mL) as described for **8** using *N,N'*-dimethylmalonamide (105 mg, 8.0×10^{-4} mol, 10 equiv.) and purified by column chromatography (silica-CH₂Cl₂/3% MeOH) to afford the purple diol-chlorin **23** in 38% yield (23 mg) and the red diol-chlorin **24** in 18% yield (10 mg). (**23**) *R_f* (silica-CH₂Cl₂/3% MeOH) = 0.32; ¹H NMR (500 MHz, CDCl₃): δ 8.65 (d, ³*J* = 5.0 Hz, 1H), 8.60 (d, ³*J* = 4.9 Hz, 1H), 8.49 (s, 2H), 8.41 (d, ³*J* = 4.9 Hz, 1H), 8.35 (d, ³*J* = 7.4 Hz, 1H), 8.26 (s, 1H), 8.22 (d, ³*J* = 7.4 Hz, 2H), 8.12 (d, ³*J* = 4.9 Hz, 1H), 8.08 (d, ³*J* = 7.4 Hz, 1H), 7.99 (s, 1H), 7.92 (d, ³*J* = 7.4 Hz, 1H), 7.85 (t, ³*J* = 7.2 Hz, 1H), 7.75-7.60 (m, 12H), 6.14 (s, 1H, exchangeable with D₂O), 5.62 (s, 1H, exchangeable with D₂O), 5.57 (q, ³*J* = 4.7 Hz, 1H, exchangeable with D₂O), 4.21 (s, 1H), 2.77 (d, ³*J* = 4.9 Hz, 3H), 2.41 (s, 3H), -1.91 (s, 1H, exchangeable with D₂O), -1.95 (s, 1H, exchangeable with D₂O) ppm; ¹³C NMR (125 MHz, CDCl₃): δ 169.4, 169.1, 156.7, 154.0, 153.4, 151.3, 141.67, 141.64, 141.48, 140.7, 140.5, 136.38, 136.29, 136.10, 135.4, 134.70, 134.56, 134.3, 133.3, 133.0, 128.6, 128.20, 128.05, 127.90, 127.85, 127.74, 127.3, 127.0, 126.22, 126.05, 125.8, 125.5, 124.2, 123.3, 114.8, 113.8, 100.6, 82.8, 77.2, 54.8, 26.60, 26.55 ppm; UV-vis (CH₂Cl₂) λ_{max} (log ε) 400 (5.19), 413 (5.14), 455 (sh), 511 (4.04), 538 (4.12), 582 (3.97), 634 (4.30) nm; HR-MS (ESI⁺, 100% CH₃CN, TOF) *m/z* calcd for C₄₉H₃₉N₆O₄ ([M·H]⁺), 775.3033 found 775.3041. (**24**): *R_f* (silica-CH₂Cl₂/3% MeOH) = 0.19; ¹H NMR (500 MHz, CDCl₃): δ 8.65 (d, ³*J* = 4.6 Hz, 1H), 8.60 (d, ³*J* = 4.7 Hz, 1H), 8.48 (s, 2H), 8.29 (d, ³*J* = 4.6 Hz, 1H), 8.19-8.14 (m, 2H), 8.11 (d, ³*J* = 5.2 Hz, 4H), 8.07 (d, ³*J* = 4.7 Hz, 1H), 8.04 (d, ³*J* = 7.3 Hz, 1H), 7.94 (d, ³*J* = 5.7 Hz, 1H), 7.74-7.66 (m, 12H), 4.59 (s, 1H, exchangeable with D₂O), 3.60 (s, 1H, exchangeable with D₂O), 3.19 (d, ²*J* = 17.5 Hz, 1H), 2.81 (d, ²*J* = 17.5 Hz, 1H), 2.24 (s, 3H), -1.92 (s, 1H, exchangeable with D₂O) ppm; ¹³C NMR (125 MHz, CDCl₃): δ 173.8, 157.0, 154.5, 153.9, 153.4, 141.72, 141.56, 141.50, 141.3, 140.22, 140.06, 136.3, 136.0, 135.0, 134.5, 134.2, 133.8, 133.3, 133.0, 128.9, 128.5, 128.05, 127.92, 127.69, 127.55, 126.98, 126.92, 125.40, 125.27, 124.3, 123.5, 113.4, 112.7, 100.3, 85.7, 44.9,

26.0 ppm; UV-vis (CH_2Cl_2) λ_{max} (log ϵ) 399 (5.17), 411 (sh), 437 (sh), 460 (sh), 508 (4.03), 535 (4.06), 583 (3.90), 634 (4.31) nm; HR-MS (ESI⁺, 100% CH_3CN , TOF) m/z calcd for $\text{C}_{47}\text{H}_{36}\text{N}_5\text{O}_3$ ($[\text{M}\cdot\text{H}]^+$), 718.2813 found 718.2815.

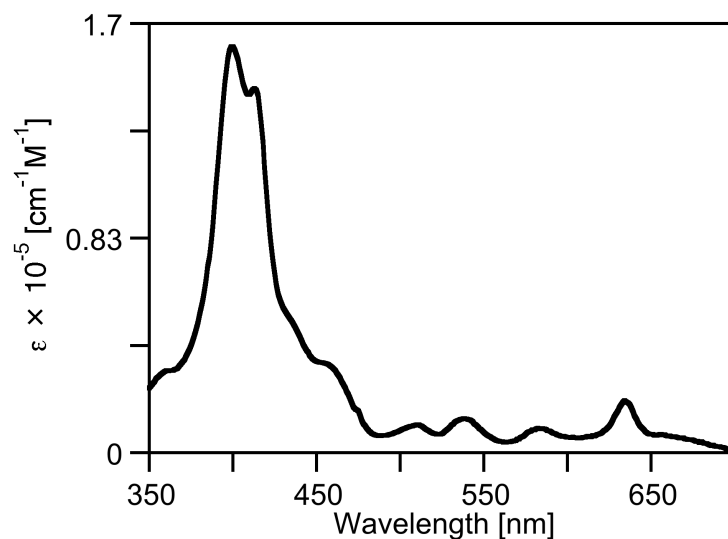


Figure 5-51. UV-vis spectrum (CH_2Cl_2) of **23**.

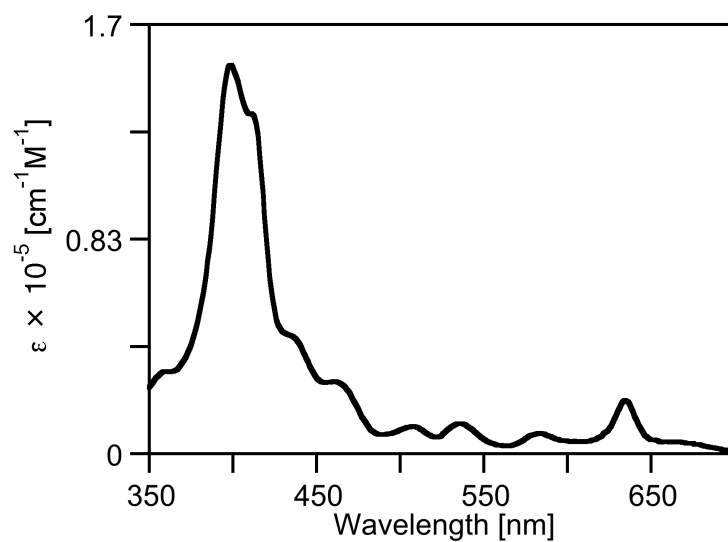


Figure 5-52. UV-vis spectrum (CH_2Cl_2) of **24**.

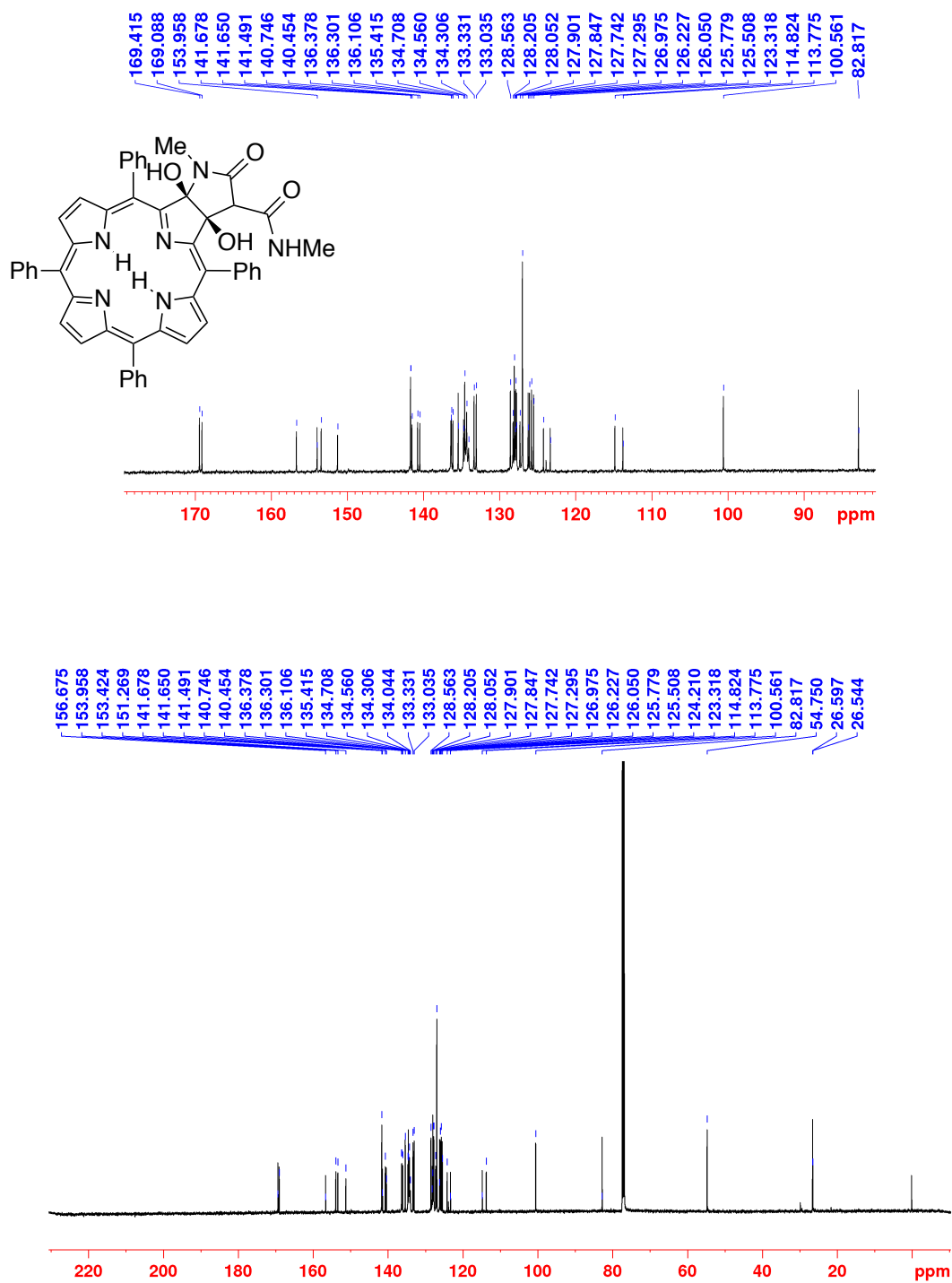


Figure 5-54. ^{13}C NMR spectrum (125 MHz, CDCl_3) of **23**.

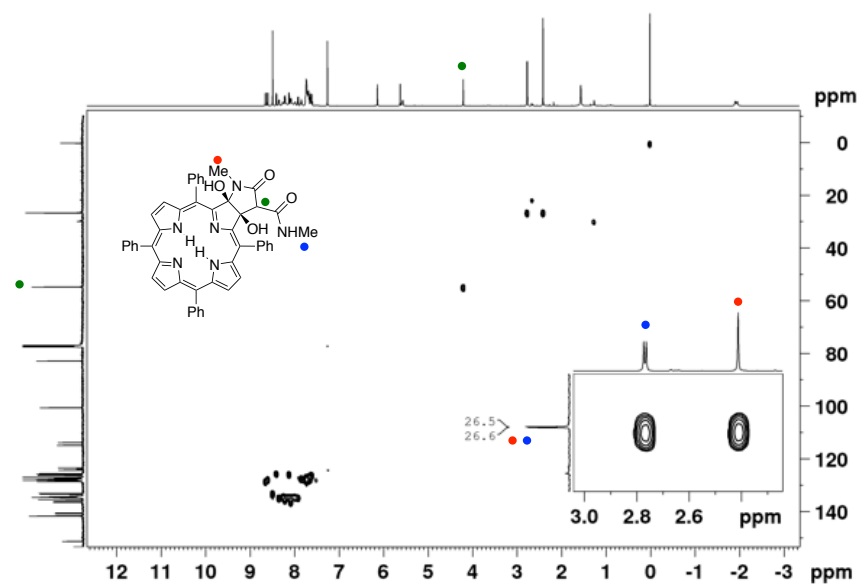


Figure 5-55. ^{13}C - ^1H HSQC spectrum (CDCl_3) of 23.

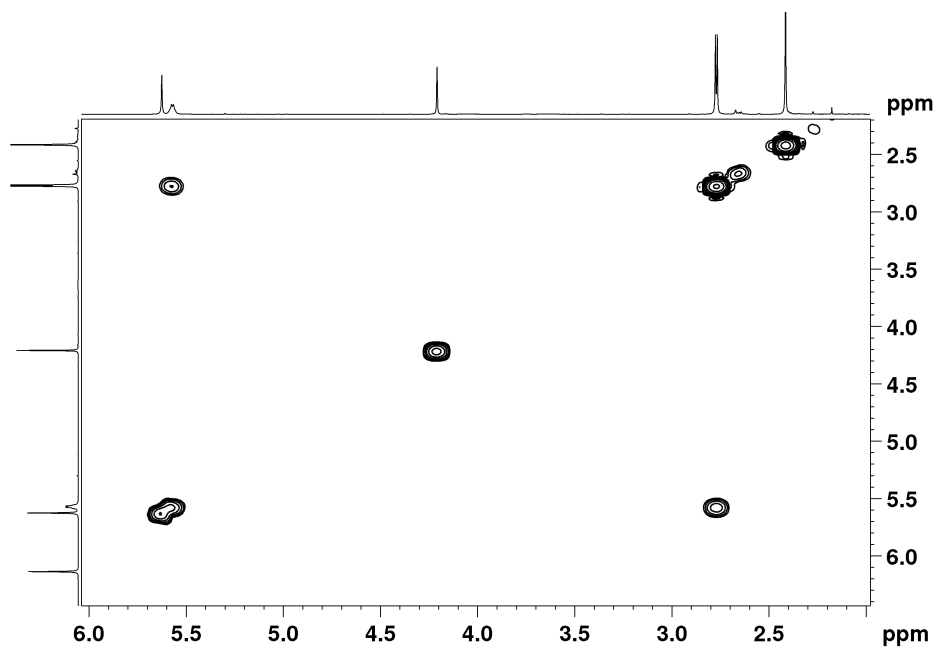
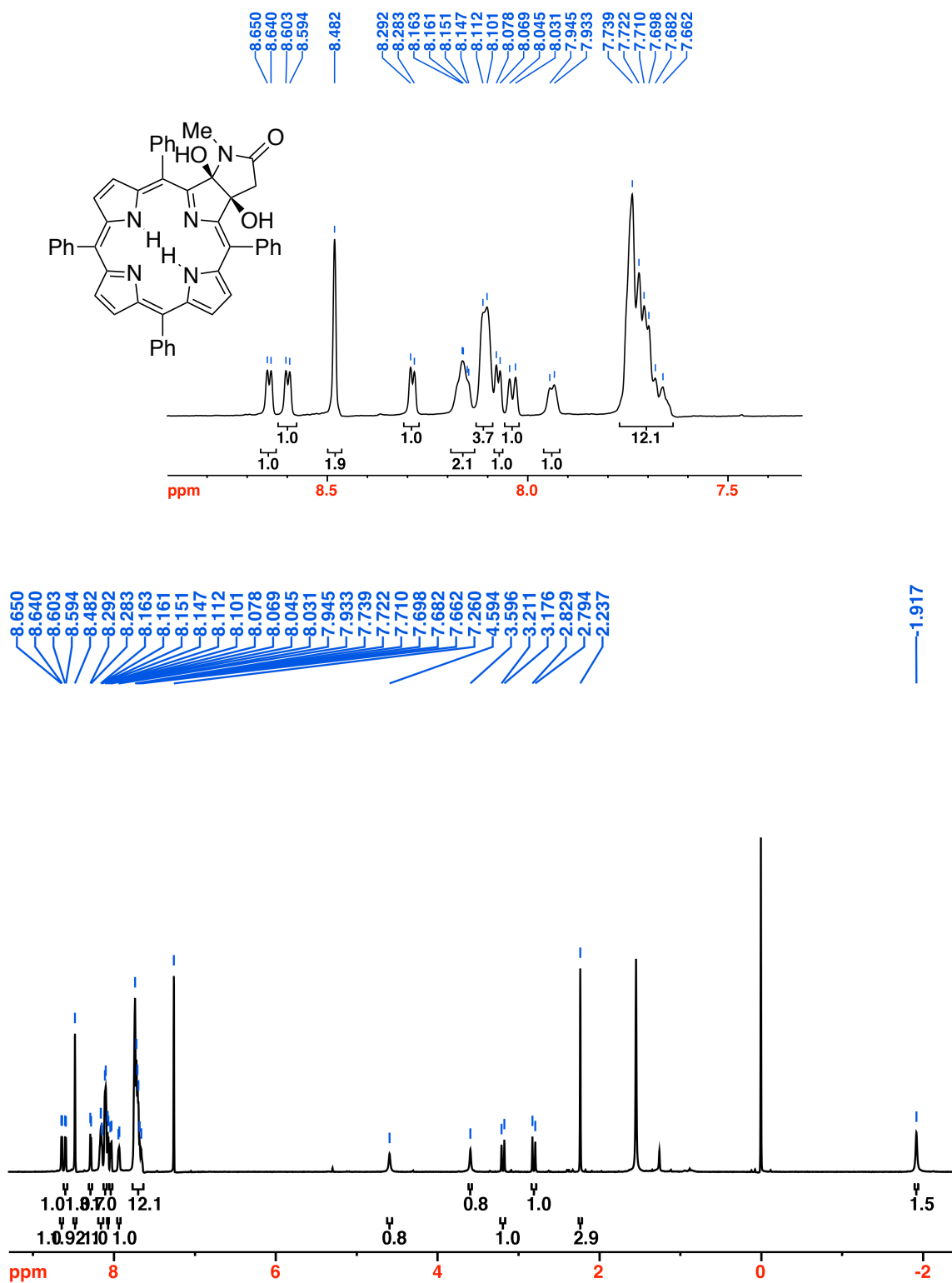


Figure 5-56. ^1H - ^1H COSY spectrum (CDCl_3) of 23.

Figure 5-57. ^1H NMR spectrum (500 MHz, CDCl_3) of **24**.

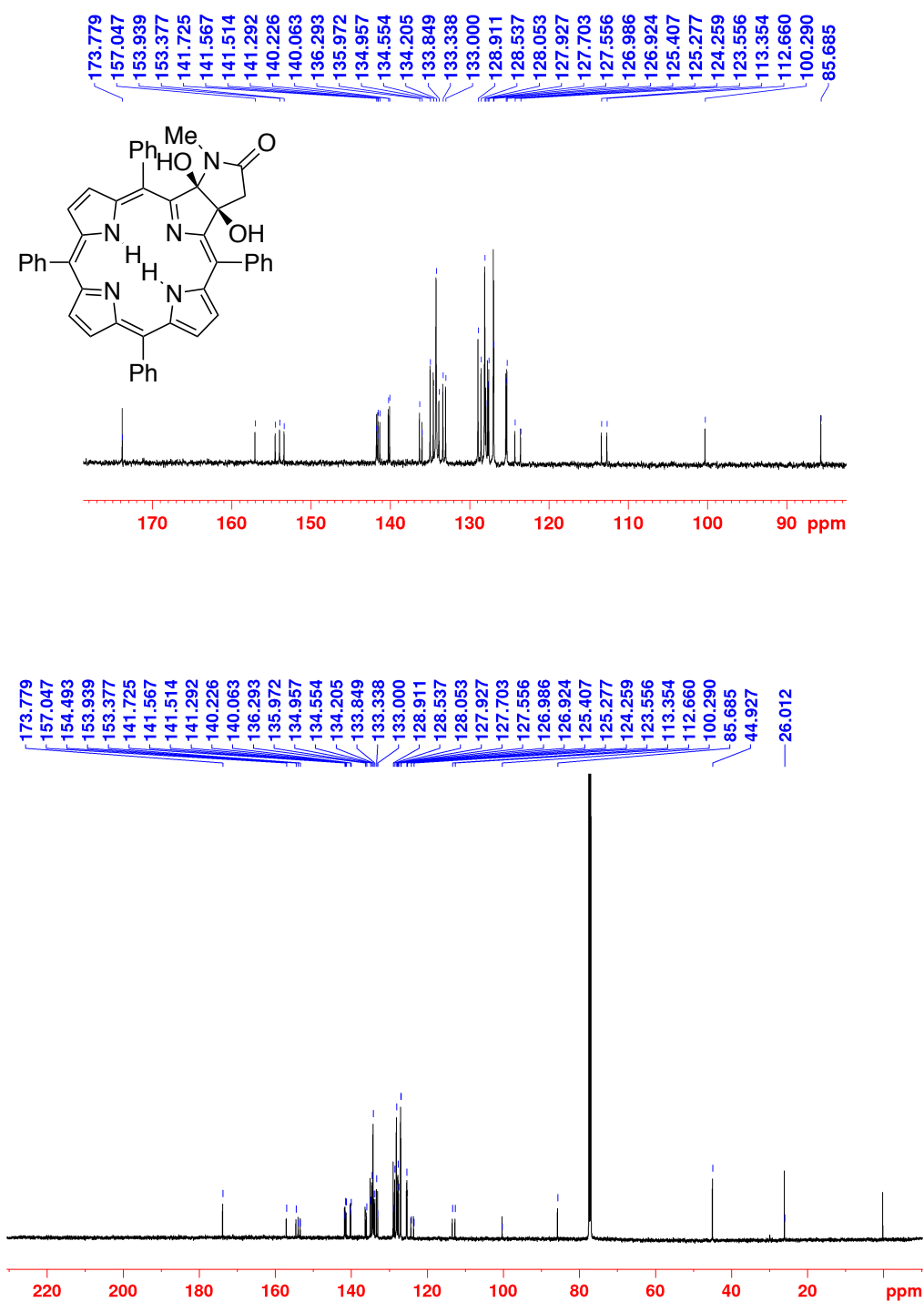


Figure 5-58. ^{13}C NMR spectrum (125 MHz, CDCl_3) of **24**.

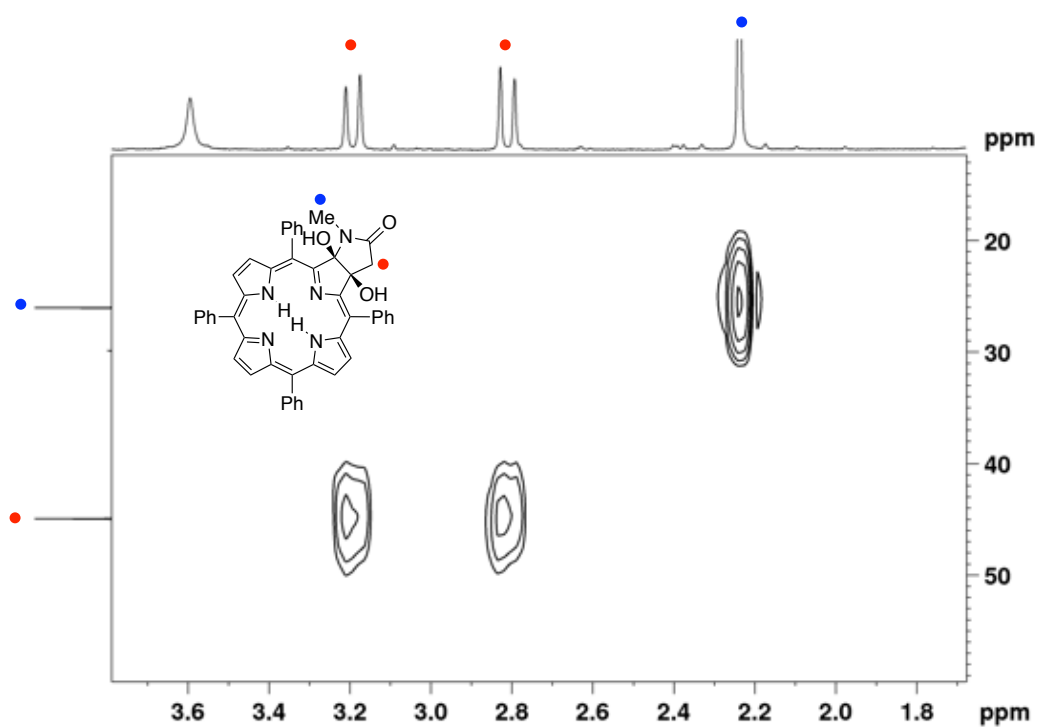


Figure 5 59. Partial ^{13}C - ^1H HSQC spectrum (CDCl_3) of **24**.

Oxidative Cleavage of Malonamide-adduct 20. Malonamide-diol **20** (42 mg, 5.6×10^{-5} mol) was dissolved in dry THF (15.0 mL) in a round bottom flask equipped with a magnetic stir bar under N₂ atmosphere. Pb(OAc)₄ (total 56.7 mg, 1.28×10^{-4} mol, 2.3 equiv.) was added in portions and the reaction mixture was stirred at ambient temperature for 45 min-1h. When the starting material was consumed, (reaction control by TLC), the solvent was evaporated and the crude mixture was purified by preparative TLC (silica-CH₂Cl₂/2% MeOH) to afford the purple **21** contaminated with a small amount of spiro-barbiturate **22** (24 mg, ~57% yield based on the mass of the main product): R_f (silica-CH₂Cl₂/2% MeOH) = 0.10; ¹H NMR (400 MHz, CDCl₃) δ 8.71 (d, ³J = 4.9 Hz, 2H), 8.58-8.52 (m, 3H), 8.38 (d, ³J = 5.2 Hz, 1H), 8.14-8.10 (m, 4H), 7.96-7.94 (m, 2H), 7.89-7.83 (m, 3H), 7.77-7.59 (m, 12H), 6.91 (s, 1H, exchangeable with D₂O), 5.42 (s, 1H, exchangeable with D₂O), -2.02 (s, 1H, exchangeable with D₂O), -2.08 (s, 1H, exchangeable with D₂O) ppm; ¹³C NMR (100 MHz, CDCl₃): δ 194.7, 166.9, 164.0, 155.98, 155.90, 154.2, 141.45, 141.26, 141.15, 141.10, 139.71, 139.61, 139.49, 138.8, 138.2, 137.9, 137.0, 134.7, 134.5, 134.32, 134.12, 134.07, 133.81, 133.64, 132.2, 129.01, 128.83, 128.6, 128.11, 128.03, 127.99, 127.87, 127.80, 127.57, 127.42, 127.36, 127.30, 127.15, 127.07, 126.91, 126.87, 124.8, 122.6, 116.6, 112.7 ppm; UV-vis (CH₂Cl₂) λ_{max} (rel I.) 334 (0.16), 420 (1.0), 522 (0.06), 562 (0.06), 590 (0.05), 642 (0.05) nm; HR-MS (ESI⁺, 100% CH₃CN, TOF) *m/z* calcd for C₄₇H₃₁N₆O₄([M·H]⁺), 743.2401 found 743.2437.

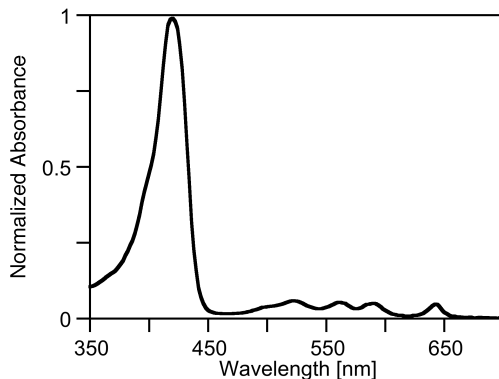


Figure 5-60. UV-vis spectrum (CH₂Cl₂) of **21**.

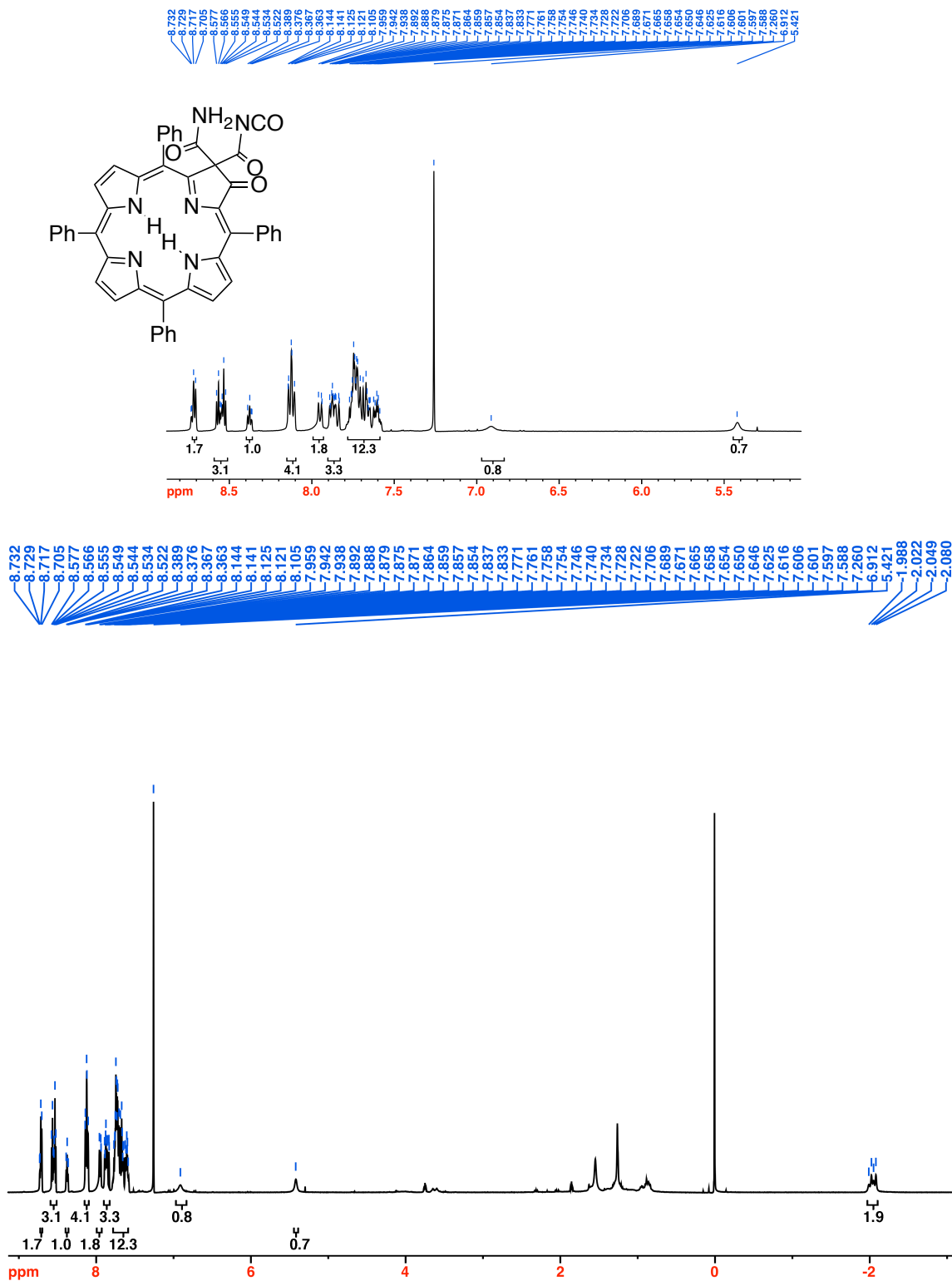


Figure 5-61. ^1H NMR spectrum (400 MHz, CDCl_3) of **21**.

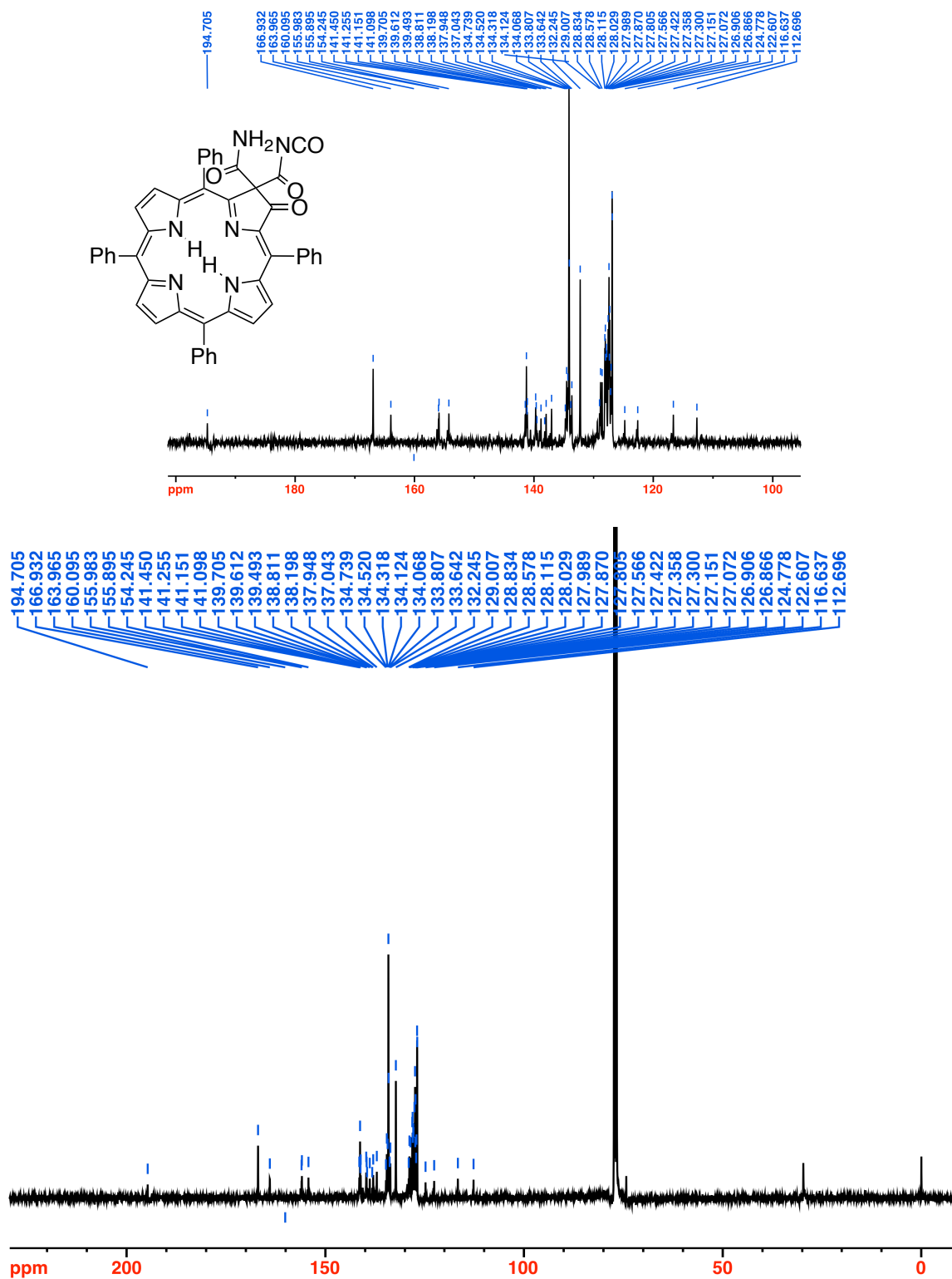


Figure 5-62. ^{13}C NMR spectrum (100 MHz, CDCl_3) of **21**.

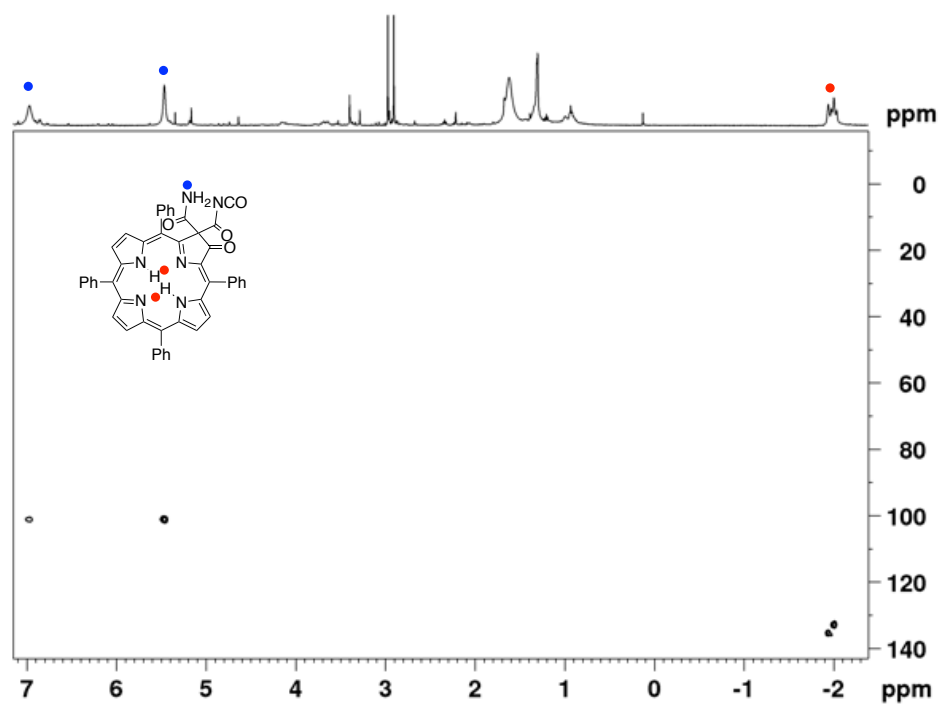


Figure 5-63. ^{15}N - ^1H HSQC spectrum (CDCl_3) of **21**.

5.4 References

- (1) Stepien, M.; Latos-Grazynski, L. *Top. Heterocycl. Chem.* **2009**, *19*, 83.
- (2) a) Sessler, J. L.; Davis, J. M. *Acc. Chem. Res.* **2001**, *34*, 989; b) Cetin, A.; Ziegler, C. J. *Dalton Trans.* **2005**, 25.
- (3) Toganoh, M.; Furuta, H. *Chem. Commun.* **2012**, *48*, 937.
- (4) a) Chmielewski, P. J.; Latos-Grazynski, L. *Coord. Chem. Rev.* **2005**, *249*, 2510; b) Gupta, I.; Ravikanth, M. *Coord. Chem. Rev.* **2006**, *250*, 468; c) Arnold, L.; Müllen, K. *J. Porphyrins Phthalocyanines* **2011**, *15*, 757; d) Lash, T. D. *J. Porphyrins Phthalocyanines* **2012**, *15*, 423; e) Brückner, C.; Akhigbe, J.; Samankumara, L. In *Handbook of Porphyrin Science*; Kadish, K. M., Smith, K. M., Guillard, R., Eds.; World Scientific: River Edge, NY, 2014; Vol. 31, p 1; f) Costa, L. D.; Costa, J. I.; Tome, A. C. *Molecules* **2016**, *21*; g) Lash, T. D. *Acc. Chem. Res.* **2016**, *49*, 471.
- (5) Brückner, C. *Acc. Chem. Res.* **2016**, accepted for publication (DOI: 10.1021/ar).
- (6) Brückner, C.; Götz, D. C. G.; Fox, S. P.; Ryppa, C.; McCarthy, J. R.; Bruhn, T.; Akhigbe, J.; Banerjee, S.; Daddario, P.; Daniell, H. W.; Zeller, M.; Boyle, R. W.; Bringmann, G. *J. Am. Chem. Soc.* **2011**, *133*, 8740.
- (7) a) Akhigbe, J.; Peters, G.; Zeller, M.; Brückner, C. *Org. Biomol. Chem.* **2011**, *9*, 2306; b) Akhigbe, J.; Samankumara, L.; Brückner, C. *Tetrahedron Lett.* **2012**, *53*, 3524.
- (8) Shimizu, S.; Zhu, H.; Kobayashi, N. *Chem. Commun.* **2011**, *47*, 3072.
- (9) Yet, L. *Chem. Rev.* **2000**, *100*, 2963–3007.
- (10) Montalban, A. G.; Baum, S. M.; Barrett, A. G. M.; Hoffman, B. M. *Dalton Trans.* **2003**, 2093.
- (11) a) Daniell, H. W.; Williams, S. C.; Jenkins, H. A.; Brückner, C. *Tetrahedron Lett.* **2003**, *44*, 4045; b) Crossley, M. J.; Burn, P. L.; Langford, S. J.; Pyke, S. M.; Stark, A. G. *J. Chem. Soc., Chem. Commun.* **1991**, 1567.
- (12) Akhigbe, J.; Brückner, C. *Eur. J. Org. Chem.* **2013**, 3876.
- (13) Hush, N. S.; Reimers, J. R.; Hall, L. E.; Johnston, L. A.; Crossley, M. J. *Ann. N.Y. Acad. Sci.* **1998**, *852*, 1.
- (14) Brückner, C.; McCarthy, J. R.; Daniell, H. W.; Pendon, Z. D.; Ilagan, R. P.; Francis, T. M.; Ren, L.; Birge, R. R.; Frank, H. A. *Chem. Phys.* **2003**, *294*, 285.
- (15) a) Akhigbe, J.; Ryppa, C.; Zeller, M.; Brückner, C. *J. Org. Chem.* **2009**, *74*, 4927; b) Brückner, C.; Rettig, S. J.; Dolphin, D. *J. Org. Chem.* **1998**, *63*, 2094; c) Banerjee, S.;

- Zeller, M.; Brückner, C. *J. Porphyrins Phthalocyanines* **2012**, *16*, 576; d) McCarthy, J. R.; Jenkins, H. A.; Brückner, C. *Org. Lett.* **2003**, *5*, 19.
- (16) Adams, K. R.; Bonnett, R.; Burke, P. J.; Salgado, A.; Valles, M. A. *J. Chem. Soc., Chem. Commun.* **1993**, 1860.
- (17) Akhigbe, J.; Haskoor, J. P.; Krause, J. A.; Zeller, M.; Brückner, C. *Org. Biomol. Chem.* **2013**, *11*, 3616.
- (18) Ryeng, H.; Ghosh, A. *J. Am. Chem. Soc.* **2002**, *124*, 8099.
- (19) Guberman-Pfeffer, M. J.; Greco, J. A.; Samankumara, L. P.; Zeller, M.; Birge, R. R.; Gascón, J. A.; Brückner, C. *J. Am. Chem. Soc.* **2017**, *139*, 548.
- (20) Manohara Reddy, S. A.; Mudgal, J.; Bansal, P.; Vasanthraju, S. G.; Srinivasan, K. K.; Rao, C. M.; Gopalan Kutty, N. *Biorg. Med. Chem.* **2011**, *19*, 384.
- (21) a) Kai, S.; Mikio, S. *Tetrahedron Letters* **1996**, *37*, 5931; b) Gerlach, B.; Montforts, F. P. *Tetrahedron Lett.* **1993**, *34*, 6369; c) Banala, S.; Sintic, P.; Kraeutler, B. *Helv. Chim. Acta* **2012**, *95*, 211.
- (22) Whiteley, M. A. *J. Chem. Soc. Trans.* **1903**, *83*, 24.

6 Substituted Imidazoloporphyrins

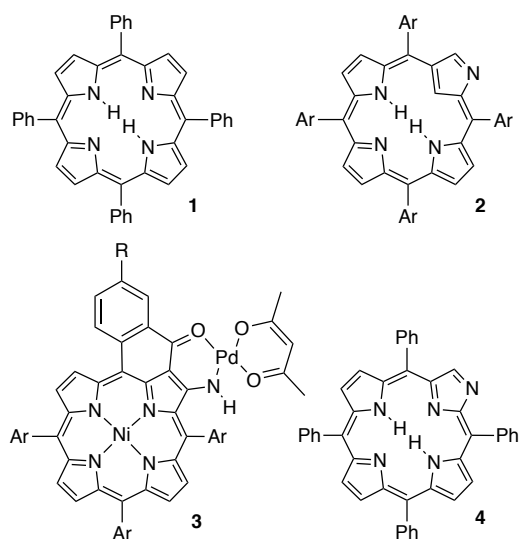
Much of the contemporary work in the area of synthetic chemistry of porphyrins, hydroporphyrins,¹ and their analogues aims at the optimization of their optical properties. Particularly prominent is the aim of generating porphyrinoids possessing NIR wavelengths of absorbance and emission because of their potential utility in medical applications;² technical applications may also utilize their altered electronics.³ Less studied are derivatives with functionalized porphyrinic macrocycles that allow their utilization in ways unknown to regular, unmodified porphyrins.

To illustrate this, while *meso*-tetraarylporphyrins such as **1** can coordinate a metal ion in their central cavity,⁴ and therefore have been used (as well as their analogues) as metal sensors (or non-reversible chemidosimeters),⁵ the binding (or release) of a metal ion is not very selective and kinetically challenging. Bearing otherwise only aromatic CH groups at their chromophore periphery, they do not interact with metals in any other way. On the other hand, the isomeric N-confused porphyrin **2** overcomes this limitation; it can readily coordinate a metal through the β -N atom on its periphery (in addition to coordination of metals to its center).⁵⁻⁶ Since metal coordination involves the chromophore, any interaction with the metal is observed by diagnostic changes in its optical properties. However, the external monodentate coordination mode is necessarily weaker than any chelation mode (using comparable donor atoms).

Ruppert, Callot, Jeandon, Richeter, and co-workers studied the construction of β -modified tetraarylporphyrin derivatives capable of forming conjugated chelates at their chromophore periphery, such as porphyrin **3**,⁷ thereby increasing its affinity toward metals. We like to stress that the focus of this discussion is not on porphyrins that were appended to, e.g., a metal ion coordination motif that allows the binding of the ion without the direct involvement of atoms of

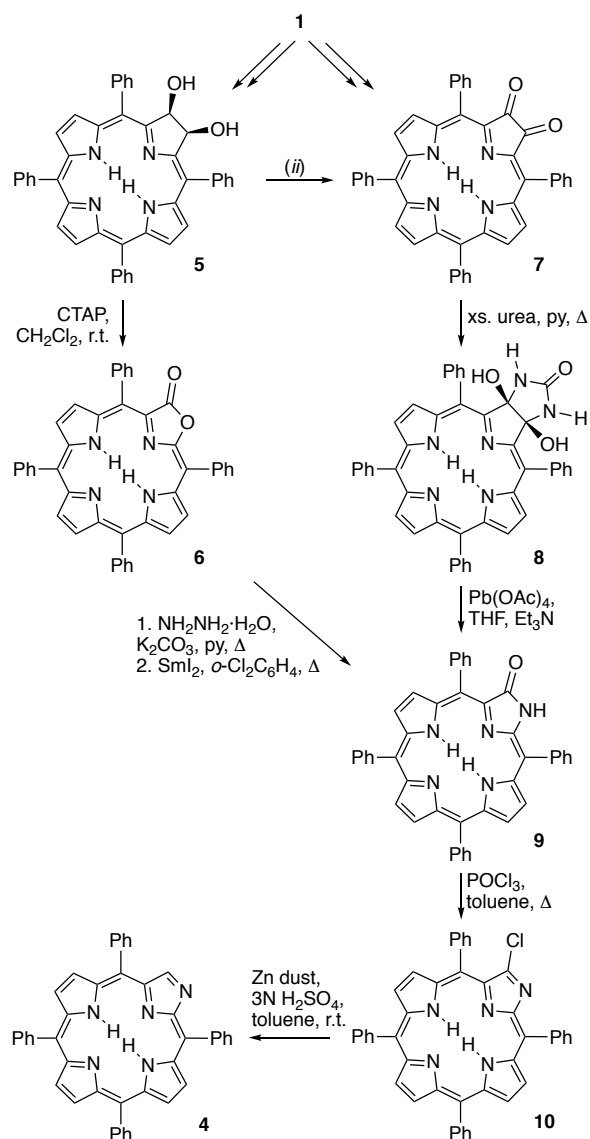
the macrocycle/chromophore, for which there are many examples.⁸ The optical response of the chromophore upon metal binding in these systems is often very weak.

Imidazoloporphyrin **4** reported by our laboratory combines the N₄-central cavity of a porphyrin with the peripheral β -N of N-confused porphyrins.⁹ The basicity of the peripheral nitrogen atom was demonstrated by the halochromic optical response upon protonation.^{9b} Thus, we predicted imidazoloporphyrin **4** to be a competent ligand for transition metals, but even though it can be accessed along three independent pathways by modification of **1** (see also below), none were efficient enough to enable us to study the coordination chemistry in any depth, nor could we investigate the derivatization of its imidazole moiety.



Porpholactones, such as the tetraphenyl derivative **6**, possess a lactone functionality in place of a CH=CH double bond at their periphery (Scheme 6-1). The electrophilicity of this functionality, particularly in the *meso*-C₆F₅-substituted and metalated derivatives, could be utilized for high pH sensing in cementitious materials, aqueous solutions, and as cyanide sensors, among others.¹⁰ The lactone moiety also changes the optical, catalytic, and bio-distribution properties of this chromophore in unexpected ways.¹¹ Porpholactones are available along a number of alternative routes.¹² The route of our choice is by step-wise oxidation of

porphyrin **1** (Scheme 6-1):^{12e} Dihydroxylation to chlorin diol **5** and diol oxidation to lactone **6**. This efficiently prepared lactone derivative served also as an intermediate toward the generation of imidazoloporphyrin **4**: Lactone **6** was reacted with hydrazine and the resulting *N*-amino-lactam intermediate reductively cleaved to porpholactam **9**; this was dehydrated/chlorinated to form chloro-imidazole **10**, that was finally hydrodehalogenated into imidazoloporphyrin **3**. Importantly in the current context, the halogen atom on chloro-imidazole **10** could potentially be used as a synthetic handle toward further modifications of the imidazoloporphyrins, but when this work was reported in 2013,^{9b} our access to porpholactam **9** via porpholactone **6** was limited enough to prohibit a full-fledged study. In 2016, we fortuitously discovered a short pathway toward porpholactam **9**:¹³ *meso*-Tetraphenyl-2,3-dioxochlorin **7**, readily available along a number of alternative pathways from porphyrin **1**,^{12a,14} formed a novel chlorin diol **8** in high yields by reaction with urea. Upon oxidative diol cleavage, it fragmented and formed porpholactam **9**. This much more economic and efficient pathway now allowed the study of its conversion to (functionalized) imidazoloporphyrin derivatives, to be presented here.



Scheme 6-1. Known synthesis of imidazoloporphyrin **3** and porpholactam **9**.

Thus, we report here the full details of the formation of the porpholactam **9** along the dione **7** \rightarrow diol **8** \rightarrow lactam **9** route mentioned as an incidental result in a preliminary report.¹³ We will then detail the conversion of porpholactam **9** to a number of imidazoloporphyrin derivatives designed to chelate transition metals at their periphery also involving the β -N atom of the imidazole moiety. In so doing, we are providing the synthetic methodology for the expansion of the utility of synthetic porphyrinoids.

6.1 Results and Discussion

6.1.1 An Efficient Synthesis of Porpholactam **9**

The regular ketone reactivity of *meso*-tetraarylporphyrin diones, such as **7**, was previously demonstrated,¹⁵ including its reaction with diamines to generate diimines.¹⁶ However, we found that the reaction of non-polar, yellow-brown **7** with urea did not generate a diimine but the non-dehydrated precursor product, a polar, magenta-colored dihydroxychlorin **8** containing an imidazolidinone moiety annulated at the β,β' -position. Diagnostic for the formation of the dihydroxychlorin structure are the preservation of the two-fold symmetry of the dione in the product and the presence of OH and NH signals in its ^1H NMR spectrum, the replacement of the pyrrolinone carbonyl signal in its ^{13}C NMR spectrum (at 188 ppm) by a signal at $\delta = 159.5$ ppm assigned to the imidazolidinone moiety, and its regular chlorin-like spectrum compared to the much broadened spectra for dione **7** (Figure 6-1),¹⁷ and a composition ($\text{C}_{45}\text{H}_{33}\text{N}_6\text{O}_3$ for MH^+ , as per HR-MS) consistent with the structural assignment. For a reproduction of the spectra of all new products, see experimental section. Chlorin **8** is available in multi-100 mg batches.

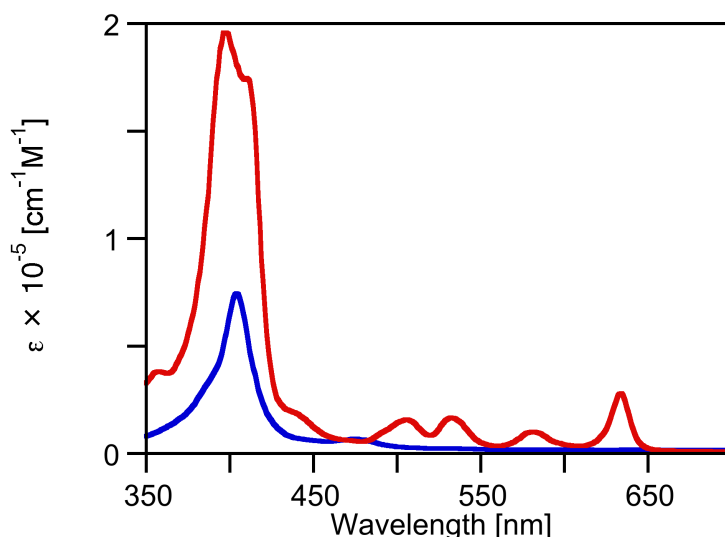


Figure 6-1. UV-vis spectra (CH_2Cl_2) of dione **7** (blue trace) and dihydroxychlorin **8** (red trace).

We previously reported multiple methods for the oxidative cleavage of the pyrroline β,β' -bond of dihydroxychlorins.¹⁸ Thus, treatment of diol **8** under classic diol cleavage reaction conditions using $\text{Pb}(\text{OAc})_4$ ¹⁹ resulted in the formation of a red, non-polar compound **9** in good yields (69%). Its porphyrin-like UV-vis spectrum (Figure 6-2), NMR spectra, and its composition as determined by HR-MS identified it to be the known porpholactam.^{9b} Evidently, the expulsion of smaller fragments $\text{CO}_2 + \text{HCN}$ from the putative pyrrole-modified derivative containing an 8-membered heterocycle, thereby establishing a stable ‘tetrapyrrolic’ architecture, drove the reaction. We have previously seen these types of ring-contraction reactions.^{9a,20} The mechanism of this reaction was not studied and is undoubtedly complex, but the fragmentation can be halted by formal *N*-methylation of the urea adduct (formation of the chlorin diol adduct from *N,N'*-dimethylurea) and the unusual 1,3,6-triazocine-2,4,8-trione-derived porphyrinoid could be isolated.¹³ This 3-step pathway toward porpholactam **9** from *meso*-tetraphenylchlorin diol **6** involving high-yielding steps (**6** \rightarrow **7** \rightarrow **8** \rightarrow **9**) is much more convenient, economic, and significantly higher yielding (overall 29% at a 50 mg scale) than the previously described 4-step synthesis from **1** (~13% along **6** \rightarrow **5** (two steps) \rightarrow **9**).

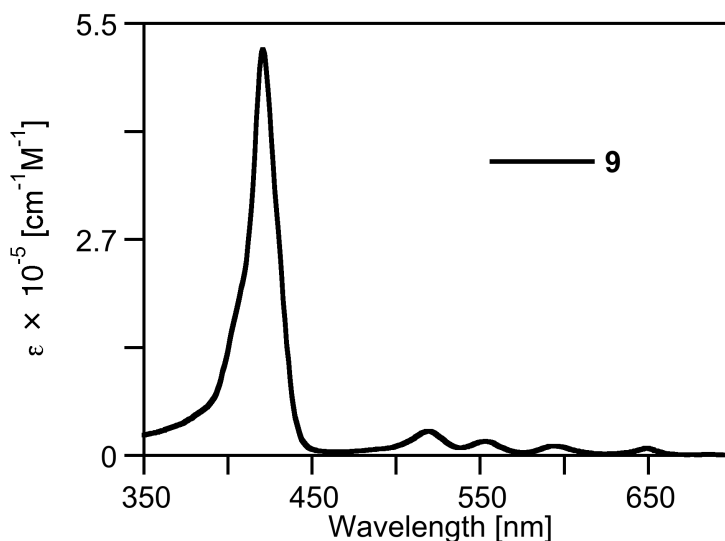


Figure 6-2. UV-vis spectrum (CH_2Cl_2) of the compound indicated.

6.1.2 Conversion of Porpholactam **8** to Reactive Imidazoloporphyrin Triflate **12**

Initial experiments on the substitution of the Cl-atom in chloro-imidazoloporphyrin **10** were disappointing. Thus, we set out to prepare the analogous triflate compound (Scheme 6-2). Parallel to the iminolization with concomitant OH-to-Cl substitution of porpholactam **8** using POCl₃ to prepare **10**, we reacted purple porpholactam **9** with trifluoromethanesulfonic anhydride (Tf₂O) in CH₂Cl₂ under an inert atmosphere at -78 °C for an iminolization with concomitant OH-to-OTf exchange. Upon warming to ambient temperature, one major nonpolar (*R_f* = 0.88, silica-CH₂Cl₂) purple compound was obtained in good yields (76%). Its composition (C₄₄H₂₉F₃N₅SO₃ for MH⁺, as determined by ESI⁺ HR-MS), corresponded to the composition of the target imidazoloporphyrin triflate **12**. Notably absent from its ¹H NMR spectrum was the diagnostic N-H peak of the porpholactam (at 9.7 ppm), any sign for a lactam carbonyl oxygen in its ¹³C NMR, and the presence of a single diagnostic peak (s at -71.1 ppm) in its ¹⁹F NMR indicating the presence of the triflate group. Once crystallized, the compound is stable and can be stored for months in the freezer.

Owing to the ready substitution of the triflate group in triflate imines,²¹ imine **12** was expected to react with a range of nucleophiles. Indeed, *in situ* substitution of the triflate group when the reaction of lactam **8** with Tf₂O was performed in the presence of pyridine generated the pyridinium-substituted imidazoloporphyrin **13** in excellent yields. Its spectroscopic and analytical data (e.g., composition of C₄₈H₃₃N₆ for MH⁺, as per ESI⁺ HR-MS) confirm its assigned structure. Significantly, its UV-vis spectral properties (λ_{max} = 683 nm) are, owing to the presence of the positive charge of the pyridinium substituent located on a β -position of the chromophore, significantly altered compared to the porphyrin-like spectra observed for **10** (λ_{max} = 655 nm) or **12** (λ_{max} = 654 nm) that are similar to each other (Figure 6-3). The influence of a cationic charge on the optical properties of the chromophore were previously also shown in β,β' -annulated imidazolium porphyrins.²²

The pyridinium-substituted imidazoloporphyrin **13** exhibit a red-shifted and hyperchromic UV-vis spectrum with much broadened Q-band region under acidic conditions (10% TFA in CH_2Cl_2) (Figure 6-3). While some features of this spectrum are similar to that of the spectra of porphyrins protonated at the central nitrogens (bathochromically shifted Soret band, reduction of the number of side bands), particularly the red-shifted Q-bands are untypical and suggestive of a protonation of the peripheral imidazole nitrogen (that may or may not be accompanied by central nitrogen protonation).^{9a,23}

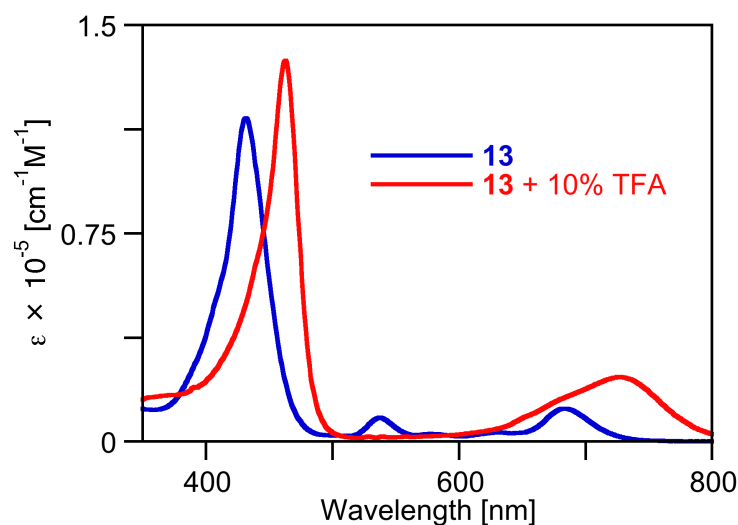
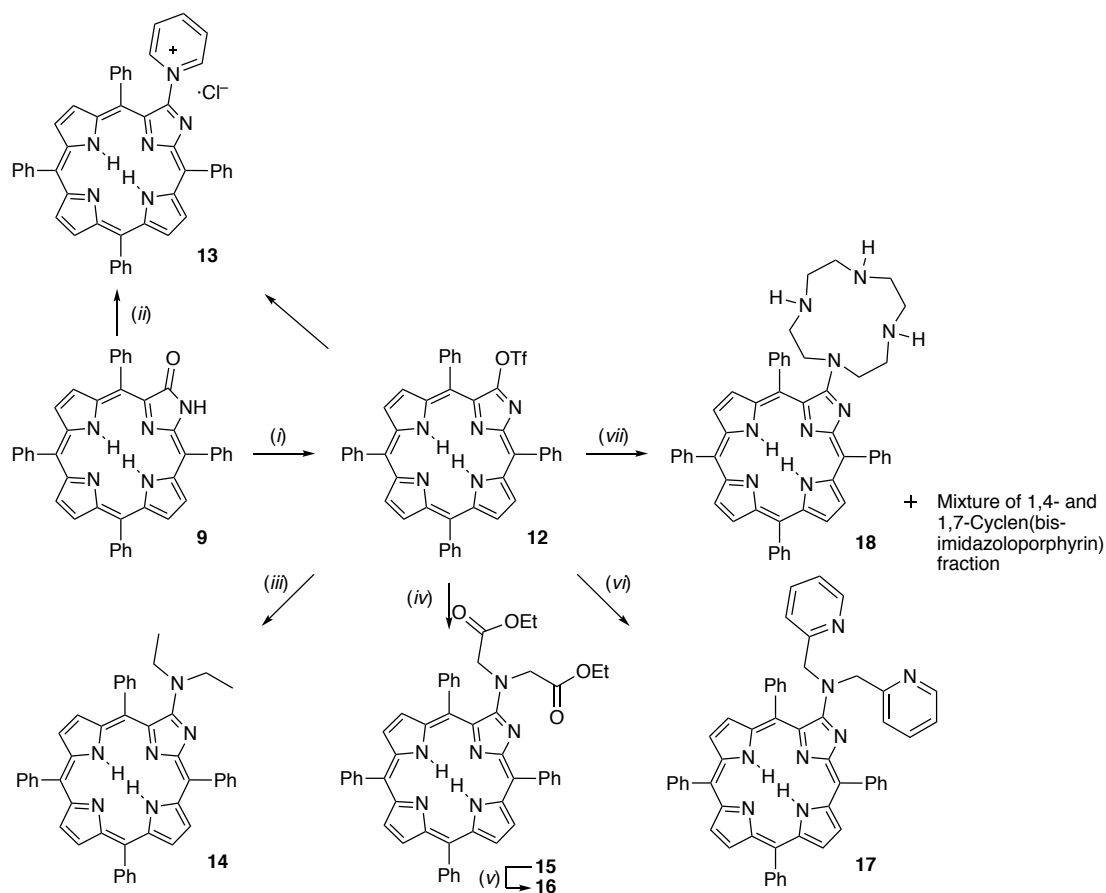


Figure 6-3. UV-vis spectra (CH_2Cl_2) of the compounds indicated.



Scheme 6-2. Conversion of porpholactam **9** to imidazoloporphyrin β -substituted derivatives. Reaction conditions: (i) Tf_2O , CH_2Cl_2 , N_2 , -78°C to 25°C (ii) Tf_2O , $\text{CH}_2\text{Cl}_2/\text{py}$, N_2 , -78°C to 25°C (iii) N,N -diethylamine, Na_2CO_3 , CH_2Cl_2 , r.t. (iv) diethyliminodiacetate, Na_2CO_3 , acetone, Δ (v) 1M KOH: THF (1:1 v/v), Δ (vi) DPA, Na_2CO_3 , CH_2Cl_2 , r.t. (vii) cyclen, Na_2CO_3 , CH_2Cl_2 , r.t.

Reaction of triflate **12** with Et_2NH (in the presence of Na_2CO_3 in CH_2Cl_2) at ambient temperature smoothly afforded the diethylamine-substituted imidazoloporphyrin **14** (Scheme 6-2). Diagnostic for the connectivity of this compound was the appearance of the signals for the two ethyl groups in its ^1H NMR spectrum; all other spectroscopic and analytical data (e.g., composition of $\text{C}_{47}\text{H}_{39}\text{N}_6$ for MH^+ , as per ESI+ HR-MS). Interestingly, the UV-vis spectrum of this compound is significantly broadened and features a split Soret band (Figure 6-4). No change in this UV-vis spectrum was observed upon addition of an excess of Et_3N , but the addition of acid leads to protonation-related changes in the spectrum that suggest that protonation had also taken place at the outside and/or the inside nitrogens of the molecule (Figure 6-4).

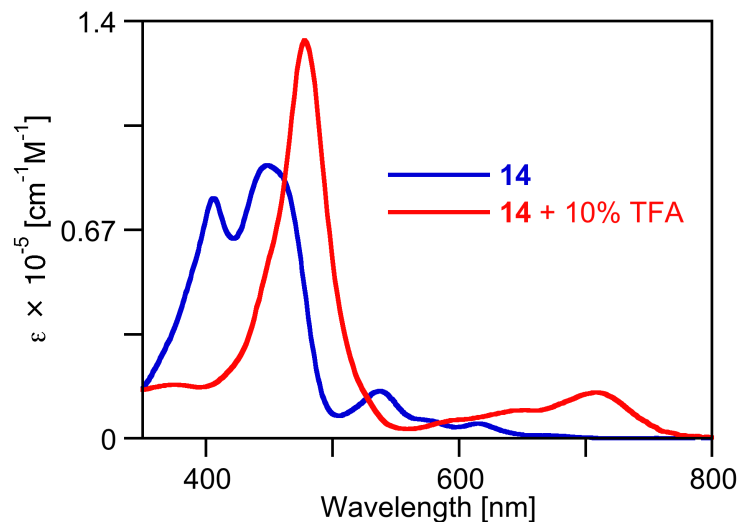
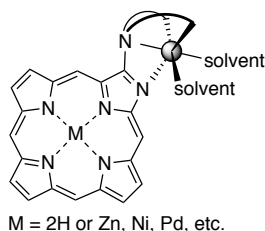


Figure 6-4. UV-vis spectra (CH_2Cl_2) of the compounds indicated.

6.1.3 Modification of Imidazoloporphyrin with Potential Chelating Motifs

With the proof of concept in hand that triflate **12** can be efficiently derivatized with amines, we investigated whether amine-based metal chelates could be introduced that would chelate a metal ion in a way that would also involve the external nitrogen donor atoms of the imidazoloporphyrin cooperatively. We thus hoped to be able to sense the presence of a specific metal ion through the changes in the optical properties of the chromophore, while the chelating interaction was designed to increase the binding affinity and selectivity of the sensor. However, we also realized that the $N_{\text{imidazole}}, N_{\text{amine}}$ -bite angle of this sensing platform might be a bit smaller than ideal.



Iminodiacetate moieties are excellent and versatile chelates. Thus, reaction of triflate imidazole **12** with diethyliminodiacetic acetate in the presence of Na_2CO_3 in hot acetone

afforded a polar brown compound after ~24 h (the reaction with the corresponding free acid was unsuccessful). The composition of the product ($C_{51}H_{43}N_6O_4$ for MH^+ , as per ESI+ HR-MS) matched that of the target chelate **15**. Also observed in its 1H NMR were the peaks corresponding to the ethyl ester groups, as well a peak at 4.4 ppm corresponding to the methylene group of the iminodiacetic acid moiety. A single crystal of **15** could be grown to ultimately confirm the connectivity of the chromophore, revealing also its slight ruffling (Figure 6-5). The $N_{imidazole}, N_{amine}$ -bite angle was measured to be 119.36.

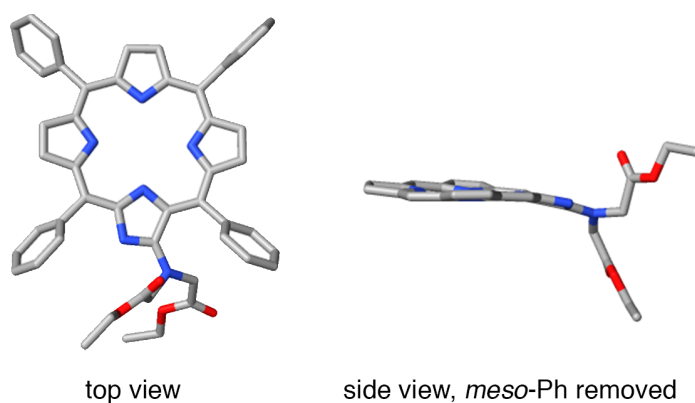


Figure 6-5. X-ray structure of substituted imidazoloporphyrin **15**, hydrogens removed for clarity.

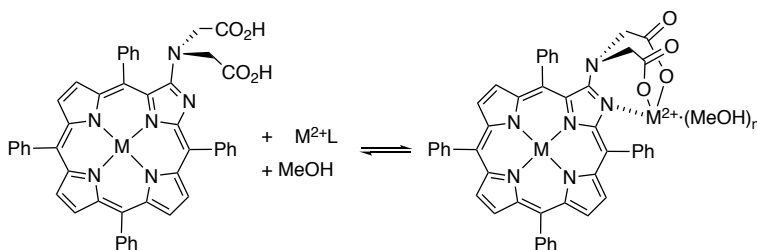
Reaction of the diester **15** under classic saponification conditions (KOH, wet THF) afforded a very polar, streaking brown product after 2 h of reflux. After neutralization of the reaction mixture and extraction into CH_2Cl_2 , the product was purified by column chromatography ($CH_2Cl_2/10\%$ MeOH) to afford a brown residue that displayed a loss of two ethanol molecules by HR-MS. The resulting free acid was only slightly soluble in $CHCl_3$ and CH_2Cl_2 , but soluble in $CH_2Cl_2/MeOH$ mixtures as well as pure MeOH. The 1H NMR of the free acid indicated a slight upfield shift but retention of the methylene peaks (~4 ppm) of the iminodiacetic acid moiety. Due to solubility issues of the free acid **16**, the NMR spectra were recorded in $CD_2Cl_2/MeOD$ mixtures and thus, the carboxylic acid and inner N-H protons were not observed.

Likewise, the DPA-substituted imidazoloporphyrin **17** could be prepared by treatment of **12** with a 50-fold molar excess of di-(2-picolyl)amine (DPA) in the presence of sodium carbonate in CH_2Cl_2 at ambient temperature. The presence of eight additional peaks in the aromatic region in the ^1H NMR spectrum, along with a peak corresponding to the methylene unit of the DPA moiety indicated successful substitution. The peaks corresponding to the DPA moiety were identified by the observation of a pair of doublets and a pair of triplets in the aromatic region exhibiting diagnostic ^1H - ^1H COSY correlations of the 2-substituted pyridine moiety (see ESI).

The triflate imidazole **12** could also be converted to the corresponding cyclen-substituted imidazoloporphyrin **18** in 62% yield, by treatment with cyclen in the presence of sodium carbonate in CH_2Cl_2 at ambient temperature. A series of four peaks in the aliphatic region of the ^1H NMR, each integrating to four protons, indicated the presence of the cyclen unit. The correct mass was confirmed by HR-MS (ESI^+ , 100% CH_3CN). Next to the main cyclen-substituted product **18**, another less polar, brown product was isolated in 16% yield with a similar but slightly broadened UV-vis spectrum than that of **18**. The HR-MS (ESI^+ , 100% CH_3CN) of the nonpolar brown compound indicated the presence of a dimeric species arising from the conjugation of two porphyrins to one cyclen unit.

6.1.4 Interaction of iminodiacetic acid-substituted imidazoloporphyrin **16** with Zn^{2+}

We hypothesized that external coordination of the iminodiacetic acid-substituted imidazoloporphyrin **16** with M^{2+} cations would lead to a spectrophotometric response associated with donation of the imidazole lone-pair to the metal cation (Scheme 6-3).



Scheme 6-3. Proposed mode of binding of substituted-imidazoloporphyrin **16** with M^{2+} cations in MeOH solution.

Indeed, titration of **16** with Zn^{2+} shows marked effects on the native UV-Vis spectrum, causing a gradual increase and sharpening of the Soret band, along with a small hypsochromic shift (Figure 6-6). The titration resulted in the gradual decrease of the first Q band and enhancement of all subsequent Q bands. All of these aspects are consistent with porphyrin metallation; however, the conditions in which these titrations were performed are not suitable for internal complexation of most metals. As such, this spectrum is indicative of peripheral metalation of **16**.

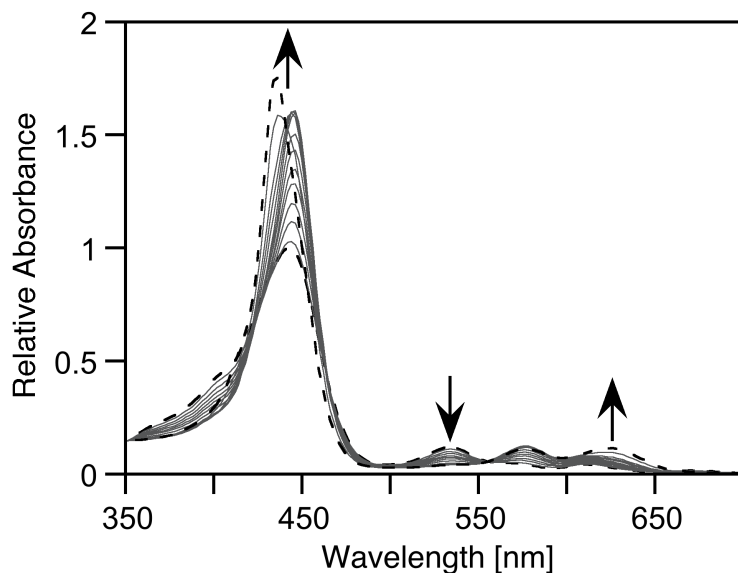


Figure 6-6. Absorbance titration of **16** with Zn^{2+} . Conditions: [**16**] 6.4×10^{-6} M, MeOH, 25 °C, aerated solution, addition of Zn^{2+} as a 1.00 mM methanolic solution.

6.2 Conclusions

In conclusion, we introduced a new and significantly more efficient (and non-obvious) synthetic pathway toward known *meso*-tetraphenylporpholactams. We demonstrated the conversion of *meso*-tetraphenylporpholactams to an imidazoloporphyrin triflate derivative that proved most useful in the preparation of imidazoloporphyrins carrying a substituted amine adjacent to the outside N atoms of the imidazole moiety. This provides a platform for the synthesis of chromophore periphery-functionalized porphyrinoids and invites the continued exploration of the reactivity of the imidazole triflate.

When choosing amines substituted with chelating units, a number of derivatives could be prepared that were designed to chelate a metal ion while also involving the outside imidazole nitrogen atom in their coordination sphere, thus setting the stage for the generation of high-affinity and selective optical metal ion chemosensors. Preliminary reports on the metal ion response of one of such system lends credence to this hypothesis, but the detailed acid/base and metal-induced optical response profiles of all the potential sensors will be reported in due course.

6.3 Experimental Section

6.3.1 Materials and Instruments

All solvents and reagents were used as received. Lactam **9** was prepared as described in the literature.¹³⁻¹⁴

6.3.2 Synthesis and Characterization

meso-Tetraphenyl-2-aza-3-trifluoromethylsulfonylporphyrin (12). To a flame-dried 25 mL round-bottom flask equipped with a septum was added 10 mL of dry CH₂Cl₂ and *meso*-tetraphenyl-2-aza-3-oxo-porphyrin **9** (21 mg, 3.35×10^{-5} mol) was dissolved under an atmosphere of dry N₂. The mixture was cooled to -78 °C and stirred for 20 min. Trifluoromethanesulfonic anhydride (300 µL) was added drop-wise *via* syringe to the reaction flask. The mixture was stirred for 20 min at -78 °C (acetone/dry ice bath), then warmed to 0 °C (ice/water bath) and stirred for an additional 20 min. The reaction mixture was allowed to warm to ambient temperature and stirred for 15 h until the starting material was consumed (reaction control by UV-vis and TLC). The reaction was quenched by addition of a saturated aq solution of sodium bicarbonate (NaHCO₃, 5 mL) and CH₂Cl₂ (5 mL). The biphasic mixture was poured rapidly in a separation funnel and the organic layer was separated from the aqueous layer. The aqueous layer was extracted with CH₂Cl₂ (2 × 5 mL), and the combined organic layers were dried over anhyd Na₂SO₄. The crude material was purified by preparative TLC (CH₂Cl₂/20% petroleum ether 30–60) to furnish **12** as a purple solid in 76% (20 mg) yield. *R*_f (silica-CH₂Cl₂) = 0.88; ¹H NMR (400 MHz, CDCl₃): δ 9.17 (d, ³*J* = 5.2 Hz, 1H), 8.96 (d, ³*J* = 5.0 Hz, 1H), 8.90 and 8.88 (two overlapping d, ³*J* = 5.0 Hz, 2H) 8.74 (s, 2H), 8.27 (d, ³*J* = 7.7 Hz, 2H), 8.20 (t, ³*J* = 7.7 Hz, 4H), 8.11 (d, ³*J* = 7.0 Hz, 2H) 7.85–7.77 (m, 12H) -2.46 (s, 1H, exchangeable with D₂O); ¹⁹F NMR (376 MHz, CDCl₃, external reference CFC₃): δ -71.1 (s) ppm; ¹³C NMR (100 MHz, CDCl₃): δ 163.6, 157.5, 157.2, 153.0, 141.6, 140.6, 140.3, 140.1, 139.3, 139.0, 138.8, 136.2, 135.7,

135.6, 134.8, 134.7, 134.5, 133.6, 130.2, 129.6, 129.0, 128.8, 128.3, 127.9, 127.8, 127.2, 127.1, 126.9, 121.6, 121.4, 121.1, 120.6, 119.2, 117.4 ppm; UV-vis (CH_2Cl_2) λ_{max} (log ϵ) 422 (5.80), 524 (4.40), 562 (3.94), 598 (3.90), 654 (4.42) nm, UV-vis (CH_2Cl_2 + 10% TFA) λ_{max} (log ϵ) 447 (5.62), 680 (4.76) nm; HR-MS (ESI⁺, cone voltage = 30 V, 100% CH_3CN , TOF) m/z calcd for $\text{C}_{44}\text{H}_{29}\text{F}_3\text{N}_5\text{SO}_3$ 764.1943 ($[\text{M}\cdot\text{H}]^+$), found 764.1983.

meso-Tetraphenyl-2-aza-3-(*N*-pyridinium)-porphyrin triflate (13). Compound **13** was prepared similarly to **12**, except that pyridine (1 mL) was also present in the reaction flask. The crude material was purified by preparative TLC (CH_2Cl_2 /5% MeOH) to furnish **13** as a purple solid in 86% yield (15.0 mg): R_f (silica- CH_2Cl_2 /10% MeOH) = 0.38; ^1H NMR (400 MHz, CDCl_3): δ 9.12 (d, 3J = 5.4 Hz, 2H), 9.05 (d, 3J = 4.9 Hz, 1H), 8.90 (d, 3J = 4.9 Hz, 1H), 8.85 (s, 2H), 8.68 (s, 2H), 8.38 (t, 3J = 7.5 Hz, 1H) 8.25 (dd, 3J = 5.8, 1.6 Hz, 2H), 8.19–8.17 (m, 4H), 7.99 (br d, 3J = 4.8 Hz, 4H), 7.83–7.76 (m, 6H) 7.61 (br d, 3J = 5.1 Hz, 3H), 7.46–7.43 (m, 3H), –1.99 (s, 1H, exchangeable with D_2O) ppm; ^{13}C NMR (100 MHz, CDCl_3): δ 159.3, 158.9, 152.8, 147.5, 145.9, 142.7, 142.2, 141.0, 140.9, 140.4, 139.5, 139.3, 137.8, 136.5, 136.4, 135.8, 135.1, 134.9, 134.8, 131.5, 130.9, 129.8, 129.5, 128.6, 128.5, 128.4, 128.3, 127.4, 127.3, 127.2, 123.5, 121.7, 121.6, 119.4 ppm; UV-vis (CH_2Cl_2) λ_{max} (log ϵ) 431 (5.07), 538 (3.93), 528 (3.45), 630 (3.51), 683 (4.07) nm, UV-vis (CH_2Cl_2 + 10 % TFA) λ_{max} (log ϵ) 463 (5.14), 728 (4.37) nm; HR-MS (ESI⁺, cone voltage = 30 V, 100% CH_3CN , TOF) m/z calcd for $\text{C}_{48}\text{H}_{33}\text{N}_6$ 693.2767 ($[\text{M}]^+$), found 693.2816.

meso-Tetraphenyl-2-aza-3-diethylamino)-porphyrin (14). To a 25 ml round bottom flask equipped with magnetic stir bar was added triflate **12** (40.1 mg, 0.0525 mmol), sodium carbonate (13.8 mg, 0.1302 mmol), diethylamine (0.10 mL) and CH_2Cl_2 (5 mL). The mixture was stirred at room temperature for 20 h. After the starting material was consumed, the solvent and excess diethylamine were evaporated and the product was purified by column chromatography

(silica-CH₂Cl₂/1% MeOH) to obtain **14** as a yellow/brown solid in 87% yield (31.5 mg): *R_f* (silica-CH₂Cl₂/5% MeOH) = 0.75; ¹H NMR (500 MHz, CDCl₃): δ 8.91 (d, ³*J* = 4.9 Hz, 1H), 8.78 (d, ³*J* = 4.9 Hz, 1H), 8.75 (d, ³*J* = 4.9 Hz, 1H), 8.70 (d, ³*J* = 4.9 Hz, 1H), 8.62 (d, ³*J* = 4.56 Hz, 1H), 8.61 (d, ³*J* = 4.56 Hz, 1H), 8.34-8.31 (m, 4H), 8.23-8.20 (m, 4H), 7.79-7.73 (m, 10H), 7.71-7.68 (m, 2H), 3.48 (q, ³*J* = 7.1 Hz, 4H), 1.01 (t, ³*J* = 7.1 Hz, 6H), -1.90 (broad s, 2H, exchangeable with D₂O) ppm; ¹³C NMR (125 MHz, CDCl₃): δ 171.6, 160.8, 155.8, 154.1, 142.38, 142.25, 142.0, 140.6, 140.2, 139.6, 138.6, 137.6, 136.1, 135.7, 134.85, 134.81, 134.73, 134.1, 133.4, 128.29, 128.25, 128.20, 127.89, 127.79, 127.66, 127.04, 126.97, 126.90, 126.86, 126.81, 126.73, 121.7, 119.6, 117.9, 116.3, 77.2, 46.2, 12.5 ppm; UV-vis (CH₂Cl₂) λ_{max} (log ε) 406 (4.89), 449 (4.95), 538 (4.19), 615 (3.64) 673 (3.16) nm; FT-IR (neat, diamond ATR): ν_{C=O} = 1522.4 cm⁻¹; HR-MS (ESI⁺, 100% CH₃CN, TOF) *m/z* calcd for C₄₇H₃₉N₆ ([M·H]⁺) 687.3236, found 687.3242.

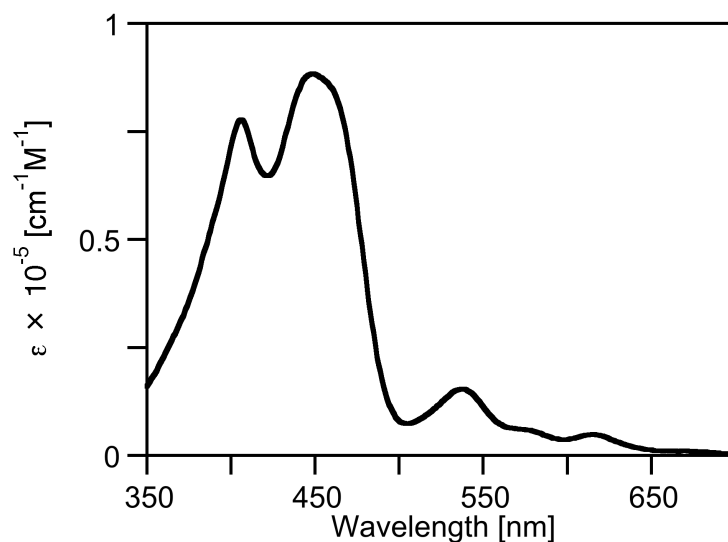
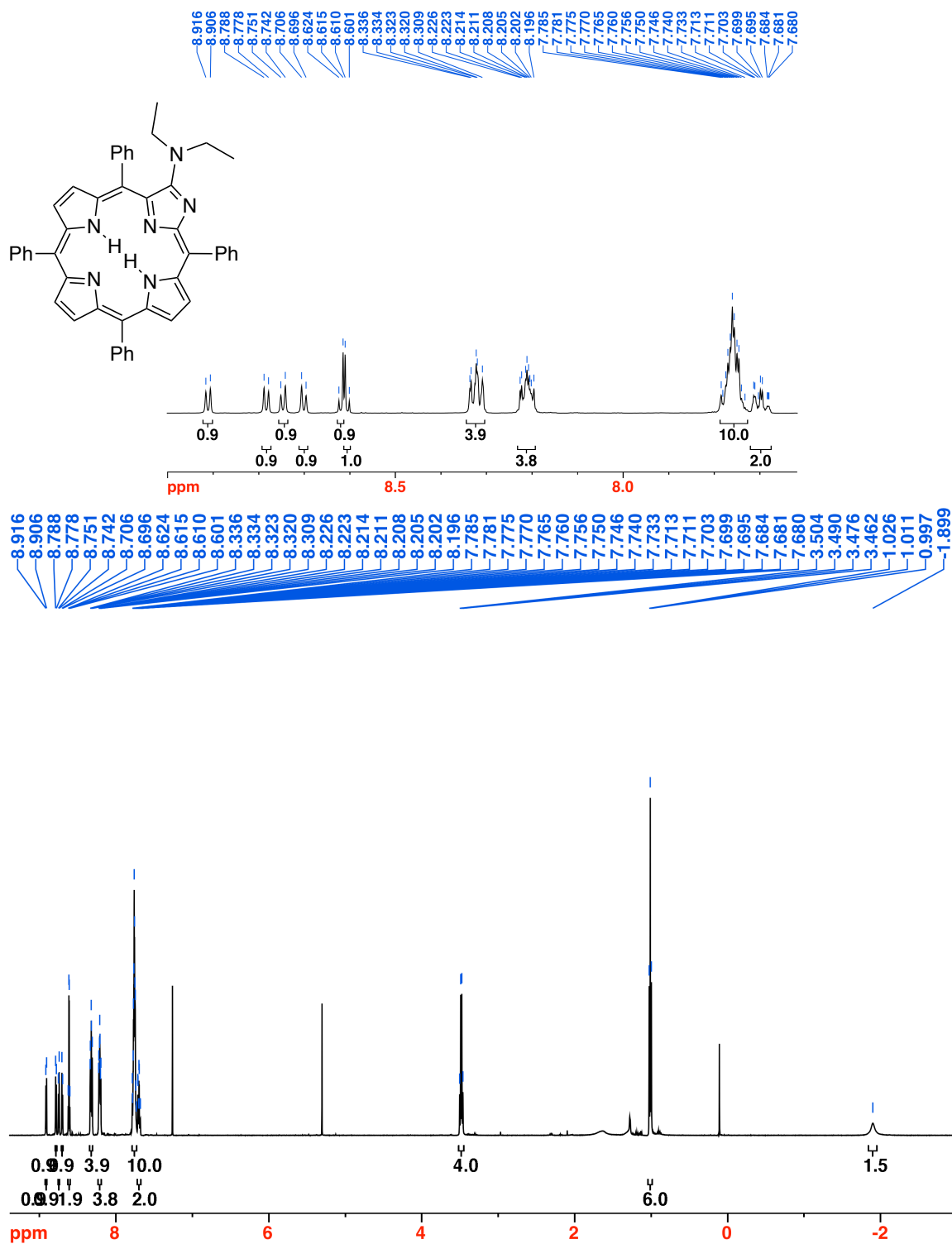


Figure 6-7. UV-vis spectrum (CH₂Cl₂) of **14**.

Figure 6-8. ^1H NMR spectrum (125 MHz, CDCl_3) of **14**.

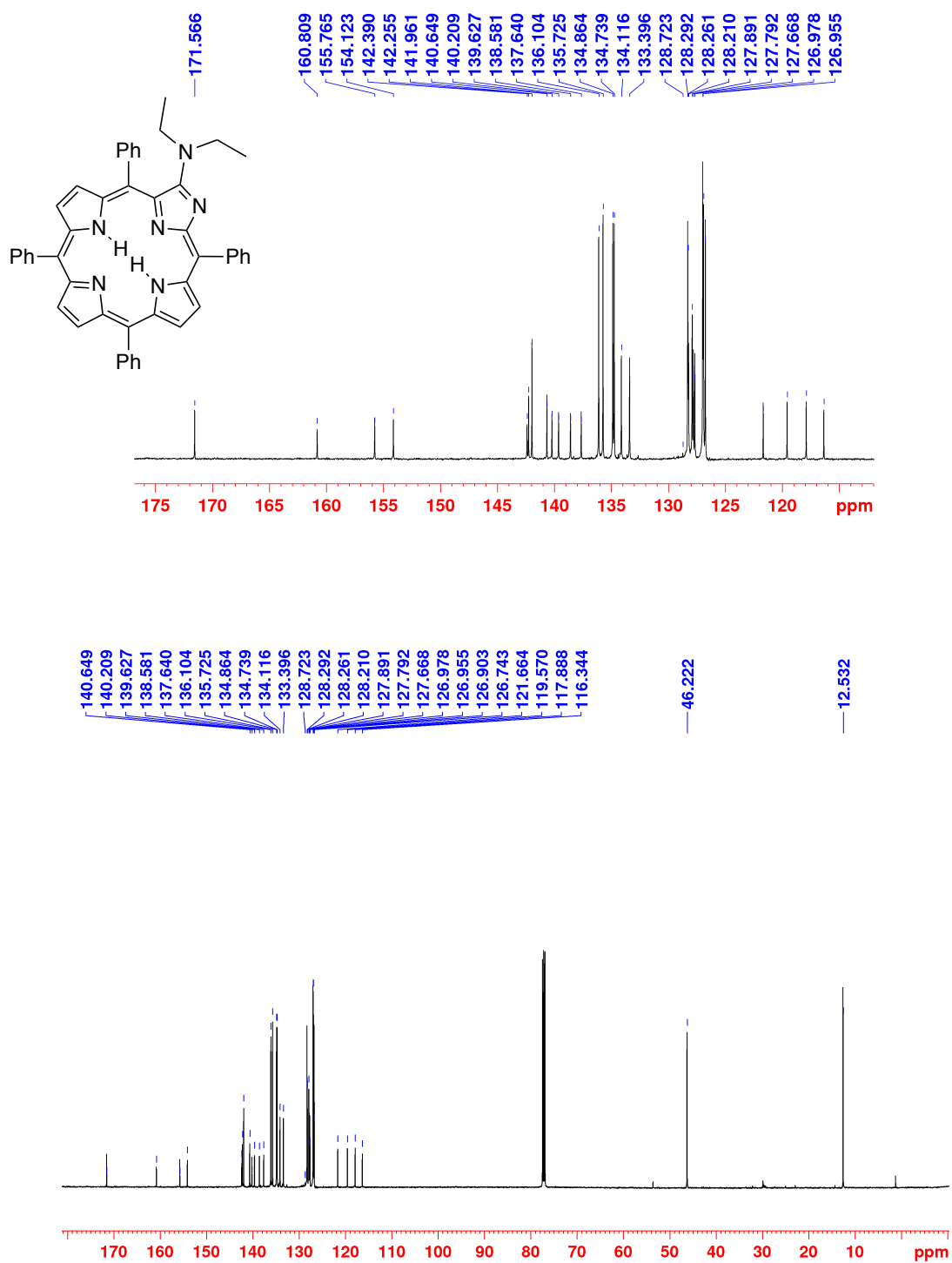


Figure 6-9. ¹³C NMR spectrum (125 MHz, CDCl₃) of 14.

meso-Tetraphenyl-2-aza-3-diethyliminodiacetate)-porphyrin (15). To a 25 ml round bottom flask equipped with magnetic stir bar was added triflate **12** (49.0 mg, 6.4×10^{-5} mol), sodium carbonate (15 mg, 1.4×10^{-4} mol, 2.2 equiv), diethyl iminodiacetate (250 μ l, 1.4 mmol, 21 equiv.) and acetone (8 mL). The mixture was heated to reflux overnight. After 23-27 h, the reaction mixture was evaporated to dryness. Flash column chromatography (silica-CH₂Cl₂/5% MeOH) afforded recovered **12** (10-13 mg, 20-27%) and **15** as a yellow/brown solid (36-39 mg, 70-76%): R_f (silica-CH₂Cl₂/2% MeOH) = 0.63; ¹H NMR (500 MHz, CDCl₃): δ 8.93 (d, ³J = 5.0 Hz, 1H), 8.83 (d, ³J = 4.9 Hz, 1H), 8.75 (two overlapping doublets, ³J = 4.5 Hz, 2H), 8.65 (s, 2H), 8.43 (d, ³J = 7.1 Hz, 2H), 8.24-8.20 (m, 6H), 7.82-7.70 (m, 13H), 4.39 (s, 4H), 4.03 (q, ³J = 7.1 Hz, 4H), 1.16 (t, ³J = 7.1 Hz, 6H), -2.11 (br s, 2H, exchangeable with D₂O) ppm; ¹³C NMR (100 MHz, CDCl₃): δ (ppm) 170.0, 158.6, 156.1, 154.6, 142.2, 141.8, 140.1, 139.9, 139.9, 139.6, 138.9, 138.0, 136.2, 134.9, 134.5, 134.4, 133.8, 133.6, 128.6, 128.5, 128.3, 128.3, 128.0, 127.9, 127.9, 127.7, 127.0, 126.97, 126.9, 126.6, 121.7, 119.9, 118.2, 117.2, 77.4, 77.2, 76.9, 60.7, 54.4, 30.0, 14.2 ppm; UV-vis (CH₂Cl₂) λ_{\max} (log ϵ) 439 (5.07), 532 (4.06), 568 (sh), 610 (3.5), 664 (3.1) nm; FT-IR (neat, diamond ATR); HR-MS (ESI⁺, 100% CH₃CN, TOF) m/z calcd for C₅₁H₄₃N₆O₄ ([M·H]⁺) 803.3346, found 803.3368.

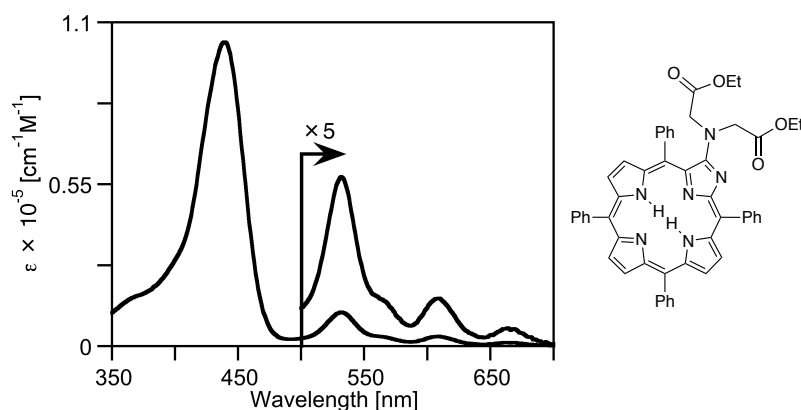
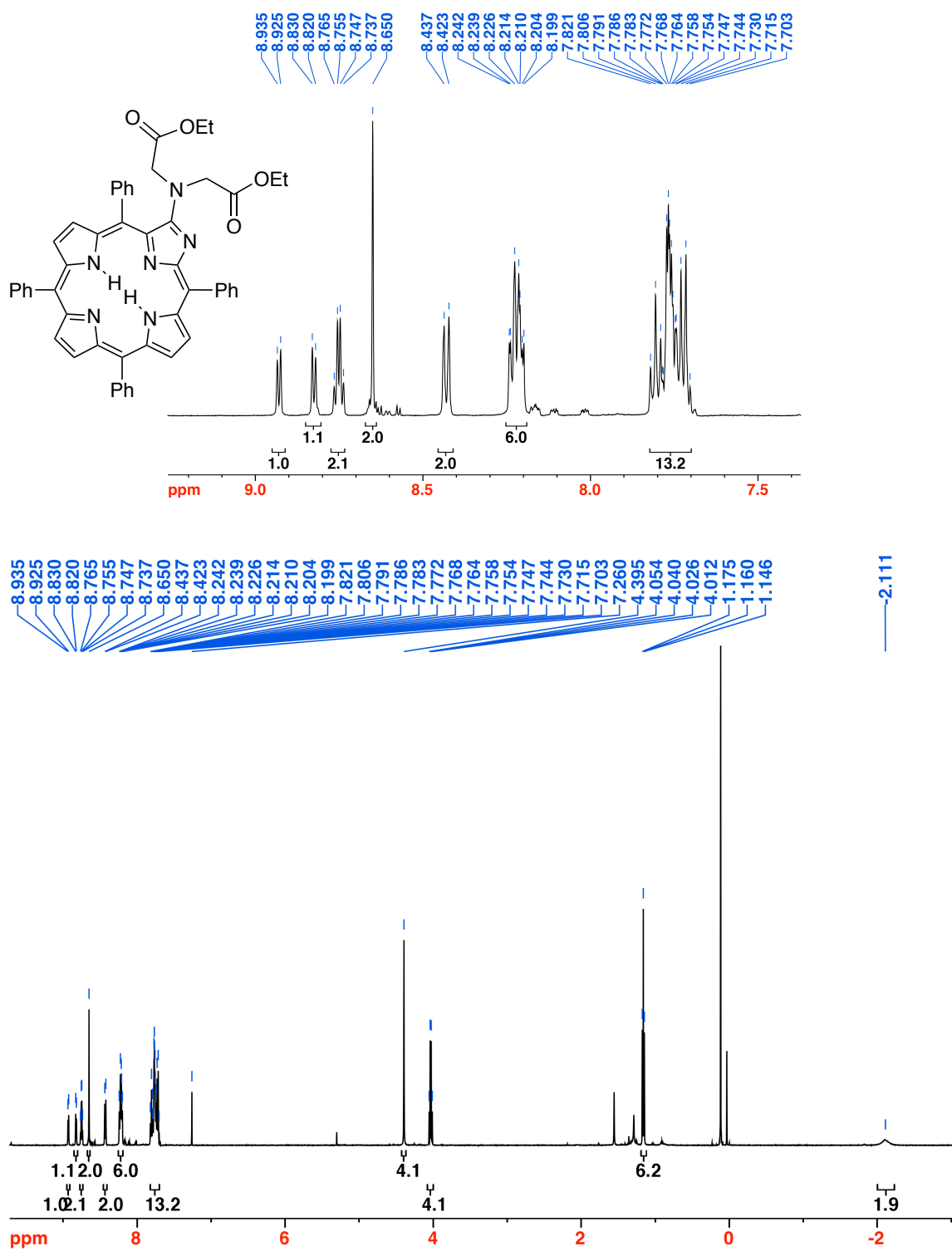


Figure 6-10. UV-vis spectrum (CH₂Cl₂) of **15**.

Figure 6-11. ¹H NMR spectrum (500 MHz, CDCl₃) of **15**.

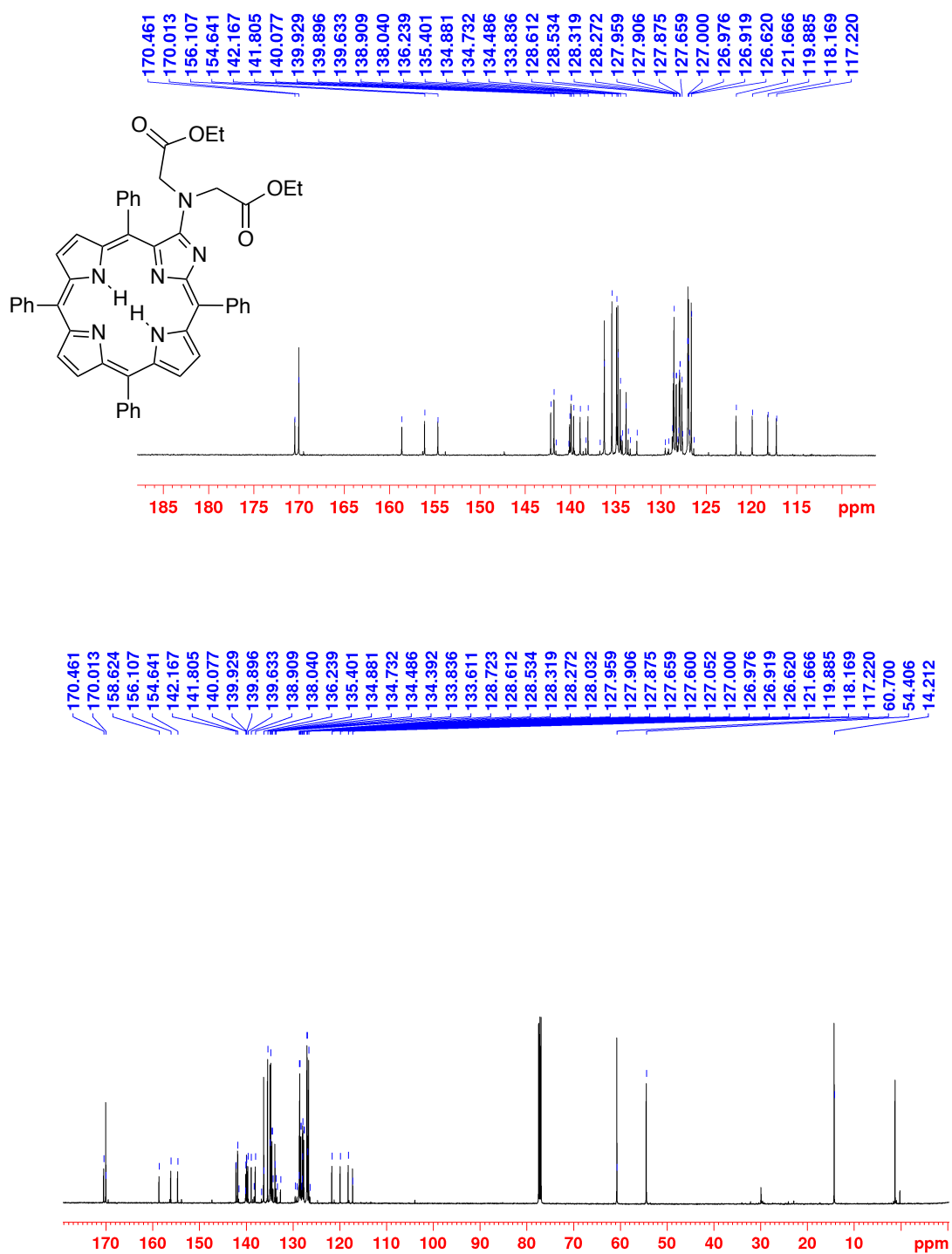


Figure 6-12. ^{13}C NMR spectrum (125 MHz, CDCl_3) of 15.

meso-Tetraphenyl-2-aza-3-dicarboxylamino-porphyrin (16). Diester **15** (35.0 mg, 4.3×10^{-5} mol) was dissolved in THF (10.0 mL) in a round bottom flask equipped with a magnetic stir bar and stirred for 5 minutes. 1M aqueous KOH (10.0 mL) was added and the reaction mixture was heated to reflux for 2 h. After the starting material was consumed (reaction control by TLC), the reaction mixture was allowed to cool and as much THF as possible was removed by rotary evaporation. 1M aqueous HCl was added to neutralize the aqueous phase, and the aqueous phase was extracted with CH_2Cl_2 (4×20.0 mL). The organic extracts were combined and evaporated to dryness. The remaining residue was purified by column chromatography (silica- CH_2Cl_2 /10% MeOH) to afford **16** as a yellow/brown solid in 80 % yield (26 mg): ^1H NMR (400 MHz, CD_2Cl_2 /10% MeOD): δ 8.92 (d, $^3J = 5.0$ Hz, 1H), 8.90 (d, $^3J = 5.0$ Hz, 1H), 8.87 (d, $^3J = 5.0$ Hz, 1H), 8.80 (d, $^3J = 5.0$ Hz, 1H), 8.65 (s, 2H), 8.32 (d, $^3J = 7.1$ Hz, 2H), 8.21-8.17 (m, 6H), 7.88 (t, $^3J = 7.4$ Hz, 2H), 7.83-7.77 (m, 10H), 3.97 (s, 4H) ppm; ^{13}C NMR (125 MHz, CD_2Cl_2 /10% MeOD): δ 171.9, 169.2, 157.0, 155.4, 153.8, 141.5, 141.0, 140.2, 139.41, 139.32, 138.8, 137.6, 135.5, 134.9, 134.67, 134.57, 134.2, 128.97, 128.79, 128.3, 128.02, 127.92, 127.3, 126.96, 126.86, 122.2, 120.4, 119.5, 115.7, 56.7 ppm; UV-vis (MeOH) λ_{max} (log ϵ) 442 (4.86), 534 (3.92), 571 (sh), 612 (3.51), 676 (3.0) nm; FT-IR (neat, diamond ATR): $\nu = 1603.5\text{ cm}^{-1}$, 1216.0 cm^{-1} , 1151.7 cm^{-1} , 796.0 cm^{-1} , 752.3 cm^{-1} , 698.5 cm^{-1} ; MS (ESI $^+$, 100% CH_3CN , TOF) m/z calcd for $\text{C}_{47}\text{H}_{35}\text{N}_6\text{O}_4$ ([MH] $^+$) 747.268, found 747.439.

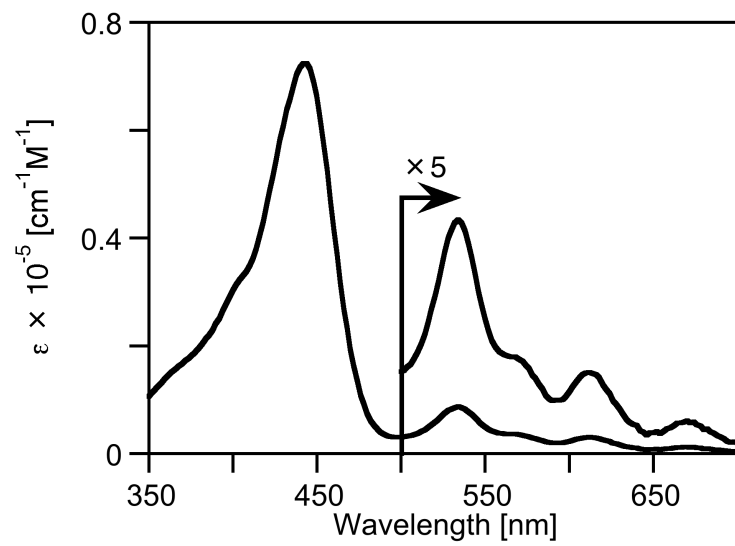


Figure 6-13. UV-vis spectrum (MeOH) of **16**.

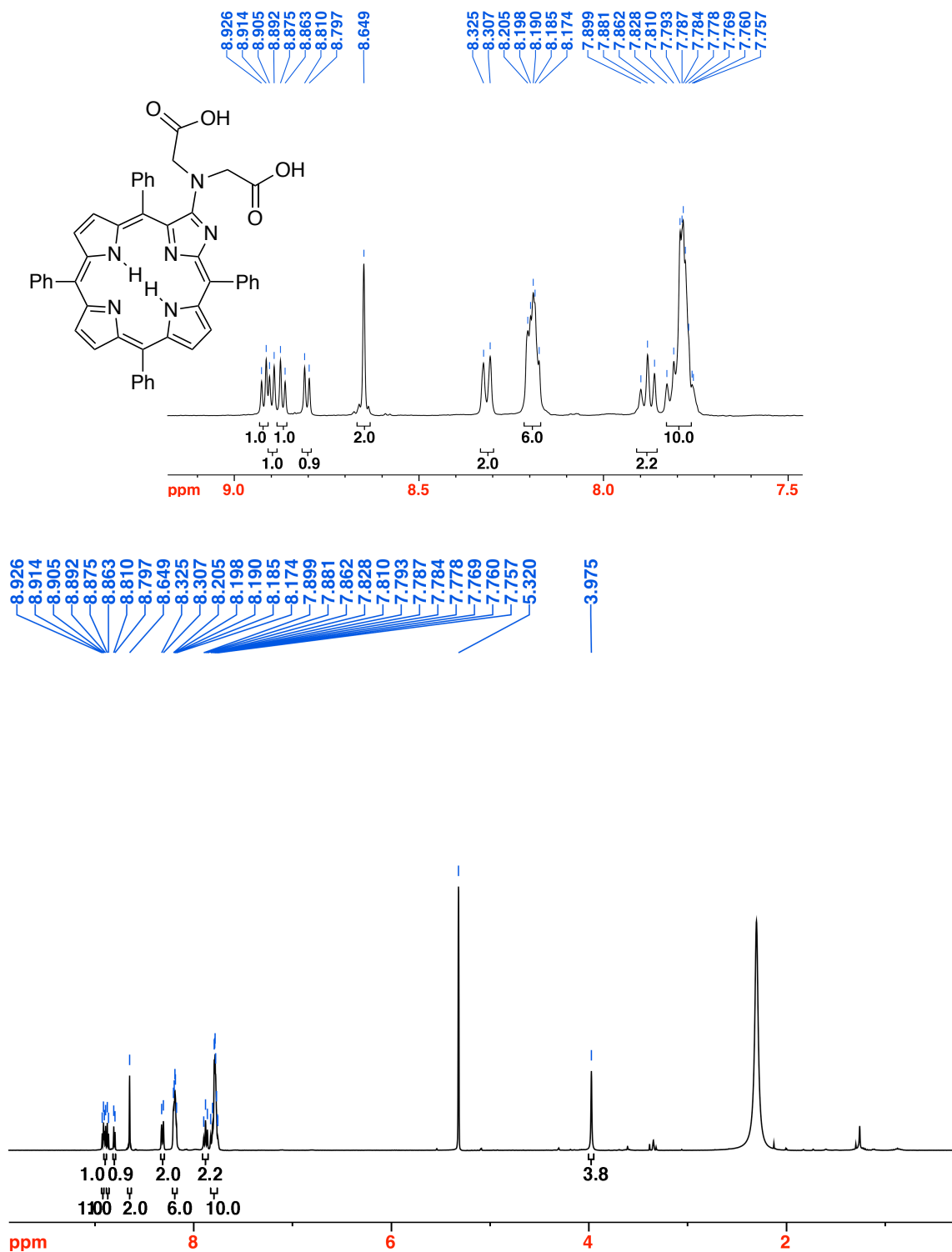


Figure 6-14. ^1H NMR spectrum (400 MHz, $\text{CD}_2\text{Cl}_2/10\%$ MeOD) of 16.

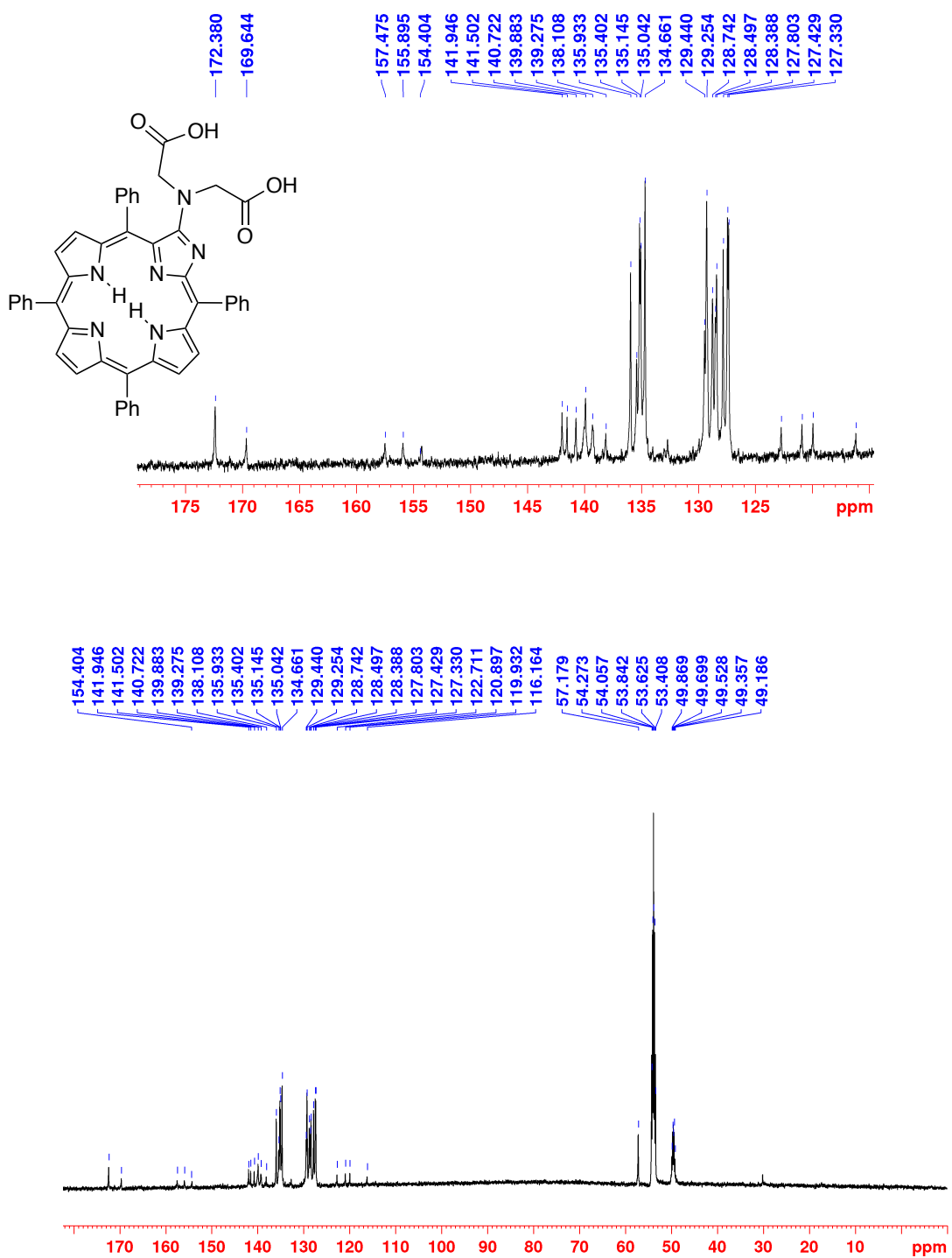


Figure 6-15. ^{13}C NMR spectrum (125 MHz, $\text{CD}_2\text{Cl}_2/10\%$ MeOH) of **16**.

DPA-substituted Imidazoloporphyrin (17). To a round-bottom flask equipped with a magnetic stir bar under N₂ was added triflate-imidazole **12** (31 mg, 4.1×10^{-5} mol), Di-(2-picolyl)amine (365 μ l, 2×10^{-3} mol, 50 equiv), Na₂CO₃ (17.0 mg, 1.6×10^{-4} , 4 equiv) and CH₂Cl₂ (10 mL). The reaction mixture was stirred for 24 h. When the starting material was consumed (reaction control by TLC), the reaction mixture was filtered through a glass frit and the filtrate washed with water (3 \times 20.0 mL). The organic layer was dried over Na₂SO₄ and the residue was purified by preparative TLC (silica-CH₂Cl₂/10% MeOH) to afford DPA-substituted imidazoloporphyrin **17** as a yellow/brown solid in 76 % yield (25 mg): *R*_f (silica-CH₂Cl₂/10% MeOH) = 0.41; ¹H NMR (400 MHz, CDCl₃): δ 8.91 (d, ³*J* = 5.0 Hz, 1H), 8.80 (d, ³*J* = 5.0 Hz, 1H), 8.72 (d, ³*J* = 4.7 Hz, 1H), 8.69 (d, ³*J* = 4.9 Hz, 1H), 8.62-8.60 (m, 2H), 8.43 (s, 2H), 8.26 (d, ³*J* = 6.7 Hz, 2H), 8.19 (dd, ³*J* = 7.2, ⁴*J* = 2.0 Hz, 6H), 7.76-7.67 (m, 12H), 7.38 (td, ³*J* = 7.7, ⁴*J* = 1.6 Hz, 2H), 7.12 (d, ³*J* = 7.8 Hz, 2H), 7.03 (dd, ³*J* = 7.0, ⁴*J* = 5.3 Hz, 2H), 4.77 (s, 4H), -2.03 (s, 2H) ppm; ¹³C NMR (125 MHz, CDCl₃): δ 171.3, 158.1, 156.1, 154.5, 149.0, 142.1, 141.84, 141.78, 140.3, 139.9, 139.7, 138.8, 137.9, 136.19, 136.03, 135.3, 134.87, 134.71, 134.4, 133.7, 128.51, 128.42, 128.31, 128.26, 127.95, 127.88, 127.5, 127.10, 127.02, 126.97, 126.91, 126.76, 123.6, 122.0, 121.8, 119.8, 118.2, 116.7, 77.4, 77.2, 76.9, 58.8 ppm; UV-vis (CH₂Cl₂) λ_{\max} (log ϵ) 403 (sh), 449 (5.17), 542 (4.07), 588 (3.77), 618 (3.71), 681 (3.66) nm, UV-vis (CH₂Cl₂ + 10% TFA) λ_{\max} (log ϵ) 473 (5.15), 629 (sh), 680 (4.40) nm; FI (DMF, $\lambda_{\text{excitation}}$ = Soret) λ_{\max} 693, 750 nm, ϕ_F (DMF) = 0.01; FT-IR (neat, diamond ATR); HR-MS (ESI⁺, 100% CH₃CN, TOF) *m/z* calcd for C₅₅H₄₁N₈ ([M·H]⁺) 813.3454, found 813.3485.

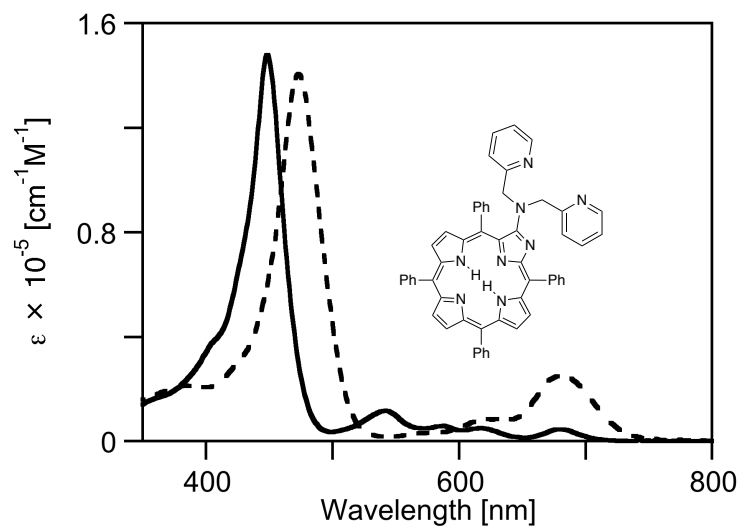
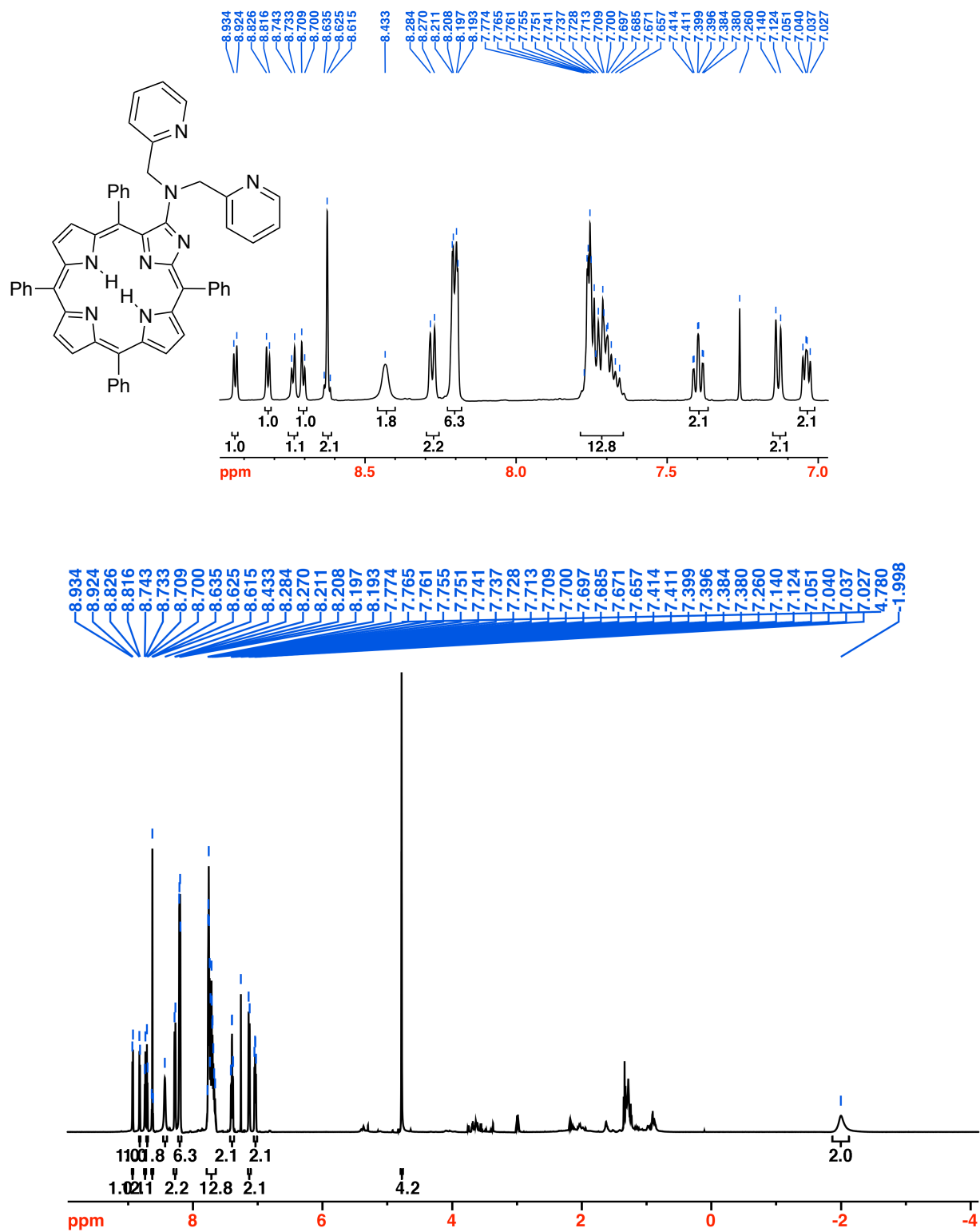


Figure 6-16. UV-vis spectrum of **17** in CH_2Cl_2 (solid trace) and $\text{CH}_2\text{Cl}_2 + 10\% \text{ TFA}$ (broken trace).

Figure 6-17. ^1H NMR (125 MHz, CDCl_3) of 17.

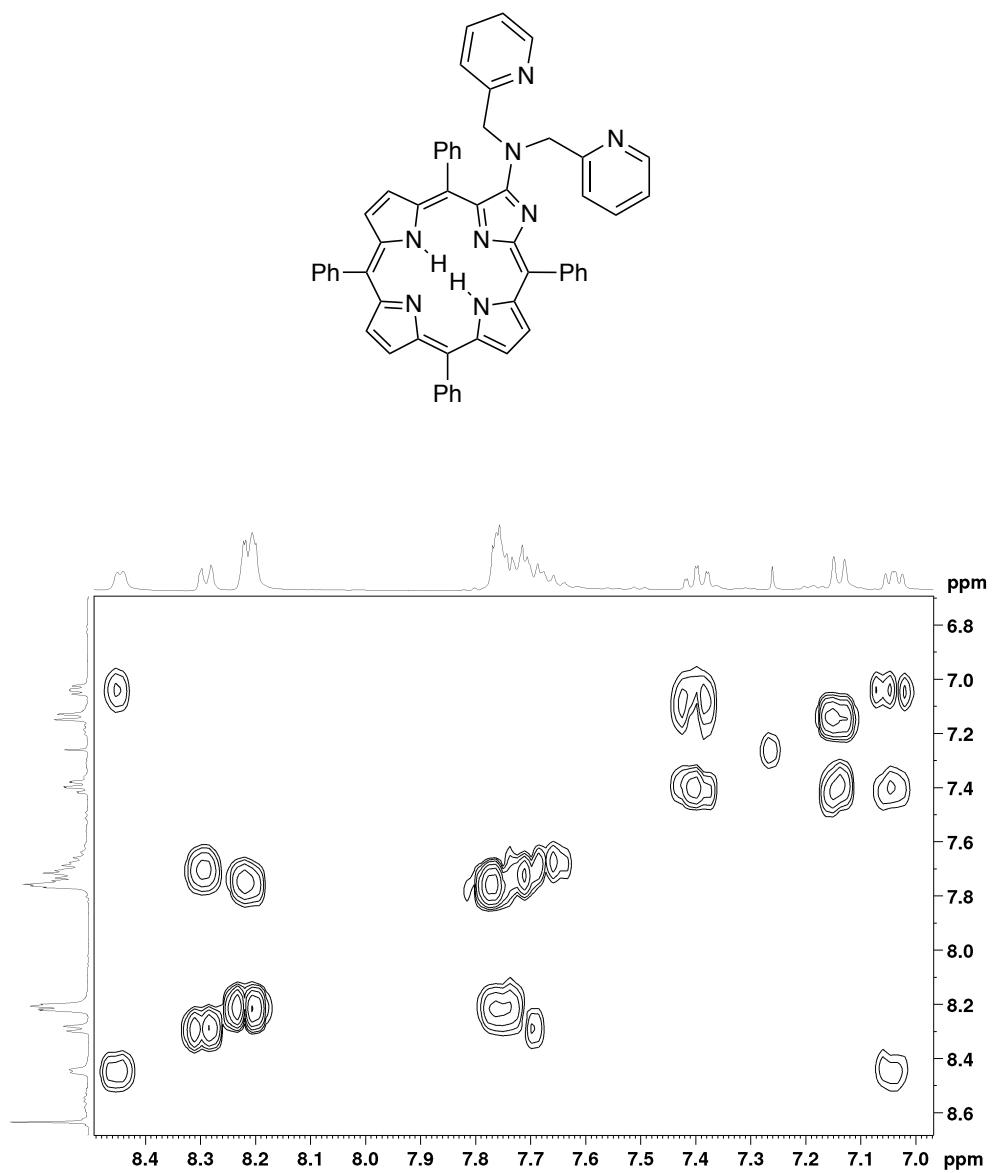


Figure 6-18. Partial H-H COSY spectrum (CDCl₃) of 17.

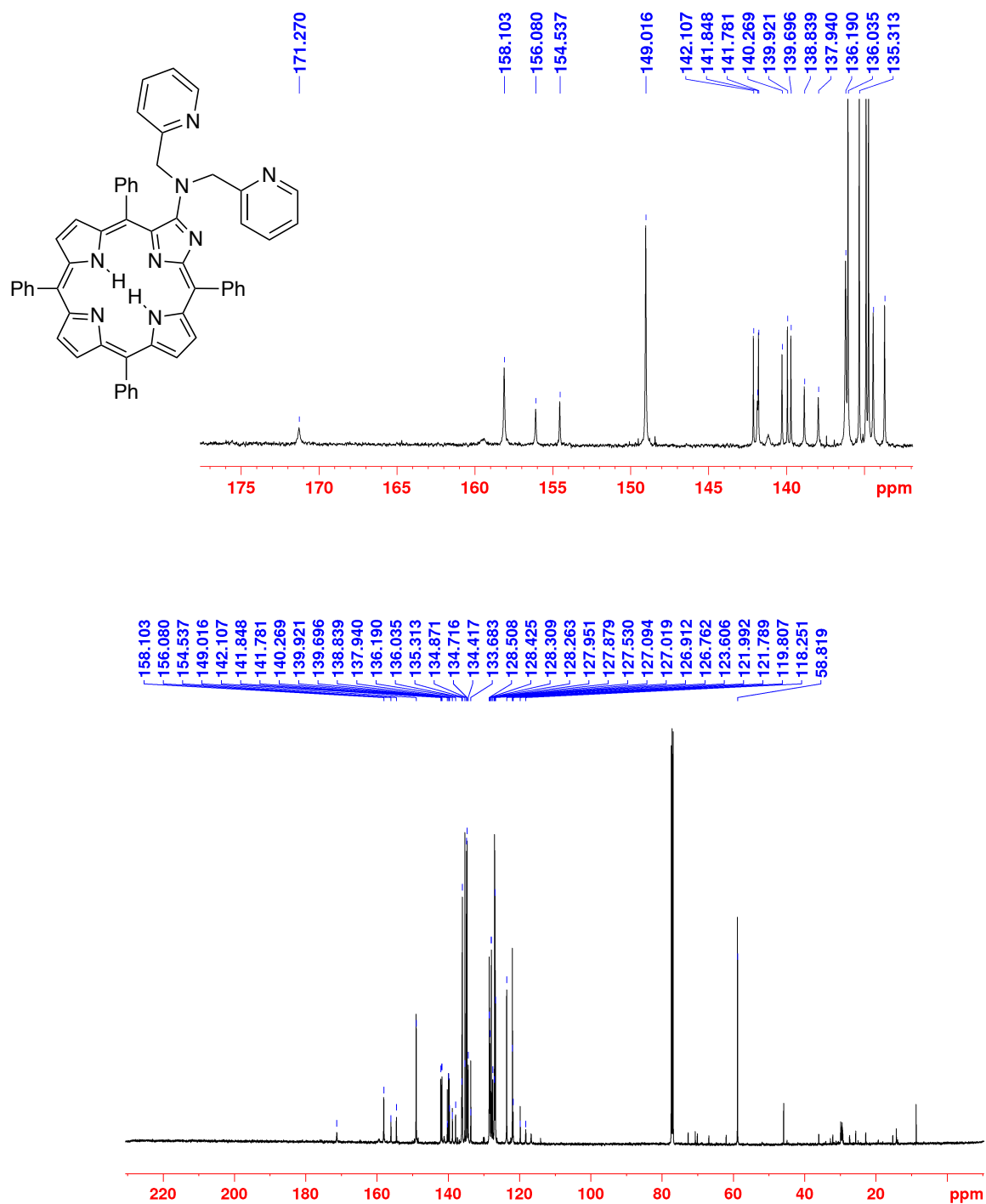


Figure 6-19. ¹³C NMR (125 MHz, CDCl₃) of 17.

Cyclen-substituted Imidazoloporphyrin (18). To a round-bottom flask equipped with a magnetic stir bar was added cyclen (7.0 mg, 4.1×10^{-5} mol, 1.6 equiv), Na_2CO_3 (11.0 mg, 1.0×10^{-4} mol, 4 equiv) and CH_2Cl_2 (3.0 mL). A solution of triflate-imidazole **12** (20.0 mg, 2.6×10^{-5} mol) in CH_2Cl_2 was added to the stirred solution under N_2 . The reaction mixture was stirred at r.t. for 2h. The reaction mixture was filtered through a glass frit and the filtrate was washed with H_2O (2×10.0 mL), brine, and dried over Na_2SO_4 . The remaining residue was purified by preparative TLC (silica- CH_2Cl_2 /10% MeOH) to afford recovered **12** (2.0 mg, 10 %), **18** (13.0 mg, 62 %), and **19** (6 mg, 16 %): (**18**) R_f (silica- CH_2Cl_2 /10% MeOH) = 0.09; ^1H NMR (500 MHz, CDCl_3): δ 8.91 (d, 3J = 5.0 Hz, 1H), 8.86 (two overlapping d, 3J = 4.1 Hz, 2H), 8.78 (d, 3J = 4.9 Hz, 1H), 8.65 (d, 3J = 4.6 Hz, 1H), 8.63 (d, 3J = 4.6 Hz, 1H), 8.27 (two overlapping d, 3J = 7.5, 7.0 Hz, 4H), 8.21-8.17 (m, 4H), 7.84 (td, 3J = 7.4, 4J = 3.4 Hz, 4H), 7.80-7.75 (m, 8H), 3.47 (s, 4H), 2.80 (s, 4H), 2.46 (s, 4H), 2.22 (s, 4H), -2.14 (s, 1H, exchangeable with D_2O), -2.24 (s, 1H, exchangeable with D_2O) ppm; ^{13}C NMR (125 MHz, CDCl_3): δ 170.5, 156.9, 155.4, 142.3, 141.8, 141.4, 140.24, 140.16, 139.49, 139.43, 139.31, 138.7, 135.4, 135.14, 135.07, 134.86, 134.79, 134.72, 134.68, 134.63, 134.3, 129.0, 128.78, 128.73, 128.66, 128.57, 128.42, 128.35, 128.28, 128.20, 128.11, 127.9, 127.5, 127.13, 127.03, 126.94, 122.4, 121.9, 120.3, 119.36, 119.29, 116.0, 51.0, 47.3, 44.0 ppm; UV-vis (CH_2Cl_2) λ_{max} (log ϵ) 438 (5.0), 533 (4.0), 570 (sh), 610 (3.54), 670 (3.58) nm, UV-vis (CH_2Cl_2 + 10% TFA) λ_{max} (log ϵ) 470 (4.9), 624 (sh), 682 (4.27) nm; FI (DMF, $\lambda_{\text{excitation}}$ = Soret) λ_{max} 678, 739 nm, ϕ_F (DMF) = 0.02; FT-IR (neat, diamond ATR); HR-MS (ESI $^+$, 100% CH_3CN , TOF) m/z calcd for $\text{C}_{51}\text{H}_{48}\text{N}_9$ ($[\text{M}\cdot\text{H}]^+$) 786.4033, found 786.4061. (**19**) R_f (silica- CH_2Cl_2) = 0.45; ^1H NMR (400 MHz, CDCl_3): δ 8.82 (d, 3J = 4.9 Hz, 1H), 8.79 (d, 3J = 4.9 Hz, 1H), 8.70 (d, 3J = 4.6 Hz, 1H), 8.67 (d, 3J = 4.6 Hz, 1H), 8.42 (d, 3J = 5.0 Hz, 1H), 8.24 (d, 3J = 6.4 Hz, 2H), 8.15 (t, 3J = 8.6 Hz, 5H), 7.85-7.74 (m, 8H), 7.59-7.54 (m, 3H), 6.40 (s, 1H), 5.88 (s, 1H), 3.36 (s, 4H), 2.61 (s, 4H), -1.92 (s, 1H, exchangeable with D_2O), -2.36 (s, 1H, exchangeable with D_2O) ppm; ^{13}C NMR (125 MHz, CDCl_3): δ 170.2, 157.6, 156.8, 155.0, 142.0,

141.5, 140.7, 140.4, 139.4, 139.0, 138.7, 138.4, 135.04, 134.98, 134.7, 134.38, 134.23, 132.9, 129.0, 128.66, 128.47, 128.36, 128.22, 128.13, 128.03, 127.94, 127.35, 127.31, 127.21, 127.13, 127.08, 126.99, 126.92, 125.9, 125.13, 125.05, 122.3, 119.8, 118.6, 115.6, 77.2, 50.4, 48.3 ppm; UV-vis (CH_2Cl_2) λ_{max} (log ϵ) 404 (sh), 438 (5.14), 570 (sh), 534 (4.29), 608 (3.86), 665 (3.58) nm, UV-vis (CH_2Cl_2 + 10% TFA) λ_{max} (log ϵ) 470 (5.18), 495 (sh), 570 (sh), 622 (sh), 679 (4.59) nm; FI (DMF, $\lambda_{\text{excitation}}$ = Soret) λ_{max} 684, 743 nm, ϕ_{F} (DMF) = 0.01; FT-IR (neat, diamond ATR); HR-MS (ESI⁺, 100% CH_3CN , TOF) m/z calcd for $\text{C}_{94}\text{H}_{75}\text{N}_{14}$ ($[\text{M}\cdot\text{H}]^+$) 1400.6330, found 1400.6337.

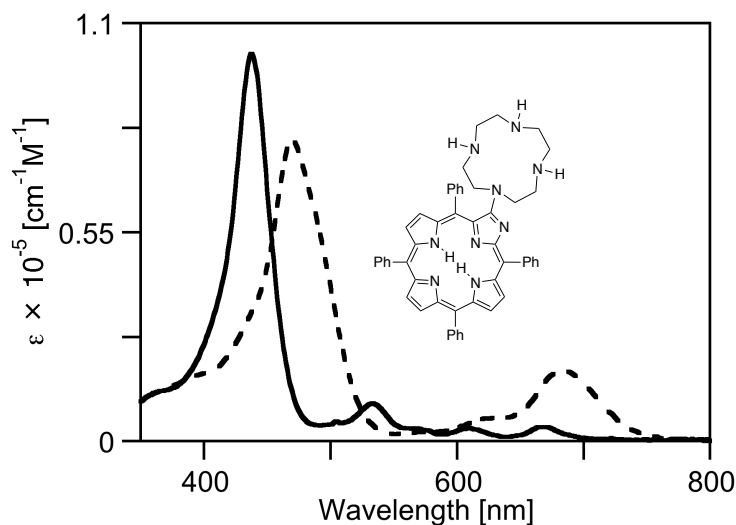
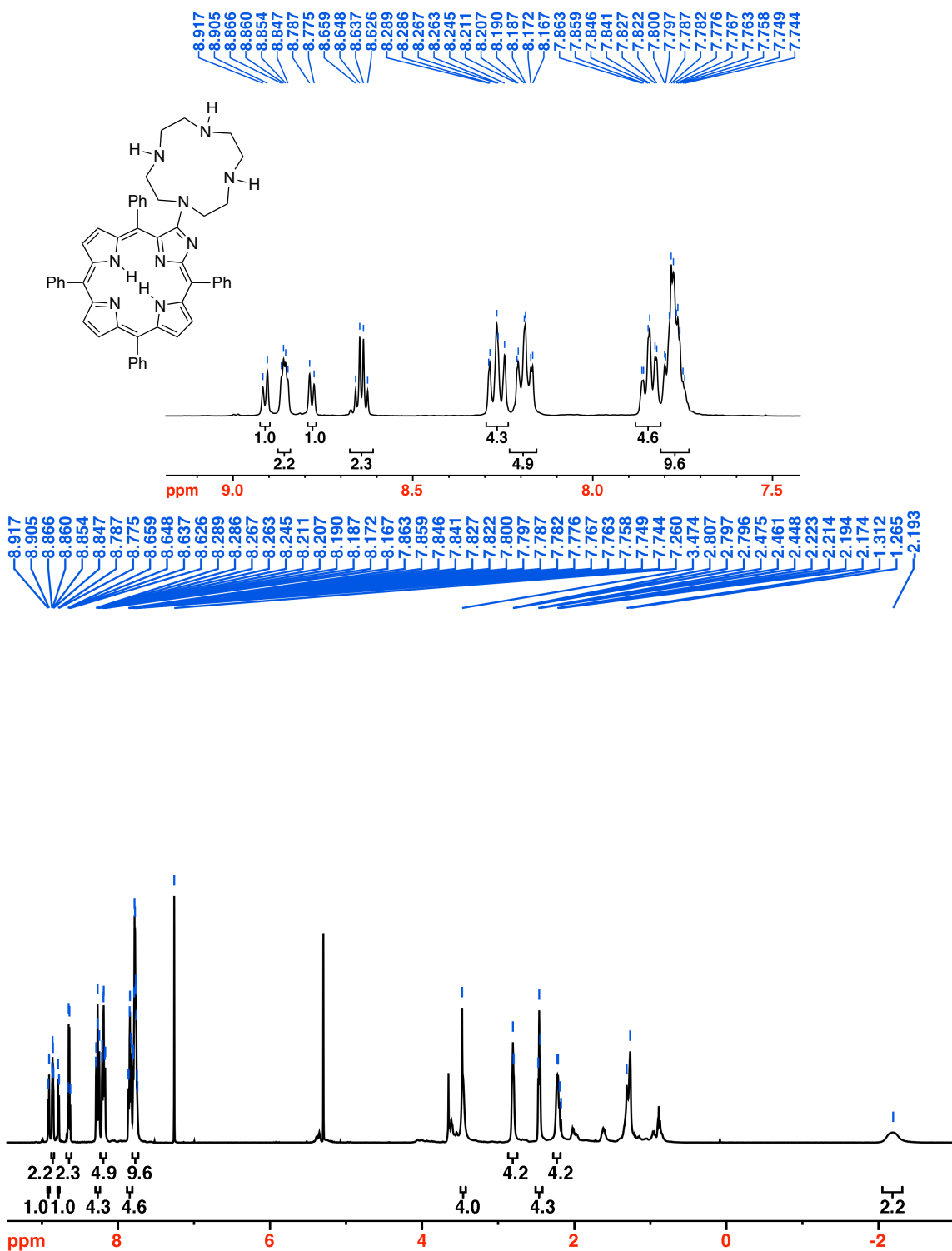


Figure 6-20. UV-vis spectrum of **18** in CH_2Cl_2 (solid trace) and CH_2Cl_2 + 10% TFA (broken trace).

Figure 6-21. ^1H NMR spectrum (500 MHz, CDCl_3) of **18**.

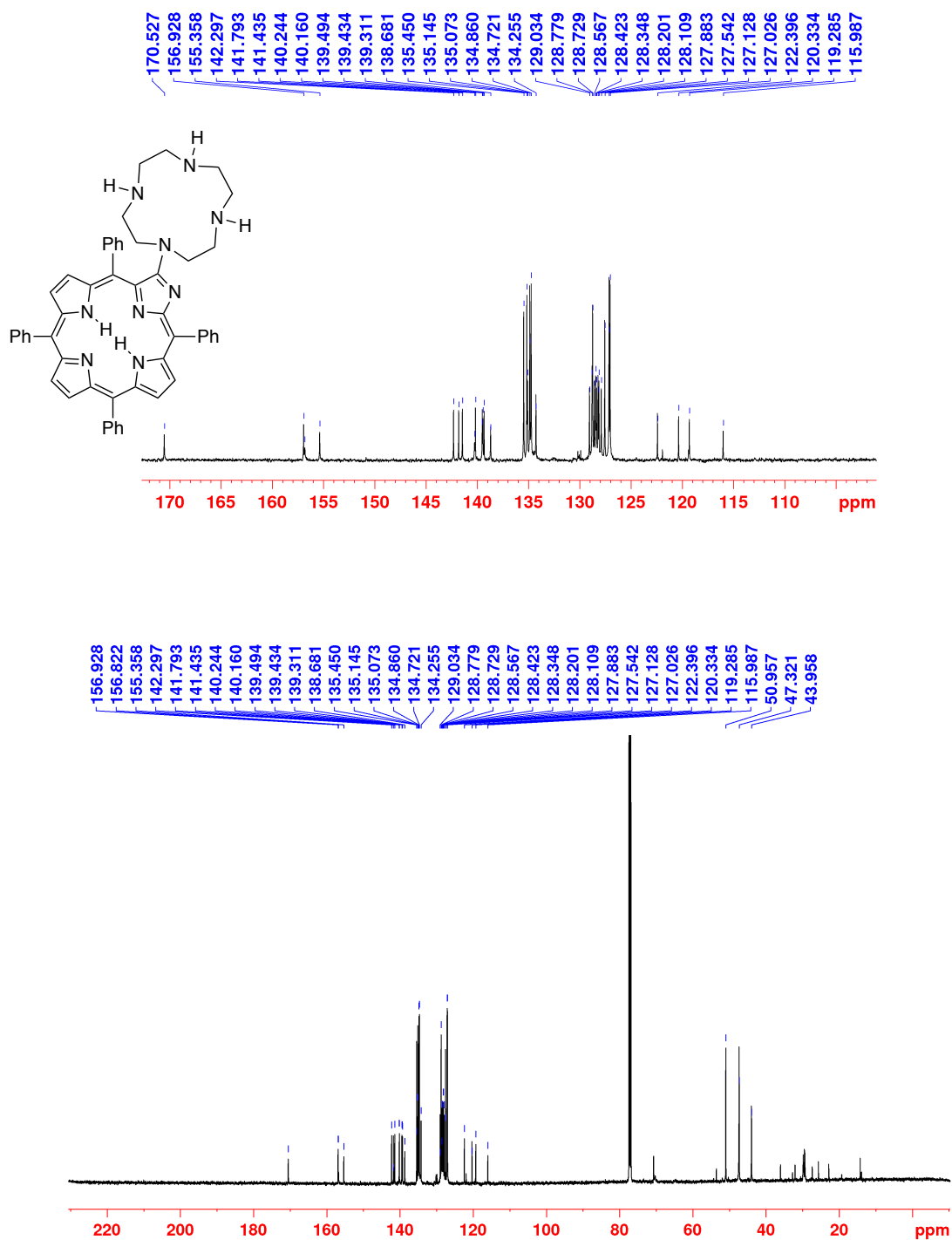


Figure 6-22. ^{13}C NMR spectrum (125 MHz, CDCl_3) of **18**.

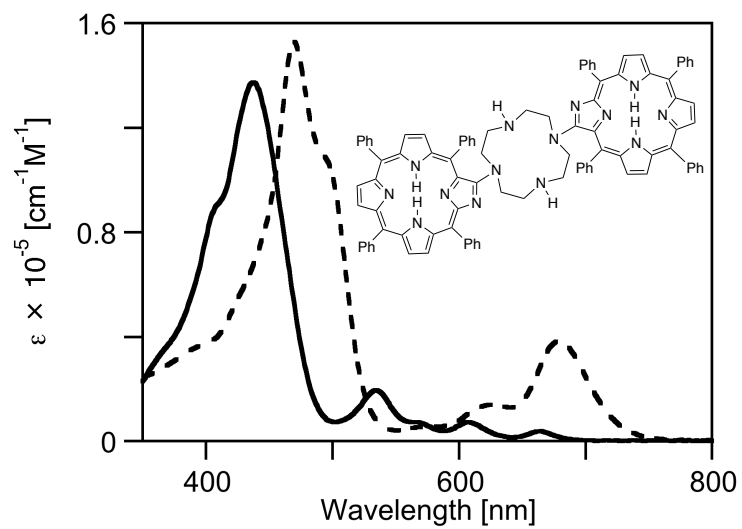


Figure 6-23. UV-vis spectrum of **19** in CH₂Cl₂ (solid trace) and CH₂Cl₂ + 10% TFA (broken trace).

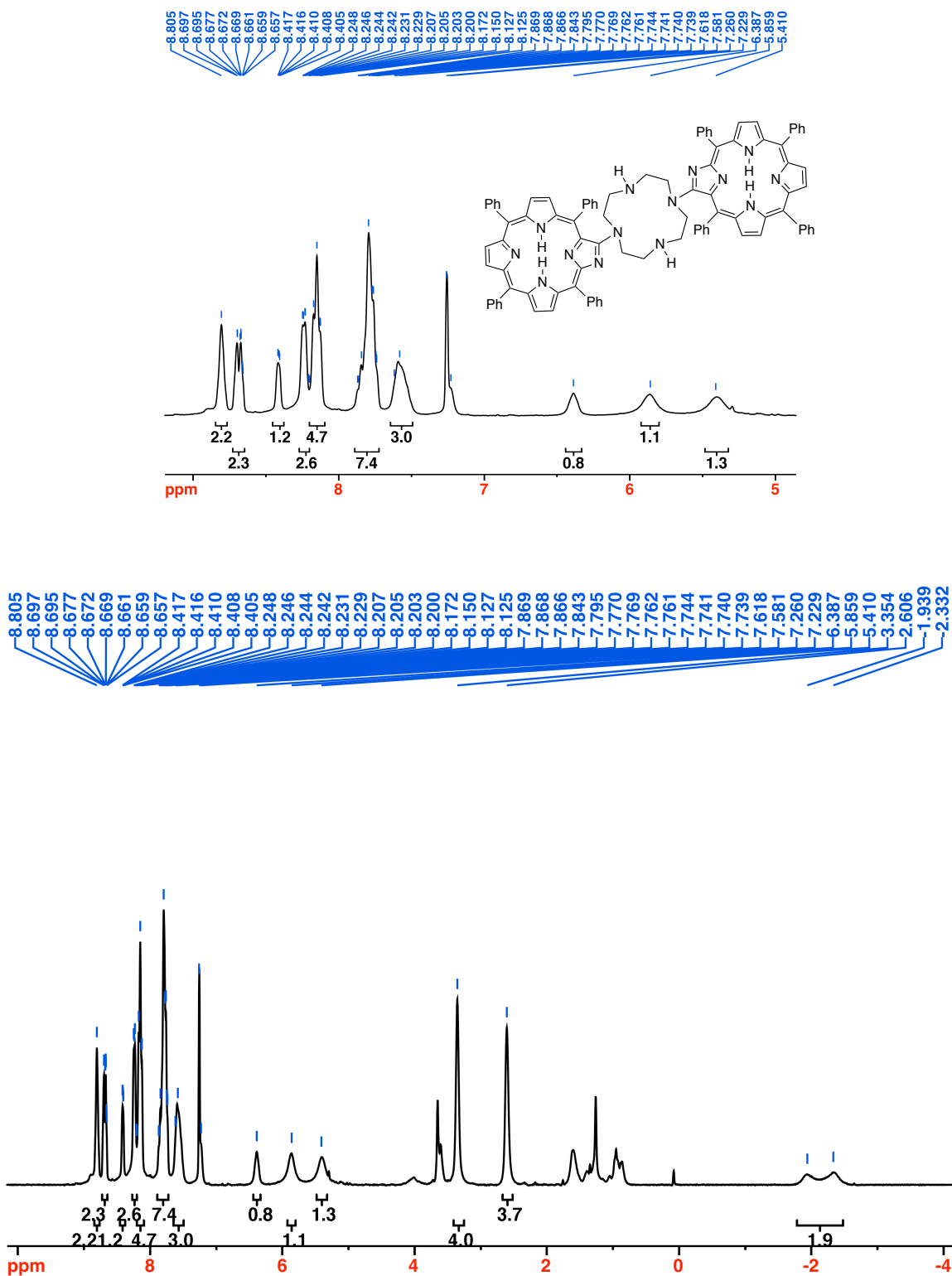


Figure 6-24. ^1H NMR spectrum (125 MHz, CDCl_3) of **19**.

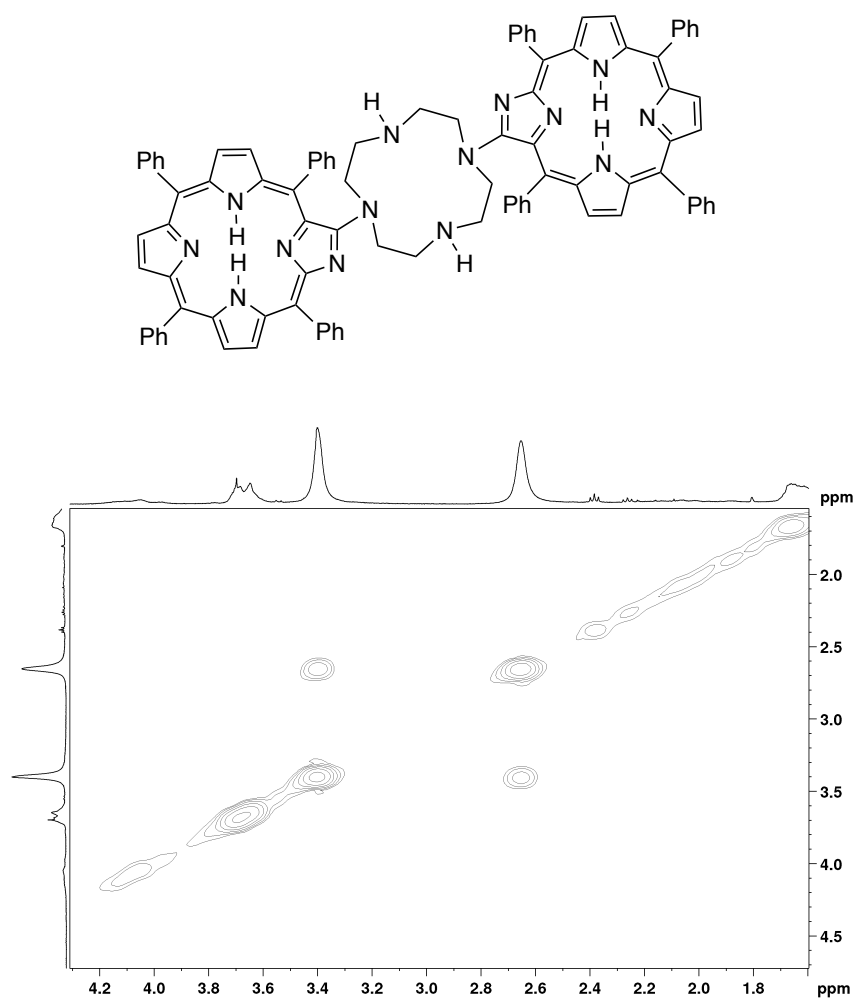


Figure 6-25. Partial ^1H - ^1H COSY spectrum (CDCl_3) of **19**.

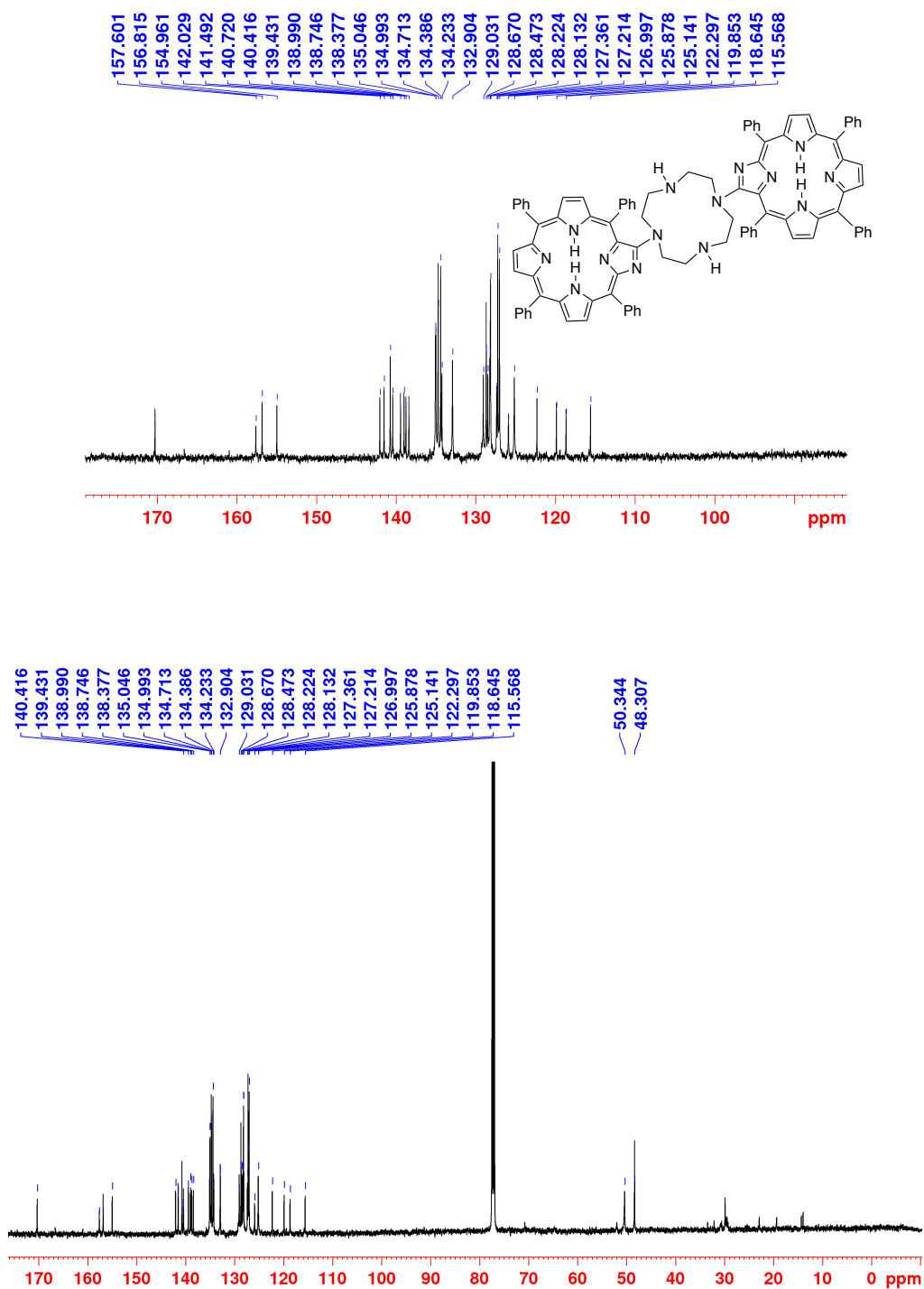


Figure 6-26. ^{13}C NMR (125 MHz, CDCl_3) of **19**.

6.4 References

- (1) a) Brückner, C.; Samankumara, L.; Ogikubo, J. In *Handbook of Porphyrin Science*; Kadish, K. M., Smith, K. M., Guillard, R., Eds.; World Scientific: River Edge, NY, 2012; Vol. 17, Chapter 76. b) Taniguchi, M.; Lindsey, J. S. *Chem. Rev.* **2017**, *117*, 344–535; c) Lindsey, J. S. *Chem. Rev.* **2015**, *115*, 6534.
- (2) a) Bonnett, R. *Chem. Soc. Rev.* **1995**, *24*, 19; b) Pandey, R. K.; Zheng, G. In *The Porphyrin Handbook*; Kadish, K. M., Smith, K. M., Guillard, R., Eds.; Academic Press: San Diego, 2000; Vol. 6, p 157; c) Brandis, A. S.; Salomon, Y.; Scherz, A. In *Chlorophylls and Bacteriochlorophylls*; Grimm, B., Porra, R. J., Rüdinger, W., Scheer, H., Eds.; Springer: Dordrecht, NL, 2006, p 485; d) de Haas, R. R.; van Gijlswijk, R. P. M.; van der Tol, E. B.; Zijlmans, H. J. M. A. A.; Bakker-Schut, T.; Bonnet, J.; Verwoerd, N. P.; Tanke, H. J. *J. Histochem. Cytochem.* **1997**, *45*, 1279; e) Schäferling, M. *Angew. Chem. Int. Ed.* **2012**, *51*, 3532; f) Huang, H.; Song, W.; Rieffel, J.; Lovell, J. F. *Frontiers Phys.* **2015**, *3*, Article #23.
- (3) a) Grätzel, M. *J. Photochem. Photobiol. C* **2003**, *4*, 145; b) Lindsey, J. S.; Mass, O.; Chen, C.-Y. *New J. Chem.* **2011**, *35*, 511; c) Suslick, K. S. In *The Porphyrin Handbook*; Kadish, K. M., Smith, K. M., Guillard, R., Eds.; Academic Press: San Diego, 2000; Vol. 4, p 41; d) Meunier, B.; Robert, A.; Pratviel, G.; Bernadou, J. In *The Porphyrin Handbook*; Kadish, K. M., Smith, K. M., Guillard, R., Eds.; Academic Press: San Diego, 2000; Vol. 4, p 119; e) Marchon, J.-C.; Ramasseul, R. In *The Porphyrin Handbook*; Kadish, K. M., Smith, K. M., Guillard, R., Eds.; Academic Press: San Diego, 2003; Vol. 11, p 75; f) Ruppel, J. V.; Fields, K. B.; Snyder, N. L.; Zhang, X. P. In *Handbook of Porphyrin Science*; Kadish, K. M., Smith, K. M., Guillard, R., Eds.; World Scientific: Hackensack, New Jersey, 2010; Vol. 10, p 1.
- (4) Buchler, J. W. In *The Porphyrins*; Dolphin, D., Ed. 1978; Vol. 1, p 389.
- (5) Ding, Y.; Zhu, W.-H.; Xie, Y. *Chem. Rev.* **2017**, *117*, 2203.
- (6) a) Harvey, J. D.; Ziegler, C. J. *Coord. Chem. Rev.* **2003**, *247*, 1; b) Toganoh, M.; Furuta, H. In *Handbook of Porphyrin Science*; Kadish, K. M., Smith, K. M., Guillard, R., Eds.; World Scientific: Singapore, 2010; Vol. 2, p 295; c) Toganoh, M.; Furuta, H. *Chem. Commun.* **2012**, *48*, 937.
- (7) a) Callot, H. J.; Ruppert, R.; Jeandon, C.; Richeter, S. *J. Porphyrins Phthalocyanines* **2004**, *8*, 111; b) Jimenez, A. J.; Jeandon, C.; Gisselbrecht, J.-P.; Ruppert, R. *Eur. J. Org. Chem.* **2009**, *2009*, 5725; c) Richeter, S.; Jeandon, C.; Gisselbrecht, J.-P.; Graff,

- R.; Ruppert, R.; Callot, H. J. *Inorg. Chem.* **2004**, *43*, 251; d) Richeter, S.; Jeandon, C.; Gisselbrecht, J.-P.; Ruppert, R.; Callot, H. J. *Inorg. Chem.* **2007**, *46*, 10241; e) Richeter, S.; Jeandon, C.; Kyritsakas, N.; Ruppert, R.; Callot, H. J. *J. Org. Chem.* **2003**, *68*, 9200; f) Richeter, S.; Christophe, J.; Jean-Paul, G.; Romain, R. In *Handbook of Porphyrin Science*; Kadish, K. M., Smith, K. M., Guillard, R., Eds.; World Scientific Publishing Company: Hackensack, New Jersey, 2010; Vol. 3, p 429; g) Jeandon, C.; Ruppert, R. *Eur. J. Org. Chem.* **2011**, 4098.
- (8) a) Gotardo, M. C. A. F.; Sacco, H. C.; Filho, J. C. S.; Ferreira, A. G.; Tedesco, A. C.; Assis, M. D. *J. Porphyrins Phthalocyanines* **2003**, *7*, 399; b) Zhang, X. A.; Lovejoy, K. S.; Jasanoff, A.; Lippard, S. J. *Proc. Natl. Acad. Sci. U. S. A.* **2007**, *104*, 10780; c) Lv, Y.; Cao, M.; Li, J.; Wang, J. *Sensors* **2013**, *13*, 3131.
- (9) a) Akhigbe, J.; Peters, G.; Zeller, M.; Brückner, C. *Org. Biomol. Chem.* **2011**, *9*, 2306; b) Akhigbe, J.; Haskoor, J. P.; Krause, J. A.; Zeller, M.; Brückner, C. *Org. Biomol. Chem.* **2013**, *11*, 3616.
- (10) a) Khalil, G. E.; Daddario, P.; Lau, K. S. F.; Imtiaz, S.; King, M.; Gouterman, M.; Sidelev, A.; Puran, N.; Ghandehari, M.; Brückner, C. *Analyst* **2010**, *135*, 2125; b) Yu, Y.; Czepukojc, B.; Jacob, C.; Jiang, Y.; Zeller, M.; Brückner, C.; Zhang, J.-L. *Org. Biomol. Chem.* **2013**, *11*, 4613; c) Worlinsky, J. L.; Zarate, G.; Zeller, M.; Ghandehari, M.; Khalil, G.; Brückner, C. *J. Porphyrins Phthalocyanines* **2013**, *17*, 836; d) Worlinsky, J. L.; Halepas, S.; Brückner, C. *Org. Biomol. Chem.* **2014**, *12*, 3991; e) Worlinsky, J. L.; Halepas, S.; Ghandehari, M.; Khalil, G.; Brückner, C. *Analyst* **2015**, *140*, 190; f) Liu, E.; Ghandehari, M.; Brückner, C.; Khalil, G.; Worlinsky, J.; Jin, W.; Sidelev, A.; Hyland, M. *A. Cement Concrete Res.* **2017**, *95*, 232.
- (11) a) Cetin, A.; Ziegler, C. J. *Dalton Trans.* **2005**, 25; b) Liang, L.; Lv, H.; Yu, Y.; Wang, P.; Zhang, J.-L. *Dalton Trans.* **2012**, *41*, 1457; c) Ke, X. S.; Yang, B. Y.; Cheng, X.; Chan, S. L. F.; Zhang, J. L. *Chem–Eur. J.* **2014**, *20*, 4324; d) Ke, X.-S.; Chang, Y.; Chen, J.-Z.; Tian, J.; Mack, J.; Cheng, X.; Shen, Z.; Zhang, J.-L. *J. Am. Chem. Soc.* **2014**, *136*, 9598; e) Tang, J.; Chen, J.-J.; Jing, J.; Chen, J.-Z.; Lv, H.; Yu, Y.; Xub, P.; Zhang, J.-L. *Chem. Sci.* **2014**, *5*, 558.
- (12) a) Crossley, M. J.; King, L. G. *J. Chem. Soc., Chem. Commun.* **1984**, 920; b) Gouterman, M.; Hall, R. J.; Khalil, G. E.; Martin, P. C.; Shankland, E. G.; Cerny, R. L. *J. Am. Chem. Soc.* **1989**, *111*, 3702; c) Jayaraj, K.; Gold, A.; Austin, R. N.; Ball, L. M.; Turner, J.; Mandon, D.; Weiss, R.; Fischer, J.; DeCian, A.; Bill, E.; Mütter, M.; Schünemann, V.; Trautwein, A. X. *Inorg. Chem.* **1997**, *36*, 4555; d) Yu, Y.; Lv, H.; Ke, X.

- Yang, B.; Zhang, J.-L. *Adv. Synth. Catal.* **2012**, *354*, 3509; e) Brückner, C.; Ogikubo, J.; McCarthy, J. R.; Akhigbe, J.; Hyland, M. A.; Daddario, P.; Worlinsky, J. L.; Zeller, M.; Engle, J. T.; Ziegler, C. J.; Ranaghan, M. J.; Sandberg, M. N.; Birge, R. R. *J. Org. Chem.* **2012**, *77*, 6480; f) Hewage, N.; Zeller, M.; Brückner, C. *Org. Biomol. Chem.* **2017**, *15*, 396.
- (13) Luciano, M.; Tardie, W.; Zeller, M.; Brückner, C. *Chem. Commun.* **2016**, *52*, 10133.
- (14) Daniell, H. W.; Williams, S. C.; Jenkins, H. A.; Brückner, C. *Tetrahedron Lett.* **2003**, *44*, 4045.
- (15) Crossley, M. J.; Burn, P. L.; Langford, S. J.; Pyke, S. M.; Stark, A. G. *J. Chem. Soc., Chem. Commun.* **1991**, 1567.
- (16) Hush, N. S.; Reimers, J. R.; Hall, L. E.; Johnston, L. A.; Crossley, M. J. *Ann. N.Y. Acad. Sci.* **1998**, *852*, 1.
- (17) Brückner, C.; McCarthy, J. R.; Daniell, H. W.; Pendon, Z. D.; Ilagan, R. P.; Francis, T. M.; Ren, L.; Birge, R. R.; Frank, H. A. *Chem. Phys.* **2003**, *294*, 285.
- (18) Brückner, C. *Acc. Chem. Res.* **2016**, *49*, 1080–1092.
- (19) a) Adams, K. R.; Bonnett, R.; Burke, P. J.; Salgado, A.; Valles, M. A. *J. Chem. Soc., Chem. Commun.* **1993**, 1860; b) Brückner, C.; Rettig, S. J.; Dolphin, D. *J. Org. Chem.* **1998**, *63*, 2094.
- (20) Akhigbe, J.; Samankumara, L.; Brückner, C. *Tetrahedron Lett.* **2012**, *53*, 3524.
- (21) Motorina, I. A.; Grierson, D. S. *Tetrahedron Lett.* **1999**, *40*, 7211.
- (22) Richeter, S.; Hadj-Aissa, A.; Taffin, C.; van der Lee, A.; Leclercq, D. *Chem. Commun.* **2007**, 2148.
- (23) Falk, J. E.; Phillips, J. N. In *Chelating Agents and Metal Chelates*; Dwyer, F. P., D.P., M., Eds.; Academic Press: New York, London, 1964, p 441.